



Objective Evaluation of Flight Simulator Motion Cueing Fidelity Through a Cybernetic Approach

Daan M. Pool

**Objective Evaluation of
Flight Simulator Motion Cueing Fidelity
Through a Cybernetic Approach**

D.M. Pool

ISBN 978-94-6186-032-3

Printed by Wöhrmann Print Service, Zutphen, The Netherlands.

Cover design by D.M. Pool.

Copyright © 2012 by D.M. Pool. All rights reserved. No part of this publication may be reproduced, stored in a retrieval system, or transmitted, in any form or by any means, electronic, mechanical, photocopying, recording, or otherwise, without the prior permission in writing from the proprietor.

Objective Evaluation of Flight Simulator Motion Cueing Fidelity Through a Cybernetic Approach

PROEFSCHRIFT

Ter verkrijging van de graad van doctor
aan de Technische Universiteit Delft.
op gezag van de Rector Magnificus prof.ir. K.C.A.M. Luyben,
voorzitter van het College voor Promoties,
in het openbaar te verdedigen
op maandag 24 september 2012 om 10.00 uur

door

Daan Marinus Pool

Ingenieur Luchtvaart en Ruimtevaart
geboren te Purmerend

Dit proefschrift is goedgekeurd door de promotor:

Prof.dr.ir. M. Mulder

Copromotor:

Dr.ir. M.M. van Paassen

Samenstelling promotiecommissie:

Rector Magnificus,	voorzitter
Prof.dr.ir. M. Mulder,	Technische Universiteit Delft, promotor
Dr.ir. M.M. van Paassen,	Technische Universiteit Delft, copromotor
Prof.dr. F.C.T. van der Helm,	Technische Universiteit Delft
Prof. F.M. Cardullo, M.Sc.,	State University of New York at Binghamton
Prof.dr.ir. J.E. Bos,	Vrije Universiteit Amsterdam
Dr. J. van der Steen,	Erasmus Universiteit Rotterdam
Dr. S.K. Advani,	International Development of Technology
Prof.dr.ir. J.A. Mulder,	Technische Universiteit Delft, reservelid



Dit onderzoek is mogelijk gemaakt door de Nederlandse Technologiestichting STW, de divisie voor toegepaste wetenschappen van de Nederlandse Organisatie voor Wetenschappelijk Onderzoek (NWO), en het technologie programma van het Ministerie van Economische Zaken.

Summary

Objective Evaluation of Flight Simulator Motion Cueing Fidelity Through a Cybernetic Approach

Daan M. Pool

Flight simulators provide a flexible, safe, efficient, and less costly alternative to real flight. For this reason, flight simulators are widely used in aviation, with applications in both pilot training and a range of research and aircraft system development programs. Due to the fact that the motion of a real aircraft induces forces and moments on pilots' bodies during flight, the importance of replicating these *physical motion stimuli* in flight simulator devices has been assumed and stressed since the very first attempts at flight simulation. Due to technological, practical, and financial limitations, perfect one-to-one replication of the physical motion stimuli that are experienced during flight in ground-based simulators is, however, not feasible.

The extent to which a simulator is capable of replicating the corresponding in-flight environment and experience is typically referred to as its *fidelity*. In addition to the quality of the simulator *motion system hardware*, the key factor that affects the fidelity of simulator motion cueing is the distortion of the aircraft motion stimuli by simulator *motion filter algorithms*. Such motion filters transform the true aircraft rotational and translational motion to a reduced representation of that motion, which is then *cued* using a simulator's motion system. The most notable of these transformations are frequency-independent *scaling*, to reduce overall magnitude of the cued simulator motion, and *high-pass filtering*, to attenuate the low-frequency motion that is especially difficult to replicate. The extent of the distortion of the true aircraft motion induced by a motion filter is largely determined by the values of its *parameters*: the *scaling gains*, high- and low-pass filter *break frequencies*, and other parameters that together define the motion filter dynamics.

It has been argued that high-fidelity simulator motion cueing is indispensable for the training of low-level manual flying skills, that is, for acquiring the correct *skill-based* manual aircraft control behavior. Current guidelines and requirements for achieving high-fidelity simulator motion cueing are, however, mostly technology-centered and largely disregard the human perceptual processes that ultimately define a simulator's fidelity. A limited understanding of human motion perception and how visual and physical motion stimuli are used

for manual control still stands in the way of formulating simulator motion cueing fidelity requirements that adequately account for this human element inherent to flight simulation.

In this thesis, simulator motion cueing fidelity is evaluated at the *behavioral* level, that is, by considering a simulator's ability to induce real-flight *pilot manual control behavior*. This is achieved by comparing pilot manual control behavior between real flight and in a moving-base simulator and analyzing the *behavioral discrepancies* that are induced in the simulator as a result of limitations in the supplied motion stimuli. For this evaluation of behavioral simulator motion fidelity, a *cybernetic approach* is adopted in which the occurring discrepancies in pilot control behavior are analyzed using *multimodal pilot models*. The multimodal pilot models that are used in this thesis for analyzing the contribution of physical motion feedback to pilot manual control behavior explicitly account for pilots' responses to *visual* and *physical motion stimuli*. Fitting such pilot models to time-domain measurements of pilot control behavior using *parameter estimation techniques* allows for the *objective* quantification of multimodal pilot control dynamics and its adaptation to variations in simulator motion fidelity. In this thesis, this approach is utilized to explicitly compare pilot control behavior during skill-based manual control tasks performed in *real flight* with control behavior observed, under a variation in motion filter settings, in a moving-base flight simulator. The simulator motion cueing settings that yield pilot control behavior that most closely matches the measured real-flight behavior are then defined to yield the highest level of behavioral simulator motion fidelity.

The manual control tasks considered for the evaluation of behavioral simulator motion fidelity are skill-based aircraft attitude *tracking tasks*. It has been shown that the control behavior adopted during such tracking tasks is sufficiently stationary and time-invariant to allow for modeling it with *quasi-linear control-theoretical models*. In the considered tracking tasks, pilot control behavior is induced using two *forcing function signals*, with the first inserted as a reference signal that is to be followed, and the second as an external disturbance on the controlled aircraft dynamics. Two different types of tracking tasks are considered in this thesis for the evaluation of behavioral simulator motion fidelity. The first are *compensatory* tracking tasks where the target and disturbance forcing functions are independent *quasi-random multisine signals*, as it has been shown that the contributions of visual and physical motion stimuli to the exhibited pilot tracking behavior can be reliably separated for such tasks. In addition, tracking tasks in which a quasi-random multisine disturbance signal is combined with a *deterministic* target forcing function that consists of multiple ramp-like changes in target attitude are also considered, as such tasks more closely resemble operational manual flying and maneuvering tasks. For these considered *ramp-tracking tasks* pilots, however, no longer use a purely compensatory control strategy. Therefore, an augmentation to the multimodal pilot models that are used for modeling compensatory tracking behavior, which accounts for this change in manual control behavior through an additional pilot feedforward response to the deterministic target forcing function signal, is proposed and evaluated.

This thesis describes a number of experiments, all performed in the SIMONA Research Simulator (SRS) at Delft University of Technology, in which pilot tracking behavior was measured under an applied variation in simulator motion cueing settings. The strongest and most consistent changes in pilot control behavior that are observed with increasing attenuation of the supplied simulator motion, both resulting from reduced motion filter gains and

increased motion filter break frequencies, are observed for pilots' responses to visually presented tracking errors. A compilation of the data from a number of simulator experiments described in this thesis and previous experiments described in literature showed that, on average, the gain of the pilot visual response reduces with around 20% between tracking with one-to-one motion feedback and tracking without physical motion feedback. In addition to this decrease in pilot gain, an around 30% increase in the amount of visual lead equalization performed by pilots, and a slight reduction in the delay of the pilot visual response were also observed as highly consistent effects of motion filter variations on pilot tracking behavior. Pilots' responses to physical motion stimuli were found to be largely unaffected by variations in motion cueing settings.

The major milestone for the research described in this thesis is the direct comparison of multimodal pilot control behavior based on in-flight and simulator measurements of pilot tracking behavior, as this allows for the true evaluation of simulator fidelity with respect to real flight. For the two roll attitude tracking tasks considered for this comparison – one with two multisine forcing function signals, the other a combined ramp-tracking and disturbance-rejection task – the in-flight measurements were collected using Delft University of Technology's Cessna Citation II laboratory aircraft. As it is known that pilot control dynamics are also affected by important task variables such as the display characteristics, sidestick manipulator, and the controlled aircraft and control system dynamics, it was attempted to match these variables as best as possible between both the experimental setups in the laboratory aircraft and the SRS. This was done to ensure that none of these factors affected the desired isolated comparison of the effects of varying motion feedback settings on pilot manual control behavior.

When comparing the considered metrics for the evaluation of in-flight and simulator measurements of pilot tracking behavior, it was found that the control behavior observed in real flight showed an obvious reliance on physical motion feedback, which clearly differentiated the adopted control strategy from that observed under conditions without physical motion feedback. A comparison of the control behavioral measurements collected in real flight and for the simulator motion cueing conditions with roll motion closest to the true aircraft roll motion in the SRS, however, showed slightly degraded task performance and decreased control activity for the in-flight tracking tasks. Furthermore, the most notable behavioral discrepancies that were observed from multimodal pilot model analysis between these sets of data were a decrease in the gain with which pilots responded to visual and physical motion stimuli, an increase in the latency of their responses to visually presented tracking errors, and a decrease in the natural frequency of the neuromuscular actuation dynamics. Using measurements of single-loop tracking behavior collected in both the laboratory aircraft and the SRS, the different neuromuscular actuation dynamics were shown to result from the different sidestick and pilot seat available in both experimental setups. The remaining observed behavioral discrepancies could not be traced back to similar discrepancies in the controlled task variables between the in-flight and simulator parts of the experiments. The fact that the physical motion feedback available in these SRS conditions was in fact equivalent to that available in real flight suggests that these behavioral discrepancies are the result of pilot-centered variables, such as motivation and stress, affecting the comparison of in-flight and simulator measurements of pilot control behavior. Thereby,

these obtained results illustrate the complexity, and perhaps the limitations, of such human-centered in-flight to simulator comparisons.

The cybernetic approach to the evaluation of simulator motion fidelity as proposed and evaluated in this thesis was found to provide valuable insight into the effects of simulator motion cueing fidelity on pilot manual control behavior. This cybernetic approach allowed for the unequivocal confirmation of both the presence and nature of the adaptation of skill-based pilot tracking behavior to variations in high-pass motion filter settings. For the compensatory roll attitude tracking task for which an explicit comparison of pilot tracking behavior measured in real flight and in a moving-base simulator was performed, it was found that, despite the fact that a perfect match of pilot control dynamics in both environments was not observed, pilot control dynamics for experimental conditions with only very limited attenuation by roll motion filters matched the baseline in-flight measurements best. This was especially reflected in behavioral metrics that were shown to most clearly reveal the adaptation of pilot control dynamics to variations in motion cueing, such as the pilot visual gain and lead time constant. Despite the modified control task due to the use of a deterministic ramp forcing function signal, the same was observed for the roll attitude ramp-tracking task for which this comparison of in-flight and simulator behavior was also performed. All experimental results described in this thesis therefore suggest that achieving the highest level of behavioral simulator motion fidelity corresponds to replicating the motion stimuli that are utilized by pilots during manual control with *as limited attenuation as possible*.

Due to the success of the adopted cybernetic approach in quantifying the behavioral adaptation induced by motion filter dynamics, important future work is thought to be the extension of the adopted methods to true operational manual control and maneuvering tasks. This requires significant extension of the models of pilot manual control behavior that are currently available, as well as demanding the development of parameter estimation techniques suitable for the identification of such models. Furthermore, to assess the severity of the behavioral adaptations observed in this thesis for the development of manual flying skills in flight simulators where limited motion stimuli are provided, it is important to explicitly analyze control-skill development, by application of the same cybernetic approach, in investigations where the transfer of such simulator training is evaluated.

Contents

Summary	vii
1 Introduction	1
1.1 Background	1
1.1.1 Flight Simulation in Aviation	1
1.1.2 Simulator Motion Cueing	3
1.1.3 Pilot Behavior and Moving-Base Simulator Training	5
1.1.4 Evaluating Simulator Motion Cueing Fidelity	7
1.2 Approach	10
1.2.1 Manual Control Behavior During Tracking	10
1.2.2 The Cybernetic Approach	12
1.3 Thesis Objective	15
1.4 Thesis Structure	18
I Pilot Model Development	23
2 Modeling Pilot Control of Aircraft Pitch Dynamics	25
2.1 Introduction	27
2.2 Pilot Compensation in Manual Control	28
2.2.1 Background	28
2.2.2 Control Task	31
2.2.3 Multimodal Pilot Model	32
2.2.4 Controlled Dynamics	34
2.2.5 Pilot Equalization	35
2.3 Experiment	37
2.3.1 Forcing Functions	37
2.3.2 Apparatus	38
2.3.3 Conditions, Participants and Experimental Procedure	40
2.3.4 Pilot Model Identification	41
2.4 Results	41
2.4.1 Identified Equalization Dynamics	41
2.4.2 Comparison with Measured Pilot Describing Functions	44
2.4.3 Variance Accounted For Evaluation	47
2.4.4 Effects of Physical Motion Feedback on Pilot Equalization	49

2.5	Discussion	52
2.6	Conclusions	53
3	Modeling Pilot Control During Ramp Tracking	55
3.1	Introduction	57
3.2	Background	58
3.2.1	Control Task	58
3.2.2	Successive Organization of Perception	60
3.2.3	Modeling Manual Control Behavior	62
3.2.3.1	Modeling Compensatory Control	62
3.2.3.2	Modeling Pursuit/Precognitive Control	62
3.3	Experiment	66
3.3.1	Apparatus	66
3.3.2	Controlled Element Dynamics	67
3.3.3	Forcing Functions	67
3.3.4	Independent Variables	69
3.3.5	Participants, Experimental Procedures, and Instructions	69
3.3.6	Dependent Measures	70
3.3.7	Hypotheses	71
3.4	Results	72
3.4.1	Measured Time Traces	72
3.4.2	Tracking Performance and Control Activity	72
3.4.3	Pilot Modeling Results for Pure Compensatory Tasks	75
3.4.4	Pilot Modeling Results for Ramp-Tracking Tasks	77
3.4.4.1	Time-Domain Pilot Model Fits	77
3.4.4.2	Pilot Model Parameter Estimates	82
3.5	Discussion	87
3.6	Conclusions	89
II	Preliminary and Previous Simulator Experiments	91
4	Effects of Heave Washout During Pitch Tracking	93
4.1	Introduction	95
4.2	Heave Motion During Pitch Maneuvering	96
4.2.1	Heave Motion Components	96
4.2.2	Heave Motion Filter	97
4.2.3	Observed Effects of Heave	99
4.3	Experiment	99
4.3.1	Method	100
4.3.1.1	The Aircraft Pitch Control Task	100
4.3.1.2	Independent Variables	101
4.3.1.3	Dependent Measures	102
4.3.1.4	Pilot Model	103
4.3.1.5	Apparatus	104

4.3.1.6	Participants and Experimental Procedures	105
4.3.2	Hypotheses	105
4.4	Results	106
4.4.1	Tracking Performance and Control Activity	106
4.4.2	Crossover Frequencies and Phase Margins	108
4.4.3	Pilot Modeling Results	111
4.4.3.1	Pilot Model Validation	111
4.4.3.2	Pilot Model Parameter Estimates	113
4.5	Discussion	117
4.6	Conclusions	119
5	Effects of Motion Filter Settings on Tracking Behavior	121
5.1	Introduction	123
5.2	Background	124
5.2.1	Simulator Motion Fidelity	124
5.2.2	Pilot Tracking Behavior	125
5.2.3	Motion Fidelity and Tracking Behavior	126
5.3	Method	127
5.3.1	Selection Criteria: Dependent Measures	127
5.3.2	Predictors: Motion Fidelity Measures	129
5.3.3	Selected Studies	130
5.3.4	Pilot Model Tuning Rule Development	133
5.3.4.1	Data Normalization	133
5.3.4.2	Linear Regression Modeling	135
5.4	Results	136
5.4.1	Predictor Variable Selection	136
5.4.2	Notable Trends in Dependent Measures	137
5.4.2.1	Tracking Performance and Control Activity	137
5.4.2.2	Crossover Frequencies and Phase Margins	138
5.4.2.3	Pilot Behavioral Parameters	140
5.5	Discussion	143
5.6	Conclusions	145
III	In-Flight to Simulator Behavioral Comparisons	147
6	Multisine-Tracking Behavior in Real and Simulated Flight	149
6.1	Introduction	151
6.2	Behavioral Simulator Motion Fidelity	152
6.2.1	Roll Tracking Task	152
6.2.1.1	Control Task	152
6.2.1.2	Forcing Functions	154
6.2.1.3	Controlled Element	155
6.2.2	Modeling Multimodal Pilot Tracking Behavior	157
6.2.3	Motion Filter and Pilot-Vehicle System Dynamics	158

6.3	Offline Pilot-Vehicle System Analysis	159
6.3.1	Analysis Setup	159
6.3.2	Analysis Parameters	160
6.3.3	Analysis Results	161
6.3.3.1	Pilot-Vehicle System Open-Loop Dynamics	161
6.3.3.2	Crossover Frequencies and Phase Margins	162
6.3.3.3	Closed-Loop Tracking Performance	167
6.4	Experiment Setup	170
6.4.1	Apparatus	170
6.4.1.1	Cessna Citation II Laboratory Aircraft	170
6.4.1.2	SIMONA Research Simulator	170
6.4.1.3	Side Stick Manipulator	172
6.4.2	Simulator Motion Cueing	172
6.4.3	Independent Variables	173
6.4.4	Participants	175
6.4.5	Experimental Procedure	175
6.4.5.1	Simulator Measurements	175
6.4.5.2	In-Flight Measurements	176
6.4.6	Dependent Measures	176
6.4.7	Hypotheses	177
6.5	Results	178
6.5.1	Subjective Motion Fidelity Ratings	179
6.5.2	Tracking Performance and Control Activity	179
6.5.3	Crossover Frequencies and Phase Margins	182
6.5.4	Pilot Control Behavior	184
6.6	Discussion	190
6.7	Conclusions	192
7	Ramp-Tracking Behavior in Real and Simulated Flight	193
7.1	Introduction	195
7.2	Control Task	197
7.2.1	Roll Ramp-Tracking Task	197
7.2.2	Forcing Functions	199
7.2.3	Aircraft Motion During Ramp-Tracking	201
7.2.4	Modeling Multimodal Ramp-Tracking Behavior	203
7.2.4.1	Feedforward Pilot Response Model	204
7.2.4.2	Compensatory Pilot Response Models	205
7.2.5	Discrete Maneuvering Analysis using Phase-Planes	206
7.3	Experiment	208
7.3.1	Apparatus	208
7.3.2	Independent Variables	208
7.3.3	Participants	209
7.3.4	Dependent Measures	210
7.3.5	Experimental Procedures	210
7.3.6	Hypotheses	211

7.4	Results	213
7.4.1	Subjective Motion Fidelity Ratings	213
7.4.2	Tracking Performance and Control Activity	214
7.4.3	Pilot Modeling Results	218
7.4.3.1	Pilot Model Quality of Fit	218
7.4.3.2	Pilot Model Parameter Estimates	221
7.5	Discussion	225
7.6	Conclusions	228
8	Roll Motion Filter Settings and Multisine-Tracking Behavior	229
8.1	Introduction	231
8.2	Background	232
8.2.1	Roll Tracking Task	232
8.2.2	Modeling Multimodal Pilot Tracking Behavior	233
8.2.3	Previously Reported Behavioral Effects of Roll Washout	235
8.2.4	Offline Prediction and Analysis of Washout Effects	237
8.2.4.1	No Pilot-Adaptation Analysis	237
8.2.4.2	Prediction of Washout Effects on Pilot Tracking	238
8.3	Experiment Setup	240
8.3.1	Apparatus	240
8.3.2	Controlled Element	240
8.3.3	Forcing Functions	241
8.3.4	Simulator Motion Cueing	242
8.3.5	Independent Variables	242
8.3.6	Participants	243
8.3.7	Experimental Procedure	243
8.3.8	Dependent Measures	245
8.3.9	Hypotheses	246
8.4	Results	247
8.4.1	Subjective Motion Fidelity Ratings	248
8.4.2	Tracking Performance and Control Activity	249
8.4.3	Crossover Frequencies and Phase Margins	252
8.4.4	Pilot Control Behavior	254
8.4.4.1	Pilot Model Parameter Estimates	255
8.4.4.2	Pilot Model Quality of Fit	258
8.4.4.3	Pilot Model Control Signal Variance Contributions	258
8.4.5	Comparisons with Offline Prediction Data	260
8.4.6	Comparisons with In-Flight Tracking Measurements	264
8.5	Discussion	266
8.6	Conclusions	269

9	Conclusions and Recommendations	271
9.1	Conclusions	273
9.1.1	Modeling and Identification of Manual Control Behavior	273
9.1.2	Effects of Motion Filter Settings on Tracking Behavior	274
9.1.3	In-Flight and Simulator Tracking Behavior Comparisons	276
9.1.4	The Cybernetic Approach	277
9.2	Recommendations	279
	References	283
A	Pilot Visual Response Modeling	303
A.1	Introduction	303
A.2	Pilot Model Structures	304
A.3	Analysis Setup	306
A.3.1	Pilot Model Simulations	306
A.3.2	Data Analysis	306
A.4	Results	307
A.4.1	Delay Sensitivity Analysis	307
A.4.2	Delay Identifiability Analysis	308
A.5	Conclusions	311
B	Pilot Model Identification Using Ramp Target Signals	313
B.1	Introduction	314
B.2	The Pilot Model Identification Problem	315
B.2.1	Control Task	315
B.2.2	Pilot Model	316
B.2.3	Parameter Estimation Procedure	318
B.3	Ramp Forcing Function Characteristics	319
B.3.1	Fourier Transforms of Ramps and Steps	319
B.3.2	Comparison with Multisine Signal	320
B.3.2.1	Time Domain	321
B.3.2.2	Frequency Domain	322
B.4	Method	324
B.4.1	Pilot Model Simulations	324
B.4.2	Forcing Functions	325
B.4.3	Identification Procedure	326
B.4.4	Dependent Measures and Hypotheses	326
B.5	Results	327
B.5.1	Example Simulation Results	327
B.5.2	Pilot Model Estimation Results	329
B.6	Discussion	334
B.7	Conclusions	335

C	In-Flight Experiment Hardware Verification Tests	337
C.1	Visual Display Delay Measurements	337
C.2	Force Stick Measurements	339
C.2.1	Static Force-Voltage Characteristic Measurements	339
C.2.2	Force Stick Describing Function Measurements	340
C.2.3	Stick Output Noise and Bias Characteristics	342
C.3	Gyro Describing Function Measurements	343
D	In-Flight Experiment Software and Timing	347
D.1	July/August 2009 Experiments	347
D.1.1	Experiment Software Setup	347
D.1.1.1	dSPACE Software	348
D.1.1.2	DUECA Software	350
D.1.1.3	UDP Communication	352
D.1.1.4	Tracking Error Calculation	353
D.1.2	Experiment Software Timing Issues	353
D.1.2.1	Software Timing Issues Evaluation	353
D.1.2.2	Timing Issues Evaluation Test Setup	355
D.2	October/December 2010 Experiments	357
D.2.1	Experiment Software Setup	357
D.2.1.1	Modifications to dSPACE Software	357
D.2.1.2	Modifications to DUECA Software	359
D.2.1.3	Modifications to UDP Communication	359
D.2.1.4	Modifications to Tracking Error Calculation	359
D.2.2	Experiment Software Timing Verification	359
E	Cessna Citation II Fly-By-Wire and Aircraft Dynamics Model	363
E.1	Model Structure and Implementation	363
E.2	Fly-By-Wire Control System Model	364
E.3	Aerodynamic Hinge Moment Model	367
E.4	Citation II Aircraft Dynamics Model	369
E.5	Comparison of Model Responses and In-Flight Measurements	370
F	Aircraft and Simulator Single-Loop Tracking Measurements	373
F.1	Introduction	374
F.2	Tracking Performance and Control Activity	374
F.3	Crossover Frequencies and Phase Margins	375
F.4	Pilot Control Behavior	375
G	Simulator Hood Tracking Measurements	379
G.1	Introduction	379
G.2	Tracking Performance and Control Activity	381
G.3	Pilot-Vehicle System Crossover Parameters	382
G.3.1	Pitch Tracking	382
G.3.2	Roll Tracking	385

G.4 Pilot Modeling Results	385
G.4.1 Pitch Tracking	385
G.4.2 Roll Tracking	389
G.5 Discussion	389
H Motion Fidelity Pilot Comments	393
I Roll Tracking Replicated Condition Comparison	405
I.1 Subjective Evaluations	406
I.2 Tracking Performance and Control Activity	408
I.3 Crossover Frequencies and Phase margins	410
I.4 Pilot Control Behavior	410
I.5 Conclusions	413
Nomenclature	415
Samenvatting	418
Acknowledgments	423
Curriculum Vitae	427
Publications	429

1

Introduction

1.1 Background

1.1.1 Flight Simulation in Aviation

The first flight simulation devices appeared almost as soon as the first functional aircraft were developed at the beginning of the 20th century [Rolfe and Staples, 1986; Allen, 1993; Allerton, 2009]. In these early days of aviation, piloting was still a highly precarious occupation due to the relative aerodynamic instability and general lack of structural strength, engine power, and safety mechanisms of the aircraft that were available. Therefore, the need for rigorous understanding of aircraft control, dynamics, and stability before attempting to fly an actual aircraft were soon recognized. The first flight simulator devices, of which two examples, the *Antoinette Learning Barrel* and the *Link Trainer* are shown in Fig. 1.1, were therefore developed to facilitate the on-ground training of flying tasks in order to bring down in-flight accident rates.

Since these early efforts, the aviation industry's reliance on flight simulators for pilot training has continuously increased [Allen, 1993; Allerton, 2009, 2010]. Due to the inherently safe environment, the increased efficiency in the repeated execution of certain maneuvers, and the reduced costs compared to in-flight training, pilots currently conduct a major part of their training in simulators, especially their training of critical and emergency maneuvers. Active airline pilots are required to attend regular simulator training sessions during the course of their careers to maintain their flying skills and to allow for monitoring their proficiency. As the culmination of simulator-based training, the first *ab initio* pilots, who during their education only received flight training in flight simulators, are currently active with a number of the world's airlines [Bürki-Cohen et al., 2001]. It has been ar-

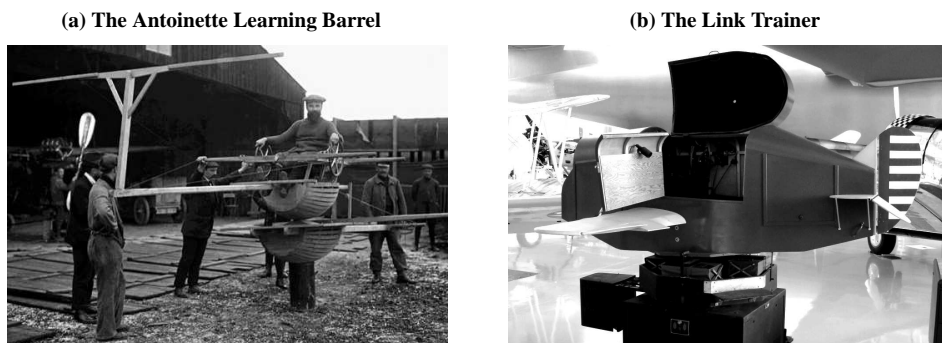


Figure 1.1. Two examples of pioneering moving-base flight simulator devices: the *Antoinette Learning Barrel* (a) [Allerton, 2009] and the *Link Trainer* (b).

gued that without flight simulators, aviation would not have been able to achieve its current impressive level of safety [Allerton, 2009].

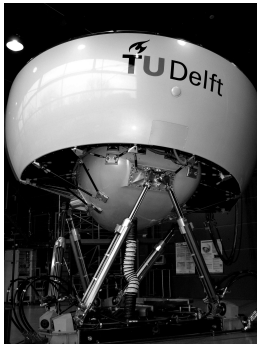
Pilot training is, however, no longer the sole function of flight simulator devices. Flight simulators have seen additional use as fundamental tools for research into flight control and control interface design [Mulder and Mulder, 2005; Borst et al., 2008; Lam et al., 2009; Lombaerts et al., 2009], aircraft handling qualities [Bray, 1964; Field et al., 2002b; Gouverneur et al., 2003; Damveld, 2009; Stroosma et al., 2011], and human motion perception and manual control behavior [Van Paassen, 1994; Schroeder, 1999; Stroosma et al., 2003; Valente Pais et al., 2010]. Mirroring the same reasons for simulator usage in pilot training, flight simulators are also found to provide a flexible, efficient, safe and cost-effective alternative to real flight for these research applications.

Most flight simulator devices include a number, if not all, of the following subsystems [Sinacori, 1978; Baarspul, 1990]: a model that simulates the dynamics of the aircraft, true-to-life flight instruments, loaded control manipulators, an out-of-the-window visual view, and a motion system to emulate the forces and moments that act on pilots' bodies during flight. The current standard in moving-base flight simulation, commonly referred to as a *full motion flight simulator*, is a device equipped with a true-to-life aircraft cockpit and flight instruments, a high-resolution and wide field-of-view outside visual system, and a hydraulically or electrically driven hexapod motion system¹. Two examples of such typical moving-base flight simulators are depicted in Fig. 1.2. Even though the large majority of the moving-base flight simulators that are currently in use resemble the devices shown in Fig. 1.2, devices with more advanced and exotic designs – such as those including centrifuge capabilities [Wentink et al., 2005; Valente Pais et al., 2009], serial robotic actuators, [Teufel et al., 2007], and extremely large linear displacement actuators [Aponso et al., 2009] – are also in use, mostly for research purposes.

For some of the subsystems of flight simulator devices, achieving a satisfactory level of correspondence with the aircraft that is to be simulated, or *simulator fidelity*, is com-

¹Hexapod motion systems, which consist of six parallel linear actuators, are also referred to as *synergistic motion systems*, *Stewart-Gough platforms*, or *Stewart platforms*. The latter two names refer to their credited inventor, Eric Gough, and the first scientific publication in which such a system is described by Stewart [1966].

(a) The SIMONA Research Simulator



(b) The CAE 7000 Full Flight Simulator



Figure 1.2. Examples of modern moving-base flight simulator devices: the SIMONA Research Simulator at Delft University of Technology (a) and the CAE 7000 commercial full flight simulator (b) [CAE, 2009].

paratively straightforward. This is for instance the case for replicating an aircraft's physical cockpit environment and flight instruments, for which simply (replicas of) real aircraft components can be installed. For other subsystems, achieving such correspondence is not nearly as straightforward, or can only be achieved at great cost. The most notable examples of simulator subsystems for which this is the case, and for which therefore still some improvements with respect to the current standard in flight simulation are possible, are those used for generating realistic out-of-the-window views and, most notably, the motion systems used for the generation of physical sensations of motion.

1.1.2 Simulator Motion Cueing

Compared to aircraft, which can move through the air virtually without limitations, moving-base flight simulators such as those depicted in Fig. 1.2 have always been severely limited in their motion envelopes. This causes the generation of motion cues in flight simulation to be an inevitable compromise between the desired level of achievable correspondence between the motion cues supplied in simulators and those perceivable in real flight, and the size and quality, and hence cost, of the simulator motion system [Schmidt and Conrad, 1970; Conrad et al., 1973; Advani et al., 1999]. For instance, the quality of the motion cues supplied in moving-base flight simulators is strongly dependent on the dynamics of the simulator motion system itself and its resulting characteristics such as latency, bandwidth, and smoothness [Chung, 2000; Advani and Hosman, 2006; Nieuwenhuizen, 2012]. In addition to these effects of motion system hardware on motion cue fidelity, a second major factor in the achieved level of simulator motion fidelity lies in the methods that are typically applied for the cueing itself.

The desire to limit the size and cost of simulator motion systems has spurred the development of smart methods for transforming the true aircraft motion to a reduced representation of that motion in flight simulators [Schmidt and Conrad, 1970; Conrad et al., 1973]. This transformation of (simulated) aircraft motion to simulator motion is commonly achieved by

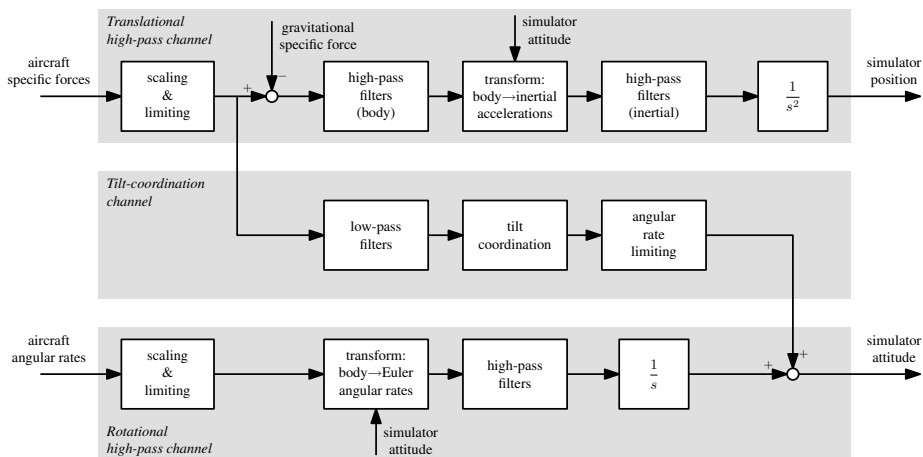


Figure 1.3. Classical simulator motion washout algorithm structure as defined by Reid and Nahon [1985].

algorithms referred to as *motion filters* or *washout algorithms*. These algorithms take their name from one of their main functions: by *filtering* the true aircraft motion they continuously “wash-out” the simulator rotational and linear accelerations to retain as much of the available motion space for cueing as possible. One of the most frequently applied and most intensively studied motion filters, referred to as the *classical washout* algorithm [Reid and Nahon, 1985, 1986a,b; Grant, 1996], is depicted in Fig. 1.3.

As shown in Fig. 1.3, the *classical washout* algorithm transforms aircraft translational specific forces and rotational rates into corresponding simulator translational and rotational motion through three different channels. The translational and rotational high-pass channels apply a combination of *scaling* and attenuation with *high-pass filters* to the aircraft translational and rotational motion, respectively, in order to reduce their absolute magnitude and to remove the low-frequency components that typically yield large amplitude simulator motion excursions [Schmidt and Conrad, 1970; Conrad et al., 1973]. In addition to these direct high-pass channels, Fig. 1.3 further shows a coupling between both these channels. This coupling is implemented to allow for better cueing of sustained low-frequency translational specific forces by tilting the simulator cabin with respect to gravity, a motion cueing strategy typically referred to as *tilt coordination*.

A large number of different motion filter algorithm designs and implementations have been proposed, including algorithms with time-varying and adaptive elements [Parrish et al., 1975; Riedel and Hofmann, 1978; Nahon et al., 1992] and motion filter designs based on linear optimal control theory [Kosut, 1979; Sturgeon, 1981; Sivan et al., 1982; Telban et al., 1999]. However, the basic attenuation of the true rotational and translational aircraft motion through frequency-independent scaling and high-pass filtering, as also performed in the high-pass channels of the classical washout algorithm shown in Fig. 1.3, is common to practically all of these proposed motion filter algorithms.

As their main function is to manipulate the true aircraft motion to the extent that it can be presented on moving-base flight simulators, motion filters by definition introduce discrepancies between the true aircraft motion and the motion perceivable in the simulator. For a given motion filter algorithm, the extent of the distortion of the true aircraft motion induced by this motion filter is determined by the values of its *parameters*: the *scaling gains*, high- and low-pass filter *break frequencies*, and other parameters that together define the motion filter dynamics. Despite the inevitable discrepancies, it is currently accepted that with a properly designed motion filter algorithm with properly tuned parameters a reasonably accurate presentation of those motion cues that are important to pilots can still be achieved in moving-base flight simulation [Grant and Reid, 1997a,b].

1.1.3 Pilot Behavior and Moving-Base Simulator Training

Due to the undeniable availability of information on the motion of the aircraft through a sensation of body motion in real flight, the standing belief has been that motion cueing in flight simulators is absolutely indispensable for achieving optimal transfer of simulator training to true aircraft control, especially for the development of low-level manual flying skills [Allen, 1993; Ray, 1996; Mulder et al., 2004; Allerton, 2009]. In addition to providing useful information to pilots, the sensation of motion in the aircraft is also argued to be disorienting and confusing to pilots in some cases, leading to the conclusion that training in the absence of this motion stimulation would not adequately prepare pilots for their true task [Gundry, 1977; Allerton, 2009]. Numerous studies have shown, however, that the increased realism intended with the motion cueing in flight simulators is not needed for all aspects of pilot training [Caro, 1973; Hosman, 1999; Hosman et al., 2001]. Intuitively, this also makes sense, as during some of the tasks that are trained in flight simulators, for instance communication with air traffic control and modification of autopilot settings, pilot behavior is most likely unaffected by the physical motion of the aircraft at all. Still, it has been argued that for a final integration of all learned skills, and for true assessment of the learned piloting behavior, full flight simulators with the capability of presenting physical aircraft motion are still required [Ray, 1996; Hosman, 1999].

Some of the controversy with respect to the requirement for simulator motion in pilot training stems from the fact that it is not a single type of *behavior* that is trained by pilots in flight simulator devices. For distinguishing between these different types of behavior that are of interest with respect to pilot training, the skills-rules-knowledge taxonomy of Rasmussen [1983] is a highly valuable concept. Rasmussen makes a distinction between three different levels of human cognitive behavior:

- *skill-based behavior*, the lowest level, represents the most elementary form of human information-processing and involves basic control tasks that are often executed intuitively or subconsciously;
- *rule-based behavior*, the intermediate level, represents human behavior that is performed based on rules and procedures that have been learned in the past; and
- *knowledge-based behavior*, the highest level, is defined as behavior that is guided by high-level cognitive problem solving skills.

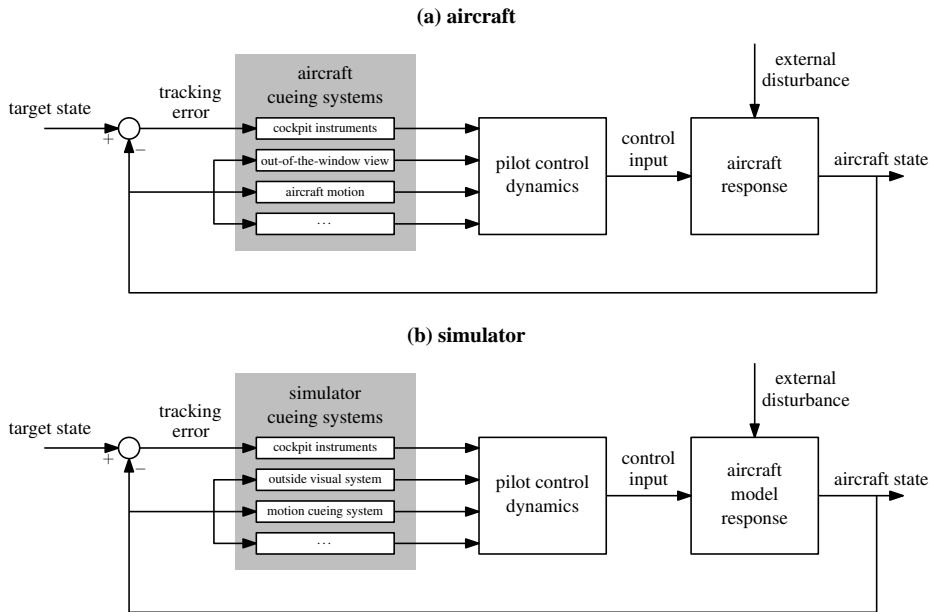


Figure 1.4. A schematic representation of a closed-loop skill-based aircraft control performed in an aircraft (a) and in a flight simulator (b).

For the training of rule-based and knowledge-based pilot behavior, it is accepted that the current generation of flight simulators sufficiently supports the transfer of learned skills to the real aircraft, also due to a reduced requirement for high-fidelity cueing of visual and motion stimuli [Caro, 1973; Durlach et al., 2000; Hettinger and Haas, 2003]. For skill-based control behavior, however, for which training involves pilots' intimate familiarization with the inherent dynamics and handling qualities of the aircraft they are to fly, it is argued that significantly higher levels of simulator fidelity are required [Hosman, 1999; Hosman et al., 2001; Hettinger and Haas, 2003]. Schematic representations of such a skill-based manual aircraft control tasks, as performed in an aircraft and in a moving-base flight simulator, are depicted in Fig. 1.4.

Fig. 1.4(a), shows a skill-based manual control task performed in a real aircraft, where a pilot is exerting control on the aircraft based on feedback information perceived from his cockpit instruments, the out-of-the-window view, his physical sensation of motion, or some other perceived cues. As indicated in Fig. 1.4(a), skill-based manual aircraft control tasks can typically be characterized as pilots' efforts to bring the state of the aircraft to a certain defined *target state*, possibly in the presence of an *external disturbance* that perturbs the controlled aircraft. The pilot's objective in such a task is therefore essentially to limit the magnitude of the *tracking error*, that is, the difference between the commanded and actual aircraft state. As described by McRuer and Jex [1967a], for achieving this objective, pilots typically identify those perceivable quantities that are suitable for achieving adequate feedback control dynamics from all available stimuli and utilize these selected stimuli in

a skill-based feedback-control strategy. Note that during such skill-based manual aircraft control, the pilot effectively closes one or multiple loops around the controlled aircraft dynamics, equivalent to how an automatic feedback-control system would be constructed by a control engineer.

Fig. 1.4(b) shows where possible differences in this closed-loop pilot-aircraft system can occur when considered in a simulator environment. In a simulator, the dynamics of the aircraft need to be simulated using a mathematical model. The accuracy of such mathematical aircraft models is typically high, especially when simulating aircraft responses well within the flight envelope, as is the case under normal operating conditions. Recently, however, some concern has arisen with respect to the fidelity of the aircraft models applied in flight simulation for simulating aircraft responses at extreme attitudes and during upset recovery [Advani et al., 2010].

Assuming an accurate model of the aircraft's dynamics, however, the main difference between Figures 1.4(a) and (b) lies in the possible effects of the simulator cueing systems that provide feedback of the aircraft state to the pilot through multiple sensory *modalities*, such as the visual and vestibular systems. Discrepancies in the cueing of these *multimodal* stimuli, for instance those resulting from the motion filter algorithms applied for simulator motion cueing, may affect the "look and feel" provided by the simulator. Numerous investigations have shown that perceived handling qualities, piloting technique, and control performance are sensitive to the way these multimodal stimuli are presented in simulators [Reid and Nahon, 1986b; Knotts and Bailey, 1988; Schroeder, 1999; Field et al., 2002b; Lee et al., 2003]. In extreme cases, it is feared that cueing discrepancies may result in pilots learning manual flying skills that allow them to adequately fly the simulator, but which do not transfer to the real aircraft. Due to the comparatively large discrepancies that occur in the presentation of physical motion stimuli in flight simulators, this concern applies especially to simulator motion cueing fidelity.

1.1.4 Evaluating Simulator Motion Cueing Fidelity

The formulation of requirements and guidelines for achieving adequate levels of simulator motion cueing fidelity has shown to be a difficult problem that the flight simulation community has struggled with for decades [Anonymous, 1980; Ashkenas, 1986; Hosman, 1999; Hosman et al., 2001]. The main reason for this difficulty is a limited understanding of human motion perception, manual control behavior, and skill-development under multimodal cueing conditions. Progress is further hampered by the strong dependency of these phenomena, on the simulated aircraft, task, and scenario, which makes it extremely difficult to draw generalized conclusions with respect to best practices for achieving a sufficient level of simulator motion fidelity.

Different definitions of *fidelity* as the metric for evaluating the quality of simulator cueing devices have been proposed [Fedderson, 1962; Sinacori, 1978; Anonymous, 1980; Hefley et al., 1981; Ashkenas, 1986]. Fig. 1.5 shows a schematic representation of these different definitions of fidelity. Note that in correspondence with Fig. 1.4, Fig. 1.5 shows two closed-loop pilot-vehicle systems, representative for skill-based manual control tasks performed in real flight and in a flight simulator, respectively. The different definitions of sim-

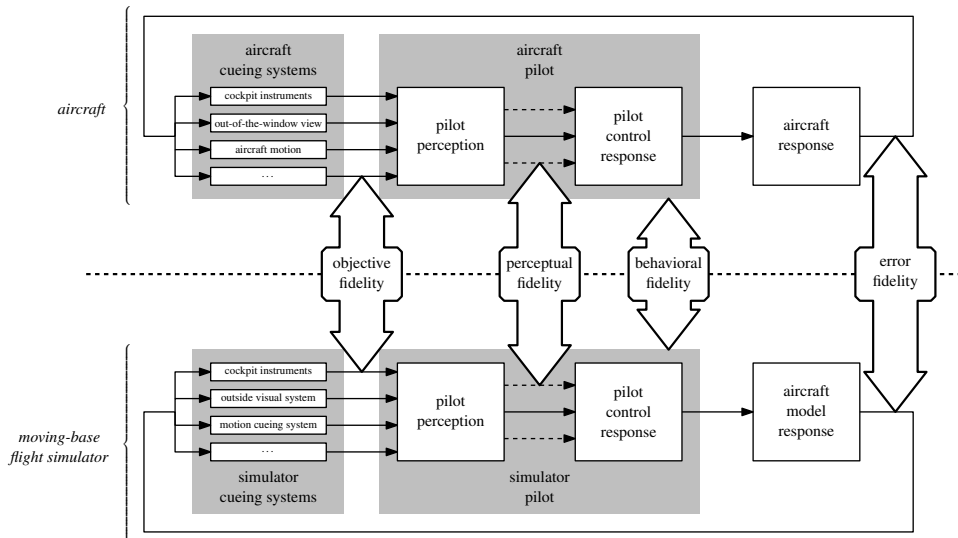


Figure 1.5. Schematic representation of how flight simulator fidelity can be evaluated at mechanical, perceptual and behavioral levels.

ulator cueing fidelity, corresponding to different locations in the closed-loop pilot-vehicle systems where these systems are compared, are indicated with white-filled arrows.

Perhaps the most workable definition of fidelity shown in Fig. 1.5 is *objective fidelity* (also referred to as *engineering fidelity*) [Anonymous, 1980; Ashkenas, 1986], which is the degree to which the simulator replicates the true aircraft in an absolute sense. Objective fidelity is therefore purely determined by the quality of the simulated aircraft dynamics and the simulator cueing systems, as can be verified from Fig. 1.5. As aircraft model fidelity is typically considered separately, objective simulator cueing fidelity is hence most often evaluated by explicitly considering the characteristics of the simulator cueing hardware. In fact, the most notable available flight simulator fidelity requirements are stated in terms of simulator hardware capabilities, for instance, by specifying lower limits for characteristics of the visual and motion systems such as time delay and bandwidth [Anonymous, 2003, 2005, 2009]. Furthermore, most of the criteria that have been proposed for evaluating simulator motion cueing fidelity also purely account for the dynamic characteristics of the motion filter algorithm and the motion system hardware [Sinacori, 1977; Schroeder, 1999; Advani and Hosman, 2006].

One drawback of evaluating simulator cueing fidelity at the objective level is that it can only be considered for each cueing component and, in case of motion cueing, degree-of-freedom *separately*. Evaluating the *total* level of objective fidelity achieved in a simulator is therefore not straightforward. Furthermore, when evaluating objective fidelity *any* discrepancy induced by the simulator cueing systems corresponds, by definition, to a degradation in fidelity. Even though optimization of simulator hardware and cueing systems may indeed go a long way in the optimization of simulator cueing fidelity, it does not take any of the

limitations of the human perceptual system into account that can be (and are) frequently exploited in flight simulators [Brown et al., 1989]. Therefore, optimizing objective fidelity does typically not result in the most efficient and cost-effective simulator cueing solution. This is especially true for simulator motion cueing. With our current level of simulator technology, increasing the objective fidelity of motion cueing systems requires ever larger and more expensive hardware.

To explicitly account for the influence of perceptual processes in the evaluation of simulator fidelity, it has alternatively been proposed to evaluate *perceptual fidelity*. As indicated in Fig. 1.5, perceptual fidelity is defined to be high when pilots' perception of stimuli presented in a simulator is indistinguishable from those perceivable during a real-flight maneuver. Hence, perceptual fidelity is *pilot-centered*, as opposed to objective fidelity. The main issue with perceptual fidelity, however, is finding an appropriate and reliable method for measuring it. One method used for evaluating perceptual fidelity is the evaluation of the perceptual errors induced by simulator cueing devices using mathematical models of the "pilot perception" block shown in Fig. 1.5. Note that this yields an evaluation of simulator fidelity similar to that performed for determining objective fidelity, where, additionally, the characteristics and limitations of the human motion perception processes that are of interest are taken into account through these perceptual models. Even though the individual perceptual sensors are perhaps sufficiently understood to allow for modeling their response [Gum, 1973; Fernandez and Goldberg, 1971; Hosman, 1996], a limited understanding of how sensory outputs of these different sensors are integrated in the brain [Gum, 1973; Sinacori, 1978; Zacharias and Young, 1981; Borah et al., 1988; Bos and Bles, 2002] still stands in the way of truly allowing for evaluation of perceptual fidelity using this approach.

An alternative method for determining perceptual fidelity has been to assess it *subjectively* by asking evaluation pilots to judge how well their perception of the stimuli provided in a simulator matches the real world case. Numerous studies have been performed in which pilots were asked to indicate their perceived level of simulator motion fidelity through subjective motion fidelity rating scales [Reid and Nahon, 1986b; Grant and Reid, 1997b; Chung et al., 1998; Mikula et al., 1999; Schroeder, 1999]. The fact that motion perception is an inherently subconscious process – that is, an activity that is normally performed without a conscious thought process – implies that the forced subjective evaluation of perceived stimuli might be difficult and not yield results that are representative for perceptual processes under "normal" conditions. Furthermore, such subjective evaluations of simulator fidelity are typically found to be strongly affected by expectation and personal preferences and biases. For instance, due to these factors, the evaluation of different simulator motion filter algorithms and motion filter parameter settings using subjective pilot indications of perceived motion fidelity has been found to be a troublesome and often unrepeatable process in a number of investigations [Parrish and Martin, 1976; Reid and Nahon, 1986b; Grant and Reid, 1997a,b; Beukers et al., 2010].

Due to the difficulties in the measuring of perceptual fidelity, it has also been suggested to evaluate a simulator's cueing fidelity by its capacity to induce similar *control errors* – that is, errors in the attained aircraft response compared to perfect maneuver execution – as observed in real flight. This definition of fidelity is typically referred to as *error fidelity* [Ashkenas, 1986], and is indicated in Fig. 1.5 with the rightmost arrow. Note from Fig. 1.5 that error fidelity is a direct result of the pilot perceptual and control response processes. For

this reason, measures of task performance have been used as pilot-centered metrics of simulator cueing fidelity in a large number of investigations [Reid and Nahon, 1986b; Zaichik et al., 1999; Schroeder, 1999; Chung, 2000; Telban et al., 2005b]. A major issue with the evaluation of this error fidelity is that when confronted with degraded simulator cueing, pilots are likely to adapt their control response dynamics to achieve the best attainable level of task performance under these modified conditions [Young, 1969; McRuer and Jex, 1967a]. Due to this behavioral adaptation, analysis of performance metrics is unlikely to capture the full extent of the effects of degraded cueing fidelity on a closed-loop pilot-vehicle system as depicted in Fig. 1.5 [Mulder et al., 2004].

The final definition of fidelity depicted in Fig. 1.5 is *behavioral fidelity*, which has been defined by Heffley et al. [1981] as “*the specific quality of a simulator that permits the skilled pilot to perform a given task in the same way that it is performed in the actual aircraft.*”. In Fig. 1.5, this is indicated as the comparison of the gray-shaded “aircraft pilot” and “simulator pilot” blocks. Behavioral fidelity is high if a simulator induces pilots to utilize the same control behavior, where the governing pilot control dynamics are based on the same selection of all available stimuli, as observed in real flight. Of all fidelity definitions depicted in Fig. 1.5, behavioral fidelity evaluates the quality of a simulator in terms that most directly apply to the skill-based manual control skills that are to be developed. Even though the measuring of pilots’ control dynamics and finding appropriate behavioral metrics for quantifying their control behavior are by no means easy tasks, it can provide a pilot-centered approach to the evaluation of simulator fidelity based solely on *objective* control behavioral measurements. For these two reasons, this thesis focuses on the evaluation of simulator motion cueing fidelity at this behavioral level.

1.2 Approach

This thesis describes an effort to evaluate simulator motion fidelity based on explicit measurements of *skill-based pilot control behavior* and its *adaptability* to the attenuation of the supplied simulator motion cues by motion filter algorithms. Furthermore, it is attempted to relate observed changes in pilot control behavior to the selected *motion filter parameters*. The originality of the work described in this thesis lies in the *objective* and *quantitative* evaluation of behavioral flight simulator motion fidelity that is performed. To facilitate this quantitative approach, this thesis focuses on skill-based control behavior in *manual tracking tasks*, as it has been shown that for such continuous and stationary control tasks the adopted pilot control dynamics can be accurately *modeled* and determined *objectively* using *system identification* and *parameter estimation techniques*.

1.2.1 Manual Control Behavior During Tracking

Based on pioneering research into manual tracking behavior by Tustin [1947] and Elkind [1956], an elaborate framework for the analysis and modeling of skill-based manual control behavior during *compensatory* tracking was formulated in the 1960s [McRuer and Krendel, 1959; Krendel and McRuer, 1960; McRuer et al., 1965; McRuer and Jex, 1967a; McRuer and Krendel, 1974]. Much of our current knowledge on skill-based manual control behavior

stems from these investigations into pilot dynamics during *single-loop* compensatory tracking tasks, where pilots performed manual control tasks with only explicit feedback of the tracking error from a visual display [Elkind, 1956; McRuer et al., 1965; McRuer and Jex, 1967a]. As also observed in the description of Fig. 1.4 in this thesis, the similarities between automatic control systems and compensatory manual control behavior were noted in these early investigations into manual tracking. This spurred the application of methods that were initially developed for the analysis and design of automatic control systems to the analysis of skill-based manual control behavior. *Forcing function signals*, which were either inserted as the *target state* or *external disturbance* shown in Fig. 1.4, were used in these experiments to induce pilot control behavior [Elkind, 1956; McRuer and Krendel, 1959]. Typically, these forcing function signals were *quasi-random multisine signals*, which were constructed as the sum of a number of individual sinusoids that spanned the frequency range over which manual control behavior was to be induced. In addition to yielding easily reproducible signals that were perceived as sufficiently random to induce only compensatory behavior, the use of such multisine forcing functions facilitated the identification of frequency-domain describing functions of the pilot control dynamics for such compensatory tracking tasks.

From such measurements, pilot control dynamics under such conditions were found to be sufficiently linear and time-invariant to allow for modeling them with *quasi-linear control-theoretical models* [McRuer et al., 1965; McRuer and Jex, 1967a]. These quasi-linear models consist of a linear part that describes pilots' responses to all relevant perceived variables using transfer function models of the adopted pilot dynamics, supplemented with a *remnant* signal that accounts for all otherwise unmodeled nonlinearities. Such quasi-linear models of single-loop compensatory tracking behavior have been used to analyze manual control behavior in many later experiments [Van Gool, 1978; Van der Vaart, 1992; Van Paassen, 1994; Sentouh et al., 2009] and have also shown to be a valuable tool for the prediction of pilot-vehicle system characteristics in a wide range of different man-machine systems and applications [Ashkenas and McRuer, 1962; Johnston and Aponso, 1988; Cameron et al., 2003].

One of the key properties of human manual control that was established from this extensive research into compensatory tracking behavior is the fact that human operators are found to *adapt* their own control dynamics to a myriad of factors. This is for instance reflected in the well-known *crossover model* described by McRuer et al. [1965], which illustrates and explains the adaptation of human manual control dynamics to the dynamics of the system (or vehicle) that is controlled. McRuer and Jex [1967a] compiled an excellent categorized overview all different variables that may affect human manual control behavior during manual control, which is reproduced in Fig. 1.6.

As can be verified from Fig. 1.6, McRuer and Jex [1967a] defined four different groups of variables that influence human manual control dynamics in a closed-loop pilot-vehicle system. The most important of these factors are the *task variables*, which define the nature and characteristics of the manual control task itself. As indicated in Fig. 1.6, important task variables are the displays and ways in which feedback information is presented to the human pilot, the applied forcing function signals, and the dynamics of the control manipulator and the controlled element. *Environmental variables*, which define the environment in which the control task is performed, can further affect a manual control system and its performance. The same holds for *operator-centered variables*, such as motivation and stress,

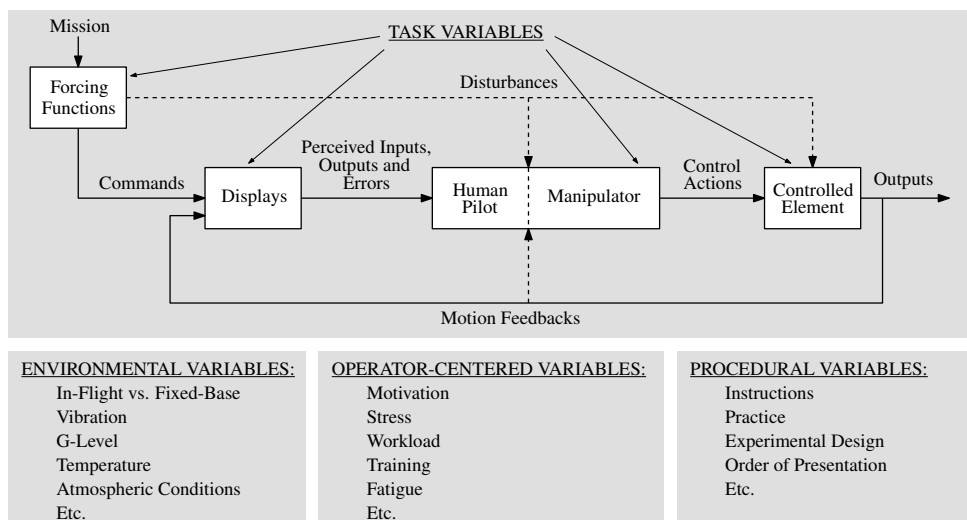


Figure 1.6. The variables that affect a pilot-vehicle system as defined by McRuer and Jex [1967a].

and *procedural variables*, such as the received instructions and the time allowed for practice. Changes in any of these variables are likely to result in adaptation of the adopted manual control dynamics and can hence affect the overall dynamics and performance of the closed-loop pilot-vehicle system.

As can be verified from Fig. 1.6, “*motion feedbacks*” is also defined as one of the important task variables that affect pilot control behavior by McRuer and Jex [1967a]. Many subsequent investigations have indeed confirmed a strong effect of the presence of physical motion feedback, and of variations in the level of fidelity with which it is presented in a simulator, on skill-based control behavior and tracking performance during manual tracking [Shirley and Young, 1968; Stapleford et al., 1969; Levison and Junker, 1977; Levison, 1978; Jex et al., 1981; Hosman, 1996; Van der Vaart, 1992; Schroeder, 1993].

1.2.2 The Cybernetic Approach

This observed adaptation of skill-based manual control behavior to variations in physical motion feedback allows for the explicit evaluation of simulator motion fidelity at the behavioral level using a *cybernetic approach*. Such a cybernetic approach involves the studying of the fundamental properties of the interaction between the human operator and his environment centered around the presented stimuli, in this case the information that is used for manual control [Wiener, 1961; Mulder, 1999]. In this thesis, this cybernetic approach is implemented by explicitly quantifying the way in which the physical motion feedback that is supplied in moving-base flight simulators affects and contributes to skill-based manual control behavior through the use of *mathematical models of multimodal pilot control behavior*.

To allow for isolated evaluation of the effects of simulator motion cueing fidelity on pilot control behavior, this thesis focuses on aircraft *attitude* tracking tasks where in addition to variables presented on a central visual display, most notably the tracking error, *only* physical motion feedback of the aircraft motion is available to pilots. A schematic representation of such an attitude tracking task with physical motion feedback, and an example of a *quasi-linear multimodal pilot model* that is used in this thesis for the analysis of manual control behavior in such a task, is depicted in Fig. 1.7.

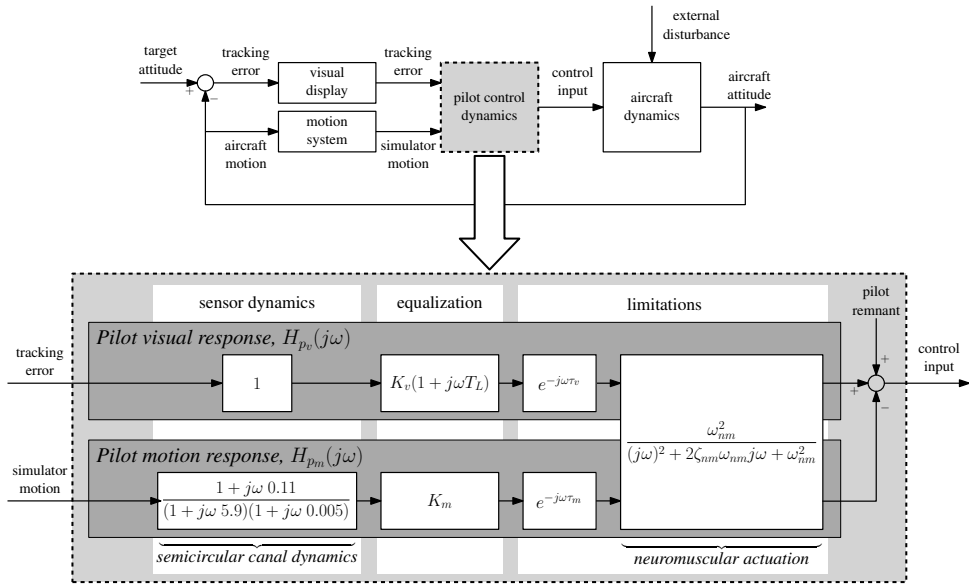


Figure 1.7. An example of a multimodal pilot model as used for quantification of pilot control behavior in this thesis.

The multimodal pilot model of Fig. 1.7 includes separate pilot visual and motion responses that account for the portions of the pilot control input that are attributable to responses to visually presented tracking errors and perceived motion feedback, respectively. The model has a multiple-input single-output structure, which relates the model inputs, the tracking error and the supplied physical motion stimulus, to the given pilot control inputs that form the model output. As the linear responses with which these input-output dynamics are modeled cannot account for the nonlinearities that are inherent to human manual control behavior, a *pilot remnant* signal is included in this model, as is also done in the quasi-linear modeling of single-loop compensatory tracking behavior [McRuer et al., 1965; McRuer and Jex, 1967a]. The multimodal pilot model shown in Fig. 1.7 is highly similar to the models proposed for capturing pilot control dynamics in the presence of physical motion feedback in a number of earlier investigations [Stapleford et al., 1969; Jex et al., 1981; Hosman, 1996; Van der Vaart, 1992; Hess, 1990b].

As indicated in Fig. 1.7, the multimodal pilot models utilized in this thesis model the pilot dynamics adopted during tracking tasks with physical motion feedback in terms of dis-

tinct contributions that are physically interpretable. For instance, the dynamics of the visual and motion perception *sensors*, that is, the eyes with which the tracking error is perceived from a visual display and the semicircular canals of the vestibular system that are sensitive to rotational motion stimulation, are explicitly accounted for in the model. It is known that the perception of physical body motion is the result of the integration of the sensations obtained from multiple modalities (vestibular, tactile, proprioceptive) [Gum, 1973; Borah et al., 1988; Zaichik et al., 1999]. Only the semicircular canal dynamics are included in the multimodal pilot model shown in Fig. 1.7, however, as it has been argued that for the perception of rotational motion the SCC are the dominant sensor [Young, 1966; Hosman and Van der Vaart, 1978]. In addition to these sensor dynamics, the model further accounts for some of the *limitations* of human manual control behavior that are found to affect pilot control dynamics, such as the time delays incurred in the perception and processing of the visual and motion information and the neuromuscular actuation dynamics. Finally, the modeled *equalization* dynamics in the visual and motion channels of the model represent pilots' interpretation and usage of the perceived information in the formulation of an appropriate control input. For example, Fig. 1.7 shows *lead* equalization dynamics in the pilot visual response path, which can describe pilots' responses to both perceived *tracking errors* and *tracking error rate*. On the other hand, the equalization dynamics in the pilot motion response channel are seen to be a pure gain, indicating a pilot response that is purely proportional to the physical motion perceived through the semicircular canals.

The multimodal pilot model shown in Fig. 1.7 has seven free model parameters: the pilot visual and motion response gains K_v and K_m , the visual equalization lead time-constant T_L , the visual and motion response delays τ_v and τ_m , and the natural frequency and damping ratio (ω_{nm} and ζ_{nm} , respectively) of the model for the neuromuscular actuation dynamics. These model parameters together fully characterize and quantify the adopted pilot control dynamics. Hence, in the cybernetic approach followed in this thesis, it is these pilot model parameters that are considered as metrics for evaluating the effects of varying motion cueing settings on pilot control behavior.

The key to using such multimodal pilot model parameters as metrics for quantifying changes in pilot control behavior is hence a *parameter estimation method* that is capable of yielding reliable and accurate estimates of these parameters based on measurements of the model in- and outputs. One of the main observations made with respect to the effects of physical motion feedback on pilot tracking behavior is that for control tasks where significant lead equalization is required for achieving satisfactory pilot-vehicle system dynamics, the availability of physical motion feedback is seen to yield a drastic reduction in the amount of visual lead equalization that is performed [Stapleford et al., 1969; Jex et al., 1981; Hosman, 1996; Van der Vaart, 1992]. Instead, part of the required lead equalization dynamics is then obtained from the available physical motion feedback information through the pilot motion response. Note that this implies that the control dynamics pilots adopt for their responses to visual and motion stimuli can have inherently similar dynamic characteristics. This causes such multimodal pilot models to typically have an *overdetermined* model structure, that is, multiple different combinations of model parameters can yield an almost identical model response and therefore provide a similarly good fit to experimental measurements [Zaal et al., 2009a]. For this reason, obtaining estimates of the parameters of a multimodal pilot model as depicted in Fig. 1.7 that allow for proper evaluation of the

relative contributions of pilots' visual and motion responses, and changes therein, is not straightforward.

A number of different identification methods have been proposed for estimating the parameters of such overdetermined multimodal pilot models. A frequently applied approach consists of two steps, in which first frequency-domain describing functions of both the pilot visual and motion responses are estimated using spectral methods [Stapleford et al., 1967; Van Paassen and Mulder, 1998]. In the second step of such a two-step approach, a parametric model as depicted in Fig. 1.7 is then fit to the obtained describing functions to obtain the estimates of the model parameters. A drawback of such a two-step approach is that estimation errors in the determination of the describing function estimates in the first step affect the reliability of the parameter estimates obtained from the second step. Furthermore, the spectral methods typically used to obtain the describing function estimates in the first step of this approach demand the use of two independent multisine forcing function signals – which are typically inserted as target and disturbance signals, see Fig. 1.7 – in order for reliable separation of the pilot visual and motion responses to be obtained [Stapleford et al., 1967; Van Paassen and Mulder, 1998]. Nieuwenhuizen et al. [2008] have shown that the estimation of frequency domain describing functions can also be performed using linear time-invariant models, such as Auto-Regressive models with an eXogeneous input (ARX). Though still requiring a second step to estimate the multimodal pilot model parameters, this approach is found to yield more accurate describing function estimates with superior frequency-domain resolution.

More recently, a one-step time-domain identification method based on maximum likelihood estimation has been developed specifically for application to the problem of estimating multimodal pilot model parameters [Zaal et al., 2009a]. With this method it is possible to estimate the parameters of a multimodal pilot model directly from the time-domain measurements, which has been shown to yield more accurate and reliable results than obtained with two-step identification methods [Zaal et al., 2009a]. A further advantage of this time-domain identification method is that, as long as sufficient excitation of both pilot visual and motion responses is retained, the forcing functions used for inducing pilot control behavior are no longer required to be independent multisine signals. For these reasons, this time-domain identification method described by Zaal et al. [2009a] is applied in this thesis for estimating the parameters of the utilized multimodal pilot models.

1.3 Thesis Objective

The first objective of this thesis is to explicitly compare measurements of skill-based pilot control behavior collected in *real flight* with measurements collected in a *moving-base flight simulator* under varying motion cueing conditions. The availability of two state-of-the-art facilities at Delft University of Technology, the SIMONA Research Simulator (SRS) and the Cessna Citation II laboratory aircraft, facilitates this direct comparison of skill-based pilot control behavior measured in real flight and in a moving-base flight simulator. The second, and main, objective of this thesis is to *trace back* discrepancies in multimodal pilot control behavior that are observed through the adopted cybernetic approach, to the way the physical motion information is presented in the simulator, that is, to variations in high-pass

motion filter parameter settings. A schematic representation of the different steps in this cybernetic approach to the assessment of simulator motion fidelity is depicted in Fig. 1.8.

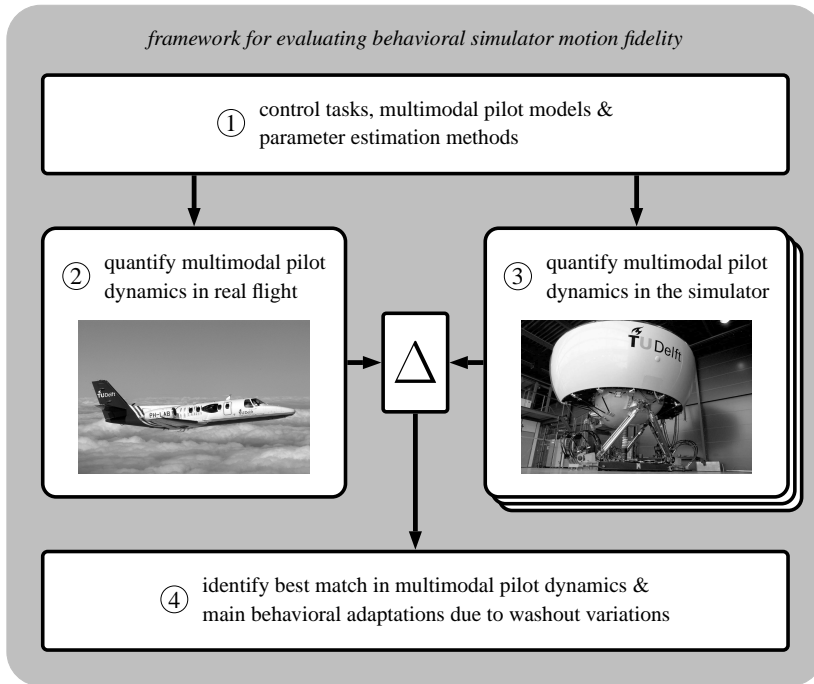


Figure 1.8. Graphical representation of the cybernetic approach adopted in this thesis.

The first step in achieving the objectives of this thesis is the selection of the control tasks that are considered for the evaluation of simulator motion fidelity (Block ① in Fig. 1.8). This task selection is coupled to the development of multimodal pilot models and corresponding parameter estimation methods that allow for application of the desired cybernetic approach. As indicated in Block ②, the selected control tasks are then performed in *real flight* to collect measurements pilot tracking behavior under conditions with *true aircraft motion feedback*. These in-flight measurements are then used as a baseline in a comparison with pilot tracking behavior, for exactly the same control tasks, observed in a moving-base flight simulator, for a wide variation in the simulator motion filter settings (Block ③). From this comparison of tracking behavior measured in real flight and in a moving-base flight simulator the behavioral discrepancies (“ Δ ”) that occur due to attenuated simulator motion stimuli will be identified and used to indicate which motion cueing settings yield the best match of true in-flight tracking behavior. These behavioral discrepancies are deduced from the comparison of the identified values of the parameters (gains, time constants, delays) of multimodal pilot models as depicted in Fig. 1.7, which together fully quantify the adopted multimodal pilot control dynamics. It should be noted that, equivalent to the definition of behavioral fidelity as proposed by Feddersen [1962]; Heffley et al. [1981]; Ashkenas [1986], the approach depicted in Fig. 1.8 is centered around the assumption that if the visual

and motion information presented in a flight simulator sufficiently matches that perceived in real flight, multimodal pilot control behavior equivalent to that exhibited in real flight will be adopted in this simulator.

For evaluating simulator motion fidelity according to the approach shown in Fig. 1.8, it is of critical importance that the accuracy of the obtained pilot model parameter estimates that are used to characterize multimodal pilot control dynamics is as high as possible. Due to the fact that tracking tasks performed with quasi-random multisine target and disturbance forcing function signals have been shown to consistently yield accurate estimates of multimodal pilot model dynamics [Stapleford et al., 1969; Nieuwenhuizen et al., 2008; Zaal et al., 2009a], such tasks are also mainly considered in this thesis. In addition, however, skill-based tracking tasks in which more deterministic target forcing function signals consisting of multiple ramp-like changes in reference attitude are also considered for evaluating behavioral flight simulator motion fidelity in this thesis. As opposed to the tracking of quasi-random signals, such *ramp forcing function signals* yield a control task, and a corresponding motion sensation, that is comparable to discrete maneuvering tasks that are often performed during operational manual aircraft control, such as a series of commanded altitude captures or turn entries and exits [Pool et al., 2009b; Zaal et al., 2010]. It should be noted, however, that the currently available models of skill-based multimodal pilot control behavior, as depicted in Fig. 1.7, have only been validated for purely compensatory tracking tasks with quasi-random multisine forcing function signals. Necessary extensions to the available multimodal pilot models that can account for possible deviations from purely compensatory control behavior that occur during such *ramp-tracking tasks* are therefore proposed and validated in this thesis (Block ① in Fig. 1.8).

In-flight measurements of skill-based tracking behavior in real flight similar to those described in this thesis have been collected in a number of earlier experiments [Smith, 1966; Newell and Smith, 1969; Mooij, 1973; Van Gool and Mooij, 1976; Hess and Mnich, 1986; Steurs et al., 2004]. In most of these earlier studies these in-flight measurements were also compared to tracking behavior measured in fixed-base or moving-base flight simulators. The in-flight experiments described in this thesis, however, clearly distinguish themselves from these earlier efforts to compare in-flight and ground-based tracking behavior for two reasons. First, the analysis methods applied in these earlier studies did not permit the separation of pilots' responses to visual and motion stimuli. Instead, pilot dynamics were analyzed based on a single, lumped, pilot describing function or estimated pilot-vehicle system dynamics. As opposed to the analysis with multimodal pilot models as performed in this thesis, analysis of such lumped describing functions does not permit true interpretation of the extent to which visual and motion information is used by pilots in skill-based tracking tasks. Hence, such an approach also does not allow for true evaluation of the possible differences between the multimodal pilot dynamics that are adopted in real flight and in ground-based simulators [Steurs et al., 2004; Kaljouw et al., 2004]. In addition to this methodological difference, a direct comparison pilot tracking behavior measured in real flight and under a wide variation in simulator motion filter parameter settings, as performed in this thesis, has not been reported before.

1.4 Thesis Structure

Fig. 1.9 shows a graphical representation of the structure of this thesis. As is clear from this figure, this thesis consists of three different parts, labeled I–III. Furthermore, a distinction is made in Fig. 1.9 between chapters that consider pilot control behavior in tracking tasks with only quasi-random forcing function signals (chapters at left) and chapters in which control behavioral measurements for tracking tasks with deterministic ramp forcing function signals are evaluated (chapters at right). First, Part I of this thesis (Chapters 2 and 3) describes two contributions to the development of the behavioral pilot models that form the foundation of the cybernetic approach adopted in this thesis (Block ① of Fig. 1.8). Part II, consisting of Chapters 4 and 5, then describes the reported effects of motion cueing variations on pilot tracking as observed in a preliminary simulator experiment performed in the SRS and in a number of earlier studies reported in literature. Part III of this thesis describes the comparison of pilot tracking behavior measured in real flight and for varying motion cueing settings in a moving-base flight simulator, as indicated by Blocks ②–④ in Fig. 1.8. Finally, the main conclusions, recommendations and some directions for future research are described in Chapter 9.

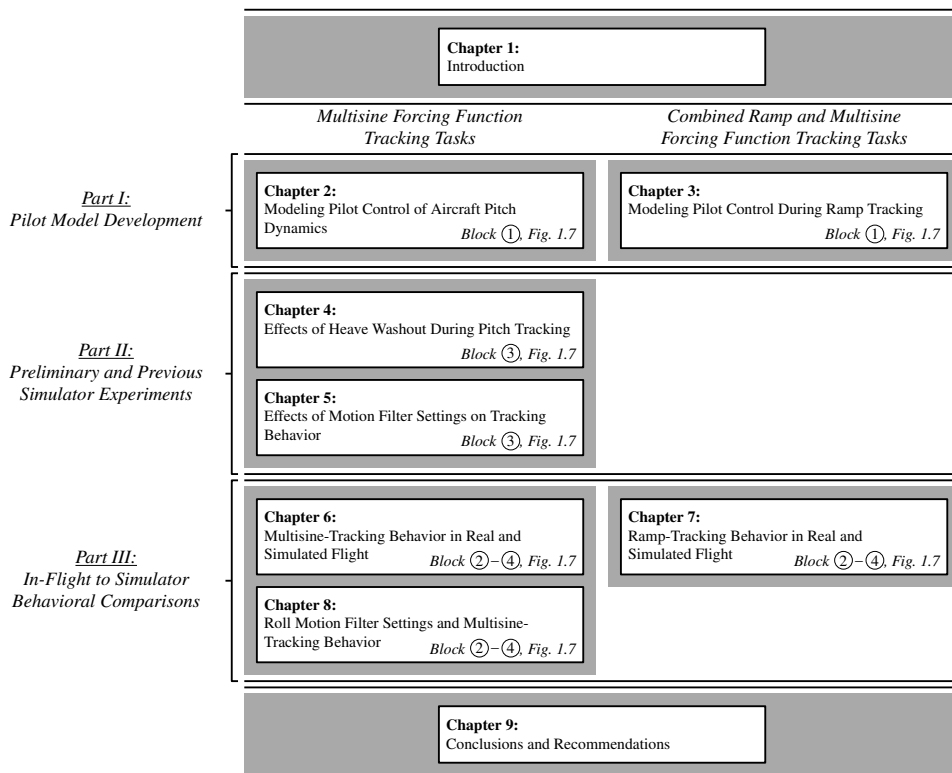


Figure 1.9. Graphical representation of the structure of this thesis.

It should be noted that all chapters of this thesis, except this introduction and the conclusions of Chapter 9, have been written as papers that were either presented at a scientific conference or that have been (or are to be) submitted for publication in scientific journals. The papers that have already been published elsewhere were included here with only minor modifications. The fact that each chapter is in fact written as a separate paper has the advantage that it allows for all individual chapters to be read separately. The first page of each chapter provides a short introduction of the scope of that chapter, how the work described there relates to the overall thesis topic and to the research described in other chapters of this thesis. A short description of the scope and contents of each chapter is provided below.

Part I: Pilot Model Development

Chapter 2 describes an extension to the models of compensatory pilot control behavior that are described in literature that was found to be required for accurate modeling of the visual pilot equalization dynamics adopted during compensatory control of typical conventional longitudinal aircraft dynamics. Using collected measurements of pilot tracking behavior for such a controlled element, the need for this pilot model extension is illustrated and shown to be required for correct interpretation of the effects of the addition of physical motion feedback based on fitted pilot model parameters.

Chapter 3 describes an experiment performed to evaluate the control behavioral consequences of using deterministic target forcing function signals consisting of multiple ramp-like changes in reference attitude for the tracking tasks as considered in this thesis. Due to the deterministic nature of these forcing function signals, it was thought to be likely that they induce a control strategy that deviates from the purely compensatory control observed for the tracking of unpredictable multisine signals. This chapter utilizes collected measurements of ramp-tracking behavior to verify if pilot model extensions are required for modeling the manual control dynamics observed in such ramp-tracking tasks.

Part II: Preliminary and Previous Simulator Tracking Experiments

Chapter 4 describes a pitch tracking experiment in which pilot control behavior was evaluated for a variation in simulator pitch and heave motion cueing. During pitch maneuvering with a conventional aircraft, significant vertical heave motion is perceivable in the cockpit in addition to the rotational pitch motion. Due to the severe limitations in presenting aircraft heave motion on typical moving-base flight simulators, aircraft heave motion cues are typically heavily attenuated by high-pass motion filters in simulator motion filter algorithms. The experiment that is described in this chapter focuses on the effects of attenuating the component heave motion that pilots may utilize during aircraft pitch control on their adopted control dynamics.

Chapter 5 gives an overview of the effects of high-pass motion filter settings on pilot tracking behavior reported in a number of experiments described in literature and this thesis. By compiling the data of these different experiments, it is attempted to identify consistent trends with varying motion cueing settings in the behavioral metrics that are typically considered for the evaluation of changes in pilot tracking behavior. Furthermore, for those behavioral metrics that consistently show significant variation with applied variations in mo-

tion filter settings, linear prediction equations are derived that allow for offline prediction of the behavioral adaptation induced by a certain high-pass motion filter setting.

Part III: Comparisons of In-Flight and Simulator Pilot Tracking Behavior

Chapter 6 describes a direct comparison of compensatory pilot roll tracking behavior measured in real flight and in a moving-base flight simulator for a roll attitude tracking task with quasi-random multisine target and disturbance forcing function signals. This experiment is a major milestone for the research described in this thesis, as it is one of the few studies in which in-flight and simulator measurements of pilot control behavior are directly compared and where pilot control behavior is analyzed using multimodal pilot models. The behavioral discrepancies that occur between real flight and under four different roll motion cueing settings in a moving-base flight simulator are objectively quantified with the adopted cybernetic approach. This chapter further includes a detailed description of the setup of this combined simulator and in-flight experiment and the experiment described in Chapter 7.

Chapter 7 provides the comparison between measurements of pilot tracking behavior collected in real flight and in a moving-base flight simulator for a roll tracking task with a deterministic ramp target forcing function signal. During this more operationally relevant control task, a number of commanded turn maneuvers are performed by pilots. Due to the coordinated nature of aircraft turn maneuvers, this yields a different motion sensation, and perhaps different usage of motion feedback for manual control, than for the compensatory roll tracking task considered in Chapter 6. The analysis of pilot control behavior for this experiment relies heavily on the model proposed for the modeling of pilot dynamics in ramp-tracking tasks in Chapter 3.

Chapter 8 describes the results of an experiment performed to collect additional reference simulator measurements for the comparison of compensatory roll tracking behavior with in-flight measurements described in Chapter 6. In this experiment pilot roll tracking behavior was measured for exactly the same roll tracking task as considered in Chapter 6. Measurements of pilot tracking behavior were collected for ten different simulator roll motion cueing settings, defined by ten different settings of a first-order high-pass roll motion filter, spanning the full range of high to low motion fidelity as defined by previously formulated motion fidelity criteria.

The research described in this thesis was performed during a six-year research project with the title “A Cybernetic Approach to Assess Simulator Fidelity”, for which a “Vidi” grant from the “Stichting voor de Technische Wetenschappen” (STW) was awarded to Prof. dr. ir. M. Mulder in 2005 (grant number 07058). Two PhD students worked on this project and both wrote separate theses. The first thesis, “Pilot Control Behavior Discrepancies Between Real and Simulated Flight Caused by Limited Motion Stimuli” by Peter Zaal [2011], was published more than a year before the completion of this thesis, and complements the work described here. It describes the majority of the work that was performed, in collaboration with the author of this thesis, in the development of the multimodal pilot models and identification techniques that are also applied in this thesis (Block ① of Fig. 1.8) and the details of the design and implementation of the custom fly-by-wire control system that was used to collect the in-flight measurements of pilot tracking behavior (Block ② of Fig. 1.8). Finally, Zaal [2011] also describes a comparison of in-flight and simulator control behavior,

equivalent to that performed for roll attitude tracking tasks in this thesis, for a pitch attitude tracking task, for which the effects of varying pitch and heave motion cueing settings on pilot control behavior were evaluated.

Part I

Pilot Model Development

2

Modeling Pilot Control of Aircraft Pitch Dynamics

The first step of the research project that has resulted in the writing of this thesis (see Fig. 1.8) involved further development of the current standard in multimodal pilot modeling and the identification techniques for estimating the parameters of such pilot models from measured data. Most of the work from this phase of the research project is described in the first thesis to come out of this research project [Zaal, 2011]. This chapter describes one further contribution made in the field of modeling of pilot control behavior during compensatory tracking. An extension to the pilot models described in literature, which was found to be required for modeling the adopted pilot equalization during control of typical longitudinal aircraft dynamics, is proposed and validated using experimental measurement data. The extension to modeling pilot control proposed in this chapter is further applied in Chapter 4 of this thesis and in other related papers [Zaal et al., 2009b,c, 2010, 2011] for modeling pilot control behavior during compensatory pitch tracking tasks.

The contents of this chapter have been published as:

Pool, D.M., Zaal, P.M.T., Damveld, H.J., Van Paassen, M.M., Van der Vaart, J.C., and Mulder, M., "Modeling Wide-Frequency-Range Pilot Equalization for Control of Aircraft Pitch Dynamics", *Journal of Guidance, Control, and Dynamics*, 34(5), 2011, pp. 1529-1542.

2.1 Introduction

Ever since the foundations for focused research into human dynamics during manual control were laid by Elkind [1956] and McRuer et al. [1965] for compensatory tracking tasks, the modeling of pilot manual control behavior has been of interest to many applications in the field of aerospace engineering ever since. Notable examples are the evaluation of aircraft handling qualities [McRuer et al., 1960; Ashkenas and McRuer, 1962; Hall, 1963; Hess, 1995; Damveld, 2009], the assessment of flight simulator cueing fidelity [Hess and Malsbury, 1991; Zeyada and Hess, 2003; Steurs et al., 2004; Zaal et al., 2009b,a; Grant and Schroeder, 2010], the design of aircraft flight control systems [Hess, 1990a], and the evaluation of manipulator characteristics [Johnston and Aponso, 1988; Mitchell et al., 1992] and perspective guidance displays [Mulder and Mulder, 2005].

One of the key characteristics of pilot tracking behavior is that human operators are seen to adapt their control behavior to a myriad of external and internal factors [McRuer and Jex, 1967a]. Perhaps the most apparent form of this adaptation is the fact that human operators are seen to modify their own equalizing control dynamics to yield an open-loop pilot-vehicle system that has the properties of a well-designed feedback control system, that is, an open-loop system with approximately single integrator dynamics over a limited frequency range around the gain crossover frequency [McRuer et al., 1965; McRuer and Jex, 1967a]. For modeling pilot dynamics in the crossover region, including this adaptation to the dynamics of the controlled element, McRuer et al. [1965] have proposed the *extended crossover model*, which includes an explicit lag-lead pilot equalization term that can be modified to model control of different types of controlled elements. Furthermore, as the validity of the *extended crossover model* was found to be restricted to a limited frequency range around crossover, McRuer et al. proposed their *precision model* for the modeling of pilot dynamics over the full range of frequencies where pilot dynamics are typically evaluated. Compared to the *extended crossover model*, the *precision model* has additional terms to model very low-frequency pilot lag and the neuromuscular actuation dynamics that are observed at frequencies well above crossover. The *precision model* further includes the same lag-lead pilot equalization term as used for capturing pilot equalization in the crossover region in the *extended crossover model*.

Recent experiments into the effects of physical motion feedback during compensatory tracking tasks have indicated that considerable changes in pilot tracking behavior under varying motion cueing settings not only occur around crossover, but also at frequencies that are well above the pilot-vehicle system crossover frequency [Nieuwenhuizen et al., 2008; Zaal et al., 2009b; Damveld, 2009; Pool et al., 2010]. Furthermore, research into the characteristics of the human neuromuscular system during manual aircraft control also focuses on pilot dynamics outside of the crossover region [Damveld et al., 2009]. A number of these experiments evaluated pilot tracking behavior for controlled elements that are representative for conventional aircraft elevator-to-pitch dynamics [Zaal et al., 2009b; Damveld, 2009; Pool et al., 2010]. Such conventional aircraft pitch dynamics have relatively complex dynamic characteristics over the frequency range where manual tracking behavior is typically evaluated due to the presence of the short-period mode. When considering pilot behavior over a wide frequency range, thereby including frequencies above and below the crossover region, it is found that the lead-lag equalization term as included in the *precision model* can

not capture the equalization dynamics adopted for compensation of the controlled element characteristics around the short-period mode.

The main objective of the present study is to define and validate an appropriate pilot equalization model that captures the adopted pilot equalization over the full measurement bandwidth during manual for a controlled element that represents the elevator-to-pitch dynamics of a small conventional jet aircraft. Furthermore, for this type of controlled element the importance of accurate modeling of the pilot equalization dynamics for quantitative evaluation of the typical effects of physical motion feedback that are observed for compensatory tracking tasks will be shown.

To achieve these objectives, measured pilot control behavior from the compensatory pitch attitude tracking task from the experiment described in [Zaal et al., 2009b] is analyzed. For this experiment, the controlled element was a linearized reduced-order model of the pitch dynamics of a Cessna Citation I Ce500 business jet. Furthermore, the pitch tracking task was performed both with and without simulator motion cues. To be able to investigate the separate contributions of the visual and vestibular systems, a combined disturbance-rejection and target-following task was performed [Stapleford et al., 1969]. To confirm that the requirement for a more complex model for pilot equalization is indeed caused by the dynamic characteristics of the considered aircraft pitch dynamics, the pitch tracking task of Zaal et al. [2009b] has been repeated for control of a system with double integrator dynamics, both with and without physical motion feedback, in the same experimental setting.

This chapter is structured as follows. First, Section 2.2 gives an overview of previous research into the modeling of pilot equalization during compensatory tracking. In addition, this section will cover the relation between controlled element dynamics and pilot equalization dynamics, which will be used to propose an extended equalization model for control of typical conventional aircraft pitch dynamics. Then, Section 2.3 describes the details of the human-in-the-loop experiments that were performed to gather the required measurements of human manual control behavior for evaluating the proposed equalization models. The model identification results are presented in Section 2.4. The chapter ends with a discussion and conclusions.

2.2 Pilot Compensation in Manual Control

2.2.1 Background

The foundations for much of the current knowledge on pilot dynamics during manual control were obtained from investigations into pilot control behavior and performance for single-loop compensatory target tracking tasks with a visually presented, random-appearing forcing function [Elkind, 1956; McRuer et al., 1965]. A schematic representation of such a single-loop compensatory control task is depicted in Fig. 2.1.

Fig. 2.1 shows a pilot exerting control (u) on a controlled element with dynamical characteristics given by $H_c(j\omega)$, based only on information of the tracking error e . This tracking error is defined as the difference between the actual state of the controlled element θ and the desired state defined by the forcing function signal f_t . Such compensatory manual con-

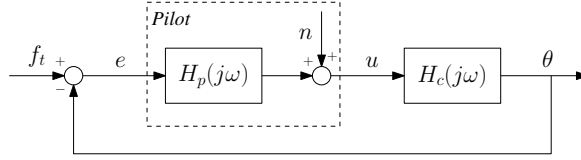


Figure 2.1. Schematic representation of a single-loop compensatory control task.

control behavior has mainly been studied for tracking tasks with unpredictable (quasi-random) forcing function signals f_t , as these force the pilot adopt to a purely compensatory control strategy [McRuer and Jex, 1967a]. Based on such measurements of $H_p(j\omega)$ for a wide variety of controlled elements, McRuer et al. [1965] formulated the most well-known of all models of human tracking behavior, the *crossover model*:

$$H_p(j\omega)H_c(j\omega) = \frac{\omega_c}{j\omega} e^{-j\omega\tau_e} \quad (2.1)$$

The model defined by Eq. (2.1) implicitly captures the adaptation of pilot dynamics to those of the controlled element, by stating that the combined pilot-vehicle dynamics approximate those of a single integrator ($K/j\omega$) around the crossover frequency ω_c , independent of the controlled element dynamics $H_c(j\omega)$. The crossover model further accounts for phase lags around crossover that can be attributed to the pilot dynamics $H_p(j\omega)$ through the equivalent pilot time delay τ_e .

Based on their *crossover model*, which has been shown capable of describing the combined pilot-vehicle dynamics in the crossover region for a wide variety in controlled element dynamics [McRuer and Jex, 1967a; McRuer, 1988], McRuer et al. [1965] further introduced a number of quasi-linear models for describing the pilot dynamics $H_p(j\omega)$ during compensatory tracking. The first of these models is the *extended crossover model*, which is given by:

$$H_p(j\omega) = K_p \underbrace{\left(\frac{T_L j\omega + 1}{T_I j\omega + 1} \right)}_{\text{pilot equalization}} e^{-j\omega\tau_e} \quad (2.2)$$

Note that the low-frequency phase correction proposed by McRuer et al. [1965], $e^{-j\alpha/\omega}$, is omitted from the *extended crossover model* as given by Eq. (2.2). As can be verified from comparison of Equations (2.1) and (2.2), the *extended crossover model* results from the required combined pilot-vehicle system dynamics defined by the crossover model. The adaptation of pilots' dynamics as a control element $H_p(j\omega)$ to the dynamics of the controlled system $H_c(j\omega)$ is captured by the pilot equalization term in the model. Depending on what type of equalization is required to satisfy Eq. (2.1) for a given controlled element, the lead-lag pilot equalization form of Eq. (2.2) may reduce to a pure lead, a pure lag, or even a pure gain. For instance, for modeling tracking behavior for single and double integrator controlled elements ($K_c/j\omega$ and $K_c/(j\omega)^2$, respectively), McRuer et al. [1965] have shown that the equalization term can be reduced to K_p and $K_p(T_L j\omega + 1)$, respectively.

Both the *crossover model* (Eq. (2.1)) and the *extended crossover model* in the form given by Eq. (2.2) were meant for analyzing pilot-vehicle system dynamics in a limited frequency range around the gain-crossover frequency of $H_p(j\omega)H_c(j\omega)$. As for instance stated by McRuer and Jex [1967a], the combined pilot-vehicle system dynamics in the crossover region “*determine the dominant closed-loop modes and response*”. This implies that for many applications, such as the prediction of closed-loop pilot-vehicle system performance, these models provide satisfactory results, despite the restricted frequency range they are applicable to.

Despite the modest contribution to the overall characteristics of the resulting combined pilot-vehicle system, pilot dynamics during tracking extend to frequencies well above and below crossover. For modeling these high and low-frequency pilot dynamics, and to allow for quantitative evaluation of changes in tracking behavior in these frequency ranges, McRuer et al. [1965] proposed a further extension to the *extended crossover model* given by Eq. (2.2). In a form that compared to its definition in [McRuer et al., 1965] omits the indifference threshold describing function, this *precision model* is given by:

$$H_p(j\omega) = \underbrace{K_p \left(\frac{T_L j\omega + 1}{T_I j\omega + 1} \right)}_{\text{pilot equalization}} \underbrace{\left(\frac{T_K j\omega + 1}{T'_K j\omega + 1} \right)}_{\text{low-freq. lag-lead}} \cdot \underbrace{\left[\frac{1}{(T_N j\omega + 1) \left(\left[\frac{j\omega}{\omega_{nm}} \right]^2 + \frac{2\zeta_{nm} j\omega}{\omega_{nm}} + 1 \right)} \right]}_{\text{neuromuscular dynamics}} \underbrace{e^{-j\omega\tau}}_{\text{delay}} \quad (2.3)$$

Note that compared to the *extended crossover model*, the *precision model* given by Eq. (2.3) includes an additional lag-lead term and an extensive model for the neuromuscular actuation dynamics. These additional elements ensure that the *precision model* allows for the modeling pilot dynamics over a wider frequency range than possible with the *crossover* and *extended crossover* models. A more subtle difference with these simpler models is the delay term $e^{-j\omega\tau}$. In the *extended crossover model*, the equivalent time delay τ_e accounts for more than just pilot time delay, as for instance the phase lags induced by the neuromuscular actuation dynamics, which also affect pilot dynamics in the crossover region, are also lumped into τ_e [McRuer et al., 1965]. As can be verified from Eq. (2.3), the explicit inclusion of the neuromuscular dynamics in the model allows for the modeling of a pure pilot time delay in the *precision model*.

As can be verified from comparison of Equations (2.2) and (2.3), McRuer et al. [1965] propose the same equalization term for both the *extended crossover model* and the *precision model* to model the adaptation of the adopted pilot dynamics to those of the controlled element. The equalization dynamics required in the crossover region for achieving satisfactory overall characteristics of the combined pilot-vehicle system are, however, not necessarily also applicable to frequencies that are well above crossover, as the dynamics of many controlled elements that are representative for manual vehicle control may show considerable

changes in their dynamic characteristics in the crossover region and for frequencies beyond crossover. For instance, controlled elements of the form $K_c/(j\omega(Tj\omega + 1))$ – which are representative for, among others, aircraft aileron-to-roll dynamics – are approximately K_c/s around crossover if $1/T > \omega_c$. However, the second-order dynamics at frequencies above $1/T$ may still require pilot lead compensation at frequencies above crossover, especially if $1/T \approx \omega_{sp}$. Moreover, previous research has indicated that marked changes in pilot dynamics at frequencies well above crossover occur due to variations in, for instance, manipulator feel-systems and dynamics [Johnston and Aponso, 1988; Mitchell et al., 1992] and the availability of physical motion feedback of the controlled element state [Nieuwenhuizen et al., 2008; Zaal et al., 2009b; Pool et al., 2010]. This chapter investigates the equalization model structure that is required for capturing pilot equalization dynamics over a wider frequency range for such applications, focusing on pitch attitude tracking tasks with a controlled element that is representative for conventional aircraft elevator-to-pitch dynamics, as for instance considered in [Zaal et al., 2009b] and [Pool et al., 2010].

2.2.2 Control Task

Fig. 2.2 shows a schematic representation of the compensatory pitch attitude control task that is considered in the present study. The tracking error e is presented to the pilot using the compensatory visual display shown in Fig. 2.3. Tracking errors, and thereby pilot control action, are induced using the target and disturbance forcing function signals, f_t and f_d , respectively.

If the pitch motion of the controlled element H_{θ,δ_e} is presented through physical motion cues in addition to the visually perceived tracking error, an additional feedback path is present that provides the pilot with explicit information on the controlled pitch attitude, θ . Pilots' responses to perceived visual tracking errors and physical pitch motion are indicated in Fig. 2.2 by the response functions $H_{pv}(j\omega)$ and $H_{pm}(j\omega)$, respectively. The main reason for using both a target and a disturbance forcing function signal in the pitch control tasks studied in this chapter is that this yields a combined target-following and disturbance-rejection task for which reliable separation and identification of $H_{pv}(j\omega)$ and $H_{pm}(j\omega)$ is possible [Stapleford et al., 1969].

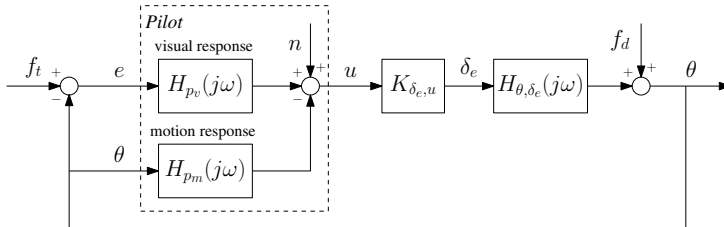


Figure 2.2. Compensatory pitch attitude control task. Note that the pilot motion response is only present if physical motion cues are supplied.

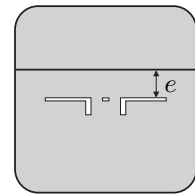


Figure 2.3. Compensatory display.

Fig. 2.2 differs from the single-loop tracking tasks considered by McRuer et al. [1965] (as can be verified from comparison with Fig. 2.1) by the presence of physical motion feed-

back – and the corresponding pilot motion response $H_{p_m}(j\omega)$ – and the disturbance signal f_d . Note, however, that if no motion feedback is available ($H_{p_m}(j\omega) = 0$) the tracking errors introduced by the target and disturbance signals – which are typically both signals with a low-pass characteristic – are indistinguishable from a compensatory display [Pool et al., 2008a]. Therefore, despite the additional disturbance signal, direct comparison with the results of McRuer et al. is still possible for the control task shown in Fig. 2.2 if no physical motion feedback is available.

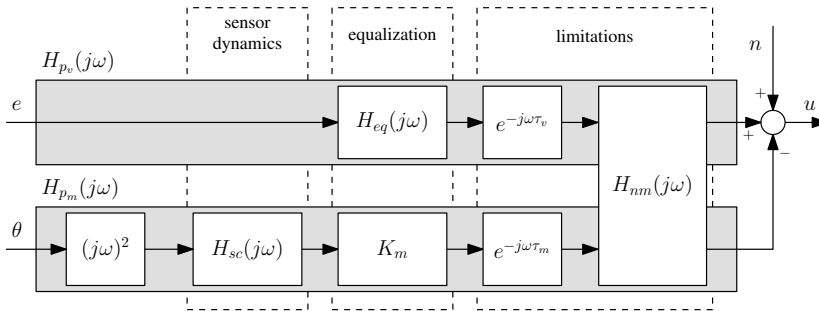


Figure 2.4. Multimodal pilot model.

2.2.3 Multimodal Pilot Model

Pilot control behavior in compensatory tracking tasks can be modeled successfully using quasi-linear pilot models [McRuer et al., 1965; McRuer and Jex, 1967a], as those indicated in Figures 2.1 and 2.2. Such models typically consist of a linear part that describes pilot responses to all relevant perceived variables, and a remnant signal n that accounts for all otherwise unmodeled nonlinearities. As for instance summarized in [Grant and Schroeder, 2010], many different model structures have been derived in past studies to represent the linear pilot's responses to perceived visual errors $H_{p_v}(j\omega)$, perceived physical motion feedback $H_{p_m}(j\omega)$, or the combination of both. Examples are the *crossover model*, *extended crossover model* and *precision model* that were introduced in Section 2.2.1, the *multi channel model* [Van der Vaart, 1992], the *descriptive model* [Hosman and Stassen, 1999], and the *structural model* [Hess, 1990b].

Fig. 2.4 depicts the multimodal pilot model adopted in the present study. The visual channel of the pilot model is based on the *precision model* [McRuer et al., 1965] and therefore largely equivalent to Eq. (2.3), where the low-frequency lag-lead term has been omitted. Similar to the $e^{-j\omega/\alpha}$ term added to the *extended crossover model* in [McRuer et al., 1965], the low-frequency lag-lead term in Eq. (2.3) is included to match pilot describing function measurements at the lowest frequencies in the measurement band (phase droop). For an unstable first-order controlled element, McRuer et al. [1965] propose that the parameters of this low-frequency lag-lead are equal to $T_K = 3.33$ s and $T'_K = 20$ s independent of the forcing function bandwidth, yielding only negligible effects at frequencies higher than the inverse lead time constant $1/T_K$, that is, 0.3 rad/s. As the additional lag-lead term in Eq. (2.3) was intended to capture such very low frequency phase lags and the measurement

bandwidth of the experiment considered in this study ranges from 0.38 to 17.56 rad/s (see Section 2.3.1), this low-frequency lag-lead term is not considered in this study.

For the pilot model defined in Fig. 2.4, the lead-lag equalization term of Eq. (2.3) has been replaced by the generic frequency response function $H_{eq}(j\omega)$, and the third-order neuromuscular term has been replaced by $H_{nm}(j\omega)$. The characteristics of $H_{eq}(j\omega)$ as considered in this study will be described in detail in Section 2.2.5. The neuromuscular term in the *precision model* proposed by McRuer et al. [1965] consists of a second-order mass-spring-damper model combined with an additional first-order lag, as can be verified from Eq. (2.3). The neuromuscular system model $H_{nm}(j\omega)$ adopted here only considers the second-order term of Eq. (2.3), yielding the following model with two parameters, the natural frequency ω_{nm} and damping ratio ζ_{nm} :

$$H_{nm}(j\omega) = \frac{1}{\left(\frac{j\omega}{\omega_{nm}}\right)^2 + \frac{2\zeta_{nm}}{\omega_{nm}}j\omega + 1} \quad (2.4)$$

Previous investigations have indicated that this model of the neuromuscular system dynamics typically suffices for approximating the neuromuscular dynamics measured in the frequency range that is considered for similar tracking tasks [Johnston and Aponso, 1988; Zaal et al., 2009b,a; Damveld et al., 2009; Pool et al., 2010].

The additional parallel motion channel of the pilot model, $H_{pm}(j\omega)$, incorporates the pilot's response to his vestibular motion sensation as proposed by Van der Vaart [1992] and Hosman and Stassen [1999] in their *multi channel model* and *descriptive model*, respectively. The dynamics of the semicircular canals (SCC), the vestibular sensors that are sensitive to angular motion, are defined by $H_{sc}(j\omega)$, which is given by:

$$H_{sc}(j\omega) = \frac{0.11j\omega + 1}{(5.9j\omega + 1)(0.005j\omega + 1)} \quad (2.5)$$

The form of Eq. (2.5), which relates angular accelerations applied to the SCC (in rad/s²) to afferent neuron firing rate (in impulses per second, ips), has been determined from sinusoidal stimulation of the vestibular organs of squirrel monkeys by Fernandez and Goldberg [1971]. The parameters of the semicircular canal model of Eq. (2.5) as used here have been adapted from those found by Fernandez and Goldberg using experimental measurements of human motion perception thresholds [Hosman and Van der Vaart, 1978]. Note that despite the possible presence of differences in SCC dynamics over different individuals, here the model of Eq. (2.5) is applied to the data from different experiment participants. This same approach was taken in a number of previous investigations into multimodal pilot control behavior [Van der Vaart, 1992; Hosman and Stassen, 1999; Zaal et al., 2009b,a; Damveld et al., 2009; Pool et al., 2010], where this assumption was found to result in only modest modeling errors. Note that in the frequency range of interest to manual vehicle control, the output of the SCC model of Eq. (2.5) is proportional to angular rate for an angular acceleration input [Fernandez and Goldberg, 1971].

2.2.4 Controlled Dynamics

In this chapter, data from two sets of experiments are compared. Both experiments evaluated the effect of motion feedback in a pitch attitude tracking task as depicted by Fig. 2.2. The first experiment evaluated the effects of pitch and heave motion cues on pilot control behavior in a pitch control task [Zaal et al., 2009b]. The controlled dynamics, $H_{\theta, \delta_e}(j\omega)$, in this experiment were the reduced-order linearized pitch dynamics of a Cessna Citation I Ce 500 business jet aircraft, in cruise in the standard atmosphere at an altitude of 10,000 ft and at an airspeed of 160 kt, as given by:

$$\begin{aligned} H_{\theta, \delta_e}(j\omega) &= K_{\theta, \delta_e} \frac{T_{\theta_2} j\omega + 1}{j\omega \left(\left(\frac{j\omega}{\omega_{sp}} \right)^2 + \frac{2\zeta_{sp}}{\omega_{sp}} j\omega + 1 \right)} \\ &= 1.38 \frac{1.01 s + 1}{j\omega (0.13(j\omega)^2 + 0.36j\omega + 1)} \end{aligned} \quad (2.6)$$

Note that Eq. (2.6) is a typical fixed-airspeed approximation of aircraft pitch attitude dynamics [Bryan, 1911], as for instance considered in many studies into longitudinal aircraft handling qualities [McRuer et al., 1960; Ashkenas and McRuer, 1962; Hall, 1963]. Furthermore, note that the units of the in- and output signals of Eq. (2.6) – δ_e and θ , respectively – are both deg. The Bode frequency response of the aircraft pitch dynamics is depicted in Fig. 2.5. Note that in the frequency range of interest, the aircraft dynamics defined by Eq. (2.6) are characterized by a lead term ($T_{\theta_2} j\omega + 1$) and the periodic short-period eigenmode. The short-period mode of this specific aircraft in the given configuration has a natural frequency ω_{sp} and damping ratio ζ_{sp} of 2.76 rad/s and 0.50, respectively. As can be verified from Eq. (2.6), the corresponding value of T_{θ_2} is 1.01 s. Note the significant magnitude peak and phase lead around the short-period frequency in Fig. 2.5. Furthermore, observe that due to the values of T_{θ_2} and ω_{sp} both features of Eq. (2.6) affect the dynamics in the frequency range where the pilot-vehicle system crossover frequency is expected to be for compensatory tracking tasks, that is, 2.5 – 5 rad/s [McRuer et al., 1965].

Previous experiments that investigated pilot manual control of aircraft pitch dynamics [Zaal et al., 2009b; Damveld, 2009; Pool et al., 2010] indicated that a pilot equalization model as defined in Eq. (2.3) is not sufficient for describing the measured pilot control behavior. To support a comparison of these findings with the results described by McRuer et al. [1965], the same pitch tracking task described in [Zaal et al., 2009b] was repeated in a later experiment with double integrator dynamics:

$$H_{\theta, \delta_e}(j\omega) = \frac{K_{\theta, \delta_e} \omega_{sp}^2 T_{\theta_2}}{(j\omega)^2} = \frac{10.62}{(j\omega)^2} \quad (2.7)$$

The frequency response of the system given by Eq. (2.7) is depicted in Fig. 2.5 in gray. Note that the gain for this double integrator system was chosen to have its frequency response coincide with the high-frequency magnitude of the Citation pitch dynamics, Eq. (2.6). Furthermore, note from Fig. 2.5(b) that the aircraft pitch dynamics given by Eq. (2.6) are stable, while those of the double integrator are not. For this reason, control of double integrator dynamics requires more stabilizing lead equalization by the pilot, thereby

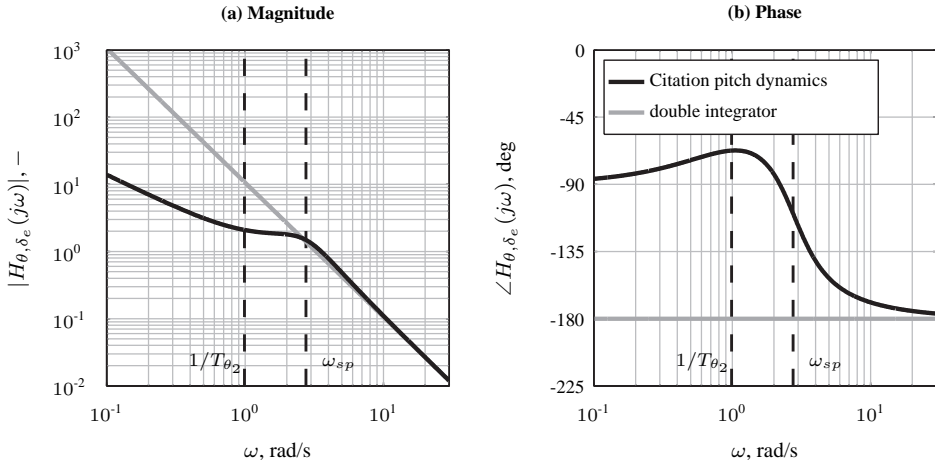


Figure 2.5. Controlled dynamics frequency responses.

making such controlled elements markedly more difficult to control [Shirley and Young, 1968].

2.2.5 Pilot Equalization

The main focus of the current chapter is on the model structure for the pilot equalization term $H_{eq}(j\omega)$ (see Fig. 2.4) required for modeling pilot dynamics during control of a system $H_{\theta, \delta_e}(j\omega)$ with dynamics given by Eq. (2.6) over a wide frequency range. The theory of manual vehicle control as compiled by McRuer et al. [McRuer et al., 1965; McRuer and Jex, 1967a; McRuer, 1988] states that pilots adapt their equalization dynamics around crossover to the controlled element dynamics to yield a pilot-vehicle system that has the properties close to those of a single integrator system around the crossover frequency. For double integrator systems as defined by Eq. (2.7), it has been shown in literature that pilot equalization takes the form of a pure lead in order to achieve these open-loop characteristics [McRuer et al., 1965].

For an expected range of ω_c between 2.5 and 5 rad/s as proposed in [McRuer et al., 1965], to achieve a pilot-vehicle system with approximate single integrator characteristics around crossover for control of dynamics as given by Eq. (2.6), pilots would need to generate lag at a frequency close to $1/T_{\theta_2}$ to compensate for the gain-like dynamics introduced by the lead term of the aircraft dynamics, as indicated in Fig. 2.6. In addition, due to the value of $\omega_{sp} = 2.76$ rad/s for the considered controlled element, it is also likely that lead equalization will be adopted to compensate for the second-order dynamics beyond the short-period mode natural frequency. Note from Fig. 2.6 that equalization dynamics $H_{eq}(j\omega)$ that include both pilot lag at low frequencies and pilot lead at high frequencies would yield a combined pilot-vehicle system, $H_{eq}(j\omega)H_{\theta, \delta_e}(j\omega)$, with approximately single integrator dynamics over the full range of frequencies considered here.

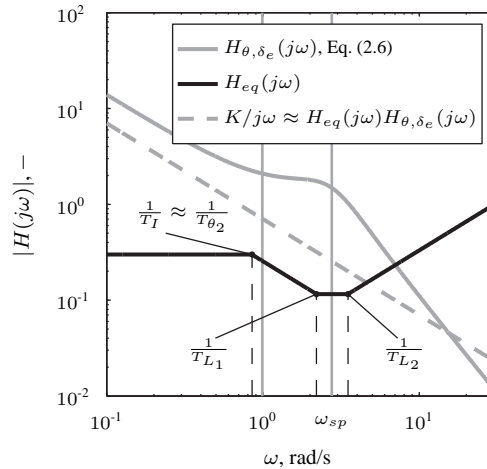


Figure 2.6. Frequency response of theoretical pilot equalization for control of aircraft pitch dynamics.

Fig. 2.6 shows the proposed pilot equalization dynamics for control of a system with dynamics described by Eq. (2.6). Eq. (2.3) defines the full equalization term of the pilot model proposed by McRuer et al. [1965] for modeling pilot behavior for a wide frequency range. Comparison of both equalization forms shows that the model of Eq. (2.3) is not capable of capturing the proposed equalization dynamics shown in Fig. 2.6. As can be verified from Fig. 2.6, an additional lead term is required to model the combination of low-frequency lag and high-frequency lead equalization in $H_{eq}(j\omega)$. As this high-frequency lead equalization is expected for this controlled element, in addition to the low-frequency lag compensation required for achieving approximately single integrator dynamics around crossover, it is anticipated that the addition of a second lead term to the equalization term $H_{eq}(j\omega)$ will allow for better modeling of the pilot equalization dynamics that are adopted for such a controlled element.

To further investigate this, four equalization models are evaluated for describing pilot control behavior in a pitch attitude tracking task in this study. These different forms of $H_{eq}(j\omega)$ are listed in Table 2.1. Equalizations A and B represent pure lead and lead-lag equalization terms that have been frequently applied in literature. Equalizations C and D both have an additional lead term, to allow for modeling of pilot equalization of the form depicted in Fig. 2.6. The difference between these is that D allows for the additional lead time constant, T_{L_2} , to have a different value than the first, – and thereby adds an extra parameter to the pilot equalization model $H_{eq}(j\omega)$ – while C assumes both lead time constants to be equal. This additional independent lead time constant allows for more freedom in the equalization model and can therefore allow for attaining a better fit than with equalization C. However, due to fact that equalization D has two mathematically identical lead terms,

it yields an overdetermined pilot model structure, which is a disadvantage from a model identification view [Zaal et al., 2009a].

Table 2.1. Definition of equalization forms.

Symb.	Form	Equalization, $H_{eq}(j\omega)$
A	lead	$K_v(T_L j\omega + 1)$
B	$\frac{\text{lead}}{\text{lag}}$	$K_v \frac{(T_L j\omega + 1)}{(T_I j\omega + 1)}$
C	$\frac{\text{lead}^2}{\text{lag}}$	$K_v \frac{(T_L j\omega + 1)^2}{(T_I j\omega + 1)}$
D	$\frac{\text{lead} \cdot \text{lead}}{\text{lag}}$	$K_v \frac{(T_{L1} j\omega + 1)(T_{L2} j\omega + 1)}{(T_I j\omega + 1)}$

Pilot lead equalization captures the pilots' response to visually perceived tracking error rate. An additional lead term in the pilot model equalization model, as is proposed here for equalizations C and D (see Table 2.1), therefore suggests modeling of pilots' responses to visually perceived accelerations. As for instance argued in [Hosman, 1996], however, the human visual system is believed to be incapable of perceiving (and inferring) acceleration. Note from Table 2.1 that for certain settings of T_I , T_L , and $T_{L_{1,2}}$ – most notably if $T_I \ll T_{L_{1,2}}$ – both equalizations C and D can yield pilot equalization dynamics proportional to $(j\omega)^2$ over a certain frequency range. As illustrated by Fig. 2.6, the effective pilot equalization for control of dynamics as defined by Eq. (2.6) would never be more than a single lead (rate perception), due to the fact that pilot lag is generated at a frequency that is well below the frequency range where lead equalization is required, that is, $T_I > T_{L_{1,2}}$. Care should, however, be taken in utilizing equalization C and D for modeling pilot control, as for certain combinations of the equalization parameters these proposed equalization terms can yield pilot equalization dynamics that are unachievable for a human pilot.

2.3 Experiment

2.3.1 Forcing Functions

The pitch tracking task considered in the experiments described in this chapter (see Fig. 2.2) was defined to be a disturbance-rejection task, where the disturbance of the pitch attitude was induced by the disturbance signal f_d . An additional target signal f_t with reduced signal power (25% of the power of f_d) was inserted as well, this to facilitate multimodal pilot model identification [Stapleford et al., 1969; Jex et al., 1978; Zaal et al., 2009a]. As in the experiments described by McRuer et al. [1965], the forcing function signals were constructed as sums of ten sinusoids:

$$f_{d,t}(t) = \sum_{k=1}^{N_{d,t}} A_{d,t}(k) \sin [\omega_{d,t}(k)t + \phi_{d,t}(k)] \quad (2.8)$$

Experimental measurement runs had a length of 110 seconds, of which only the final 81.92 seconds were used as the measurement data. Removal of the run-in time from the measurement runs ensured stationary measurements of pilot tracking, as initial transient and stabilization effects were no longer present after 10 seconds of tracking. The sinusoid frequencies, ω_t and ω_d , were distributed more or less evenly spaced on a logarithmic scale over the frequency range of 0.3 to 18 rad/s. The frequencies were defined as integer multiples of the experimental measurement time base frequency – $\omega_m = 2\pi/T_m$, with $T_m = 81.92$ seconds – to allow for pilot model identification using spectral methods [Stapleford et al., 1969].

The frequency, amplitude, and phase distributions ($\omega_{d,t}(k)$, $A_{d,t}(k)$, and $\phi_{d,t}(k)$) were the same as those used in a previous experiment [Zaal et al., 2009b]. The frequencies, amplitudes, and phases of the target and disturbance signals are summarized in Table 2.2. The amplitude distributions of f_t and f_d are depicted in Fig. 2.7(a); Fig. 2.7(b) shows a part of the time traces of both forcing function signals. Note from Fig. 2.7(b) that f_d yields maximum pitch attitude excursions of no more than 3 degrees.

Table 2.2. Experiment forcing function properties.

		disturbance, f_d			target, f_t			
k	n_d	ω_d	A_d	ϕ_d	n_t	ω_t	A_t	ϕ_t
–	–	rad/s	deg	rad	–	rad/s	deg	rad
1	5	0.383	1.343	1.530	6	0.460	0.698	1.288
2	11	0.844	1.016	5.967	13	0.997	0.488	6.089
3	23	1.764	0.506	1.000	27	2.071	0.220	5.507
4	37	2.838	0.258	6.117	41	3.145	0.119	1.734
5	51	3.912	0.157	6.145	53	4.065	0.080	2.019
6	71	5.446	0.095	2.692	73	5.599	0.049	0.441
7	101	7.747	0.060	1.895	103	7.900	0.031	5.175
8	137	10.508	0.043	3.153	139	10.661	0.023	3.415
9	171	13.116	0.036	3.570	194	14.880	0.018	1.066
10	226	17.334	0.030	3.590	229	17.564	0.016	3.479

2.3.2 Apparatus

The experiments were performed in the SIMONA Research Simulator (SRS) at Delft University of Technology, see Fig. 2.8. The SRS motion system was used to present the subjects with rotational pitch motion cues during specific conditions of both experiments. The vertical motion cues that are typically coupled to conventional aircraft pitch rotations [Zaal et al., 2009b] were not presented. The pitch motion of the simulator was driven directly by the pitch motion of the simulated controlled element, that is, no motion filter was applied. The time delay associated with the motion cues generated by the SRS motion base is 30 ms [Berkouwer et al., 2005].

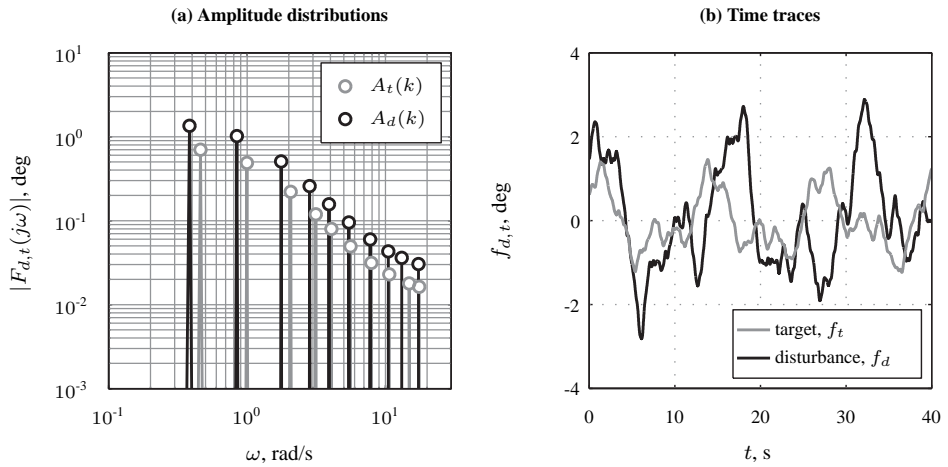


Figure 2.7. Target and disturbance forcing function spectra and time traces.

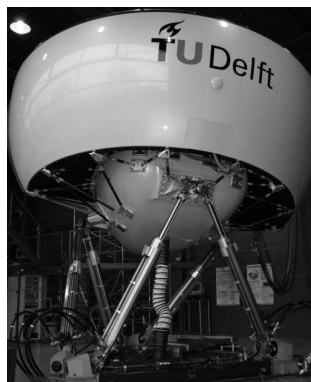


Figure 2.8. The SIMONA Research Simulator.

The pitch tracking error the participants were to minimize during the tracking tasks was presented on the primary flight display (PFD) in the SRS cockpit. As depicted in Fig. 2.3, the instantaneous value of the tracking error e was depicted as the vertical displacement of a moving horizontal line with respect to a fixed aircraft symbol, which was centered on the display. The update rate of the PFD was 60 Hz and the time delay associated with the generation of visual images on the SRS cockpit displays has been determined to be 20 – 25 ms [Stroosma et al., 2007].

In both experiments, subjects controlled the pitch dynamics with a sidestick with electrical control loading. The sidestick had no break-out force and a maximum deflection of 14 deg. The stiffness of the stick was set to 1.1 N/deg for stick deflections under 9 deg and to 2.6 N/deg for larger stick excursions. The stick roll axis, which was not used during the experiment, was kept fixed at the zero position. A selectable gain – indicated with the symbol $K_{\delta_e, u}$ in Fig. 2.2 – controlled the scaling between the sidestick deflection u and the elevator input to the controlled dynamics, δ_e . To give optimal control authority for both types of controlled dynamics, this gain was set to -0.2865 or -0.4011 for the Citation pitch and double integrator controlled elements, respectively.

2.3.3 Conditions, Participants and Experimental Procedure

Data from four different experimental conditions are evaluated in this chapter. As indicated in Table 2.3, the modeling of pilot control behavior will be compared for the aircraft pitch dynamics Eq. (2.6) and the double integrator dynamics Eq. (2.7) depicted in Fig. 2.5. For direct comparison with the results described by McRuer et al. [1965] and evaluation of the interpretation of observed effects of physical motion feedback on the adopted pilot dynamics, the control task is performed both with and without additional pitch motion feedback.

Table 2.3. Experimental conditions.

	no motion	motion
aircraft dynamics, Eq. (2.6)	C1	C2
double integrator dynamics, Eq. (2.7)	C3	C4

Five subjects performed the four experimental conditions listed in Table 2.3. All participants were students or staff of the Faculty of Aerospace Engineering. Two subjects were pilots and all had extensive experience with similar manual control tasks from previous human-in-the-loop experiments.

Participants were instructed to minimize the pitch tracking error, that is, the signal that was presented on the visual display. Five repetitions of each experimental condition per subject were performed to collect the measurement data. Before collecting the measurements, all subjects performed a considerable number of training runs, until their proficiency in performing the tracking task had stabilized at a constant level of tracking performance. After each run subjects were informed of their tracking score – defined as the root-mean-square of the error signal e – in order to motivate them to improve their tracking performance during initial familiarization and to maintain a constant level of performance after their proficiency had stabilized.

2.3.4 Pilot Model Identification

The parameters of the multimodal pilot model depicted in Fig. 2.4 were estimated using a time-domain maximum likelihood estimation (MLE) procedure [Zaal et al., 2009a] for all experimental conditions listed in Table 2.3. As explained in detail by Zaal et al. [2009a], this identification procedure yields more consistent parameter estimates than obtained by frequency-domain methods based on Fourier coefficients (FC) or linear time-invariant models (ARX) [Nieuwenhuizen et al., 2008]. The free parameters in this estimation procedure were the pilot perceptual time delays (τ_v and τ_m), the neuromuscular frequency and damping ratio (ω_{nm} and ζ_{nm}), the pilot motion gain (K_m), and the parameters of the pilot visual equalization transfer function (K_v , T_I and T_L – or T_{L1} and T_{L2} for equalization D). Note that for conditions C1 and C3, where no motion cues were available to the participants, only the model for the pilot visual response $H_{p_v}(j\omega)$ (see Fig. 2.4) was fit to the data. For each condition of every subject, the averaged time-domain data over the measurement interval (see Section 2.3.1) of the five measurement runs were used as input to the estimation algorithm, to remove part of the remnant present in these measured signals before estimating the model parameters. The same MLE parameter estimation procedure for estimating pilot model parameters has been used in [Beerens et al., 2009] to successfully replicate some of the results of the experiments of [McRuer et al., 1965].

For all experimental conditions listed in Table 2.3 four different pilot models were fit to each data set, corresponding to the pilot equalization structures listed in Table 2.1. Since the modeling efforts in the original work of McRuer et al. [McRuer et al., 1965; McRuer and Jex, 1967a] were based on experiments without physical motion cues, the main comparison of required pilot model equalization structures will be performed using the experimental conditions without physical motion (C1 and C3). The accuracy of the pilot model identification results for the different equalization structures is further evaluated using the model variance accounted for (VAF) [Zaal et al., 2009a]. The VAF indicates the amount of variance in the measured pilot control signal that is captured by the linear model fit and expresses it in the form of a percentage (0–100%). An additional evaluation of the suitability of the different equalization structures will be performed for the conditions where the aircraft pitch dynamics were controlled by comparing the identified lead and lag time constants for all equalization structures with the known characteristic frequencies of the controlled element. These results are then used to indicate which of the equalization forms listed in Table 2.1 are found to be most suitable for evaluation of the effects of physical motion feedback on control behavior.

2.4 Results

2.4.1 Identified Equalization Dynamics

Figs. 2.9 and 2.10 depict the magnitude responses of the identified pilot equalization dynamics $H_{eq}(j\omega)$, averaged over all subjects, for the no-motion conditions and control of the double integrator and aircraft dynamics (conditions C3 and C1), respectively. Note that the pilot equalization frequency responses shown in Figs. 2.9 and 2.10 were obtained from identification of the full visual response of the pilot model of Fig. 2.4 using MLE, according

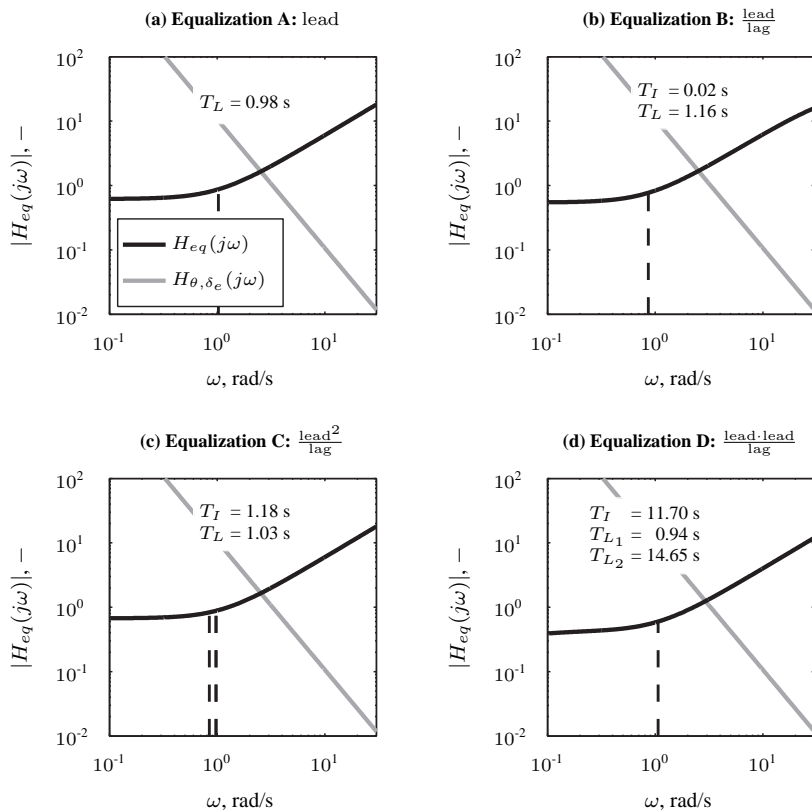


Figure 2.9. Average estimated pilot model equalization frequency response functions $H_{eq}(j\omega)$ for control of double integrator dynamics (condition C3).

to the identification procedure detailed in Section 2.3.4. The four different graphs in each figure show the identified frequency responses of the four forms of $H_{eq}(j\omega)$ listed in Table 2.1. Vertical dashed black lines indicate the frequencies that correspond to the average estimated equalization lag and lead time constants, whose numerical values are also given in each figure. The frequency responses of the controlled element dynamics $H_{\theta,\delta_e}(j\omega)$, which were calculated from Equations (2.6) and (2.7), are depicted in gray for reference.

For control of double integrator dynamics it is well-known that pilots generate lead, typically starting from frequencies well below the pilot-vehicle system crossover frequency to achieve single integrator dynamics in the crossover region [McRuer et al., 1965]. McRuer et al. [1965] reported pure lead equalization with a value of T_L of 5 sec for single-loop double integrator control. Other investigations have reported visual lead time constants between 1 and 3 sec, depending on the bandwidth of the applied forcing function signals [Van der Vaart, 1992; Beerens et al., 2009; Zollner et al., 2010]. Fig. 2.9 shows that the equalization dynamics found for a double integrator controlled element in this experiment compare well

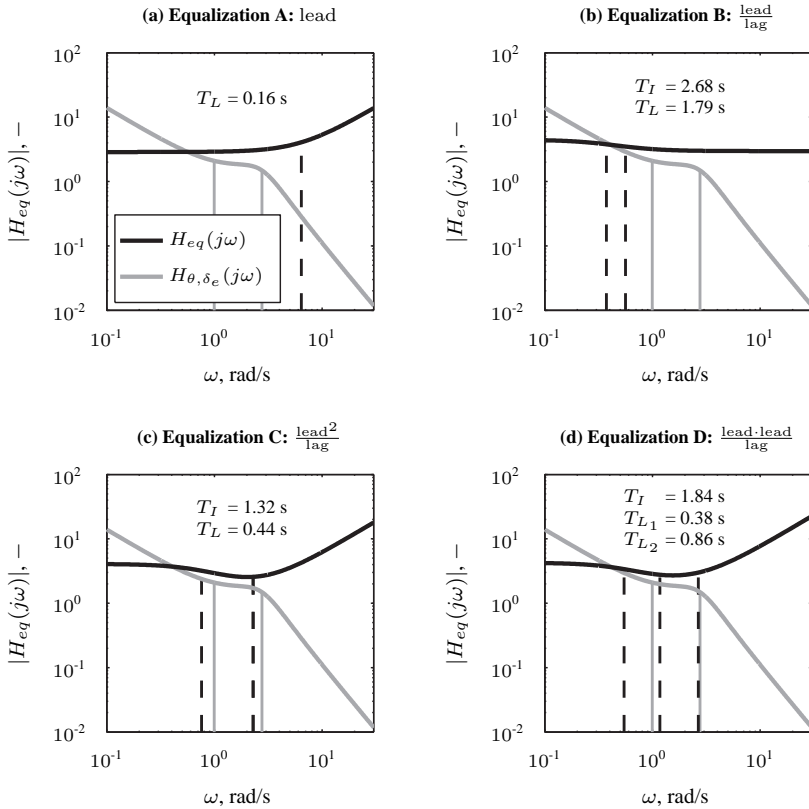


Figure 2.10. Average estimated pilot model equalization frequency response functions $H_{eq}(j\omega)$ for control of aircraft dynamics (condition C1).

with these previous findings, since all pilot equalization forms yield a frequency response of $H_{eq}(j\omega)$ that is approximately a single lead with a lead time constant of around 1 sec.

Note that the parameters of the more extensive forms of $H_{eq}(j\omega)$ (B–D) are estimated to yield an overall response equivalent to that of the pure lead equalization, A. For equalization B this is achieved by setting the value of T_I to approximately zero, thereby yielding only a minor effect of the additional lag term at very high frequencies. For the equalization structures with additional lead terms (C and D), the same effective reduction to $K_v(T_L j\omega + 1)$ is obtained by either canceling the effect of the additional lead term by setting $T_I \approx T_L$ (C) or by setting T_I and T_{L_2} to values outside of the frequency range of interest (D). As the added complexity of equalization forms B–D is not found to yield differences in the estimated pilot equalization dynamics, Fig. 2.9 therefore suggests that, a pure lead equalization term (A) is sufficient for modeling $H_{eq}(j\omega)$ for control of double integrator dynamics over a wide frequency range, as also found for pilot behavior in the crossover region by McRuer et al. [1965].

As explained in Section 2.2.5, equalization forms C and D allow for capturing the low-frequency lag and high-frequency lead equalization that is required for modeling pilot equalization dynamics if compensation for the aircraft pitch dynamics given by Eq. (2.6) is performed over a wide frequency range. As can be verified from Fig. 2.10, the estimates of $H_{eq}(j\omega)$ obtained using both these equalization forms indeed show pilot lag starting from 0.7 rad/s and pilot lead compensation starting from around 2 – 3 rad/s. As $T_I > T_{L_{1,2}}$, the resulting pilot equalization dynamics captured with equalizations C and D indeed never provide more than a first order lead (rate perception), as pointed out as an important condition for application of these equalization forms in Section 2.2.5. Note from Fig. 2.10(d) that for equalization D the average identified dynamics of $H_{eq}(j\omega)$ are similar to the fit obtained for equalization C (Fig. 2.10(c)), even though the average values of T_{L_1} and T_{L_2} were found to differ considerably. It should be noted that the average difference in the identified values for both lead time constants mainly results from the data from one participant. For the data from all other participants only very small differences between the values of T_{L_1} and T_{L_2} were observed: on average the difference between both identified lead time constants of equalization D for these four participants was 0.05 sec.

As can be verified from Figures 2.10(a) and (b), equalizations A and B are found to provide a fit of the equalization dynamics that is different from the results obtained with equalizations C and D. Equalization A is found to capture only high-frequency pilot lead compensation, which only affects frequencies that are well above crossover, thereby yielding pure gain equalization dynamics in the crossover region. The lead-lag equalization model (B) captures only the adopted low-frequency lag equalization.

2.4.2 Comparison with Measured Pilot Describing Functions

In addition to estimating the parameters of the pilot model using MLE, pilot describing functions were calculated with the Fourier coefficients method [Stapleford et al., 1969]. This nonparametric identification method allows for analytical calculation of pilot describing functions in the frequency domain and does therefore not require selection of an appropriate pilot model structure. FC describing function estimates are used here as a second independent measurement of the adopted pilot dynamics, to validate the pilot model fits obtained for the different equalization forms with MLE, as presented in Figures 2.9 and 2.10.

Figures 2.11 and 2.12 show the average pilot visual response functions for conditions C3 and C1, respectively, obtained from the identification of the pilot model of Fig. 2.4 using MLE. In both figures, only the estimated equalizations A-C are shown, as the model fits obtained for C and D are found to be similar for both controlled elements, see Figures 2.9 and 2.10. In addition to these identified pilot model frequency responses, the averaged FC estimates of the corresponding pilot describing functions are provided in Figures 2.11 and 2.12 for reference. Finally, also the average pilot-vehicle system crossover frequencies determined for both controlled elements using the describing function measurements are depicted as vertical solid lines. Note that these average crossover frequencies were found to be 2.93 rad/s and 3.36 rad/s for conditions C3 and C1, respectively, which is consistent with the measurements from [McRuer and Jex, 1967a], where crossover frequencies of around 3

rad/s are reported for double integrator control and higher values for more stable controlled elements.

For the double integrator controlled element, Fig. 2.11 shows that the pure lead equalization dynamics that resulted from identification of the different equalization models as depicted in Fig. 2.9 yield a pilot model that corresponds well with the calculated frequency-domain pilot describing function. Note from Fig. 2.11 that the measured pilot dynamics indeed show lead equalization that extends to frequencies well above ω_c . As no apparent discrepancies with the describing function are observed over the full range of measurement frequencies, this indicates that a pure lead equalization term is sufficient for capturing pilot dynamics during control of double integrator dynamics over a wide frequency range.

As shown in Fig. 2.12(a), the magnitude response of the average FC describing function estimate found for control of the aircraft pitch dynamics of Eq. (2.6) has a shape that is consistent with the hypothetical pilot equalization depicted in Fig. 2.6. It shows decreasing magnitudes of $H_{p_v}(j\omega)$ at low frequencies, suggesting pilot lag equalization in that frequency range. The describing function phase response shown in Fig. 2.12(b) also shows around 20 deg of pilot phase lag at low frequencies. The describing function further shows a high-frequency pilot response that is similar to that observed for the double integrator controlled element in Fig. 2.11 and indicates pilot lead compensation that is seen start from frequencies around, or even just below, the crossover frequency.

As can be observed in Fig. 2.12, the lead-lag equalization (B, see Table 2.1) provides an acceptable fit of the low frequency phase lag. As this equalization form does not allow for the modeling of high-frequency lead in addition to the lag at low frequencies (see also Fig. 2.10(b)), a degradation in model fit is observed for the higher frequencies. This yields a model fit in which the lack of high-frequency lead is partly compensated for by selecting a very low value for the neuromuscular damping ratio ζ_{nm} , as evident from the sharp phase drop of visible for equalization B at 10 rad/s in Fig. 2.12(b). The pilot equalization with only a lead term (A) is able to capture the high-frequency magnitude response (Fig. 2.12(a)) with reasonable accuracy. A significant deviation from the estimated describing function can, however, be observed in the gain and phase responses below crossover (Fig. 2.12(a) and (b), respectively). Equalization C, with its additional lead term, is able to capture both the low-frequency lag and high-frequency lead compensation observed in the Fourier coefficients estimate of $H_{p_v}(j\omega)$ and provides a model fit over the entire range of measured frequencies that shows the least deviations from the average describing function.

As a further verification of this observation, Fig. 2.13 depicts the same data shown in Fig. 2.12 for condition C1 for the aircraft pitch dynamics tracking tasks performed with physical pitch motion feedback (C2). Fig. 2.13 shows the describing function estimates of both the pilot visual and motion responses, in addition to the frequency responses of the visual and motion channels of the multimodal pilot model depicted in Fig. 2.4. Again the average identified model frequency responses for equalizations A-C are depicted. Note from Figures 2.13(c) and (d) that only minor differences in the estimated pilot motion responses $H_{p_m}(j\omega)$ occur for the different equalization forms. Fig. 2.13, however, shows the same differences in the success with which the different equalization forms are able to capture the adopted pilot dynamics for the pilot visual channel $H_{p_v}(j\omega)$ as visible in Fig. 2.12. Despite the fact that the estimated responses to motion feedback are hardly affected by the equalization form selected for $H_{p_v}(j\omega)$ for the data presented here, this choice still

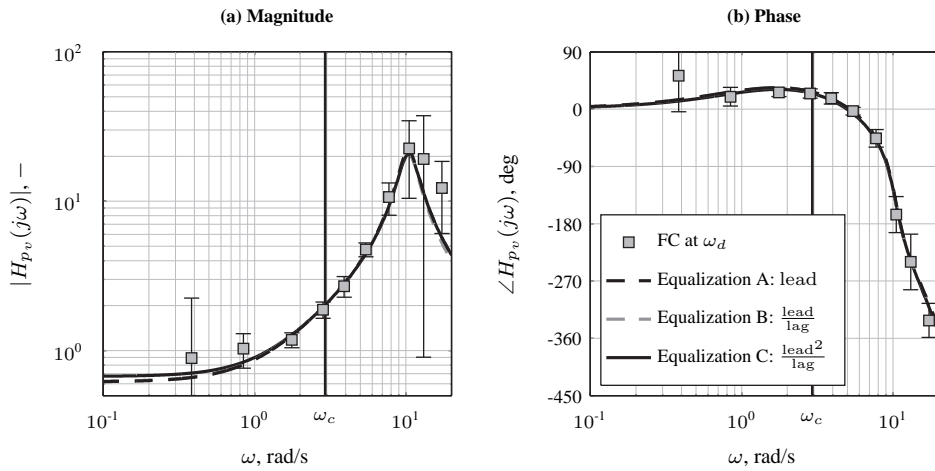


Figure 2.11. Mean pilot model frequency responses estimated with different equalization settings for double integrator dynamics (five subjects, condition C3).

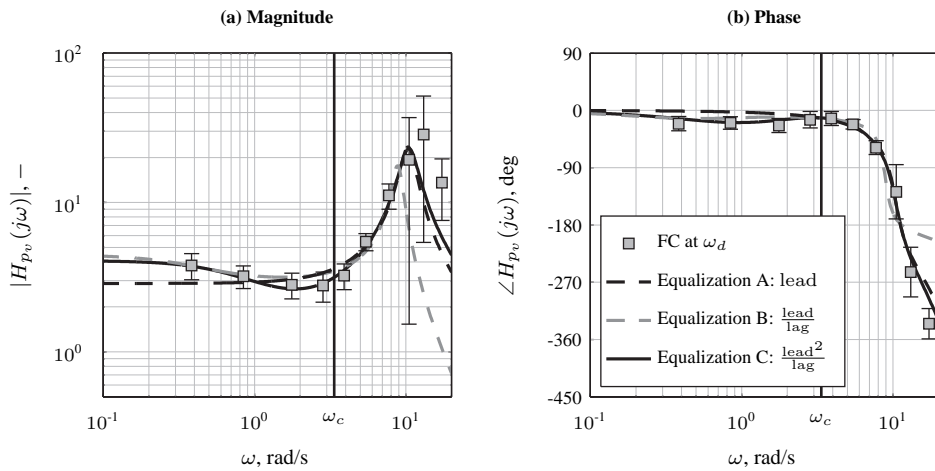


Figure 2.12. Mean pilot model frequency responses estimated with different equalization settings for aircraft pitch dynamics (five subjects, condition C1).

influences the interpretation of the effects of physical motion feedback on pilot behavior, as will be further discussed in Section 2.4.4.

2.4.3 Variance Accounted For Evaluation

Figures 2.12-2.13 showed differences in the accuracy with which the different equalization forms listed in Table 2.1 allowed for in matching frequency-domain pilot describing function estimates. In this section, the accuracy with which pilot dynamics can be modeled over the full measurement bandwidth will be evaluated further in the time domain by considering the pilot model VAF for the different equalization models. Fig. 2.14 depicts the mean pilot model VAF obtained for the two different controlled elements and the four evaluated pilot equalization models. The VAF values for the fits of only $H_{p_v}(j\omega)$ to data from the no-motion conditions C1 and C3 are shown in Fig. 2.14(a), while Fig. 2.14(b) presents the VAF of the full pilot model of Fig. 2.4 with the different forms of $H_{eq}(j\omega)$ for conditions C2 and C4. A one-way repeated measures Analysis of Variance (ANOVA) was performed to investigate possible differences in the VAF values obtained for the different equalization forms, where a p -value lower than 0.05 was considered as a significant effect, while a p -value between 0.05 and 0.1 was considered to indicate a marginally significant effect. The data for condition C3 showed problems with sphericity, so for the data from that condition the conservative Greenhouse-Geisser sphericity correction was applied [Field, 2005].

As expected from the results shown in Fig. 2.9, the different equalization settings yield approximately the same pilot model fit for the double integrator dynamics (conditions C3 and C4), with average VAFs of around 82% for the no-motion tasks and 88% for the tasks with physical motion feedback. ANOVA results for these conditions indicate no significant effect of the selected equalization from on the pilot model VAF for condition C3 ($F(1.05, 4.22) = 1.43, p > 0.05$), while for C4 a significant effect was observed: $F(3, 12) = 3.85, p < 0.05$. Using post-hoc tests (pairwise comparisons), for which the Bonferroni adjustment for multiple comparisons was applied [Field, 2005], this latter significant effect was found to result from the slightly lower VAF values found for the lag-lead equalization (B), see Fig. 2.14(b). Fig. 2.14 thereby confirms the observation made from the results presented in Fig. 2.9, that is, that for modeling double integrator control behavior over the full measurement bandwidth the addition of extra lead and lag terms to the pure lead equalization form A does not improve the quality of pilot model fit.

For the aircraft dynamics, Fig. 2.14 shows that the achieved VAF is on average found to be 2–5% higher for equalizations C and D. This increase in VAF is comparable for both the data from the no-motion and motion conditions (C1 and C2), as expected from the comparison with measured describing functions shown in Figures 2.12 and 2.13. The variation in VAF with the selected equalization form is found to be highly significant: $F(3, 12) = 6.83, p < 0.05$ and $F(3, 12) = 18.52, p < 0.05$ for conditions C1 and C2, respectively. Post-hoc analysis showed that for both the no-motion and motion data, the most significant pairwise comparisons were those between the VAF values of equalizations A-B and C-D. Furthermore, compared to equalization C, the additional freedom in the equalization model provided by the two separate lead time constants in equalization D (see Table 2.1) was not found to yield significantly more accurate modeling of pilot behavior for control of the considered aircraft pitch dynamics for both condition C1 and C2. Fig. 2.14 even shows a minor

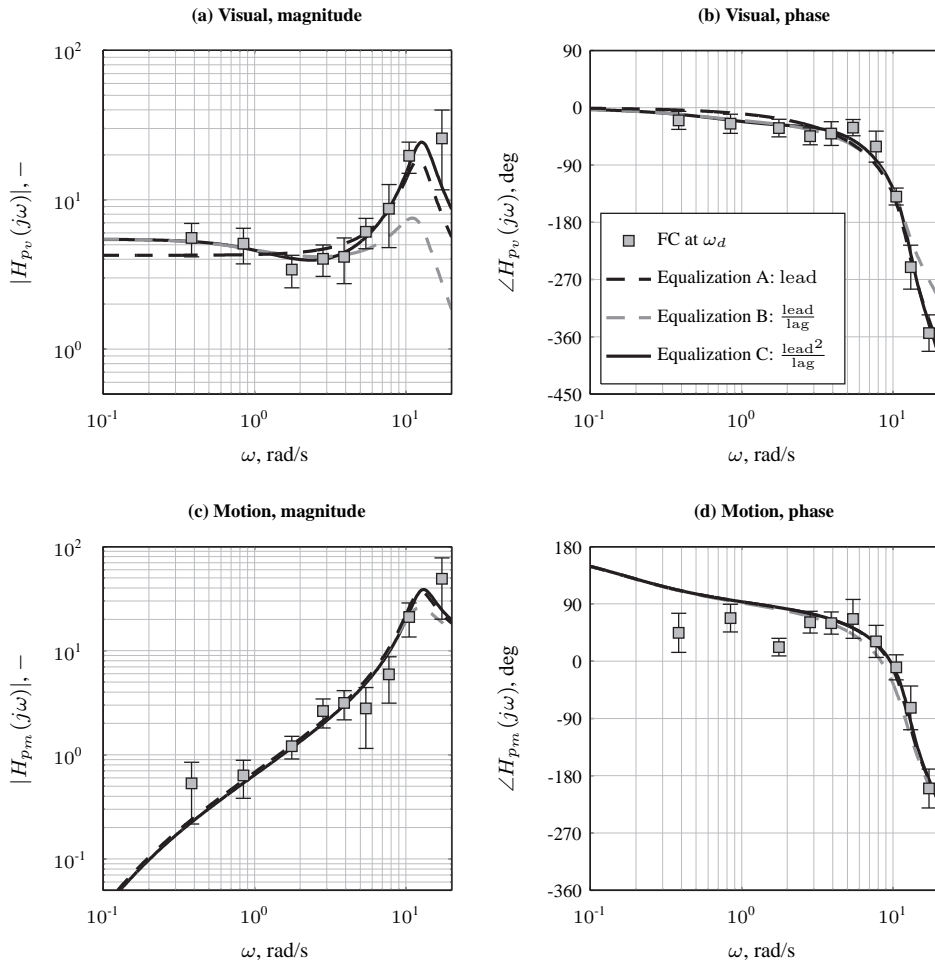


Figure 2.13. Mean pilot model frequency responses estimated with different equalization settings for aircraft pitch dynamics (five subjects, condition C2).

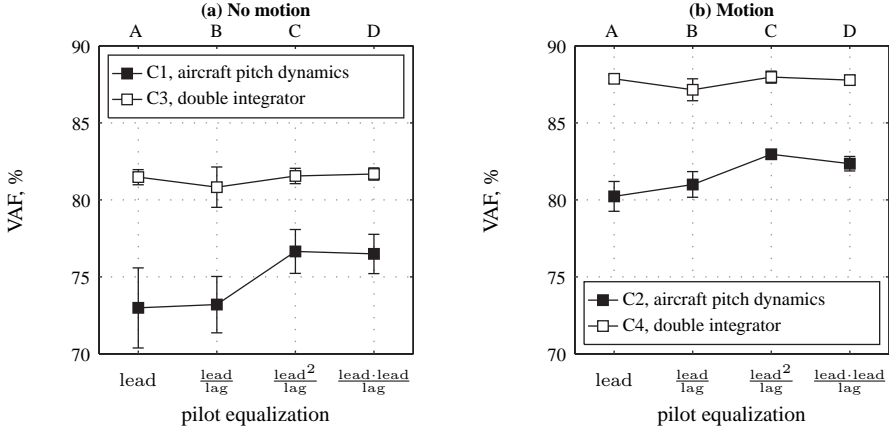


Figure 2.14. Mean pilot model VAF for different equalization settings (five subjects, motion and no motion).

reduction in model VAF if equalization D is used. This indicates the second independent lead term is unneeded for modeling pilot behavior for the considered aircraft pitch dynamics and even negatively affects the quality of the obtained pilot model identification results, as suggested in Section 2.2.5.

Based on the results shown in Figs. 2.9 to 2.14 it can be concluded that equalization forms A and C yield the most concise pilot models that are capable of representing the adopted pilot dynamics over the complete measurement range for control of double integrator and the aircraft pitch dynamics considered in this study, respectively.

2.4.4 Effects of Physical Motion Feedback on Pilot Equalization

Other experiments that investigated the effects of physical motion feedback on pilot tracking behavior revealed considerable changes in pilot behavior, especially in pilots’ responses to visually presented tracking errors ($H_{p_v}(j\omega)$, see Fig. 2.4) at the higher frequencies in the measurement bandwidth [Nieuwenhuizen et al., 2008; Zaal et al., 2009b; Pool et al., 2010]. In addition to the adaptation of the neuromuscular actuation dynamics as reported in [Zaal et al., 2009b] and [Pool et al., 2010], the most defining effect of physical motion feedback on compensatory tracking behavior that is typically observed is a decrease in visual lead equalization, which is allowed for due to the additional lead compensation that is available from the vestibular response $H_{p_m}(j\omega)$, see Fig. 2.13. The human vestibular system – that is, the SCC for rotational motion as considered here, see Section 2.2.3 – provides a much more efficient way of providing lead information than can be obtained from visual lead equalization, due to the smaller time delay associated with vestibular perception compared to visual lead perception [Hosman and Stassen, 1999].

The results presented in Sections 2.4.1 to 2.4.3 showed that for modeling pilot control behavior over the full measurement bandwidth for the typical aircraft pitch dynamics given

by Eq. (2.6), the use of equalization C as the pilot equalization dynamics $H_{eq}(j\omega)$ yielded the best modeling results, as indicated by higher VAF values and better correlation with measured pilot describing functions. For modeling control of double integrator dynamics, no additions to the pure lead equalization term, proposed by McRuer et al. [1965] for modeling equalization around crossover, were found to be required when considering pilot equalization over a wider frequency range. The average parameters of the multimodal pilot model defined in Fig. 2.4 that were estimated for all four experimental conditions, using these two settings for the equalization term $H_{eq}(j\omega)$, are summarized in Table 2.4.

Table 2.4. Average pilot model parameters for each condition.

Cond.	$H_{eq}(j\omega)$	K_v —	T_L s	T_I s	K_m deg/ips	τ_v s	τ_m s	ω_{nm} rad/s	ζ_{nm} —
C1	C	4.07	0.44	1.32	—	0.21	—	10.50	0.14
C2	C	5.65	0.32	0.90	3.79	0.26	0.19	12.74	0.18
C3	A	0.62	0.98	—	—	0.23	—	10.41	0.14
C4	A	1.44	0.38	—	3.55	0.28	0.17	12.78	0.18

The average pilot model identification results presented in Table 2.4 show nearly identical values for the parameters of the neuromuscular actuation model given by Eq. (2.4) for both controlled elements, both for the conditions without and with motion feedback (C1 and C3, and C2 and C4, respectively). These results suggest similar adaptation of the high-frequency neuromuscular actuation dynamics when motion feedback is made available across different controlled elements. In addition, the parameters of the pilot motion response $H_{pm}(j\omega)$ – the pilot motion gain K_m and the motion delay τ_m – and the 0.05 sec increase in τ_v observed for the conditions with motion feedback are also found to be largely invariant for the two considered controlled elements.

Of special interest to the application of pilot modeling considered in this chapter are the observed changes in the identified pilot equalization parameters. For the double integrator controlled element, for which equalization form A (pure lead) was adopted, these equalization parameters are the visual gain K_v and the visual lead time constant T_L . As can be verified from Table 2.4, the effect of physical motion feedback on these equalization parameters consists of a decrease in T_L from 0.98 sec for condition C3 to 0.38 sec for condition C4 – that is, a decrease of nearly 40% – which is allowed for by the alternative lead compensation available from the SCC. Furthermore, the presence of physical motion feedback is found to yield a large increase in the value of the pilot visual gain, which indicates pilots were able to respond to visually presented tracking errors with a much higher gain for condition C4. These results of physical motion feedback on pilot dynamics during control of double integrator systems are consistent with previous research [Hosman and Stassen, 1999; Van der Vaart, 1992].

To illustrate the importance of the proposed pilot equalization term extension for the interpretation of such changes in pilot equalization dynamics due to the presence of physical motion feedback for the considered aircraft pitch dynamics, Fig. 2.15 depicts the average values of T_I and T_L that were identified using equalizations A, B, and C for conditions C1 and C2. Furthermore, these identified parameter values are compared to the corresponding

characteristic time constants of the controlled aircraft pitch dynamics. As suggested by McRuer et al. [McRuer et al., 1965; McRuer and Jex, 1967a], the amount of visual lag and lead equalization adopted during tracking is related to the characteristics of the controlled element. For the aircraft pitch dynamics of the form given by Eq. (2.6), these characteristics are defined by the values of the aircraft dynamics lead time constant T_{θ_2} and the inverse short-period frequency $1/\omega_{sp}$, respectively. Note that as equalization A does not have a lag term, no data for this equalization is shown in Fig. 2.15(a). The variance bars in Fig. 2.15 depict the 95% confidence intervals of the mean identified parameters.

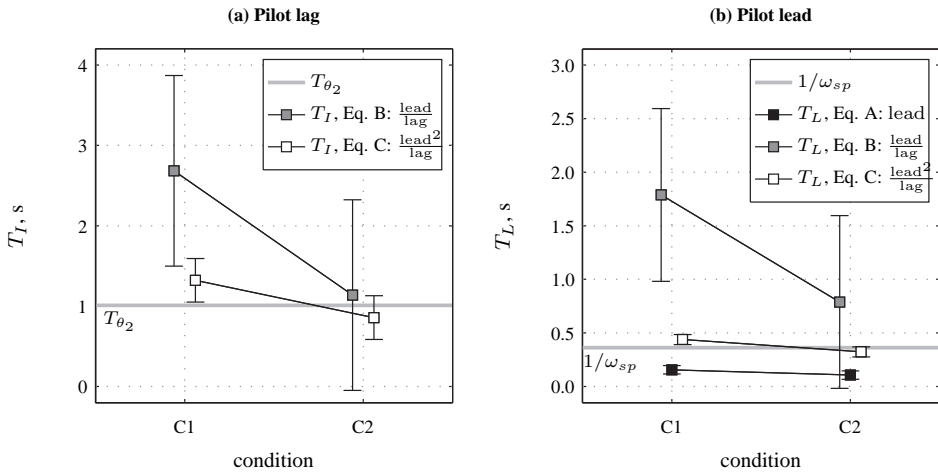


Figure 2.15. Pilot lag and lead constants compared to aircraft dynamics characteristic frequencies (conditions C1 and C2, equalization A-C).

In line with the differences observed in the average pilot model frequency responses depicted in Figures 2.12 and 2.13, Fig. 2.15 shows that considerable differences in the identified values of T_I and T_L are found when attempting to capture the full bandwidth pilot dynamics with equalizations A-C. Equalization A shows comparatively low values of T_L due to the fact that only high-frequency lead is captured by this equalization model, while the low-frequency lag compensation visible in the measured describing functions is not accounted for. The results for equalization B show very high values T_I and T_L , and also more spread in the obtained identification results than observed for the other equalization forms. Note that for condition C1 the pilot lead time constants identified with equalization B are found to be even higher on average than those observed for the double integrator controlled element for condition C3, see Table 2.4. Fig. 2.15 shows that for equalization C the identified pilot lag and lead time constants are found to be closest to the values of the characteristic time constants of $H_{\theta, \delta_e}(j\omega)$, as would be expected for compensation of the controlled element dynamics [McRuer et al., 1965; McRuer and Jex, 1967a]. Fig. 2.15(a) shows that for both conditions C1 and C2 T_I is found to be around T_{θ_2} . In addition, the identified values for the pilot lead constant shown in Fig. 2.15(b) indicate a strong correlation between T_L and $1/\omega_{sp}$.

In addition, as visible from the matches of identified pilot models with the measured describing functions depicted in Figures 2.12 and 2.13, the identified results for equalization C shown in Fig. 2.15 also allow for quantitative evaluation of changes in the adopted equalization over a wide frequency range. As can be verified from Table 2.4, the values of T_L estimated for condition C1 are found to be slightly higher than $1/\omega_{sp}$, implying pilot lead is on average generated starting at slightly lower frequencies than required for exact compensation of the aircraft dynamics. For condition C2, T_L is found to be below ω_{sp} and around 27% lower than the lead time constants found for condition C1. As expected based on the overview of the magnitude of effects of physical motion feedback given in [Shirley and Young, 1968], the decrease in visual lead equalization observed for the aircraft pitch dynamics is smaller than that observed for the double integrator controlled element. A more modest increase in pilot gain (see Table 2.4), a 38% increase compared to the more than doubling of K_v observed for the double integrator system, further confirms this reduced effect of physical motion feedback for this controlled element. The results shown in Fig. 2.15 indicate that equalization C yields pilot model identification results that allow for valid quantification and the most intuitive interpretation of changes in pilot control behavior over a wide frequency range for the considered aircraft pitch dynamics.

2.5 Discussion

The study described in this chapter emphasizes the value of the quasi-linear models introduced by McRuer et al. [1965] for describing and analyzing pilot control behavior during compensatory tracking, not only in the frequency range around the pilot-vehicle system crossover frequency, but also for the full range of frequencies over which pilot dynamics are of interest. Many studies have shown that these models are capable of modeling manual control behavior during tracking tasks with pure gain, single integrator, double integrator, or more complex controlled elements representative for different types of vehicle systems [McRuer and Jex, 1967a; McRuer, 1988; Grant and Schroeder, 2010]. In addition, pilot model estimation results from the current study confirm that the lead-lag pilot equalization term included in this model suffices for describing the pilot equalization that is adopted over a wide frequency range during control of double integrator dynamics.

However, for a controlled element that is representative for conventional aircraft elevator-to-pitch dynamics, measured pilot describing functions indicate that the pilot equalization term included in the *precision model* described in [McRuer et al., 1965] does not allow for modeling of the adopted equalization dynamics over a frequency range that extends beyond the crossover region. Describing function measurements show that pilots compensate for the dynamics of this controlled element around the short-period mode natural frequency by performing both low-frequency lag and high-frequency lead equalization, where the latter extends to frequencies well above crossover. The addition of a second lead term to the lead-lag pilot equalization transfer function proposed for the *precision model* is found to provide the required freedom for modeling this combination of pilot lag and lead equalization dynamics. Furthermore, using an analysis of the VAF of the obtained pilot model fits for varying equalization models, this additional lead term was found to yield a signifi-

cant increase in the accuracy with which manual control behavior can be modeled for such aircraft pitch dynamics.

For the aircraft pitch dynamics considered in the present study, for which the natural frequency of the short-period mode was in the crossover region, it was found that the lead time constant of this additional lead term could be coupled to the lead term already present in the model, yielding an equalization transfer function with a single lag and a squared lead term (equalization C). Even though the time constants of both lead terms are not necessarily equal, no improvement in model fit was observed for an equalization with two independent lead terms (D) for the presented data. Differences in the values of both lead time constants for this equalization model were found to be small for the data from all subjects except one. Furthermore, the extra model parameter, combined with the fact that both lead terms are – from a model identification perspective – mathematically identical, leaves the pilot model identification problem overdetermined. Note, however, that depending on the adopted pilot-vehicle system crossover frequency and the value of the short-period natural frequency for such a controlled element, the additional independent lead time constant might still need to be considered for modeling the adopted pilot equalization dynamics. Evaluation of the applicability of the proposed equalization model extension to controlled elements of this form, but with different values for the short-period mode natural frequency, is planned for future research.

Previous experiments have shown considerable changes in pilot dynamics, especially in pilots responses to visually presented tracking errors, at frequencies above crossover when physical motion feedback of the controlled element state is made available [Nieuwenhuizen et al., 2008; Zaal et al., 2009b; Damveld, 2009; Pool et al., 2010]. To show the importance of selecting an appropriate equalization model for the interpretation of these effects of physical motion feedback on pilot control behavior over a wide frequency range, measured effects of providing rotational pitch motion cues were compared for the considered aircraft pitch dynamics and a double integrator controlled element. For the aircraft pitch dynamics, measured pilot describing functions indicate that pilots select the same combination of low-frequency lag and high-frequency lead equalization for tasks with and without physical motion cues. Furthermore, by comparing identified pilot model lead and lag time constants with the characteristic modes of the aircraft pitch dynamics, the extended pilot equalization model with a squared lead term was found to provide a quantification of pilot control behavior over a wide frequency range that best reflects observed changes in the adopted lead and lag equalization and explicitly shows human adaptation to the dynamics of the controlled element, as proposed by McRuer et al. [McRuer et al., 1965; McRuer and Jex, 1967a; McRuer, 1988]. The effects of motion feedback on pilot control behavior as presented in this chapter, which were quantified using the proposed pilot model extension, are found to be consistent with findings from previous research [Shirley and Young, 1968; Hosman and Stassen, 1999; Zaal et al., 2009b; Pool et al., 2010].

2.6 Conclusions

Using frequency-domain describing function measurements of pilot tracking behavior, both with and without physical motion feedback, it was shown that for a controlled element that is

representative for conventional aircraft pitch dynamics an extended pilot model equalization term is needed for modeling the adopted equalization dynamics over the full measurement frequency range. These describing function measurements show that pilots perform a combination of low-frequency lag and high-frequency lead compensation, the latter extending to frequencies well above crossover, to compensate for the characteristics of such aircraft pitch dynamics that result from the short-period mode. It is found that an extended pilot model equalization term, which consists of a squared lead and a single lag term, provides the most accurate and consistent results for the modeling of pilot manual control behavior for such aircraft dynamics. Furthermore, compared to equalization models that lack the second lead term, this extended equalization term was also found to yield a significant increase in the average quality of fit of the pilot model to time-domain data. Finally, using a comparison with measurements for a double integrator controlled element, it is shown that the proposed equalization model allows for intuitive quantitative evaluation of the effects of physical motion feedback on pilot tracking behavior, most notably the high-frequency adaptation of pilots' responses to visually presented tracking errors.

3

Modeling Pilot Control During Ramp Tracking

To extend the evaluation of the effects of simulator motion cueing variations on pilot manual control behavior to other control tasks than compensatory tracking tasks with quasi-random forcing function signals, tracking tasks with target forcing functions that consist of a number of discrete ramp-like changes in target attitude are also considered in this thesis. Tracking such alternative reference signals yields a control task that is similar to discrete maneuvering tasks that are often performed during real manual aircraft control. Due to the deterministic nature of such ramp forcing function signals, they may induce a control strategy that deviates from the purely compensatory control observed for the tracking of an unpredictable multisine signal and hence require a different pilot model structure for modeling measured control behavior. In this chapter, this is evaluated by considering manual control behavior for single-loop pitch tracking tasks (no physical motion feedback) where participants were asked to track target signals consisting of four ramp-like changes in target pitch attitude.

The contents of this chapter have been published as:

Pool, D. M., Van Paassen, M. M., and Mulder, M., "Modeling Human Dynamics in Combined Ramp-Following and Disturbance-Rejection Tasks", *Proceedings of the AIAA Guidance, Navigation, and Control Conference*, Aug. 2-5, Toronto, Canada, 2010, AIAA-2010-7914

3.1 Introduction

The theory of Successive Organization of Perception (SOP) put forth by McRuer et al. [1968] defines three different levels of manual control behavior that can be adopted during manual tracking tasks. Depending on the defining features of the control task, such as the display format and the applied forcing functions, human operators may revert to compensatory, pursuit, or precognitive control strategies, or could be switching between any combination of these SOP levels. Most research into human manual control behavior has focused on purely compensatory control, a typical type of behavior found for control tasks where tracking errors were induced by quasi-random forcing function signals. Considerable success has also been achieved in the modeling of compensatory manual control in both single-loop [Elkind, 1956; McRuer et al., 1965] and multimodal control tasks [Jex et al., 1978; Hosman, 1996; Zaal et al., 2009c]. Despite the fact that most real-life manual control tasks are not purely compensatory, but induce pursuit or precognitive control strategies [McRuer et al., 1968], modeling of these higher levels of manual control behavior has received significantly less attention and has not nearly been as successful as that of compensatory tracking.

This chapter focuses on manual control behavior in manual control tasks where a deterministic reference trajectory, defined as a number of discrete ramp-like changes in target attitude, is to be tracked using a pursuit display. In addition, a quasi-random disturbance signal is applied to perturb the controlled element dynamics. Compared to the control tasks that are typically used for studying the effects of physical motion feedback during manual control, where two quasi-random forcing function signals are applied [Stapleford et al., 1969; Jex et al., 1978; Zaal et al., 2009c], such ramp target signals yield more realistic manual control tasks, similar to in-flight maneuvers such as a turn entry or altitude change [Zaal et al., 2008; Pool et al., 2009b]. Furthermore, it is shown in Appendix B that, depending on ramp forcing function signal design, reliable identification of the multimodal pilot models that are used for modeling compensatory manual control under such multimodal cueing conditions is possible using measurements taken during combined ramp-tracking and disturbance-rejection tasks.

For repetitive manual tracking of such deterministic ramp-like reference signals using a pursuit display, however, it is likely that human operators will develop a control strategy that corresponds to a SOP level that exceeds purely compensatory tracking. First, despite the fact that the use of a pursuit display does not directly imply the adoption of pursuit behavior by a human operator [Wasicko et al., 1966; Hess, 1981], the use of a pursuit display in combination with ramp signals with predictable maneuver times and rates of change does provide ample opportunity for pursuit tracking. In addition, human operators may be able to acquire such familiarity with the reference signal and controlled element dynamics that it allows for generation of open-loop precognitive control inputs [Pew et al., 1967; McRuer et al., 1968; McRuer and Krendel, 1974; McRuer, 1980; Yamashita, 1989, 1990]. Many researchers have illustrated the differences between compensatory and pursuit tracking behavior with experimental measurements [Chernikoff et al., 1955; Elkind, 1956; Wasicko et al., 1966; McRuer and Jex, 1967b; Allen and Jex, 1968; Hess, 1981]. Convincing experimental evaluations of precognitive behavior during tracking are, however, sparse. In addition, models have been proposed for modeling both pursuit and precognitive tracking

behavior, see for instance [McRuer et al., 1968], but have generally not been validated by fitting them to experimental measurements of tracking behavior.

Due to the adaptive nature of human control behavior [McRuer et al., 1968; Young, 1969], it is likely that the type of control behavior (compensatory, pursuit, precognitive) that is adopted in the ramp-tracking tasks considered in this chapter is dependent on both the characteristics of the ramp signals (steepness, magnitude) and the controlled element dynamics. In addition, previous experimental work has hinted at suppression of pursuit operation when an additional disturbance forcing function signal is present [Reid, 1970], as disturbances on the controlled element can only be attenuated using compensatory control. It is the purpose of this chapter to evaluate if the considered ramp-tracking tasks induce a control strategy that differs from pure compensatory tracking and to determine how this depends on the key characteristics of the control task. This is done by fitting a dual-mode model for human ramp-tracking behavior, similar to the models proposed by McRuer et al. [1968] and Allen and McRuer [1979] for pursuit and precognitive tracking behavior, to collected human-in-the-loop measurements of ramp-tracking behavior. The model used for this analysis includes a compensatory response that captures compensatory control inputs, and a feedforward response on the target signal that can account for possible additional pursuit and precognitive control inputs.

This chapter describes an experiment in which single-loop ramp-tracking behavior is measured for control of both single and double integrator dynamics. Ramp-tracking tasks with ramp target signals with two different ramp steepnesses are considered, both with and without the presence of an additional quasi-random disturbance signal that perturbs the controlled element. The considered ramp target signals are identical to two of the ramp signal settings also evaluated in Appendix B. Note that the effects of physical motion feedback on manual control, which are the main focus of this thesis, are not considered in this study. Rather, the focus of this chapter lies on the human dynamics that occur during ramp-tracking with only visually presented information, to which the effects of additional motion feedback are expected to be added in later work.

This chapter is structured as follows. First, Section 3.2 provides a detailed description of the manual control task and gives an overview of the the pertinent literature on modeling manual control behavior for the considered type of control task. Then, Section 3.3 describes the details of the human-in-the-loop experiment that was performed to gather the required measurements of human manual control behavior. The results of this experiment are presented in Section 3.4. The chapter ends with a discussion and conclusions.

3.2 Background

3.2.1 Control Task

This chapter considers manual control behavior in a pitch-attitude tracking task performed with a pursuit display. Fig. 3.1 depicts a schematic representation of such a manual control task, where a human operator controls the pitch attitude θ of the controlled element with dynamics $H_c(s)$. Two forcing function signals are indicated in Fig. 3.1: the target forcing function f_t defines the reference trajectory that should be followed as closely as possible,

while f_d represents an external disturbance that works on the controlled element. Note from Fig. 3.1 that due to the use of a pursuit display, as depicted in Fig. 3.2, the operator can use information on the target signal f_t , the tracking error e , and the controlled element state θ to achieve a suitable control input u .

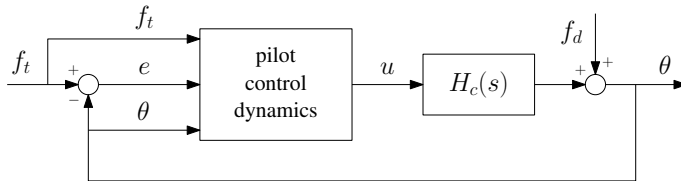


Figure 3.1. Schematic representation of a combined target-following and disturbance-rejection task performed with a pursuit display.

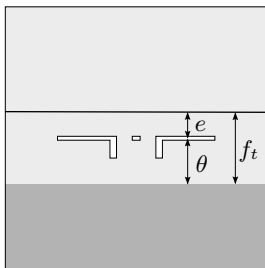


Figure 3.2. Pursuit display.

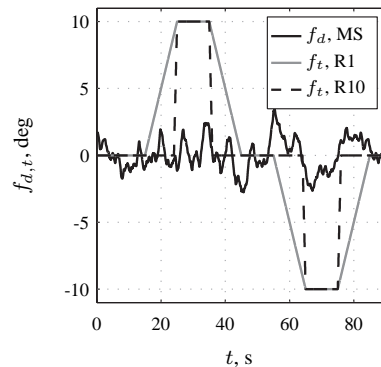


Figure 3.3. Time traces of the multisine disturbance forcing function (MS) and both ramp target forcing function signals (R1 and R10).

Pursuit tracking tasks similar to the one depicted in Fig. 3.1 have been studied extensively [Wasicko et al., 1966; McRuer et al., 1968; Allen and McRuer, 1979; Hess, 1981], but mainly for control tasks with quasi-random target forcing function signals (f_t) and without external disturbances (f_d). As a continuation of previous research [Zaal et al., 2008; Pool et al., 2009b], this chapter addresses manual control behavior for tracking tasks in which the target signal is composed of a series of discrete ramp-like changes in reference attitude and where an additional quasi-random disturbance signal is present. Fig. 3.3 depicts the two ramp target forcing functions (R1 and R10, which have different ramp steepnesses) and the quasi-random multisine disturbance signal (MS) that are considered in this chapter. The details of these forcing function signals are provided in Section 3.3.

Human dynamics during compensatory tracking have been shown to be highly adaptable to the dynamics of the controlled element $H_c(s)$ [McRuer et al., 1965]. As a similar

dependence on $H_c(s)$ is also likely with respect to the development of higher levels of control behavior in the considered ramp-tracking and disturbance-rejection task [McRuer et al., 1968], this chapter investigates ramp-tracking control behavior for both single and double integrator controlled element dynamics, given by:

$$H_c(s) = \frac{K_c}{s}, H_c(s) = \frac{K_c}{s^2} \tag{3.1}$$

3.2.2 Successive Organization of Perception

In the 1960s, McRuer et al. [1968] developed their theory of Successive Organization of Perception (SOP). This SOP theory defines three distinct levels of skill-based manual control behavior that can be adopted during manual tracking, depending on the nature and characteristics of the control task. Block-diagram representations of these three levels of manual control behavior are depicted in Fig. 3.4.

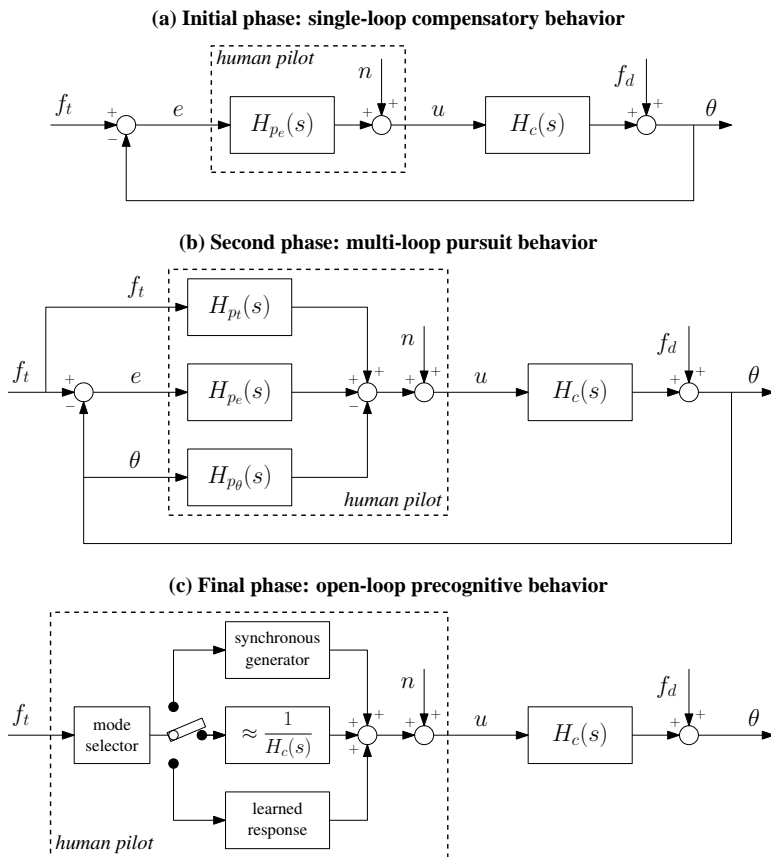


Figure 3.4. The different phases in the Successive Organization of Perception. Adapted from [McRuer et al., 1968].

The lowest level of manual control behavior is referred to as compensatory behavior, which is depicted in Fig. 3.4(a). During compensatory control, the human operator only acts on the perceived tracking error e , thereby closing a single loop around the controlled element $H_c(s)$. Compensatory behavior is, for instance, adopted during control tasks where tracking errors induced by an unpredictable quasi-random forcing function signal are depicted on a compensatory display [McRuer et al., 1965].

If information other than the tracking error e is also available to the human operator, such as for instance provided on the pursuit display shown in Fig. 3.2, he may choose to utilize pursuit tracking behavior as depicted in Fig. 3.4(b). Even though the explicit presentation of f_t and θ on a pursuit display would allow the human operator to also operate on both those quantities, thereby utilizing a multi-loop control strategy, this is no guarantee for the adoption of a pursuit tracking strategy. As rightly pointed out by Hess [1981], a distinction needs to be made between the variables that are made available to a human operator and the internal organization of the control strategy he adopts during manual control.

The ultimate stage in the SOP process depicted in Fig. 3.4 is precognitive control. As indicated in Fig. 3.4(c), precognitive control behavior is observed in control tasks where the level of familiarity with the controlled element and the commanded maneuver allows for responding with a preprogrammed learned response upon a certain trigger provided by the reference signal f_t . Fig. 3.4(c) shows that different mechanisms may underly the execution of such a precognitive response. A clear example of is the tracking of a forcing function signal consisting of a single sinusoid, for which, given enough practice, operators are typically found to respond quicker than can be expected given the latency inherent to a closed-loop compensatory response [Pew et al., 1967]. Note that this instance of precognitive control behavior corresponds to the block labeled “synchronous generator” in Fig. 3.4(c).

Manual control tasks with predictable forcing function signals as considered in this chapter (see Fig. 3.3) are an example of a control task that, given extensive training and familiarization, would also support the utilization of a precognitive control strategy. The key characteristic of precognitive behavior, which distinguishes it from for instance pursuit tracking, is that it involves an open-loop response to a trigger or recognized pattern in f_t that is entirely independent of the perceivable information at the moment it is given and depends solely on the human operator’s internal representation of the control task.

The taxonomy of control behavior summarized in the SOP theory and Fig. 3.4 is a useful starting point for the evaluation of control behavior in the combined ramp-tracking and disturbance-rejection tasks studied in this chapter. As can be verified from all three block diagrams depicted in Fig. 3.4, a disturbance signal on the controlled element output can only be attenuated through a compensatory feedback control strategy. Even though the presence of an additional disturbance forcing function has been reported to affect pursuit tracking operation [Reid, 1970], to what extent the presence of such a disturbance signal interferes with the human dynamics required for following of ramp target signals is as of yet unknown. The same holds for the modeling of these pilot control dynamics.

3.2.3 Modeling Manual Control Behavior

3.2.3.1 Modeling Compensatory Control

The modeling of compensatory control behavior as depicted in Fig. 3.4(a) has been well established since the work of McRuer et al. [1965]. Using measurements of pilot dynamics for a multitude of different controlled elements and forcing function signals, McRuer et al. developed models and accompanying sets of rules of thumb that have proven to be widely applicable for describing compensatory pilot dynamics. Here, the following model, which is based on the work of McRuer et al. [1965], is used for modeling compensatory manual tracking dynamics:

$$H_{pe}(s) = K_{pe} (1 + sT_{Le}) e^{-s\tau_e} H_{nm}(s) \quad (3.2)$$

In Eq. (3.2), $K_{pe}(1 + sT_{Le})$ represents the pilot equalization characteristic, as discussed in detail in Chapter 2. Note that in the original model as described in [McRuer et al., 1965] this equalization characteristic was defined as a lead-lag transfer function. McRuer et al. [1965], however, established that human operators adapt their equalization characteristics to yield an open-loop system ($H_{pe}(s)H_c(s)$) with approximately single integrator dynamics around gain-crossover. This implies that for single integrator controlled element dynamics, the equalization characteristic as given in Eq. (3.2) is reduced to only the proportional gain K_{pe} . For double integrator dynamics, low-frequency lead needs to be generated to achieve K/s dynamics around crossover. Therefore, the full equalization characteristic listed in Eq. (3.2) is needed for describing human dynamics during compensatory double integrator control. Note, however, that lag equalization is required for neither controlled elements and has therefore been omitted from Eq. (3.2). The delay parameter τ_e accounts for any delays internal to the pilot that accumulate in generating a compensatory control input. Finally, the transfer function $H_{nm}(s)$ represents the combined dynamics of the neuromuscular actuation and the manipulator, which are approximated here as a second-order mass-spring-damper system [Damveld et al., 2009]:

$$H_{nm}(s) = \frac{\omega_{nm}^2}{s^2 + 2\zeta_{nm}\omega_{nm}s + \omega_{nm}^2} \quad (3.3)$$

The neuromuscular frequency ω_{nm} and damping factor ζ_{nm} are free parameters of this compensatory model, as are K_{pe} , τ_e , and T_{Le} (the latter for double integrator control only).

3.2.3.2 Modeling Pursuit/Precognitive Control

Compared to the modeling of compensatory manual control behavior, the modeling of pursuit and precognitive tracking has received only moderate attention [Wasicko et al., 1966; McRuer et al., 1968; McRuer and Krendel, 1974; Allen and McRuer, 1979; Hess, 1981]. One of the reasons for this is the fact that during both pursuit tracking and control tasks where precognitive inputs are given, the adopted control strategy is no longer defined as pure tracking error minimization based on a single explicitly presented variable. Control behavior for these higher SOP levels might involve multiple responses to (implicitly or

explicitly) perceived or internally generated variables, as is, for instance, clear for a pursuit display configuration as presented in Fig. 3.2. This fact makes the modeling of such multimodal control behavior significantly more complex than the modeling of purely compensatory behavior [Wasicko et al., 1966; Hess, 1981].

For pursuit tracking, Wasicko et al. [1966] have shown that due to the fact that $e = f_t - \theta$, pursuit control behavior can be captured by considering only two of the three pilot responses depicted in Fig. 3.4(b), $H_{p_t}(s)$, $H_{p_e}(s)$, and $H_{p_\theta}(s)$. Allen and McRuer [1979] have proposed to model pursuit control behavior with only the $H_{p_t}(s)$ and $H_{p_e}(s)$ channels depicted in Fig. 3.4(b), that is, as a closed-loop compensatory control strategy combined with feed-forward control operations on the target signal. In an excellent overview of adaptation in manual control, Young [1969] also proposed that the dominant characteristics of pilot pursuit tracking behavior can be modeled with only $H_{p_t}(s)$ and $H_{p_e}(s)$: *“In the pursuit situation [the human operator] has performance blocks acting on the error, input and response, although it is established that the response block is probably not used for anything except perhaps controlled element adaptation.”* Wasicko et al. [1966] and McRuer and Jex [1967b] have shown with describing function measurements that this is indeed a likely model structure for pursuit tracking behavior.

The development of methods for modeling precognitive control behavior has received far less attention than those for pursuit tracking. The purely open-loop precognitive response representation proposed by McRuer et al. [1968] as depicted in Fig. 3.4(c) is only feasible if the human operator’s internal representation of the reference signal f_t and the controlled element dynamics $H_c(s)$ allows for perfect execution of the appropriate control response. For the ramp-tracking tasks considered in this chapter, and perhaps for most applications in manual tracking, this can, however, be expected to hardly ever be the case.

This is also recognized by McRuer et al. [1968], who argue that for the tracking of a step reference signal a combination of open-loop precognitive and closed-loop compensatory behavior is adopted. This is illustrated by Fig. 3.5(a), which shows that after an inevitable delay in the human operator response (phase I), the occurrence of a step in the reference signal results in an initial, possibly precognitive, rapid response (phase II) with which the controlled system response is brought to the step’s final value A . McRuer et al. [1968] argue that this initial response, which in most instances will not result in perfect tracking of the step input, is followed by a final, compensatory, error reduction phase (III), with which the controlled element response is stabilized around A .

For ramp tracking, as considered in this chapter, a similar combined response as proposed by McRuer et al. [1968] for step tracking can be anticipated, see Fig. 3.5(b). This hypothetical response to a ramp input shows a time delay phase (I) and a compensatory error reduction phase (III) equivalent to that shown for step tracking in Fig. 3.5(a). Furthermore, a rapid response that largely eliminates the difference between the controlled element output and the ramp input, which is very similar to phase II of the step-tracking response, is indicated as phase IIa. For ramp tracking, however, an additional phase IIb is also shown in Fig. 3.5(b). As indicated by phase IIb, Once the controlled element output is sufficiently close to the reference signal, the human operator might end up in a state where he merely matches the rates of change of θ and f_t as visible on the pursuit display shown in Fig. 3.2. This would require a different control strategy than hypothesized for phase IIa. Note that the proportion of time spent in phases IIa and IIb depends on the characteristics of the ramp

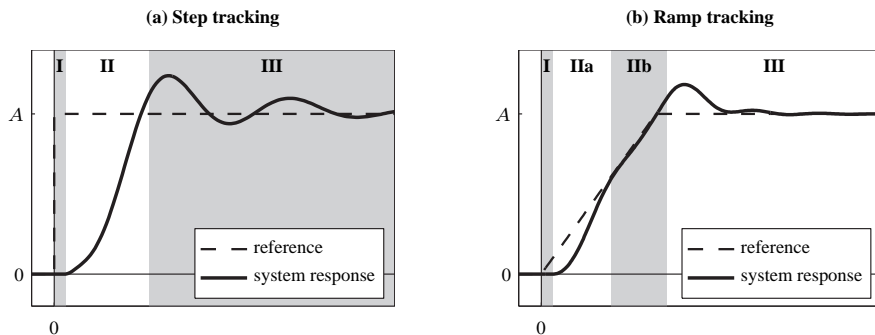


Figure 3.5. Hypothetical responses of controlled element output during manual tracking of step and ramp target signals. Adapted from [McRuer et al., 1968].

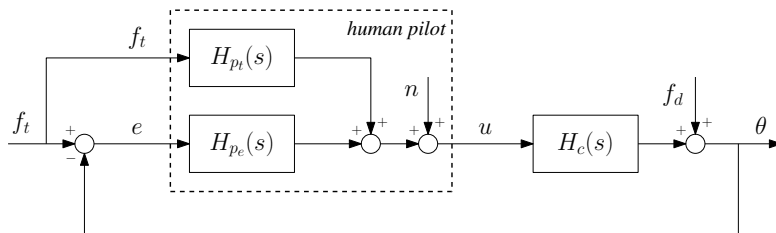


Figure 3.6. Two-channel model of pursuit/precognitive control. Adapted from [McRuer et al., 1968].

signal. For instance, for very steep ramp signals that approximate a step input phase IIb might never be reached, as the reference signal might already have reached its maximum value A before the system response has caught up.

For modeling the dual-mode control behavior that may be anticipated for step tracking based on Fig. 3.5(a), where the human operator is hypothesized to switch between precognitive and compensatory tracking upon a certain trigger, McRuer et al. [1968] propose a control theoretic structure that includes both $H_{p_t}(s)$ and $H_{p_e}(s)$ equal to that proposed by Allen and McRuer [1979] for pursuit tracking, see Fig. 3.6. Therefore, previous work on pursuit tracking and precognitive control behavior suggests that the control theoretical structure with a closed-loop compensatory response $H_{p_e}(s)$ and an open-loop feedforward response $H_{p_t}(s)$ shown in Fig. 3.6 might be appropriate for modeling pilot dynamics during both these modes of operation. Due to this hypothesized equivalence of the models for pursuit and precognitive operation for the considered ramp-tracking tasks, it may prove difficult to separate both. For this reason, in this chapter the feedforward response $H_{p_t}(s)$ will in the remainder of this chapter no longer be referred to as either pursuit or precognitive, but merely used to capture any feedforward behavior that is observed in addition to the compensatory response $H_{p_e}(s)$.

For the modeling of the compensatory response in the two-channel model of Fig. 3.6, some authors have suggested to use the form of Eq. (3.2) [Wasicko et al., 1966; McRuer

et al., 1968], thereby assuming similar compensatory human dynamics as encountered for pure compensatory control. For modeling possible additional pursuit or precognitive control action, an equivalent feedforward pilot response on the target signal is proposed for both. Reflecting the internal representation of the controlled element dynamics required for both pursuit and precognitive behavior [McRuer et al., 1968; Neilson et al., 1988], it has been argued that the feedforward response $H_{p_t}(s)$ for both pursuit and precognitive behavior should approximate the inverse of the controlled element dynamics. This yields $H_{p_t}(s)H_c(s) \approx 1$ [Wasicko et al., 1966; McRuer et al., 1968; Hess, 1981], which, as can be verified from Fig. 3.6, will ensure θ approximates f_t , yielding $e \approx 0$. Due to the fact that it is anticipated that the applied feedforward control inputs are, however, likely not perfect for both the pursuit and precognitive modes, in this chapter the following model for the total feedforward response $H_{p_t}(s)$ is proposed:

$$H_{p_t}(s) = K_{p_t} \frac{1}{H_c(s)} H_{eq_t}(s) e^{-s\tau_t} \quad (3.4)$$

In Eq. (3.4), K_{p_t} and τ_t are the gain and time delay associated with this feedforward response. These parameters are equivalent to K_{p_e} and τ_e in the compensatory model of Eq. (3.2). Further dynamics of $H_{p_t}(s)$ are then governed by the inverse controlled element dynamics and the transfer function $H_{eq_t}(s)$, which represents equalization performed by the operator on the target signal, analogous to the lead equalization in Eq. (3.2), or limitations in generating the feedforward response prohibit achieving $H_{p_t}(s)H_c(s) \approx 1$. Here it is proposed, as a starting point for further investigation, to set $H_{eq_t}(s)$ to:

$$H_{eq_t}(s) = \frac{1}{1 + sT_{I_t}} \quad (3.5)$$

This first-order lag is included in the model for $H_{p_t}(s)$ to allow for capturing lags that may accumulate in this feedforward channel. These lags could result, for instance, from limitations on the inversion of $H_c(s)$ by the human operator, or, as it is unlikely that human operators will attempt to precisely follow f_t , especially for steep changes in reference value, represent internal filtering or smoothing of the input. Note from comparing Equations (3.2) and (3.4) that the neuromuscular actuation dynamics are not included in the latter model for the feedforward response. The reason for this is that the human operator is implicitly assumed to be capable of accounting for his own neuromuscular actuation dynamics through the feedforward, thereby effectively canceling the effect of $H_{nm}(s)$ on $H_{p_t}(s)$. Again, if this cancellation of $H_{nm}(s)$ is not fully achieved, the remaining dynamics are also captured by the feedforward equalization term, Eq. (3.5).

To visualize the responses the model of Eq. (3.4) is capable of describing, Fig. 3.7 shows theoretical control inputs for both ramp signals depicted in Fig. 3.3, and for both single and double integrator controlled elements. For generating the data shown in Fig. 3.7, the following parameter values have been used: $K_{p_t} = 1$, $\tau_t = 0.3$ sec, and $T_{I_t} = 0.05$ s.

It should be noted that the model for ramp tracking behavior proposed in this section does not include the explicit switching between the feedforward and compensatory responses as, for instance, proposed by McRuer et al. [1968]. Instead, Fig. 3.6 shows a two-channel model of pilot behavior for which both $H_{p_e}(s)$ and $H_{p_t}(s)$ are continuous time-invariant processes that are driven by e and f_t , respectively. For the application to

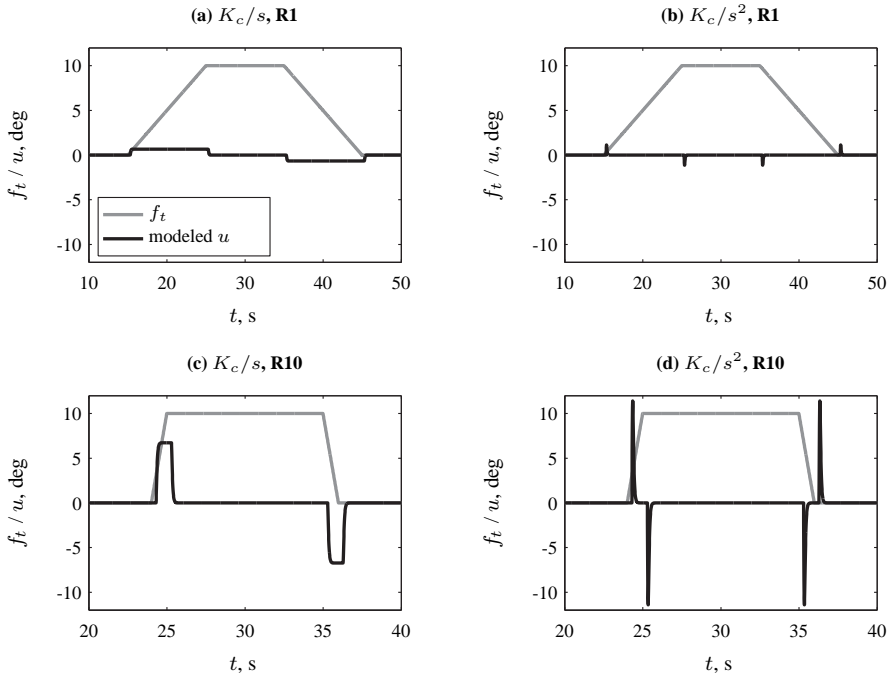


Figure 3.7. Example feedforward control inputs resulting from the proposed model of Eq. (3.4).

control tasks with ramp target forcing functions as those depicted in Fig. 3.3, however, the feedforward response $H_{p_t}(s)$, which is driven by f_t , is implicitly disabled when there is no change in the reference signal value. Hence, as also visible in Fig. 3.7, the modeled feedforward response $H_{p_t}(s)$ for this case will still only contribute to the model output during the intervals where feedforward control operations are anticipated.

3.3 Experiment

3.3.1 Apparatus

To gather the data needed for testing the model proposed for ramp-tracking behavior in Section 3.2.3, an experiment was performed in the SIMONA Research Simulator (SRS) at Delft University of Technology, see Fig. 3.8. During the tracking tasks performed for this experiment, both the motion system and the outside visual system of the simulator were switched off. The (foveal) pursuit display (see Fig. 3.2) was projected on the primary flight display (PFD) in the SRS cockpit. The PFD update rate was 60 Hz and the time delay of the image generation on this PFD has been measured to be in the order of 20-25 ms (including the projection) using a custom visual delay measurement system [Stroosma et al., 2007].

Participants used the pitch axis of a Moog FCS Ecol-8000 electrical sidestick to give their control inputs, u . The sidestick was adjusted to have no break-out force and a maxi-

imum deflection of ± 13 deg in pitch. Stick stiffness was set to 1.5 N/deg over the full range of pitch stick deflections. Manipulator inertia and inherent damping were equal to 0.0031 Ns^2/deg and 0.035 Ns/deg , respectively. The roll axis of the sidestick was locked during the experiment.

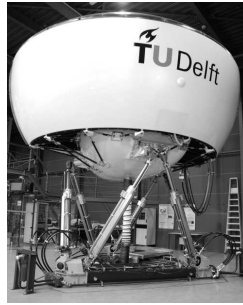


Figure 3.8. The SIMONA Research Simulator.

3.3.2 Controlled Element Dynamics

As already stated in Section 3.2, the feedforward part of precognitive and pursuit control behavior is hypothesized to be proportional to the inverse of the controlled element dynamics, $H_{pt}(s)H_c(s) \approx 1$ [Wasicko et al., 1966; McRuer et al., 1968; Hess, 1981]. For this reason, two different controlled elements were considered in this experiment: single (K_c/s) and double (K_c/s^2) integrator dynamics (Eq. (3.1)). The controlled element gain K_c was tuned to yield similarly optimal control authority with respect to the disturbance signal (see Fig. 3.3) for both controlled elements within the range of sidestick inputs (± 13 deg). For the single integrator dynamics K_c was set to 1.5, while for the double integrator K_c was taken equal to 8.

3.3.3 Forcing Functions

The target and disturbance forcing function signals that were applied in the experiment are depicted in Fig. 3.3. The ramp target signals, both consisting of one positive and one negative commanded pitch excursion, are the same as those considered in the theoretical investigation into multimodal pilot identification using such forcing function signals described in Appendix B. This previous work indicated improved identification results for target signals with steeper ramps. In addition, as both pursuit and precognitive control are modeled with a response ($H_{pt}(s)$) to which the target signal f_t is the input, control inputs were also expected to change as a function of ramp signal steepness, as illustrated by Fig. 3.7. For these reasons, two levels of ramp steepness were considered in this experiment: 1 and 10 deg/s. Note that these two values of ramp steepness represent the extreme values of those considered in Appendix B, the former being relatively benign, the latter practically approximating a step input. These two ramp target forcing function signals are referred to in the following as R1 and R10, respectively, and are shown in Fig. 3.3.

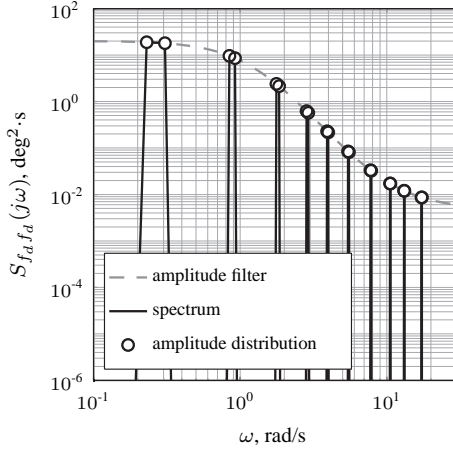


Figure 3.9. Quasi-random disturbance forcing function spectrum and amplitude distribution.

Table 3.1. Multisine disturbance forcing function data.

n_d	ω_d	A_d	ϕ_d
—	rad/s	deg	rad
3	0.230	0.959	1.269
4	0.307	0.935	2.677
11	0.843	0.686	4.523
12	0.920	0.648	1.122
23	1.764	0.342	4.159
24	1.841	0.323	1.700
37	2.838	0.174	1.408
38	2.915	0.167	6.271
51	3.912	0.106	5.993
52	3.988	0.103	0.606
71	5.446	0.0643	0.366
72	5.522	0.0630	4.849
101	7.747	0.0402	0.906
102	7.823	0.0398	4.481
137	10.508	0.0291	1.474
138	10.585	0.0289	5.883
171	13.116	0.0243	3.882
172	13.192	0.0242	5.161
225	17.257	0.0206	0.813
226	17.334	0.0205	4.344

The time trace of the multisine disturbance signal f_d , referred to as MS in the remainder of this chapter, is also depicted in Fig. 3.3. This signal was generated as a sum of $N_d = 20$ sinusoids:

$$f_d(t) = \sum_{k=1}^{N_d} A_d(k) \sin[\omega_d(k)t + \phi_d(k)] = \sum_{k=1}^{N_d} A_d(k) \sin[n_d(k)\omega_m t + \phi_d(k)] \quad (3.6)$$

The sinusoid frequencies ω_d were chosen to cover the complete frequency range of interest for evaluation of pilot dynamics (0.1-20 rad/s). To allow for measurement of frequency-domain pilot describing functions for the compensatory pilot dynamics $H_{p_e}(s)$ and evaluation of coherence of pilot control with respect to the disturbance signal [Damveld et al., 2009], pairs of neighboring frequencies were selected that all fit an integer number of times (n_d) into the experimental measurement time T_m . All sinusoid frequencies were therefore integer multiples of the experimental measurement base frequency $\omega_m = 2\pi/T_m$. The experimental measurement time for this experiment was 81.92 seconds, yielding a base frequency of $\omega_m = 0.0767$ rad/s.

Sinusoid amplitudes A_d were defined according to the same low-pass filter amplitude distribution used in previous experiments [Zaal et al., 2009b; Damveld et al., 2009]. Amplitudes were scaled to yield a disturbance signal with a time-domain variance of 1.5 deg^2 . The spectrum of f_d , showing this low-pass distribution, is depicted in Fig. 3.9. The filter frequency response is depicted in gray, while the full spectrum of f_d is depicted in black. Circular markers indicate the magnitudes of $S_{f_d f_d}(j\omega)$ equivalent to the selected sinusoid

amplitudes A_d . The sinusoid phases ϕ_d were selected from a large number of randomly generated sets of phases to yield a disturbance signal with average cresting – average maximum absolute forcing function excursion, rate and acceleration – and an approximately Gaussian distribution [Damveld, 2009; Damveld et al., 2010]. The numerical values for all disturbance forcing function parameters are listed in Table 3.1.

3.3.4 Independent Variables

Due to their hypothesized effect on manual control behavior for the control task depicted in Fig. 3.1, three different independent variables were varied in the experiment: the controlled element dynamics, the steepness of the ramps in the target forcing function signal, and the presence of the quasi-random disturbance signal. For both single and double integrator controlled elements, the tracking task was performed in a baseline compensatory configuration where only f_d was present ($f_t = 0$). A further four conditions for each controlled element resulted from the factorial variation of ramp signal steepness (R1 and R10) and the presence of the multisine disturbance signal (MS). This yielded a total number of ten experimental conditions, which are listed in Table 3.2.

Table 3.2. Experimental conditions.

Symbol	$H_c(s)$	f_t	f_d
S1		–	MS
S2	$\frac{K_c}{s}$	R1	–
S3		R1	MS
S4		R10	–
S5		R10	MS
D1		–	MS
D2	$\frac{K_c}{s^2}$	R1	–
D3		R1	MS
D4		R10	–
D5		R10	MS

In the following, these different experimental conditions – that is, combinations of settings for $H_c(s)$, f_t , and f_d – will be referred to using the symbols listed in Table 3.2. For instance, the pure compensatory conditions for single and double integrator controlled elements are indicated by S1 and D1, respectively.

3.3.5 Participants, Experimental Procedures, and Instructions

Six subjects were asked to perform the tracking task for the ten experimental conditions listed in Table 3.2. All participants were students or staff of the Faculty of Aerospace Engineering and all had extensive experience with manual tracking tasks from previous human-in-the-loop experiments. All participants were male, and their ages ranged from 25 to 47 years old.

As indicated in Table 3.3, all subjects performed the experiment in two separate sessions, which were both completed in the same week. Each session consisted of all variations in target and disturbance forcing function settings (see Table 3.2) for one of the controlled

elements. For both controlled elements, the different forcing function conditions were randomized over the different subjects according to a balanced Latin square design. In addition, half of the participants performed the single integrator control tasks (gray shaded cells in Table 3.3) in the first session, while the other half first performed the double integrator control tasks.

Table 3.3. Experiment Latin square design.

subject	session I					session II				
1	S5	S1	S2	S3	S4	D5	D3	D4	D2	D1
2	D1	D4	D5	D3	D2	S3	S4	S5	S1	S2
3	S1	S2	S3	S4	S5	D4	D2	D3	D1	D5
4	D2	D5	D1	D4	D3	S2	S3	S4	S5	S1
5	S4	S5	S1	S2	S3	D3	D1	D2	D5	D4
6	D1	D4	D3	D2	D5	S1	S2	S4	S3	S5

The individual tracking runs of the experiment lasted 90 seconds, of which the last 81.92 seconds were used as the measurement data. For each experimental condition, participants' tracking performance was monitored by the experimenter. When participants had reached a constant operating point, five repetitions at this constant level of tracking performance were collected as the measurement data. Typically, two short breaks (max. 30 minutes) were taken during each session, always after finishing the measurements for one condition and before starting the next. On average, each session took 2.5-3 hours to complete.

Participants were instructed to continuously attempt to minimize the pitch tracking error e presented on the visual displays, by minimizing the deviation of the target line with respect to the aircraft symbol (see Fig. 3.2). After each run subjects were informed of their tracking score, defined by the root mean square (RMS) of the error signal e , in order to provide them with feedback of their level of performance, during both the training and measurement phases of the experiment.

3.3.6 Dependent Measures

During the experiment, the time traces of the error signal e , the control signal u , and the pitch attitude θ were recorded for each measurement run. From these measured time traces, several dependent measures are calculated to give insight into the effects of the independent variables that were manipulated during the experiment on the measured manual control behavior. First, tracking performance and control activity – expressed as the time-domain variances (σ^2) of the error and control signals, respectively – are evaluated briefly for comparison with compensatory measurements from previous work [McRuer et al., 1965].

The main dependent measures considered in this chapter, however, are those related to the models of manual control behavior introduced in Section 3.2.3. Using time-domain identification methods [Zaal et al., 2009a], the compensatory ($H_{p_e}(s)$) and feedforward ($H_{p_i}(s)$) models proposed in this section have been fit to the measured time traces separately, in order to show to what extent these models capture the measured control inputs for the different conditions. In addition, the fit of the proposed combined model of pilot ramp-tracking behavior as depicted in Fig. 3.6, which includes both these compensatory

and feedforward responses, is also evaluated in this chapter. It should be noted that the feedforward lag time constant T_{I_t} was kept constant in the fitting of the combined model, due its limited contribution to the model response, which made estimation of this parameter difficult. For the fits of the combined model, this parameter was therefore kept fixed at the approximately constant values obtained for both controlled elements over the different ramp forcing function settings.

In addition to the estimated model parameters, the extent to which the identified models succeed in describing the measured control inputs u is quantified. For this, two measures of the quality of the time-domain model fit are considered. The first is the model variance accounted for (VAF), which can be calculated from the measured and modeled control signals – u and \hat{u} , respectively – according to:

$$\text{VAF} = \left[1 - \frac{\sum_{k=1}^N (u(k) - \hat{u}(k))^2}{\sum_{k=1}^N u^2(k)} \right] \times 100\% \quad (3.7)$$

The VAF defines the percentage of the measured control signal u that is explained (or captured) by the model. As can be verified from Eq. (3.7), the VAF is calculated as the sum of the squared modeling error $(u(k) - \hat{u}(k))^2$, normalized by the sum-of-squares of the measured control signal u . As the sum-of-squares of u is expected to vary widely over the different ramp-tracking tasks considered in the experiment, as is intuitive from observation of the hypothetical ramp-tracking responses presented in Fig. 3.7, also the mean square error (MSE) between u and \hat{u} is considered. The MSE is defined as:

$$\text{MSE} = \frac{1}{N} \sum_{k=1}^N (u(k) - \hat{u}(k))^2 \quad (3.8)$$

3.3.7 Hypotheses

It is anticipated that due to the repetitive tracking of deterministic target input signals, some evidence of feedforward operations on the target signal – either resulting from pursuit or precognitive control behavior – can be observed from the behavioral measurements. Especially for the conditions without the quasi-random disturbance signal (S2, S4, D2, and D4), the combination of the pursuit display and the predictable target signals is expected to allow for a control strategy in which $H_{p_t}(s)$ is dominant.

Furthermore, it is expected that the presence of the quasi-random disturbance signal might put more emphasis on the compensatory control loop the human operator needs to close, thereby possibly (partly) suppressing open-loop feedforward control in favor of a more stable closed-loop. This would suggest tracking performance and compensatory pilot model parameters for conditions S3/S5 and D3/D5 are anticipated to be similar to those found for the pure compensatory conditions S1 and D1, respectively. Due to its less prominent effect on task performance, this effect is expected to be largest for the lowest steepness ramp signal (R1). Furthermore, the marginally stable double integrator controlled element also requires more emphasis on compensatory stabilization than the single integrator control tasks. For this reason, reduced prominence of feedforward control inputs is expected to be found for the ramp-tracking tasks performed with double integrator dynamics.

The suspected decrease in the adoption of feedforward control for the experimental conditions where the disturbance signal is present and for the K_c/s^2 controlled element is expected to be apparent from changes in the fitted parameters of the proposed combined compensatory and feedforward model. Reduced values of K_{pt} and increased values of T_{I_t} indicate reduced effectiveness of the feedforward response and are hence expected to be found for these experimental conditions.

3.4 Results

3.4.1 Measured Time Traces

Fig. 3.10 presents sample time traces of the tracking error, control input, and pitch attitude recorded during the experiment for subject 1 in control of single integrator dynamics. Each row of graphs depicts these three signals for each of the five variations in forcing function settings (see Table 3.2). Each graph depicts the forcing function signal (scaled down for the graphs of e and u for plotting purposes) in gray. The time-domain average of the five collected measurements of the depicted variable is depicted in black. Note that for each set of time traces, the graphs for the different experimental conditions have the same scaling of the vertical axis, to allow for straightforward qualitative comparison. Furthermore, note that only 40 seconds of the total run length (90 seconds) are depicted here, which include only the first (positive) ramp-like excursion and the corresponding return to zero.

First of all, Fig. 3.10 shows the effect of the disturbance signal on the recorded signals. Where for the conditions where f_d is not present (S2 and S4) the depicted signals only show activity around the interval where a ramp in f_t occurs, the disturbance signal continuously induces tracking errors and hence control inputs. Furthermore, Fig. 3.10 also shows an effect of ramp signal steepness. Figures 3.10(j) and (m) show significant build-up of the tracking error directly after the occurrence of a R10 ramp due to the delay in the operator's response, as illustrated by Fig. 3.5. As can be verified from Figures 3.10(d) and (g), the effect of the R1 ramps on the tracking error is of markedly lower magnitude.

The corresponding graphs of the control signal u show a similar strong effect of the varying ramp signal steepness, which is especially visible for the conditions where the disturbance signal is present (S3 and S5). For condition S5, the control inputs that are performed in response to the target signal clearly stand out from those needed to attenuate the disturbance, while they appear to be lost in the compensatory control action for conditions S3. Finally, note from the time traces of the pitch attitude θ that overshoots in the following of the ramp signals are typically larger for the steeper ramps (S4 and S5) than for R1 (S2 and S3). Highly similar measurements to those depicted in Fig. 3.10 were also obtained for the double integrator dynamics and for the other participants in the experiment.

3.4.2 Tracking Performance and Control Activity

To evaluate the average effect of the independent variables of the experiment on the tracking error and control input signals, Fig. 3.11 depicts the means of the tracking error and control input variance (σ_e^2 and σ_u^2 , respectively) taken over the six experiment participants. The

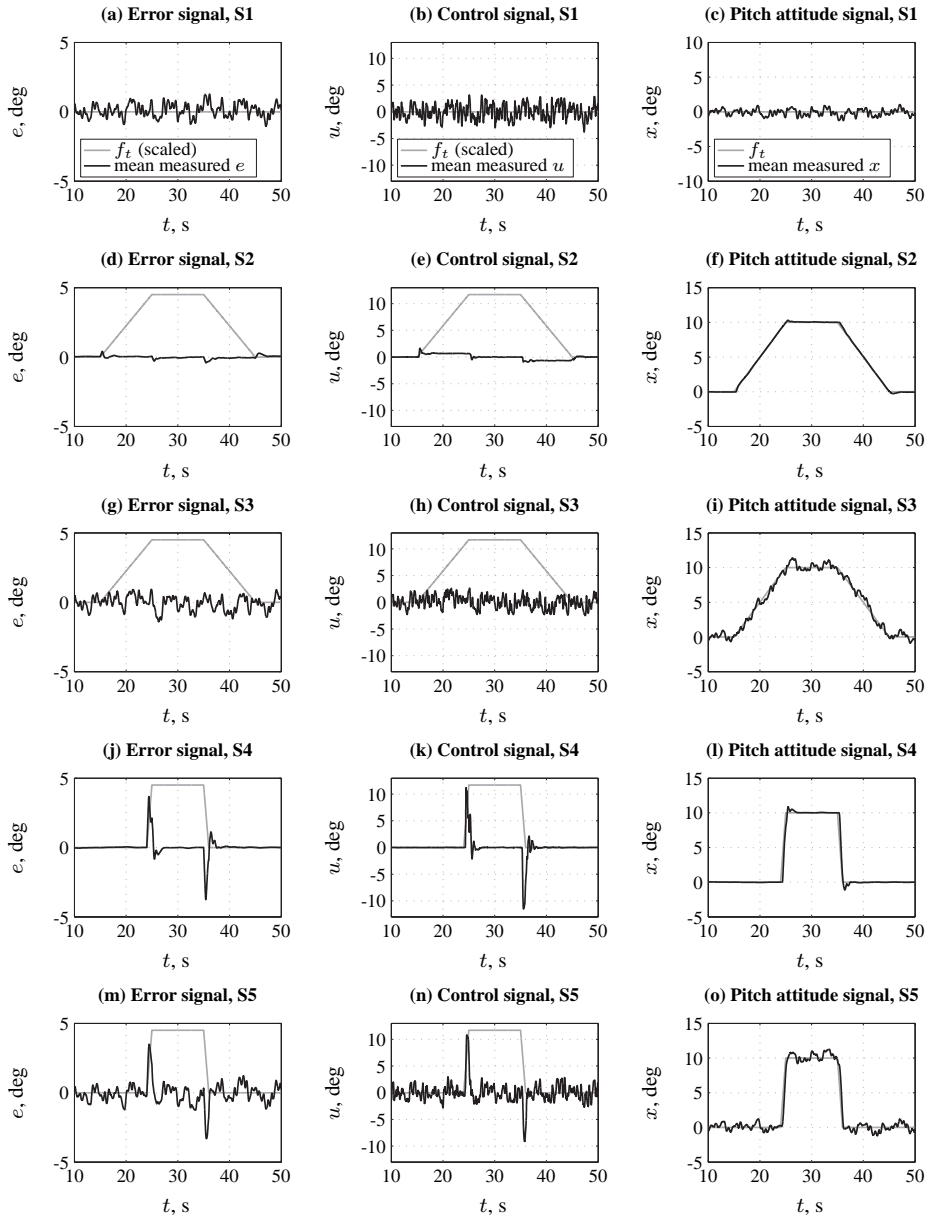


Figure 3.10. Measured time traces of e , u , and θ for control of single integrator dynamics (conditions S1-S5, subject 1).

variance bars indicate the corresponding 95% confidence intervals. The depicted data has been corrected for between-subject variance.

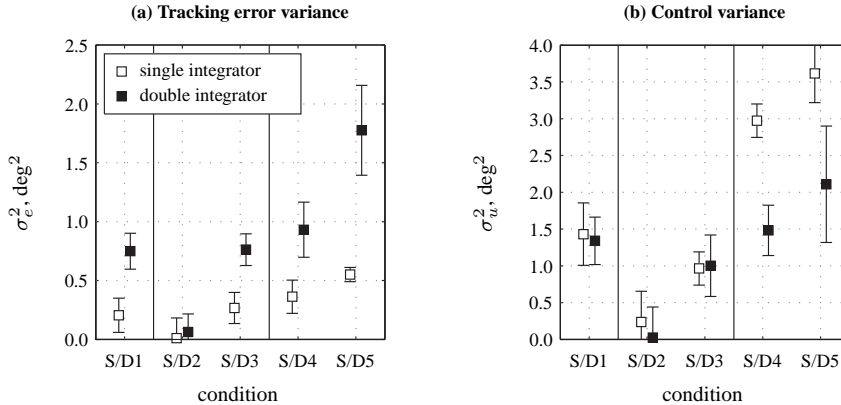


Figure 3.11. Average tracking performance and control activity.

Fig. 3.11(a) shows that tracking performance was found to be significantly worse (higher σ_e^2) for the double integrator controlled element, $F(1, 5) = 55.98$, $p < 0.05$. This is an expected result based on previous work [McRuer et al., 1965; Shirley and Young, 1968; Junker and Replegle, 1975], due to the fact that double integrator dynamics are significantly more difficult to control than single integrator dynamics. Fig. 3.11(a) also shows that σ_e^2 is significantly affected by the applied variation in forcing function signals ($F(4, 20) = 43.79$, $p < 0.05$). For instance, the tracking errors for conditions S2 and D2, where only the R1 ramp signal was present, are very small compared to those for the other conditions. This shows that participants were able to track this low-steepness ramp signal very accurately, as can also be verified from Fig. 3.10. For the steeper ramp signal (conditions S4 and D4) tracking errors were found to be markedly larger. This can be attributed to the more rapid build-up of tracking error for these steeper ramps, which already yields appreciable tracking errors within in the human operator's reaction time (compare the ramp and step responses during phase I shown in Fig. 3.10).

As is clear from Fig. 3.11(a), the observed effects of the applied differences in the forcing function signals are found to be largely independent of the effect of the considered variation in $H_c(s)$. Still, a statistically significant interaction between the effects of the different controlled elements and forcing function signals on σ_e^2 was found, $F(4, 20) = 37.97$, $p < 0.05$. This interaction effect is attributable to the much larger increase in tracking error variance due to the addition of the multisine disturbance signal observed from condition D4 to D5 than found between S4 and S5. For the low ramp steepness conditions, on the other hand, the addition of the disturbance signal during ramp tracking is seen to increase tracking error variance by approximately the error variance found for the S1 and D1 conditions. Note from Fig. 3.11(a) that this implies almost equal tracking performance for the S/D1 and S/D3 conditions for both controlled elements. Post-hoc tests (pairwise comparisons) confirmed the absence of significant differences between the measured tracking error variances for these sets of conditions.

Fig. 3.11(b) depicts the measured control signal variance for all conditions of the experiment. Note that control activity for the condition with only the disturbance signal (MS) is found to be almost equal for the single and double integrator controlled elements. This confirms the selection of appropriate values for the controlled element gain K_c as described in Section 3.3.2. Overall, a strong effect of the different forcing function settings on σ_u^2 is found, $F(4, 20) = 54.65$, $p < 0.05$. Fig. 3.11(b) shows very low control activity for both controlled elements for the conditions with only the R1 target, as also expected from Fig. 3.7. Surprisingly, control activity is found to be slightly lower for the control tasks with both the R1 target and the disturbance signal (S3 and D3) than for the corresponding conditions with only the disturbance signal (S1 and D1). For tracking of the steeper ramp signal, consistently higher control activity is found, which would be expected from the peaks during ramp tracking depicted in Fig. 3.10.

Differences in the measured control signal variances for both controlled elements are only observed for the conditions with the R10 ramp signals, yielding both a significant main effect of $H_c(s)$ ($F(1, 5) = 23.11$, $p < 0.05$) and a significant interaction with the applied forcing function settings ($F(4, 20) = 19.54$, $p < 0.05$). As is clear from Fig. 3.11(b), control activity is found to be markedly higher for the single integrator data (conditions S4 and S5) than for the D4 and D5 conditions.

3.4.3 Pilot Modeling Results for Pure Compensatory Tasks

For the conditions where no ramp target signal was present, but only the effects of the quasi-random disturbance signal were to be attenuated (that is, S1 and D1), a compensatory control task equivalent to those considered by McRuer et al. [1965] is obtained. Therefore, pilot control behavior for these conditions can be described with the compensatory pilot model described in Section 3.2.3.1. Fig. 3.12 depicts the frequency responses of the fits of Eq. (3.2) to data from conditions S1 and D2 for subject 1. In addition to the model fit shown in gray, Fig. 3.12 also depicts the describing function estimate, calculated at the frequencies of f_d .

Fig. 3.12 shows that the estimated describing functions, which are independent of the selected pilot model, correspond well with the frequency responses of the fitted compensatory pilot models. In addition, note that the VAFs of the pilot model fits for conditions S1 and D1 are around 75 and 85%, respectively, indicating that the remnant n is confirmed to contribute a typical 20-25% to the variance of the control signal u [Zaal et al., 2009a].

Furthermore, Fig. 3.12 shows the marked difference between the compensatory control of single and double integrator dynamics, as expected based on the work of McRuer et al. [1965]. As can be verified from Fig. 3.12(a) and (c) human dynamics for control of a K_c/s system are approximately those of a pure gain, with the peak attributed to the combined neuromuscular and manipulator dynamics just above 10 rad/s. In comparison, Fig. 3.12(b) and (d) (condition D1) show control behavior where significant phase lead is generated by the human operator, to compensate for the controlled double integrator dynamics [McRuer et al., 1965].

Model fits highly similar to those shown in Fig. 3.12 were obtained for the other participants in the experiment. Table 3.4 presents the average estimated compensatory model parameters for conditions S1 and D1, in addition to the average VAF of the model fit. The

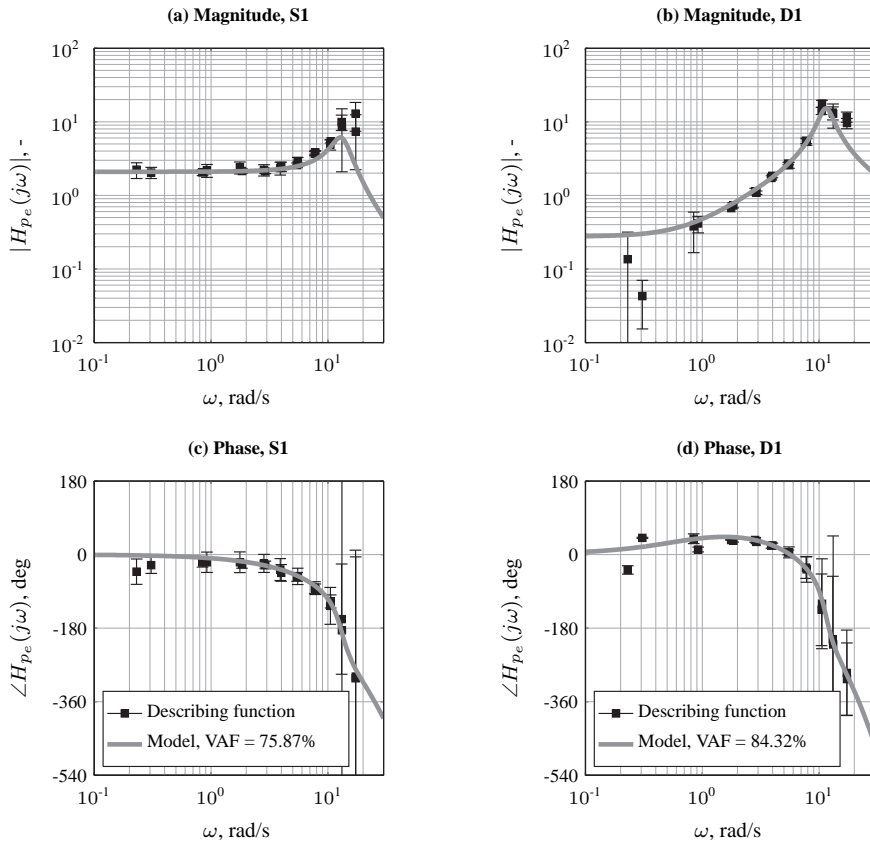


Figure 3.12. Example pilot describing functions and compensatory model fits for compensatory conditions (S1 and D1, subject 1).

Table 3.4. Average compensatory parameters and model VAF for conditions S1 and D1.

Condition	K_{pe}	T_{Le}, s	τ_e, s	$\omega_{nm}, \text{rad/s}$	ζ_{nm}	VAF, %
S1	1.95	—	0.16	13.93	0.16	84.36
D1	0.25	1.33	0.23	11.33	0.18	86.03

final column of Table 3.4 indicates an average model VAF of around 85% for both the S1 and D1 conditions. Furthermore, the estimated parameter values listed in Table 3.4 reflect the different control behavior shown in Fig. 3.12. On average participants were generating low-frequency lead for frequencies above 0.75 rad/s for condition D1, at the cost of a marked increase in the compensatory time delay τ_e . These results are highly consistent with those reported in [McRuer et al., 1965] and later publications on compensatory manual control [Stapleford et al., 1969; Hosman, 1996; Van der Vaart, 1992; Beerens et al., 2009; Zollner et al., 2010].

3.4.4 Pilot Modeling Results for Ramp-Tracking Tasks

To investigate the need for extending models of compensatory tracking behavior for the ramp-tracking tasks considered in this chapter, the compensatory model given by Eq. (3.2) and the feedforward model given by Eq. (3.4) were fit to measured time traces of the control signal u individually, in addition to the combined model that includes both $H_{p_t}(s)$ and $H_{p_e}(s)$, see Fig. 3.6. This section first evaluates the fit provided by these different models in the time domain, both qualitatively by evaluating the model responses with respect to measured control signal time traces and quantitatively using the VAF and MSE of the obtained model fits. Then the identified model parameters obtained from the different model forms are compared and differences in the estimated parameters of the combined model over the different experimental conditions are evaluated.

3.4.4.1 Time-Domain Pilot Model Fits

To investigate to what extent the models for $H_{p_t}(s)$ and $H_{p_e}(s)$ proposed in Section 3.2.3.2 can individually describe measured control inputs for the experimental conditions where a ramp target signal was present, these models were both fit to the average time traces of u . These average measurements were obtained by averaging the five repeated time-domain measurements of this signal for each subject. Note that the full time traces of u were used to fit one set of parameters, yielding parameter estimates based on control inputs for all four ramp-like changes in reference attitude occurring in the target signal (see Fig. 3.3). Fig. 3.13 depicts typical results of fitting the model of Eq. (3.4) to measurements of u for all ramp-tracking conditions where the disturbance signal was not present, that is, S2, S4, D2, and D4 (see Table 3.2). Fig. 3.14 shows the fit of the compensatory model of Eq. (3.2) to the same experimental data. Note that in both figures the VAF of the presented pilot model fit is indicated in the legend of each graph. The results shown in Figures 3.13 and 3.14 were obtained for subject 1, but highly similar results were obtained for all other participants.

Note from Fig. 3.13 that the model of Eq. (3.4) is able to capture the initial control input given after a ramp in the target signal for all four pure ramp-tracking conditions. As for instance visible in Fig. 3.13(b) and (d), the fit of the proposed model for $H_{p_t}(s)$ also captures the delay in the control response, as defined in Fig. 3.5(b). Fig. 3.13, however, also illustrates that the model for $H_{p_t}(s)$ is not capable of explaining all measured control inputs. For all conditions, the measured time traces of u show some overshoots and additional oscillatory inputs compared to the modeled control signals. In addition, as illustrated best by Fig. 3.13(c), even in the absence of f_d the double integrator controlled element dynam-

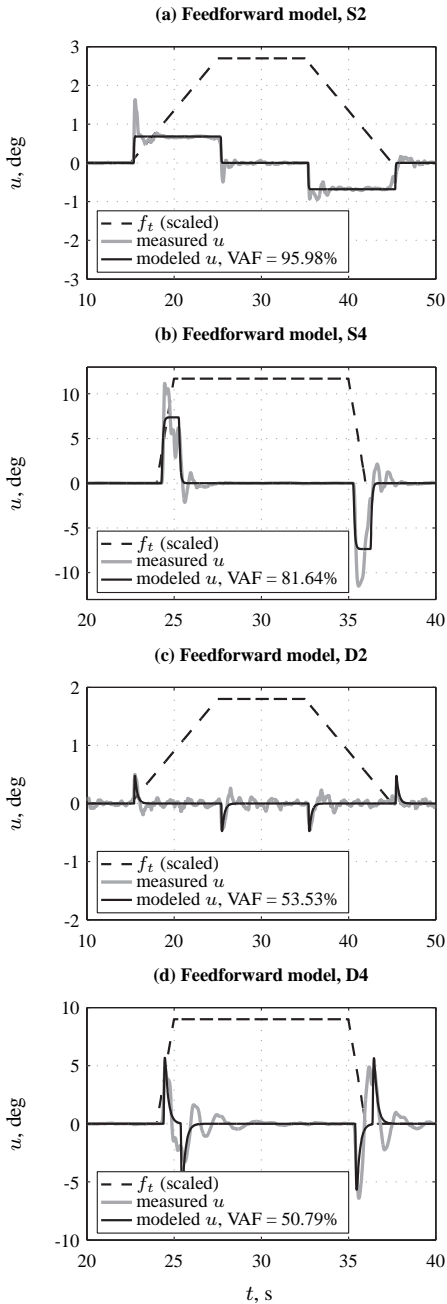


Figure 3.13. Feedforward control signal fits for pure ramp-tracking conditions (S2, S4, D2, and D4) for subject 1.

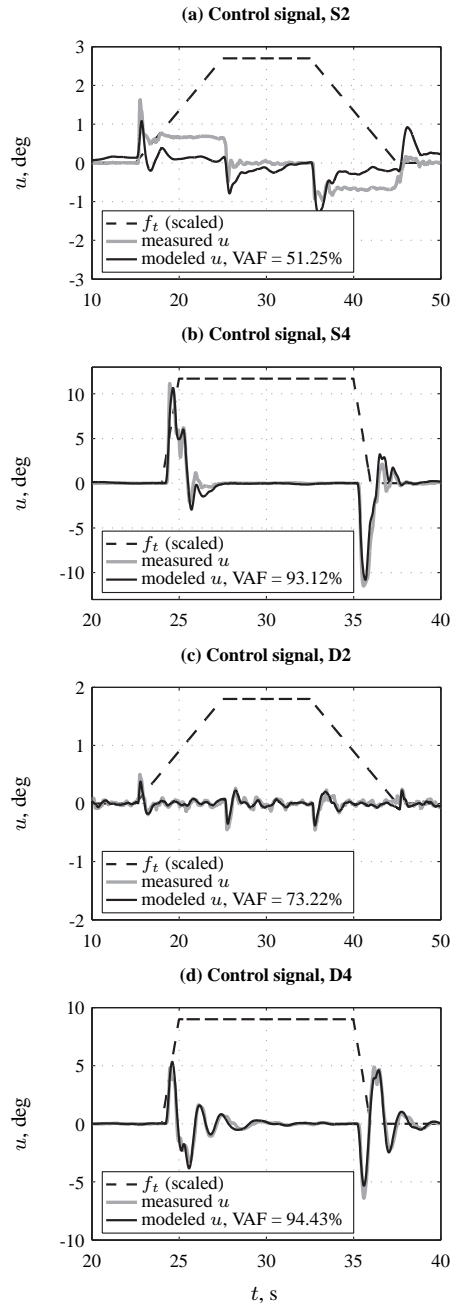


Figure 3.14. Compensatory control signal fits for pure ramp-tracking conditions (S2, S4, D2, and D4) for subject 1.

ics required significant (compensatory) control inputs for stabilization, also during periods where the ramp target signal was constant.

Fig. 3.14 depicts the resulting modeled control signals for the purely compensatory model of pilot tracking behavior given by Eq. (3.2). Fig. 3.14(a) shows that for condition S2, the control inputs given to follow the R1 target signal can not be explained by the compensatory control model. The reason for this is the fact that, except for small errors due to the time between the occurrence of a ramp and the first control input, ramp tracking errors are negligible, as can be verified from Fig. 3.10(e). Note, however, by comparing Figures 3.13(a) and 3.14(a), that the compensatory model does capture the overshoots and slight oscillations present in the measured time traces of u that the model for $H_{p_t}(s)$ cannot describe.

Surprisingly, the model time traces depicted in Fig. 3.14 for the remaining three conditions reveal that the complete measured control signals – that is, both the initial and the final error-reducing compensatory control inputs (so, phases II and III in Fig. 3.5(b)) – are captured at reasonably high accuracy by the compensatory model of Eq. (3.2). This especially holds for the conditions with the steeper R10 ramps. The similarity of the error and control signals for condition S4 depicted in Fig. 3.10 explains this, as enough tracking errors build up to fit the model for $H_{p_e}(s)$ on. Note, however, that despite the accurate fits of the compensatory model it can not be concluded that pure compensatory control behavior was utilized for these conditions. For instance, with parameter values that differ from those expected for pure compensatory tracking (see Table 3.4), the model of Eq. (3.2) might be able to at least partially capture a non-compensatory behavior. Furthermore, judging the results shown in Fig. 3.13, the total measured control input could also be a weighted sum of both the $H_{p_e}(s)$ and $H_{p_t}(s)$ responses. This will be addressed in more detail in the discussion of the estimated model parameters in Section 3.4.4.2. Fig. 3.14, however, does show that the model of Eq. (3.2) is highly capable of capturing the oscillatory control inputs the model for $H_{p_t}(s)$ fails to describe, thereby suggesting that a compensatory tracking behavior component is present for all considered experimental conditions.

Fig. 3.15 shows the time-domain fits of the combined compensatory and feedforward model depicted in Fig. 3.6 for all experimental conditions except the pure compensatory conditions S1 and D1. Again, only data and model fits obtained for subject 1 are presented for brevity.

Note from comparison of the model fits shown in Fig. 3.15 for the conditions without the disturbance signal (conditions S2, S4, D2, and D4) with those presented in Figures 3.13(a)-(b) and 3.14(a)-(b) that the combined model captures more of the measured control signal than the individually fitted compensatory and feedforward responses. This is especially visible for the S2 condition, where the combined model is shown able of modeling both the block-shaped input captured by the feedforward model in Fig. 3.13(a) and the more high-frequency oscillations accounted for by the model for $H_{p_e}(s)$, see Fig. 3.14(a). This is also reflected in higher VAF values for all of the combined model fits compared to those shown in Figures 3.13 and 3.14 for these four conditions.

Fig. 3.15 further shows that also for all ramp-tracking tasks performed with the additional disturbance signal present (S3, S5, D3, and D5) the combined feedforward and compensatory model provides a good fit to the measured control signal time traces, with VAFs higher than 80% for all four conditions. As is clear from Figures 3.15(c) and (d), for both

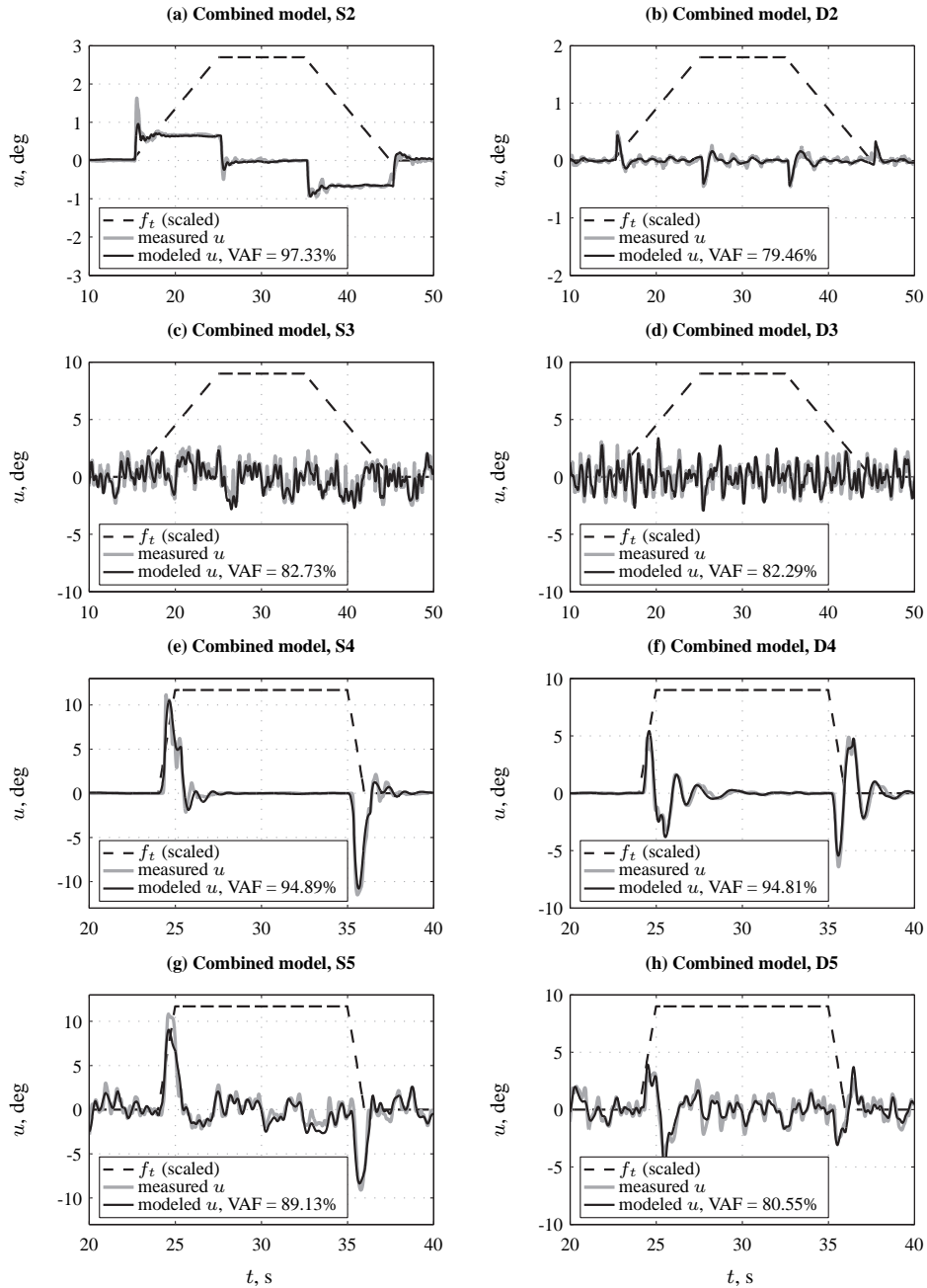


Figure 3.15. Combined compensatory and feedforward model control signal fits for conditions S2-S5 and D2-D5 (subject 1).

considered controlled elements the control inputs given for compensatory attenuation of the disturbance forcing function signal dominate those required for following the low-steepness R1 ramp signal. For the R10 ramp signal, for which more pronounced control inputs are required, far more evidence for a response to the ramp target signal is visible in the measured control signals, as can be verified from Figures 3.15(g) and (h). This suggests that for control tasks where the steepness (or power, see Appendix B) of the applied ramp forcing function signals is increasingly more dominant over that of external disturbances, the proposed combined feedforward and compensatory pilot model will likely show increasingly more benefit for modeling measured tracking behavior.

This observation is tested through further evaluation of the average pilot model VAF and MSE corresponding to the fits of the three considered pilot models, which are presented in Fig. 3.16. For each experimental condition, Fig. 3.16 shows the average VAF and MSE over the data from the six participants for the pure compensatory model (Eq. (3.2)), the pure feedforward model (Eq. (3.4)), and the combined model using white, gray, and black-filled markers, respectively. The variance bars indicate the 95% confidence intervals of the presented means. For the calculation of these confidence intervals the presented data were compensated for between-subject variability.

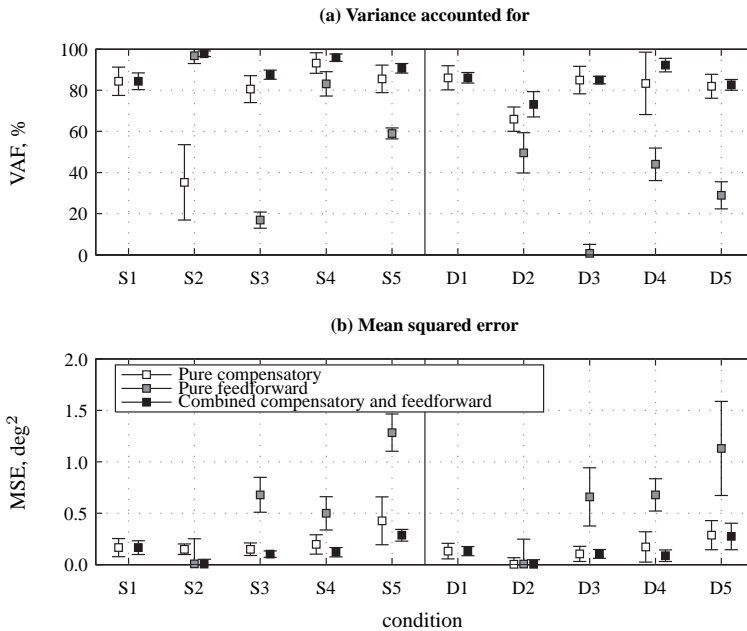


Figure 3.16. Average VAF and MSE of the fits of the pure compensatory, pure feedforward, and combined pilot models for all experimental conditions.

Fig. 3.16 shows that for the pure disturbance-rejection conditions (S1 and D1) the pure compensatory and combined models result in the same pilot model fit, as for this condition f_t , and hence the output of the feedforward channel $H_{p_t}(s)$, is equal to zero. For the ramp-tracking conditions, the pure feedforward model is found to result in the lowest VAFs

and highest MSEs, indicating the worst quality of fit, for all conditions except S2. The pure compensatory model fits are found to provide comparatively high VAFs and low MSEs, only showing compensatory model VAFs lower than those measured for pure compensatory tracking (conditions S1 and D1) for conditions S2 and D2. However, Fig. 3.16 shows that the combined model on average yields the most accurate fit of the time-domain measurements of u for all ramp-tracking conditions. It should be noted, however, that especially for the conditions with the K_c/s^2 controlled element and the disturbance signal present (conditions D3 and D5) the improvement in fit with respect to the pure compensatory model is only comparatively modest. The quality-of-fit results presented in Fig. 3.16 thereby suggest a diminishing effect of feedforward control contributions with increasing controlled element order and increasing power of external disturbances.

3.4.4.2 Pilot Model Parameter Estimates

Figures 3.17 and 3.18 show the estimated parameters for the feedforward model of Eq. (3.4) and the compensatory model given by Eq. (3.2), respectively, for all three fitted pilot models. As also done in Fig. 3.16, the estimated parameters corresponding to fits of the pure compensatory model, the pure feedforward model, and the combined model are presented using white, gray, and black-filled markers, respectively. Note that as the feedforward model parameters were not estimated for the pure compensatory model and those of the compensatory model were not estimated for the pure feedforward model, both Figures 3.17 and 3.18 only show data for two of the three considered model fits.

Fig. 3.17(a) shows the estimated values for the feedforward gain K_{p_t} obtained from fitting the pure feedforward model (gray markers) and the combined model (black markers). The estimates of K_{p_t} obtained for the pure feedforward model presented in Fig. 3.17(a) show values around or slightly above 1 for the single and double integrator controlled elements, respectively. Recall that for optimal feedforward control dynamics K_{p_t} should be around unity, as then $H_{p_t}(s)H_c(s) \approx 1$. On the other hand, except for condition S2, the feedforward gain values corresponding to the fits of the combined model are found to be around half those found for the pure feedforward model, suggesting that the pilot control response can not fully be attributed to the feedforward response in the pure feedforward model, but partly results from compensatory control.

For both fitted models, the estimates of K_{p_t} for the conditions where the R1 ramp signal was to be followed in the presence of the disturbance signal (S3 and D3) show the largest spread or values that are not consistent with those obtained for the other experimental conditions. This is what would be expected based on the time-domain model fits shown in Fig. 3.15 for these conditions, as the measured control signal time traces suggest a negligible contribution of the response that can be described with the feedforward model. The estimated feedforward gains for the combined feedforward and compensatory model show lower values for the double integrator controlled element than observed for the single integrator conditions. Furthermore, when considering the data for all experimental conditions, K_{p_t} is found to decrease for the steeper ramp signals and with the addition of the disturbance signal. Both these variations in K_{p_t} over the different controlled elements and forcing function settings are found to be statistically significant: $F(1, 5) = 10.09$, $p < 0.05$ and $F(3, 15) = 27.07$, $p < 0.05$, respectively. Furthermore, note that both the significant ef-

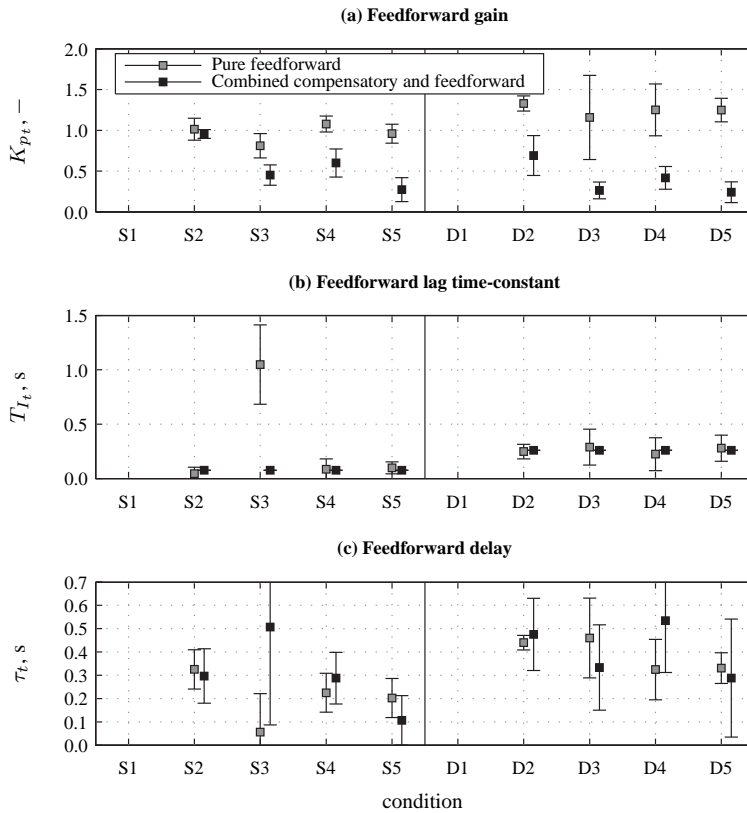


Figure 3.17. Average feedforward pilot model parameters for all experimental conditions.

fect of the controlled element dynamics and the reduction in K_{pt} for the conditions with f_d present are consistent with the hypothesis that decreased feedforward response power is adopted for control tasks where more emphasis on compensatory control is required.

As explained in Section 3.3.6, the feedforward lag time-constant T_{L_t} was only estimated for the pure feedforward model. As is clear from Fig. 3.17(b), this parameter was kept fixed for the combined model at values that were found to be representative for ramp-tracking with single and double integrator controlled element dynamics from the pure feedforward model fits. The values of T_{L_t} that were estimated for the pure feedforward model indeed show approximately constant values for both controlled elements over all different forcing function settings. Except for condition S3, for which it is anticipated that too little information on the pilot feedforward response is present in the recorded pilot control signal time traces (see Fig. 3.15(c)) for accurate estimation of the feedforward model parameters, T_{L_t} is found to on average be around 0.076 s for the single integrator controlled element. For the double integrator measurements, feedforward lag time-constants of around 0.26 s are measured. The larger feedforward lag time-constant values found for the double integrator data indicate that for this controlled element the ramp-tracking control inputs given

through the feedforward response showed larger deviations from the optimal feedforward ($H_{p_t}(s)H_c(s) \approx 1$). This is consistent with the increased emphasis on compensatory control behavior anticipated for this controlled element. As explained in Section 3.3.6, due to the invariance of T_{I_t} over the different experimental conditions, this parameter was kept fixed at the reported values for both controlled elements in the fitting of the combined feedforward and compensatory model.

Fig. 3.17(c) shows the estimated feedforward delay parameters τ_t for both models that include the pilot feedforward response. As also observed for the feedforward gain and lag time-constant, the estimated results for the S3 condition show significant spread and parameter values that are not consistent with those estimated for the other conditions. For both controlled elements, the estimated feedforward delay parameters obtained from fitting the pure feedforward model show lower values for τ_t for the conditions with the R10 ramps, suggesting a faster initial response for these steeper ramp signals. As can be verified from Fig. 3.17(c), this trend is not observable in the estimates of τ_t obtained from fitting the combined model. Due to the significant spread in the estimated values of τ_t , no significant effects of the applied variation in both controlled element dynamics and forcing function signals are observed on the feedforward delay parameters estimated with the combined pilot model. Based on the estimated values for the feedforward delay parameter presented in Fig. 3.17(c) it can therefore only be concluded that the delay in the feedforward response is in the range of 0.2-0.4 s.

Fig. 3.18 presents the estimated compensatory model parameters, including those of the neuromuscular actuation dynamics given by Eq. (3.3), for the pure compensatory and combined model fits. Estimated parameters for the pure compensatory and combined models are indicated with white and black markers, respectively.

Fig. 3.18(a) shows that the pure compensatory and combined models yield highly comparable estimates of the compensatory pilot gain K_{p_e} for conditions S1, S3, and S5. Similar consistency, but at a much lower value of K_{p_e} , is observed for all double integrator conditions. Note that for the double integrator conditions, the variance bars of the presented K_{p_e} data suggest that the compensatory pilot gain could become negative. This is, however, not the case. No negative values of K_{p_e} were measured and the depicted variance bars result from the correction for between-subject variance that was applied to the data from all experimental conditions for the calculation of the presented 95% confidence intervals.

The pure compensatory model fits for the S2 and S4 conditions, where f_d was not present, show values of K_{p_e} that are considerably higher and show markedly more spread than those found for the other single integrator conditions. As is especially visible from the time-domain fit of the compensatory model for condition S2 – as presented in Fig. 3.14 – these discrepancies in the estimated compensatory model parameters are the result of this model's inability to describe the measured data for these conditions. The fact that the values of K_{p_e} obtained from fitting the combined model, which as shown in Fig. 3.15 provides a much better representation of the measured control inputs, are distinctly different from those resulting from the fits of the pure compensatory model is further proof of this. Though still showing larger spread, on average the combined model fit for condition S4 is even found to yield estimated values of K_{p_e} that are consistent with those observed for S1, S3, and S5. The comparatively low K_{p_e} found from the fitted combined model for condition S2, however, suggests reduced emphasis on compensatory control for this condition compared

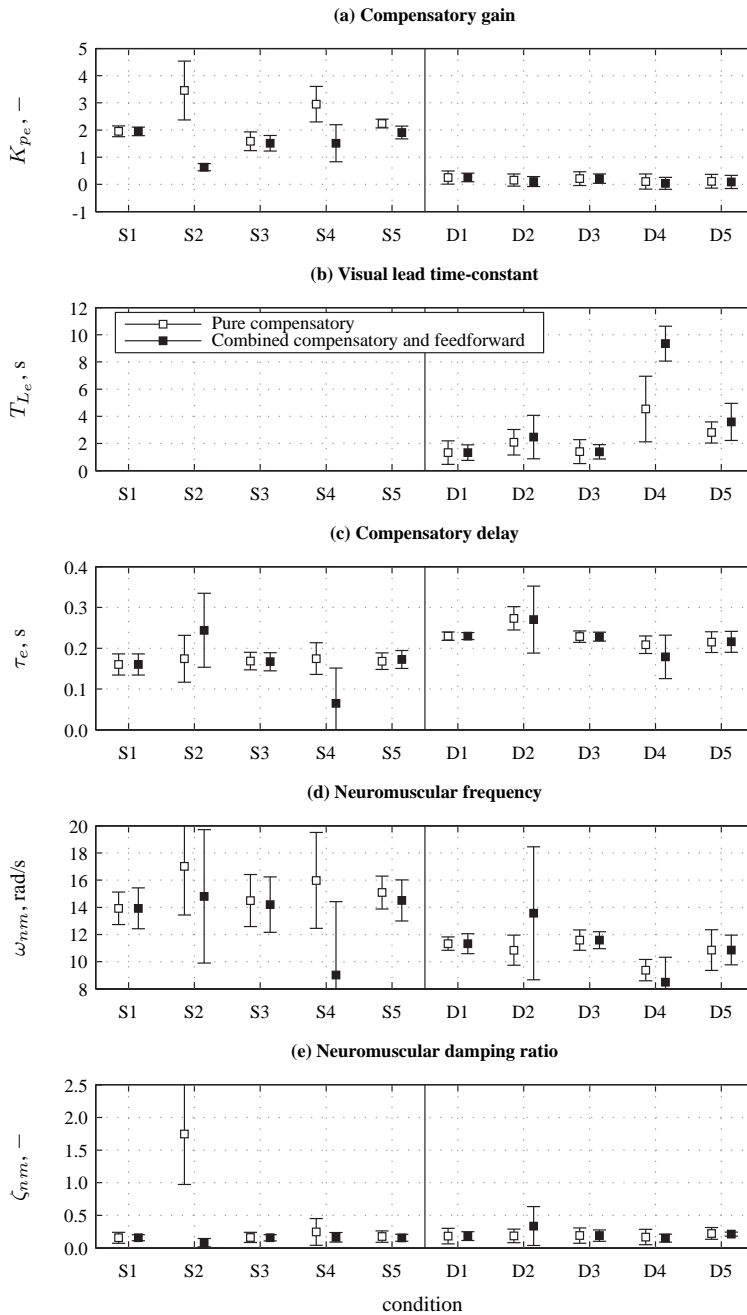


Figure 3.18. Average compensatory pilot model parameters for all experimental conditions.

to all other single integrator tasks. The observed difference in the estimated compensatory gains for both controlled elements was found to be statistically significant, $F(1, 5) = 82.12$, $p < 0.05$. Furthermore, note that the slight drop in K_{pe} for condition S3 compared to the pure compensatory condition S1 is consistent with the observed reduction in control activity (see Fig. 3.11) for this condition. Fig. 3.18(a) therefore suggests that this decreased control activity is the result of the selection of a reduced crossover frequency for the compensatory loop in the presence of the R1 ramp signal. Note that this decrease in compensatory gain is not found to occur for the steeper R10 ramp forcing functions.

As in compensatory tracking lead equalization is only required for controlled elements that are approximately K/s^2 in the crossover region [McRuer et al., 1965], the lead term in the compensatory pilot model of Eq. (3.2) was only included for the double integrator ramp-tracking tasks performed in the current experiment. Hence, Fig. 3.18(b) only shows estimated values of the visual lead time-constant for conditions D1-D5. Similar to the estimates of K_{pe} for conditions S2 and S4, the estimated values of T_{Le} are also found to show less consistent results for the conditions where the disturbance signal was not present (D2 and D4). The values of T_{Le} obtained for conditions D1 and D3 with both the pure compensatory and combined pilot models are very similar and highly consistent with values reported for previous experiments that considered tracking tasks with double integrator controlled elements, such as [McRuer et al., 1965; Hosman, 1996; Van der Vaart, 1992; Beerens et al., 2009] and Chapter 2. Finally, both fitted models consistently predict a considerable increase in T_{Le} , to 3-3.5 s, for condition D5 compared to the values measured for D1 and D3. This would suggest that for following the steep R10 ramp signals in the presence of the disturbance signal, the participants performed markedly more lead equalization in the compensatory loop.

Figures 3.18(c), (d), and (e) depict the estimated values of the compensatory time delay τ_e and the neuromuscular actuation model parameters (Eq. (3.3)). These parameters show largely the same variation over the different experimental conditions as observed for K_{pe} and T_{Le} . Estimates with deviating values and increased spread are obtained for the conditions where the disturbance signal was not present, especially for the control tasks performed with the single integrator controlled element. For the other conditions, Fig. 3.18(c) shows average values of τ_e of around 0.15 s for the control tasks with the K_c/s dynamics. For the double integrator control tasks, however, consistently higher values of τ_e of around 0.23 s are observed, a significant effect: $F(1, 5) = 67.97$, $p < 0.05$. As also recognized for the pure compensatory conditions S1 and D1 in Section 3.4.3, this difference in compensatory time delay between control of K_c/s and K_c/s^2 systems has been reported in previous research and is a direct result of the required lead equalization during control of the latter system [McRuer et al., 1965; McRuer and Jex, 1967a]. The neuromuscular model natural frequency ω_{nm} (see Fig. 3.18(d)) also shows to be affected by the controlled element dynamics and is found to be around 14 and 11.5 rad/s for the K_c/s and K_c/s^2 tasks, respectively. The damping ratio ζ_{nm} is found to be approximately constant over both controlled elements at around 0.2.

3.5 Discussion

This chapter investigated the modeling of human dynamics in control tasks where predictable target forcing function signals, consisting of multiple ramp-like changes in reference attitude, are tracked using a pursuit display. Based on the SOP theory described by McRuer et al. [1968], it would be expected that the use of predictable forcing function signals might result in the adoption of a partially precognitive control strategy. In addition, the use of a pursuit display would theoretically allow for using a pursuit tracking strategy. For these reasons, the requirement for extending commonly applied compensatory tracking models for more complex control tasks, such as the ramp-tracking tasks studied in this chapter, was investigated. For this investigation, an experiment was performed in which control behavior was measured in tracking tasks with single and double integrator controlled element dynamics. These control tasks were performed with two different ramp target forcing function signals with ramp steepnesses of 1 and 10 deg/s. In addition, the effects of the presence of an additional quasi-random disturbance signal on the adopted control strategy were evaluated.

Previous work that considered manual control behavior for more complex tasks than pure compensatory tracking – most notably the work of Wasicko et al. [1966], Allen and McRuer [1979], and McRuer and Krendel [1974] – suggests that both pursuit and precognitive control can be modeled using a model of human behavior that combines closed-loop compensatory control with open-loop feedforward operations on the reference signal. These previous studies also proposed, but did not provide compelling validation with experimental measurements, that for optimal feedforward control performance the adopted feedforward control dynamics should be proportional – and most preferably equal – to the inverse of the controlled element dynamics. As human feedforward control dynamics were anticipated to not be perfect, this chapter proposed a model that yielded a feedforward response proportional to the inverse of the controlled element dynamics, but filtered by a first-order lag and a pure time delay. In the proposed combined compensatory and feedforward model, this feedforward model was combined with a model of compensatory tracking behavior as proposed and validated by McRuer et al. [1965].

The proposed combined compensatory and feedforward model was tested by fitting it to time-domain measurements of tracking behavior collected for all ramp-tracking conditions of the experiment. In addition, the model fit and model parameter estimates obtained for this combined model were compared to the results obtained from fitting only the individual compensatory and feedforward response models to the same data. This comparison of fitted models showed that for all conditions performed with the single integrator dynamics, the proposed combined model best reproduced the measured control inputs, as indicated by the highest VAF and lowest MSE values of all three fitted models. The strength of the contribution of the modeled feedforward response was found to be greatest for the conditions that required the least compensatory control inputs, most notably for the condition with single integrator dynamics, the low-steepness 1 deg/s ramp signal, and no disturbance forcing function signal. For the double integrator control tasks, the improvement in model fit achieved with the combined model compared to the pure compensatory model was found to be only modest. Estimated model parameters for the combined model indicate a reduction in the gain of the feedforward response for the conditions where the disturbance signal

was present. Furthermore, this gain was also found to be significantly lower for the ramp-tracking tasks performed with the double integrator dynamics than for all corresponding conditions with single integrator controlled element. These results are consistent with the observations made from the VAF and MSE comparison with the pure compensatory and feedforward models. The results presented in this chapter therefore confirm the hypothesis that for control tasks where increased compensatory control behavior is required – for instance for the conditions where the low-steepness ramp signal was combined with the quasi-random disturbance and for all double integrator control tasks – reduced feedforward control power is adopted. This further implies that, to some extent, pure compensatory modeling of manual control behavior might still be acceptable for such conditions.

The measurement of pure compensatory pilot dynamics for both single and double integrator controlled element dynamics during tracking with only the quasi-random disturbance signal yielded estimates of the compensatory model parameters that are highly consistent with previous research [McRuer et al., 1965]. In addition, for the data from the tasks where the same disturbance signal was applied in addition to a ramp target signal, highly similar compensatory model estimates were obtained, suggesting nearly constant compensatory human operator dynamics, even for tasks where behavior was found to be not purely compensatory. However, for the single integrator ramp-tracking tasks where the disturbance signal was not present (conditions S2 and S4), the estimated parameters of the proposed combined model indicate different human compensatory control dynamics, especially a somewhat lower compensatory gain, for these cases that required less compensatory control inputs. To what extent compensatory control dynamics are equivalent for purely compensatory control and when additional pursuit or precognitive control strategies are applied, as suggested by McRuer and Krendel [1974] and Wasicko et al. [1966], is deemed an important question with respect to increasing our understanding of human manual control behavior. The experimental measurements presented in this chapter are not sufficiently conclusive to support such a generalization, but future experiments are planned to further address this question explicitly.

McRuer et al. [1968] did not only propose the different levels of the SOP theory to make a distinction between the different types of control behavior that can be adopted, but also as a set of consecutive stages in skill development during manual tracking. They hypothesize that upon being confronted with an unfamiliar control task, human operators first utilize the lowest SOP level of compensatory behavior. Then, depending on whether the defining features of the control task allow for it, familiarization with the control task may induce transition to the pursuit and precognitive levels. In the current experiment, ramp-tracking behavior was measured in an experiment in which each condition was evaluated completely, that is, training was performed and measurements were taken, before moving on the next condition. The proposed model was fitted to measurement data for subject who had extensively familiarized themselves with the control task they were to perform and had reached the end of their learning curve. Hence, for the behavior measured in this experiment the subjects received ample opportunity for reaching the higher levels of tracking behavior as proposed by the SOP theory. For manual control tasks performed in an operational environment, it is seldom that exactly the same control task or maneuver is executed repetitively. Even though extensive familiarity with the controlled element is likely still present in most cases, the performed maneuvers are likely not identical every time. One important question

that therefore needs to be addressed for extending the results of this research to operationally relevant conclusions is how strong this effect of training and skill development on the development of a feedforward control strategy, as modeled in this chapter, is.

The current experiment data and the fitted behavioral models suggest a decreasing contribution of feedforward control inputs with a decrease in the relative control power required for following the ramp target signal and that required for compensatory disturbance rejection. The same is observed when comparing measurements taken with single and double integrator controlled elements, likely due to the fact that for the latter more (compensatory) controlled element stabilization is typically required. The current experiment only considered a severely limited number of different measurement conditions to evaluate both these effects and more experimental measurements are required for fully understanding these adaptation processes. In a follow-up study to the experiment considered in this chapter, which is described by Drop [2011], the effect of varying the relative power of the applied ramp target and multisine disturbance signals on measured pilot control dynamics during single-integrator control is evaluated over a wider range than considered for the experiment in this paper. Research is currently being performed to clarify the relation between feedforward control dynamics and controlled element dynamics during ramp-tracking tasks. Eventually, this research effort is expected to yield an extension the theory of manual control as compiled by McRuer et al. [1965] for purely compensatory tracking, including extended behavioral models and practical mathematical rules for offline tuning of these models to specific task variables, to more complex and operationally relevant control tasks.

3.6 Conclusions

The modeling of manual control behavior in control tasks where predictable forcing function signals, such as signals consisting of multiple ramp-like changes in target attitude, are applied could require models of human behavior that account for both compensatory behavior and feedforward operations on the reference signal. This chapter described the results of an experiment and corresponding modeling effort aimed at revealing if such dual-mode models are indeed required for modeling the tracking of ramp signals. Due to the expected effect of these task variables on the benefit and occurrence of this combined compensatory and feedforward control strategy, target signals with different ramp steepnesses were considered in the experiment, as well as both single and double integrator controlled element dynamics. Furthermore, due to possible suppression of such a dual-mode control strategy when an additional quasi-random disturbance forcing function is present, which can only be attenuated through compensatory control, the different ramp signal and controlled element settings were also evaluated both with and without such an external disturbance being present. Only a marginal improvement in model fit with the combined compensatory and feedforward model compared to a purely compensatory model of tracking behavior was observed for the experimental conditions performed with the double integrator controlled element dynamics and those where the control inputs required for ramp-tracking were small compared to those required for attenuating the disturbance signal. This suggests that in the presence of comparatively large external disturbances, or for marginally stable controlled element dynamics, a predominantly compensatory control strategy is adopted for the con-

sidered ramp-tracking tasks performed with a pursuit display. For single integrator control tasks where the ramp signal power is sufficiently large with respect to the external disturbances that need to be attenuated, however, the proposed combined compensatory and feedforward model of pilot control dynamics was found to provide a consistently more accurate fit of measured control inputs than a pure compensatory model, thereby suggesting use was made of a control strategy more complex than purely compensatory tracking.

Part II

Preliminary and Previous Simulator Experiments

4

Effects of Heave Washout During Pitch Tracking

With the limited motion space available in typical moving-base flight simulators, perhaps the largest discrepancies between the true aircraft motion and the motion cues presented in the simulator are observed for the vertical degree-of-freedom. Due to the significant amount of vertical aircraft motion that results from such maneuvers, longitudinal aircraft control tasks were therefore thought to be of special interest to the research described in this thesis. For this reason, two of the first experiments performed in this project focused on the effects of the available motion cues on pilot tracking behavior during aircraft pitch attitude control tasks. The first – which is described in [Zaal et al., 2009b] and [Zaal, 2011] – measured the individual and combined effects of the perceivable rotational pitch and vertical heave motion cues, by independently varying their presence in a simulated pitch control task. The research described in this chapter was performed as a follow-up to the experiment of Zaal et al. [2009b] to explicitly evaluate the effects of varying heave motion filter settings on pilot tracking. Together with the experiment performed by Zaal et al. [2009b], this experiment thereby served as an important reference for the comparison between pitch tracking behavior measured in real flight and for varying motion cueing settings in a flight simulator, as described in detail in the thesis by Zaal [2011]. Furthermore, the measured effects of variations in heave washout filter settings observed in this chapter are also included in the literature overview of reported effects of washout on pilot tracking behavior and performance described in Chapter 5.

The contents of this chapter have been published as:

Pool, D.M., Zaal, P.M.T., Van Paassen, M.M., and Mulder, M., “Effects of Heave Washout Settings in Aircraft Pitch Disturbance Rejection”, *Journal of Guidance, Control and Dynamics*, Vol. 33, No. 1, Jan-Feb, 2010, pp. 29-41.

4.1 Introduction

Compared to aircraft, flight simulators are severely limited in their motion envelope. This causes the generation of motion cues in flight simulation to be an inevitable compromise between the desired level of motion cue fidelity and the available motion space. Since the 1970s, it has become common practice to use washout algorithms for transforming aircraft rotational and linear accelerations to simulator motion [Schmidt and Conrad, 1970]. Such washout algorithms typically use linear high- and low-pass filters to attenuate simulated aircraft motion states both in magnitude (scaling) and in phase (washout). In addition to the attenuation of the real aircraft motions, the washout performed by motion filters is also known to result in false motion cues [Grant and Reid, 1997a].

Numerous studies in literature have shown that simulator washout filter settings affect pilots' perception and acceptance of simulator motion [Ringland and Stapleford, 1971; Jex et al., 1978; Reid and Nahon, 1986b; Schroeder, 1999; Gouverneur et al., 2003; Telban et al., 2005b]. In addition, it has been shown that the design and tuning of motion washout filters is heavily dependent on the maneuver that is to be simulated [Hosman et al., 1979]. Therefore, insight into the effects of the rotational and linear motion components involved in a specific maneuver, and their effect on pilots' motion perception and control behavior, is required for proper motion washout filter design. To achieve the optimal level of simulator motion fidelity, those motion components that provide important feedback to the pilot must be replicated at high accuracy, while those that are less likely to affect pilots' control behavior can be attenuated to save valuable simulator motion space.

An example of a piloting task for which this relative importance of the different perceivable motion components is of interest, is a manual aircraft pitch attitude stabilizing task. Zaal et al. [2009b] describe an experiment in which the effects of two different vertical motion components on pilot control behavior in a pitch attitude disturbance-rejection task have been investigated, which they referred to as "pitch-heave" and "c.g. heave". The first results from the fact that pilots are generally seated well in front of the aircraft center of pitch rotation and that rotational pitch accelerations therefore cause correlated vertical (heave) accelerations at the pilot station. In addition, changes in pitch attitude cause vertical motion of the aircraft center of gravity, which yields a second component of the total heave motion. The results described in [Zaal et al., 2009b] indicate that, because similar information can be deduced from rotational pitch motion and the pitch-heave motion component, pilot control behavior is affected by both these motion cues in a similar way.

The effects of pitch-heave on pilot performance and control behavior found by Zaal et al. [2009b] were, however, significantly lower in magnitude than those of rotational pitch motion. In that experiment, pitch motion was presented one-to-one, as it would rarely exceed plus or minus 5 degrees, but the heave motion was filtered using a third-order linear high-pass filter. This motion filter was required for attenuating the high-magnitude low-frequency c.g. heave motion and, to allow for fair comparison of both heave motion components, was also used to filter the pitch-heave accelerations. The relatively lower magnitude of the effects of pitch-heave may therefore be partly explained by the heave motion filter used in this experiment.

This chapter describes an investigation into the effects of heave washout filter settings on pilot control behavior in the same pitch tracking task as was studied by Zaal et al. [2009b].

By varying the parameters of the heave washout filter, some insight into the effects of the gain and phase attenuation induced by such linear filters on pilot skill-based control behavior can be obtained. Due to the significant correlation between pitch and pitch-heave motion during aircraft pitch maneuvering, it can be anticipated that the effects of degrading heave motion cues by washout will have less impact when pitch motion is also present.

In this chapter, first some of the details of the considered pitch attitude disturbance-rejection task will be described and, using data from the experiment performed by Zaal et al. [2009b], the effect of the washout filter adopted in this previous experiment on the supplied heave motion cues will be illustrated. Then, the setup of the current human-in-the-loop experiment that was performed in the SIMONA Research Simulator (SRS) at Delft University of Technology will be described in detail. In this experiment, different heave motion attenuation settings were tested, to allow for evaluation of the effects of heave washout on pilot control behavior. Objective measurements of pilot control behavior from the current experiment will be presented and compared to results of the experiment described in [Zaal et al., 2009b]. The chapter ends with a discussion and conclusions.

4.2 Heave Motion During Pitch Maneuvering

During aircraft pitch maneuvering, pilots' motion sensation will not consist solely of physical pitch rotation. Due to aircraft geometry and dynamical responses, some additional linear motion will also be perceivable, most notably vertical heave motion. In this section, the heave motion cues associated with aircraft pitch control, the heave motion filter, and some of the main trends that were observed in the experiment described by Zaal et al. [2009b] will be discussed.

4.2.1 Heave Motion Components

As indicated in Fig. 4.1, Zaal et al. [2009b] made a distinction between two components of the total vertical motion at the pilot station. The first, referred to as “pitch-heave” motion and indicated with the symbol a_{z_θ} in Fig. 4.1, represents the vertical motion that is a direct result of the pitch rotation and the distance between the pilot station and the center of gravity, l . A second contribution to the vertical motion pilots perceive during pitch maneuvering, referred to as “c.g. heave” ($a_{z_{c.g.}}$), results from changes in aircraft altitude that are caused by the changes in aircraft pitch. Note that this breakdown into vertical motion of the aircraft c.g. and heave motion with respect to the c.g. could alternatively have been performed using the instantaneous center of pitch rotation as described in literature [Field et al., 2002a]. However, due to the modest size of the aircraft considered in this study, a Cessna Citation I, the difference between both definitions is small.

The two distinct components of heave motion identified in [Zaal et al., 2009b] yield highly different motion sensations at the pilot station. For pure pitching maneuvers, the pitch-heave accelerations are linearly related to the second derivative of the aircraft pitch attitude through:

$$a_{z_\theta} = -l\ddot{\theta} \quad (4.1)$$

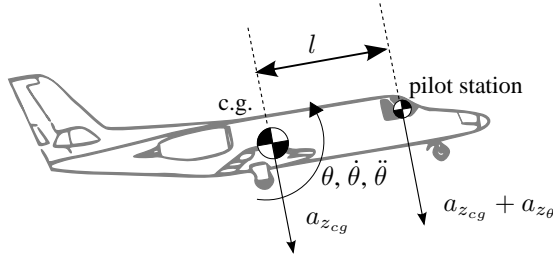


Figure 4.1. Motion cues at the center of gravity and pilot station during a pitch maneuver.

As indicated by this relation, the pitch-heave component of the vertical motion at the pilot station essentially provides a vertical presentation of the aircraft's pitching motion. For a Cessna Citation I, the distance between the aircraft center of gravity and the pilot station is approximately 3.2 meters. As a result, the magnitude of this heave motion component is relatively modest: for pitch attitudes between ± 5 deg, only ± 0.28 meters of vertical motion space would be required for one-to-one presentation of the pitch-heave motion.

The pitch-heave accelerations a_{z_θ} are a high-pass response to elevator control inputs. The c.g. heave component of the vertical motion, however, is a high-magnitude low-pass response to an elevator input. As changes in aircraft altitude are typically in the order of meters, one-to-one presentation of this component of vertical motion is not possible in most full-motion flight simulators. The analysis of pilot control behavior described by Zaal et al. [2009b] revealed that pilot control behavior during pitch tracking is affected by both pitch-heave and c.g. heave motion. The investigation of the effects of heave washout on pilot control behavior described in this paper, however, requires a baseline condition in which heave motion is presented one-to-one. Therefore, the center of gravity heave component of the vertical linear motion during pitch maneuvering could not be considered in the current study.

4.2.2 Heave Motion Filter

A linear high-pass heave motion filter, as typically adopted in motion base flight simulators, was used for attenuating the aircraft heave motion in the experiment of Zaal et al. [2009b]. To achieve significant low-frequency attenuation, a third-order high-pass filter was used, whose transfer function is given by:

$$H_{mf}(s) = K_{mf} \frac{s^2}{s^2 + 2\zeta_{n_{mf}}\omega_{n_{mf}}s + \omega_{n_{mf}}^2} \frac{s}{s + \omega_{b_{mf}}} \quad (4.2)$$

In Eq. (4.2), K_{mf} represents the motion filter gain, which was set to 0.6. The filter break frequencies, $\omega_{n_{mf}}$ and $\omega_{b_{mf}}$, and the damping factor $\zeta_{n_{mf}}$, which together define the dynamical characteristics of the washout filter, were fixed to 1.25 and 0.3 rad/s, and 0.7, respectively.

This washout filter was required for attenuation of the c.g. heave component of the total vertical motion, but not for the pitch-heave motion component. Despite the fact that

pitch-heave motion could be replicated one-to-one for the Citation I aircraft used in the experiment of Zaal et al. [2009b], both heave motion components were attenuated by the washout filter of Eq. (4.2), to allow for fair comparison of their respective effects on pilot control behavior during pitch tracking.

Fig. 4.2 depicts the frequency response of the high-pass filter of Eq. (4.2). In addition, the average spectrum of the aircraft pitch-heave accelerations measured by Zaal et al. for their seven subjects is shown alongside (circles indicate disturbance signal frequencies). Note the high-pass characteristic of the pitch-heave accelerations. Furthermore, observe that the motion filter corner frequencies were chosen such that the main filter amplitude attenuation did not affect the frequencies where the pitch-heave acceleration had the most power. Finally, note from Fig. 4.2 that both filter break frequencies were also selected to be significantly below the short-period frequency of the Citation dynamics, $\omega_{sp} = 2.76$ rad/s.

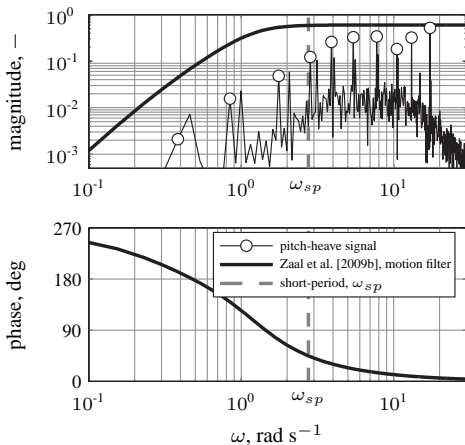


Figure 4.2. Average pitch-heave acceleration spectrum compared to frequency response of the [Zaal et al., 2009b] heave motion filter.

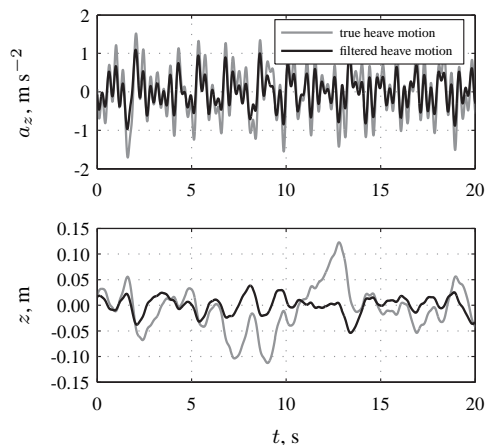


Figure 4.3. Comparison of sample heave acceleration and displacement time traces for true and filtered heave motion (Zaal et al. [2009b]'s motion filter).

Fig. 4.2 suggests that when the pitch-heave accelerations are attenuated by the motion filter defined by Eq. (4.2), the resulting motion cues will not have been attenuated much in the frequency range where they hold the most power. This is further illustrated by the top graph in Fig. 4.3, which shows a comparison of unfiltered and filtered pitch-heave acceleration time traces. Note that the gain attenuation of 0.6 is clearly visible, but hardly any phase shift is observable from the acceleration time traces. As illustrated by the bottom graph of Fig. 4.3, this no longer holds when the acceleration signals are integrated to vertical position, as the washout clearly reduces the magnitude of the simulator excursions.

4.2.3 Observed Effects of Heave

One of the main findings of the experiment described by Zaal et al. [2009b] was that rotational pitch motion and translational pitch-heave motion were found to have highly similar effects on pilot performance and control behavior during pitch tracking. As the pitch-heave acceleration component is directly related to pitch acceleration through Eq. (4.1), this was hypothesized before the experiment was performed. The magnitude of the effects of $a_{z\theta}$ on pilot control behavior and performance were, however, found to be significantly lower than those observed for rotational pitch motion. This is illustrated in Fig. 4.4, where the time-domain variances of the tracking error signal and the pilot control signal are depicted as measures of pilot performance and control activity, respectively.

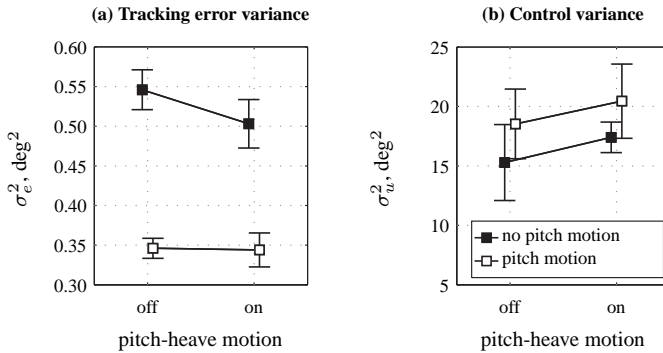


Figure 4.4. Effects of pitch and pitch-heave motion on tracking performance and control activity (data from [Zaal et al., 2009b]).

Fig. 4.4 clearly illustrates that both tracking performance and control activity were found to increase when rotational pitch motion was made available (lower σ_e^2 signifies better tracking performance). In addition, note the similar but reduced effect of the addition of pitch-heave motion, which is most clearly observed for the error variance data shown in Fig. 4.4(a). Highly similar trends were visible in the underlying pilot control behavior. From the analysis of the motion filter used by Zaal et al. [2009b] for their experiment, this reduced magnitude of the effects of pitch-heave motion compared to rotational pitch motion is believed to be at least partly due to the use of this motion filter. This warrants more research into the effect of motion washout filters on pilot control behavior in attitude control tasks.

4.3 Experiment

An experiment was performed on the SIMONA Research Simulator (SRS) at Delft University of Technology, to investigate the influence of heave motion attenuation on pilot control behavior in a pitch tracking task. This section describes the experimental method and hypotheses. The control task, experimental procedures, and apparatus of the current

experiment are equal to those of the experiment described in [Zaal et al., 2009b], to allow for valid comparison of both sets of results.

4.3.1 Method

4.3.1.1 The Aircraft Pitch Control Task

To investigate the effects of heave motion attenuation on pilot behavior during aircraft pitch control, control behavior was evaluated in the pitch control task depicted in Fig. 4.5. In this task, a pilot controls the pitch angle θ of the controlled element ($H_{\theta, \delta_e}(s)$) by compensating for deviations from the desired pitch attitude by minimizing the tracking error e as shown on a compensatory display (Fig. 4.6). In addition to this visual information, continuous feedback of physical pitch and pitch-heave motion is available. This yields a pilot response, which is a summation of a visual response $H_{p_e}(j\omega)$, a pitch motion response $H_{p_\theta}(j\omega)$, a pitch-heave motion response $H_{p_{a_z}}(j\omega)$, and a remnant signal n , that accounts for the nonlinear behavior.

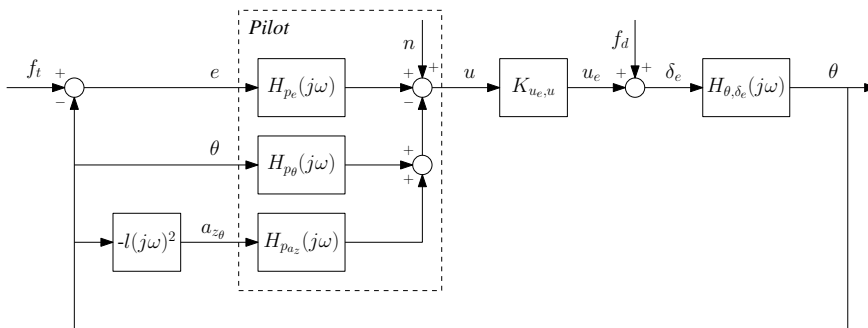


Figure 4.5. Schematic representation of a closed-loop pitch control task with pitch and pitch-heave motion cues.

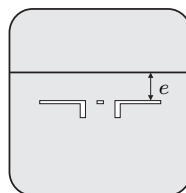


Figure 4.6. Compensatory display.

The controlled dynamics for the pitch attitude control task are the elevator to pitch attitude dynamics of a Cessna Citation I Ce500, linearized at an altitude of 10,000 ft and an airspeed of 160 kt. The transfer function of this controlled element is given by:

$$H_{\theta, \delta_e}(s) = -10.6189 \frac{s + 0.9906}{s(s^2 + 2.756s + 7.612)} \tag{4.3}$$

Table 4.1. Experiment forcing function properties.

disturbance, f_d				target, f_t			
$n_d, -$	$\omega_d, \text{rad/s}$	A_d, deg	ϕ_d, rad	$n_t, -$	$\omega_t, \text{rad/s}$	A_t, deg	ϕ_t, rad
5	0.383	0.344	-1.731	6	0.460	0.698	1.288
11	0.844	0.452	4.016	13	0.997	0.488	6.089
23	1.764	0.275	-1.194	27	2.071	0.220	5.507
37	2.838	0.180	4.938	41	3.145	0.119	1.734
51	3.912	0.190	5.442	53	4.065	0.080	2.019
71	5.446	0.235	2.274	73	5.599	0.049	0.441
101	7.747	0.315	1.636	103	7.900	0.031	5.175
137	10.508	0.432	2.973	139	10.661	0.023	3.415
171	13.116	0.568	3.429	194	14.880	0.018	1.066
226	17.334	0.848	3.486	229	17.564	0.016	3.479

The control input scaling gain $K_{u_e, u}$, which defined the scaling of stick deflections to model elevator inputs, was set to -0.2865 to yield optimal control authority. To induce pitch attitude tracking errors that pilots needed to compensate for, target and disturbance forcing function signals – denoted with the symbols f_t and f_d in Fig. 4.5, respectively – were inserted into the closed-loop system as shown in Fig. 4.5. These forcing function signals were constructed as quasi-random sum-of-sines signals, as also used in many previous research efforts [McRuer et al., 1965; McRuer and Jex, 1967a; McRuer and Krendel, 1974; Van der Vaart, 1992; Hosman, 1996]. The same target and disturbance signals as adopted by Zaal et al. [2009b] were also used for this experiment, yielding a control task in which the disturbance-rejection element was dominant. The sum-of-sines signals were constructed according to:

$$f_{d,t}(t) = \sum_{k=1}^{N_{d,t}} A_{d,t}(k) \sin(\omega_{d,t}(k)t + \phi_{d,t}(k)), \quad (4.4)$$

where the subscripts d and t indicate the disturbance or target forcing function, respectively. In Eq. (4.4), $A(k)$, $\omega(k)$ and $\phi(k)$ indicate the amplitude, frequency and phase of the k^{th} sine in f_d or f_t . N indicates the number of sines in the signals. The properties of the sine components of both forcing function signals are given in Table 4.1.

4.3.1.2 Independent Variables

This study aims to investigate the effects of heave washout settings on the usefulness of the pitch-heave component of heave motion during pitch attitude disturbance-rejection. As, for the control task described in Section 4.3.1.1, no washout filter is in fact required for replicating the pitch-heave accelerations a_{z_θ} in the SRS, the effects of a linear washout filter in heave can be compared to a full motion case. Five different heave washout settings will be considered in this experiment. The motion filter gains and break frequencies for these five experimental conditions are depicted graphically in Fig. 4.7.

Heave conditions K0.0 and K1.0 represent conditions with no heave motion and one-to-one heave motion, respectively. The combination of heave filter break frequency and gain that was used for the experiment described in [Zaal et al., 2009b] is depicted by condition

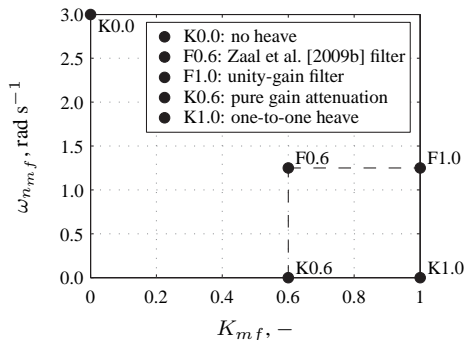


Table 4.2. Heave motion filter settings.

condition	K_{mf}	$\omega_{n_{mf}}$ rad/s	$\omega_{b_{mf}}$ rad/s	$\zeta_{n_{mf}}$
K0.0	0	—	—	—
F0.6	0.6	1.25	0.3	0.7
F1.0	1	1.25	0.3	0.7
K0.6	0.6	—	—	—
K1.0	1	—	—	—

Figure 4.7. Graphical representation of heave motion filter conditions.

F0.6. Heave filter F1.0 has the same break frequency as used for F0.6, but has unity gain. K0.6 has the same gain as condition F0.6, but with a break frequency of zero. These conditions are expected to reveal if a possible reduction in usefulness of the heave motion is a result of the gain attenuation (K_{mf}) or of the phase shifts induced by the washout, whose impact can be characterized by the value of the break frequencies $\omega_{n_{mf}}$ and $\omega_{b_{mf}}$.

The properties of the five heave filters used in the experiment are summarized in Table 4.2. All five heave conditions will be performed with and without the presence of one-to-one rotational pitch motion cues, as an interaction between heave filter settings and the availability of pitch motion is anticipated. This means a total of 10 conditions were performed in the experiment.

4.3.1.3 Dependent Measures

A number of dependent measures from the experiment were considered to be of interest. First of all, the variances of the recorded error signal e and control signal u were calculated as measures of tracking performance and control activity in the time domain, respectively. In addition, a multimodal pilot model – defined in detail in Section 4.3.1.4 – was fitted to the time-domain data using a genetic maximum likelihood (MLE) procedure [Zaal et al., 2009a]. To evaluate the accuracy of the pilot model in the time domain, the variance accounted for (VAF) was calculated using the measured pilot control signal and the output of the linear pilot model [Nieuwenhuizen et al., 2008]. The changes in pilot model parameters were used to quantify changes in pilot control strategy for the different attenuations of heave motion. The performance of the attenuation of the disturbance and target errors was evaluated by calculating the crossover frequencies and phase margins of the disturbance and target open-loop response, respectively.

4.3.1.4 Pilot Model

The structure of the quasi-linear pilot model used in this study is shown in Fig. 4.5. It consists of parallel linear responses to all perceived visual and physical motion cues, supplemented with a remnant signal n to account for all nonlinearities. The model of the pilot visual response, given by Eq. (4.5), is based on the work of McRuer et al. [1965] and was shown to be suitable for modeling pilot control of the aircraft dynamics defined in Eq. (4.3) in Chapter 2 of this thesis.

$$H_{p_e}(j\omega) = K_v \frac{(1 + T_L j\omega)^2}{1 + T_I j\omega} e^{-j\omega\tau_v} H_{nm}(j\omega) \quad (4.5)$$

In Eq. (4.5), K_v and τ_v represent the pilot visual gain and visual perception time delay, respectively. The visual equalization characteristic is defined using the lead and lag constants, T_L and T_I . The neuromuscular actuation dynamics are included through the neuromuscular system model $H_{nm}(j\omega)$, which is assumed to be a second-order mass-spring-damper system:

$$H_{nm}(j\omega) = \frac{\omega_{nm}^2}{(j\omega)^2 + 2\zeta_{nm}\omega_{nm}j\omega + \omega_{nm}^2} \quad (4.6)$$

The dynamics of the neuromuscular system are characterized with the second-order system natural frequency and damping ratio, ω_{nm} and ζ_{nm} , which are both free parameters of the pilot model. The pilot model for the no motion condition of the experiment (F0.0, without pitch motion) consisted solely of Eqs. (4.5) and (4.6).

In literature, pilots' responses to physical motion cues have often been described with models that included only contributions from the human vestibular motion sensors [Van der Vaart, 1992; Hosman, 1996; Zaal et al., 2009b], that is, the semicircular canals for rotational motion and the otoliths for linear motion (specific forces). Pilot vestibular motion responses to rotational motion have for instance been modeled successfully as:

$$H_{p_\theta}(j\omega) = K_m(j\omega)^2 H_{sc}(j\omega) e^{-j\omega\tau_m} H_{nm}(j\omega), \quad (4.7)$$

in numerous previous experiments in which the effects of rotational motion feedback on pilot tracking behavior was evaluated [Van der Vaart, 1992; Hosman, 1996; Pool et al., 2008b; Praamstra et al., 2008; Zaal et al., 2009b; Nieuwenhuizen et al., 2008; Zaal et al., 2009c]. In Eq. (4.7), K_m and τ_m are the pilot motion response gain and time delay, respectively. The frequency response function $H_{sc}(j\omega)$, with $T_{sc_1} = 0.11$ s, $T_{sc_2} = 5.9$ s, and $T_{sc_3} = 0.005$ s, represents the response of the human semicircular canals to rotational acceleration inputs, as described in literature [Hosman, 1996]:

$$H_{sc}(j\omega) = \frac{1 + T_{sc_1}j\omega}{(1 + T_{sc_2}j\omega)(1 + T_{sc_3}j\omega)} \quad (4.8)$$

Eq. (4.7) describes a pilot's response to rotational motion from a physical perspective, by making use of knowledge of the underlying physical motion perception processes. Due to the fact that the semicircular canals are sensitive to rotational accelerations, and that their dynamics are a single integrator in the frequency range of interest for human manual

vehicular control, the model defined by Eq. (4.7) effectively provides additional pilot lead – that is, a response to rotational velocity – in parallel to the lead generated from the visual response (Eq. (4.5)). Despite the fact that the otoliths are sensitive to specific forces and yield a sensation of linear acceleration [Hosman, 1996], pilots are known to integrate these sensed accelerations to rates during manual control tasks to yield a lead contribution that is highly similar to that obtained from the semicircular canals [Hosman et al., 2005].

This additional lead from the vestibular sensors is often stated to be superior to visual lead due to the lower perceptual latency [Hosman, 1996]. Previous experiments, which investigated control behavior in control tasks similar to the one depicted in Fig. 4.5, have indeed shown that pilots substitute lead from physical motion stimuli, if available, for the lead generated from visual information [Zaal et al., 2009b,c]. For the experiment described in this paper, it is hypothesized that this additional lead information is present in both the rotational pitch motion and the vertical pitch-heave motion. Therefore, the contribution of the pitch and heave motion channels of the pilot model were combined. To achieve this, both motion response channels are defined to take the form of a pure lead with a time delay on the pitching motion:

$$H_{p_\theta}(j\omega) = K_m j\omega e^{-j\omega\tau_m} H_{nm}(j\omega) \quad (4.9)$$

$$H_{p_{az}}(j\omega) = \frac{-1}{l(j\omega)^2} H_{p_\theta}(j\omega) = \frac{-K_m}{lj\omega} e^{-j\omega\tau_m} H_{nm}(j\omega) \quad (4.10)$$

For conditions with only heave motion, Eq. (4.10), which includes the distance between the center of gravity and the pilot station l , is included in the pilot model. For conditions where pitch motion is present (including those with additional heave), only Eq. (4.9) is used for modeling the pilot motion response. This approach allows for comparison of the pilot model parameters that are of interest – mainly the visual lead constant T_L and the motion gain K_m – over all conditions of the experiment. A validation of this modeling approach will be provided in Section 4.4.3.1 using experimental data.

4.3.1.5 Apparatus

The experiment was performed in the SRS at Delft University of Technology, see Fig. 4.8. Pitch and heave motion cues were generated with the six degree-of-freedom SRS motion system, which consists of six hydraulic actuators in a hexapod configuration. The SRS motion system latency is 30 ms [Berkouwer et al., 2005].

Subjects were seated in the right pilot seat. The compensatory visual display shown in Fig. 4.6 was depicted on the right primary flight display in the SRS cockpit. The time delay associated with the generation of visual images on the cockpit displays has been determined to be around 20-25 ms [Stroosma et al., 2007].

A sidestick with electrical control loading was used to give control inputs to the controlled aircraft dynamics, Eq. (4.3). The sidestick was defined to have no breakout force and a maximum pitch axis deflection of ± 14 degrees. The stick roll axis was kept fixed at the zero position. The stiffness of the stick was set to 1.1 N/deg for stick deflections under 9 degrees, and to 2.6 N/deg for larger stick excursions.

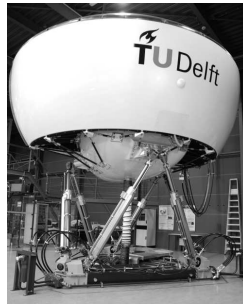


Figure 4.8. The SIMONA Research Simulator.

4.3.1.6 Participants and Experimental Procedures

Seven subjects participated in the experiment. All participants were male and their ages ranged from 23 to 47 years old. Four of the participants had experience as pilots of single or multi-engine aircraft. The others had extensive experience with manual vehicle control tasks from previous human-in-the-loop experiments. Before the start of the experiment, the participants were briefed on the objective of the experiment and the experimental method. The main instruction to the subjects was to minimize the pitch tracking error e presented on the visual display, within their capabilities. After the end of each experiment run the subjects were informed of their score in order to motivate them to perform at their maximum level of performance.

The experiment had a balanced Latin square design, that is, the conditions were presented in quasi-random order. The subjects were trained on the task until they performed at a stable level of performance. When five repetitions of each condition had been collected at a stable performance level, the experiment was terminated. No fixed number of training runs was defined prior to the experiment. On average, 9 to 10 repetitions of each experimental condition were sufficient to gather the measurement data. Typically, each subject performed 16 runs, that is, two repetitions of all conditions, in between breaks. This allowed each subject to complete the experiment in approximately 4 hours.

An individual experiment run was defined to last 90 seconds, of which the final 81.92 seconds were used as the measurement data. The first 8.08 seconds of data from each run were discarded for analysis, to remove the initial transient response resulting from pilots stabilizing the system dynamics. Data were logged at a frequency of 100 Hz.

4.3.2 Hypotheses

Based on the experiment described in [Zaal et al., 2009b] and other experiments on the effects of motion attenuation on pilot performance and control behavior [Steurs et al., 2004; Dehouck et al., 2006], some hypotheses can be formulated. Filtering pitch-heave motion is hypothesized to yield lower tracking performance. This decrease is expected to be less when, in addition, rotational pitch motion is present. As both types of motion give the same information, the pitch motion then compensates for the lower fidelity pitch-heave motion.

For the pilot model parameters it is hypothesized that as the fidelity of the motion is increased, the visual and physical motion perception gains will increase. In addition, the visual lead is thought to decrease, as the additional motion cues provide a more efficient source of lead information. The disturbance crossover frequency is thought to increase, accompanied by a decrease in disturbance phase margin. For the target crossover frequency and phase margin the opposite trend to the disturbance crossover frequency and phase margin is anticipated when motion fidelity is increased. Furthermore, it is hypothesized that one-to-one pitch-heave motion affects pilot performance and control behavior in the same order of magnitude as one-to-one rotational pitch motion.

4.4 Results

This section presents the results of the human-in-the-loop experiment. First, the effects of variation of pitch and heave motion on tracking performance and control activity are presented. Second, pilot-vehicle system crossover frequency and phase margin – with respect to both the disturbance and target signals used in the control task – are presented as measures of combined pilot-vehicle system stability and bandwidth. Finally, changes in pilot control behavior over the different motion conditions are analyzed explicitly using the multimodal pilot model introduced in Section 4.3.1.4. The statistical significance of the results is identified, where possible, using a two-way repeated-measures analysis of variance (ANOVA) that considers the effects of pitch and heave motion cues as separate factors.

4.4.1 Tracking Performance and Control Activity

Fig. 4.9 depicts the mean tracking performance and control activity – expressed in terms of the variances of the error and control signals, e and u – for the ten conditions of the experiment. Black data points indicate measurements for conditions without pitch motion; data from the corresponding heave motion conditions with additional pitch motion are depicted with white squares. Variance bars indicate the 95% confidence intervals of the means for each condition over the seven experiment subjects. For calculation of the confidence intervals, the data were corrected for between-subject effects. Repeated-measures ANOVA results for the data depicted in Fig. 4.9 are summarized in Table 4.3.

From Fig. 4.9(a) a clear difference in achieved tracking performance for runs with and without pitch motion can be observed. This decrease in σ_e^2 when pitch motion cues were available is a highly significant effect, $F(1, 6) = 41.15$, $p < 0.05$. In addition, heave motion fidelity was also found to affect control task performance significantly ($F(1.3, 8.0) = 22.24$, $p < 0.05$), as increased heave motion fidelity clearly yielded lower error signal variances. Note from Table 4.3 that Mauchly's test indicated a violation of the sphericity assumption for the main effect of heave on σ_e^2 and that thus the conservative Greenhouse-Geisser correction was applied.

The effect of heave motion settings on tracking performance is found to be significantly reduced when pitch motion cues are also available. Addition of heave motion is still found to increase performance, but the effect is much smaller than for the corresponding conditions without pitch. This reduced effect of heave motion fidelity for conditions with pitch motion

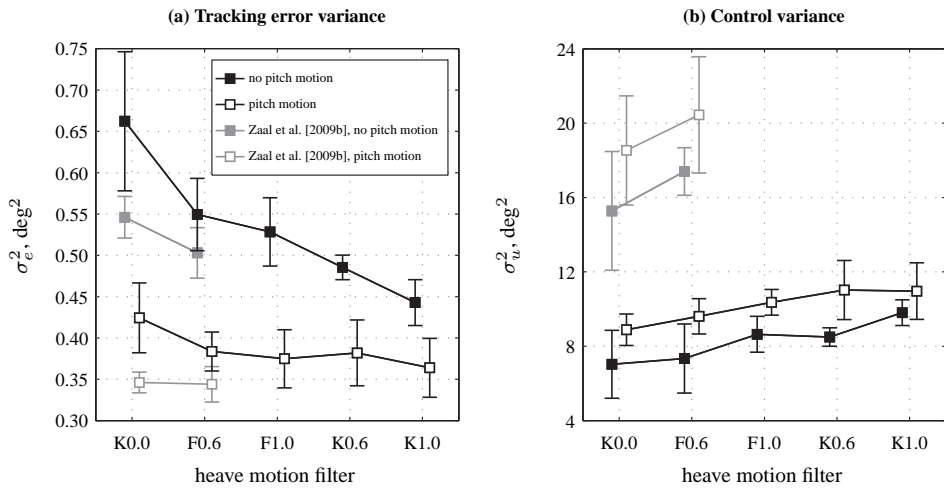


Figure 4.9. Mean tracking performance and control activity.

Table 4.3. Two-way repeated-measures ANOVA results for tracking performance and control activity.

Independent variables	Dependent measures					
	σ_e^2			σ_u^2		
Factor	df	F	Sig.	df	F	Sig.
pitch	1,6	41.15	**	1,6	9.24	**
heave	1,3,8,0 ^{gg}	22.24	**	1,6,9,8 ^{gg}	6.95	**
pitch × heave	4,24	10.74	**	4,24	1.22	—

** = highly-significant ($p < 0.05$) gg = Greenhouse-Geisser sphericity correction
 * = significant ($0.05 \leq p < 0.1$)
 — = not significant ($p \geq 0.1$)

is also evident from the significant interaction found for both types of motion cues from the ANOVA, $F(4, 24) = 10.74, p < 0.05$.

Fig. 4.9(b) clearly shows increased control activity both with increased heave fidelity and when additional pitch motion cues are made available. These effects of pitch and heave on σ_u^2 are both significant: $F(1, 6) = 9.24, p = 0.023$ and $F(1.6, 9.8) = 6.95, p = 0.016$, respectively. In addition, the increase in control activity with increasing heave fidelity is found to be more or less equal in magnitude with and without availability of pitch motion, which is also supported by the insignificant interaction between pitch and heave motion found for σ_u^2 , $F(4, 24) = 1.22, p = 0.33$.

The gray data shown in Fig. 4.9 depict the error and control signal variances measured during the experiment of Zaal et al. [2009b] for the K0.0 and F0.6 heave motion conditions, which were shared by both experiments. Note that the observed trends between these conditions are highly similar for both sets of data, but that the average tracking performance for these shared conditions was clearly better during the previous experiment than found from the current data. Average control activity is also found to be markedly higher for the data from [Zaal et al., 2009b]. To illustrate the origin of this discrepancy, average tracking performance and control activity for the K0.0 and F0.6 conditions from the current experiment are depicted in Fig. 4.10 alongside the individual subject data from [Zaal et al., 2009b], shown in gray.

Fig. 4.10 illustrates that three of the subjects that performed the experiment of Zaal et al. [2009b] can be characterized as achieving above average tracking performance (low σ_e^2) and adopting a comparatively high-gain control strategy (high σ_u^2). The data measured during the current experiment nicely coincide with the data from the remaining participants of the previous experiment. For the current experiment, a more homogeneous group of subjects was used, as all of them were comparatively low-gain controllers. Note that despite the clear offset in the data of the different participants in Fig. 4.10, the observed trends are remarkably consistent for all subjects, especially for the error signal variance σ_e^2 . This same consistency was also observed for the data from the current experiment.

4.4.2 Crossover Frequencies and Phase Margins

As indicated in Section 4.3.1.1, the control task studied in this experiment was a combined disturbance-rejection and target-following task, in which the disturbance-rejection element was made dominant by downscaling the target forcing function signal. For such a combined task, the suppression of tracking errors induced by both forcing function signals determines overall closed-loop system performance. The crossover frequencies and phase margins of the open-loop response functions with respect to both target and disturbance signals can give an indication of pilot-vehicle system performance and stability [Jex et al., 1978]. These target and disturbance open-loop response functions can be calculated from time-domain measurements according to [Zaal et al., 2009b]:

$$H_{ol,d}(j\omega_d) = -\frac{U_e(j\omega_d)}{\delta_e(j\omega_d)}, \quad H_{ol,t}(j\omega_t) = \frac{\theta(j\omega_t)}{E(j\omega_t)} \quad (4.11)$$

In Eq. (4.11), $U_e(j\omega_d)$, $\delta_e(j\omega_d)$, $\theta(j\omega_t)$, and $E(j\omega_t)$ represent the Fourier transforms – evaluated at the frequencies of the sinusoids in either f_d or f_t – of the signals u_e , δ_e ,

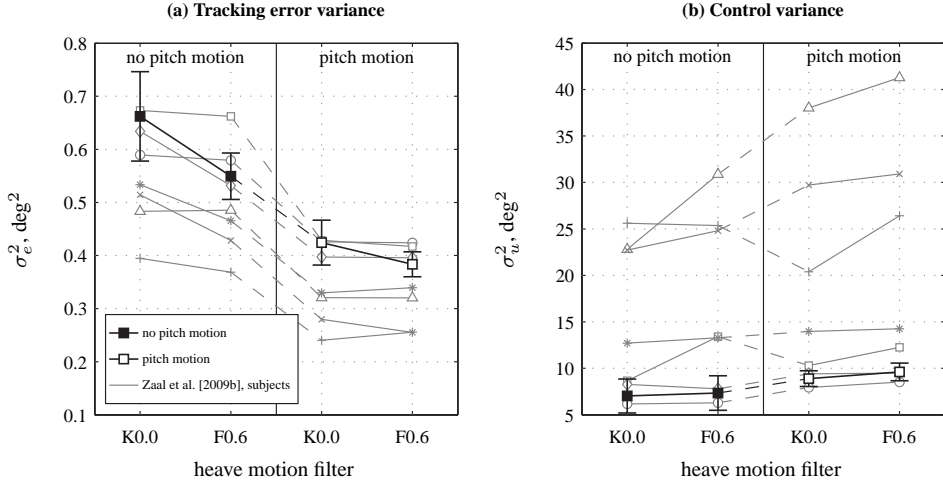


Figure 4.10. Comparison of mean tracking performance and control activity during current experiment with individual subject data from the experiment of Zaal et al. [2009b] for identical motion conditions.

θ , and e as defined in Fig. 4.5. Fig. 4.11 depicts the average crossover frequencies and phase margins that have been determined from $H_{ol,d}(j\omega_d)$ and $H_{ol,t}(j\omega_t)$. The error bars again indicate the 95% confidence intervals of the means for each condition over the seven subjects. Furthermore, for calculation of the 95% confidence intervals, subject means of the data shown in Fig. 4.11 have been corrected, in order to account for between-subject effects. Table 4.4 summarizes the ANOVA results for the crossover data depicted in Fig. 4.11. Data from the experiment described in [Zaal et al., 2009b] are shown in gray for reference. Note again the offset between the data from both experiments, which reflects the influence of the subjects with high-gain control strategies in the gray data.

First of all, note from Fig. 4.11 and Table 4.4 that the presence of pitch motion significantly affects both target and disturbance-loop crossover frequencies and phase margins. A clear increase in $\omega_{c,d}$ of approximately 1 rad/s is observed when pitch motion is made available ($F(1, 6) = 176.15, p < 0.05$), which is accompanied by a significant reduction of disturbance-loop phase margin $\varphi_{m,d}$ ($F(1, 6) = 23.40, p < 0.05$) of around 10 deg. Pitch motion cues are found to induce the opposite changes in the target open-loop response function: a significant decrease in crossover frequency ($F(1, 6) = 40.37, p < 0.05$) and a significant increase in phase margin ($F(1, 6) = 24.49, p < 0.05$) are observed in Figures 4.11(b) and (d), respectively.

The variation in heave motion cues over the different experimental conditions also induced some significant changes in the crossover frequencies and phase margins shown in Fig. 4.11. Table 4.4 indicates that the increase in disturbance crossover frequency with increasing heave motion fidelity observed in Fig. 4.11(a) is statistically significant, $F(4, 24) = 24.52, p < 0.05$. Similar to the effects of pitch motion observed above, a marginally significant decreasing trend in disturbance phase margin ($F(4, 24) = 2.78, p = 0.05$) is also

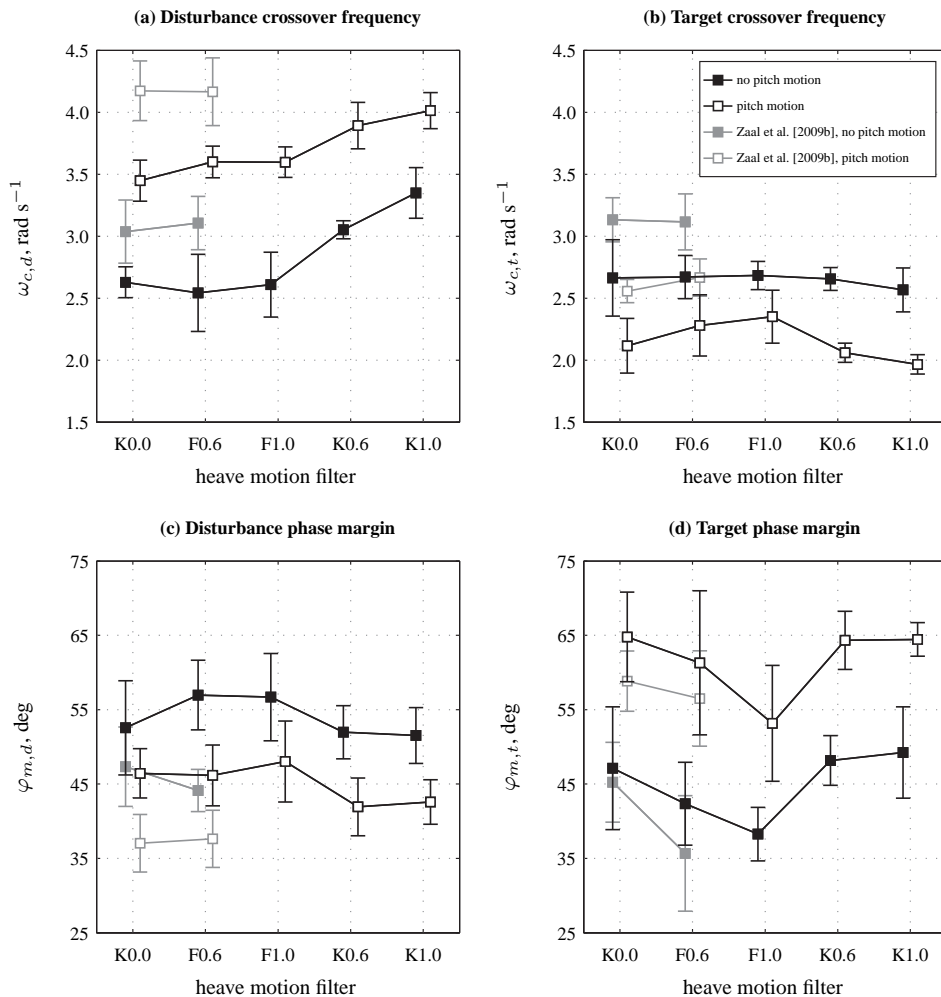


Figure 4.11. Mean disturbance and target loop crossover frequency and phase margin.

Table 4.4. Two-way repeated-measures ANOVA results for crossover data.

Independent variables	Dependent measures											
	$\omega_{c,d}$			$\varphi_{m,d}$			$\omega_{c,t}$			$\varphi_{m,t}$		
Factor	df	F	Sig.	df	F	Sig.	df	F	Sig.	df	F	Sig.
pitch	1,6	176.15	**	1,6	23.40	**	1,6	40.37	**	1,6	24.49	**
heave	4,24	24.52	**	4,24	2.78	*	1,8,10.5 ^{gg}	3.34	*	1,7,10.4 ^{gg}	9.06	**
pitch × heave	4,24	2.44	*	4,24	0.83	—	4,24	1.15	—	4,24	0.40	—

** = highly-significant ($p < 0.05$)

* = significant ($0.05 \leq p < 0.1$)

— = not significant ($p \geq 0.1$)

gg = Greenhouse-Geisser sphericity correction

observed. Note that, compared to the no-heave conditions (K0.0), $\omega_{c,d}$ and $\varphi_{m,d}$ are not significantly different for the washout conditions (F0.6 and F1.0), both with and without pitch motion. Rather, the sharp changes in disturbance crossover frequency and phase margin for the conditions where heave motion without washout was present (K0.6 and K1.0), are the cause of the significant main effects listed in Table 4.4.

The target-loop crossover frequency is found to be significantly less affected by varying levels of heave motion fidelity than $\omega_{c,d}$. A slight decreasing trend is observed with increasing heave fidelity, mainly for the conditions where pitch motion was available in addition to unfiltered heave, but this effect is only marginally significant, $F(1.8, 10.5) = 3.34$, $p = 0.08$. The target phase margin is seen to decrease when filtered heave motion cues are made available (K0.6) and reduces even further when the filter gain is increased to unity (K1.0). For the conditions where heave motion was presented without washout, $\varphi_{m,t}$ is seen to increase again to roughly the same level as when no heave motion was available. As can be verified from Table 4.4, this is a highly significant effect, $F(1.7, 10.4) = 9.06$, $p < 0.05$.

As is clearly visible from Fig. 4.11, the trends in target and disturbance loop crossover frequency and phase margin observed for the different levels of heave motion fidelity appear to be independent of the availability of additional pitch motion. This observation is supported by the ANOVA results listed in Table 4.4, as the interaction of pitch and heave shows no significant effects on any of the crossover parameters. For the disturbance crossover frequency, this interaction is close to statistically significant ($F(4, 24) = 2.44$, $p = 0.074$), however, which can be explained by the fact that the increase in $\omega_{c,d}$ with heave motion fidelity appears slightly larger when pitch motion is not available.

Finally, note that all main trends in target and disturbance-loop crossover frequency and phase margin with the addition of pitch and heave motion cues as shown in Fig. 4.11 – that is, an overall increase in $\omega_{c,d}$ and $\varphi_{m,t}$ and a corresponding decrease in $\omega_{c,t}$ and $\varphi_{m,d}$ – are highly similar to findings from other experiments [Hosman, 1996; Van der Vaart, 1992; Zaal et al., 2009b,c; Pool et al., 2008b].

4.4.3 Pilot Modeling Results

The marked variation in crossover frequencies and phase margins described in Section 4.4.2 hints at significant changes in pilot control behavior over the different motion conditions. To quantify these possible shifts in pilot control strategy, a multimodal pilot model has been fit to the measurement data using a time-domain maximum likelihood estimation technique [Zaal et al., 2009a].

4.4.3.1 Pilot Model Validation

The use of the generic model given by Equations (4.9) and (4.10) for describing pilots' responses to pitch and heave motion cues is a simplification compared to physical models as the one defined by Eq. (4.7). Fig. 4.12 shows average pilot model frequency responses that were estimated for the condition with only pitch motion (pitch motion, K0.0) for both the physical and generic pilot motion response models. The visual response model was that of Eq. (4.5) for both model fits. In addition to these model frequency responses, pilot

describing functions calculated using a Fourier coefficients estimation method [Stapleford et al., 1969; Van Paassen and Mulder, 1998] are shown for reference.

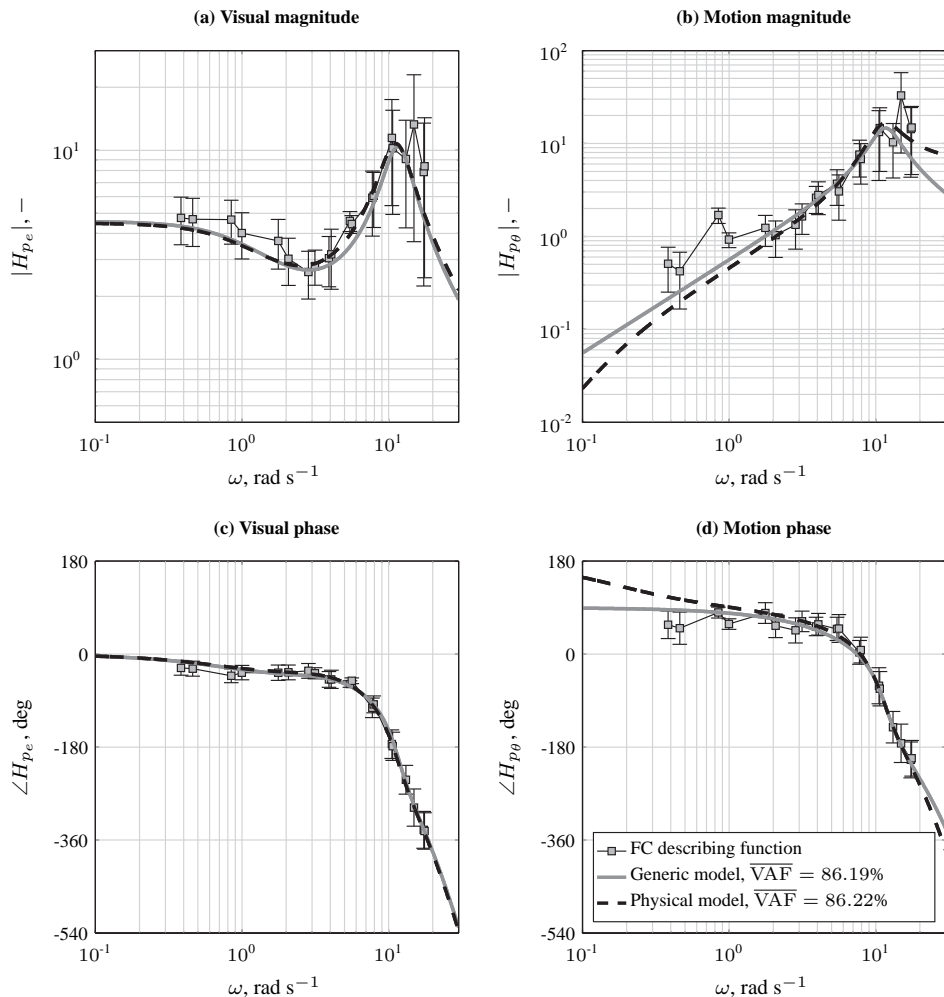


Figure 4.12. Comparison of generic and physical pilot model fits for the condition with pitch and K0.0 heave motion.

Fig. 4.12 shows that the generic pilot model provides a fit to the measurement data that is highly comparable to the fit of the physical model. The difference in VAF for both models is less than 0.1%. The VAF is a measure often used in system identification for indicating the percentage of the variance in the measured model output signal that can be explained by the model [Nieuwenhuizen et al., 2008]. This small difference in VAF for both models depicted in Fig. 4.12 indicates that they perform equally well in describing the measured pilot control signal for the condition with only pitch motion. For modeling pilot heave motion responses

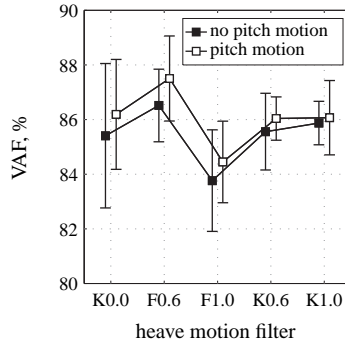


Figure 4.13. Mean pilot model variance accounted for (VAF).

similar negligible differences were found between using a physical model, which included otolith dynamics, and the generic model of Eq. (4.10).

To further illustrate the accuracy of the pilot modeling approach adopted in this paper, Fig. 4.13 depicts the mean pilot model variance accounted for, for all conditions of the experiment. Fig. 4.13 shows that the linear part of the pilot model is able to describe around 86% of the variance in the control signal u , and therefore provides an accurate fit, for all conditions. The slightly decreased VAF found for the conditions with the unity gain washout filter (F1.0) suggests slightly decreased linearity of pilot control behavior for this condition. This may have been caused by the high gain on the filtered heave cues in this condition, which made the desired heave motion but also the false cues generated by the washout more perceivable.

4.4.3.2 Pilot Model Parameter Estimates

Fig. 4.14 depicts the mean pilot-model parameter estimates for all ten conditions of the experiment. The error bars indicate the 95% confidence intervals of the means taken over all seven participants of the experiment. The repeated-measures ANOVA results are given in Tables 4.5 to 4.7. Note that the two-way repeated-measures ANOVA used to analyze all other dependent measures could not be performed for the pilot model motion gain K_m and time delay τ_m , because these parameters are not available for the no motion condition. For these two parameters, a one-way repeated-measures ANOVA was performed instead, with a single factor (“motion”) that had nine levels, see Table 4.7.

Fig. 4.14(a) shows that the pilot visual gain K_v was found to increase both when pitch motion was made available and with increasing level of heave fidelity. As can be verified from Table 4.5, both these effects were found to be statistically significant: $F(1, 6) = 14.60$, $p < 0.05$ and $F(4, 24) = 6.89$, $p < 0.05$, respectively. In addition, Fig. 4.14(a) clearly shows reduced effect of heave fidelity on K_v if pitch motion is also present. This interaction between pitch and heave motion was also found to be significant: $F(4, 24) = 3.24$, $p = 0.029$.

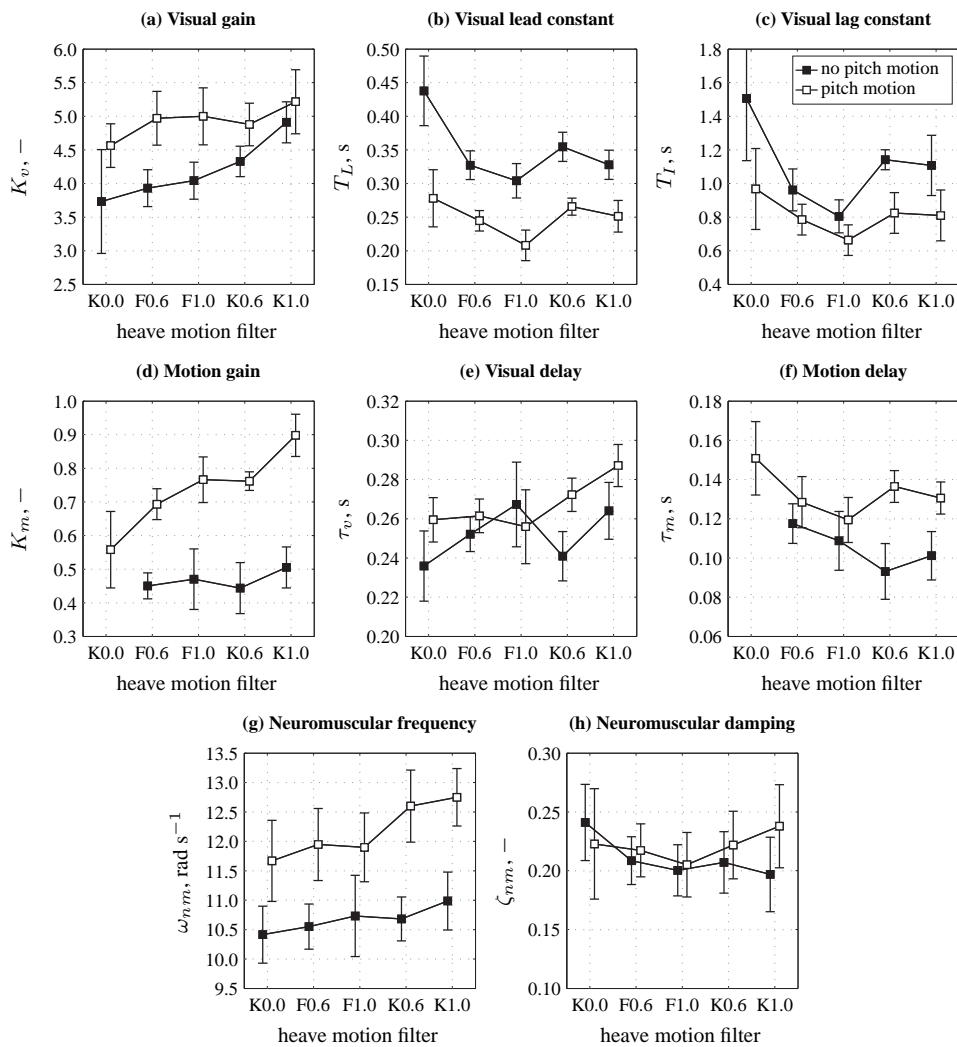


Figure 4.14. Mean pilot model parameters.

Table 4.5. Two-way repeated-measures ANOVA results for visual channel model parameters.

Independent variables	Dependent measures											
	K_v			T_L			T_I			τ_v		
Factor	df	F	Sig.	df	F	Sig.	df	F	Sig.	df	F	Sig.
pitch	1,6	14.60	**	1,6	51.10	**	1,6	17.26	**	1,6	10.43	**
heave	4,24	6.89	**	4,24	29.21	**	1,2,7,2 ^{gg}	11.24	**	4,24	5.73	**
pitch × heave	4,24	3.24	**	4,24	5.12	**	4,24	3.26	*	4,24	4.45	**

Table 4.6. Two-way repeated-measures ANOVA results for neuromuscular system model parameters.

Independent variables	Dependent measures					
	ω_{nm}			ζ_{nm}		
Factor	df	F	Sig.	df	F	Sig.
pitch	1,6	22.01	**	1,6	0.37	—
heave	1,6,9,6 ^{gg}	5.04	**	1,4,8,7	1.72	—
pitch × heave	4,24	2.67	*	4,24	2.99	*

Table 4.7. One-way repeated-measures ANOVA results for motion channel model parameters.

Independent variables	Dependent measures					
	K_m			τ_m		
Factor	df	F	Sig.	df	F	Sig.
motion	8,48	30.88	**	8,48	10.69	**

** = highly-significant ($p < 0.05$) gg = Greenhouse-Geisser sphericity correction
 * = significant ($0.05 \leq p < 0.1$)
 — = not significant ($p \geq 0.1$)

The pilot visual lead and lag time constants (see Figures 4.14(b) and (c)) show highly similar trends over the different conditions of the experiment. Such apparent coupling between T_L and T_I has also been observed in the experiment of Zaal et al. [2009b]. The visual lead time constant is found to decrease significantly if pitch motion cues are available, $F(1, 6) = 51.01$, $p < 0.05$. A generally decreasing trend in T_L is also visible with increasing heave fidelity, which is also found to be highly significant: $F(4, 24) = 29.21$, $p < 0.05$. Finally, also a statistical significant interaction was found for T_L ($F(4, 24) = 5.11$, $p < 0.05$), which is caused by the comparatively high value of the visual lead constant for the no motion condition. The effects of pitch and heave motion on the lag time constant T_I were found to be similar to those found for T_L , but slightly less statistically significant (see Table 4.5). A high-pass motion filter as defined by Eq. (4.2) introduces some phase lead on the supplied heave accelerations, (see Fig. 4.2). Figures 4.14(b) and (c) clearly show that the visual lead and lag constants are found to be markedly lower for the conditions with heave washout, that is F0.6 and F1.0, than for the equivalent conditions without washout (K0.6 and K1.0). This marked decrease in the amount of visual lead pilots generated for conditions F0.6 and F1.0 seems to indicate that the presence of a high-pass washout filter reduces the amount of visual lead compensation required from pilots for stable attitude control, and thereby clearly affects their adopted control strategy.

The identified values for the pilot motion gain shown in Fig. 4.14(d) show an increase in K_m when pitch motion is made available. In addition, K_m is found to increase further with increasing heave fidelity when pitch motion is also available. These two trends are responsible for the statistically significant effect of the supplied motion on the pilot motion gain shown in Table 4.7, $F(8, 48) = 30.88$, $p < 0.05$. Post-hoc analysis indeed revealed that no significant differences in K_m were present for the conditions without pitch motion (black data in Fig. 4.14(d)).

Despite the fact that changes in both pilot model time delays appear to be relatively modest from Figures 4.14(e) and (f), the ANOVAs performed on the values found for both parameters revealed the changes are significant effects (see Tables 4.5 and 4.7, respectively). Both delays are found to be slightly higher for the conditions where pitch motion was available. In addition, a decreasing trend in τ_m with increasing heave fidelity can be observed from Fig. 4.14(f).

The final two pilot model parameters shown in Fig. 4.14 are the neuromuscular system eigenfrequency ω_{nm} and damping factor ζ_{nm} . The neuromuscular frequency is found to increase both with the addition of pitch motion and with increasing heave fidelity. Despite the relatively large error bars shown in Fig. 4.14(g), both these effects were statistically significant: $F(1, 6) = 22.01$, $p = 0.003$ and $F(1.60, 9.59) = 5.04$, $p = 0.037$ for pitch and heave, respectively. Such increases in ω_{nm} with increasing motion strength have also been reported for other experiments [Pool et al., 2008b; Zaal et al., 2009b]. As can be judged from Table 4.6, no significant main effects were found for the neuromuscular system damping factor ζ_{nm} .

4.5 Discussion

Seven subjects participated in an experiment investigating the effects of heave washout settings on pilot performance and control behavior in a pitch attitude disturbance-rejection task. The effect of heave motion fidelity was investigated by independently adjusting the gain and break frequency of a third-order linear washout filter. All heave motion conditions were performed with and without additional rotational pitch motion. The current experiment has shown that the relatively small impact of pitch-heave on pilot control behavior, compared to rotational pitch motion, found in a previous experiment performed by Zaal et al. [2009b] was a result of the heave washout filter used in that study. Here, almost equal performance and pilot control behavior were observed for the conditions with only rotational pitch and only one-to-one pitch-heave motion, as expected from the linear relation between both motion cues.

Pilot performance and control activity are found to be significantly reduced if the heave motion is attenuated using a washout filter. If rotational pitch motion is available, the reduction is markedly smaller. The presence of washout is seen to degrade performance and control activity more than pure gain attenuation. In addition, the control strategy of the pilot is found to be significantly affected when heave motion is attenuated, as seen by a change in disturbance and target crossover frequencies and phase margins. The disturbance crossover frequency is significantly increased when the fidelity of the heave motion is increased.

This change in control strategy is also reflected by significant changes in the identified pilot model parameters. With increasing heave motion fidelity, the visual and motion perception gains of the pilot model are seen to increase, while the visual lead decreases. The increase in motion perception gain and the decrease in visual lead constant observed for conditions with increased heave motion fidelity indicate that pilots will clearly prefer the availability of lead information from these heave motion cues. Additionally, by increasing heave motion fidelity, the visual and physical motion perception time delays increase and decrease, respectively. This is further evidence of an increase in the usefulness of the motion cues when the fidelity is increased. Crossover frequencies, phase margins, and pilot model parameters show similar trends with and without additional pitch motion.

The conditions with washout on the supplied heave motion (F0.6 and F1.0) show some interesting results for the pilot visual lead in addition to the observed global trends. The visual lead for these conditions is lower compared to the conditions where the heave motion is attenuated with only a gain. This could be explained by the fact that extra lead information is present due to the high-pass washout filter characteristics, as can be seen in Fig. 4.2. The extra lead that results from the presence of washout reduces the need for the pilot to perform lead equalization, allowing the visual lead constant to be reduced. However, this effect on the generated visual lead does not seem to affect the remaining dependent measures.

Overall, it can be concluded that all attenuation of the heave motion as considered in this experiment resulted in changes in pilot control behavior. Even a reduction in heave motion gain to a value of 0.6, which is still stated to be quite acceptable in some publications, already shows significant degradation of tracking performance, pilot crossover frequency, and the contribution of motion feedback to pilot control behavior, as indicated by a reduction in the pilot model motion perception gain. The effect of the phase attenuation caused by the addition of heave washout is clearly seen to further increase this discrepancy in pilot con-

rol behavior with respect to the condition with one-to-one heave motion. Though lower in magnitude, these effects of heave motion fidelity are still observable even when additional one-to-one pitch motion cues are available. As, within the limitations of the current experiment, the condition where both pitch and pitch-heave motion were presented one-to-one is arguably the most representative of real flight, these findings suggest that it is highly preferable to present motion cues that pilots might rely on in continuous aircraft control tasks at the highest achievable level of motion fidelity.

Only part of the total vertical aircraft motion that occurs during pitch maneuvering was, however, considered in the current study. Heave motion originating from movement of the aircraft center of gravity was not simulated in the current experiment, as it can not be represented one-to-one. Based on the findings of Zaal et al. [2009b], center of gravity heave is hypothesized to act as a disturbance on the remaining motion components during pitch control and could therefore degrade pilot tracking performance compared to the condition with one-to-one rotational pitch and pitch-heave motion. In that experiment, a non-significant decrease in performance was observed with the addition of filtered c.g. heave motion, in addition to a surprising increase in the amount of lead pilots generated visually, that is, opposite effects to those found for pitch and pitch-heave motion. The addition of this c.g. heave could therefore result in different results on the effects of pitch-heave and rotational pitch motion on pilot performance and control behavior as described in this paper. Future experiments, in which pilot control behavior for tracking tasks similar to the one described here will be compared in real flight and in the simulator, are expected to show how the effects of simulator washout measured in the current experiment compare to true in-flight pilot control behavior.

The pilot model used in the present study contains a generic motion perception channel with only a lead term. This motion perception channel is applied for modeling both the perception of heave and rotational pitch motion, as both are shown to effectively yield additional pilot lead. In the case of heave motion, only a factor is added to compensate for the distance between the center of gravity and the pilot station. The proposed model proved to be accurate in replicating the measured time-domain data, as is indicated by the high VAF for all conditions. Furthermore, due to the difficulty in separating pilot responses to the proprioceptive, somatosensory, and vestibular stimuli that result from physical motion cueing, the physical pilot models described in literature often attribute the total pilot motion response to the dominant motion sensor, that is, the vestibular system for rotational motion. Alternatively, the generic model used in this study lumps all separate contributions together in a single generic model structure, which may be a preferred approach in future experiments on pilot modeling.

The current study was performed for a Cessna Citation I aircraft, which has a relatively small distance of 3.2 m between the center of gravity and the pilot station, while for typical airliners this distance can be more than ten times larger. This also yields a much higher magnitude of the pitch-heave component for an airliner, compared to the small aircraft used in this experiment. In some dependent measures, such as pilot performance, the trend in the data as a result of the heave motion attenuation was reduced when rotational pitch motion was present. This may suggest that rotational pitch motion is more dominant than pitch-heave motion if both are present. If the pitch-heave motion is larger in magnitude compared to the current experiment, however, the trend as a result of the pitch-heave attenuation could

also be more pronounced when rotational pitch motion is present. This topic may be covered in future research.

4.6 Conclusions

An experiment was performed to investigate how pilot performance and control behavior in an aircraft pitch control task are affected by attenuation of the associated heave motion by a high-pass washout filter. When both are presented one-to-one, the effects of pitch and heave motion on pilot control behavior were found to be highly similar. Pilot performance and control activity are found to be significantly reduced, however, when the heave motion is filtered or only attenuated with a gain. This reduction is smaller in magnitude if rotational pitch motion is available in addition to the heave motion. The additional phase attenuation caused by the third-order heave washout filter is found to affect tracking performance and pilot control behavior more than pure gain attenuation. The changes in crossover frequencies, phase margins, and the estimated pilot model parameters show that if the fidelity of the heave motion is increased, pilots will rely more on these motion cues to improve their task performance. This is mainly reflected by an increase in visual and motion perception gains, and a decrease in pilot visual lead.

5

Effects of Motion Filter Settings on Tracking Behavior

A number of studies predating the work described in this thesis have been performed into the effects of high-pass motion filter settings on pilot tracking behavior. In some of these studies, these effects were measured for manual control tasks similar to those considered in this thesis using comparable methods and compatible behavioral metrics. This chapter describes an effort to combine the measured results of some of these individual experiments and to identify consistent trends in typical metrics that are considered for the evaluation of changes in pilot tracking behavior: estimated pilot model parameters, pilot-vehicle system crossover frequencies and phase margins, and measures of tracking performance and control activity. Data from a number of studies available in literature at the time of writing of this chapter, which include those of the experiments described in Chapters 4 and 6, are included in this compilation effort. Furthermore, from this compiled data an attempt is made to develop a set of equations that capture the observed trends in the data and can be used to predict changes in the considered behavioral metrics based on parameters that define the high-pass motion filter settings. The prediction equations derived in this chapter are evaluated in Chapter 8 by comparing their results with behavioral measurements for a roll tracking task for which a large number of different motion filter settings were tested.

The contents of this chapter are to be published as:

Pool, D.M., Damveld, H.J., Van Paassen, M.M., and Mulder, M., "Prediction of Behavioral Pilot Model Parameters for Given Motion Filter Settings", *Journal of Guidance, Control, and Dynamics*.

5.1 Introduction

Much of our current knowledge on human manual control behavior has come from the considerable database of behavioral measurements that have been collected for single-loop compensatory tracking tasks [McRuer et al., 1965]. Using this extensive database, it has been shown that single-loop pilot tracking behavior during compensatory tracking tasks can be modeled at high accuracy using quasi-linear pilot models [McRuer et al., 1965; McRuer and Jex, 1967a]. The fitting of such quasi-linear pilot models to measurements of pilot tracking behavior has allowed for a quantitative evaluation of changes in pilot dynamics due to a number of different factors, thereby increasing our understanding of human operation during manual control. Furthermore, rules have been developed that allow for intuitive tuning of such single-loop models of pilot tracking behavior to the defining features of the considered control task, such as the dynamics of the controlled element and the characteristics of the applied forcing function signals [McRuer et al., 1965; McRuer and Jex, 1967a]. This set of rules thereby allows for prediction of pilot control behavior during tracking for certain combinations of controlled elements and forcing function signals without having to resort to experimental evaluation of pilot control behavior and has shown its merit in various areas of human-machine interaction research.

The presence of physical motion feedback of the controlled element state has been shown to yield pilot control behavior during compensatory control tasks that is markedly different from that observed for single-loop tasks where motion feedback is not available [Shirley and Young, 1968; Jex et al., 1978]. To the question to what extent, and exactly how, pilot tracking behavior is affected by the application of simulator motion cueing strategies as commonly adopted in full-motion flight simulation, however, no satisfactory answer has yet been found [Schroeder and Grant, 2010; Grant and Schroeder, 2010]. To answer this question, and to allow for the prediction of changes in pilot behavior due to a selected simulator motion cueing strategy, a set of rough tuning rules for incorporating the approximate effects of cueing settings on pilot behavior into pilot models – preferably validated through extensive experimental measurements – would be a valuable tool. Unfortunately, largely due to the complexity of human perceptual processes and manual control behavior in multimodal environments, such a standardized set of rules for pilot model tuning that includes the effects of the supplied physical motion cues does not exist yet.

The research described in this thesis attempts to contribute to solving this problem by tracing observed changes in measured pilot tracking behavior during tracking tasks with physical motion feedback back to the selected flight simulator motion cueing settings. The final objective of this study is to use these measurements of pilot behavior, and a comparison with measurements of true in-flight tracking behavior, to define a behavioral flight simulator motion fidelity criterion. Given a certain control task or maneuver, this criterion is meant to allow for selecting a flight simulator motion cueing setting that will yield pilot behavior that is as close to that observed in real flight as possible. Despite not being representative for all aspects of aircraft control, compensatory tracking tasks where physical motion feedback is available in addition to visual error information are used in this study to evaluate the underlying multimodal motion perception and integration processes that are important during manual aircraft control. Similar to the single-loop case studied by McRuer et al. [1965], these multimodal tracking tasks have been shown to allow for the modeling, and thereby the

explicit quantification, of changes in pilot control strategy by using quasi-linear multimodal pilot models [Stapleford et al., 1969; Jex et al., 1978].

This chapter provides the results of an effort to compile data from a number of experiments from which measurements of multimodal pilot behavior under varying motion cueing conditions are available. Data have been collected from a number of investigations performed at Delft University of Technology – [Steurs et al., 2004; De Vroome et al., 2009; Van Wieringen et al., 2011] and the experiments described in Chapters 4 and 6 – and from a number of studies found in literature [Stapleford et al., 1969; Bergeron, 1970; Jex et al., 1978; Van Gool, 1978; Bray, 1985]. This chapter provides a short overview of the scope and setup of all these different experiments. The main objective of this chapter, however, is to use the total set of collected data to identify consistent trends in typical dependent measures of pilot control strategy and the parameters that define the applied motion cueing setting. The main dependent measures by which the effect of simulator motion cueing on pilot tracking behavior are evaluated in this chapter are:

1. tracking performance and control activity
2. pilot-vehicle system crossover frequencies and phase margins
3. identified multimodal pilot model parameters

A relation is sought between these different dependent measures of pilot tracking behavior and typical metrics that quantify the level of simulator motion attenuation by the motion filter. Examples of metrics that are considered are the motion filter parameters (gain, break frequency) and motion filter gain and phase distortion at a certain frequency, for example, the 1 rad/s evaluation frequency proposed by Sinacori [1977]. A rudimentary set of pilot model tuning rules will be obtained by fitting a linear regression through combinations of dependent measures and motion fidelity metrics for which a clear correlation is present.

5.2 Background

5.2.1 Simulator Motion Fidelity

Due to severe limitations on the motion capabilities of flight simulators, motion washout algorithms are required for attenuating and limiting the simulated aircraft motion. A large diversity in washout algorithms has been developed over the years [Schmidt and Conrad, 1970; Reid and Nahon, 1985; Telban et al., 2000]. One of the biggest challenges, however, has been finding an appropriate criterion for the evaluation of simulator motion cueing fidelity and defining the minimum requirements for simulator motion cueing for pilot training and other flight simulator applications.

One of the first efforts to define a structured and practical methodology for the assessment of simulator motion fidelity was the work of Sinacori [1977], who proposed a motion fidelity criterion based on the combination of motion filter gain and phase distortion introduced by motion filters at a frequency of 1 rad/s. This frequency, though still the topic of much debate, was selected as much of the activity during manual aircraft control was thought to be centered around this frequency range. The criterion proposed by Sinacori was

later modified and validated by Schroeder [1999] using subjective motion fidelity assessments for various helicopter tasks.

Hess et al. [1993] defined a more analytical methodology for evaluating simulator motion fidelity from the effect of a motion filter on the dynamics of the combined simulator, aircraft, and pilot system in a flight simulator. For a helicopter lateral translational maneuver, Hess et al. showed that their chosen criterion was indeed sensitive to variations in motion cueing fidelity. Hess and Marchesi [2009] later showed this analytical method to also be applicable to other types of aircraft and maneuvers.

The most recent effort into the formulation of a standard for the assessment of flight simulator motion fidelity is the work of Advani and Hosman [2006]. Their proposed motion fidelity criterion, which is currently being included in the ICAO 9625 manual for the qualification of flight simulator devices [Anonymous, 2009], considers the dynamics of the simulator motion hardware in addition to those of the motion cueing algorithm, and evaluates the total motion cueing dynamics over a frequency range that is thought to be important for manual aircraft control.

The work described in this thesis is part of a research effort that attempts to develop a framework for assessing simulator motion fidelity from measurements of pilot control behavior. By measuring changes in pilot control behavior that result from applied changes in simulator motion cueing it is hoped that some experimental validation of the criteria proposed for evaluating simulator motion fidelity can be provided.

5.2.2 Pilot Tracking Behavior

Fig. 5.1 shows a generalized and extensive schematic representation of a closed-loop aircraft manual tracking task performed in a flight simulator environment, which is valid for the tracking tasks performed in all of the studies into the effects of motion filter dynamics on pilot behavior considered in this chapter. The target and disturbance forcing function signals that induce pilot tracking behavior and thereby define the type of tracking task under consideration (target following, disturbance rejection, or the combination of both) are depicted in Fig. 5.1 with the symbols f_t and f_d , respectively. As can be verified from Fig. 5.1, a distinction is made between simulator, pilot, and controlled element dynamics. Simulator dynamics include the characteristics of the simulator visual and simulator motion cueing systems ($H_{sv}(s)$ and $H_{sm}(s)$, respectively), in addition to the dynamics of the applied motion filter which are indicated by the $H_{mf}(s)$ block.

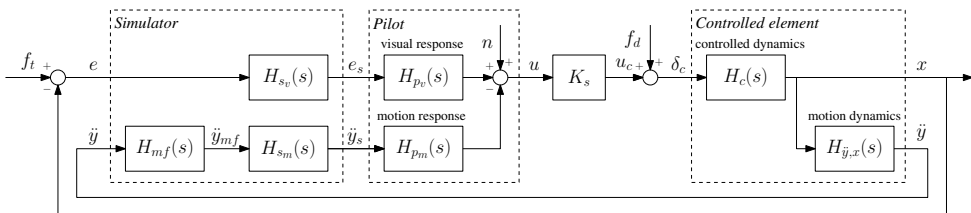


Figure 5.1. Schematic representation of a compensatory tracking task with motion feedback.

As can be verified from Fig. 5.1, this study considers control tasks for which pilot control behavior can be represented as the sum of two parallel responses to visual and motion information [Stapleford et al., 1969]. The pilot visual response $H_{p_v}(s)$ captures pilots' control dynamics in response to presented tracking errors e_s , while the pilot motion response $H_{p_m}(s)$ models pilots' responses to cued motion information \ddot{y}_s . The remnant n , which accounts for the portion of the pilot control input u that is not correlated with the forcing function signals – resulting, among others, from pilot-injected noise and nonlinear and non-steady control operations [McRuer and Jex, 1967a] – completes this quasi-linear model of pilot tracking behavior.

The controlled element dynamics are defined to consist of two separate parts: the controlled dynamics and the motion dynamics. The former, $H_c(s)$, are the dynamics that drive the vehicle state that is controlled by the pilot, x . The motion dynamics $H_{\dot{y},x}(s)$ define the transformation from the controlled state x to the variable that enters the pilot's motion response channel $H_{p_m}(s)$. When $H_{p_m}(s)$ captures pilots' responses to angular or translational cues perceived through the vestibular system (through the semicircular canals or otoliths, respectively)[Hosman, 1996] – as is the case for most control tasks considered in this chapter – motion cueing provides pilots with feedback of the acceleration of the controlled element state, so $H_{\dot{y},x}(s) = s^2$. However, more extensive transformations between controlled state and motion feedback quantities exist in some studies, for instance for the aircraft pitch control tasks with variation in the coupled heave motion cueing considered in Chapter 4 and [Zaal et al., 2009b]. Finally, the gain K_s accounts for the scaling of pilot control inputs, such as results from a control input to control surface deflection gearing ratio, that is present in some of the considered studies.

5.2.3 Motion Fidelity and Tracking Behavior

As can be verified from Fig. 5.1, the closed-loop pilot-vehicle system dynamics in a closed-loop control task will be affected by the presence of a motion filter. For instance, the following relations can be derived from Fig. 5.1 for the disturbance and target open-loop responses, whose crossover frequencies and phase margins can be used for assessing closed-loop pilot-vehicle system performance and stability for disturbance rejection and target-following, respectively [Jex et al., 1978]:

$$\begin{aligned} H_{ol,d}(s) &= -\frac{U_c(s)}{\delta_c(s)} \\ &= [H_{s_v}(s)H_{p_v}(s) + H_{\dot{y},x}(s)H_{mf}(s)H_{s_m}(s)H_{p_m}(s)] K_s H_c(s) \end{aligned} \quad (5.1)$$

$$H_{ol,t}(s) = \frac{X(s)}{E(s)} = \frac{H_{s_v}(s)H_{p_v}(s)K_s H_c(s)}{1 + H_{\dot{y},x}(s)H_{mf}(s)H_{s_m}(s)H_{p_m}(s)K_s H_c(s)} \quad (5.2)$$

Similarly, the corresponding closed-loop forcing function to error responses, which are indicative of the success of the closed-loop system depicted in Fig. 5.1 in attenuating f_d and following f_t , are given by:

$$\begin{aligned}
H_{e,fd}(s) &= \frac{E(s)}{F_d(s)} \\
&= \frac{-H_c(s)}{1 + [H_{s_v}(s)H_{p_v}(s) + H_{\ddot{y},x}(s)H_{mf}(s)H_{s_m}(s)H_{p_m}(s)] K_s H_c(s)}
\end{aligned} \tag{5.3}$$

$$\begin{aligned}
H_{e,ft}(s) &= \frac{E(s)}{F_t(s)} \\
&= \frac{1 + H_{\ddot{y},x}(s)H_{mf}(s)H_{s_m}(s)H_{p_m}(s)K_s H_c(s)}{1 + [H_{s_v}(s)H_{p_v}(s) + H_{\ddot{y},x}(s)H_{mf}(s)H_{s_m}(s)H_{p_m}(s)] K_s H_c(s)}
\end{aligned} \tag{5.4}$$

First of all, Equations (5.1) to (5.4) indicate that the effect of the motion filter dynamics $H_{mf}(s)$ on these open-loop and closed-loop relations depends on the dynamics of all other elements shown in Fig. 5.1. In addition, compared to the case where no motion filter is present ($H_{mf}(s) = 1$), pilots may adapt their control dynamics in response to a motion filter with certain dynamics being introduced to (partially) compensate for the effect the motion filter dynamics have on the closed-loop system. The most elementary example that can be given is the case where motion cues are attenuated by a pure gain, $H_{mf}(s) = K$. As long as the gain does not cause the motion cues to become smaller than human motion perception thresholds [De Vroome et al., 2009], pilots could simply respond to the lower magnitude motion information (\ddot{y}_s) with a higher gain. If they succeed in increasing the gain of $H_{p_m}(s)$ with approximately $1/K$, this means the governing open-loop and closed-loop dynamics remain approximately the same, as can be verified from Eqs. (5.1) to (5.4).

Much like the work of Hess et al. [1993], this project is concerned with the effects of the presence of a motion filter on the dynamics of the closed-loop pilot-vehicle system as depicted in Fig. 5.1. However, unlike previous work on this topic, the focus is on investigating how changes in these closed-loop dynamics resulting from the presence of such a motion filter might induce changes in pilot control behavior and to obtain quantitative measurements of these changes in pilot behavior from human-in-the-loop evaluations.

5.3 Method

5.3.1 Selection Criteria: Dependent Measures

A large number of studies have been dedicated to the evaluation of the effects of simulator motion cueing on pilot performance, motion perception, and control behavior. An excellent recent overview of a large number of these studies is given by Schroeder and Grant [2010]. For the current chapter, only a specific subset of the large body of literature on the effects of motion filters is of interest due to the focus on measured changes in pilot behavior. The main requirement for a study to be included in this overview is that it should provide data for some behavioral metric measured over a number of different motion cueing conditions, most preferably in terms of explicit measurements of pilots' control dynamics. The pilot visual and motion responses – $H_{p_v}(j\omega)$ and $H_{p_m}(j\omega)$, respectively – accounted for in Fig. 5.1

are typically modeled with linear models that can be deduced from or are equivalent to the equations given by:

$$H_{p_v}(j\omega) = K_v \frac{(1 + T_L j\omega)^2}{1 + T_I j\omega} e^{-j\omega\tau_v} H_{nm}(j\omega) \quad (5.5)$$

$$H_{p_m}(j\omega) = K_m H_m(j\omega) e^{-j\omega\tau_m} H_{nm}(j\omega) \quad (5.6)$$

$$H_{nm}(j\omega) = \frac{1}{\left(\frac{j\omega}{\omega_{nm}}\right)^2 + \frac{2\zeta_{nm}}{\omega_{nm}} j\omega + 1} \quad (5.7)$$

Eq. (5.5) defines the most elaborate form of the modeled pilot response to visual cues considered in this study, consisting of a pure gain, a lead-lag equalization element, a pure delay term, and the low-pass neuromuscular actuation dynamics model given by Eq. (5.7). As detailed in Chapter 2, the full lead-lag equalization element shown Eq. (5.5) is required for capturing pilot dynamics during control of certain conventional aircraft pitch dynamics, but may, for instance, be reduced to a pure first-order lead or a pure gain for controlled elements that have approximately double or single integrator dynamics in the crossover region, respectively [McRuer et al., 1965].

For modeling of pilots' responses to motion information, typically models of the form of Eq. (5.6) are adopted. Similar to the model for the pilot visual response, these models also include pure gain and pure delay terms and the same neuromuscular actuation model. In addition, Eq. (5.6) includes the further unspecified $H_m(j\omega)$ term, which represents further possible contributions to the pilot motion dynamics $H_{p_m}(j\omega)$ such as (vestibular) sensory dynamics and possible equalization dynamics, similar to the lead-lag element in Eq. (5.5). In this chapter, analysis of pilot tracking behavior is limited to relative changes in the measurements of the pilot motion gain K_m and delay τ_m . For this reason, the remaining dynamics of pilots' motion responses as modeled in Eq. (5.6) by $H_m(j\omega)$ are not further considered.

Table 5.1 lists the full set of dependent measures selected for the overview of motion filter effects provided by this chapter. In addition to the parameters of the considered behavioral models of pilot behavior listed in the final column of Table 5.1, two additional groups of dependent measures are considered: performance measures and pilot-vehicle system crossover characteristics. In many studies into the effects of motion cueing on pilot behavior, performance measures such as the variance of the recorded tracking error and control signals are considered as dependent measures, as these metrics are often found to signal underlying changes in pilot behavior. Similarly, pilot-vehicle system crossover parameters reveal how possible changes in pilot behavior affect the dominant characteristics of the combined open-loop pilot-vehicle system in the important frequency range around gain crossover [McRuer et al., 1965]. Note that due to the different open-loop response definition for target-following and disturbance-rejection tasks [Jex et al., 1978], see Equations (5.1) and (5.2), crossover frequencies and phase margins for both target-following and disturbance-rejection loops are separated.

Table 5.1. Considered dependent measures.

Category	Symbol	Definition
<i>Performance Measures</i>	σ_e^2	Tracking error variance
	σ_u^2	Control input variance
<i>Crossover Characteristics</i>	$\omega_{c,d}$	Disturbance crossover frequency
	$\omega_{c,t}$	Target crossover frequency
	$\varphi_{m,d}$	Disturbance phase margin
	$\varphi_{m,t}$	Target phase margin
<i>Behavioral Parameters</i>	K_v	Pilot visual (error) gain
	T_L	Pilot visual lead time constant
	T_I	Pilot visual lag time constant
	K_m	Pilot motion gain
	τ_v	Pilot visual delay
	τ_m	Pilot motion delay
	ω_{nm}	Neuromuscular system natural frequency
	ζ_{nm}	Neuromuscular system damping ratio

5.3.2 Predictors: Motion Fidelity Measures

For attenuating the simulated aircraft motion and for washing out flight simulator motion typically a combination of gain attenuation and high-pass filtering is adopted in flight simulation [Schmidt and Conrad, 1970]. Due to the fact that the required amount of attenuating and filtering is highly dependent on the vehicle, maneuver, simulator axis, and perhaps even the pilot who is executing the maneuver, there is quite some variation in the dynamics of the adopted washout filter dynamics ($H_{mf}(j\omega)$ in Fig. 5.1). For the studies considered in this chapter, washout dynamics vary from zeroth order (pure gain) to third-order high-pass filters:

$$\text{zeroth order: } H_{mf}(s) = K \quad (5.8)$$

$$\text{first order: } H_{mf}(s) = K \frac{s}{s + \omega_n} \quad (5.9)$$

$$\text{second order: } H_{mf}(s) = K \frac{s^2}{s^2 + 2\zeta_n\omega_n s + \omega_n^2} \quad (5.10)$$

$$\text{third order: } H_{mf}(s) = K \frac{s^2}{s^2 + 2\zeta_n\omega_n s + \omega_n^2} \frac{s}{s + \omega_b} \quad (5.11)$$

The washout filter order has a dominant effect on the level of fidelity of the supplied simulator motion cues. For constant parameter settings, motion fidelity decreases with increasing filter order, as increasingly more low-frequency motion is attenuated and phase distortion increases rapidly for higher order filters. The level of motion fidelity is of course also affected by the parameters of the different washout filters listed in Eq. (5.8) to (5.11)

define the level of supplied motion fidelity. Generally higher filter gains K and lower (dominant) break frequencies ω_n correspond to higher fidelity motion cueing [Sinacori, 1977].

The objective of this study is to relate measured changes in any of the dependent measures listed in Table 5.1 to some important measure of simulator motion fidelity. If a clear correlation exists between some combination of dependent measure and fidelity measure, this means that this fidelity measure can be used as a predictor for the observed change in the dependent measure. A natural first choice for measures of motion fidelity are of course the washout filter parameters: the filter gain K , the filter break frequency ω_n , the filter damping ratio ζ_n , and the additional first-order filter break frequency ω_b . The dominant parameters with the largest effect on the washout filter dynamics are the filter gain K and (for third-order filters) the filter break frequency ω_n . Hence, these two parameters were selected as a first set of possible predictor variables.

Filter parameters, however, do not account for the effect of filter order. This makes comparison of the level of motion fidelity by evaluating these parameters between studies with different order washout filters difficult. This was also recognized by Sinacori [1977], who therefore proposed the usage of the gain and phase distortion at a frequency of 1 rad/s induced by the motion filter as indicators of motion fidelity:

$$K_S = |H_{mf}(j\omega)| \quad \text{with} \quad \omega = 1 \text{ rad/s} \quad (5.12)$$

$$\phi_S = \angle H_{mf}(j\omega) \quad \text{with} \quad \omega = 1 \text{ rad/s} \quad (5.13)$$

The motion filter gain and phase distortion at a certain evaluation frequency are, of course, a function of the filter order in addition to the filter parameters. Furthermore, it should be noted that in addition to the filter order, ϕ_S is only affected by the washout dynamics and hence the selected value of ω_n (assuming constant ζ_n and ω_b). The absolute value of $H_{mf}(j\omega)$, however, is not only affected by the filter gain K , but also by the filter break frequency ω_n . This makes K_S a metric that captures, to some extent, the cumulative effect of variations in filter gain and break frequency.

In addition to the motion filter gain and phase distortion at 1 rad/s as given by Eqs. (5.12) and (5.13), also other evaluation frequencies – such as 0.5 and 2, and 3 rad/s – were considered as fidelity metrics in this study. This chapter, however, will only analyze trends in the dependent measures as a function of K_S and ϕ_S , as the other evaluation frequencies were not found to yield markedly different results for the considered set of experimental measurements.

5.3.3 Selected Studies

Tables 5.2 and 5.3 present the details of the ten studies with translational and rotational motion cueing variations, respectively, that have so far been included in the data base considered in this chapter. In addition to a short description of the considered control task, Tables 5.2 and 5.3 present the motion filter dynamics and the different sets of motion filter parameters evaluated in each study. Fig. 5.2 further depicts the motion filter dynamics evaluated in all studies in the form of the motion fidelity criterion proposed by Sinacori [1977], using the definition of the different fidelity regions proposed by Schroeder [1999].

Table 5.2. Studies with translational motion cueing variation included in the literature overview.

Symb. Ref.	Control Task	Filter	Filter Settings
T.A Chapter 4	Conventional aircraft pitch control task (target-following and disturbance-rejection, latter dominant), Cessna Citation controlled element dynamics, varying translational heave cueing, heave cues represent motion wrt. aircraft center of gravity, additional 1-to-1 rotational pitch motion on/off	$K \frac{s^2}{s^2 + 2\zeta_n \omega_n s + \omega_n^2}$	T.A1: $K = 0.0$
			T.A2: $K = 0.6$
			T.A3: $K = 1.0$
			T.A4: $K = 0.6$
			T.A5: $K = 1.0$
T.B [Van Wieringen et al., 2011]	Conventional aircraft pitch control task (target-following and disturbance-rejection), Boeing 747 controlled element dynamics, varying translational heave cueing, heave cues represent motion wrt. aircraft center of gravity, additional 1-to-1 rotational pitch motion on/off	$K \frac{s^2}{s^2 + 2\zeta_n \omega_n s + \omega_n^2}$	T.B1: $K = 0.0$
			T.B2: $K = 0.5$
			T.B3: $K = 0.7$
			T.B4: $K = 0.3$
T.C [Bray, 1985]	Helicopter translational heave control task, varying heave motion cueing, separate target-following and disturbance-rejection tasks, helicopter dynamics with "good" and "slightly degraded" vertical responses	$K \frac{s^2}{s^2 + 2\zeta_n \omega_n s + \omega_n^2}$	T.C1: $K = 1.0$
			T.C2: $K = 1.0$
			T.C3: $K = 1.0$
T.D [Steurs et al., 2004]	Conventional aircraft pitch attitude target-following task, Cessna Citation controlled element dynamics, varying translational heave cueing, heave cues represent motion wrt. aircraft center of gravity, three levels of additional rotational pitch cueing ($K = 0.0, 0.5,$ and 1.0)	$K \frac{s^2}{s^2 + 2\zeta_n \omega_n s + \omega_n^2}$	T.D1: $K = 0.0$
			T.D2: $K = 0.1$
			T.D3: $K = 0.5$

Table 5.3. Studies with rotational motion cueing variation included in the literature overview.

Symb. Ref:	Control Task	Filter	Filter Settings
R.A [Chapter 6]	Conventional aircraft roll control task (combined target-following and disturbance-rejection task), Cessna Citation controlled element dynamics, varying rotational roll cueing, no compensation for lateral specific force cues resulting from simulator roll	$K \frac{s-1}{s+\omega_n}$	R.A.1 : $K = 0.0$ R.A.2 : $K = 0.5$ R.A.3 : $K = 1.0$ R.A.4 : $K = 1.0$ $\omega_n = 0.5 \text{ r/s}$ $\omega_n = 0.5 \text{ r/s}$ $\omega_n = 0.0 \text{ r/s}$
R.B [De Vroome et al., 2009]	Pitch attitude control task (dominant target-following and dominant disturbance-rejection tasks performed separately), double integrator controlled element dynamics, pure scaling of the supplied pitch motion cues (no washout)	K	R.B.1 : $K = 0.25$ R.B.2 : $K = 0.5$ R.B.3 : $K = 0.75$ R.B.4 : $K = 1.0$
R.C [Stapleford et al., 1969]	Roll attitude control task (combined target-following and disturbance-rejection task), two controlled elements: $K/(s^2 + 10)$ and K/s^2 , priority III conditions	$K \frac{s-1}{s+\omega_n}$	R.C.1 : $K = 1.0$ R.C.2 : $K = 1.0$ R.C.3 : $K = 1.0$ $\omega_n = 0.5 \text{ r/s}$ $\omega_n = 1.0 \text{ r/s}$ $\omega_n = 2.0 \text{ r/s}$
R.D [Bergeron, 1970]	Two-axis pitch and yaw attitude disturbance-rejection task, single integrator controlled element dynamics in both axes, pure scaling of the supplied pitch motion cues (no washout)	K	R.D.1 : $K = 0.0$ R.D.2 : $K = 0.0625$ R.D.3 : $K = 0.125$ R.D.4 : $K = 0.25$ R.D.3 : $K = 0.5$ R.D.4 : $K = 1.0$
R.E [Jex et al., 1978]	Conventional aircraft roll attitude control task (combined target-following and disturbance-rejection task), controlled element representative of a higher aircraft	$K \frac{s-1}{s+\omega_n}$ and $K \frac{s^2}{s^2+2\zeta_n\omega_n s+\omega_n^2}$	R.E.1 : $K = 1.0$ R.E.2 : $K = 1.2$ R.E.3 : $K = 1.0$ R.E.4 : $K = 0.7$ R.E.5 : $K = 0.53$ R.E.6 : $K = 0.0$ $\omega_n = 0.85 \text{ r/s}$ $\omega_n = 1.0 \text{ r/s}$ $\omega_n = 0.4 \text{ r/s}$ $\zeta_n = 0.7$ 2 nd order
R.F [Van Gool, 1978]	Conventional aircraft pitch and roll attitude disturbance-rejection tasks (performed separately), controlled element representative of a DCC9-10 in the landing/approach configuration	$K \frac{s^2}{s^2+2\zeta_n\omega_n s+\omega_n^2}$	R.F.1 : $K = 1.0$ R.F.2 : $K = 1.0$ R.F.3 : $K = 1.0$ R.F.4 : $K = 0.0$ $\omega_n = 0.2 \text{ r/s}$ $\omega_n = 0.25 \text{ r/s}$ $\omega_n = 0.5 \text{ r/s}$ $\zeta_n = 1.0$ $\zeta_n = 1.0$ $\zeta_n = 1.0$

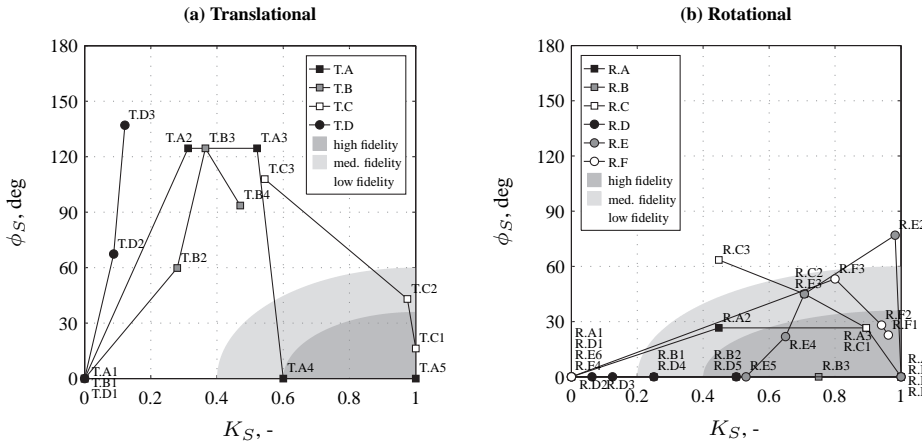


Figure 5.2. Compiled translational and rotational motion filter settings from literature evaluated against simulator motion fidelity criteria from literature [Sinacori, 1977; Schroeder, 1999].

Note from Tables 5.2 and 5.3 and Fig. 5.2 that more studies that evaluated pilot tracking behavior with variations in rotational cueing are available than those that considered different translational motion cueing settings. Furthermore, translational motion is typically a lot more problematic with respect to the cueing in flight simulators than rotational motion, due to the large stroke required for presenting, especially low-frequency, aircraft translational motion. This is also observable from Fig. 5.2, which shows that the motion filter settings that were evaluated for rotational cueing (Fig. 5.2(b)) were typically less restrictive – that is, were closer to the dark gray high-fidelity region – than those considered for translational cueing experiments (Fig. 5.2(a)).

5.3.4 Pilot Model Tuning Rule Development

5.3.4.1 Data Normalization

The goal of this study is to obtain a quantitative indication of the magnitude of pilot behavioral adjustments in response to the presence of a motion filter with certain dynamics. The collected behavioral measurements from the studies listed in Tables 5.2 and 5.3, thereby combining measurements that were taken for variations in translational and rotational motion cueing, will therefore be used to see if consistent variations in any of the dependent measures listed in Table 5.1 and any of the predictor variables introduced in Section 5.3.2 can be found. For a dependent measure Z and a predictor variable Y , this means that we are looking for a prediction equation $Z(Y)$.

It should be noted that differences in the defining characteristics of the compensatory control tasks (for example, controlled element dynamics, forcing function signals, and adopted display formats) naturally lead to large offsets in some of the dependent measures listed in Table 5.1. For instance, a controlled element with double integrator dynamics as used in the experiment of De Vroome et al. [2009] requires markedly more pilot lead

equalization (higher T_L) than typical aircraft pitch and roll dynamics as controlled in the experiment of Van Gool [1978]. As the relative change in the considered dependent measures due to changes in motion filter dynamics is of interest to this study, the data from all dependent measures has been normalized with the mean of this dependent measure over all conditions for each experiment. For values of a dependent measure Z taken from an experiment with N_z different motion filter conditions, this gives:

$$\bar{Z}[n] = \frac{Z[n]}{\frac{1}{N_z} \sum_{k=1}^{N_z} Z[k]} \quad \text{with } n = 1 \dots N_z \quad (5.14)$$

To illustrate the necessity of this normalization, Fig. 5.3 shows a side-by-side comparison of the raw data and the result of the normalization of all measurements for the pilot visual lead time constant T_L . Note from Fig. 5.3(b) that due to the normalization according to Eq. (5.14), the normalized dependent measure represents the percentage-wise variation in the dependent measure over the range of the selected predictor.

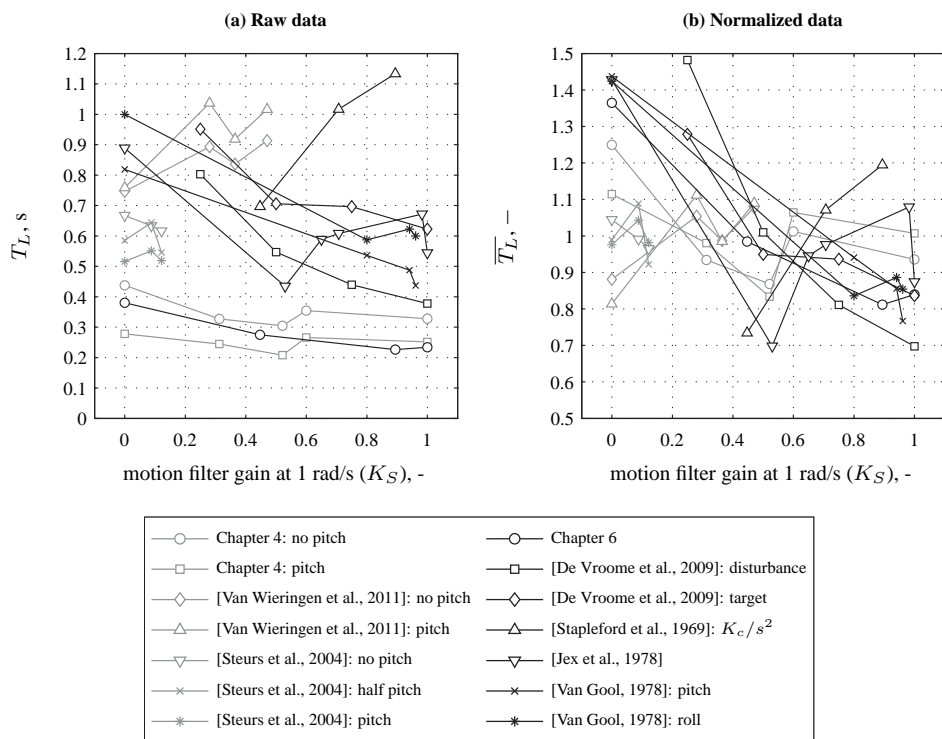


Figure 5.3. Example data normalization according to Eq. (5.14) for pilot visual lead time constant T_L .

5.3.4.2 Linear Regression Modeling

For all dependent measures, the normalized data were tested for correlation with the considered measures of motion filter characteristics (see Section 5.3.2) by calculating Pearson's correlation coefficient R . For absolute values of R of 0.3 and higher, the correlation between two variables is considered to be of "medium" strength, while $R > 0.5$ is typically referred to as a "strong" correlation [Cohen, 1977; Field, 2005]. Still, as argued by Cohen [1977] the interpretation of the magnitude of R is heavily dependent on the field of research. In the physical sciences, typically very high values of R are found, while Cohen [1977] claims that for many applications in the behavioral sciences correlation coefficients larger than 0.6 are rarely observed due to markedly larger spread in typical obtained measurements.

Due to the variation in the experiments from which data is compiled here, the typically low numbers of participants for which data was collected, and the considerable measurement noise typically present in behavioral measurements as considered here, a correlation coefficient larger than 0.3 was deemed to be strong enough to allow for modeling of the trend in the data using a linear regression. In addition, when evaluating the statistical significance of the linear correlations it was found that for all occurrences of $R > 0.3$ the correlation was found to be statistically significant. Note, however, that $R = 0.3$ indicates that $0.3^2 = 0.09 = 9\%$ of the variance in the measured data can be explained with a linear regression. This linear regression represents a relation between the normalized dependent measure \bar{Z} and the independent (predictor) variable Y given by:

$$\bar{Z}(Y) = \beta(Y - Y_{ref}) + \alpha_{Y_{ref}} \quad (5.15)$$

In Eq. (5.15), Y_{ref} represents the reference value of the predictor variable Y , with respect to which the trend in Z is to be predicted. The symbols β and $\alpha_{Y_{ref}}$ are the linear regression coefficient and offset, which are determined by fitting the model of Eq. (5.15) to the normalized data using a least-squares fitting procedure. It should be noted that for data as presented in Fig. 5.3(b) a different choice in Y_{ref} (for instance $K_S = 0$ or $K_S = 1$) affects the value of $\alpha_{Y_{ref}}$ for the corresponding regression model, but not the value of β . When converting Eq. (5.15) back to the non-normalized dependent measure $Z(Y)$ (note that $\alpha_{Y_{ref}} = \bar{Z}(Y_{ref})$ and use Eq. (5.14)) an equation results that can be used for linear prediction of the considered dependent measure based on the parameters of the fitted linear regression:

$$Z(Y) = Z(Y_{ref}) \left[\frac{\beta}{\alpha_{Y_{ref}}} (Y - Y_{ref}) + 1 \right] \quad (5.16)$$

In Eq. (5.16), $Z(Y_{ref})$ represents the value of the dependent measure at the reference value of Y . For a control task where pilot behavior and pilot-vehicle system performance and crossover characteristics are known for a reference predictor setting, $Z(Y_{ref})$, this allows for prediction of changes in Z for other values of Y according to Eq. (5.16). Note from Eq. (5.16) that the coefficient that defines the magnitude of the change in Z due to a variation in Y is given as the fraction of β and $\alpha_{Y_{ref}}$, and hence is dependent on the choice of the reference predictor value Y_{ref} .

5.4 Results

5.4.1 Predictor Variable Selection

As explained in Section 5.3.4, four different variables were considered as predictors for observed trends in the dependent measures listed in Table 5.1: the motion filter gain K , the (dominant) motion filter break frequency ω_n , the motion filter gain at 1 rad/s K_S , and the motion filter phase distortion at 1 rad/s ϕ_S . For all combinations of dependent measure and predictor variables plots as those depicted in Fig. 5.3 were evaluated to investigate possible correlation between the two considered metrics. Furthermore, the correlation coefficients R calculated for all considered combinations of dependent measures and predictors were calculated and are presented in Table 5.4.

Table 5.4. Correlation coefficients for all considered combinations of dependent measure and predictor. Bold font indicates $|R| > 0.3$.

Dependent Measures	Predictor			
	K	ω_n	K_S	ϕ_S
σ_e^2	-0.30	0.47	-0.60	0.18
σ_u^2	0.53	0.12	0.54	-0.17
$\omega_{c,d}$	0.37	-0.61	0.69	-0.52
$\omega_{c,t}$	-0.09	0.57	-0.26	0.38
$\varphi_{m,d}$	-0.02	0.49	-0.30	0.41
$\varphi_{m,t}$	0.05	-0.47	0.28	-0.42
K_v	0.39	-0.17	0.60	-0.18
T_L	-0.33	-0.05	-0.49	0.06
T_I	-0.62	-0.23	-0.33	-0.57
K_m	-0.17	0.18	-0.12	-0.16
τ_v	0.31	-0.41	0.40	-0.25
τ_m	-0.41	-0.20	-0.30	-0.05
ω_{nm}	0.27	0.06	0.35	-0.23
ζ_{nm}	0.25	-0.49	0.27	-0.03
Mean $ R $	0.28	0.33	0.37	0.25

Each column in Table 5.4 presents the values of R for one of the considered dependent measures (see Table 5.1). The final column of Table 5.4 shows the average absolute correlation coefficient calculated across all dependent measures. As can be verified from this final column, the strongest average $|R|$ across all dependent measures is present for the motion filter gain at 1 rad/s (K_S). Based on this strongest average correlation across all dependent measures – although a number of medium and strong correlations are also found for the other predictors and considering that the average correlation coefficient for ω_n is nearly as high as found for K_S – the choice is made in this chapter to focus on K_S as the most promising predictor variable.

Another reason for favoring K_S as the predictor in this chapter can be observed from Tables 5.2 and 5.3 and Fig. 5.2. Some of the included studies considered pure-gain motion filter dynamics K [Bergeron, 1970; De Vroome et al., 2009], so no variation in ω_n and ϕ_S was available for these experiments. Furthermore, as explained in Section 5.3.2, K_S is the only considered predictor variable that is a function of both the motion filter gain

(K) and filter characteristics (ω_n). Though different combinations of K and ω_n can still give the same value for this predictor, K_S is still selected here as the most promising of the considered predictor variables because of this property. All results presented in this chapter, and also the derived pilot model tuning rules, will utilize K_S as the predictor.

It should be noted that the frequency of 1 rad/s at which K_S was selected for correspondence with the fidelity criteria of Sinacori [1977] and Schroeder [1999], but that evaluation of the filter dynamics at other frequencies in the range of interest to manual control (see Section 5.3.2) yielded highly similar results.

For prediction of changes in behavior due to variations in motion cueing, here the condition where no motion filter is present, yielding one-to-one presentation of motion cues, will be considered as the baseline. For the selected predictor variable this corresponds to the case where $K_S = 1$. Naturally, tuning rules could also be defined with respect to the no-motion case ($K_S = 0$), but for interpreting the effects of motion filters on pilot behavior, the chosen convention was thought to be more intuitive. Substitution of $Y = K_S$ and $Y_{ref} = K_{S_{ref}} = 1$ in Eq. (5.16) results in the following structure for the linear prediction equations that will be derived in this chapter:

$$Z(K_S) = Z(1) \left[\frac{\beta}{\alpha_1} (K_S - 1) + 1 \right] \quad (5.17)$$

In Eq. (5.17), $Z(1)$ represents the value of the considered dependent measure for the reference case where $K_S = 1$. The symbols β and α_1 are the parameters of the fitted linear regression model (see Section 5.3.4.2).

5.4.2 Notable Trends in Dependent Measures

5.4.2.1 Tracking Performance and Control Activity

Fig. 5.4 presents the normalized tracking error and control input variance data for the studies included in this overview. Fig. 5.4 depicts the normalized data for both dependent measures as black markers, while the linear regression that was fit through the data is shown as a solid gray line. The legend entry for the measured data lists the value of R and its statistical significance (if $p < 0.05$, the correlation is statistically significant); the entry for the fitted regression lists the corresponding estimated values of the regression parameters β and α_1 .

As can be verified from Fig. 5.4, for both σ_e^2 and σ_u^2 a strong correlation ($|R| > 0.5$) with the variation in K_S is present. Fig. 5.4 shows that an increase in K_S is found to yield improved tracking performance (lower σ_e^2) and increased control activity (higher σ_u^2). Substitution of the fitted values of β and α_1 (indicated in the bottom legend entries in Fig. 5.5) in the prediction equation given by Eq. (5.17) yields the following tuning rules for σ_e^2 and σ_u^2 :

$$\sigma_e^2(K_S) = \sigma_e^2(1) [-0.48 (K_S - 1) + 1] \quad (5.18)$$

$$\sigma_u^2(K_S) = \sigma_u^2(1) [0.17 (K_S - 1) + 1] \quad (5.19)$$

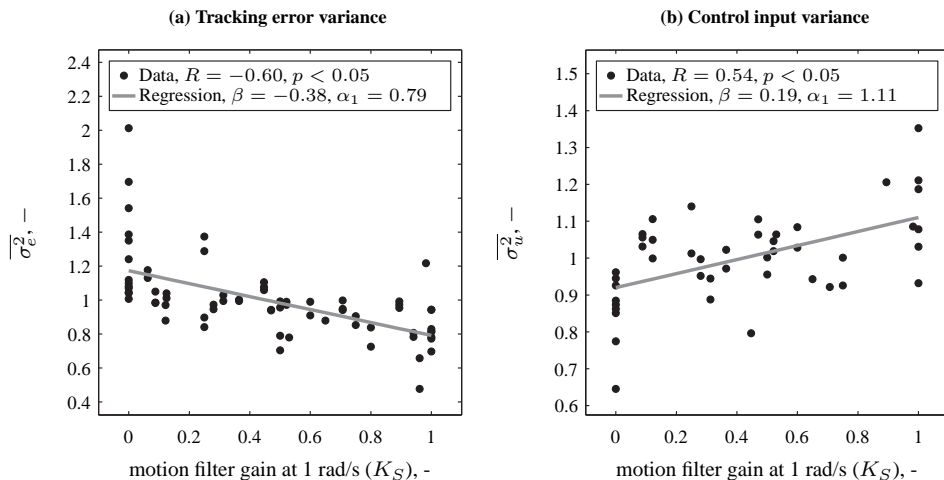


Figure 5.4. Variation in tracking performance and control activity as a function of K_S .

In Eqs. (5.18) and (5.19), $\sigma_e^2(1)$ and $\sigma_u^2(1)$ represent the level of tracking performance and control activity for the case where $K_S = 1$, respectively. As can be verified from Fig. 5.4(a) and Eq. (5.18), tracking performance on average degrades by 48% for $K_S = 0$ compared to $K_S = 1$. Similarly, Eq. (5.19) shows that control input variance is found to decrease by 17% under the same variation of K_S .

5.4.2.2 Crossover Frequencies and Phase Margins

Figures 5.5 and 5.6 show the compiled data and fitted linear regressions for the target and disturbance open-loop crossover frequencies and phase margins, respectively. As can be verified from the correlation coefficients listed in Table 5.4, only the crossover frequency and phase margin of the disturbance open-loop response show $|R| > 0.3$ with K_S . Fig. 5.5(a) shows a strong positive correlation between $\omega_{c,d}$ and K_S , indicating disturbance crossover frequencies are typically found to increase with increasing K_S . For the corresponding phase margin, the reverse trend is observed from Fig. 5.6(a), as $\varphi_{m,d}$ is found to reduce with increasing motion filter gain at 1 rad/s. The target crossover frequency and phase margin data presented in Figures 5.5(b) and 5.6(b), respectively, still show smaller and opposite trends with K_S than observed for the corresponding disturbance open-loop parameters. Note that these trends are consistent with the results reported in a number of the individual studies that were included, [De Vroome et al., 2009; Bray, 1985] and Chapter 4. These trends, however, do not sufficiently correlate with the variation in K_S ($|R| < 0.3$) to meet the requirement for tuning rule development. This gives the following tuning rules for $\omega_{c,d}$, $\omega_{c,t}$, $\varphi_{m,d}$, and $\varphi_{m,t}$, corresponding to the data shown in Figures 5.5 and 5.6:

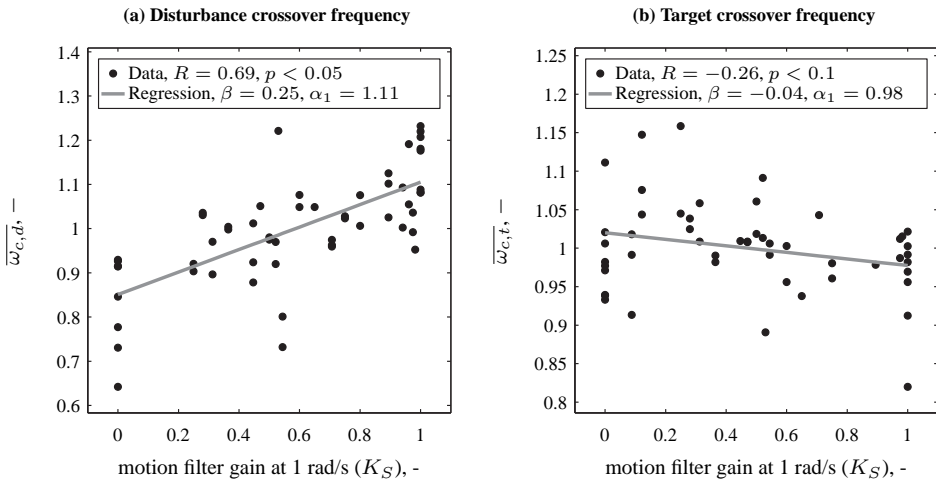


Figure 5.5. Variation in the disturbance and target open-loop crossover frequencies as a function of K_S .

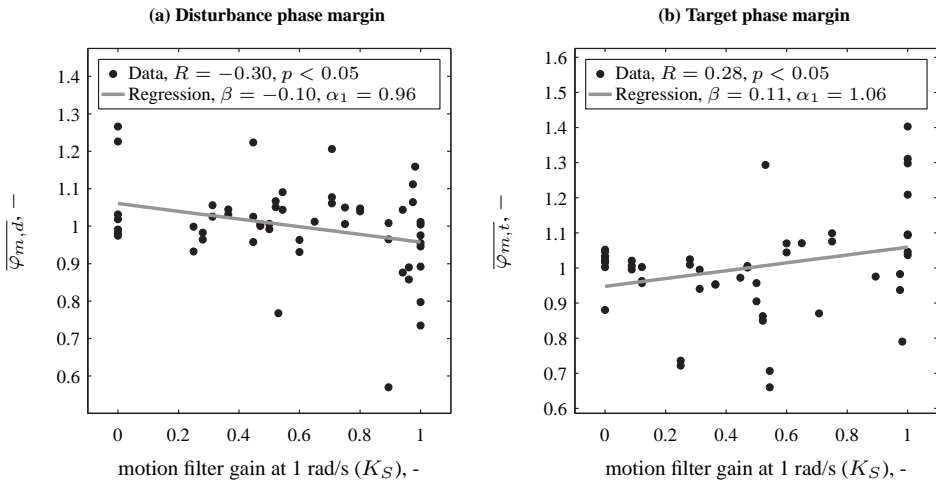


Figure 5.6. Variation in the disturbance and target open-loop phase margins as a function of K_S .

$$\omega_{c,d}(K_S) = \omega_{c,d}(1) [0.23(K_S - 1) + 1] \quad (5.20)$$

$$\omega_{c,t}(K_S) = \omega_{c,t}(1) \quad (5.21)$$

$$\varphi_{m,d}(K_S) = \varphi_{m,d}(1) [-0.10(K_S - 1) + 1] \quad (5.22)$$

$$\varphi_{m,t}(K_S) = \varphi_{m,t}(1) \quad (5.23)$$

Eq. (5.20) indicates a variation of around 23% over the range of K_S values from 0 to 1 for $\omega_{c,d}$. For the disturbance phase margin $\varphi_{m,d}$, see Eq. (5.22), this variation is found to be around 10%.

5.4.2.3 Pilot Behavioral Parameters

Fig. 5.7 shows the normalized measurement data as a function of K_S for the three most interesting pilot model parameters of the visual response channel with respect to the effects of motion cueing variations: the pilot visual gain K_v , the pilot visual lead time constant T_L , and the pilot visual time delay τ_v . For T_I too little data was thought to be available for identifying a consistent trend, as only the experiments described in Chapter 4 and [Van Wieringen et al., 2011] provide data for this parameter.

Fig. 5.7 shows a strong positive correlation with K_S for the pilot visual gain K_v , while for T_L and τ_v medium values for the correlation coefficient are found ($0.3 < R \leq 0.5$). Pilot visual gains are consistently found to be higher for higher values of K_S , indicating pilots respond with a higher gain to visually presented tracking errors when motion cueing is of higher fidelity, a finding that is indeed reported in many studies. Here, an average change in K_v of nearly 20% is found over the full range of K_S .

One of the most consistent effects that is reported in many studies that investigate the effects of motion feedback on manual control behavior is that the presence of motion feedback allows for a reduction in the amount of visual lead equalization that pilots need to adopt, see for instance [Hosman, 1996; Van der Vaart, 1992; De Vroome et al., 2009; Zaal et al., 2009b] and Chapters 2, 4, and 6. This reduction in visual lead stems from the fact that the motion cues, which are, for instance, perceived with the vestibular system, provide information on the rates of the controlled element state directly, thereby removing the requirement to generate lead visually [Shirley and Young, 1968; Hosman, 1996]. Fig. 5.7(b) shows that this is also apparent from the collected data of all experiments listed in Tables 5.2 and 5.3. Values for the visual lead time constant T_L are seen to increase with decreasing K_S , with a total variation of 29% over the full range of $K_S = 0$ to 1.

A correlation with $R > 0.3$ is also found for the pilot visual delay τ_v . Even though the trend in this dependent measure is not as large as those found for K_v and T_L (only 7% variation for K_S ranging from 0 to 1), still a highly consistent increase in τ_v is observed with increasing K_S . This effect is often seen to occur in series with a reduction in the amount of visual lead equalization (lower T_L), and is believed to result from the fact that due to the added information from motion feedback, a control strategy that requires less workload,

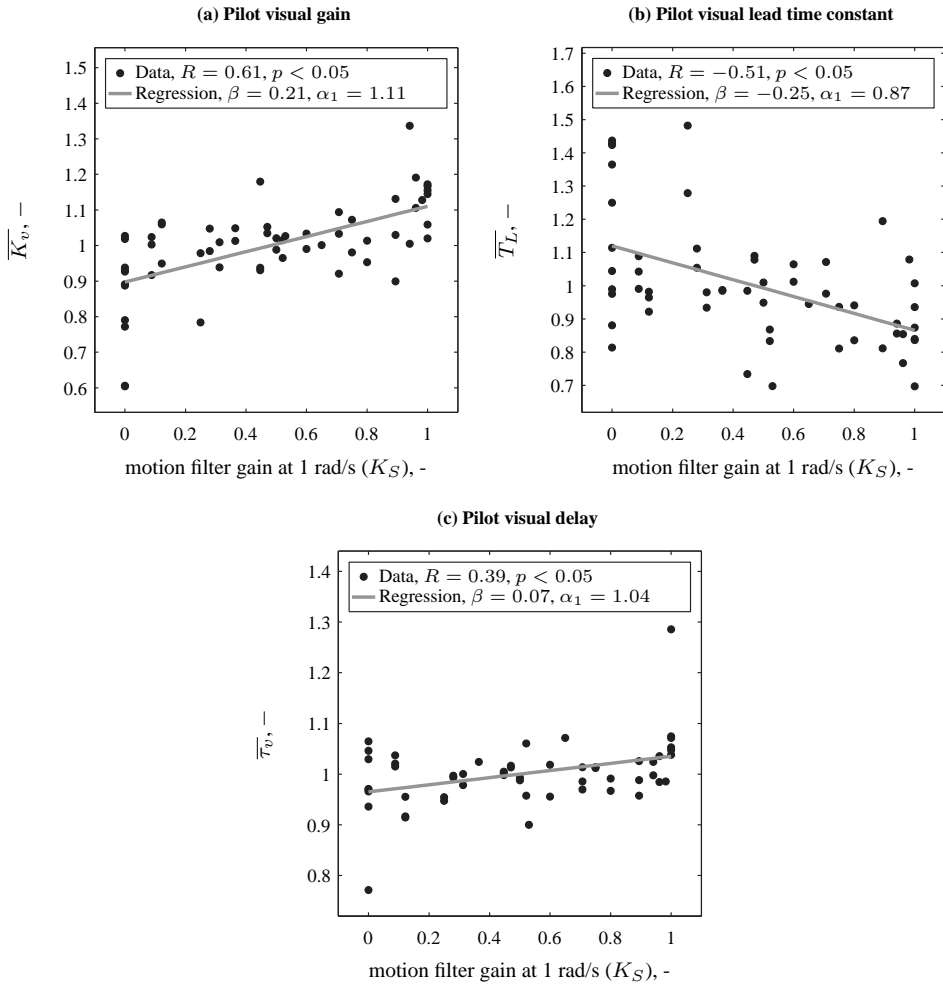


Figure 5.7. Variation in pilot model visual response parameters as a function of K_S .

but induces more high-frequency phase lag in the pilot visual control response $H_{p_v}(j\omega)$, is permissible without significantly affecting the dominant closed-loop characteristics.

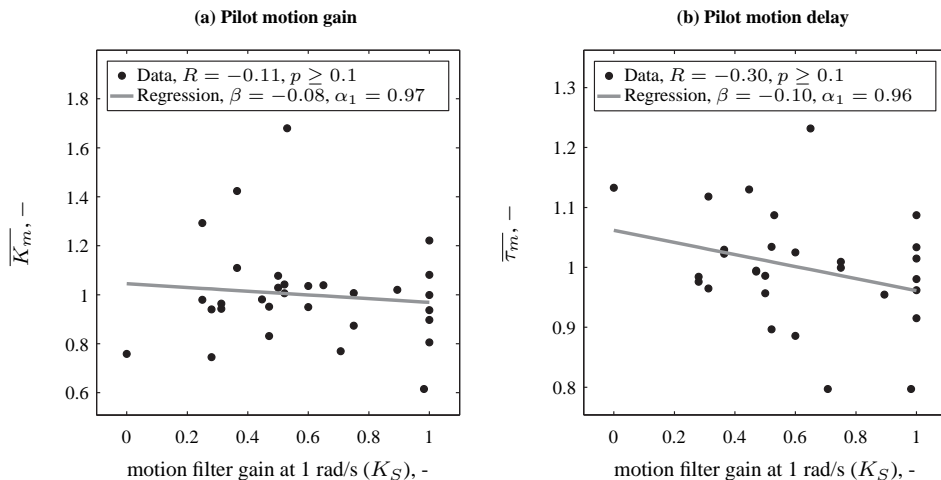


Figure 5.8. Variation in pilot model motion response parameters as a function of K_S .

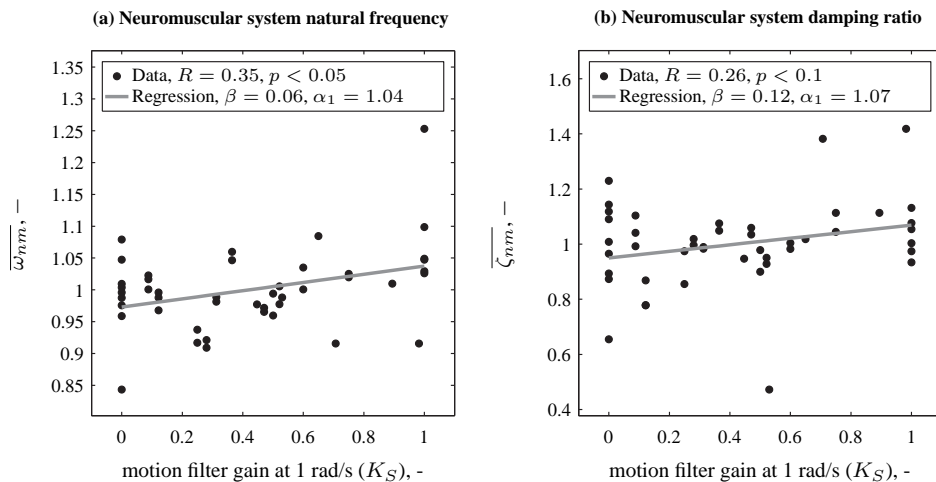


Figure 5.9. Variation in neuromuscular actuation parameters as a function of K_S .

Fig. 5.8 shows the data and fitted regressions for the two defining parameters of the pilot model motion response channel, the pilot motion gain K_m and the pilot motion time delay τ_m . The collected data for the pilot motion gain K_m and τ_m are not found to yield values of $|R| > 0.3$ (though τ_m is close). Especially the nearly constant values of K_m under a variation of K_S are notable, as this implies that pilots appear to be unable to increase their K_m to compensate for reductions in motion cue magnitude, as suggested in Section 5.2.3.

These results for the pilot motion gain therefore suggest a reducing contribution of motion feedback to pilot control behavior with reducing K_S .

The collected results for the two pilot model parameters that are typically used for quantification of the neuromuscular actuation dynamics as given by Eq. (5.7) are shown in Fig. 5.9. As can be verified from Fig. 5.9, an increasing trend with increasing K_S is observed for both the neuromuscular system natural frequency ω_{nm} and damping ratio ζ_{nm} , however, only for ω_{nm} a correlation $R > 0.3$ is found. Increased ω_{nm} has been argued to indicate an increase in muscle co-contraction [Damveld et al., 2009], which would imply pilots hold a tighter grip on the manipulator for increasing motion fidelity and motion amplitudes.

The linear pilot model parameter tuning equations that can be derived from the linear regression models fit to the data presented in Figures 5.7 to 5.9 are given by:

$$K_v(K_S) = K_v(1) [0.19 (K_S - 1) + 1] \quad (5.24)$$

$$T_L(K_S) = T_L(1) [-0.29 (K_S - 1) + 1] \quad (5.25)$$

$$K_m(K_S) = K_m(1) \quad (5.26)$$

$$\tau_v(K_S) = \tau_v(1) [0.069 (K_S - 1) + 1] \quad (5.27)$$

$$\tau_m(K_S) = \tau_m(1) \quad (5.28)$$

$$\omega_{nm}(K_S) = \omega_{nm}(1) [0.058 (K_S - 1) + 1] \quad (5.29)$$

$$\zeta_{nm}(K_S) = \zeta_{nm}(1) \quad (5.30)$$

Again, Eqs. (5.24) to (5.30) indicate the change in the values of K_v to τ_m relative to the case where $K_S = 1$. Hence, the parameters $K_v(1)$ to $\zeta_{nm}(1)$ indicate the values of these pilot model parameters that would be suitable for pilot control behavior when motion cues are presented one-to-one ($K_S = 1$).

5.5 Discussion

This chapter presented the results of an effort to develop some rudimentary tuning rules for adaptation of pilot behavioral tracking model parameters to variations in motion feedback. Data from a number of studies that investigated the effects of variations in motion cueing settings on pilot tracking behavior and performance were compiled, compared to selected measures of motion cueing fidelity, and used to fit linear regression models for those combinations of predictor variables and dependent measures for which a sufficiently strong correlation was observed. Using the motion filter gain at 1 rad/s as the predictor variable, a set of mathematical equations was obtained that allows for tuning multimodal pilot model parameters to a selected motion filter setting, granted that the pilot dynamics for the control task where no motion filter is present in the motion feedback path are known.

The choice of the predictor variable to use for pilot model tuning rules as attempted in this chapter is a very important and complicated one, as it essentially requires a single numerical metric that summarizes the total motion filter dynamics. Here the motion filter gain at 1 rad/s (K_S) was selected as the most promising predictor variable, as this metric is indeed affected by both variations in motion cue scaling (motion filter gain K) and motion cue filtering (motion filter break frequency ω_n). However, it should be noted that this choice of metric also has some drawbacks. For instance, the choice of the 1 rad/s evaluation frequency implies that all motion filters for which $\omega_n \ll 1$ rad/s essentially become pure gain attenuation filters, as in that case K_S is not affected by the filter dynamics governed by ω_n . Therefore, a more in-depth investigation of this effect of the frequency at which K_S is evaluated than described here, and the testing of further possible predictor variables, is thought to be valuable to the work described in this chapter.

In this chapter, only linear regression models were fit to the collected data, thereby yielding a set of linear prediction or interpolation equations to adjust pilot model parameters. In reality, it is unlikely that only linear variations of parameters that define pilot control behavior with respect to a selected predictor variable will occur. However, for investigating for which dependent measures this might be appropriate and for deriving valid higher-order prediction models from collected data as used in this study, a significantly larger number of measurements is needed.

The observed trends in the dependent measures for which tuning equations have been derived in this chapter are mostly highly consistent over the different experiments considered in this study. There are, however, some exceptions that result from differences in the defining elements of the considered control tasks, which should be taken into account when applying the equations from this chapter. One notable example is the observed reduction in the pilot visual lead time constant T_L with increasing K_S . This trend is consistent over studies in which the controlled element state is the dominant motion cue that is perceivable to the pilot. For control tasks for which this is not the case, most notably for pitch tracking tasks with conventional aircraft as considered in a number of previous studies [Steurs et al., 2004; Zaal et al., 2009b; Van Wieringen et al., 2011], where heave motion is the dominant motion cue rather than rotational pitch motion, an opposite trend in T_L is observed. This is believed to be a result of the fact that this heave motion provides less useful motion feedback to pilots than only rotational pitch motion would. Such effects, however, are not yet explicitly included in the tuning rules as described in this chapter.

It should be noted that predicting human manual control behavior is always going to remain a difficult problem, mainly due to the sheer number of factors that affect the adopted control strategy [McRuer and Jex, 1967a]. Hence, the equations for predicting changes in tracking performance, pilot-vehicle crossover frequencies, and behavioral pilot model parameters as developed in this chapter should always be used with some caution. The tuning rules developed in this chapter will be updated when new sets of data are added to the database.

5.6 Conclusions

Using data from ten different investigations into the effects of motion filter characteristics on pilot tracking behavior and performance, this chapter developed a rudimentary set of tuning rules that can be used to predict changes in tracking performance, pilot-vehicle system crossover frequencies and phase margins, and the values of behavioral pilot model parameters that reflect pilots' adaptation to a selected motion filter setting. The motion filter gain at 1 rad/s, which is also used as a metric in a well-known criterion for evaluating simulator motion cueing fidelity, was found to be the most promising metric to use for the prediction of changes in pilot control strategy. Consistent changes in pilot behavior due to variations in motion filter dynamics that were revealed for the data used in this study include increased pilot visual gains, reduced pilot visual lead equalization, and increased pilot visual response delays when the predicted level of motion fidelity is increased. Linear regression models were fit to data for these parameters to define a set of mathematical equations that can be used to predict the values of these parameters for a specific motion filter setting.

Part III

In-Flight to Simulator Behavioral Comparisons

6

Multisine-Tracking Behavior in Real and Simulated Flight

A major milestone for the research described in this thesis is the measurement of pilot tracking behavior in real flight. These in-flight tracking behavior measurements are used as a baseline for evaluating changes in behavior that result from varying motion cueing settings in a flight simulator. Three different tracking tasks were performed in the Cessna Citation II laboratory aircraft: a pitch tracking task with two multisine forcing functions, a roll tracking task with two multisine forcing functions, and a roll tracking task with a ramp target signal. For all these three tasks, the pilots for whom in-flight behavioral measurements were collected also performed the same tracking tasks for a small number of different motion cueing settings in the SIMONA Research Simulator at Delft University of Technology. The comparison of in-flight and simulator measurements for the pitch tracking task is described in [Zaal et al., 2011] and Zaal [2011]'s thesis. For the roll tracking tasks, this chapter includes the details of the experimental setup and the results of the multisine roll tracking task. The data from the roll ramp tracking tasks are analyzed in Chapter 7.

The contents of this chapter are to be published as:

Pool, D. M., Zaal, P. M. T., Damveld, H. J., Van Paassen, M. M., and Mulder, M., "Evaluating Simulator Motion Fidelity using In-Flight and Simulator Measurements of Roll Tracking Behavior", *Journal of Guidance, Control, and Dynamics*.

6.1 Introduction

It is an accepted fact that human manual control behavior is a highly adaptive process and that the control dynamics human operators utilize for a certain control task are a function of a large number of variables internal and external to the operator [McRuer and Jex, 1967a]. In this chapter this knowledge is used to evaluate behavioral simulator motion fidelity using measurements of pilot tracking behavior. For evaluating behavioral motion fidelity, objective measurements of pilot tracking behavior are collected in real flight, and for exactly the same control task but with varying simulator motion cueing settings in a flight simulator. The in-flight measurements, for which the supplied motion feedback is by definition equal to the true aircraft motion, are to be used as the baseline for evaluating changes in pilot tracking behavior that result from changes in simulator motion cueing settings. Through this approach, it is hoped that some validation of existing criteria proposed for evaluating simulator motion fidelity, such as those proposed by Sinacori [1977] and Schroeder [1999], can be provided from a behavioral perspective.

With the objective of evaluating simulator motion fidelity against the motion cues perceivable in real aircraft, a number of studies have been performed that explicitly compared pilot tracking behavior in real flight and in a representative flight simulator setup [Smith, 1966; Newell and Smith, 1969; Mooij, 1973; Van Gool and Mooij, 1976; Steurs et al., 2004]. Despite the fact that good correspondence between in-flight and simulator behavior was obtained for many of these efforts, none of them resulted in definitive conclusions on differences in usage of visual and physical motion cues on pilot tracking behavior and, hence, simulator motion fidelity. The main reason for this is the fact that the techniques utilized in these studies for measuring pilot dynamics only allowed for identification of a lumped pilot describing function, which represented the cumulative effects of pilots' responses to visual and motion information.

This chapter will evaluate simulator motion fidelity from a behavioral perspective for a compensatory roll tracking task with physical roll motion feedback. A combined target-following and disturbance-rejection task, with two independent quasi-random sum-of-sines forcing function signals, is used as such a task allows for reliable separation of pilot visual and motion responses using both frequency-domain and time-domain identification methods [Stapleford et al., 1969; Zaal et al., 2009a]. Measurements of pilot tracking behavior in the same roll tracking task are taken in Delft University of Technology's (DUT) Cessna Citation II laboratory aircraft and in the SIMONA Research Simulator (SRS) for varying roll motion cueing settings. By comparing measured tracking behavior over these different experimental conditions it is attempted to indicate when pilots start adapting their tracking behavior to changes in washout filter dynamics.

The roll tracking task selected for evaluating behavioral motion fidelity in this chapter is especially suitable for this purpose as the aircraft roll motion cues can be presented 1-to-1 on the SRS motion base, allowing for explicit comparison of pilot behavior with full aircraft roll motion in both facilities [Schroeder and Grant, 2010]. The experiment described in the current chapter was performed using the same experimental setup as the pitch tracking experiments described in [Zaal et al., 2011; Zaal, 2011].

This chapter is structured as follows. First, Section 6.2 will provide the details of the roll attitude tracking task considered in this study for evaluating simulator roll motion fidelity.

Here also the multimodal pilot model, which is a key element in the proposed behavioral evaluation of motion fidelity, is introduced. Then Section 6.3 presents the results of an offline pilot model analysis performed to assess the effect of introducing washout filter dynamics in the closed-loop pilot-vehicle system and how this affects its open-loop and closed-loop dynamics. The details of the experiment performed to measure pilot tracking behavior in real flight and in a flight simulator for a variation in roll motion cueing are described in Section 6.4. The experimental results, and a comparison of these experimental measurements with the results of the offline analysis, are then presented in Section 6.5. The chapter ends with a discussion and conclusions.

6.2 Behavioral Simulator Motion Fidelity

6.2.1 Roll Tracking Task

6.2.1.1 Control Task

Fig. 6.1 shows a schematic representation of the closed-loop aircraft roll tracking task considered for the evaluation of flight simulator motion fidelity in this chapter. Fig. 6.1 distinguishes between cueing, pilot, and controlled aircraft dynamics. The pilot controls the roll attitude ϕ of an aircraft with roll dynamics given by $H_c(s)$, for which he receives visual feedback of the tracking error e and physical motion feedback of the controlled aircraft roll acceleration $\ddot{\phi}$. The tracking error information is presented using the compensatory display shown in Fig. 6.2. The cueing dynamics include the dynamic characteristics of the visual and motion cueing systems ($H_{s_v}(s)$ and $H_{s_m}(s)$, respectively) used to present information to the pilot, in addition to the dynamics of an applied motion filter, which are indicated by the $H_{mf}(s)$ block. The target and disturbance forcing function signals that are used to induce compensatory tracking behavior are depicted with the symbols f_t and f_d , respectively.

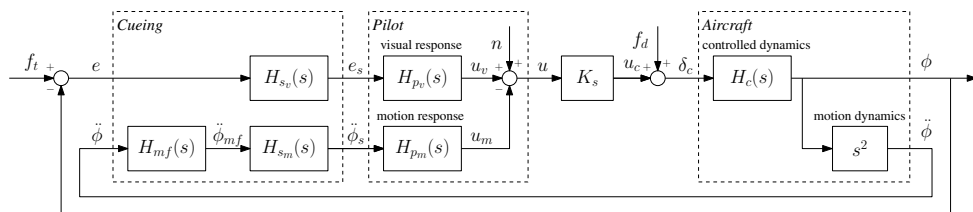


Figure 6.1. Schematic representation of the compensatory roll tracking task with motion feedback.

As explained in detail in Section 6.2.1.3, for the roll tracking task considered in this chapter the controlled element dynamics $H_c(s)$ were the combined Cessna Citation II roll and fly-by-wire (FBW) control system dynamics as representative for Delft University of Technology's Cessna Citation II laboratory aircraft. Furthermore, pilot control inputs u , which were defined as the output voltage of the sidestick manipulator used for the in-flight tracking tasks (see Section 6.4.1.1), are weighed by a gain $K_s = 0.3$ before being used as a FBW command.

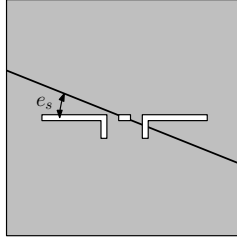


Figure 6.2. Compensatory roll tracking display.

Pilot tracking behavior for compensatory tracking tasks with physical motion feedback of the controlled element state as depicted in Fig. 6.1 can be represented as the sum of two parallel responses to visual and motion information [Stapleford et al., 1969]. The pilot visual response $H_{p_v}(s)$ captures pilots' control dynamics in response to presented tracking errors e_s , while the pilot motion response $H_{p_m}(s)$ models pilots' responses to cued motion information $\ddot{\phi}_s$. The remnant signal n , which accounts for all nonlinear contributions to the pilot control input u [McRuer and Jex, 1967a], completes this quasi-linear model of pilot tracking behavior.

This chapter discusses a comparison of measurements of pilot tracking behavior for the roll tracking task shown in Fig. 6.1 taken in real flight and in a flight simulator for varying settings of a first-order high-pass roll washout filter, as is commonly applied for rotational degrees of freedom in moving-base flight simulation. The dynamics of such a high-pass motion filter are given by:

$$H_{mf}(s) = \frac{s^2 \phi_{mf}(s)}{s^2 \phi(s)} = K_{mf} \frac{s}{s + \omega_{mf}} \quad (6.1)$$

The first-order filter given by Eq. (6.1) has two parameters: the motion filter gain K_{mf} and the filter break frequency ω_{mf} . Together with the dynamics of the motion cueing system, $H_{s_m}(s)$, the motion filter dynamics $H_{mf}(s)$ cause a discrepancy between the true aircraft roll accelerations $\ddot{\phi}$ and the roll accelerations to which the pilot is subjected, $\ddot{\phi}_s$. As explained in more detail in Section 6.4, for the in-flight tracking tasks, which are performed in DUT's Cessna Citation II laboratory aircraft, no motion filter and motion cueing dynamics are present ($H_{mf}(s) = 1$ and $H_{s_m}(s) = 1$). For the simulator tracking tasks performed in the SIMONA Research Simulator (SRS) at DUT, the motion cueing dynamics are approximately equal to a pure delay of 30 ms [Berkouwer et al., 2005], $H_{s_m}(s) = e^{-s\tau_{sm}} = e^{-0.03s}$, while a variation in the settings of $H_{mf}(s)$ is considered.

The visual cueing dynamics $H_{s_v}(s)$ are also assumed to be a pure time delay. The delay in the presentation of the visual tracking error information was determined for both experimental setups using the custom delay measurement system described in [Stroosma et al., 2007]. For both the visual cueing delay was found to be around 25 ms, giving $H_{s_v}(s) = e^{-s\tau_{sv}} = e^{-0.025s}$.

6.2.1.2 Forcing Functions

To allow for reliable separation of the pilot visual and motion responses $H_{p_v}(s)$ and $H_{p_m}(s)$ using both frequency domain [Stapleford et al., 1969] and time-domain [Zaal et al., 2009a] pilot model identification techniques, the target and disturbance forcing functions used to induce pilot tracking behavior in the control task depicted in Fig. 6.1 were two independent quasi-random multisine signals. Both signals were constructed as the sum of $N_{d,t} = 10$ individual sinusoids as defined by:

$$f_{d,t}(t) = \sum_{k=1}^{N_{d,t}} A_{d,t}(k) \sin [\omega_{d,t}(k)t + \phi_{d,t}(k)] \quad (6.2)$$

In Eq. (6.2), $A_{d,t}(k)$, $\omega_{d,t}(k)$, and $\phi_{d,t}(k)$ represent the amplitude, frequency and phase shift of the k^{th} sinusoid in the forcing function signal. The disturbance and target forcing function signals consisted of sinusoids with interleaving frequencies to obtain two independent multisine signals. All forcing function frequencies were defined as integer multiples of the measurement window base frequency $\omega_m = 2\pi/T_m$, where T_m is the measurement window, which for this experiment was equal to 81.92 s. Forcing function frequencies were then related to ω_m through $\omega_{d,t}(k) = \omega_m n_{d,t}(k)$, where $n_{d,t}(k)$ represents the integer factor. Forcing function amplitudes had a low-pass characteristic, defined by the magnitude characteristic of the same second order low-pass filter also used in [Zaal et al., 2009b; Pool et al., 2010]. The target forcing function amplitudes were scaled to yield a signal with a variance of 0.4 deg^2 . The disturbance signal was pre-shaped with the inverse of the controlled element dynamics and scaled to yield a perturbation of the roll attitude with the desired low-pass characteristic and a variance of 0.4 deg^2 . The forcing function phases were selected from a large number of randomly generated sets of phases according to the method described in [Damveld et al., 2010] to yield signals with an approximately Gaussian distribution and an average crest factor. The numerical values of all forcing function properties are given in Table 6.1.

Table 6.1. Multisine disturbance and target forcing function properties.

disturbance, f_d				target, f_t			
n_d	ω_d , rad/s	A_d , V	ϕ_d , rad	n_t	ω_t , rad/s	A_t , deg	ϕ_t , rad
5	0.383	0.014	-1.764	6	0.460	0.698	1.288
11	0.844	0.023	2.792	13	0.997	0.489	6.089
23	1.764	0.026	-1.575	27	2.071	0.220	5.507
37	2.838	0.026	4.641	41	3.145	0.119	1.734
51	3.912	0.029	5.512	53	4.065	0.078	2.019
71	5.446	0.035	2.687	73	5.599	0.049	0.441
101	7.747	0.049	2.321	103	7.900	0.031	5.175
137	10.508	0.068	3.821	139	10.661	0.023	3.415
171	13.116	0.090	4.363	194	14.880	0.018	1.066
226	17.334	0.123	4.558	229	17.564	0.016	3.479

6.2.1.3 Controlled Element

Pilot tracking behavior is known to be adaptable to the dynamics of the controlled element [McRuer et al., 1965; McRuer and Jex, 1967a]. For the experiment described in this chapter, the controlled element dynamics $H_c(s)$ are defined as the combination of Cessna Citation II aileron to roll dynamics and the dynamics of the custom fly-by-wire (FBW) system that was developed for this laboratory aircraft, whose characteristics are described in detail in [Zaal et al., 2009d; Zaal, 2011]. As explained in more detail in Section 6.4.1, for the tracking tasks analyzed in this chapter the FBW system was used to achieve aircraft aileron deflections δ_a equal to the tracking task control commands δ_c (see Fig. 6.1), that is, the sum of the disturbance signal f_d and the weighted control input u_c .

Due to limiting of control commands δ_c by the FBW system, either because of physical limitations of system components or resulting from saturation limits imposed for safety reasons, the FBW system has nonlinear dynamics. For the FBW system dynamics, a nonlinear structural model has been developed and identified using in-flight measurements [Mulder et al., 2009]. However, this limiting by the FBW system can be avoided by ensuring that δ_c stays well away from system limitations. With the forcing function signals defined for the roll tracking tasks (see Section 6.2.1.2), this was mostly the case and as shown in [Zaal et al., 2010, 2011], the dynamics of the FBW system can be modeled as a pure gain with a delay over the full range of forcing function frequencies.

For the Cessna Citation II roll dynamics no mathematical model was available. Therefore, data from the experiment of [Zaal et al., 2010] and further test-flight data were used to identify linearized aircraft roll dynamics for the flight condition for which the in-flight measurements were collected ($V = 160$ kt, $h = 17,000$ ft). Typically, conventional aircraft aileron-to-roll dynamics are given by the following transfer function:

$$\frac{\phi(s)}{\delta_a(s)} = K_\phi \frac{\frac{s^2}{\omega_\phi^2} + \frac{2\zeta_\phi}{\omega_\phi} s + 1}{s(T_r s + 1) \left(\frac{s^2}{\omega_d^2} + \frac{2\zeta_d}{\omega_d} s + 1 \right)} \quad (6.3)$$

In Eq. (6.3), T_r represents the time constant of the roll subsidence mode, while the second-order denominator term defined by the natural frequency ω_d and damping factor ζ_d represents the dutch roll. The second-order numerator term typically partially cancels out the dutch roll mode poles ($\omega_\phi \approx \omega_d$), leaving aileron-to-roll dynamics that are approximately K/s below a frequency of $1/T_r$, and resemble K/s^2 for higher frequencies.

For modeling the Cessna Citation II aileron-to-roll dynamics, the standard form of Eq. (6.3) was found to be too extensive. Especially due to the partial cancellation of the periodic numerator and denominator terms, yielding an overdetermined model structure, the estimation of the model given by Eq. (6.3) proved impossible. Instead, a reduced transfer function form, where the second-order numerator term and the first-order roll subsidence mode pole were approximated as a first-order lead, was fit to the available data. When including the FBW system dynamics, the full linearized controlled element dynamics for the roll tracking task studied in this chapter are then given by:

$$\begin{aligned}
 H_c(s) &= \frac{\phi(s)}{\delta_c(s)} = K_\phi \frac{T_\phi s + 1}{s \left(\frac{s^2}{\omega_\phi^2} + \frac{2\zeta_\phi}{\omega_\phi} s + 1 \right)} e^{-\tau_\phi s} \\
 &= 0.29 \frac{0.51s + 1}{s \left(\frac{s^2}{2.70^2} + \frac{2 \cdot 0.81}{2.70} s + 1 \right)} e^{-0.09s}
 \end{aligned} \tag{6.4}$$

Note that Eq. (6.4) represents a controlled element with approximately K/s dynamics below ω_ϕ and approximately K/s^2 dynamics above ω_ϕ . For the fitted value of $\omega_\phi = 2.70$ rad/s, this transition from single to double integrator dynamics occurs in the 1-5 rad/s frequency range where the pilot-vehicle system crossover frequency is expected [McRuer et al., 1965]. Hence, it is likely that pilots will show lead equalization to compensate for the high-frequency K/s^2 dynamics. Finally, note that the FBW system delay was found to be equal to 0.09 s.

Fig. 6.3 shows a frequency-domain comparison of the fitted model given by Eq. (6.4) and describing function estimates obtained for the controlled element dynamics at the frequencies of the disturbance forcing function for the data from [Zaal et al., 2010]. Note that the fitted model corresponds very well with the measured describing function estimates. Furthermore, the controlled element model variance accounted for (VAF), the percentage of measured model response explained by the model [Zaal et al., 2009a], was found to be higher than 98%, indicating that the model of Eq. (6.4) is able to capture the time-domain response of the combined FBW system and Cessna Citation II roll dynamics during the roll tracking tasks studied in this chapter at high accuracy. More details on the verification of the aircraft model given by Eq. (6.4) can be found in Appendix E.

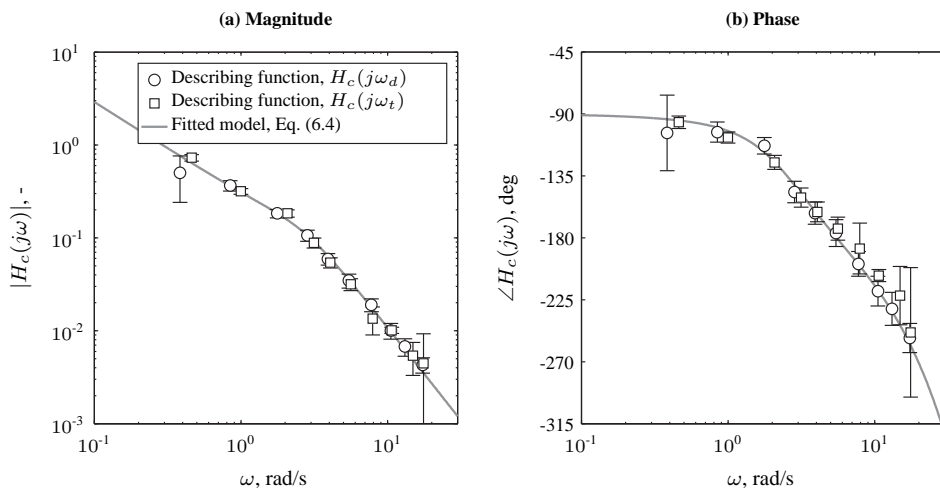


Figure 6.3. Comparison of the frequency response of the identified FBW system and Cessna Citation II roll dynamics with an average estimated frequency domain describing function.

6.2.2 Modeling Multimodal Pilot Tracking Behavior

For control tasks where continuous physical motion feedback of the controlled variable was available, it has been shown in many previous investigations that pilot tracking behavior can be successfully modeled with a model consisting of parallel visual and motion responses [Stapleford et al., 1969; Jex et al., 1978; Hosman, 1996; Van der Vaart, 1992], as depicted in Fig. 6.1. Fig. 6.4 shows the definition of the pilot visual and motion responses, indicated with $H_{pv}(s)$ and $H_{pm}(s)$ in Fig. 6.1, respectively, used for modeling multimodal pilot tracking behavior in the roll tracking task studied in this chapter.

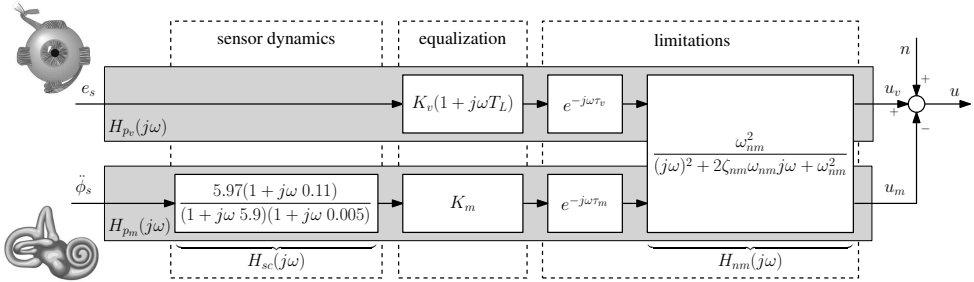


Figure 6.4. The multimodal pilot model used for modeling pilot control of aircraft roll attitude.

Note from Fig. 6.4 that the multimodal pilot model consists of separate terms that capture sensory dynamics, pilot equalization dynamics, and pilot limitations. The model for the pilot visual response $H_{pv}(j\omega)$ is based on McRuer et al.'s precision model [McRuer et al., 1965]. Note that as pilot lead equalization is expected for the controlled element given by Eq. (6.4), the visual equalization dynamics are modeled with a gain-lead element [McRuer et al., 1965]. Furthermore, a pure time delay is assumed to be associated with a response to visually presented tracking errors, and the control input given by the pilot is further assumed to be limited by the combined neuromuscular actuation and manipulator dynamics $H_{nm}(j\omega)$. Note that $H_{nm}(j\omega)$ is modeled as a second-order mass-spring-damping system, which has been shown to be an acceptable model of the lumped dynamics associated with neuromuscular actuation [McRuer et al., 1965; Zaal et al., 2009b; Damveld et al., 2009].

The model for the pilot motion response $H_{pm}(j\omega)$ assumes a pilot response proportional to the output of the semicircular canals of the vestibular system. The model for $H_{pm}(j\omega)$ therefore has the supplied roll acceleration $\ddot{\phi}_{mf}$ as the input. The supplied roll acceleration is converted to an afferent neuron firing rate by the semicircular canal dynamics $H_{sc}(j\omega)$, whose dynamics as shown in Fig. 6.4 are taken from previous investigations into manual control in multimodal environments [Hosman, 1996]. This afferent firing rate, whose unit is here defined as impulses per unit of time (IPUT), is known to be proportional to rotational velocity over a fairly wide frequency range [Fernandez and Goldberg, 1971; Hosman, 1996]. Note from Fig. 6.4 that the same normalization of the semicircular canal dynamics as proposed by Groen et al. [2006] is considered here, which ensures that $H_{sc}(j\omega)$ has unity magnitude at 1 rad/s and hence has dynamics that approximate $1/s$ in the frequency range between $1/5.9$ and $1/0.11$ rad/s. Therefore, the considered model for the semicircular canal

dynamics differs from the model used in Chapters 2 and 4 by the gain of 5.97, which ensures this property. As a result of this convention, the pilot motion response gain K_m has the unit V/IPUT, as can be verified from Fig. 6.4. Finally, equivalent to the model for the pilot visual response, a pure delay and the neuromuscular actuation dynamics are also included in the model for $H_{p_m}(j\omega)$.

It is known that human roll motion perception is the result of more than just the perception with the semicircular canals [Hosman, 1996]. For instance, pilots may also respond to changes in the lateral specific force or somatosensory cues that result from the rotational roll motion instead of or in addition to the actual roll accelerations. Still, as for instance shown in Chapter 4, the pilot motion response is typically found to be proportional to the rate of the controlled element state over a wide frequency range, independent of the degree of freedom of the cued and perceived motion. Note that such a response proportional to the supplied roll rate $\dot{\phi}_s$ also results from the proposed form of $H_{p_m}(j\omega)$ shown in Fig. 6.4 over the 0.1-10 rad/s frequency range where the semicircular canal dynamics are approximately K/s .

For fitting the model of Fig. 6.4 to measured data for e , $\ddot{\phi}_{mf}$, and u , the semicircular canal dynamics are assumed to be fixed. This leaves a total of seven model parameters to be estimated: the pilot model gains K_v and K_m , the visual lead time constant T_L , the pilot visual and motion delays τ_v and τ_m , and the parameters of the neuromuscular actuation model ω_{nm} and ζ_{nm} .

6.2.3 Motion Filter and Pilot-Vehicle System Dynamics

As proposed by McRuer et al. [1965] in the crossover model, human operators adapt their own dynamics to those of the controlled element to achieve a combined pilot-vehicle system with desirable characteristics, especially in the frequency range around the pilot-vehicle system crossover frequency. For control tasks that are more complicated than the single-loop compensatory tracking tasks for which the crossover model was developed, there may be more elements in the closed-loop control task that affect the pilot-vehicle system dynamics. For instance, as can be verified from Fig. 6.1, for the roll tracking task with motion feedback considered in this chapter, the closed-loop pilot-vehicle system dynamics are also affected by the presence of a motion filter and the visual and motion cueing dynamics. To illustrate this, the following relations can be derived from Fig. 6.1 for the disturbance and target open-loop responses, whose crossover frequencies and phase margins are often used for assessing closed-loop pilot-vehicle system performance and stability for disturbance rejection and target-following, respectively [Jex et al., 1978]:

$$H_{ol,d}(s) = -\frac{U_c(s)}{\delta_c(s)} = [H_{s_v}(s)H_{p_v}(s) + s^2H_{s_m}(s)H_{p_m}(s)] K_s H_c(s) \quad (6.5)$$

$$H_{ol,t}(s) = \frac{\phi(s)}{E(s)} = \frac{H_{s_v}(s)H_{p_v}(s)K_s H_c(s)}{1 + s^2H_{m_f}(s)H_{s_m}(s)H_{p_m}(s)K_s H_c(s)} \quad (6.6)$$

Note from Eqs. (6.5) and (6.6) that if the pilot motion response $H_{p_m}(s)$ is set to 0, which indicates no use was made of motion feedback, both these relations reduce to the single-loop

open-loop response $H_{ol}(s) = H_{s_v}(s)H_{p_v}(s)K_sH_c(s)$. If $H_{p_m}(s) \neq 0$, however, it is clear that if pilot behavior remains constant, a change in the dynamics of the motion filter $H_{m_f}(s)$ will result in changes in the dynamics of both the disturbance-rejection and target-following open-loop systems as defined by Eqs. (6.5) and (6.6), respectively.

If this gives undesirable pilot-vehicle system dynamics, pilots might then adapt their control dynamics in response to the presence of a motion filter with certain dynamics to (partially) compensate for the effect of $H_{m_f}(s)$ on the closed-loop system. The most elementary example of this would be the case where motion cues are attenuated by a pure gain, $H_{m_f}(s) = K_{m_f}$, compared to where they are presented 1-to-1 ($K_{m_f} = 1$). As long as the gain does not cause the motion cues to become smaller than human motion perception thresholds [De Vroome et al., 2009], pilots could simply respond to the lower magnitude motion information ($\ddot{\phi}_{m_f}$) with a higher gain K_m . If they succeed in increasing the gain of $H_{p_m}(s)$ with around $1/K_{m_f}$, this means the open-loop dynamics as given by Eqs. (6.5) and (6.6) remain approximately the same.

Similarly, a motion filter with certain dynamics also affects the corresponding closed-loop forcing function to error responses given by:

$$H_{e,f_d}(s) = \frac{E(s)}{F_d(s)} = \frac{-H_c(s)}{1 + [H_{s_v}(s)H_{p_v}(s) + s^2H_{m_f}(s)H_{s_m}(s)H_{p_m}(s)]K_sH_c(s)} \quad (6.7)$$

$$H_{e,f_t}(s) = \frac{E(s)}{F_t(s)} = \frac{1 + s^2H_{m_f}(s)H_{s_m}(s)H_{p_m}(s)K_sH_c(s)}{1 + [H_{s_v}(s)H_{p_v}(s) + s^2H_{m_f}(s)H_{s_m}(s)H_{p_m}(s)]K_sH_c(s)} \quad (6.8)$$

H_{e,f_d} and H_{e,f_t} as given by Eqs. (6.7) and (6.8) are indicative of the success of the closed-loop system depicted in Fig. 6.1 in attenuating f_d and following f_t . Changes to these closed-loop responses due to $H_{m_f}(s)$ may yield unsatisfactory performance of the closed-loop pilot-vehicle system, especially if they result in degraded performance around crossover, thereby perhaps forcing pilots to change their own control dynamics to alleviate these effects.

6.3 Offline Pilot-Vehicle System Analysis

6.3.1 Analysis Setup

To evaluate the effect of the dynamics of a motion filter in the motion feedback path of the closed-loop control task (see Fig. 6.1) on the overall pilot-vehicle system dynamics, an offline control-theoretic analysis was performed. The parameters used to define the pilot-vehicle system dynamics for the roll attitude control task considered in this chapter are taken from a previous experiment that measured roll tracking behavior in real flight ([Zaal et al., 2010]) and will be provided in Section 6.3.2.

Using these pilot dynamics that are appropriate for the case where $H_{m_f}(s) = 1$ it is possible to evaluate the effect of changes in motion filter dynamics on the performance and stability of the pilot vehicle system, assuming no pilot adaptation. Even though it is not possible to infer how pilots will adapt their control dynamics in response to the introduction

of a motion filter with certain dynamics, such an analysis does give insight into how important pilot-vehicle system characteristics are affected by $H_{mf}(s)$. For instance, Eqs. (6.5) to (6.8) give some of the important open-loop and closed-loop transfer functions that are related to pilot-vehicle system performance and stability. To evaluate the discrepancies, which in the remainder of this chapter will be referred to with the symbol “ Δ ”, that occur in these transfer functions as a result of varying $H_{mf}(s)$, the following relation is defined:

$$\Delta H(s) = \frac{H(s)|_{H_{mf}(s)}}{H(s)|_{H_{mf}(s)=1}} \quad (6.9)$$

Eq. (6.9) shows how a change in a generic transfer function $H(s)$ that is a function of the motion filter dynamics $H_{mf}(s)$ with respect to the case where no motion filter is present ($H_{mf}(s) = 1$) can be evaluated. Similarly, for a derived quantitative measure X – which could for example be the achieved tracking performance expressed as the variance of the error signal e (σ_e^2) or the disturbance open-loop crossover frequency $\omega_{c,d}$ – a similar “ Δ ” can be defined as:

$$\Delta X = X|_{H_{mf}(s)} - X|_{H_{mf}(s)=1} \quad (6.10)$$

Using Eqs. (6.9) and (6.10) this section will attempt to quantify the effect of a first-order high-pass motion filter with dynamics $H_{mf}(s)$ as given by Eq. (6.1) on the pilot-vehicle system depicted in Fig. 6.1. Seven different quantitative measures of pilot-vehicle system performance and stability (X in Eq. (6.10)) will be analyzed in this section:

- The target and disturbance open-loop crossover frequencies, $\omega_{c,d}$ and $\omega_{c,t}$
- The target and disturbance open-loop phase margins, $\varphi_{m,d}$ and $\varphi_{m,t}$
- The tracking error signal variance σ_e^2 and the separate variance contributions of the disturbance and target forcing functions, $\sigma_{e,d}^2$ and $\sigma_{e,t}^2$

For the analysis of the effect of $H_{mf}(s)$ only first-order high-pass motion filter dynamics as given by Eq. (6.1) were considered. The two motion filter parameters, the motion filter gain K_{mf} and the filter break frequency ω_{mf} were varied independently over a range of typical values. For K_{mf} values between 0 and 1 (steps of 0.05) were considered, while the effect of the filter break frequency was evaluated for ω_{mf} ranging from 0 to 3 rad/s, with 0.1 rad/s increments.

6.3.2 Analysis Parameters

The dynamics and settings of most of the elements in the closed-loop control task depicted in Fig. 6.1, such as the controlled element dynamics $H_c(s)$ and the forcing function signals f_d and f_t , have already been defined in Section 6.2.1. The only important element to define for the analysis that will be performed in this section are the dynamics of the pilot visual and motion responses $H_{pv}(s)$ and $H_{pm}(s)$. For this analysis, parameters for the multimodal pilot model described in Section 6.2.2 were taken from [Zaal et al., 2010], which presents identified pilot model parameters (pilot 2) for an in-flight roll attitude tracking task

performed in DUT's Cessna Citation II laboratory aircraft with quasi-random target and disturbance forcing function signals (condition C3). The pilot model parameters that were used to set $H_{p_v}(s)$ and $H_{p_m}(s)$ for the analysis are listed in the left column of Table 6.2.

Table 6.2. Offline analysis parameters and derived measures.

Analysis parameters			Derived measures		
Symbol	Value	Unit	Symbol	Value	Unit
K_v	0.3749	V/deg	$\omega_{c,d}$	2.6147	rad/s
T_L	0.2230	s	$\omega_{c,t}$	1.5244	rad/s
K_m	0.0869	V/IPUT	$\varphi_{m,d}$	53.5120	deg
τ_v	0.2740	s	$\varphi_{m,t}$	64.9336	deg
τ_m	0.1290	s	σ_e^2	0.2688	deg ²
ω_{nm}	9.5930	rad/s	$\sigma_{e,d}^2$	0.1052	deg ²
ζ_{nm}	0.1920		$\sigma_{e,t}^2$	0.1636	deg ²
			σ_u^2	0.0617	V ²
K_{mf}	1.0		$\sigma_{u,d}^2$	0.0366	V ²
ω_{mf}	0.0	rad/s	$\sigma_{u,t}^2$	0.0251	V ²

The difference in the pilot model gains K_v and K_m listed in Table 6.2 compared to the data presented in [Zaal et al., 2010] results from the fact that Zaal et al. considered the signal u_c as the pilot model output instead of u . Furthermore, the inputs to the pilot model were considered in rad rather than deg, yielding a difference in the values of K_v and K_m of $\pi/(180K_s)$. Finally, due to the different gain of the semicircular canal dynamics model used in the multimodal pilot model in this chapter (see Section 6.2.2), the value of K_m differs an additional factor $1/5.97$ with the value reported by [Zaal et al., 2010].

In addition to the pilot model parameters used for the analysis, Table 6.2 also shows the reference values of the quantitative measures that will be analyzed for the reference case where $K_{mf} = 1$ and $\omega_{mf} = 0$ rad/s, yielding $H_{mf}(s) = 1$. These values are calculated from the model of the control task of Fig. 6.1 using the listed settings of the pilot model and motion filter parameters. The values obtained for the target and disturbance loop crossover frequencies and phase margins, and the fact that the disturbance loop shows a higher crossover frequency and a lower phase margin, are consistent with previous research [Hosman, 1996; Van der Vaart, 1992; Zaal et al., 2009b,c; Pool et al., 2010; Zaal et al., 2011]. Also the fact that tracking errors resulting from a disturbance signal are more effectively attenuated than those resulting from a target signal (both signals here resulted in a total error variance of 0.4 deg^2 if not compensated for) is consistent with earlier findings [Hosman, 1996; Van der Vaart, 1992; Zaal et al., 2009c, 2011].

6.3.3 Analysis Results

6.3.3.1 Pilot-Vehicle System Open-Loop Dynamics

Figures 6.5 and 6.6 depict the discrepancies according to the definition of Eq. (6.9) that would occur in the pilot-vehicle system disturbance and target open-loop responses as defined by Equations (6.5) and (6.6) without pilot adaptation for variations in the filter break

frequency ω_{mf} and the filter gain K_{mf} , respectively. Note that for the data shown in Fig. 6.5, the filter gain is equal to $K_{mf} = 1$. Similarly, Fig. 6.6 shows data for a variation in K_{mf} for the case where no washout is present ($\omega_{mf} = 0$ rad/s). In all graphs in Figures 6.5 and 6.6 the gray shaded area indicates the crossover region, that is, the 1-5 rad/s range where the pilot-vehicle system crossover frequency is typically located for compensatory tracking.

Fig. 6.5 shows that the introduction of a washout filter in the motion feedback path degrades both the characteristics of $H_{ol,d}(s)$ and $H_{ol,t}(s)$. For the disturbance open-loop response, for which the visual and motion feedback paths are parallel, an almost constant decrease in open-loop magnitude in the crossover region, which increases with increasing ω_{mf} , can be observed in Fig. 6.5(a). For $\omega_{mf} = 2$ rad/s the open-loop gain is seen to reduce with a factor of around 0.7 in the crossover region. In addition to this discrepancy in open-loop gain, Fig. 6.5(c) also shows an increase in the disturbance open-loop phase lag, mainly in the lower frequency range and extending into the lower part of the crossover region.

For the target open-loop $H_{ol,t}(s)$ a different effect of ω_{mf} on the open-loop magnitude is observed. As can be verified from Fig. 6.5(b), rather than an approximately constant discrepancy in open-loop gain as observed for $H_{ol,d}(s)$, a steepening of the slope of the open-loop response in the crossover region is found to occur for $H_{ol,t}(s)$ with increasing ω_{mf} . Note that this is consistent with the increased target open-loop phase lag visible in Fig. 6.5(d). The drop in open-loop phase is found to be larger for the target open-loop than for $H_{ol,d}(s)$.

A decrease in the gain of a pure-gain washout filter is also seen to affect the disturbance and target open-loop responses, see Fig. 6.6. For the disturbance open-loop, decreasing K_{mf} is seen to yield a slight reduction in the gain of $H_{ol,d}(s)$ at the higher frequencies in the crossover region and a marked drop in the open-loop phase that increases with frequency. Fig. 6.6(c) shows that for low K_{mf} this drop in open-loop phase reaches over 30 deg in the crossover region, that is, a reduction of $\varphi_{m,d}$ to 40% of its nominal value (see Table 6.2). For the target open-loop, Fig. 6.6(b) shows a strong increase in the low-frequency gain of $H_{ol,t}(s)$ with decreasing K_{mf} , which extends well into the crossover region. A decrease in open-loop phase that increases with frequency, similar to yet slightly smaller than observed for $H_{ol,d}(s)$, is further visible in Fig. 6.6(d).

Figures 6.5 and 6.6 show that when a pilot does not adapt his control behavior to the introduction of a washout filter with a certain gain K_{mf} and break frequency ω_{mf} , this leads to changes in the disturbance and target open-loop dynamics that are typically associated with degraded pilot-vehicle system dynamics. The most prominent examples are the observed reduction in the gain of $H_{ol,d}(s)$ and the increased magnitude of the target open-loop, which have been reported to signal decreasing tracking performance [McRuer et al., 1965; Hosman, 1996; Pool et al., 2008a]. Furthermore, the decreased phase of both in the crossover region is indicative of reduced stability margins and closed-loop damping.

6.3.3.2 Crossover Frequencies and Phase Margins

Figures 6.5 and 6.6 presented the individual effects of variations in K_{mf} and ω_{mf} on the disturbance and target open-loop responses. For the full variation in both motion filter parameters considered for the offline analysis (see Section 6.3.1), Figures 6.7 and 6.8 show

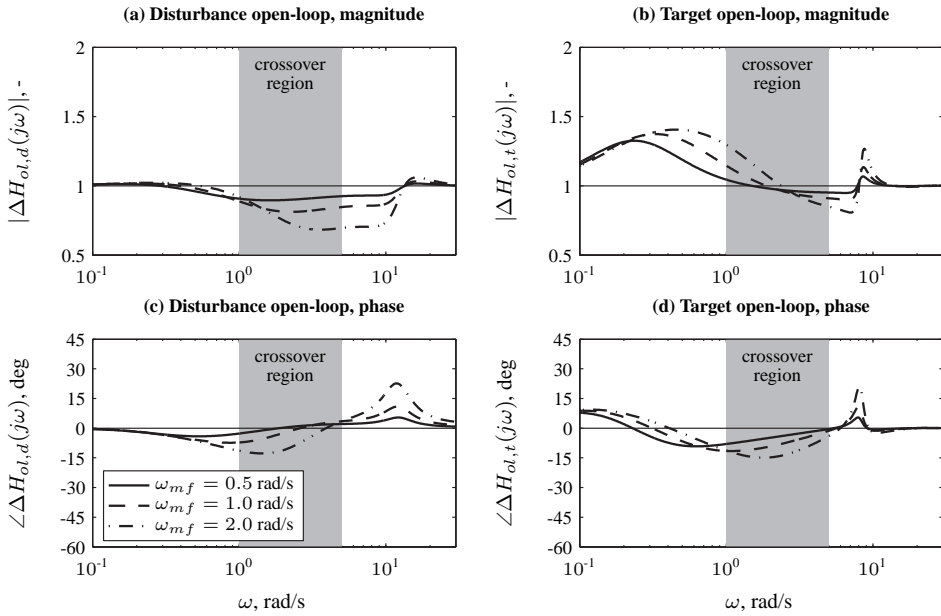


Figure 6.5. Offline analysis prediction of the discrepancies in the pilot-vehicle system open-loop responses as a function of ω_{mf} for $K_{mf} = 1$.

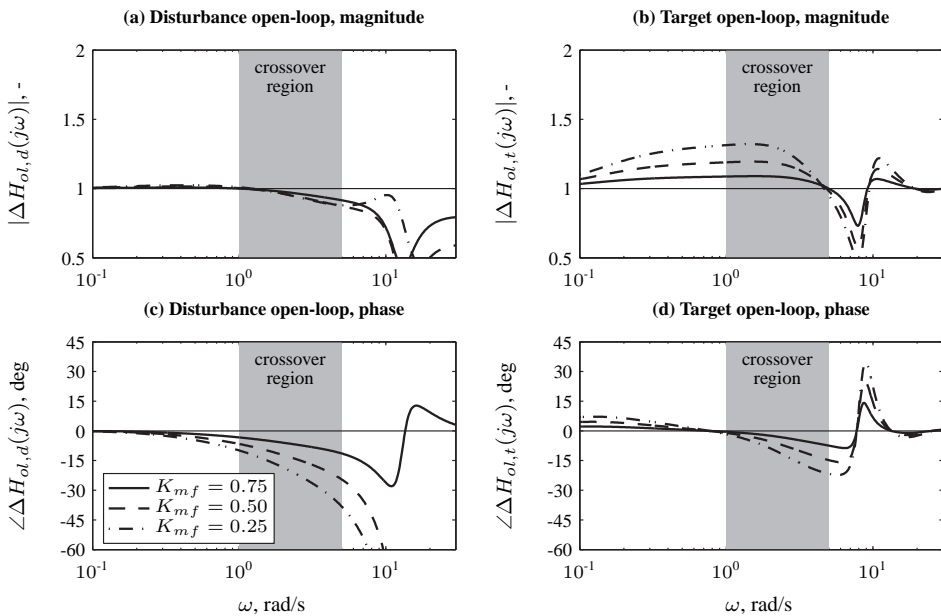


Figure 6.6. Offline analysis prediction of the discrepancies in the pilot-vehicle system open-loop responses as a function of K_{mf} for $\omega_{mf} = 0$ rad/s.

the corresponding changes in the disturbance and target open-loop crossover frequencies, respectively. For both measures, graph (a) shows the two-dimensional variation as a function of both motion filter parameters, while graphs (b) and (c) show curves that represent the observed discrepancies along trajectories A-C and D-F, respectively, as indicated in graph (a) with dashed black lines. Note that trajectories C and D correspond to the data presented in Figures 6.5 and 6.6, respectively.

In line with the data presented in Figures 6.5 and 6.6, Fig. 6.7 shows that the disturbance crossover frequency is highly sensitive to changes in ω_{mf} and is seen to decrease with increasing motion filter break frequency. The largest discrepancies in $\omega_{c,d}$ are seen to occur for $K_{mf} = 1$, for which a drop in disturbance crossover frequency of nearly 0.8 rad/s is observed around $\omega_{mf} = 2$ rad/s, a 30% drop compared to the nominal value listed in 6.2. Fig. 6.7(b) shows that the sensitivity to changes in ω_{mf} largely disappears for values of the filter break frequency above 1.5-2 rad/s. Furthermore, Figures 6.7(a) and (b) show a clear effect of the interaction between K_{mf} and ω_{mf} on the disturbance crossover frequency. For instance, the total variation in $\omega_{c,d}$ along intersections B and C – which correspond to $K_{mf} = 0.5$ and $K_{mf} = 1$, respectively – is approximately equal to 0.3 and 0.8 rad/s, respectively, over the full range of considered values for ω_{mf} . Furthermore, Fig. 6.7(c) clearly shows that if no washout is present ($\omega_{mf} = 0$ rad/s), $\omega_{c,d}$ increases with increasing K_{mf} , as expected from Eq. (6.5), while already for modest filter break frequency settings the opposite trend is observed.

The discrepancies in the open-loop dynamics presented in Figures 6.5 and 6.6 showed that the magnitude of the target open-loop response $H_{ol,t}(s)$ was affected more strongly by changes in K_{mf} than by changes in ω_{mf} . This same effect is also clearly visible in Fig. 6.8(a), where the largest variation in the target open-loop crossover frequency $\omega_{c,t}$ is observed a direction parallel to the longitudinal K_{mf} axis. Fig. 6.8(c) shows an almost linear increase in $\omega_{c,t}$ with decreasing motion filter gains, a trend on which the different values of ω_{mf} for trajectories D-F are found to only have minor impact. Note that the nearly 1 rad/s increase in $\omega_{c,t}$ observed for very low values of K_{mf} is especially large compared to the nominal value of $\omega_{c,t} = 1.52$ rad/s listed in Table 6.2.

Figures 6.9 and 6.10 show the variation in the disturbance and target open-loop phase margin that result from changes in the motion filter gain and break frequency in the same format as that used for Figures 6.7 and 6.8. It should be noted, however, that the presented predictions of changes in $\varphi_{m,d}$ and $\varphi_{m,t}$ are less directly a result of K_{mf} and ω_{mf} than those obtained for $\omega_{c,d}$ and $\omega_{c,t}$. This is caused by the fact that the phase margin is calculated at the corresponding crossover frequency. The phase of the open-loop transfer functions given by Equations (6.5) and (6.6) typically continuously decreases with increasing frequency. Therefore, a change in phase margin as shown in Figures 6.9 and 6.10 always results from the combined effects of the discrepancies in the open-loop phase responses caused by K_{mf} and ω_{mf} (as shown in Figures 6.5 and 6.6) and the change in the corresponding crossover frequency value.

Fig. 6.9 shows a clear example of this. The increase in disturbance open-loop phase margin visible for $K_{mf} > 0.75$ and $0 < \omega_{mf} < 2.5$ rad/s does not result from reduced phase lag in $H_{ol,d}(s)$, as Figures 6.5 and 6.6 both show phase lag increases with increasing ω_{mf} and decreasing K_{mf} , respectively. This gain in $\varphi_{m,d}$ is the result of the decrease in $\omega_{c,d}$, on average 0.5 rad/s for this range of values of K_{mf} and ω_{mf} , as shown in Fig. 6.7.

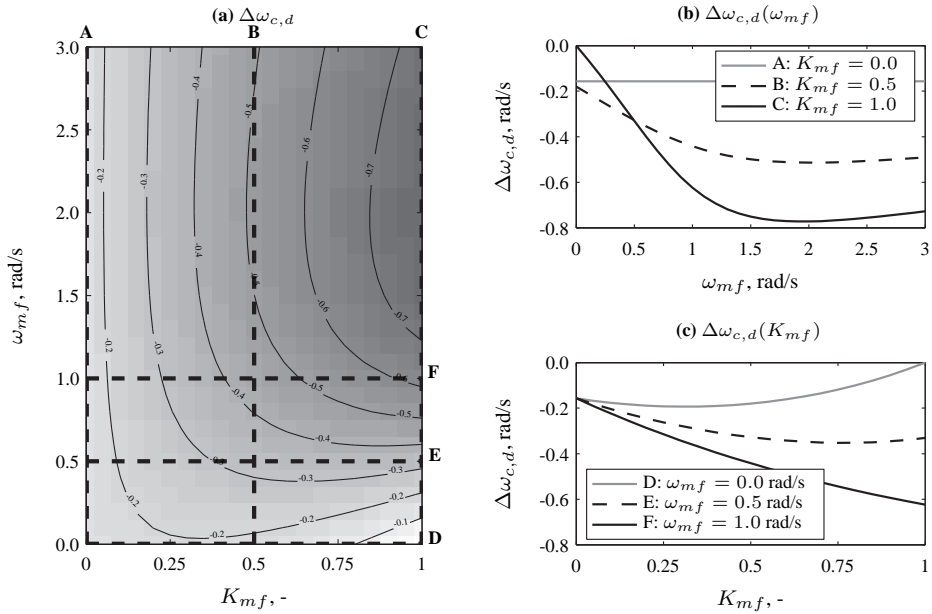


Figure 6.7. Offline analysis prediction of the discrepancies in disturbance crossover frequency as a function of K_{mf} and ω_{mf} .

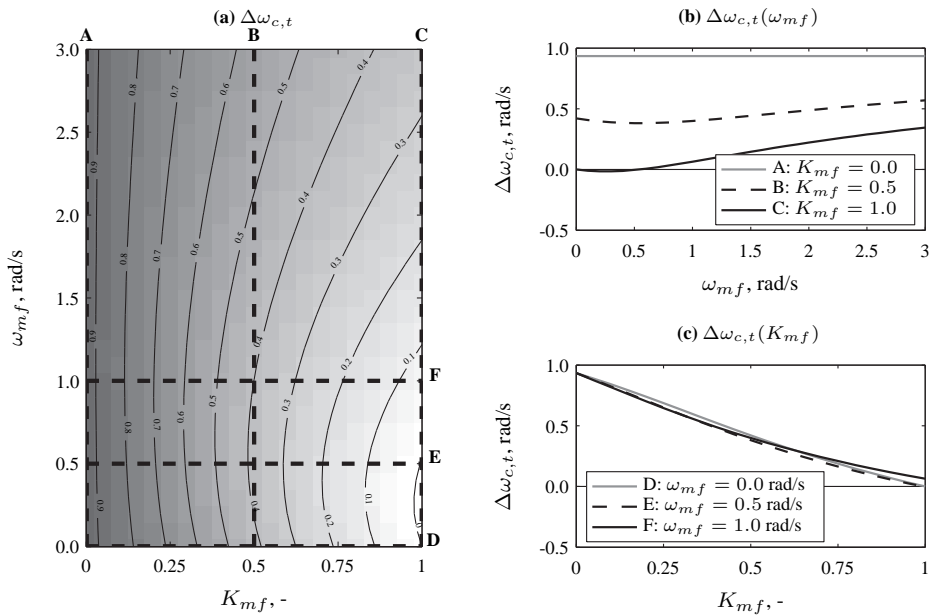


Figure 6.8. Offline analysis prediction of the discrepancies in target crossover frequency as a function of K_{mf} and ω_{mf} .

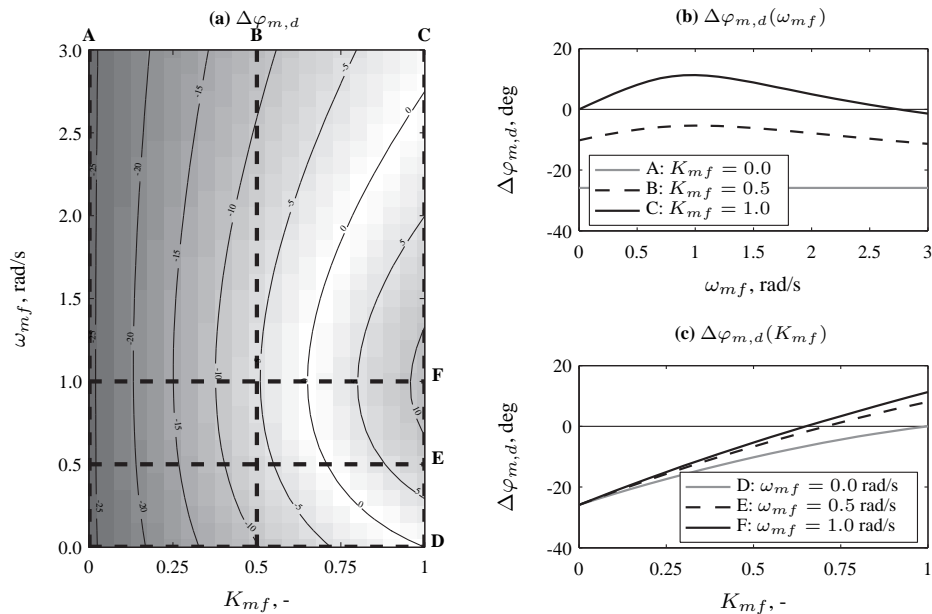


Figure 6.9. Offline analysis prediction of the discrepancies in disturbance phase margin as a function of K_{mf} and ω_{mf} .

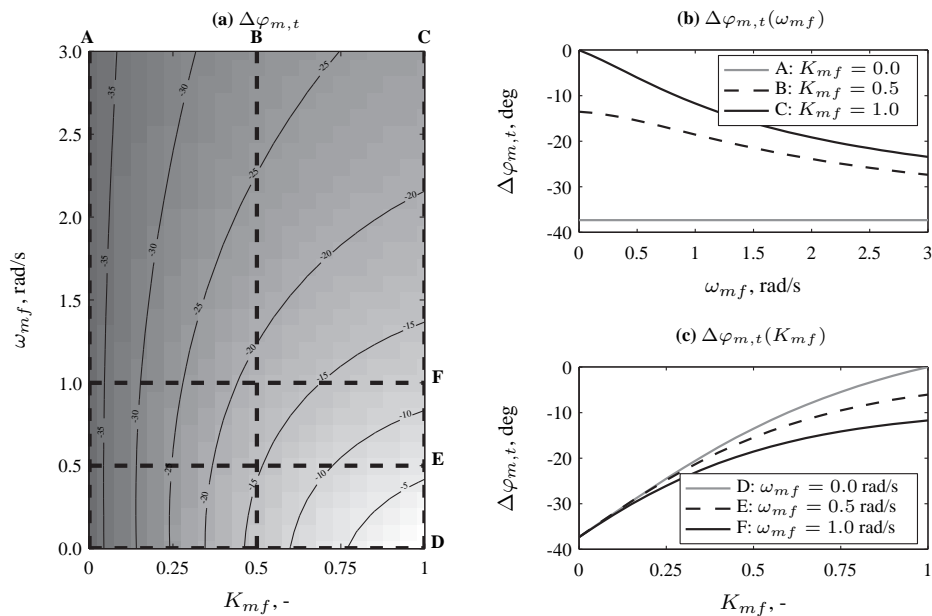


Figure 6.10. Offline analysis prediction of the discrepancies in target phase margin as a function of K_{mf} and ω_{mf} .

The decrease in $\varphi_{m,d}$ with decreasing K_{mf} shown in Fig. 6.9(c), around 30 deg over the full range of considered motion filter gains, however, confirms the drop in open-loop phase observed in Fig. 6.6(c).

As can be verified from Fig. 6.10, the target phase margin $\varphi_{m,t}$ is found to decrease as a result of both decreasing K_{mf} and increasing ω_{mf} . Figures 6.10(b) and (c) show that the largest variation in $\varphi_{m,t}$ occurs for $K_{mf} = 1$, for which a drop of around 25 deg is observed between $\omega_{mf} = 0$ and 3 rad/s. For $K_{mf} = 0.5$ the effect of ω_{mf} is found to be smaller (around 15 deg reduction over the full range of ω_{mf}), however, with added phase lag that results from the drop in K_{mf} .

Figures 6.7 to 6.10 show that with no adaptation of pilot dynamics, increasing ω_{mf} and decreasing K_{mf} both lead to changes in the disturbance and target crossover frequencies and phase margins, and hence to changes in pilot-vehicle system performance and stability. The decrease in $\omega_{c,d}$, the increase in $\omega_{c,t}$, and the decrease in both phase margins for settings of K_{mf} and ω_{mf} that correspond to a lower level of motion fidelity are all indicators of unfavorable changes to the dynamic characteristics of the pilot-vehicle system.

6.3.3.3 Closed-Loop Tracking Performance

Degraded pilot-vehicle system crossover frequencies and stability margins during compensatory tracking are typically found to result in degraded tracking performance, especially in the frequency range around crossover [McRuer et al., 1965; McRuer and Jex, 1967a]. Figures 6.11 and 6.12 show the discrepancies in the closed-loop disturbance-to-error and target-to-error responses as defined by Equations (6.7) and (6.8), respectively, for the same variation in ω_{mf} and K_{mf} for which the discrepancies in the corresponding open-loop responses are presented in Figures 6.5 and 6.6.

Figures 6.11 and 6.12 show that both increasing ω_{mf} and decreasing K_{mf} yields increased magnitude of both $H_{e,f,d}(s)$ and $H_{e,f,t}(s)$ in the crossover region, which indicates degraded tracking performance. Note that as the degradation in closed-loop error attenuation is strongest in the 1-5 rad/s frequency range, these effects of varying motion filter dynamics are mainly felt for control tasks and forcing function signals that induce significant control power in this frequency range. The example frequency responses shown in Figures 6.11 and 6.12 suggest that the degradation in tracking performance resulting from reducing K_{mf} is larger than the effect of increasing ω_{mf} , as the peaking in the crossover region is much more severe for the former as can be judged from Fig. 6.12.

Figures 6.13 and 6.14 show the corresponding variation in the disturbance and target components of the tracking error variance – $\sigma_{e,d}^2$ and $\sigma_{e,t}^2$, respectively – that result for the full variation in the motion filter gain and break frequency considered in the offline analysis. Figures 6.13 and 6.14 confirm the dominant effect of K_{mf} on closed-loop pilot vehicle system performance suggested by Figures 6.11 and 6.12, as both $\sigma_{e,d}^2$ and $\sigma_{e,t}^2$ are found to increase markedly with decreasing K_{mf} while remaining comparatively constant with changes in motion filter break frequency. Note from comparison of Figures 6.13(c) 6.14(c) that $\sigma_{e,d}^2$ is more sensitive to small reductions in K_{mf} from 1, while for $\sigma_{e,t}^2$ the effect of K_{mf} is less pronounced for $K_{mf} > 0.5$. It should be noted that the degradation in tracking performance observed in Figures 6.13 and 6.14 is marked, considering the reference values of $\sigma_{e,d}^2 = 0.11 \text{ deg}^2$ and $\sigma_{e,t}^2 = 0.16 \text{ deg}^2$ for $K_{mf} = 1$ and $\omega_{mf} = 0 \text{ rad/s}$ (see Table 6.2).

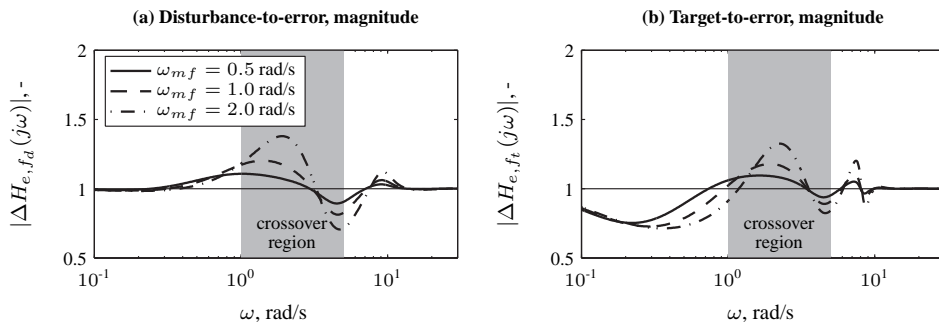


Figure 6.11. Offline analysis prediction of the discrepancies in the closed-loop forcing function-to-error responses as a function of ω_{mf} for $K_{mf} = 1$.

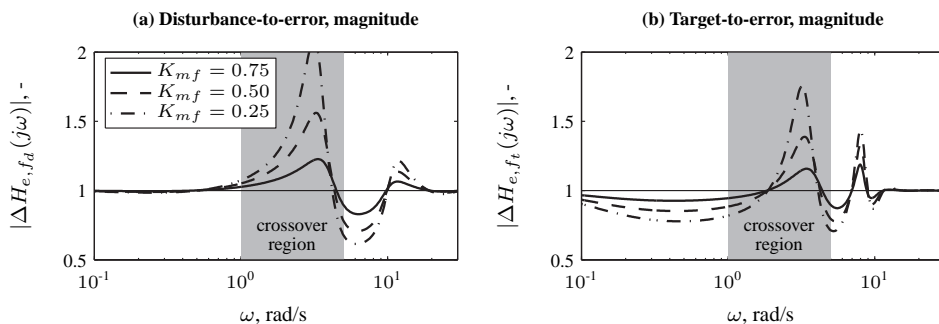


Figure 6.12. Offline analysis prediction of the discrepancies in the closed-loop forcing function-to-error responses as a function of K_{mf} for $\omega_{mf} = 0$ rad/s.

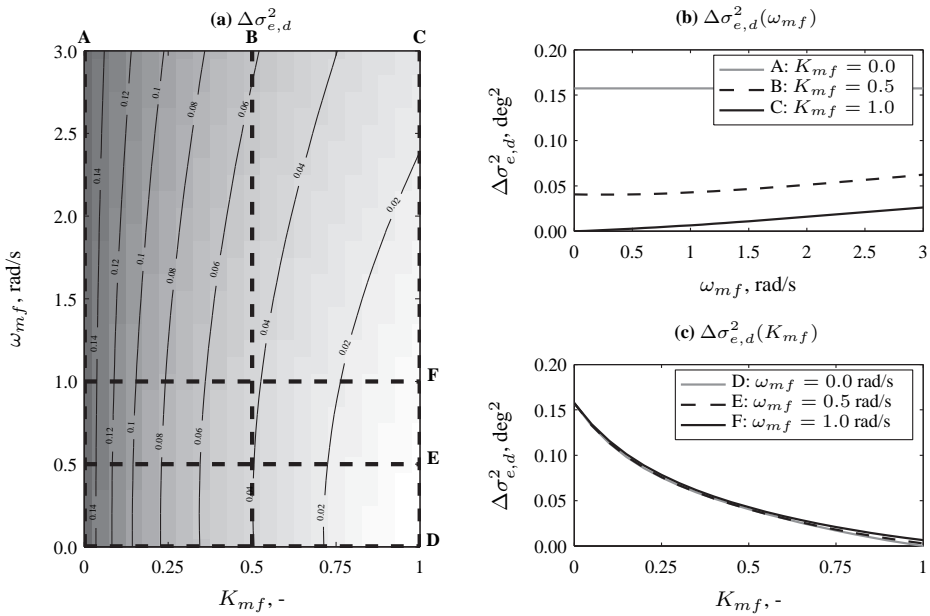


Figure 6.13. Offline analysis prediction of the discrepancies in disturbance tracking error variance as a function of K_{mf} and ω_{mf} .

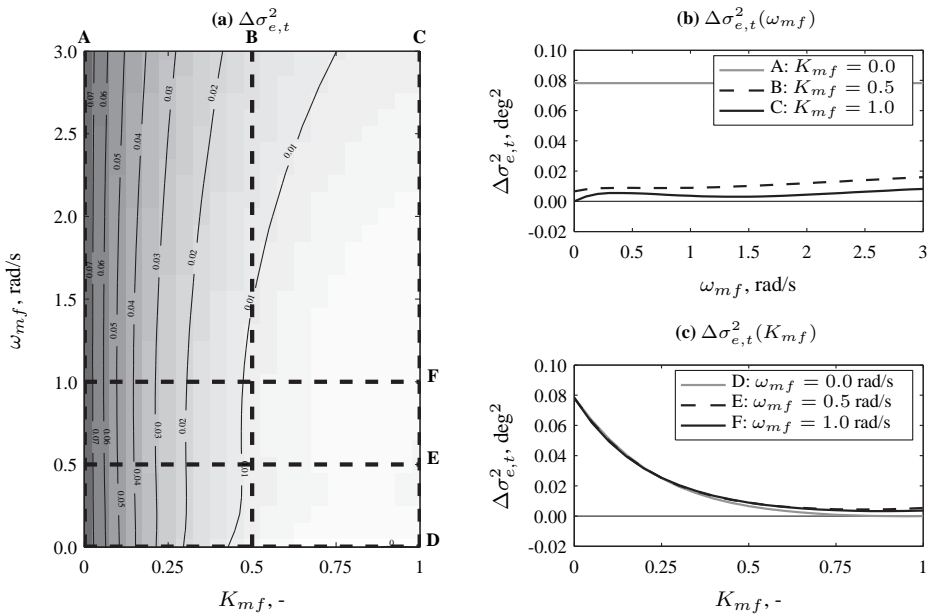


Figure 6.14. Offline analysis prediction of the discrepancies in target tracking error variance as a function of K_{mf} and ω_{mf} .

6.4 Experiment Setup

6.4.1 Apparatus

6.4.1.1 Cessna Citation II Laboratory Aircraft

For the experiment performed to measure pilot tracking behavior both in-flight and for varying roll motion cueing settings in a flight simulator, two different facilities were used. The first is the Cessna Citation II laboratory aircraft that is owned by the Faculty of Aerospace Engineering of Delft University of Technology and the Netherlands' National Aerospace Laboratory (NLR) shown in Fig. 6.15. The Citation II is a twin-jet business aircraft with two Pratt & Whitney JT15D-4 turbofan engines. The maximum operating altitude of the aircraft is 43,000 ft and the maximum cruising speed is 385 kt. In addition to a custom Flight Test Instrumentation System (FTIS) that is available in the aircraft [Zaal et al., 2009d], extra sensors can be installed on a nose boom, roof rack, or external pod underneath the aircraft.

The experimental setup in the laboratory aircraft used for the current experiment was highly similar to that used for the earlier experiments described in [Zaal et al., 2010] and [Zaal et al., 2011]. The aircraft was equipped with a nose boom with alpha and beta vanes, which allowed for more accurate measurements of the undisturbed angle of attack and the sideslip angle, respectively, during the experiment. At the right pilot seat a programmable LCD display was installed in front of the instrument panel, see Fig. 6.17. This LCD display was used to present the compensatory display shown in Fig. 6.2 to the pilots. The update rate of the LCD display was 60 Hz and, as also stated in Section 6.2.1, the latency of this display (including the projection) was measured to be 25 ms.

Fig. 6.17 further shows the side stick manipulator that was used for the experiment. This BG Systems JF force stick was used to give control inputs during the in-flight tracking tasks. As explained in detail in [Zaal et al., 2009d, 2010], the side stick commands and the disturbance forcing function signal were fed to a custom Experiment Computer present in the aircraft, which in turn used the electrical actuators of the Honeywell SP-200 (4008519-941) automatic control system to move the aircraft control surfaces. Note that as the mechanical control architecture is used by the automatic control system, side stick inputs and the disturbance forcing function signal yielded movement of the control column (see Fig. 6.17). To avoid effects of this moving control column and pilots' view of the outside world on their control strategy during the pitch tracking task, participants were required to wear a hood (see Fig. 6.19) that limited their field of view to the LCD display during the in-flight measurements.

6.4.1.2 SIMONA Research Simulator

The flight simulator portion of the experiment was performed in the SIMONA Research Simulator (SRS) at Delft University of Technology, see Fig. 6.16. The SRS has a hydraulic six degree-of-freedom hexapod motion system, which was used to supply participants with the considered pitch and heave motion cues. Details of the motion cueing implementation for this experiment are given in Section 6.4.2. The time delay of the motion cues generated by the SRS motion base is no more than 30 ms [Berkouwer et al., 2005].



Figure 6.15. The Cessna Citation II laboratory aircraft.



Figure 6.16. The SIMONA Research Simulator.



Figure 6.17. The Cessna Citation II laboratory aircraft cockpit.



Figure 6.18. The SIMONA Research Simulator cockpit.



Figure 6.19. Experiment pilot wearing the hood during in-flight measurements.

As can be verified from Fig. 6.18, the experimental setup in the SRS was highly similar to that in the Citation. Participants were seated in the right pilot seat and used a Moog FCS Ecol-8000 electrical side stick to give control inputs. The compensatory display (Fig. 6.2) was shown on the primary flight display (PFD) directly in front of them. No other visual cues, for instance from the outside visual system, were provided during the experiment. The PFD update rate was 60 Hz and the delay in the image generation on the PFD in the SRS has been measured to be in the order of 25 ms, that is, approximately equal to the delay of the LCD display used for the Citation experiments.

6.4.1.3 Side Stick Manipulator

Due to the limited space available in the Citation cockpit, a force stick was used for the experiment. As opposed to a deflection stick, a force stick has very high stiffness and no manipulator deflections are required for giving a control input. Rather, the control input given by the pilot is proportional to the force applied to the manipulator. For the force stick installed in the Citation cockpit the output voltage, which was used as the pilot control input u (see Fig. 6.1), was between ± 2.5 V. As detailed in Appendix C, the relation between applied force and output voltage was determined from static measurements, where known weights were used to induce known stick forces. The resulting output voltage u was then measured. The force-voltage characteristic of the Citation force stick was found to be approximately linear over the full range of u . The electrical side stick in the SRS was configured to have the same characteristics as the Citation force stick, that is, a linear force-voltage characteristic with a gradient of 14 N/V. Note that the stiffness in the roll axis of the force stick was lower than the stiffness in the pitch axis (24 N/V) as used for the experiment of [Zaal et al., 2011]. The electrical side stick in the SRS was also configured as a force stick and set to have exactly the same force-output characteristics as the Citation force stick.

6.4.2 Simulator Motion Cueing

During the roll tracking tasks performed in the SRS simulator roll motion equivalent to that present in the Citation was presented. As can be verified from Fig. 6.20, the axis around which the SRS cabin performs roll motion – X_s , which completes the right-handed simulator reference frame indicated by Y_s and Z_s and points forward through the Upper Gimbal Point (UGP) – is located 0.55 m to the left and 1.2075 m below the design position of the right pilot's eye. As also indicated in Fig. 6.20, the axis around which the Cessna Citation II laboratory aircraft performed rolling motion was measured to be closer to the right pilot position. To achieve the same lateral and vertical specific forces at the pilot eye position directly due to rotational accelerations around the axis of roll rotation, the simulator roll axis was displaced 0.215 m in lateral direction and -0.2025 m in vertical direction.

As explained in Section 6.2.1, roll motion cues were presented for varying settings of the first-order washout filter given by Eq. (6.1). In the simulator part of the experiment, four different roll cueing conditions were evaluated, which will be explained in detail in Section 6.4.3.

In addition to the simulator roll motion cueing, a pre-positioning filter similar to that adopted in [Beukers et al., 2010] was used to move the SRS to the trim pitch attitude θ_0

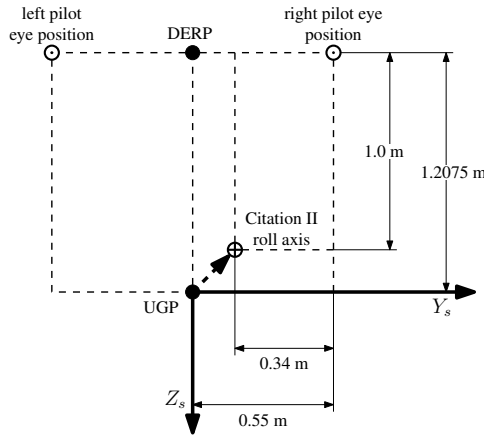


Figure 6.20. Positioning of the axis of simulator roll motion with respect to the SRS Upper Gimbal Point (UGP), Design Eye Reference Point (DERP), and the right pilot eye position.

of the Citation in the flight condition in which the experiment was performed ($V = 160$ kt, $h = 17,000$ ft). This trim pitch attitude to which the simulator was pre-positioned was equal to 4.34 deg. The pre-positioning filter was defined as:

$$H_{pp}(s) = \frac{s^2}{s^2 + 2\zeta_{n_{pp}}\omega_{n_{pp}}s + \omega_{n_{pp}}^2} \cdot \frac{s}{s + \omega_{b_{pp}}} \tag{6.11}$$

The values of the parameters of Eq. (6.11) were set to $\omega_{n_{pp}} = 1.0$ rad/s, $\zeta_{n_{pp}} = 1.0$, and $\omega_{b_{pp}} = 2.0$ rad/s. The pre-positioning was done before the start of each measurement run. Note that also for the tracking tasks performed without roll motion cueing (see Section 6.4.3) the SRS was pre-positioned to θ_0 .

6.4.3 Independent Variables

This chapter presents the results of an experiment that investigates the effect of flight simulator motion cueing on pilot control behavior in the roll attitude tracking task shown in Fig. 6.1. This experiment was designed to allow for comparison of in-flight measurements of pilot tracking behavior with those obtained in the SRS for different motion cueing settings. The different conditions under which pilot control behavior during roll tracking was evaluated in this combined in-flight and simulator experiment are listed in Table 6.3.

First of all, the middle four conditions listed in Table 6.3 indicate the four different simulator roll motion cueing settings for which pilot tracking behavior was evaluated in the SRS. For these conditions, labeled as S0-S3, the corresponding values of the roll motion filter gain K_{mf} and break frequency ω_{mf} are listed in the final column of Table 6.3 in the format (K_{mf}, ω_{mf}) .

As can be verified from Table 6.3, S0 was a condition with no simulator motion feedback, performed to allow for direct comparison with earlier work on single-loop compensatory tracking behavior [McRuer et al., 1965; McRuer and Jex, 1967a]. As motion feed-

Table 6.3. Experimental conditions.

condition	apparatus	description	filter, (K_{mf}, ω_{mf})
C0	Citation	aircraft no motion	(0,0)
S0	SIMONA	no motion	(0,0)
S1	SIMONA	medium-fidelity filter	(0.5,0.5)
S2	SIMONA	high-fidelity filter	(1,0.5)
S3	SIMONA	simulator 1-to-1 motion	(1,0)
CIT	Citation	aircraft 1-to-1 motion	—

back is increasingly attenuated by a motion filter, human operators are typically seen to revert to a control strategy that approximates single-loop compensatory control [Jex et al., 1978; Pool et al., 2010], hence it was found important to evaluate S0 as a reference measurement. On the other hand, S3 indicates the condition in which aircraft roll motion cues were presented 1-to-1, that is, $H_{mf} = 1$.

The remaining two conditions, S1 and S2, indicate two different settings of the high-pass washout filter of Eq. (6.1): both had a break frequency of 0.5 rad/s and filter gains of 0.5 and 1, respectively. Fig. 6.21 depicts the characteristics of the four motion cueing settings tested in the SRS against the simulator motion fidelity criterion proposed by Sinacori [1977], with fidelity regions as suggested by Schroeder [1999]. As can be observed from Fig. 6.21 condition S2 (1,0.5) represents a high fidelity filter setting according to the criterion proposed by Schroeder, while condition S1 would be considered medium fidelity.

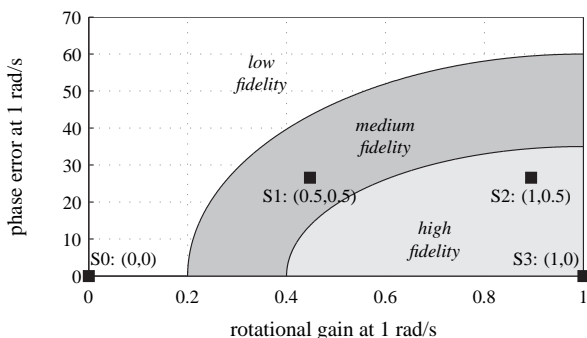


Figure 6.21. Evaluation of the rotational simulator motion fidelity criterion proposed by Sinacori [1977], with modified fidelity regions from [Schroeder, 1999], for the different experimental conditions.

The condition indicated with CIT in Table 6.3 indicates the in-flight roll tracking tasks performed in the Citation II laboratory aircraft. As the true aircraft motion was presented to the pilots in this condition, no motion filter dynamics are listed in Table 6.3. Note, however, that the physical roll motion to which pilots were subjected for the CIT and (1,0) conditions was equivalent.

Finally, Table 6.3 lists one further condition that was performed in the Citation laboratory aircraft: C0. For this condition the roll tracking task was performed using the experimental setup utilized for the in-flight measurements of condition CIT, but pilots were controlling the same model of the Citation and FBW system dynamics used in the SRS conditions rather than the aircraft itself. Condition C0 was performed on the ground and therefore yielded a condition that should be equivalent to S0, and therefore allowed for direct comparison of pilot tracking behavior in both cockpit setups. Even though extreme care was taken to ensure the important elements of the experimental setups in the Citation and SRS were as equal as possible (as detailed in Section 6.4.1), these additional measurements were performed to quantify possible discrepancies in control behavior due to remaining differences in the experimental setup and the environment in which pilot control was measured. It should be noted that for condition C0 the participants did not wear the hood they were required to wear during the in-flight measurements.

6.4.4 Participants

Seven subjects performed the roll attitude tracking task of Fig. 6.1 under the six conditions listed in Table 6.3. At the time of the experiments, all participants were active Cessna Citation II pilots employed by Delft University of Technology and all except one had experience with similar tracking tasks from previous simulator and in-flight experiments. The participants' flight experience ranged from 1,500-14,000 hrs on a multitude of different aircraft. Their ages ranged from 34 to 72 years ($\mu = 51.1$, $\sigma = 14.3$).

6.4.5 Experimental Procedure

All participants performed the simulator part of the experiment before the in-flight and no-motion measurements in the Citation laboratory aircraft were taken. During both the in-flight and simulator parts of the experiment, participants performed a number of training runs – typically 4-6 repetitions of each experimental condition – until their proficiency in performing the tracking task had reached a consistent level. Then five more repetitions of each experimental condition were collected as the measurement data.

6.4.5.1 Simulator Measurements

During the simulator part of the experiment the motion conditions listed in Table 6.3 (S0-S3) were presented in random order (Latin square) throughout both the training and measurement phases of the experiment. Breaks were taken regularly, on average after every 16 tracking runs (four repetitions of all conditions), to avoid fatigue. As explained in Section 6.4.2, the simulator was prepositioned to the aircraft trim pitch attitude before each tracking run was started, even for the condition without any further motion cues, S0. The experimenter then counted down from three and started the run. Directly after a run ended the simulator was tilted back to zero pitch attitude, after which participants were required to give a subjective judgment of motion fidelity for the run they just completed (see Section 6.4.6). After this subjective evaluation was completed participants were informed of their tracking score, defined as the root mean square of the tracking error signal e as recorded for the last run.

6.4.5.2 In-Flight Measurements

During the in-flight measurements, two pilots were always required for each flight. One pilot functioned as the safety pilot and was responsible for monitoring the aircraft during the experiment and ensuring the aircraft was in the desired trim state (velocity, altitude) before each run. The other pilot, referred to as the experiment pilot, performed the experiment.

The two conditions of the in-flight part of the experiment (see Table 6.3) were always performed in the same order. Before take-off, the measurements for the C0 condition were taken. The main reason for taking these measurements first was that this allowed for initial re-familiarization with the control task in a more controlled environment than available during flight. In addition, it was thought to reduce the number of training runs required for the in-flight measurements.

For condition C0, the experimenter initiated the start of a run (after counting down from three), as was also the case during the simulator part of the experiment. For the CIT condition, where the experiment pilot actually controlled the aircraft, the experiment pilot started the tracking runs himself using the pilot interface shown above the LCD screen in Fig. 6.17. For more details on this pilot interface, please refer to [Zaal et al., 2009d, 2010]. After completion of an in-flight tracking run, the FBW system would disengage itself, after which the safety pilot would take control of the aircraft and bring it back in the desired trim state for the next run of the experiment. The experimenter then notified the experiment pilot of his performance for the last run.

6.4.6 Dependent Measures

A number of different dependent measures are considered for this experiment to evaluate the effects of the variation in motion fidelity on pilot control behavior and tracking performance. First of all, during the conditions of the experiment performed in the SRS, participants were asked to give a subjective indication of the level of motion fidelity for each tracking run. For this, the rating scale depicted in Fig. 6.22 was used. On this visual analogue scale (VAS) the participants gave their motion fidelity rating by drawing a vertical line through the horizontal bar of the scale, which had a total length of 10 cm. For these experiments, which were designed to allow for an objective evaluation of simulator motion fidelity, these subjective ratings merely served as a reference.

How would you rate motion fidelity for this condition with respect to the aircraft?

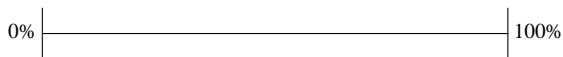


Figure 6.22. Visual analogue motion fidelity rating scale.

In addition to the subjective motion fidelity ratings, a number of objective measures of pilot tracking performance, control activity and control strategy were considered. Tracking performance and control activity were evaluated from the time-domain variances of the recorded time traces of the pitch tracking error (e) and pilot control signal (u), respectively.

In addition, using a spectral method described in [Jex et al., 1978], the contributions of the target and disturbance forcing functions and pilot remnant to these signal variances were evaluated separately.

To assess changes in pilot-vehicle system open-loop dynamics, frequency-domain describing function estimates were calculated at the forcing function frequencies [Stapleford et al., 1969; Jex et al., 1978] for the disturbance and target open-loop responses as given by Eqs. (6.5) and (6.6), respectively. From these frequency-domain describing functions, the values of the disturbance and target loop crossover frequencies ($\omega_{c,d}$ and $\omega_{c,t}$) and phase margins ($\varphi_{m,d}$ and $\varphi_{m,t}$) were then calculated.

Finally, for explicitly evaluating changes in pilot control strategy over the different experimental conditions, the multimodal pilot model introduced in Section 6.2.2 was fit to the experimental measurement data using the time-domain parameter estimation procedure described in [Zaal et al., 2009a]. As shown in Fig. 6.4, the input to the visual channel of the pilot model was the measured tracking error signal e , while the model output was the measured pilot control input u . For the in-flight tracking tasks, no measurement of $\ddot{\phi}$ was available to be used as the input of the pilot model motion channel $H_{p_m}(s)$. Therefore, the aircraft roll rate $\dot{\phi}$, which was measured for the in-flight tracking tasks using an on-board IMU, was used as the input to $H_{p_m}(s)$ for the model identification and an extra differentiator was added to the model for the pilot motion dynamics. For the data from the SRS conditions also the supplied simulator roll rates, so ϕ_s , were used for the identification of the multimodal pilot model.

Before being used for model identification, the high-frequency noise present in all signals – that is, the noise above 30 rad/s, so well above the highest frequency sinusoids in f_t and f_d , see Table 6.1 – was filtered out. The five repetitions of these signals collected for each subject and condition were then averaged, to yield one identification data set for each condition and participant. It should be noted that for conditions S0 and C0 only the visual response of the model, $H_{p_v}(s)$ was fit to measurements of e and u , as no motion feedback was available for these conditions.

6.4.7 Hypotheses

The experiment described in this chapter attempts a challenging comparison of pilot control behavior in two different environments: a real in-flight cockpit and a full-motion flight simulator. As pointed out by McRuer and Jex [1967a] human operator behavior for a certain control task is affected by a multitude of variables, of which environmental factors – such as vibration level, temperature, ambient lighting conditions, etc. – form an important group. Differences in pilot control behavior resulting from differences in such environmental factors would complicate the interpretation of the effect of motion cueing on pilot behavior as made in this chapter.

To assess possible differences in control strategy that resulted from the difference in experimental setup and environmental factors, an additional single-loop roll tracking task was performed in the setup used for the in-flight part of the experiment (condition C0, see Table 6.3). The measurements taken for this condition can be compared directly to those taken for the equivalent S0 condition in the SRS. As explained in detail in Section 6.4.1, extreme care was taken to ensure the conditions under which the in-flight and flight simulator exper-

iments were performed were as similar as possible. Hence, differences in control strategy observed for the S0 and C0 conditions were expected to be relatively minor compared to the effect of the variation in motion cueing.

The variation in simulator motion cueing evaluated for the comparison with in-flight measurements of pilot tracking behavior consists of a no-motion and a 1-to-1 roll cueing setting, in addition to two conditions with simulator roll washout. Based on the significant effects of motion feedback on pilot tracking behavior in similar tracking tasks reported in previous studies [Shirley and Young, 1968; Jex et al., 1978; Stapleford et al., 1969; Van der Vaart, 1992; Hosman, 1996; Zaal et al., 2009b; Pool et al., 2010; Zaal et al., 2011] it is expected that clear differences in tracking performance and control behavior will be observable between conditions (0,0) and (1,0). Evaluation of the two roll motion conditions with first-order washout against the motion fidelity criterion proposed by Schroeder [1999] (see Fig. 6.21) suggests that condition S1 (0.5,0.5) yields medium motion fidelity, while S2 (1,0.5) yields high motion fidelity. Here it is expected that this difference will also be visible in the measured tracking behavior, yielding behavior closest to the no-motion tracking behavior of condition (0,0) for S1. Correspondingly, only minor differences in pilot tracking behavior compared to tracking with 1-to-1 motion are expected for condition S2.

Finally, comparison of the results of the offline pilot-vehicle system analysis described in Section 6.3 with the experimental measurements is believed to provide a method for objectively pointing out pilot adaptation over the different conditions of the experiment. Based on the results of this offline analysis, it is expected that adaptation of pilot tracking behavior compared to the measurements for 1-to-1 motion occurs for both the no-motion condition (0,0) and the condition with the filter with a break frequency of 0.5 rad/s and a gain of 0.5 (0.5,0.5).

6.5 Results

This section presents the main experimental results from both the in-flight and simulator parts of the experiment. This section only compares the data for the four conditions performed in the SRS and the in-flight tracking tasks (CIT). A comparison of the reference single-loop tracking measurements taken in the Citation setup (condition C0) and the SRS (S0) can be found in Appendix F.

Data are presented as the mean over all seven experiment participants and error bars indicating the 95% confidence interval of the mean. As the experiment had a within-subjects design, the data have been corrected for between-subject variability for calculating the 95% confidence intervals. All the calculated dependent measures were analyzed using a one-way repeated-measures analysis of variance (ANOVA) to reveal statistically significant effects. Before analyzing data with an ANOVA, data were checked for normality using a Kolmogorov-Smirnov test. Furthermore, Mauchly's test of sphericity was performed to check if the assumption of sphericity was met. If for a certain dependent measure the sphericity assumption was not met, the conservative Greenhouse-Geisser sphericity correction was applied in the interpretation of the ANOVA results. For data with a distribution significantly different from normal, as indicated by the performed Kolmogorov-Smirnov tests, a nonparametric Friedman's ANOVA was performed instead of an ANOVA.

6.5.1 Subjective Motion Fidelity Ratings

Fig. 6.23 shows the subjective motion fidelity ratings collected with the VAS shown in Fig. 6.22. No normalization of the measured ratings was performed: the data in Fig. 6.23 show the true percentages measured from the VAS rating scales for each subject.

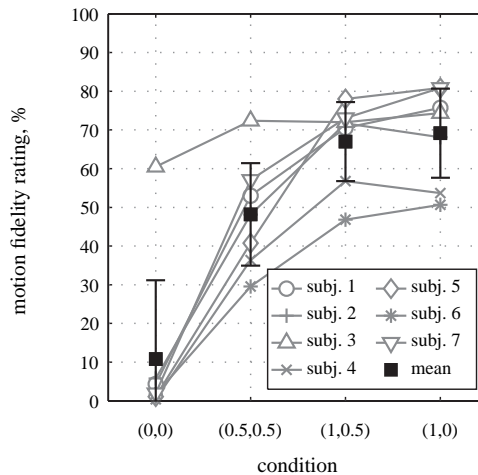


Figure 6.23. Mean subjective motion fidelity ratings for roll multisine tracking.

Fig. 6.23 shows that the different subjects were relatively consistent in their ratings, all rating the no-motion condition (0,0) the lowest and the motion cueing settings closest to the 1-to-1 case ((1,0.5) and (1,0)) the highest. Only the ratings given by subject 3 stand out, as he used a markedly smaller portion of the scale than the other subjects. Due to the data from subject 3, the ratings for conditions S0 were found to show a distribution significantly different from normal, $D(7) = 0.53$, $p < 0.05$. For this reason, nonparametric tests had to be applied to assess the statistical significance of the presented rating results. A Friedman's ANOVA showed a significant main effect of the applied variation motion cueing settings on the subjective fidelity ratings, $\chi^2(3) = 17.91$, $p < 0.05$. Pairwise comparisons of the ratings for all experimental conditions performed using Wilcoxon Signed Ranks tests revealed strong differences between the given ratings for all different motion cueing conditions, except those for (1,0.5) and (1,0). With a minimum p -value of 0.018, however, none of the six pairwise comparisons were found to be statistically significant at the adjusted significance level according to the Bonferroni correction for multiple comparisons ($\alpha = 0.05/6 = 0.008$).

6.5.2 Tracking Performance and Control Activity

Fig. 6.24 shows the measured error and control signal variances for the different experiment conditions. These are analyzed here as measures of tracking performance and control activ-

ity, respectively. The bars shown in Fig. 6.24 show the average total error and control signal variances as the total height of the bars. The error bars indicate the 95% confidence intervals of the means of σ_e^2 and σ_u^2 . The differently colored portions of each bar indicate the contributions of the disturbance signal f_d , the target signal f_t , and pilot remnant n to these signal variances. These different components were calculated using the spectral method described in [Jex et al., 1978]. The dashed gray and solid black lines in Fig. 6.24 show the predicted disturbance variance components and the sum of the disturbance and target variance components, respectively, from the offline analysis described in Section 6.3. Note that these trends indicate the change in these measures that would occur without adaptation of control behavior from what is appropriate for condition (1,0). Furthermore, note that the contribution of remnant to σ_e^2 and σ_u^2 is not included in these offline analysis predictions.

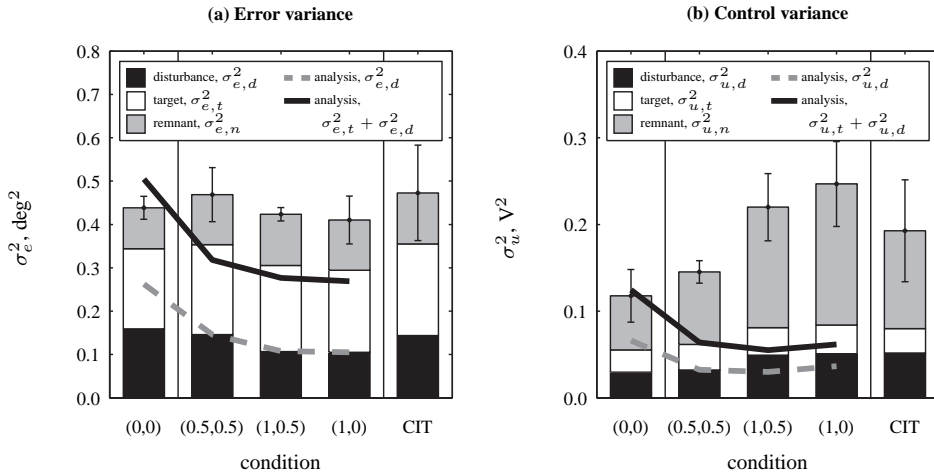


Figure 6.24. Mean error and control signal variance decompositions for roll multisine tracking.

Table 6.4. Statistical analysis results for tracking error and control signal variances.

Dependent measures	Statistical analysis results		
	Test	Results	Sig.
σ_e^2	Friedman's ANOVA	$\chi^2(4) = 13.94, p < 0.05$	**
$\sigma_{e,d}^2$	One-way repeated-measures ANOVA ^{gg}	$F(1.4, 8.4) = 5.17, p < 0.05$	**
$\sigma_{e,t}^2$	One-way repeated-measures ANOVA	$F(4, 24) = 0.79, p \geq 0.05$	—
$\sigma_{e,n}^2$	Friedman's ANOVA	$\chi^2(4) = 6.97, p \geq 0.05$	—
σ_u^2	One-way repeated-measures ANOVA ^{gg}	$F(1.2, 7.3) = 7.95, p < 0.05$	**
$\sigma_{u,d}^2$	One-way repeated-measures ANOVA	$F(4, 24) = 9.79, p < 0.05$	**
$\sigma_{u,t}^2$	One-way repeated-measures ANOVA	$F(4, 24) = 1.18, p \geq 0.05$	—
$\sigma_{u,n}^2$	One-way repeated-measures ANOVA ^{gg}	$F(1.2, 7.1) = 7.06, p < 0.05$	**

** = significant ($p < 0.05$) gg = Greenhouse-Geisser sphericity correction
 — = not significant ($p \geq 0.05$)

The statistical analysis results that correspond to the experimental data presented in Fig. 6.24, including test results for both the total error and control signal variances and the different variance components, are listed in Table 6.4. Note that the data for the total error variance σ_e^2 and its remnant component σ_n^2 were found to show distributions significantly different from normal for a number of experimental conditions. Hence, nonparametric tests were applied to analyze the variation over the different experimental conditions for these dependent measures.

Fig. 6.24(a) shows only a modest variation in tracking error variance over the different experimental conditions. When comparing tracking performance for the different conditions performed in the SRS with motion cueing ((0.5,0.5) to (1,0)), a slight decreasing trend with increasing motion fidelity is observed, indicating more accurate tracking, as also reported for a number of other tracking studies in literature (see Chapter 5). The decrease in tracking error variance observed here mainly results from a decrease in the disturbance component $\sigma_{e,d}^2$, which suggests increasing the level of simulator motion fidelity allowed pilots to achieve more accurate disturbance rejection. Notable is that tracking performance for (0.5,0.5) is found to be slightly worse than for the no-motion case. Fig. 6.24(a) further shows that tracking performance for the in-flight tracking tasks of the CIT condition was found to be worse than that achieved for the conditions that were closest in terms of the supplied motion information, (1,0.5) and (1,0). The total error variance and the different variance components for the CIT condition are remarkably similar to those measured for (0.5,0.5).

The statistical analyses performed on the tracking error variance data (see Table 6.4) show that both the total error variance σ_e^2 and the disturbance error variance component $\sigma_{e,d}^2$ vary significantly over the different experimental conditions. Pairwise comparisons indicate that the measured $\sigma_{e,d}^2$ for conditions (1,0.5) and (1,0) is significantly different from that measured for the no-motion condition (0,0). Similarly, pairwise comparisons evaluated for σ_e^2 using the nonparametric Wilcoxon Signed Ranks test also indicated that the strongest observed differences were those between the relatively high tracking error variance found for condition (0.5,0.5) and the data for both conditions with a unity motion filter gain. The total tracking error variance and the disturbance error variance component measured for the in-flight condition (CIT) were both not found to be significantly different from their values obtained for any of the SRS conditions.

The control signal variances presented in Fig. 6.24(b) show a much stronger variation over the different experimental conditions than observed for σ_e^2 . For the different conditions performed in the SRS, a clear increase in σ_u^2 is observed with increasing simulator motion fidelity, which mainly results from increases in the disturbance and remnant components. This is confirmed by the ANOVA results shown in Table 6.4, which indicate that the variations in σ_u^2 , $\sigma_{u,d}^2$, and $\sigma_{u,n}^2$ over the different experimental conditions are all statistically significant. Compared to the highest motion fidelity SRS conditions, measured control activity for the in-flight tracking tasks is found to be markedly lower. Fig. 6.24(b) suggests that this drop in control signal variance mainly results from a lower average remnant component $\sigma_{u,n}^2$. Post-hoc tests, however, showed no significant differences in σ_u^2 , $\sigma_{u,d}^2$, and even $\sigma_{u,n}^2$ between conditions (1,0.5), (1,0), and CIT.

Finally, comparison with the offline analysis results for the components of σ_e^2 and σ_u^2 that are correlated with both forcing function signals, indicated with the solid black and

dashed gray lines in Fig. 6.24, shows that the predictions of the tracking error variance for condition (1,0) are more accurate than those for the control signal variance. Experimental measurements that differ markedly from the predicted data indicate that for conditions for which this is the case, participants adapted their control strategy (pilot dynamics) compared to the reference (1,0) case. Evaluation of the predicted trends and the experimental measurements in Fig. 6.24 shows that these clearly differ for the no-motion condition (0,0). The predicted worsening of tracking performance for condition (0.5,0.5) is also consistent with the experimental data, however, the measured drop in $\sigma_{u,d}^2$ is not present in the predicted data. As both tracking performance and control activity predictions match well for condition (1,0.5), comparison of experimental and offline analysis results for σ_e^2 and σ_u^2 suggests a change in pilot tracking behavior for conditions (0,0) and (0.5,0.5) compared to (1,0).

6.5.3 Crossover Frequencies and Phase Margins

Fig. 6.25 shows the disturbance and target open-loop crossover frequencies and phase margins that were measured for the different experimental conditions. In addition to the means and 95% confidence intervals, which are indicated with the solid square markers and the error bars, respectively, Fig. 6.25 also shows the measurements for the individual subjects. The dashed black lines indicate the offline analysis data, taken from the data shown in Figures 6.7 to 6.10, for the different motion filter settings evaluated in the experiment.

Fig. 6.25 shows that despite the fact that marked differences in the crossover frequencies and phase margins can be observed between the different participants, the variation over the different experimental conditions is very similar for all participants. For the four conditions performed in the SRS, an increase in roll motion fidelity is seen to yield an increase in the disturbance open-loop crossover frequency $\omega_{c,d}$ and a decrease in the corresponding phase margin $\varphi_{m,d}$. The effects on the crossover frequency and phase margin of the target open-loop are found to be less pronounced, however, a slight decrease in $\omega_{c,t}$ and a small increase in $\varphi_{m,t}$ are observed with increasing motion fidelity. Compared to the condition with 1-to-1 roll motion in the SRS, the in-flight measurements for the CIT condition show lower disturbance crossover frequencies and phase margins, in addition to a small drop in $\varphi_{m,t}$. The lower disturbance crossover frequency is consistent with the reduced control activity observed for the CIT measurements in Fig. 6.24.

As expected from Fig. 6.25, only the differences in the disturbance crossover frequency and phase margin over the different experimental conditions are found to be statistically significant, see Table 6.5. For $\omega_{c,d}$, post-hoc tests only show a significant difference between two groups of conditions: the low-fidelity conditions (0,0) and (0.5,0.5), and the high-fidelity conditions (1,0.5), (1,0), and CIT. Despite the consistently smaller value for $\omega_{c,d}$ obtained from the in-flight measurements, this implies that the difference in the disturbance crossover frequency for conditions (1,0) and CIT is not statistically significant. Pairwise comparisons performed on the disturbance phase margin data show that the same holds for $\varphi_{m,d}$. Still, considering the consistency of both effects over the data from the different participants, the fact that the differences in both parameters between the SRS and in-flight data are not found to be statistically significant is believed to be a result of the relatively small number of available samples and the spread in the measurements.

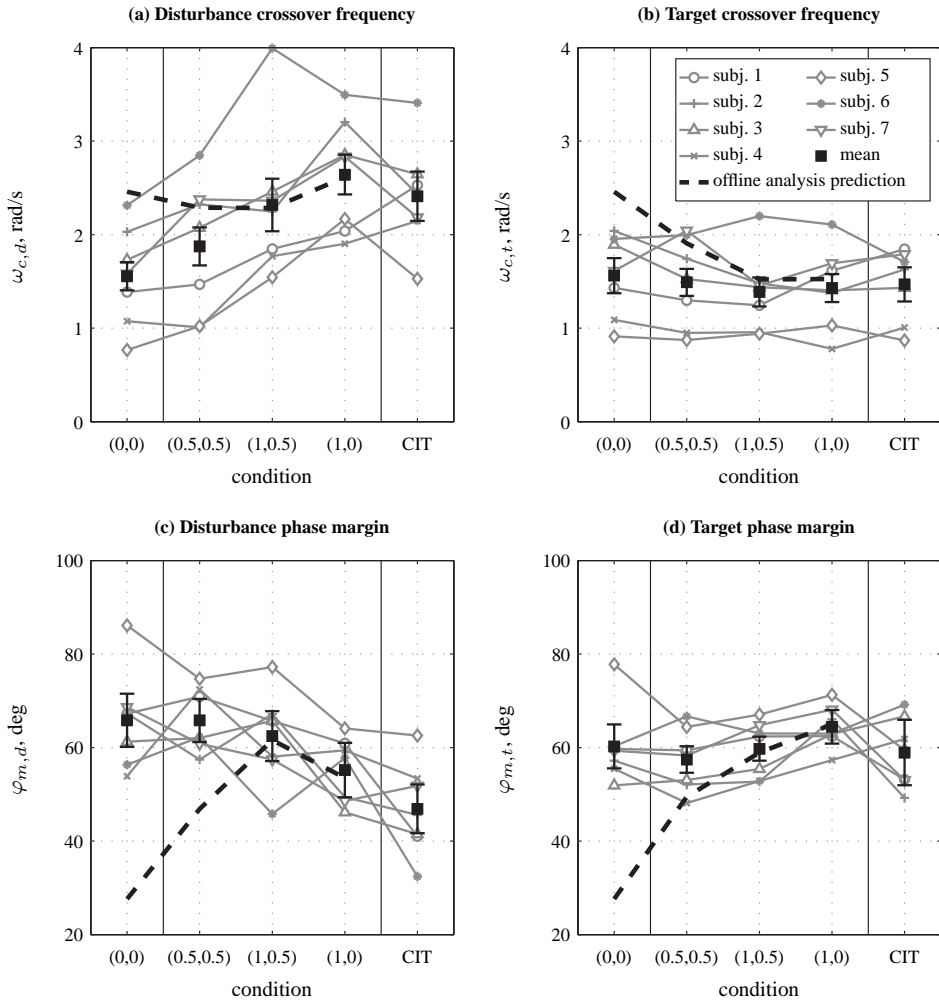


Figure 6.25. Average disturbance and target crossover frequencies and phase margins.

Table 6.5. One-Way Repeated Measures ANOVA results for crossover data.

Dependent measures	ANOVA statistics		
	df	F	Sig.
$\omega_{c,d}$	1.74,10.46 ^{gg}	16.38	**
$\varphi_{m,d}$	4,24	13.40	**
$\omega_{c,t}$	4,24	0.40	—
$\varphi_{m,t}$	4,24	1.57	—

** = significant ($p < 0.05$) gg = Greenhouse-Geisser sphericity correction
 — = not significant ($p \geq 0.05$)

Finally, comparison of the measured crossover frequencies and phase margins with the predictions from the offline analysis yields some interesting observations. First of all, the predicted crossover frequencies and phase margins match the measurements for the (1,0) very well, as expected for the prediction made based on the data from [Zaal et al., 2010]. Second, the offline analysis data for condition (1,0.5) are also highly consistent with the experimental measurements and even correctly predicts the magnitudes of the drop in $\omega_{c,d}$, the increases in $\varphi_{m,d}$ and $\varphi_{m,t}$, and the constant $\omega_{c,t}$ compared to the data for condition (1,0). For the other two conditions, (0,0) and (0.5,0.5), marked differences between the experimental measurements and the offline analysis predictions are observed. Compared to the predictions for these conditions, the experimental measurements show lower disturbance and target crossover frequencies and do not reflect the same drop in $\varphi_{m,d}$ and $\varphi_{m,t}$. The clear match between offline analysis and experimental results observed for both conditions (1,0) and (1,0.5), and the mismatch that is seen to occur for the low motion fidelity conditions, provides strong evidence that pilots only changed their control dynamics compared to the case where one-to-one motion is available for conditions (0,0) and (0.5,0.5). Note that this conclusion was also drawn from the comparison of experimental and offline analysis results for the tracking error and control signal variances presented in Fig. 6.24.

6.5.4 Pilot Control Behavior

Figures 6.26 and 6.27 shows the estimated values of parameters of the multimodal pilot model of Fig. 6.4 that were obtained by fitting the model to data from all experimental conditions. In addition to the seven parameters of the pilot model, Fig. 6.26(c) also shows the product of the pilot visual gain and the visual lead time constant $K_v T_L$, which represents the gain with which pilots responded to visual error rate information. As also done in Fig. 6.25, both the means and 95% confidence intervals are shown, in addition to the individual subject data. The corresponding ANOVA results for all eight parameters are listed in Table 6.6. Finally, the parameter values used in the offline analysis described in Section 6.3, which are representative for tracking with 1-to-1 roll motion cues (condition (1,0)) and were taken from [Zaal et al., 2010], are depicted in each graph with a dashed black line.

For the data from the different motion cueing conditions performed in the SRS, a number of changes in pilot tracking behavior are clear from Figures 6.26 and 6.27. First, Figures 6.26(a) and (b) show the same decrease in pilot visual gain and increase in visual lead time constant for decreasing motion fidelity also reported in earlier investigations, as summarized in Chapter 5. For reference, Fig. 6.26(b) shows the inverse of the frequency where the controlled element dynamics transition from approximately single to approximately double integrator dynamics (ω_ϕ , see Section 6.2.1.3). Note that, as expected, for the no-motion condition (0,0) pilots on average generate lead starting around ω_ϕ to compensate for the second-order controlled element dynamics. For conditions where physical roll motion feedback is available, the identified visual lead time constants are seen to drop below $1/\omega_\phi$, indicating less lead is generated visually in the presence of physical motion feedback, as also reported in many earlier investigations (see for example Chapters 2 and 4).

As can be observed from Fig. 6.26(c), the increase in T_L and decrease in K_v nearly perfectly offset each other to yield a constant $K_v T_L$ over all SRS conditions. Note that this implies a low-frequency gain adaptation of the pilot visual response, while $H_{p_v}(j\omega)$ remains

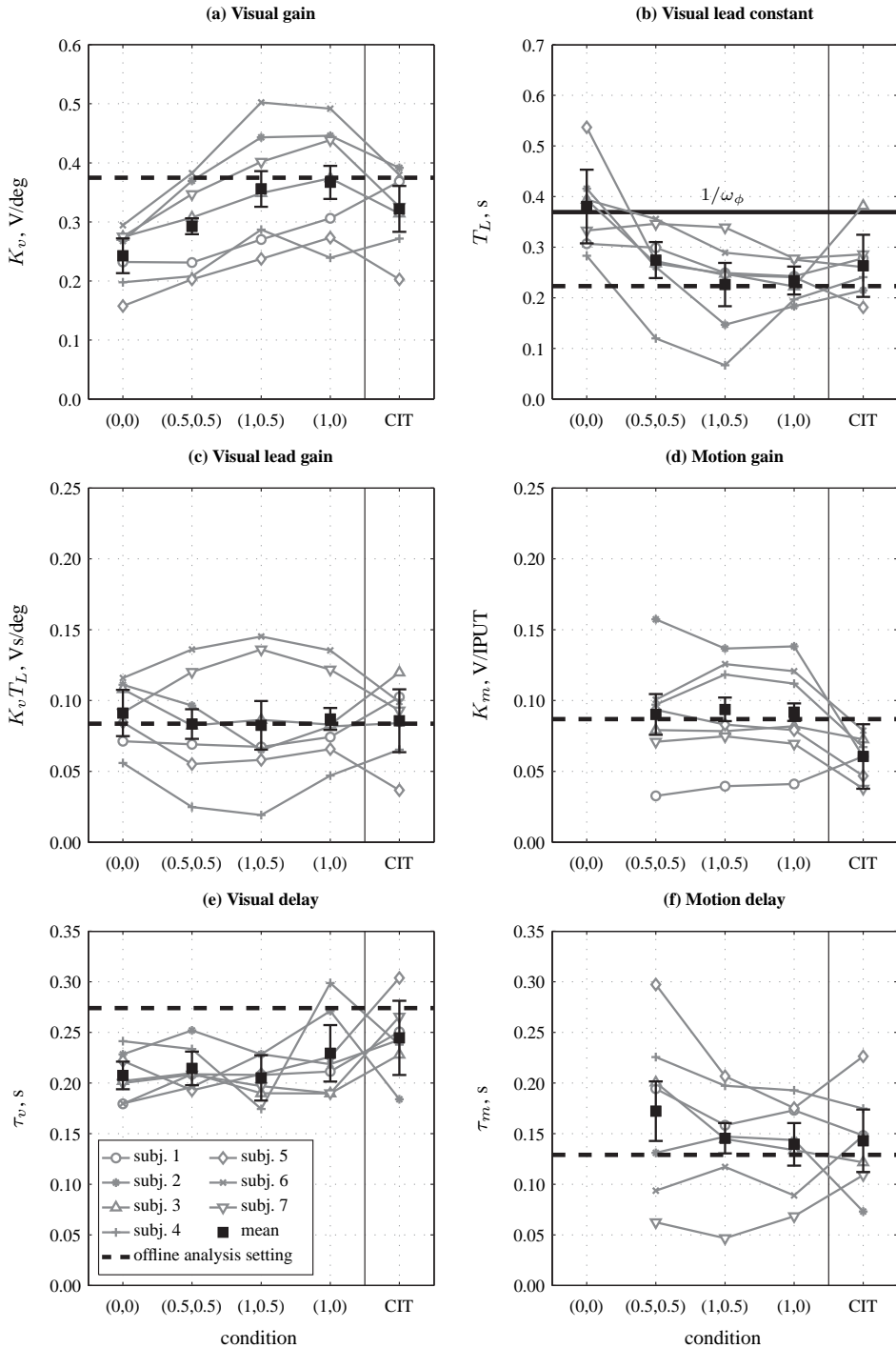


Figure 6.26. Mean estimated multimodal pilot model parameters.

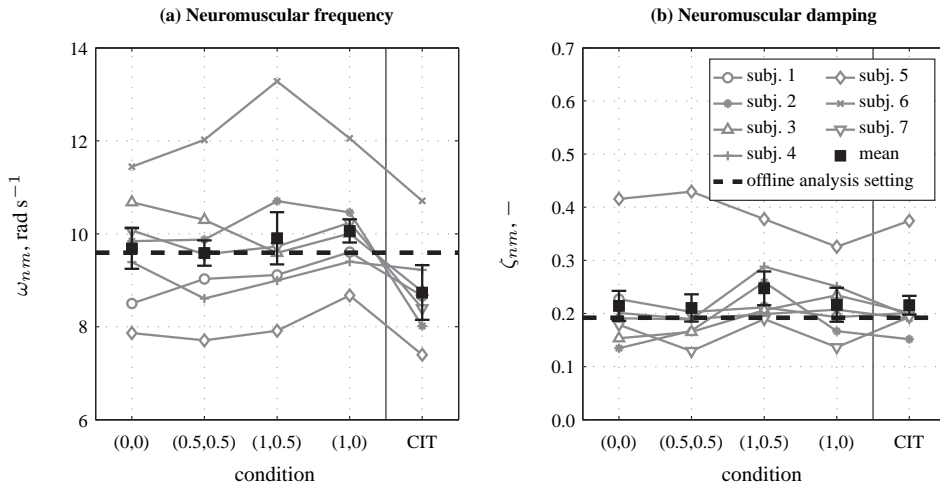


Figure 6.27. Mean estimated neuromuscular actuation model parameters.

Table 6.6. One-Way Repeated Measures ANOVA results for multimodal pilot model parameters.

Dependent measures	ANOVA statistics		
	df	F	Sig.
K_v	4,24	14.33	**
T_L	4,24	7.09	**
$K_v T_L$	4,24	0.23	—
K_m	1.31, 7.86 ^{gg}	5.37	**
τ_v	4,24	2.15	—
τ_m	3,18	1.62	—
ω_{nm}	4,24	6.39	**
ζ_{nm}	4,24	1.42	—

** = significant ($p < 0.05$) gg = Greenhouse-Geisser sphericity correction
 — = not significant ($p \geq 0.05$)

largely unaffected at the higher frequencies, where the gain is equal to $K_v T_L$. The pilot motion gain K_m , whose identified values are shown in Fig. 6.26(d), is also found to remain approximately constant over the different SRS conditions. Note that this implies pilots did not simply compensate for the lower motion cueing gain of the (0.5,0.5) condition by increasing their motion response gain. Furthermore, note that due to the chosen convention in the model for $H_{sc}(j\omega)$ (see Section 6.2.2), the absolute values of $K_v T_L$ and K_m can be compared directly, as both parameters define the gain of a response proportional to rotational velocity in the frequency range covered by the experiment forcing functions. A comparison of Figures 6.26(c) and (d) suggests that, for the considered roll tracking task, the effective lead contributions of the pilot visual and motion responses are almost equal.

Figures 6.26(e) and (f) present the identified values of the visual and motion time delay parameters, τ_v and τ_m . Except perhaps for slightly increased values of τ_v for (1,0) and of τ_m for (0.5,0.5), both pilot model delay parameters remain approximately constant at 0.2 and 0.15 s for τ_v and τ_m , respectively. The identified values of the second-order neuromuscular actuation model parameters, which are depicted in Fig. 6.27, also appear to remain approximately constant for the different simulator motion cueing conditions. The neuromuscular frequency ω_{nm} , however, does show slightly higher values for the conditions with the largest motion amplitudes ($K_{mf} = 1$), a finding also reported for other experiments, such as the one described in Chapter 4.

Comparing the estimates of all eight parameters depicted in Figures 6.26 and 6.27 for the in-flight tracking tasks (CIT) with those of the 1-to-1 roll motion condition performed in the SRS (1,0), some differences that are highly consistent over the different participants can be observed. First of all, Figures 6.26(a) and (d) indicate that both the pilot visual and motion gains K_v and K_m are found to be consistently lower for the in-flight tracking data. This indicates that the pilots responded to both visually presented tracking errors and to physical motion stimuli with a lower gain than they did in the simulator. These decreased gains are consistent with the reduced control activity and disturbance crossover frequencies that were also observed for the CIT condition.

For pitch tracking tasks performed in the same setup as the roll tracking tasks described in this chapter, Zaal et al. [2011] reported increased pilot delays for the in-flight measurements compared to those taken for the simulator conditions with the highest level of motion fidelity. For the pilot visual delay τ_v this increase was found to be appreciable, with an average of 50 ms. As can be verified from Figures 6.26(e) and (f), such increased pilot delays are not clear from the in-flight roll tracking data. The spread in the estimates of τ_v in presented in Fig. 6.26, however, is appreciable, especially for conditions (1,0) and CIT. When comparing the average delays of conditions (1,0.5) and CIT, a difference in delay similar to that noted by Zaal et al. [2011] is observed.

Finally, also the neuromuscular frequency ω_{nm} shows identified values that are around 1.5 rad/s lower for the in-flight data than for the simulator conditions. Zaal et al. [2011] reported a similar difference in neuromuscular actuation dynamics between measurements taken in the setups in the laboratory aircraft and flight simulator, especially for the reference single-loop tracking measurements taken in both setups. As can be verified from Appendix F, such a drop in neuromuscular frequency is also the sole difference observed between the reference single-loop tracking measurements taken in both experimental setups for the roll tracking task investigated here. For this reason, this change in ω_{nm} is not considered to be

an effect of possible differences in motion cueing, but merely an artifact of remaining differences between both experimental setups, most notably the sidestick and possible differences in posture resulting from different chairs and cockpit geometries.

As can be verified from Table 6.6, the variations in K_v , T_L , K_m , and ω_{nm} over the different experimental conditions are found to be statistically significant. Pairwise comparisons indicate that K_v is not significantly different for conditions (1,0.5), (1,0), and CIT. The visual gains for conditions (1,0.5) and (1,0) are, however, found to be significantly different from the values of K_v found for both (0,0) and (0.5,0.5), indicating a clear effect of simulator motion fidelity on pilot control gain. For both K_v and ω_{nm} post-hoc tests indicate that the sole significant difference in the data for these parameters is caused by the lower values measured for the in-flight tracking tasks. For K_m , this could not be proven with post-hoc tests, which showed no statistically significant differences between any of the experimental conditions. This is likely due to the large spread in the identified parameter values for K_m , which is at least partly the result of the data from subject 1, who shows a trend in K_m not consistent with the data from the other subjects.

Fig. 6.28 shows the variance accounted for (VAF) corresponding to the pilot model parameter estimates presented in Figures 6.26 and 6.27. As can be verified from Fig. 6.28, a strong between-subject effect is present, with average VAF values over all conditions for the different subjects ranging between 70 and almost 90%. On average, however, the VAFs for the different experimental conditions are not found to differ significantly, $F(4, 24) = 0.50$, $p = 0.74$, indicating the pilot model fits describe the data equally well for all evaluated conditions.

The multimodal pilot model fits obtained for the different experimental conditions allow for a final evaluation of the contribution of the supplied motion feedback to the observed pilot tracking behavior. By separately evaluating the contributions of the fitted $H_{p_v}(j\omega)$ and $H_{p_m}(j\omega)$ to the modeled pilot control signal u , indicated as u_v and u_m in Figures 6.1 and 6.4, the variances of both these contributions can be calculated and compared. Fig. 6.29(a) shows the averages of $\sigma_{u_v}^2$ and $\sigma_{u_m}^2$ obtained for all experimental conditions, while Fig. 6.29(b) depicts the fraction of both as a measure of the relative contribution of physical motion feedback to u .

Fig. 6.29(a) shows that for the flight simulator conditions both the visual and motion contributions to the control signal variance are seen to increase with increasing motion fidelity, which is consistent with the previously reported increased pilot visual gains K_v and control activity σ_u^2 . For the in-flight tracking tasks of the CIT condition, $\sigma_{u_v}^2$ is found to be similar to the values found for (1,0) and (1,0.5), even though the variation of $\sigma_{u_v}^2$ is not found to be statistically significant, $F(1.6, 9.7) = 4.11$, $p = 0.057$. The contribution of the motion response, however, is found to be nearly 50% lower for the CIT condition than for the high-fidelity simulator conditions. The change in $\sigma_{u_m}^2$ over the different experimental conditions is found to be statistically significant: $F(1.5, 9.0) = 8.22$, $p < 0.05$.

The pilot model channel variance fractions for the different experimental conditions shown in Fig. 6.29(b) show that for the simulator conditions (0,0) to (1,0) the increase in $\sigma_{u_m}^2$ is dominant over the increase observed for the visual contribution $\sigma_{u_v}^2$. This shows a relatively larger effect of the information received from physical motion feedback on pilot tracking behavior for the conditions with a higher level of simulator motion fidelity. For the CIT condition, the variance fraction is found to be only slightly higher than observed

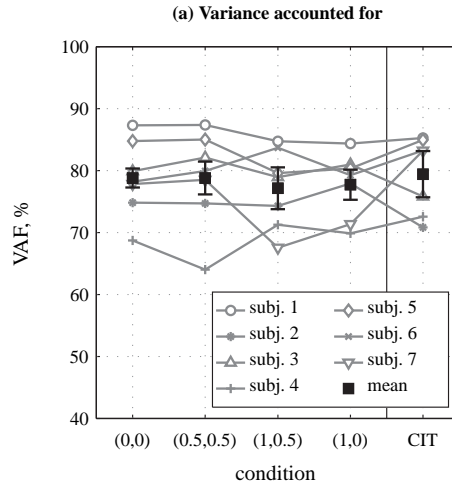


Figure 6.28. Mean pilot model variance accounted for.

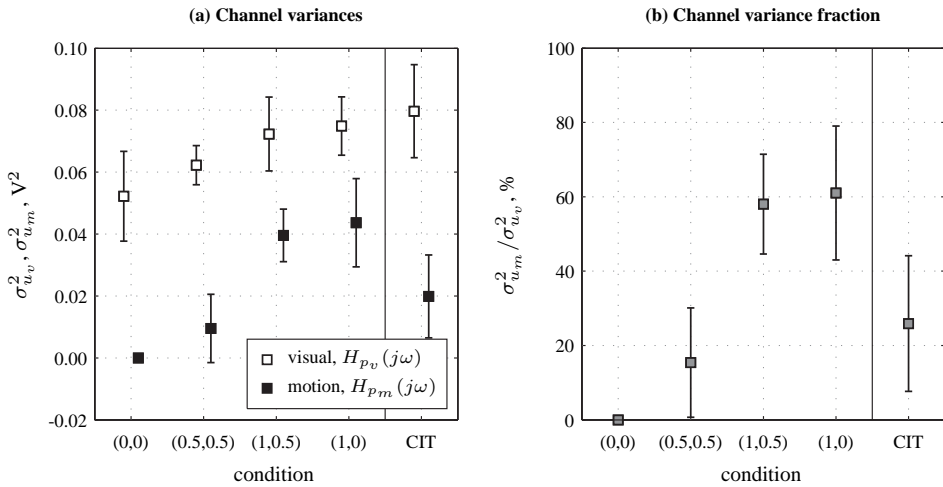


Figure 6.29. Mean pilot model channel output variances and variance fraction.

for the low-fidelity (0.5,0.5) condition performed in the SRS. This shows pilots made comparatively less use of physical motion feedback during the in-flight tracking tasks than they do under high-fidelity motion cueing conditions in the flight simulator. The variation of $\sigma_{u_m}^2 / \sigma_{u_v}^2$ shown in Fig. 6.29(b) is found to be statistically significant, $F(1.3, 7.6) = 8.95$, $p < 0.05$.

6.6 Discussion

Seven experienced pilots participated in an experiment where a comparison was made between multimodal pilot roll attitude tracking behavior measured in real flight and for varying motion cueing settings in a moving-base flight simulator. The in-flight tracking measurements, for which pilots were controlling a real aircraft and hence the perceived roll motion was the true aircraft motion, were to serve as the baseline to evaluate changes in behavior resulting from degraded simulator motion fidelity against. Due to the adaptability of pilot tracking behavior to a myriad of factors internal and external to the pilot, the utmost care was taken to ensure the differences in the experimental setups and conditions under which the in-flight and simulator measurements were collected were minimal, to allow for proper isolation of the effect of motion cueing variations on pilot tracking behavior.

The results from the simulator part of the experiment suggest clear effects of variations in simulator motion fidelity on pilot tracking behavior. Pilot control activity, disturbance open-loop crossover frequency and the gain with which pilots respond to visually presented tracking error information are all seen to significantly increase with increasing motion fidelity. The effects of variations in motion fidelity on pilot tracking behavior observed for this roll tracking task are highly consistent with previous experiments, such as those described in [Van Gool, 1978; Jex et al., 1978] and Chapters 5 and 4. In addition, the subjective motion fidelity ratings taken during the simulator experiments using a VAS rating scale showed the pilots were also able to distinguish between the evaluated high and low-fidelity motion cueing settings.

Comparison of the in-flight and simulator tracking measurements showed that pilot tracking behavior in real flight was found to be very similar to tracking behavior in a moving-base flight simulator. Despite the care taken to minimize differences between the in-flight and simulator parts of the experiment, however, differences in tracking performance, control activity, and pilot control strategy were still observed. Tracking performance was found to be slightly worse in the aircraft compared to the condition with one-to-one roll motion fidelity performed in the simulator. In addition, consistently lower values were observed for the control signal variance (control activity), the disturbance open-loop crossover frequency, and the gains with which pilots respond to both visual and motion information. The observed difference in neuromuscular actuation dynamics, which showed that the neuromuscular system natural frequency ω_{nm} was around 1.5 rad/s lower for the in-flight tracking tasks than in the simulator, was traced back to a difference in the experimental setups used for both parts of the experiment using a comparison of reference single-loop (no motion feedback) tracking tasks performed in both the experimental setups in the laboratory aircraft and the flight simulator (see Appendix F).

The observed differences in multiple dependent measures related to pilot tracking behavior between the in-flight measurements and the high-fidelity simulator conditions indicate that pilots were performing less high-bandwidth and high-gain control in real flight, resulting in relatively poorer performance for the roll tracking task. The extensive validation of the hard- and software used for both experiments (see Appendices C and D) and the aircraft and fly-by-wire control system models used for collecting the flight simulator measurements (see Appendix E) and further pilot-in-the-loop tests performed to evaluate the effect of the hood pilots wore during the in-flight measurements (Appendix G) suggest the source of the observed behavioral discrepancies does not lie in factors external to the pilot, but might be caused by factors internal to the pilots that are difficult to control in an experimental setting. The reduced control gain observed in the behavioral measurements from the in-flight tracking tasks could for instance also result from the pilots performing the control task a bit more careful in the aircraft than they did in the simulator. For instance, in a recent paper Schroeder and Grant [2010] claim that comparison of measurements taken in real flight and in a simulator environment might be inherently flawed as “*some argue that the pilot’s mindset is different in the two environments*”. Behavioral differences that result from such operator-centered factors [McRuer and Jex, 1967a] are impossible to separate and signal for the approach taken in this chapter, and therefore could heavily complicate the comparison between behavioral measurements attempted here.

When focusing on the differences in pilot tracking behavior observed from the simulator measurements, thereby taking the condition where 1-to-1 roll motion cues were presented as the baseline for evaluating changes in control strategy, the offline analysis of effects of the washout filter dynamics on the closed-loop pilot-vehicle system described in this chapter is found to provide valuable insights. Especially for interpreting changes in pilot-vehicle system crossover frequencies and phase margins, which can result both from the applied changes in washout filter settings and adapted pilot dynamics, the comparison of offline analysis predictions and experimental measurements was found to aid in pointing which motion filter settings resulted in different pilot tracking behavior than observed with 1-to-1 motion feedback. Especially the correct prediction of changes in crossover parameters that result from the motion filter dynamics for high-fidelity condition (1,0.5), for which pilot model analysis indeed showed no change in pilot dynamics, give faith in this approach. As such an offline analysis requires knowledge of the pilot dynamics for this reference case, possible broader application of this method requires more knowledge on pilot dynamics under varying conditions and simple procedures for adapting pilot models to defining control task characteristics such as controlled element dynamics and forcing function signal characteristics.

The four motion cueing settings evaluated in the simulator part of the experiment, of which one was a no-motion case and another supplied pilots with 1-to-1 roll motion, only allow for a limited evaluation of the effect of different motion filter gain and break frequency settings on pilot tracking behavior. The two experimental conditions where a roll washout filter was present – that is, conditions (0.5,0.5) and (1,0.5), both with a filter break frequency of 0.5 rad/s and filter gains of 0.5 and 1, respectively – do show potentially interesting results, for instance for the validation of accepted simulator motion fidelity criteria using behavioral measurements. According to the motion fidelity criteria proposed by Sinacori [1977] and Schroeder [1999], the (0.5,0.5) and (1,0.5) conditions evaluated in this

experiment represent medium and high motion fidelity motion filter settings, respectively. The fact that for the roll tracking task considered in this chapter pilot tracking behavior with the high-fidelity motion filter was found to be equivalent to behavior measured with 1-to-1 motion, while significant differences in behavior were observed for the condition with the medium-fidelity filter, is consistent with and adds to the validity of these previously developed fidelity criteria. The limited variation in motion filter gain and break frequency values tested in this experiment does, however, severely limit the conclusions that can be drawn from this research with respect to optimal selection of motion filter parameters. Still more measurements of pilot tracking behavior under different motion filter settings are believed to be required to support the drawing of such conclusions. The follow-up experiment described in Chapter 8 was performed to provide a first step towards this goal, by evaluating pilot tracking behavior for the same roll tracking task as analyzed here for a larger number of different roll motion filter settings.

6.7 Conclusions

To allow for evaluating the effect of changes in simulator motion fidelity on pilot tracking behavior, an experiment was performed in which a roll tracking task was performed both in real flight and in a moving-base flight simulator for a number of different roll motion cueing settings. The considered roll tracking task was especially suited for this comparison of in-flight and simulator measurements, as the roll motion during the task could be presented 1-to-1 in the simulator. The utmost care was taken to minimize differences in the experimental setups used for collecting the measurements in the aircraft and the simulator. Still, pilots were found to utilize a more low-gain control strategy during the in-flight tracking tasks than they did for the 1-to-1 simulator motion configuration, resulting in consistent discrepancies in pilot tracking behavior that are not attributable to differences in motion cueing. The simulator part of the experiment, aided by an offline analysis of the effect of changes in washout dynamics on the dynamic characteristics of the pilot-vehicle system, was found to show clear changes in pilot tracking behavior under variations in roll motion cueing. Enhanced disturbance-rejection performance and increased disturbance open-loop crossover frequencies were found for conditions with better motion fidelity. In addition, the gains with which pilots responded to both visual and motion information were shown to be larger with high-fidelity roll motion, leading to an increased contribution of motion feedback to pilot control behavior when roll motion approximated the 1-to-1 case. The experimental results further confirm the classification of the considered motion filter settings according to previously proposed simulator fidelity criteria, thereby providing further validation of these criteria using objective measurements of pilot behavior.

7

Ramp-Tracking Behavior in Real and Simulated Flight

Chapter 6 described a comparison of multimodal pilot roll tracking behavior measured in the Cessna Citation II laboratory aircraft and in the SIMONA Research Simulator. For the roll tracking task considered in Chapter 6, the applied target and disturbance forcing function signals were independent quasi-random multisine signals, yielding a tracking task where purely compensatory tracking behavior was adopted. The same roll tracking task was also performed with an additional deterministic target signal – consisting of a number of ramp-like excursions in commanded roll attitude – that was superimposed on the multisine target forcing function used for the roll tracking task of Chapter 6. For this roll ramp-tracking task also use was made of a display with a pursuit configuration. This yielded a more operationally relevant roll tracking task where pilots were required to perform a series of commanded turn entries and exits, for which evaluation of the effect of motion feedback on pilot tracking behavior was also thought to be of interest. Though stretching the currently available knowledge of manual control behavior and analysis methods, as explained in more detail in Chapter 3, such a more realistic maneuvering task is believed to be a valuable addition to the research project this thesis is the result of. This chapter applies the same methodology as also applied in Chapter 6 to the collected ramp-tracking measurements. For the analysis of pilot tracking behavior in this ramp-tracking task extensive use is made of the concepts and models introduced in Chapter 3.

7.1 Introduction

The evaluation of behavioral motion fidelity presented in this thesis mainly considers the effects of simulator motion fidelity on compensatory tracking behavior. The main reason for this is that during purely compensatory tracking, pilots' control behavior is sufficiently stationary and linear to allow for modeling it with quasi-linear time-invariant control theoretical models [McRuer and Jex, 1967a]. Furthermore, for compensatory tracking tasks with physical motion feedback, it has been shown that reliable separation of pilots' responses to visual and motion information is possible using frequency-domain [Stapleford et al., 1969] and time-domain identification methods [Zaal et al., 2009a], allowing for objective evaluation of changes in pilot control behavior. As illustrated by the experimental results reported in Chapters 5, 6, and 8, significant changes in compensatory pilot behavior are typically observed with varying motion fidelity.

Most studies that evaluated the effects of varying simulator motion fidelity through other methods than the behavioral approach taken in this thesis considered manual flying tasks as pilots would also perform regularly in real flight [Reid and Nahon, 1986a,b; Telban et al., 2005b]. For example, a number of investigations have considered the requirements for lateral yaw, roll, and sway motion cueing for helicopter sidestep maneuvers [Hess et al., 1993; Chung et al., 1998; Mikula et al., 1999] and yaw attitude capture tasks [Schroeder, 1996, 1999; Hosman et al., 2005; Grant et al., 2006; Ellerbroek et al., 2008]. Similarly, for fixed-wing aircraft operational flying tasks such as take-offs and landings [Heffley et al., 1981; Heffley and Schulman, 1981; Heffley et al., 1982; Reid and Nahon, 1986b; Pouliot et al., 1998; Groen et al., 2001; Telban et al., 2005b] and decrab maneuvers [Groen et al., 2007; Beukers et al., 2010] are typically considered for evaluating simulator motion cueing settings. These discrete maneuvering tasks are typically selected for these evaluations of simulator motion because of their operational relevance and the suspected importance of physical motion feedback in these situations. Furthermore, these maneuvering tasks tend to result in aircraft motion that is difficult to replicate on a moving-base flight simulator with a limited workspace.

Instead of explicitly evaluating changes in pilot behavior during these flying tasks, most of the studies that evaluated simulator motion fidelity for operational flying tasks relied on subjective pilot ratings and metrics of task performance (as indirect indicators of changes in pilot control behavior) to compare different levels of simulator motion fidelity. Some analysis methods and metrics for evaluating and quantifying control behavior during discrete maneuvering tasks have been proposed [Heffley, 1982; Ferguson et al., 1984] and applied for interpreting pilot control strategies during, among others, manual landing flares and helicopter sidestep or bob-up maneuvers. These techniques, however, have never been convincingly applied for objective evaluation of the effects of variations in simulator motion fidelity on pilot control behavior in discrete maneuvering tasks. Furthermore, none of the studies that considered simulator motion fidelity for operational flying tasks included an explicit comparison of these flying tasks performed in real flight and in a moving-base flight simulator environment that would allow for a strong evaluation of the effects of varying levels of simulation fidelity with respect to the true in-flight case.

Chapter 6 and Zaal [2011] describe comparisons of in-flight measurements of compensatory tracking behavior for roll and pitch tracking tasks, respectively, with those collected

in a moving-base flight simulator for varying motion cueing settings. This chapter applies the same methodology to a roll tracking task where, in addition to quasi-random target and disturbance forcing function signals, an additional deterministic reference signal is used that consists of a number of ramp-like changes in target roll attitude. The additional ramp target signal, with maximum absolute reference values of positive or negative 10 deg, induces a control task in which two commanded turn entry and exit maneuvers are performed. This yields a control task that more resembles a real flying task than the compensatory tracking tasks with only multisine forcing function signals considered in Chapter 6 and [Zaal, 2011]. This chapter describes the results of a combined in-flight and simulator experiment that evaluated pilot control behavior for this roll attitude ramp-tracking task. This experiment was performed in exactly the same experimental setups in the Cessna Citation II laboratory aircraft and SIMONA Research Simulator (SRS) at Delft University of Technology as the compensatory roll and pitch attitude tracking tasks described in Chapter 6 and [Zaal, 2011]. Similar to the experiment described in Chapter 6, for the ramp-tracking tasks performed in the SRS five different motion cueing conditions were evaluated. These different motion cueing settings consisted of a no-motion task, equivalent to the ramp-following tasks evaluated in Chapter 3, and four conditions with a first-order high-pass roll washout filters, for which a factorial evaluation of motion filter gains of 1 and 0.5 and filter break frequencies of 0.5 and 1 rad/s was considered.

As described in more detail in Chapter 3, given the predictable nature of the maneuvers executed during such a ramp-tracking task it is likely that pilots will not use a purely compensatory control strategy. It is likely that they will at least partly revert to an open-loop or feedforward control strategy during the ramp-tracking portions of the control tasks to execute these maneuvers successfully. For modeling and quantifying changes in ramp-tracking behavior with varying motion cueing settings, the extension to compensatory pilot models proposed in Chapter 3 for control tasks with ramp forcing function signals is considered. Furthermore, the extent to which the disturbance-rejection and ramp-following elements of the control task, and the effects the supplied motion feedback has on both, can be separated using the methodology adopted in this thesis is evaluated. It has been argued that a difference may exist between the function of physical motion feedback for vehicle motion originating external to the pilot, typically referred to as “disturbance motion”, and for “maneuvering motion” as a direct result of pilot control inputs [Gundry, 1977; Heffley et al., 1981; Schroeder et al., 2000]. The addition of a ramp forcing function signal yields a control task in which the maneuvering motion might be more important than the compensatory tasks considered in the rest of this thesis, thereby possibly yielding different conclusions with respect to the effects of degraded simulator motion fidelity on pilot control behavior.

This chapter is structured as follows. First, Section 7.2 describes the details of the considered roll attitude ramp-tracking task and the multimodal pilot model proposed for modeling pilot tracking behavior during this task. Section 7.3 describes the details of the combined in-flight and simulator experiment that was performed for collecting measurements of pilot behavior in the considered ramp-tracking task. Note, however, that due to the fact that these measurements were collected in the same experimental setups in the Citation II laboratory aircraft and the SIMONA Research Simulator (SRS) at Delft University of Technology, Section 7.3 only describes those aspects of the experiment described in this chapter that differ from those described for the experiment of Chapter 6. Section 7.4

presents the experimental results obtained from the collected ramp-tracking data. Finally, this chapter ends with a discussion and conclusions.

7.2 Control Task

7.2.1 Roll Ramp-Tracking Task

Fig. 7.1 depicts the roll attitude ramp-tracking task with roll motion feedback considered for evaluating simulator motion fidelity from a behavioral perspective in this chapter. Similar to the compensatory roll tracking task considered in Chapter 6, Fig. 7.1 shows a pilot controlling the roll attitude of an aircraft with aileron-input-to-roll dynamics given by $H_c(s)$. The target and disturbance forcing functions – which the pilot is to follow and attenuate, respectively, in order to minimize the tracking error e – are indicated with the symbols f_t and f_d . In addition to this tracking error, the pilot is also presented with explicit visual feedback of the current aircraft roll ϕ and the target forcing function f_t from the pursuit display shown in Fig. 7.2.

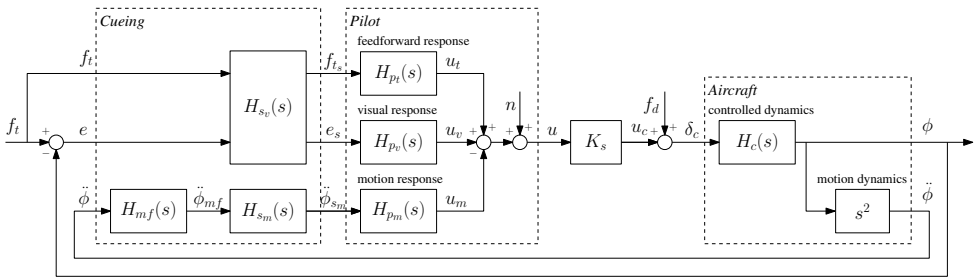


Figure 7.1. Schematic representation of the considered roll ramp-tracking task with motion feedback.

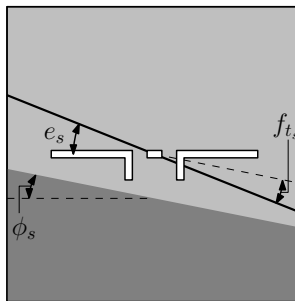


Figure 7.2. Pursuit roll tracking display.

The controlled aircraft dynamics in the roll tracking task considered in this chapter are the combined fly-by-wire (FBW) control system and Cessna Citation II roll dynamics also utilized for the experiment of Chapter 6. The nonlinear model of these aircraft dynamics, which was developed for performing the roll tracking task in a simulator environment, is

described in detail in Appendix E. This model was determined for the flight condition in which the in-flight measurements were collected, at an altitude h of 17,000 ft and an airspeed V of 160 kt. A linearization of these controlled element dynamics is given by:

$$\begin{aligned} H_c(s) &= \frac{\phi(s)}{\delta_c(s)} = K_\phi \frac{T_\phi s + 1}{s \left(\frac{s^2}{\omega_\phi^2} + \frac{2\zeta_\phi}{\omega_\phi} s + 1 \right)} e^{-s\tau_\phi} \\ &= 0.29 \frac{0.51s + 1}{s \left(\frac{s^2}{2.70^2} + \frac{2 \cdot 0.81}{2.70} s + 1 \right)} e^{-0.09s} \end{aligned} \quad (7.1)$$

As was shown in more detail in Chapter 6, the controlled element given by Eq. (7.1) has approximately K/s dynamics at low frequencies, approximately K/s^2 dynamics at frequencies above $\omega_\phi = 2.7$ rad/s, and includes a fly-by-wire control system response latency of 90 ms. The control input scaling gain K_s , which scaled pilot control inputs u to fly-by-wire control commands u_c (see Fig. 7.1), was equal to 0.3.

Similar to the comparison of in-flight and simulator measurements of compensatory tracking behavior described in Chapter 6, this chapter considers a comparison of ramp-tracking behavior measured in real flight using Delft University of Technology's Cessna Citation II laboratory aircraft and in the SIMONA Research Simulator (SRS) for varying motion cueing settings. As explained in more detail in Section 7.2.3, pure simulator roll motion cueing is considered for providing physical motion feedback in the considered ramp-tracking task. Equivalent to the variation in simulator motion cueing considered in Chapter 6, the effects of attenuating simulator roll motion with a first-order high-pass washout filter on pilot ramp-tracking behavior are evaluated. This first-order roll washout filter is given by:

$$H_{mf}(s) = \frac{s^2 \phi_{mf}(s)}{s^2 \phi(s)} = K_{mf} \frac{s}{s + \omega_{mf}} \quad (7.2)$$

The symbols K_{mf} and ω_{mf} represent the filter gain and filter break frequency, respectively. For a high-pass filter as given by Eq. (7.2), decreasing K_{mf} and increasing ω_{mf} yields larger discrepancies between the filtered roll motion ϕ_{mf} and the true aircraft roll motion ϕ . Note that by definition $H_{mf}(s) = 1$ for the in-flight ramp-tracking tasks.

To account for differences in the cueing of visual and motion information in both experimental setups, the visual and motion cueing dynamics $H_{sv}(s)$ and $H_{sm}(s)$ are included in Fig. 7.1. Using the custom visual delay measurement system described by Stroosma et al. [2007], the delay in the visual presentation of the display shown in Fig. 7.2 was measured to be around 25 ms in both the experimental setups, yielding $H_{sv}(s) = e^{-s\tau_{sv}} = e^{-0.025s}$. The motion cueing dynamics of the SRS are known to approximate a pure delay of 30 ms [Berkouwer et al., 2005], giving $H_{sm}(s) = e^{-s\tau_{sm}} = e^{-0.03s}$. As for the ramp-tracking tasks performed in real flight the perceived motion resulted from the true aircraft motion, by definition $H_{sm}(s) = 1$ for the in-flight tasks.

As will be explained in more detail in Section 7.2.4, pilot behavior in the multimodal ramp-tracking task shown in Fig. 7.1 is modeled with three linear responses to perceived variables, supplemented with a pilot remnant signal n . First, analogous to the analyses of

pursuit tracking behavior by Wasicko et al. [1966] and Allen and McRuer [1979] and the investigation into ramp-tracking behavior described in Chapter 3, ramp-tracking behavior based on the information presented on a pursuit display is modeled with two independent responses to the target forcing function and the tracking error. In addition to these responses to f_t and e , an additional pilot response to the supplied simulator roll motion $\ddot{\phi}_{sm}$ is also considered for the multimodal control task considered in this chapter. The contributions of these pilot feedforward, visual, and motion responses to the total pilot control input u are indicated with the symbols u_t , u_v , and u_m in Fig. 7.1, respectively.

7.2.2 Forcing Functions

For studying manual control behavior, the applied target and disturbance forcing functions, indicated with f_t and f_d in Fig. 7.1 have two important functions. First of all, they force the occurrence of manual control behavior by inducing tracking errors e that need to be compensated and thereby to a large extent define the nature of the control task [McRuer et al., 1965; Damveld et al., 2010]. Furthermore, especially for multimodal control tasks where pilots' responses to multiple perceived variables are evaluated, the applied forcing function signals provide the excitation of the pilot-vehicle system required to ensure that these different pilot responses can be measured accurately [Stapleford et al., 1969; Zaal et al., 2009a].

With respect to the first function of forcing function signals, most research into manual control behavior has been performed with quasi-random forcing functions, for which forcing function signal bandwidth [McRuer et al., 1965; Beerens et al., 2009; Damveld, 2009] and whether the forcing function signal was inserted as a target or disturbance signal [Hosman and Stassen, 1999; Van der Vaart, 1992; Zaal et al., 2009c] have been shown to affect pilot tracking behavior. Such quasi-random forcing functions induce stationary tracking behavior that can be argued to not be directly representative for pilot control behavior during the manual control tasks that typically occur during operational manual aircraft control.

In an attempt to extend the methods applicable to modeling compensatory tracking for modeling pilot control behavior in more realistic control tasks, Chapter 3 described an experiment in which tracking behavior was measured for purely visual (no motion feedback) control tasks where a target signal consisting of multiple ramp-like changes in target attitude was used, in addition to an applied disturbance forcing function. This chapter attempts to extend the single-loop measurements of manual ramp-tracking behavior described in Chapter 3 to a situation with physical motion feedback, effectively yielding a control task in which pilots are required to perform a number of commanded turn maneuvers in the presence of an external disturbance.

Similar to the approach taken in earlier experiments into the effects of motion feedback on compensatory pilot tracking behavior [Stapleford et al., 1969; Jex et al., 1978; Zaal et al., 2009c], in this chapter a combined target-following and disturbance-rejection task is considered due to the desire to separate pilots' visual and motion responses, as indicated in Fig. 7.1. To maintain the presence of two independent multisine forcing functions, as required for separating pilots' responses to visual and physical motion feedback, it was decided to utilize a target forcing function signal that combined multiple discrete ramp-like changes in target roll attitude with a superimposed quasi-random target signal (see

Fig. 7.3(a) for the experiment described in this chapter. The ramp target forcing function signal, referred to in the remainder of this chapter as $f_{t_{ramp}}$, was defined to command two roll attitude changes, one to 10 deg and one to -10 deg, with a maximum roll rate of 3 deg/s. As opposed to the truly discrete ramp-like changes commanded by the ramp forcing functions of Chapter 3, the ramp forcing function signal used for the experiment in this chapter had smooth transitions between the horizontal and slanted portions of the signal, as indicated in Fig. 7.3(a).

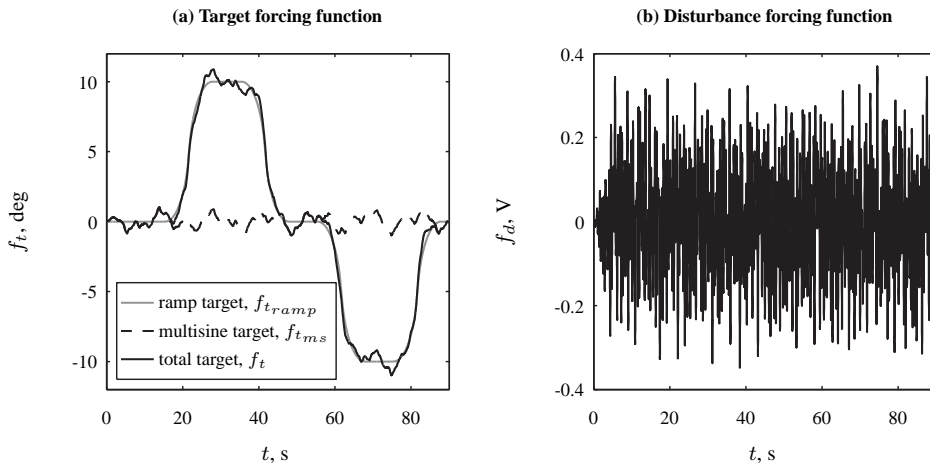


Figure 7.3. Target and disturbance forcing function time traces.

The same multisine target and disturbance forcing functions – indicated with symbols $f_{t_{ms}}$ and f_d , respectively – as used for the compensatory roll tracking experiment of Chapter 6 were also applied for this experiment. These multisine forcing function signals were defined as sums of $N_{d,t} = 10$ sinusoids according to:

$$f_{d,t_{ms}}(t) = \sum_{k=1}^{N_{d,t}} A_{d,t}(k) \sin [\omega_{d,t}(k)t + \phi_{d,t}(k)] \quad (7.3)$$

The sinusoid frequencies $\omega_{d,t}$, amplitudes $A_{d,t}$, and phases $\phi_{d,t}$ were the same as those used for the experiment described in Chapter 6. The power of the multisine target signal was, however, scaled down with a factor 0.5 by multiplying the target signal amplitudes by $\sqrt{0.5}$, yielding variances of $f_{t_{ms}}$ and the effective roll attitude disturbance induced by f_d of 0.2 and 0.4 deg², respectively. The properties of the multisine target and disturbance forcing function sinusoids are listed in Table 7.1. Time traces of the multisine ($f_{t_{ms}}$) and the total target forcing function (f_t) are shown in Fig. 7.3(a). The time trace of the disturbance signal, as inserted before the controlled element dynamics (see Fig. 7.1), is depicted in Fig. 7.3(b).

Table 7.1. Multisine disturbance and target forcing function properties.

disturbance, f_d				target, f_t			
n_d	ω_d , rad/s	A_d , V	ϕ_d , rad	n_t	ω_t , rad/s	A_t , deg	ϕ_t , rad
5	0.383	0.014	-1.764	6	0.460	0.494	1.288
11	0.844	0.023	2.792	13	0.997	0.345	6.089
23	1.764	0.026	-1.575	27	2.071	0.156	5.507
37	2.838	0.026	4.641	41	3.145	0.084	1.734
51	3.912	0.029	5.512	53	4.065	0.056	2.019
71	5.446	0.035	2.687	73	5.599	0.035	0.441
101	7.747	0.049	2.321	103	7.900	0.022	5.175
137	10.508	0.068	3.821	139	10.661	0.016	3.415
171	13.116	0.090	4.363	194	14.880	0.013	1.066
226	17.334	0.123	4.558	229	17.564	0.012	3.479

7.2.3 Aircraft Motion During Ramp-Tracking

Fig. 7.4 shows recorded time traces of the aircraft attitude (ϕ , θ , ψ), angular rates (p , q , r), and the specific forces at the aircraft center of gravity (f_x , f_y , f_z) during a roll attitude ramp-tracking task with the forcing functions defined in Section 7.2.2 performed in real flight. The depicted data were collected using the Honeywell VG-14 vertical gyro and an inertial measurement unit (IMU), consisting of three AlliedSignal QA3000 accelerometers and three LITEF μ FORS fiber optic rate gyros, that are part of the flight test instrumentation system (FTIS) installed in the Cessna Citation II laboratory aircraft. For reference, the ramp target signal is depicted alongside the recorded time traces with a dashed gray line. Note that $f_{t_{ramp}}$ has been scaled to fit the graphs for the angular rates and specific forces. Fig. 7.4(d) further shows the trim pitch attitude determined for the flight condition in which the in-flight experiments were performed ($h = 17,000$ ft, $V = 160$ kt), $\theta_0 = 4.34$ deg as indicated with the dashed black line.

Figures 7.4(a) and (d) show that during the ramp-tracking task the aircraft roll attitude ϕ varied as commanded by $f_{t_{ramp}}$, while the aircraft pitch attitude θ was maintained at its trim value. Fig. 7.4(g) further shows that the offset roll attitudes of ± 10 deg induced a change of nearly 20 deg in aircraft heading. Figures 7.4(b), (e), and (h) show that the dominant angular rate cue perceivable during the ramp-tracking task is the aircraft roll rate p . The pitch rate q is seen to be very small, while the yaw rate r only shows some constant (low-frequency) offsets that are proportional to the changes in roll attitude ϕ . Finally, Figures 7.4(c), (f), and (i) also show comparatively little variation in the perceivable specific forces during the turn maneuvers induced by $f_{t_{ramp}}$. The lateral specific force f_y shows small peaks at the turn entries and exits, but specific forces are seen to be close to zero during the turns themselves, as expected for this coordinated maneuver [Ariel and Sivan, 1984; Reid and Nahon, 1985].

Given that the human vestibular system is sensitive to angular accelerations (semicircular canals) and specific forces (otoliths) [Fernandez and Goldberg, 1971; Hosman and Van der Vaart, 1978; Hosman, 1996], Fig. 7.4 shows that the important motion cues to replicate in a moving-base flight simulator for the selected ramp-tracking task are the rotational roll motion and the (coordinated) lateral specific force. In one of the first structured research effort into simulator motion cueing, Schmidt and Conrad [1970] already stress the

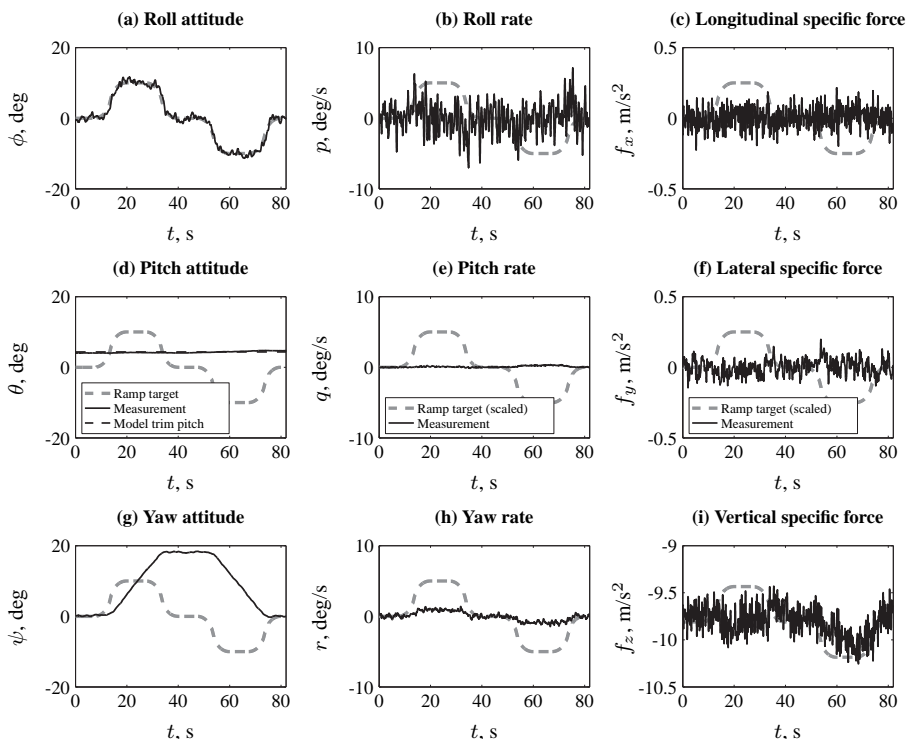


Figure 7.4. In-flight recordings of aircraft attitude, angular rate, and specific force for the ramp-tracking task considered in this chapter.

importance of coordinating rotational and translational motion cueing, and propose different schemes for doing so. As for instance described by Telban et al. [2005a], motion cueing for coordinated maneuvers involves the minimization of the perceivable specific forces, either through reducing and washing-out the simulator angular motion, through compensating simulator translational motion, or a combination of both.

As explained in Section 7.2.1, in this chapter pure simulator roll motion will be considered, where the simulator roll motion is washed-out during the turn maneuvers by applying a first-order high-pass roll motion filter as defined by Eq. (7.2). Fig. 7.5 shows what this implies for the simulator angular motion and specific forces, by presenting time traces of the simulator roll attitude ϕ and lateral specific force f_y for three different values of the roll motion filter break frequency ω_{mf} for $K_{mf} = 1$. The simulator motion resulting from using filter break frequencies of 0, 0.5, and 1 rad/s are shown, in addition to the true aircraft motion that is depicted with a solid gray line.

Fig. 7.5 shows that one-to-one motion, corresponding to a break frequency setting of 0 rad/s, would perfectly replicate the aircraft roll motion, but would yield a comparatively large lateral specific force of around 2 m/s^2 during the period where $\phi \approx 10 \text{ deg}$. Washing-out the simulator roll motion by increasing ω_{mf} is seen to markedly reduce the perceivable specific forces resulting from simulator tilt. As is clear from Fig. 7.5(a), how-

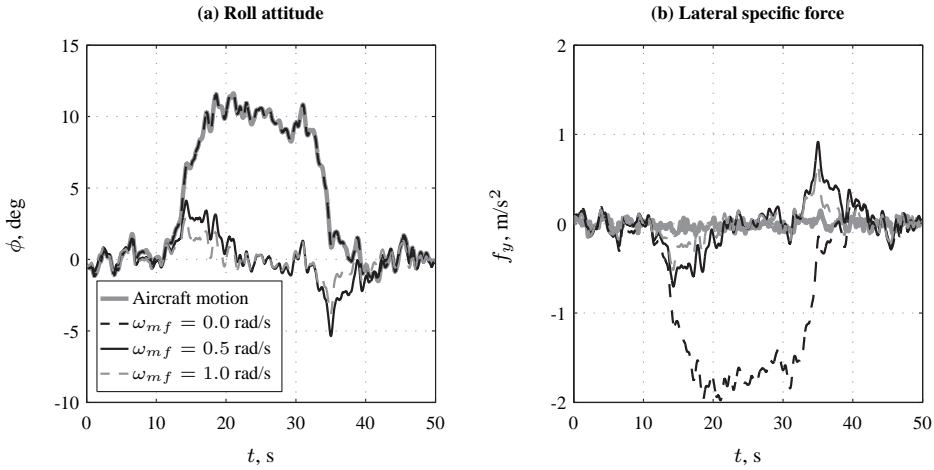


Figure 7.5. Example simulator roll attitude and lateral specific force cues for different first-order roll motion filter break frequencies.

ever, this roll washout also introduces differences between the aircraft and simulator roll attitude responses.

7.2.4 Modeling Multimodal Ramp-Tracking Behavior

As shown in Fig. 7.1, in this chapter pilot control behavior for the considered is modeled with three independent responses, indicated with $H_{p_t}(s)$, $H_{p_v}(s)$, and $H_{p_m}(s)$. Compared to the multimodal pilot model used in Chapter 6 for modeling pilot roll tracking behavior, the proposed model for multimodal ramp-tracking behavior only differs in the presence of the feedforward response $H_{p_t}(s)$. In Chapter 3 it was shown that the addition of such a feedforward response to a traditional model of compensatory tracking behavior successfully captured measured control inputs for ramp-tracking tasks. For this reason, a similar approach is taken in this chapter for modeling pilot control behavior in the considered ramp-tracking task with motion feedback, where the compensatory multimodal pilot model of Chapter 6 is extended with a feedforward response as proposed in Chapter 3. The transfer function models proposed for modeling the three pilot responses indicated in Fig. 7.1 are given by:

$$H_{p_t}(s) = \frac{U_t(s)}{F_{t_{ramp}}(s)} = K_t \frac{1}{H_c(s)K_s} e^{-s\tau_t} \quad (7.4)$$

$$H_{p_v}(s) = \frac{U_v(s)}{E_s(s)} = K_v (T_L s + 1) e^{-s\tau_v} H_{nm}(s) \quad (7.5)$$

$$H_{p_m}(s) = \frac{U_m(s)}{\phi_{s_m}(s)} = K_m H_{sc}(s) e^{-s\tau_m} H_{nm}(s) \quad (7.6)$$

In Equations (7.4) to (7.6), the symbols $U_t(s)$, $U_v(s)$, and $U_m(s)$ indicate the Laplace transforms of the control signal contributions u_t , u_v , and u_m , respectively. Similarly, $F_{t_{ramp}}(s)$, $E_s(s)$, and $\ddot{\phi}_{s_m}(s)$ indicate the Laplace transforms of the signals that are used as the inputs to the three pilot model channels, $f_{t_{ramp}}$, e_s , and $\ddot{\phi}_{s_m}$, respectively.

7.2.4.1 Feedforward Pilot Response Model

Eq. (7.4) gives the proposed model for the pilot feedforward response. In Chapter 3 it was shown that during ramp tracking, pilots select their feedforward response $H_{pt}(s)$ to be proportional to the inverse of the controlled element dynamics $H_c(s)$, as this ensures adequate following of the target signal through the feedforward. In this chapter, a target signal f_t is considered that consists of a signal made-up of multiple ramp-like changes in roll attitude – much like the ramp signals considered in Chapter 3 – with a superimposed multisine target signal. As the feedforward control inputs observed for ramp-tracking in Chapter 3 were only found during pilots' responses to the ramps in the used target signals, here the input to the feedforward response of the pilot model is also taken to be the ramp target signal $f_{t_{ramp}}$ and not the total target signal f_t .

Furthermore, note from Eq. (7.4) that the control input scaling gain is considered as a part of the controlled element compensation term. This convention ensures a “perfect” feedforward response, yielding $\phi = f_{t_{ramp}}$, for $K_t = 1$ and $\tau_t = 0$ s. The feedforward gain K_t and time delay τ_t are the free parameters of the model for $H_{pt}(s)$ and will be used in this chapter for evaluating changes in the pilot feedforward response dynamics. The proposed model for $H_{pt}(s)$ contains no further equalization dynamics in the feedforward response, as were considered for the ramp-tracking tasks evaluated in Chapter 3. Note that this implies that for the model of Eq. (7.4) all phase shifts induced by the pilot feedforward response will be attributed to the included delay term.

As explained in Section 7.2.1, the controlled element dynamics $H_c(s)$ are approximately K/s at low frequencies and approximately K/s^2 at frequencies above ω_ϕ . As $f_{t_{ramp}}$ predominantly has power at low frequencies, as shown for slightly different ramp forcing function signals in Appendix B, it is acceptable to not use the full controlled element dynamics as given by Eq. (7.1) in the model for $H_{pt}(s)$, but a low-frequency approximation given by:

$$H_c(s) = \frac{K_\phi/\omega_\phi^2}{s} \quad (7.7)$$

Fig. 7.6 shows a comparison of the frequency responses of the full controlled element dynamics and the low-frequency approximation given by Equations (7.1) and (7.7), respectively. As is clear from Figures 7.6(a) and (b), the dynamics of the reduced controlled element dynamics given by Eq. (7.7) approximate the true controlled element dynamics very well at frequencies up to 1 rad/s.

Fig. 7.6(c) shows a comparison of the modeled time traces of the feedforward control signal u_t (see Fig. 7.1) that are obtained with the full and reduced controlled element dynamics. These signals were obtained by simulating Eq. (7.4) with $f_{t_{ramp}}$ as the input and with $K_t = 1$ and $\tau_t = 0$ s. As indicated by the depicted ramp target forcing function time trace (dashed gray data), only the response of $H_{pt}(s)$ to the first positive ramp-like excursion of $f_{t_{ramp}}$ is depicted. As is clear from Fig. 7.6(c), the differences in the feedforward

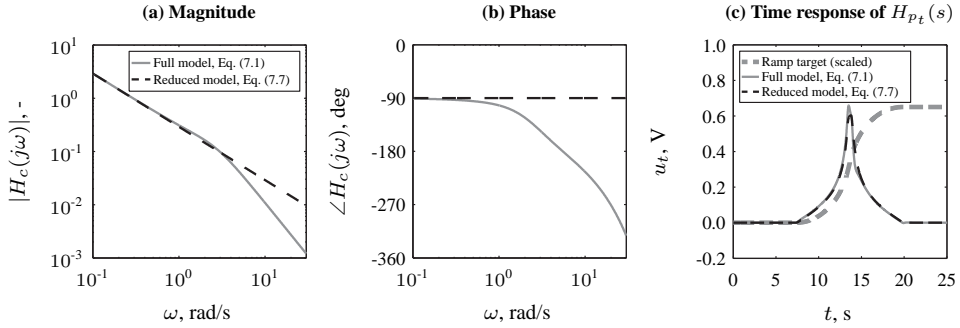


Figure 7.6. Comparison of the frequency responses of the full controlled element dynamics model and the reduced controlled element dynamics model and the modeled feedforward responses resulting from their implementation in the multimodal pilot model feedforward channel.

control signals u_t provided by using either the full or reduced controlled element dynamics in Eq. (7.4) are only very small. Hence, in the remainder of this chapter, Eq. (7.7) is used with Eq. (7.4) in the proposed model for $H_{p_t}(s)$.

7.2.4.2 Compensatory Pilot Response Models

The compensatory part of the proposed pilot model, as given by Equations (7.5) and (7.6), is the same model used for describing pilots' responses to visually presented tracking errors (e_s) and physical (simulator) roll motion accelerations ($\ddot{\phi}_s$) in Chapter 6. The pilot visual response $H_{p_v}(s)$ is modeled with a model based on the Precision Model proposed by McRuer et al. [1965]. The lead equalization term ($T_L s + 1$) is included to capture pilot lead equalization that is performed to compensate for the approximately K/s^2 dynamics of the controlled element given by Eq. (7.1) above ω_ϕ . In addition to the lead time constant T_L , the parameters of this visual response model are the pilot visual gain K_v and time delay τ_v . As can be verified from Eq. (7.5), a model for the neuromuscular actuation and manipulator dynamics $H_{nm}(s)$ associated with generation of a pilot response are also accounted for. These neuromuscular dynamics are modeled as a two-parameter second-order mass-spring-damper system:

$$H_{nm}(s) = \frac{\omega_{nm}^2}{s^2 + 2\zeta_{nm}\omega_{nm}s + \omega_{nm}^2} \quad (7.8)$$

As indicated by Eq. (7.6), $H_{p_m}(s)$ is modeled as a response that is proportional to the output of the semicircular canal dynamics $H_{sc}(s)$ to a rotational roll acceleration input [Hosman, 1996; Van der Vaart, 1992]. Similar to the visual response model of Eq. (7.5), the free parameters of the model for $H_{p_m}(s)$ are the pilot motion gain K_m and delay τ_m and it also includes the neuromuscular actuation model given by Eq. (7.8). The semicircular canal dynamics are modeled as a second-order transfer function that relates a rotational acceleration input to an afferent neuron firing rate, which is here defined to have impulses per unit of time (IPUT) as a unit. Over the frequency range between 0.1-6 rad/s, this afferent

firing rate is known to be proportional to rotational velocity [Fernandez and Goldberg, 1971; Hosman and Van der Vaart, 1978]. The model for $H_{sc}(s)$ used in this chapter, which is the same as that considered in Chapter 6, is given by:

$$H_{sc}(s) = 5.97 \frac{0.11s + 1}{(5.9s + 1)(0.005s + 1)} \quad (7.9)$$

In total, the three-channel pilot model proposed for describing ramp-tracking behavior with motion feedback in this chapter, as described by Equations (7.4) to (7.6), has nine free model parameters that will be used for characterizing pilots' control strategies under varying motion cueing settings. These free model parameters are the three response channel gains (K_t , K_v , and K_m) and time delays (τ_t , τ_v , and τ_m), the visual lead time constant T_L , and the neuromuscular actuation model natural frequency and damping ratio (ω_{nm} and ζ_{nm}).

7.2.5 Discrete Maneuvering Analysis using Phase-Planes

For analyzing human manual control behavior during discrete vehicle maneuvering tasks, some authors have proposed to evaluate the executed maneuvers using their phase-plane representations, in which the change in the controlled vehicle state is plotted against its rate [Heffley, 1982; Heffley et al., 1982; Ferguson et al., 1984; Schroeder, 1999; Ellerbroek et al., 2008]. From these phase-plane trajectories, the characteristic dynamics of the executed maneuvers can be read, compared, and quantified using metrics such as the maximum velocity attained during the maneuver and the maximum overshoot at the desired end position.

Fig. 7.7(a) shows a typical recorded time trace of the roll attitude ϕ during the ramp-tracking task considered in this chapter, depicted with a solid black line. The ramp target signal $f_{t_{ramp}}$ and the total target signal f_t are indicated with dashed black and solid gray lines, respectively. The four ramp segments of $f_{t_{ramp}}$, during which a change in ϕ of ± 10 deg is commanded, are numbered ① to ④. Fig. 7.7(b) shows the corresponding phase-plane representation of the ramp-tracking run plotted in Fig. 7.7(a). Note that the phase-plane representations of the ramp and total target forcing functions are depicted with the same colors as used in Fig. 7.7(a) and that the different ramp maneuvers are again indicated with symbols ① to ④.

As for instance shown by Heffley [1982], Ferguson et al. [1984], and Ellerbroek et al. [2008], the characteristics of the phase-plane representation of discrete maneuvers can be used to assess the performance with which these maneuvers are executed. Such an approach could have proven valuable for assessing ramp-tracking performance under varying motion cueing settings as considered in this chapter. However, as indicated by the example ramp-tracking phase-plane shown in Fig. 7.7(b), the presence of the multisine disturbance and target forcing functions result in considerable variation in the phase-plane trajectories on top of the discrete maneuvers commanded by $f_{t_{ramp}}$. Given that the roll rate and roll attitude deviations induced by the selected multisine forcing function signals are comparatively large compared to those commanded by the ramp target signal, they are thought to interfere too much with phase-plane analysis of the ramp-tracking maneuvers. Therefore, such phase-plane analysis of the executed ramp-tracking maneuvers will not be further considered in this chapter. Instead, this chapter relies on the multimodal pilot model proposed

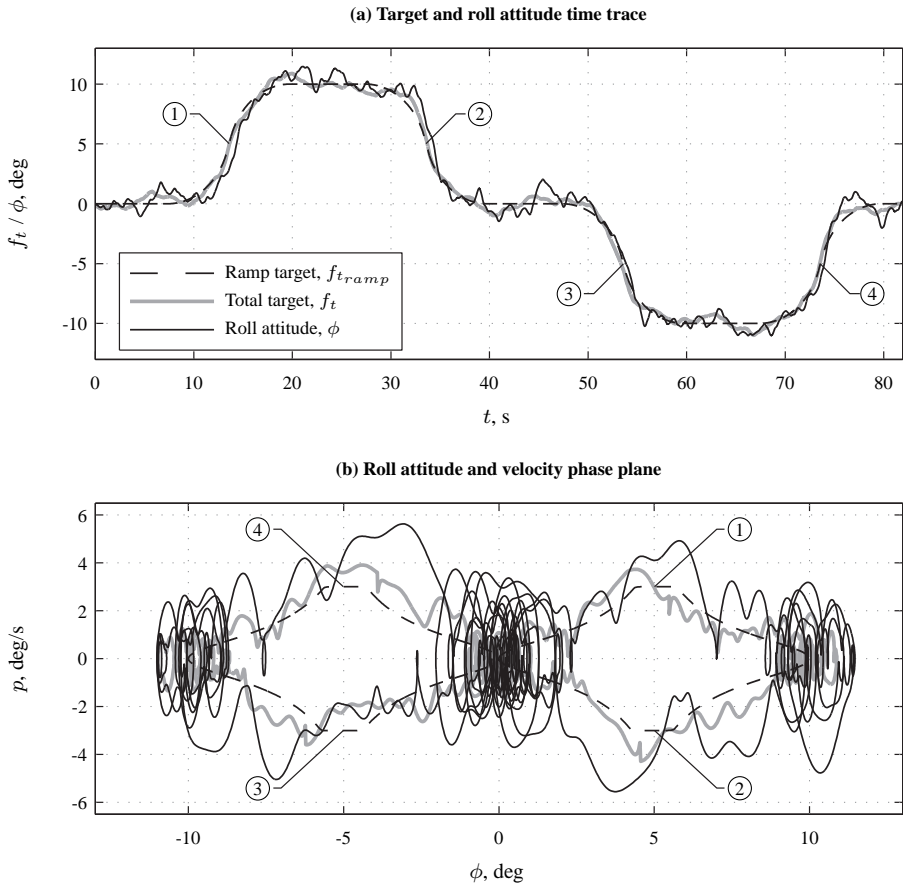


Figure 7.7. Example ramp-tracking roll attitude time trace and phase-plane.

in Section 7.2.4 for quantifying changes in pilot ramp-tracking behavior under varying roll motion cueing settings.

7.3 Experiment

7.3.1 Apparatus

This section will provide the details of the experiment performed to measure the effect of varying levels of simulator motion fidelity on pilot ramp-tracking behavior, with a comparison to tracking behavior for exactly the same control task measured in real flight. As this experiment was performed in the same experimental setups in the Cessna Citation II laboratory aircraft and the SIMONA Research Simulator (SRS) available at Delft University of Technology as used for the experiment described in Chapter 6, only comparatively brief descriptions of some aspects of these experimental setups are described here. For more details, please refer to Section 6.4.1.

In the Citation II laboratory aircraft a BG Systems JFf force stick was installed at the right pilot seat, with which control inputs u to the fly-by-wire control system were given (for details, see [Zaal et al., 2009d] and [Zaal, 2011]). As described in Appendix C, the roll axis of this force stick had an approximately linear applied force-output voltage characteristic with a gradient of around 14 N/V over the full range of attainable output voltages (± 2.5 V). In the SRS, the characteristics of this BG Systems JFf force stick were mimicked on a Moog FCS Ecol-8000 electrical side stick that was installed next to the right pilot seat in the SRS cabin. In both experimental setups, LCD displays mounted directly in front to the right pilot seats were used for presenting pilots with the visual display shown in Fig. 7.2. The update rates of both displays were 60 Hz and, as also explained in Section 7.2.1, the delay associated with the visual presentation on both these displays was measured to be around 25 ms (see [Stroosma et al., 2007] and Appendix C). In the simulator part of the experiment, simulator roll motion cues were provided using the hydraulic six degree-of-freedom hexapod motion system of the SRS. The motion base dynamics of the SRS are known to be approximately a unity gain with a delay of 30 ms over the frequency range important for this experiment [Berkouwer et al., 2005].

7.3.2 Independent Variables

This chapter considers pilot control behavior during the roll attitude ramp-tracking task shown in Fig. 7.1 for six different experimental conditions, see Table 7.2. First of all, pilot ramp-tracking behavior is measured in real flight, with the true aircraft motion as depicted in Fig. 7.4, for the CIT condition. Furthermore, for the simulator measurements collected for comparison with the in-flight measurements, five different simulator roll motion cueing settings were considered. As can be verified from Table 7.2, these five SRS conditions represent a variation in the characteristics of the first-order high-pass roll motion filter defined by Eq. (7.2).

The first SRS condition listed in Table 7.2 is the no-motion condition SR0. In this condition the participants received no physical simulator motion information, yielding a

Table 7.2. Experimental conditions.

condition	apparatus	description	filter, (K_{mf}, ω_{mf})
SR0	SRS	no motion	(0,0)
SR1	SRS	low gain, strong washout	(0.5,1)
SR2	SRS	low gain, weak washout	(0.5,0.5)
SR3	SRS	high gain, strong washout	(1,1)
SR4	SRS	high gain, weak washout	(1,0.5)
CIT	Citation	aircraft 1-to-1 motion	—

ramp-tracking task similar to those considered in Chapter 3. Conditions SR1-SR2 represent a factorial evaluation of two settings for both the motion filter gain K_{mf} and the filter break frequency ω_{mf} . For the filter gain values of 1 and 0.5 were considered, while filter break frequencies of 0.5 and 1 rad/s were evaluated. Note that one-to-one simulator roll motion, as considered for the compensatory roll tracking tasks described in Chapter 6 is not considered here, because of the significant lateral specific forces due to roll tilt that would be perceivable for pure roll motion cueing (see Fig. 7.5). The five considered simulator motion cueing settings are depicted in the rotational motion fidelity criterion proposed by Sinacori [1977], with the modified fidelity regions proposed by Schroeder [1999], in Fig. 7.8. Note from Fig. 7.8 that when purely considering the roll motion filter settings, SR4 would correspond to a high level of motion fidelity, while SR2 and SR3 are both considered to be medium fidelity. Condition SR1 and the no-motion setting SR0 are both low-fidelity according to the criterion regions proposed by Schroeder [1999].

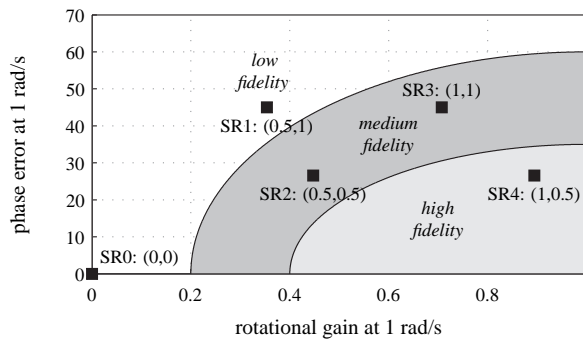


Figure 7.8. Evaluation of the rotational simulator motion fidelity criterion proposed by Sinacori [1977], with modified fidelity regions from [Schroeder, 1999], for the different experimental conditions.

7.3.3 Participants

The same seven Citation II pilots that performed the experiment described in Chapter 6 were the participants in the current experiment. At the time of the in-flight and simulator exper-

iments, all participants were active Cessna Citation II pilots employed by Delft University of Technology and all except one had experience with similar tracking tasks from previous simulator and in-flight experiments. The participants' flight experience ranged from 1,500-14,000 hrs on a multitude of different aircraft. Their ages ranged from 34 to 72 years ($\mu = 51.1$ years, $\sigma = 14.3$ years).

7.3.4 Dependent Measures

A number of different dependent measures are considered for evaluating the effects of varying roll motion fidelity for the roll ramp-tracking task evaluated in this chapter. First of all, for all experimental conditions performed in the SRS (SR0-SR4, see Table 7.2), the participants were asked to give a subjective indication of the level of motion fidelity using the same verbal analogue scale (VAS) described in Chapter 6. On this rating scale, the pilots had to give a subjective motion fidelity rating by drawing a vertical line through a horizontal 10 cm axis that ranged from 0-100% correspondence of the simulator motion to what would be expected in the real aircraft.

In addition to these subjective motion fidelity ratings, objective metrics of how the pilots performed the considered ramp-tracking task under the different experimental conditions listed in Table 7.2 were considered. First, the attained tracking performance and control activity were evaluated from the variances of the tracking error and control signals, σ_e^2 and σ_u^2 , respectively. Furthermore, using the spectral technique proposed by Jex et al. [1978], the contributions of the multisine target and disturbance forcing functions to these signal variances, and the remainder that in this case contains both pilot remnant and contributions resulting from $f_{t_{ramp}}$, are separated. In addition, to further quantify the contribution of the ramp target signal to the observed levels of tracking performance and control activity, the total σ_e^2 and σ_u^2 are also evaluated separately during and outside of the portions of the tracking runs where $f_{t_{ramp}}$ induced a change in reference roll attitude.

Finally, the model of multimodal pilot ramp-tracking behavior described in Section 7.2.4 is fitted to time-domain measurements of $f_{t_{ramp}}$, e , $\ddot{\phi}_{sm}$, and u using the time-domain identification procedure described in [Zaal et al., 2009a]. For fitting the pilot model, the time-domain averages of the five repeated measurements of these signals that were collected for each condition were used. Note that as no physical motion feedback was present for condition SR0, only the pilot feedforward and visual responses ($H_{p_t}(s)$ and $H_{p_v}(s)$, respectively) were included in the pilot model that was fit to the data from this condition. The estimated parameter values for the nine parameters of this pilot model are used to explicitly evaluate changes in pilot control behavior under the different experimental conditions. Before analyzing the observed changes in pilot control behavior using these pilot model parameter estimates, some validation of the proposed model of ramp-tracking behavior will be provided by evaluating the fit of the model to the time-domain measurements of u and using the model variance accounted for (VAF), as for instance defined in Chapter 3.

7.3.5 Experimental Procedures

As was also the case for the experiment of Chapter 6, all participants performed the simulator part of the experiment before the measurements of in-flight ramp-tracking behavior

were collected. During both the in-flight and simulator parts of the experiment, participants were first trained until their proficiency in performing the tracking task had reached a consistent level. Their tracking performance was monitored by the experimenter by evaluating the root mean square of the tracking error signal e . For the ramp-tracking task, reaching a stable level of tracking performance required, on average, around five repetitions of the experimental conditions evaluated in the in-flight and simulator parts of the experiment. Five further measurements were then collected for each experimental condition as the measurement data at this consistent level of tracking performance.

In the simulator part of the experiment, the participants were presented with the five different roll motion cueing settings (SR0-SR4, see Table 7.2) in a random order, which was defined using a balanced Latin square, throughout both the training and measurement phases of the experiment. As explained in more detail in Chapter 6, before each tracking run the simulator was repositioned in pitch to the trim pitch attitude of the aircraft during the in-flight measurements ($\theta = 4.34$ deg). The experimenter initiated each tracking run after counting down from three. After each tracking run, the simulator was tilted back to zero pitch, after which the pilots were asked to fill out the subjective motion fidelity rating form for the run they had just completed. After indicating they had completed their subjective motion fidelity rating, the participants were informed of their tracking performance (root mean square of e) for the completed tracking run.

As opposed to the additional single-loop measurements collected in the experimental setup in the Citation II laboratory aircraft for the compensatory roll tracking task considered in Chapter 6, only in-flight measurements (condition CIT) of pilot control behavior were collected for the ramp-tracking task considered in this chapter. Given that the in-flight pitch and roll tracking measurements described in Zaal [2011] and Chapter 6 were collected on the same day as the ramp-tracking measurements considered here, there was not enough time to also perform these reference measurements for the roll ramp-tracking task. As described in more detail in Chapter 6, two pilots performed the in-flight control tasks on each four-hour flight. One pilot, referred to as the safety pilot, ensured the aircraft was in the desired flight condition (altitude, velocity) before the start of a tracking run. The other pilot, referred to as the experiment pilot, would engage the fly-by-wire control system used for the in-flight experiments and initiate and perform a tracking run. When a tracking run was completed the experiment software would disengage the fly-by-wire control system, after which the safety pilot would again be in control of the aircraft. The experimenter then notified the experiment pilot of his performance for the last run.

For the in-flight ramp-tracking tasks the participants were required to wear a hood (see Appendix G) that limited their field of view to the LCD display on which the pursuit display shown in Fig. 7.2 was presented, to avoid effects of this moving control column and pilots' view of the outside world on their control strategy during the pitch tracking task. During the ramp-tracking tasks performed in the SRS, the participants did not wear this hood.

7.3.6 Hypotheses

As also done for a compensatory roll tracking task with two multisine forcing functions in Chapter 6, this chapter attempts a comparison between pilot control behavior measured in real flight and in a moving-base flight simulator for a more operationally relevant control

task that also involves the manual tracking of discrete ramp-like changes in roll attitude. In addition to subjective motion fidelity ratings, quantitative measurements of pilot control behavior, obtained from fitting a proposed behavioral pilot model thought to be appropriate for such a task, are used to evaluate the effects of varying simulator motion fidelity. As also shown in Chapter 6, comparing pilot control behavior measured in real flight and in a simulator environment is challenging, even for a control task for which the models that can be used for describing human behavior have been validated extensively. Here such a behavioral comparison is described for a control task for which pilot behavior has been studied significantly less extensively.

For the compensatory disturbance-rejection function performed by the pilots, reducing the level of simulator motion fidelity is typically found to result in reduction in the gain with which pilots respond to visual error information and an increase in the amount of visual lead equalization that is performed, as can be verified from, for instance, Chapters 5 and 6. As the same multisine disturbance and target forcing function signals used for the experiment of Chapter 6 are still utilized for the ramp-tracking task considered in this chapter in addition to $f_{t_{ramp}}$ it is expected that the effects of varying motion filter settings on pilot tracking behavior might be highly similar to those observed in Chapter 6. This will especially hold for the estimated parameters of the compensatory portion of the proposed model for multimodal ramp-tracking behavior (the visual and motion responses $H_{p_v}(s)$ and $H_{p_m}(s)$) and for the contributions of $f_{t_{ms}}$ and f_d to the error and control signal variances. Overall, despite the added ramp-tracking element, it is therefore anticipated that the ramp-tracking task considered in this chapter may show effects of varying washout settings on pilot control behavior that are highly similar to those described in Chapters 5 and 6 for tracking tasks with only multisine forcing function signals.

The combined ramp-tracking and disturbance-rejection task considered in this chapter differs from the purely compensatory roll tracking task that was used for evaluating behavioral simulator motion fidelity in Chapter 6 in the ramp-tracking element that has been added to the task. As explained in Chapter 3 and Section 7.2.4 this has consequences for the type of control behavior that is adopted for such a task and how this should be modeled. Furthermore, as explained in Section 7.2.3, the variation in roll motion fidelity and especially filter break frequency settings may show an effect on pilot behavior during ramp-tracking because of manipulation of the simulator roll motion by the roll motion washout. Here it is hypothesized that similar to compensatory tracking, pilot ramp-tracking behavior is affected by variations in roll motion washout. Degraded roll motion fidelity and especially increased values of ω_{mf} are expected to show a degradation in ramp-tracking performance and feedforward ramp-tracking behavior that shows larger discrepancies with optimal feedforward operation ($H_{p_t}(s) \approx 1/H_c(s)$). For conditions where degraded feedforward response dynamics occur, the fits of the proposed multimodal ramp-tracking pilot model are therefore anticipated to show reduced values of the feedforward gain K_t and increased values of the feedforward time delay τ_t .

Finally, when comparing the in-flight measurements of pilot tracking behavior with measurements taken in the SRS, it was found in Chapter 6 that pilot tracking behavior for the high-fidelity roll motion cueing setting referred to in this chapter as SR4 (identical to condition S2 in Chapter 6) closely matched the in-flight measurements. Still, consistently lower pilot response gains, increased visual delays τ_v , and lower neuromuscular frequencies

were observed for the tracking behavior measured in real flight compared to all simulator measurements. For this reason, similar differences between the control behavior measured for the CIT condition and for all conditions evaluated in the SRS are also anticipated for the considered ramp-tracking task. Based on the analysis of the aircraft motion that is typical for the ramp-tracking task considered in this chapter and on the typical effects of variations in simulator motion washout on pilot tracking behavior, however, it is anticipated that the high-fidelity roll motion cueing condition SR4 ($K_{mf} = 1$ and $\omega_{mf} = 0.5$ rad/s) will show the smallest behavioral discrepancies with respect to the in-flight measurements.

7.4 Results

This section presents the results of the combined in-flight and simulator experiment in which simulator roll motion fidelity was evaluated for a combined roll attitude ramp-tracking and disturbance-rejection task. The experiment had a within-subjects design and, as explained in Section 7.3.2, only considered a variation in one independent variable, that is, the different roll motion cueing settings for which ramp-tracking behavior and performance was evaluated. One-way repeated measures analyses of variance (ANOVA) were performed to evaluate possible significant variations in the considered metrics over the different experimental conditions. However, if for any of the considered metrics the measured data was found to show a sample distribution significantly different from normal (as indicated by a Kolmogorov-Smirnov test) for at least one experimental condition, a nonparametric Friedman's ANOVA was used for evaluating statistical significance instead of the repeated measures ANOVA [Field, 2005].

7.4.1 Subjective Motion Fidelity Ratings

Fig. 7.9 shows the subjective motion fidelity ratings collected for all experimental conditions performed in the SRS using the VAS rating scale. The gray data show the average ratings provided by the seven experiment participants, while the black markers and variance bars indicate the means over the data of all participants and the corresponding 95% confidence intervals of the mean, respectively.

As can be verified from Fig. 7.9, for the no-motion condition SR0 the subjective motion fidelity ratings typically show very low values, indicating little correspondence between the supplied simulator motion and the motion feedback expected in the aircraft. The sole exception to this is subject 3, who on average rated this condition at around 80% correspondence to true aircraft motion. On average, the highest motion fidelity ratings were given for both conditions with a roll motion gain of 1 (SR3 and SR4). The slightly higher mean rating observed for condition SR4 indicates that the pilots, on average, perceived this condition to yield the highest level of simulator motion fidelity for the task they were to perform. Still, some of the subjects – most notably subjects 3 and 7 – indicated they felt a reduced roll motion gain of 0.5 yielded higher simulator motion fidelity than the $K_{mf} = 1$ conditions SR3 and SR4. Due to this disagreement between the ratings given by the different experiment participants, the spread in the average rating data is found to be comparatively large, especially for the $K_{mf} = 0.5$ conditions SR1 and SR2.

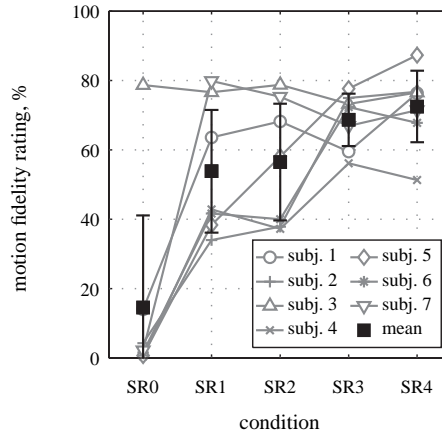


Figure 7.9. Mean subjective motion fidelity ratings for roll ramp tracking.

A Kolmogorov-Smirnov test performed on the subjective ratings shown in Fig. 7.9 indicated that the ratings for condition SR0 showed a distribution that significantly differs from normal ($D(7) = 0.37$, $p < 0.05$) due to the extremely high ratings provided by subject 3. Despite the comparatively large spread in the data, a Friedman's ANOVA still showed that the motion fidelity ratings changed significantly over the different experimental conditions, $\chi^2(4) = 10.2$, $p < 0.05$. Wilcoxon signed-rank tests were used to evaluate possible significant differences between the ratings given for individual conditions. For these ten pairwise comparisons a Bonferroni correction was applied, yielding an adjusted level of significance for these tests of 0.005 (0.05/10). Though not significant at the corrected significance level, only the comparisons between the no-motion ratings and those for all conditions with roll motion feedback were found to show close-to-significant differences.

7.4.2 Tracking Performance and Control Activity

Fig. 7.10 presents the average tracking error and control signal variances, σ_e^2 and σ_u^2 , which are considered as metrics for assessing changes in the attained level of tracking performance and control activity, respectively. The average total error and control signal variances measured for all experimental conditions are indicated by the total height of the bars in Fig. 7.10 and the presented variance bars show the corresponding 95% confidence intervals of the means of σ_e^2 and σ_u^2 . Using the spectral technique described by Jex et al. [1978], the contributions of the multisine disturbance and target forcing functions to these signal variances have been evaluated separately. The averages of these disturbance and target variance components are presented as the black and white-filled portions of the bars in Fig. 7.10, respectively. The parts of the error and control signal variances that are not correlated with f_d and $f_{t.m.s}$ are indicated with the gray portions of the bars. For control tasks that only consider multisine forcing function signals, such as the roll tracking task considered by Jex

et al. [1978], this component is attributable to pilot remnant. It should be noted, however, that for the ramp-tracking task considered in this chapter the remnant components $\sigma_{e,n}^2$ and $\sigma_{u,n}^2$ also include the contributions of f_{ramp} , as this ramp signal's contribution is not distinguishable from remnant in the frequency-domain, as it does not provide excitation at a number of discrete frequencies (see Appendix B).

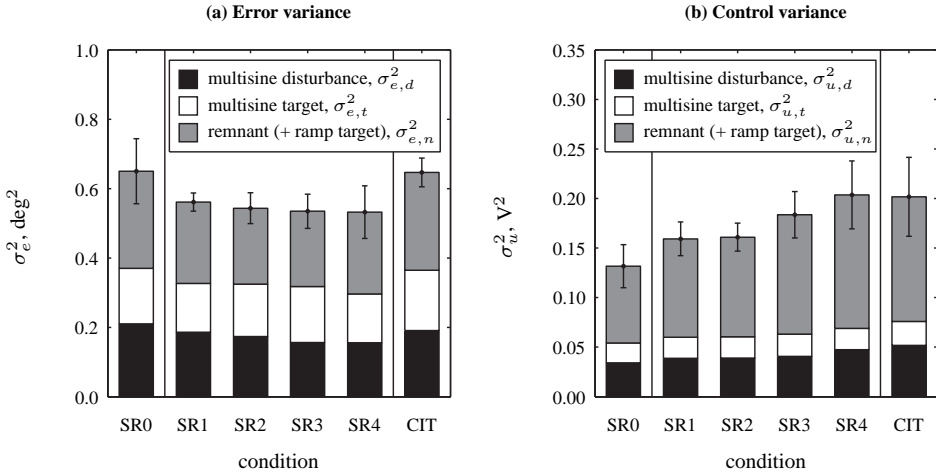


Figure 7.10. Average tracking error and control signal variance decompositions for all experimental conditions.

Fig. 7.10(a) shows that the total tracking error variance was found to be markedly lower for all conditions performed with roll motion feedback in the SRS (SR1-SR4) compared to the no-motion measurements of condition SR0. Furthermore, σ_e^2 is found to decrease slightly with increasing simulator roll motion fidelity, however, this effect is only comparatively minor. Similar to the observation made for the pure multisine roll tracking task considered in Chapter 6, tracking performance for the in-flight CIT condition was found to be considerably worse than observed for those motion conditions evaluated in the SRS that are high fidelity according to the criterion of Schroeder [1999]. For the ramp-tracking task considered here, σ_e^2 measured in-flight is on average found to be approximately equal to the level of tracking performance attained for the no-motion task in the SRS (SR0). Due to the comparatively bad task performance attained by pilot 5, there are severe issues with σ_e^2 data normality for a number of experimental conditions. A Friedman's ANOVA indicates that the observed variation in total tracking performance is statistically significant, $\chi^2(5) = 16.4$, $p < 0.05$. Pairwise comparisons (Wilcoxon signed-rank tests) indicate that this significant effect is mainly attributable to the lower σ_e^2 observed for conditions SR1-SR4 compared to conditions SR0 and CIT.

The different components of σ_e^2 show largely the same trend over the different experimental conditions as observed for the total error variance. Compared to the data for condition SR0, $\sigma_{e,d}^2$, $\sigma_{e,t}^2$, and $\sigma_{e,n}^2$ are all found to be slightly lower for all conditions performed with roll motion feedback in the SRS. Furthermore, the in-flight measurements (condition

CIT) are found to result in average variance components that are almost equivalent to those of the no-motion condition SR0. This variation over the different experimental conditions was found to be statistically significant for $\sigma_{e,t}^2$ and $\sigma_{e,n}^2$: $F(5, 30) = 2.90, p < 0.05$ and $F(5, 30) = 2.81, p < 0.05$, respectively. Mauchly's Test indicated that the assumption of sphericity was violated for the $\sigma_{e,d}^2$ data: $\chi^2(14) = 38.58, p < 0.05$. With application of the conservative Greenhouse-Geisser sphericity correction, the observed variation in $\sigma_{e,d}^2$ is not found to be statistically significant, $F(1.3, 7.7) = 3.17, p \geq 0.05$.

Equivalent to the results reported in Chapter 6, Fig. 7.10(b) shows a clear increase in control signal variance with decreasing motion attenuation (from SR0 to SR4) over the different SRS conditions. In addition, σ_u^2 measured for the in-flight condition CIT is found to be highly similar to the control activity measured for the high-fidelity roll motion setting SR4, as also observed for the multisine roll tracking task considered in Chapter 6. Due to the comparatively high control activity registered for subject 2 (mean of σ_u^2 for subject 2 over all conditions: 0.36 deg^2), Kolmogorov-Smirnov tests indicated violation of the normality assumption for the σ_u^2 data for nearly all experimental conditions. A Friedman's ANOVA indicated that the increasing trend in control signal variance shown in Fig. 7.10(b) is highly statistically significant: $\chi^2(5) = 25.5, p < 0.05$.

When considering the different contributions to σ_u^2 , Fig. 7.10(b) shows that $\sigma_{u,d}^2$ and $\sigma_{u,n}^2$ also show the increasing trend with increasing motion fidelity observed for the total control signal variance. This increasing trend was found to be significant for $\sigma_{u,n}^2$ ($\chi^2(5) = 24.6, p < 0.05$), however, Mauchly's Test indicated a violation of the sphericity assumption for $\sigma_{u,d}^2$: $\chi^2(14) = 32.89, p < 0.05$. With application of the Greenhouse-Geisser sphericity correction the variation in $\sigma_{u,d}^2$ was not found to be statistically significant, $F(1.8, 10.8) = 3.90, p \geq 0.05$. As can also be verified from Fig. 7.10(b), the multisine target control signal variance component was found to remain approximately constant over the different experimental conditions, $F(2.2, 13.4) = 1.45, p \geq 0.05$.

The variance component data presented in Fig. 7.10 does not allow for separate evaluation of the contribution of $f_{t_{ramp}}$ to σ_e^2 and σ_u^2 due to the fact that this signal introduces power at all frequencies. To still allow for some evaluation of the contribution of the ramp target signal to the error and control signal variances, these have been calculated over the time windows where the ramp target signal commands a maneuver from $\phi = 0$ to ± 10 deg or back. Fig. 7.11 shows example time traces of the tracking error and control signals. In addition, to indicate the location of the different ramps in $f_{t_{ramp}}$, the (scaled) ramp target signal is plotted in Fig. 7.11 with a dashed black line. The windows where $f_{t_{ramp}}$ induces a change in roll attitude, defined to span 8 s around the midpoint of the ramps, are indicated with the gray shaded areas. Note from Fig. 7.11 that both e and u show comparatively larger excursions within these ramp windows than during the stages where $f_{t_{ramp}}$ is constant.

Fig. 7.12 shows the tracking error and control signal variances calculated within the gray-shaded areas depicted in Fig. 7.11 (black markers) and outside of the gray-shaded areas (white markers). Furthermore, σ_e^2 and σ_u^2 calculated over the complete run, corresponding to the total height of all bars depicted in Fig. 7.10, are indicated with horizontal gray bars for each condition. Note from Fig. 7.12 that for both σ_e^2 and σ_u^2 the variation in the depicted ramp window variances follows largely the same trend as observed for the total error and control signal variances in Fig. 7.10. As shown in Fig. 7.12(a), the tracking error variances

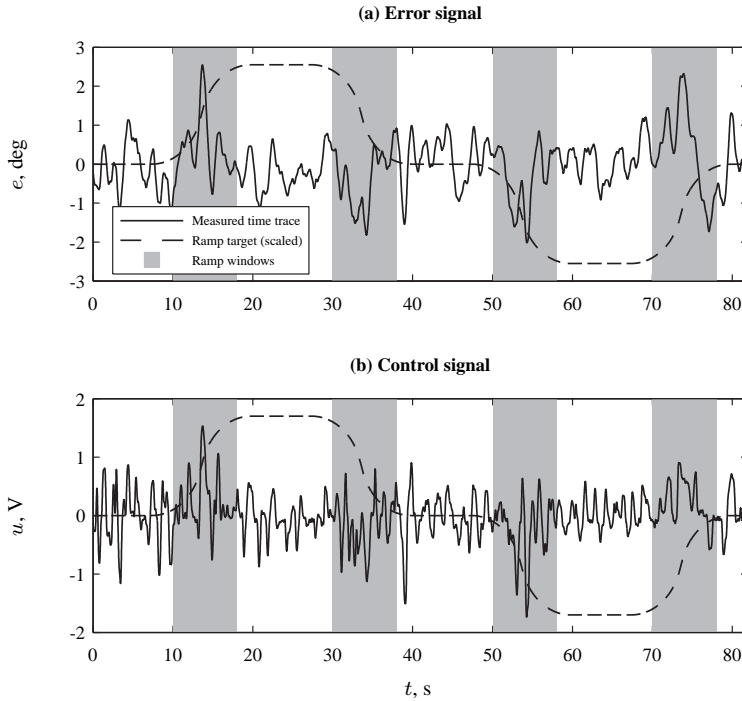


Figure 7.11. Example tracking error and control signal time traces with the windows defined for evaluation of the additional contribution of the ramp target forcing function signal to these signals (subject 1, CIT condition, run 1).

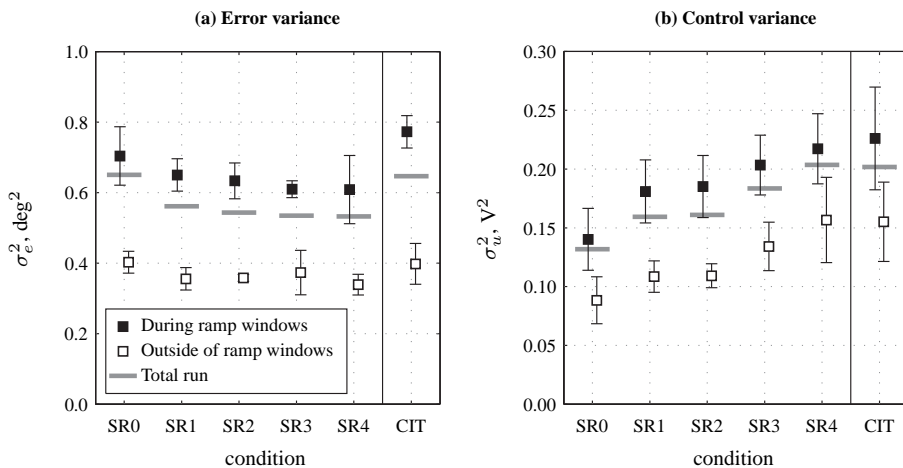


Figure 7.12. A comparison of the tracking error and control signal variances within and outside of the ramp windows.

is found to consistently be around 0.3 deg^2 higher during the ramp windows than outside of them. Similarly, a consistent increase in σ_u^2 within the ramp windows of over 0.05 V^2 is also observed from Fig. 7.12(b). The clear differences between the values of σ_e^2 and σ_u^2 measured within and outside of the ramp windows suggest a significant contribution of $f_{t_{ramp}}$ to the measured tracking performance and control activity. Furthermore, the fact that both the variances measured within and outside of the ramp windows show largely the same trend over the different experimental conditions suggests that ramp-tracking performance and behavior are affected in a similar fashion by varying simulator motion cueing settings as observed for tracking tasks with only multisine forcing function signals in Chapter 6.

7.4.3 Pilot Modeling Results

To evaluate possible changes in pilot control behavior over the different experimental conditions, the multimodal pilot model described in Section 7.2.4 was fit to (measured) time traces of $f_{t_{ramp}}$, e , $\ddot{\phi}_{sm}$, and u . First, the quality-of-fit of the proposed model for multimodal ramp-tracking behavior will be evaluated in this section. Then, the obtained estimates of the model parameters will be used for quantifying changes in pilot control behavior due to the applied variation in roll motion cueing.

7.4.3.1 Pilot Model Quality of Fit

As for instance explained in Chapters 2 and Chapter 3, the variance accounted for (VAF) is a metric that is typically used for evaluating the quality-of-fit of fitted pilot models. The VAF indicates the fraction of the variance of the measured model output signal, in this case the pilot control signal u , that is explained by the fitted model and expresses it as a percentage. A VAF of 100% indicates that the model fully explains the measured signal. Fig. 7.13 shows the VAF values obtained for the fits of the multimodal pilot model described in Section 7.2.4 to the measured data for all experimental conditions. Equivalent to the format of Fig. 7.9, the individual subject data is shown in gray and the mean VAF over all participants is depicted with black square markers.

Fig. 7.13 shows that the VAF values obtained for the fits of the multimodal ramp-tracking pilot model do not differ significantly over the different experimental conditions. A repeated measures ANOVA performed on the VAF data confirms this, $F(5, 30) = 2.07$, $p \geq 0.05$. On average, VAFs of around 85% are obtained for all conditions of the experiment, which is highly similar to the VAFs that are typically obtained for purely compensatory tracking tasks [Zaal et al., 2009a].

The model proposed for modeling multimodal ramp-tracking behavior in Section 7.2.4 differs from the models typically used for describing compensatory tracking behavior with motion feedback (see, for instance, Chapter 6) only by the presence of the feedforward response $H_{p_t}(s)$, as given by Eq. (7.4). In Chapter 3 it was shown that the addition of such a feedforward response significantly improved the modeling of ramp-tracking behavior, compared to purely compensatory models of manual control behavior. To also evaluate this for the multimodal ramp-tracking task considered in this chapter, a pilot model that only considered the pilot visual response $H_{p_v}(s)$ and the motion response $H_{p_m}(s)$, thereby yielding exactly the same model of compensatory behavior as considered in Chapter 6, was also fit

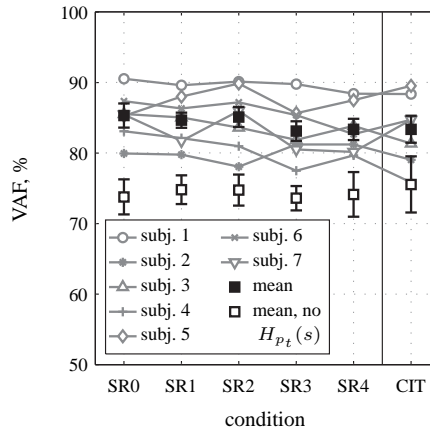


Figure 7.13. Mean multimodal ramp-tracking pilot model variance accounted for.

to the same measurement data. The VAF values of the fits of this model without $H_{pt}(s)$ are shown in Fig. 7.13 with white-filled square markers. As can be verified from Fig. 7.13, not considering the pilot feedforward response $H_{pt}(s)$ causes an average reduction of over 10% in the model VAF, indicating a severely reduced capacity of this purely compensatory model's ability to describe the measured ramp-tracking behavior.

The reason for this is illustrated by Fig. 7.14, which depicts a comparison of the measured control signal u , shown in gray, with the time traces of the feedforward (u_t , see Fig. 7.1) and compensatory ($u_v + u_m$) contributions to the total model output and the total control signal modeled by the proposed multimodal ramp-tracking pilot model. Note that in Fig. 7.14 example model responses for three different experimental conditions – SR0, SR4, and CIT – are presented. For the other conditions highly similar responses were obtained, but these are not shown for brevity. Note that Fig. 7.14 only shows the time traces for the first (positive) excursion in roll attitude commanded by $f_{t_{ramp}}$ and the corresponding return to $\phi = 0$ deg.

As can be verified from Figures 7.14(a), (d), and (g), the control response modeled by the feedforward dynamics $H_{pt}(s)$ accurately matches the off-zero excursions in the measured u around the occurrence of a ramp in $f_{t_{ramp}}$. As also shown for ramp-tracking tasks performed with single integrator controlled element dynamics in Chapter 3, these ramp-tracking responses can not be fully explained using a compensatory model of pilot tracking behavior. As can be verified from Figures 7.14(c), (f), and (i), combining this modeled feedforward response with a compensatory control response (Figures 7.14(b), (e), and (h), respectively) yields a total model fit that captures both the control inputs given to follow $f_{t_{ramp}}$ and those corresponding to compensatory attenuation of tracking errors induced by $f_{t_{ms}}$ and f_d . Omitting the pilot feedforward response, as done for the VAFs indicated with the white markers in Fig. 7.13, yields a total model fit that is only marginally better than the fits shown for the compensatory part of the total pilot model in Figures 7.14(b), (e), and (h).

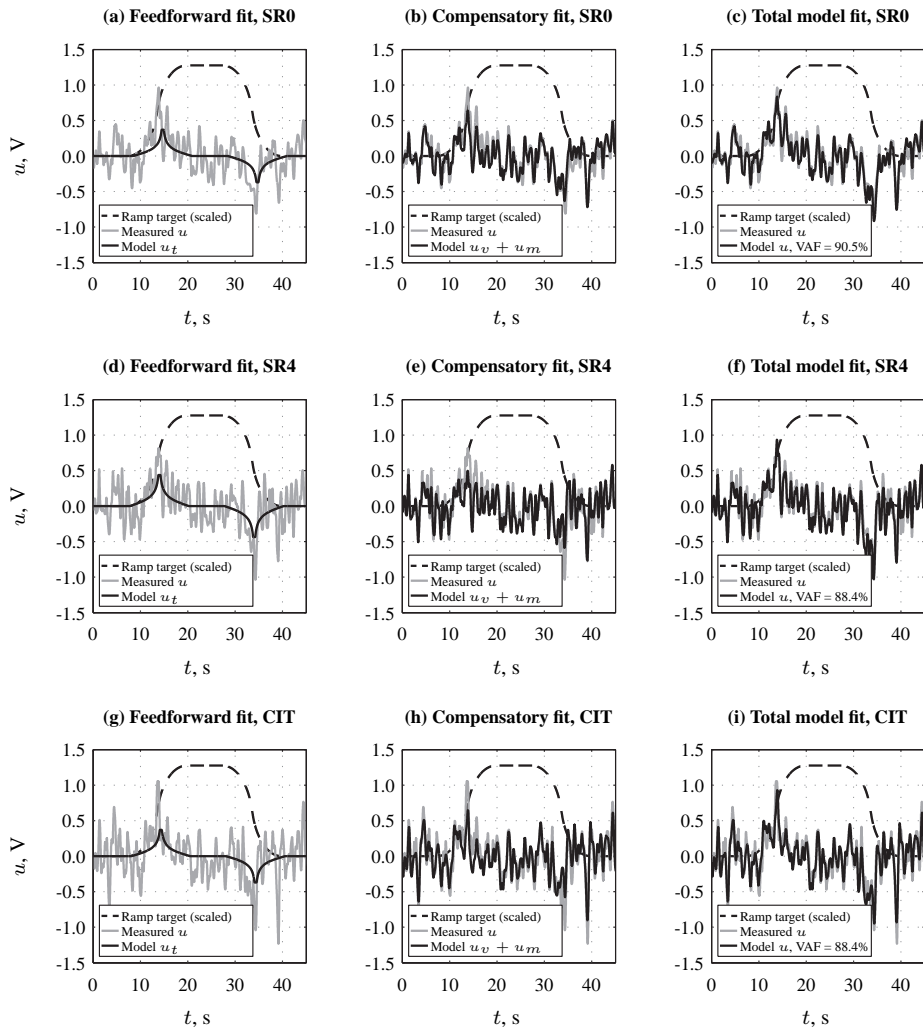


Figure 7.14. Example responses of the feedforward and compensatory portions of the fitted model of pilot multimodal ramp-tracking behavior (subject 1, conditions SR0, SR4, and CIT).

7.4.3.2 Pilot Model Parameter Estimates

Figures 7.13 and 7.14 showed that the proposed model for describing multimodal ramp-tracking behavior was found to accurately capture measured pilot control inputs, both those given to attenuate tracking errors from both multisine forcing function signals and those given for following the ramp target signal. In this section, the corresponding estimates of the nine pilot model parameters are analyzed to reveal possible changes in pilot control behavior over the different experimental conditions and as a result of the applied variation in roll motion cueing settings.

Fig. 7.15 shows the estimates of the two parameters of the model for the pilot feedforward response defined by Eq. (7.4), the feedforward gain K_t and the feedforward time delay τ_t . Fig. 7.15 shows the estimated parameters for the different experiment participants in gray to illustrate inter-subject differences. The average over the seven participants and the corresponding 95% confidence intervals are indicated with the black square markers and variance bars, respectively.

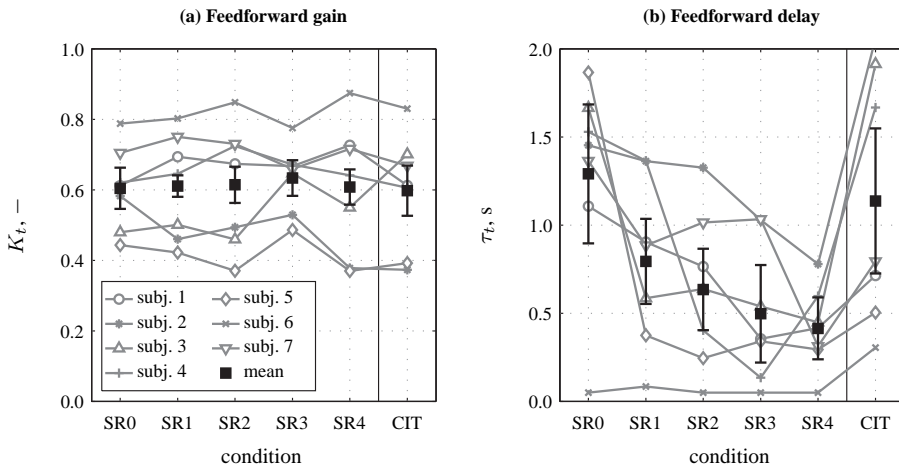


Figure 7.15. Mean estimated pilot feedforward response model parameters.

In previous experiments that evaluated ramp-tracking behavior, such as the experiment of Chapter 3, it was shown that the gain of the pilot feedforward response tends to vary for different controlled elements and ramp signals with different steepnesses. In this chapter, the same controlled element and $f_{t_{ramp}}$ were considered for all experimental conditions. Instead a variation in the supplied roll motion cueing was considered, for which the varying strength of the roll washout, as illustrated in Section 7.2.3, was anticipated to affect the pilot feedforward response dynamics. As can be verified from Fig. 7.15(a), K_t is found to remain approximately constant at around 0.6 for all experimental conditions including the in-flight ramp-tracking task (CIT). A repeated-measures ANOVA performed on the presented values of K_t confirmed that there was no significant change in the pilot feedforward gain over the different experimental conditions, $F(5, 30) = 0.27, p \geq 0.05$.

Fig. 7.15(b) shows the estimated values of the feedforward delay parameter τ_t . Note that τ_t alone defines the phase characteristics of the considered model for $H_{p_t}(s)$: no further lag or lead equalization dynamics are considered in the model for the pilot feedforward response given by Eq. (7.4). Over the different SRS conditions, Fig. 7.15(b) shows a clear decrease in τ_t with increasing roll motion fidelity, on average showing feedforward delays of around 0.4 s in the presence of high-fidelity roll motion cueing (SR4) and extremely high values of around 1.3 s for the no-motion condition SR0. The comparatively high values of the feedforward response delay presented in Fig. 7.15(b), which are all higher than the values of around 0.3 reported for the ramp-tracking tasks analyzed in Chapter 3, are the result of the fact that in the model used for $H_{p_t}(s)$ all phase shifts in the feedforward response are attributed to τ_t . Despite this modeling insufficiency, the trend in τ_t over the different SRS conditions visible in Fig. 7.15(b) still indicates that, on average, the experiment participants achieved a ramp-tracking response with reducing phase lag with increasing simulator roll motion fidelity. For the in-flight ramp-tracking tasks (condition CIT), however, the estimated feedforward delay parameters show clearly increased values compared to those measured for the conditions with high and medium-fidelity roll motion in the SRS, with values of τ_t that are almost as high as those observed for SR0. This indicates that for the in-flight ramp-tracking tasks there was a comparatively large delay in the response to a ramp target input, which is consistent with the increased σ_e^2 observed for the CIT condition in Fig. 7.10. The overall variation in τ_t over the six experimental conditions was found to be statistically significant: $F(5, 30) = 6.87, p < 0.05$. Pairwise comparisons indicate that the most significant differences between individual experimental conditions are observed for the conditions performed with motion feedback in the SRS (SR1-SR4) and the SR0 and CIT conditions.

Fig. 7.16 shows the estimated values of the parameters of the pilot error and motion response models included in the model proposed for describing multimodal ramp-tracking behavior in Section 7.2.4. Again, note that this part of the proposed pilot model is identical to the multimodal pilot model considered in Chapter 6 for modeling pilot tracking behavior in a compensatory roll tracking task with physical roll motion feedback and two multisine forcing functions. As explained in Section 7.3.6, given the fact that the same disturbance forcing function was present in the ramp-tracking task as used for the experiment of Chapter 6, it was expected that the pilots would show similar adaptation of their compensatory control dynamics given by $H_{p_v}(s)$ and $H_{p_m}(s)$ as observed there.

The estimates of the two parameters that showed to be the most sensitive to changes in roll motion cueing in Chapter 6, the pilot visual gain K_v and the visual lead time constant T_L , are shown in Figures 7.16(a) and (b), respectively. For the SRS conditions, these figures show increasing values of K_v and decreasing values of T_L with increasing roll motion fidelity. Furthermore, the pilot visual gains and lead time constants obtained from the in-flight measurements are found to be highly similar to those observed for the high roll motion fidelity condition SR4. Similar to the conclusions drawn in Chapter 6, these effects on K_v and T_L are found to be highly statistically significant: $F(5, 30) = 10.68, p < 0.05$ and $F(5, 30) = 4.48, p < 0.05$, respectively. Note that the estimated values for both parameters – ranging from 0.2-0.35 for K_v and from around 0.2-0.37 for T_L – are nearly identical to those measured for the experiment described in Chapter 6. This indicates that pilots selected visual response dynamics ($H_{p_v}(s)$) for the ramp-tracking task considered in this chapter that

are equivalent to those adopted for purely compensatory tracking. Finally, also note from comparing the estimated visual lead time constants with the value of $1/\omega_\phi$ indicated in Fig. 7.16(b) that for the no-motion condition SR0 the pilots on average performed visual lead equalization to nearly fully compensate for the K/s^2 controlled element dynamics above ω_ϕ . Consistent with many previous investigations, for instance [Shirley and Young, 1968; Jex et al., 1978; Hosman, 1996; Van der Vaart, 1992; Zaal et al., 2009b], for the conditions with roll motion feedback the availability of physical roll motion information is found to allow for a reduction in T_L .

Fig. 7.16(c) presents the estimated values of the gain of the pilot motion response $H_{p_m}(s)$. For the SRS conditions, a slight reduction in K_m is observed when moving from the high-fidelity condition SR4 towards lower levels of simulator motion fidelity. Furthermore, the lowest values of K_m are observed for the in-flight CIT condition. For SR0 the estimates of K_m showed a distribution significantly different from normal (Kolmogorov-Smirnov test, $D(7) = 0.39$, $p < 0.05$). A Friedman's ANOVA indicated no significant differences in the pilot motion gain over the different experimental conditions, $\chi^2(4) = 8.34$, $p \geq 0.05$. Note from comparison with the data presented in Chapter 6 that also the estimated values of K_m presented in Fig. 7.16(c) match those observed for compensatory tracking without the ramp target signal very well.

Figures 7.16(d) and (e) show the estimated values of the pilot visual and motion response delays τ_v and τ_m . The visual delay is found to be around 0.2 s for all experimental conditions, with slightly higher averages of around 0.25 s for conditions SR3 and CIT. Note that especially this approximately 50 ms increase in τ_v observed for the CIT conditions is highly consistent with the results of Chapter 6. Due to markedly varying inter-subject differences over the six experimental conditions, Mauchly's Test indicated a violation of the sphericity assumption for the τ_v data presented in Fig. 7.16(d), $\chi^2(14) = 27.54$, $p < 0.05$. After applying the Greenhouse-Geisser sphericity correction, the pilot visual delay was not found to differ significantly over the considered experimental conditions, $F(2.0, 12.0) = 2.73$, $p \geq 0.05$. Mirroring the results obtained for the experiment of Chapter 6, Fig. 7.16(e) shows pilot model delays of around 0.15 s for the conditions with the highest level of roll motion fidelity (CIT included) and slightly elevated values under conditions with lower-fidelity roll motion cueing. This increase in τ_m with decreasing simulator roll motion fidelity is found to be a statistically significant effect, $F(4, 24) = 4.69$, $p < 0.05$.

Fig. 7.17 presents the estimated values of the two parameters of the neuromuscular actuation model defined by Eq. (7.8). Fig. 7.17(a) shows that the neuromuscular frequency ω_{nm} is found to be approximately constant for all SRS conditions at slightly above 9 rad/s. Slightly lower values of ω_{nm} are obtained for the in-flight ramp-tracking tasks (CIT), but the drop in ω_{nm} is not as sharp as observed for the purely compensatory in-flight roll tracking task considered in Chapter 6. Overall, no significant variation in the neuromuscular frequency is observed over the different experimental conditions, $F(5, 30) = 1.20$, $p \geq 0.05$.

Chapter 6 reported slightly increased values of the neuromuscular damping ratio ζ_{nm} for the conditions with a unity roll motion gain, an effect which was, however, not found to be statistically significant. Fig. 7.17(b) shows that a similar increase in ζ_{nm} is observed here for condition SR3 and SR4, indicating slightly better damped neuromuscular actuation dynamics for these conditions. As is clear from Fig. 7.17(b), the distribution of measured values for ζ_{nm} differs significantly from a normal distribution for all conditions due to the

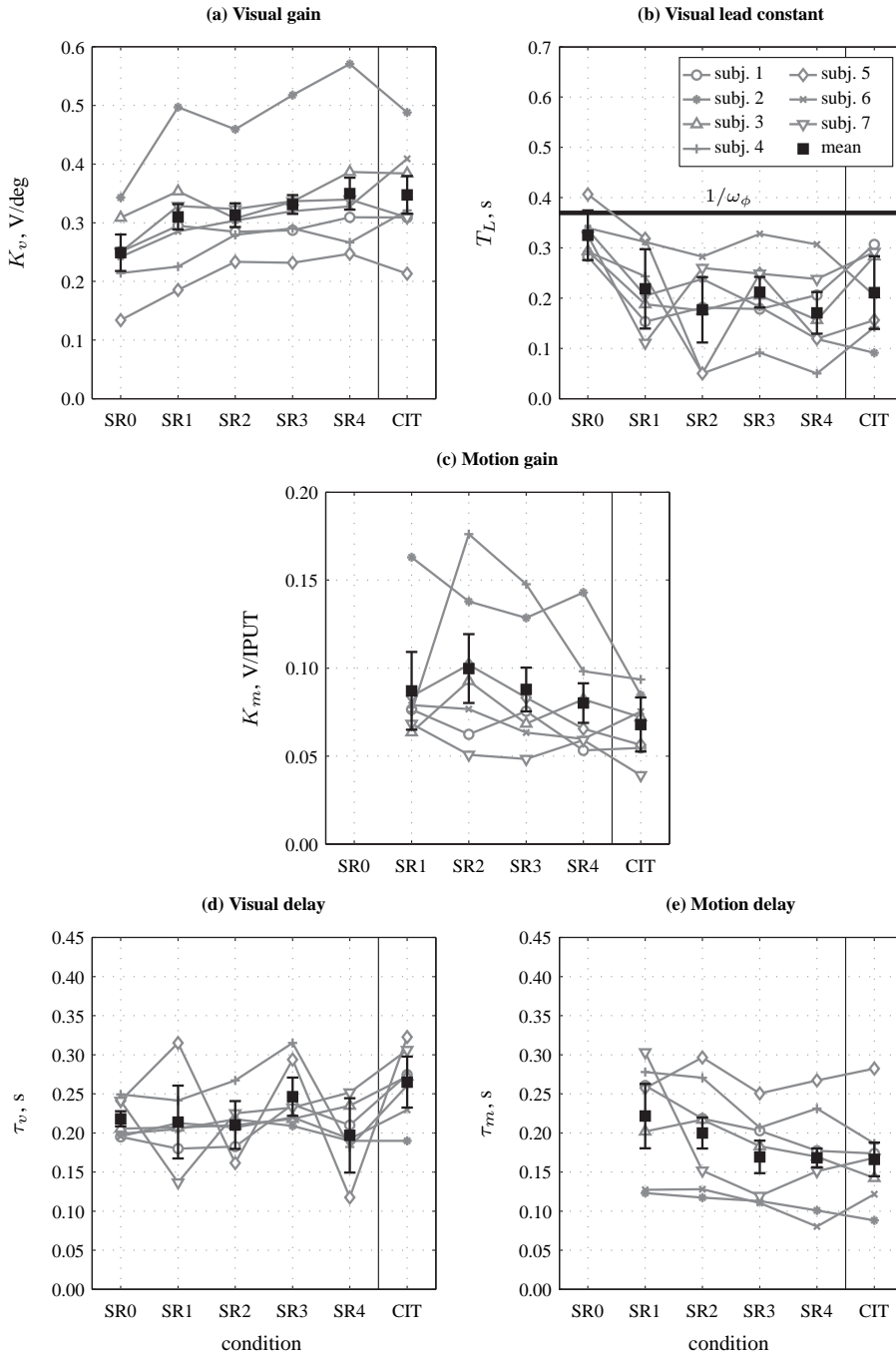


Figure 7.16. Mean estimated error and motion response model parameters.

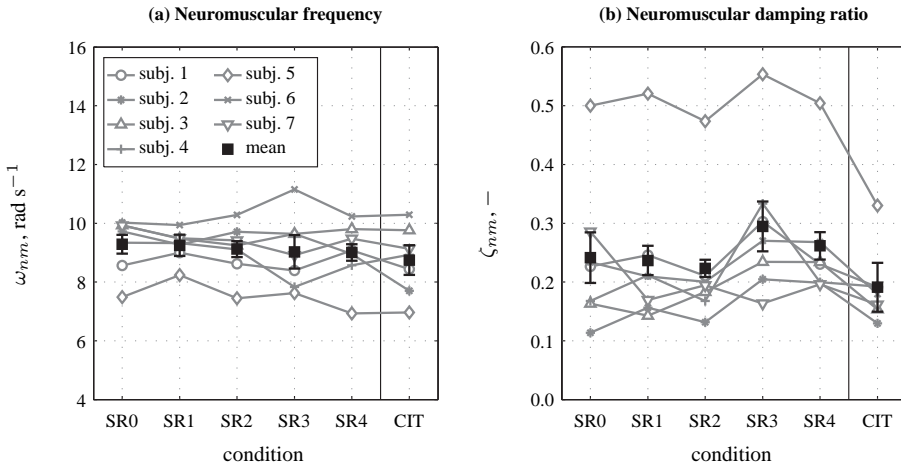


Figure 7.17. Mean estimated neuromuscular actuation model parameters.

comparatively high values measured for subject 5. A nonparametric Friedman ANOVA indicates a significant variation over the different conditions $\chi^2(5) = 19.00, p < 0.05$. Pairwise comparisons (Wilcoxon signed-rank tests) confirm that the most significant differences between individual conditions result from the consistently higher values for ζ_{nm} found for the conditions with unity roll motion cueing gain in the SRS (SR3 and SR4).

7.5 Discussion

This chapter evaluated the effects of varying roll motion settings on pilot control behavior in roll tracking task with quasi-random multisine disturbance and target forcing functions and a superimposed ramp target forcing function that commanded a number of 10 deg changes in roll attitude. For this evaluation, measurements of control behavior were collected in the SIMONA Research Simulator (SRS) and in real flight using TU Delft’s Cessna Citation II laboratory aircraft. Five different roll motion cueing settings were evaluated in the simulator part of the experiment, including a no-motion condition. The remaining four conditions consisted of a factorial variation in the gain (values of 0.5 and 1) and break frequency (values of 0.5 and 1 rad/s) for the first-order roll motion filter that was used for washing-out the simulator roll motion and thereby limiting the perceivable lateral specific forces due to simulator roll tilt.

For quantifying possible changes in pilot control behavior due to variations in roll motion cueing a three-channel model of pilot control behavior was proposed for the considered multimodal ramp-tracking task. Compared to the models of compensatory tracking behavior applied in earlier research that measured the effects of differences in simulator motion fidelity for tracking tasks with only quasi-random multisine forcing function signals, this proposed model for ramp-tracking behavior included an additional feedforward response channel that accounted for pilot feedforward operations on the deterministic ramp target

signal. In Chapter 3 strong evidence of such a feedforward response was found for single-loop (no motion feedback) ramp-tracking tasks. The data from the experiment described in this chapter suggest that this is also the case for ramp-tracking tasks performed with motion feedback, as a pilot model that did not include the proposed feedforward response was found to explain markedly less of the measured pilot control inputs.

For the pilot feedforward response a model was proposed that provided a response proportional to that of the inverse of the controlled element dynamics, scaled by the pilot feedforward gain K_t and delayed by the pilot feedforward delay τ_t . No further equalization dynamics, such as the feedforward lag term considered in Chapter 3, were included in the proposed model for the feedforward response. The values of the feedforward time delay parameter obtained from fitting the final proposed model to measured data were found to be comparatively large, reaching values of higher than 1.0 s for the SR0 and CIT conditions. Given the lack of further assumed dynamics in the feedforward response model, the phase characteristics of this model are only affected by variations in τ_t so that all further lags incurred in the pilot feedforward response are attributed to this delay parameter in the proposed model. The high estimated values of τ_t suggest that extension of the proposed feedforward response model, for instance with further equalization dynamics as also considered in Chapter 3, is in fact required. Addressing this extended modeling of the pilot feedforward response for the ramp-tracking task considered in this chapter is heavily recommended for future work.

Analysis of the adopted control strategy for the different experimental conditions performed in the SRS using the proposed multimodal model of pilot ramp-tracking behavior showed highly similar pilot adaptation as observed for the roll tracking task with only quasi-random multisine forcing function signals considered in Chapter 6. Increasing the roll motion filter break frequency and reducing the roll motion gain was found to result in a decreased gain of pilots' response to visually presented tracking errors and an increase in the amount of visual lead equalization that was performed. As can be verified from Chapter 5, both these effects are highly typical for tracking with reduced fidelity of the supplied physical motion feedback. The reason for this equivalence of the observed behavioral variation for the ramp-tracking task considered in this chapter with these previous measurements is a result of the fact that, in addition to the ramp target signal, also multisine target and disturbance signals were still present in this task. The presence of these two quasi-random forcing function signals ensured pilots still needed to exhibit largely the same compensatory control behavior as adopted for the multisine tracking task of Chapter 6.

The estimated pilot model parameters that characterize the pilot feedforward control dynamics in the proposed model, the pilot feedforward gain and time delay, showed significant differences in the pilot feedforward response over the different experimental conditions, in addition to the observed variation in the compensatory behavioral component. The gain of the feedforward response was found to remain approximately constant for all experimental conditions (including the in-flight ramp-tracking tasks). For the feedforward time delay, however, significantly higher values were observed for the experimental conditions with reduced motion fidelity compared to the considered high-fidelity roll motion condition. This increased response delay suggests a more sluggish and less optimal pilot feedforward response under conditions of reduced motion fidelity. Consistent with this increased feedfor-

ward response delay, the tracking error variance was also found to be largest for conditions with the highest feedforward delays, indicating reduced tracking performance.

The control behavior measured for the in-flight ramp-tracking tasks was found to match the simulator measurements reasonably well. Tracking performance, however, was found to be poorer for the in-flight ramp-tracking tasks than observed for all conditions with motion feedback performed in the SRS and, in fact, found to be almost equal to the level of tracking performance attained for the no-motion SRS condition. Comparatively high pilot feedforward and visual response delays were observed for the in-flight ramp-tracking tasks, in addition to slightly reduced pilot motion response gains, which can explain this degraded tracking performance. Despite the fact that some disagreement was present between the opinions of the different pilots that performed the experiment, subjective motion fidelity ratings indicated that, on average, the pilots indicated that the considered high-fidelity roll motion condition (unity gain and 0.5 rad/s break frequency) yielded simulator motion closest to that perceived in real flight. Except for the three parameters listed above, the remaining estimated pilot model parameters also showed comparatively small differences between this high-fidelity SRS condition and the in-flight measurements. For this reason, this condition is concluded to yield the best simulator motion fidelity, from an objective behavioral analysis perspective, for the ramp-tracking task considered in this chapter.

The variation in motion cueing settings evaluated in the simulator part of the experiment described in this chapter considered of different sets filter gain and break frequencies for a first-order high-pass roll washout filter. Using only simulator roll motion, the motion filter setting that most closely replicated the aircraft roll and translational motion was sought. This chosen implementation of the motion cueing for a coordinated maneuver as induced by the used ramp forcing function signal, which relies on the high-pass roll motion filter for ensuring zero lateral specific forces by washing-out the simulator roll motion, is the most simple method for replicating the aircraft motion typical for such maneuvers on a moving-base flight simulator. Extensive research has led to more advanced motion cueing implementations that have been proposed for such coordinated lateral maneuvers [Schmidt and Conrad, 1970; Ariel and Sivan, 1984; Reid and Nahon, 1985; Telban et al., 2005a; Chung et al., 1998; Mikula et al., 1999]. Further research into the effects of simulator motion cueing settings on pilot control behavior in maneuvering tasks similar to the one analyzed in this chapter should therefore focus on the evaluation of these proposed methods for achieving satisfactory motion cueing for coordinated rotational and translational motion cues.

This chapter briefly evaluated a method for evaluating changes in pilot control behavior during discrete maneuvering tasks proposed by Heffley [1982]. This method, with which the executed discrete maneuvers are evaluated using their phase-plane representation, has shown its merit for pointing out differences in the way some fixed-wing and rotorcraft discrete maneuvering tasks were performed under varying experimental conditions in a number of earlier investigations [Heffley, 1982; Ferguson et al., 1984; Schroeder, 1999; Ellerbroek et al., 2008]. For the ramp-tracking task considered in this chapter, however, the presence of the quasi-random forcing function signals was found to render analysis of ramp-tracking behavior using the maneuvers' phase-plane representation impossible because of the considerable distortion of the phase-plane profiles due to these additional forcing function signals. Given that the analysis of pilot control behavior with the proposed multimodal

ramp-tracking pilot model suggested differences in the control behavior adopted during ramp-tracking under variations in roll motion cueing, analysis of the execution of the ramp-tracking portion of this control task with the method proposed by Heffley [1982] is still expected to provide additional insight. This could, for instance, be tested with further ramp-tracking experiments with varying physical motion feedback settings with no further, or much smaller, quasi-random forcing function signals.

7.6 Conclusions

This chapter described the results of an experiment that was performed to evaluate the effects of varying levels of simulator motion fidelity on pilot control behavior in a combined roll attitude ramp-tracking and disturbance-rejection task. Control behavioral measurements for this task were collected from seven experienced pilots both in real flight, using a Cessna Citation II laboratory aircraft, and for five different settings of a first-order high-pass roll washout filter in a moving-base flight simulator. Changes in pilot control behavior due to variations in the level of simulator motion fidelity were analyzed through the fitting of a multimodal pilot model that included an additional feedforward response for modeling ramp-tracking behavior. This explicit quantification of changes in control behavior showed largely the same effects of degrading motion fidelity as observed for tracking tasks with only quasi-random forcing function signals, most notably a decrease in the gain with which pilots respond to visually presented tracking errors and an increase in visual lead equalization. The fitted feedforward response parameters further indicated increased latency in the pilot ramp-tracking control inputs with decreasing motion fidelity levels. Overall, control behavior for a high-fidelity roll motion condition, with a unity gain and a break frequency of 0.5 rad/s for the first-order roll washout filter, was found to be closest to that measured in real flight. Subjective motion fidelity ratings collected for the ramp-tracking tasks performed in the flight simulator also showed that the pilots, on average, indicated that this condition provided simulator motion cues that were closest to those available in real flight. Still, compared to the behavioral measurements for this high-fidelity roll motion cueing setting, degraded tracking performance and a significant increase in the feedforward ramp-tracking response delay were observed for the ramp-tracking tasks performed in real flight.

8

Roll Motion Filter Settings and Multisine-Tracking Behavior

Chapter 6 presented the results of a comparison between pilot roll tracking behavior measured in real flight in TU Delft's Cessna Citation II laboratory aircraft and measurements taken for varying roll motion cueing conditions in the SIMONA Research Simulator (SRS). In the simulator part of the experiment described in Chapter 6 only a limited number of four different roll motion cueing settings could be evaluated, which also limited the conclusions that could be drawn with respect to recommendations for selecting motion filter parameters based on these behavioral measurements. This chapter therefore describes an additional experiment that was performed in the SRS, which featured the same roll tracking task considered in Chapter 6 with a much larger number of evaluated roll motion cueing settings. The four conditions of the experiment of Chapter 6 were repeated in the experiment described in this chapter. An explicit side-by-side comparison of the results from both experiments for these overlapping conditions is not included in this chapter, but can be found in Appendix I.

The contents of this chapter are to be published as:

Pool, D. M., Damveld, H. J., Van Paassen, M. M., and Mulder, "Effects of Motion Filter Gain and Break Frequency Variations on Pilot Roll Tracking Behavior", *Journal of Guidance, Control, and Dynamics*.

8.1 Introduction

Flight simulator motion excursions are typically limited by applying high-pass washout filters to the simulated aircraft motion. Reducing the washout filter gain and increasing the filter break frequency typically lead to larger discrepancies between the true aircraft motion and the motion cued in the simulator, which can result in reduced motion fidelity. With the severely limited motion envelopes available in most current moving-base flight simulators, the selection of washout filter parameter settings typically involves a trade-off between retaining a sufficiently high motion gain, while limiting the phase distortion induced by the washout filter. This trade-off is also reflected in the commonly applied motion fidelity criteria proposed by Sinacori [1977] and Schroeder [1999], which define levels of simulator motion fidelity in terms of the gain and phase distortion induced by the high-pass motion filter at 1 rad/s.

However, selecting a proper combination of filter gain and break frequency is still a problem for which no all-purpose solution or even a structured and well-motivated approach is available. One of the main reasons for this is our limited understanding of human motion perception processes that play a role in simulator cueing. In this chapter, an attempt is made to tackle the problem of motion filter parameter selection from a behavioral standpoint, by focusing on the effect of washout filter settings on skill-based pilot manual control behavior. Pilot tracking behavior is known to be highly adaptable to a large number of factors internal and external to the pilot [McRuer and Jex, 1967a]. Here, it is attempted to exploit this adaptability by measuring pilot dynamics during tracking in order to reveal for which motion filter gain and break frequency settings pilots adapt their control strategy. Despite the fact that such an approach can be applied to, and likely results in different results for, all degrees of freedom that need to be considered in flight simulation, this chapter focuses on pilot tracking behavior in roll tracking tasks with physical roll motion feedback.

A number of previous studies have considered and measured pilot tracking behavior in a roll tracking task under a variation in motion cueing settings to this same end, [Jex et al., 1978; Van Gool, 1978; Stapleford et al., 1969; Ringland and Stapleford, 1971] and Chapter 6. However, none of these studies have considered a true factorial variation in washout gain and break frequency, thereby precluding the drawing of conclusions that are of interest to simulator motion cueing. Furthermore, with the exception of the experiment described in Chapter 6, none of these investigations made use of measurements of pilot tracking behavior collected in real flight to compare the measured effects of motion filter variations in a flight simulator against.

The objective of this chapter is to evaluate, and explicitly compare, the effects of independently varying motion filter gain and break frequency settings on pilot tracking behavior. To achieve this, an experiment is described in which pilot tracking behavior is measured for a factorial variation in roll motion filter gain and break frequency settings. Three settings for both motion filter parameters are evaluated in the experiment, in addition to a reference no-motion (single-loop tracking) condition, yielding a total number of ten roll motion filter settings that range from high to low motion fidelity according to the criteria proposed by Sinacori [1977] and Schroeder [1999]. From this experiment data conclusions will be drawn as to where, from a behavioral point of view, the focus of washout filter tuning should

be: on minimizing gain distortion, the impact of washout filtering on the supplied simulator motion cues, or both.

For this evaluation of behavioral simulator motion fidelity the same compensatory roll tracking task with Cessna Citation II roll dynamics as investigated in Chapter 6 is considered, for a number of reasons. First, in the experiment of Chapter 6 a combined target-following and disturbance-rejection task with two quasi-random multisine forcing function signals was considered, as such a task allows for analysis of pilot tracking behavior using estimated frequency-domain describing functions [Stapleford et al., 1967] and fitted multimodal pilot model parameters [Zaal et al., 2009a]. These methods yield objective measurements that give insight into whether, and how, pilot tracking behavior is affected by certain changes in motion filter settings. Second, the motion profiles resulting from the combined target-following and disturbance-rejection task can be presented one-to-one on the simulator, thereby allowing for collecting behavioral measurements for a true reference condition with one-to-one roll motion cues as is very desirable for such human-in-the-loop measurements [Schroeder and Grant, 2010]. Finally, as the same Cessna Citation II pilots who also performed the experiment of Chapter 6 were to perform the current experiment, this allows for a straightforward comparison of the current flight simulator measurements with the in-flight measurements of roll tracking behavior described in Chapter 6.

This chapter is structured as follows. First, some background information on the combined target-following and disturbance-rejection task that is considered for evaluating the effects of motion filter gain and break frequency variations on pilot tracking behavior is provided in Section 8.2. This section also describes the multimodal pilot model used for quantifying changes in pilot tracking behavior, and gives a summary of some of the previously developed methods for predicting changes in pilot control behavior due to changes in washout settings. Section 8.3 describes the setup of the experiment that was performed to measure pilot tracking behavior for ten different roll motion cueing settings in a moving-base flight simulator. The experimental results are presented in Section 8.4, where the current findings are also compared to previously proposed offline prediction analysis results (see Chapters 5 and 6) and the in-flight roll tracking results reported in Chapter 6. The chapter ends with a discussion and conclusions.

8.2 Background

8.2.1 Roll Tracking Task

Fig. 8.1 shows a schematic representation of the compensatory aircraft roll tracking task considered in this chapter. It is a combined target-following and disturbance-rejection task, where the target and disturbance forcing functions – f_t and f_d , respectively – are independent quasi-random multisine signals to allow for measurement of two describing functions using spectral methods [Stapleford et al., 1967]. The pilot's task is to minimize the tracking error e , which is continuously induced by the target and disturbance forcing function signals. The pilot is shown to provide control inputs u to the controlled element dynamics based on visually presented tracking error information (e) and feedback of the controlled element roll acceleration ($\ddot{\phi}$) through the simulator motion system. The measurements of pilot tracking

behavior for the control task shown in Fig. 8.1 described in this chapter are collected using the SIMONA Research Simulator (SRS) at Delft University of Technology. For the SRS, the visual and motion cueing dynamics – indicated with the $H_{s_v}(s)$ and $H_{s_m}(s)$ blocks in Fig. 8.1 – are modeled as pure delays of 25 and 30 ms, respectively [Stroosma et al., 2007; Berkouwer et al., 2005].

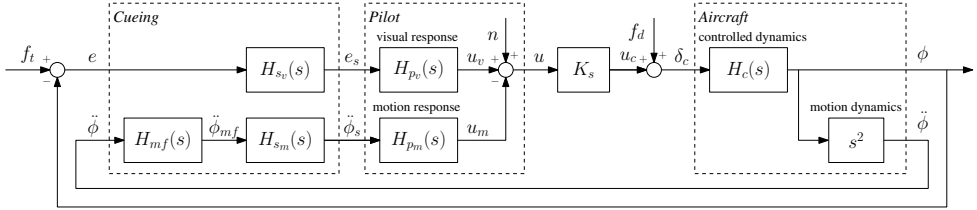


Figure 8.1. Schematic representation of a compensatory roll attitude tracking task with motion feedback.

As can be verified from Fig. 8.1, the dynamics of a roll motion filter that transforms the aircraft model roll accelerations $\ddot{\phi}$ into the roll accelerations that are cued in the simulator $\ddot{\phi}_{mf}$ are also included in the motion cueing dynamics. In this chapter, a first-order high-pass roll washout filter, which is often applied for cueing rotational degrees-of-freedom in moving-base flight simulators [Schmidt and Conrad, 1970; Sinacori, 1973; Grant and Reid, 1997a; Hagiwara et al., 2008], is considered:

$$H_{mf}(s) = \frac{s^2 \phi_{mf}(s)}{s^2 \phi(s)} = K_{mf} \frac{s}{s + \omega_{mf}} \quad (8.1)$$

Eq. (8.1) also shows the two parameters that need to be set for this first-order washout filter: the filter gain K_{mf} and the filter break frequency ω_{mf} . The filter gain K_{mf} can be used to apply a frequency-independent scaling to the aircraft roll accelerations. The break frequency ω_{mf} controls the washout dynamics: it defines the amount of low-frequency gain attenuation and the low-frequency phase distortion induced by $H_{mf}(s)$.

The controlled element dynamics $H_c(s)$ in the roll tracking task analyzed in this chapter are a linear approximation of the nonlinear model of the combined fly-by-wire control system and Cessna Citation II roll dynamics used for the experiment of Chapter 6. The details of these linearized roll dynamics will be provided in Section 8.3.2. Finally, K_s indicates the control input gain, which is equal to 0.3 for the roll tracking task considered in this chapter.

8.2.2 Modeling Multimodal Pilot Tracking Behavior

Pilot tracking behavior in combined target-following and disturbance-rejection tasks with physical motion feedback as considered in this chapter has been shown to be successfully modeled with the two-channel model structure depicted in Fig. 8.1 [Stapleford et al., 1969]. Pilot tracking behavior is modeled as two parallel linear responses, one to visually presented tracking errors and another to roll acceleration cues received through physical motion stimulation, indicated with the symbols $H_{p_v}(s)$ and $H_{p_m}(s)$ in Fig. 8.1, respectively. In addition, a remnant signal n , which accounts for all nonlinear contributions to the pilot control signal

u [McRuer and Jex, 1967a], completes this quasi-linear model of multimodal pilot tracking behavior.

A more detailed representation of the multimodal pilot model considered in this chapter is shown in Fig. 8.2. As can be verified from Fig. 8.2, the pilot visual response $H_{pv}(s)$ is modeled with a gain-lead equalization characteristic, a pure time delay τ_v , and a model for the neuromuscular actuation and manipulator dynamics $H_{nm}(s)$. This model is based on the models for single-loop compensatory tracking behavior proposed by McRuer et al. [1965]. The equalization transfer function $K_v(1 + T_L s)$ allows for capturing the lead equalization that is adopted by pilots to achieve desired open-loop characteristics around the crossover frequency for controlled elements that are approximately K/s^2 at frequencies sufficiently close to the crossover region [McRuer et al., 1965]. As will be shown in Section 8.3.2, this is also the case for the controlled element considered in this chapter.

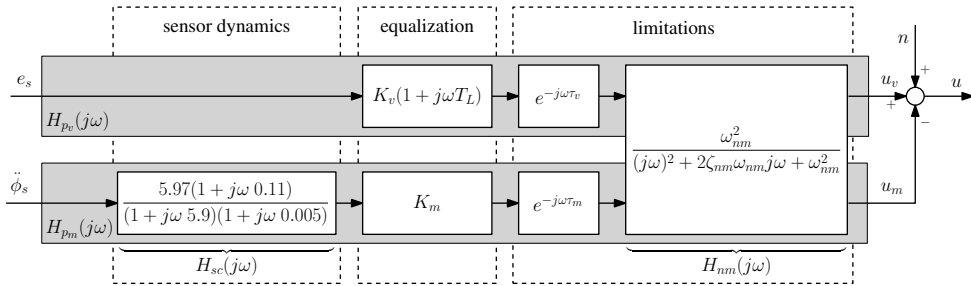


Figure 8.2. The multimodal pilot model used for modeling pilot control of aircraft roll attitude.

As proposed by Hosman [1996] and Van der Vaart [1992] – and as successfully applied in many later investigations into multimodal pilot tracking behavior, for instance [Zaal et al., 2009b,c, 2010] and Chapters 4 and 6 – pilots’ responses to rotational roll motion feedback are modeled as a response proportional to the perceived roll motion, that is, the output of the semicircular canals of the vestibular system. Despite the fact that it is known that other sensory systems, such as the proprioceptive and somatosensory systems, are also available for physical motion perception, physiological research has suggested that the vestibular system is the dominant sensor for physical motion stimulation [Benson, 1990]. Furthermore, as shown in detail in Chapter 4, measured describing functions for pilots’ physical motion responses have been shown to be modeled accurately with a model that only considers the vestibular response. Similar to the model for the pilot visual response, the model of $H_{pm}(s)$ used here accounts for a time delay in the response to the roll motion cues and for the neuromuscular actuation dynamics $H_{nm}(s)$. The model for the semicircular canal dynamics $H_{sc}(s)$, which relates the input simulator roll accelerations $\ddot{\phi}_s$ to an afferent neuron firing rate with unit impulses per unit of time (IPUT), is the same as that used in Chapters 6 and 7. The parameters of this model of the semicircular canal dynamics, which are taken from previous research [Hosman, 1996; Groen et al., 2006], are assumed to be constants of the multimodal pilot model.

In total, the pilot model shown in Fig. 8.2 has seven free parameters that characterize pilot tracking behavior under certain conditions: the pilot visual gain K_v , the visual lead time-constant T_L , the pilot motion gain K_m , the pilot visual and motion delays τ_v and τ_m ,

and the neuromuscular actuation model's natural frequency ω_{nm} and damping ratio ζ_{nm} . For direct correspondence with the experiment described in Chapter 6, where the control signal u was defined as the output voltage of the sidestick manipulator that formed the input to the Cessna Citation II laboratory aircraft fly-by-wire control system, the control signal in the current experiment is also defined in Volt (V). Note that because of this convention, the pilot visual and motion gains have the units V/deg and V/IPUT, respectively. The multimodal pilot model shown in Fig. 8.2 is used here to objectively quantify changes in pilot tracking behavior that may result from changes in the motion filter dynamics $H_{mf}(s)$, by estimating its seven parameters based on time-domain measurements of e , $\dot{\phi}_{mf}$, and u [Zaal et al., 2009a].

8.2.3 Previously Reported Behavioral Effects of Roll Washout

A number of previous studies have explicitly investigated the effects of different roll washout settings on compensatory tracking behavior for tracking tasks highly similar to the one studied in this chapter (see Section 8.2.1). As described in Chapter 5, even more studies provide relevant measurements of the effects of variations in motion cueing settings on pilot tracking behavior, however, only investigations that considered roll tracking and variations in roll motion cueing are summarized here.

First, Stapleford et al. [1969] and Ringland and Stapleford [1971] describe the results of the same experiment that considered pilot roll tracking behavior under variations in controlled element dynamics, roll and coordinated sway washout settings. Furthermore, they also varied the presence of an additional multisine target forcing function, in addition to the disturbance signal that was present in all experimental conditions. The tested roll washout filters were first-order high-pass filters with unity gain. Three different filter break frequencies were evaluated: 0.5, 1, and 2 rad/s. Even though measurements to evaluate the effects of roll washout were only collected with three pilots (describing function data for only one), Stapleford et al. [1969] and Ringland and Stapleford [1971] report a slight reduction in pilot gain and crossover frequency for the highest break frequency setting (2 rad/s). In addition, degraded tracking performance was observed for two of the three subjects for the conditions with break frequencies of 1 rad/s and higher. Without further elaboration, Stapleford et al. [1969] indicate that the presence of a washout filter might not always degrade tracking performance by stating that with increasing the motion filter break frequency “*the amplitude of the roll response at the lower frequencies is decreased and the phase lead is increased. The reduced amplitude should degrade the pilot's use of this cue but the increased lead is helpful.*”

Jex et al. [1978] considered a combined target-following and disturbance-rejection task much like the one studied here, where the controlled element dynamics were those of a typical (loaded) fighter aircraft. The participants in this experiment were not experienced pilots, but a later experiment performed with pilot subjects [Jex et al., 1979] showed no differences between the results obtained for both groups of subjects, except for the reduced training required for the pilot group. A wide variety of different roll motion cueing conditions was considered, ranging from conditions with one-to-one roll motion and one with pure gain attenuation to conditions with first- and second-order washouts. Compared to the conditions with one-to-one or scaled roll motion (no washout), tracking performance was

found to be worse when roll washout was present. Analysis of measured pilot describing functions showed that the most notable effect of roll washout was observed for the target open-loop describing function, where the presence of a washout filter was found to cause a clear increase in low-frequency gain and phase lag. Based on the presented comparison of subjective ratings and behavioral tracking measurements, the condition with the first-order washout combined with gain attenuation was concluded to be the best washout configuration for a roll-only flight simulator. As suggested roll washout parameters to use for this case Jex et al. [1978] propose to use a motion filter gain between 0.5 and 0.7 and first-order break frequency between 0.3 and 0.5 rad/s.

Van Gool [1978] evaluated the effects of different motion filter break frequency settings for both pitch and roll tracking tasks with a DC9-10 aircraft model (landing configuration, 120 kts). The evaluated pitch and roll washouts were second-order high-pass filters with unity gain and damping ratio, for which the filter break frequency was varied from 0.1, 0.25, 0.5 to ∞ (fixed base) rad/s. Due to the use of only a disturbance forcing function in this experiment only a single (lumped) pilot describing function could be determined for evaluation of the effects of the washout variation on pilot tracking behavior. Pilot describing functions showed no differences for filter break frequencies ranging from 0.1 to 0.5 rad/s, however, compared to the fixed-base results all conditions with roll motion feedback showed increased low-frequency gain and crossover frequencies and reduced high-frequency phase lag. As also no differences in tracking performance and subjective pilot ratings were observed between the three conditions with break frequencies ranging from 0.1 to 0.5 rad/s, it was concluded that pilot tracking behavior in the considered disturbance-rejection tasks is negligibly influenced by variations in the filter break frequency.

Finally, Chapter 6 describes an experiment in which pilot tracking behavior was measured for the same combined target-following and disturbance-rejection task with a Cessna Citation II controlled element as considered in this chapter. Pilot tracking behavior for four different roll motion cueing conditions is compared in Chapter 6: a fixed-base and a one-to-one roll motion condition, supplemented with two conditions with a first-order roll washout filter with a break frequency of 0.5 rad/s and filter gain settings of 1 and 0.5. Subjective motion fidelity ratings, measured tracking performance, and the estimated parameters of the same pilot model introduced in Section 8.2.2 all indicate no significant differences between the conditions with one-to-one roll motion and the unity-gain filter with a 0.5 rad/s break frequency. Note that these results are consistent with the findings of Jex et al. [1978] and Van Gool [1978], who also report no significant effects on pilot tracking behavior for filters with break frequencies of 0.5 rad/s or lower. The experiment of Chapter 6, however, does show a change in pilot tracking behavior and performance towards those measured for the fixed-base configuration for the condition where the roll motion filter gain was equal to 0.5. Using multimodal pilot model analysis, it was shown that this effect of degrading roll motion fidelity was mainly visible from decreased pilot visual response gains and increased visual lead equalization. These results suggest that the filter gains between 0.5 and 0.7 as proposed by Jex et al. [1978] could still result in a significant adaptation of pilot tracking behavior in some cases.

8.2.4 Offline Prediction and Analysis of Washout Effects

Earlier work has provided some useful tools to aid in the analysis of the effects of variations in washout filter parameters on pilot tracking behavior performed in this chapter. First, in Chapter 6 a method is described that allows for assessing the effect of changes in pilot tracking behavior on the crossover frequencies and phase margins of the disturbance and target open-loop responses, by separating it from the effect of the applied variation in the washout dynamics itself on these parameters. In addition, Chapter 5 provides some equations that can be used to predict changes in pilot behavioral parameters, and open-loop system crossover frequencies and phase margins, based on a compilation of the measured results of a number of previous experiments. Both these methods will be concisely described in the following, and their results will be compared to the current experimental measurements in Section 8.4.

8.2.4.1 No Pilot-Adaptation Analysis

For a combined target-following and disturbance-rejection task as depicted in Fig. 8.1, two open-loop responses can be evaluated to assess the closed-loop system's performance and stability in the attenuation of the disturbance forcing function f_d and in the following of a reference signal f_t [Jex et al., 1978]. From Fig. 8.1 the following equations can be derived for these disturbance and target open-loop responses:

$$\begin{aligned} H_{ol,d}(s) &= -\frac{U_c(s)}{\delta_c(s)} \\ &= [H_{s_v}(s)H_{p_v}(s) + H_{\dot{y},x}(s)H_{m_f}(s)H_{s_m}(s)H_{p_m}(s)] K_s H_c(s) \end{aligned} \quad (8.2)$$

$$H_{ol,t}(s) = \frac{X(s)}{E(s)} = \frac{H_{s_v}(s)H_{p_v}(s)K_s H_c(s)}{1 + H_{\dot{y},x}(s)H_{m_f}(s)H_{s_m}(s)H_{p_m}(s)K_s H_c(s)} \quad (8.3)$$

As can be verified from Equations (8.2) and (8.3), the disturbance and target open-loop transfer functions $H_{ol,d}(s)$ and $H_{ol,t}(s)$, and hence the crossover frequencies and phase margins derived from them, are affected by both changes in the pilot responses $H_{p_v}(s)$ and $H_{p_m}(s)$, and the dynamics of the washout filter $H_{m_f}(s)$. This implies that observed changes in the disturbance and target open-loop crossover frequencies ($\omega_{c,d}$ and $\omega_{c,t}$) and phase margins ($\varphi_{m,d}$ and $\varphi_{m,t}$) do not directly reflect changes in pilot control behavior, but can also be caused by differences in $H_{m_f}(s)$ directly.

To assess this problem, a method was proposed and applied in Chapter 6 that evaluated the change in the crossover frequencies and phase margins that would result from only varying the dynamics of $H_{m_f}(s)$, that is, assuming no adaptation of the pilot dynamics to compensate for to this variation in washout dynamics. With knowledge of baseline pilot tracking behavior ($H_{p_v}(s)$ and $H_{p_m}(s)$) for the case where physical motion cues are presented one-to-one, evaluating Equations (8.2) and (8.3) for both this one-to-one case ($H_{m_f}(s) = 1$) and for a certain washout setting $H_{m_f}(s)$ allows for quantification of the direct effect of the washout filter dynamics on $\omega_{c,d}$, $\omega_{c,t}$, $\varphi_{m,d}$, and $\varphi_{m,t}$.

The required settings of $H_{p_v}(s)$ and $H_{p_m}(s)$ that are representative for the case where $H_{m_f}(s) = 1$ were taken from a previous experiment, described by Zaal et al. [2010], for

the analysis performed in Chapter 6. Here, due to the similarity between both experiments, the choice is made to use the measurements for the one-to-one roll motion condition from the experiment described in Chapter 6 instead. The pilot model parameters and the derived measures for both these reference settings are listed in Table 8.1. As can be verified from Table 8.1, the difference between the reference parameters that were used in Chapter 6 and those used here is comparatively minor.

Table 8.1. Offline analysis parameters and derived measures.

Analysis parameters				Derived measures			
Symbol	Unit	Value		Symbol	Unit	Value	
		Ch. 6	Current			Ch. 6	Current
K_v	V/deg	0.37	0.37	$\omega_{c,d}$	rad/s	2.61	2.90
T_L	s	0.22	0.23	$\omega_{c,t}$	rad/s	1.52	1.46
K_m	V/INPUT	0.087	0.092	$\varphi_{m,d}$	deg	53.51	54.36
τ_v	s	0.27	0.23	$\varphi_{m,t}$	deg	64.93	71.13
τ_m	s	0.13	0.14	σ_e^2	deg ²	0.27	0.25
ω_{nm}	rad/s	9.59	10.06	$\sigma_{e,d}^2$	deg ²	0.11	0.099
ζ_{nm}	—	0.19	0.21	$\sigma_{e,t}^2$	deg ²	0.16	0.15
				σ_y^2	V ²	0.062	0.081
K_{mf}	—	1.0	1.0	$\sigma_{y,d}^2$	V ²	0.037	0.057
ω_{mf}	rad/s	0.0	0.0	$\sigma_{u,t}^2$	V ²	0.025	0.024

8.2.4.2 Prediction of Washout Effects on Pilot Tracking

In Chapter 5 data from a number of experiments that measured pilot tracking behavior under different motion cueing conditions was used to formulate linear prediction equations that can be used to assess changes in selected behavioral parameters based on knowledge of the washout filter settings. The most suitable predictor variable was found to be the motion filter gain distortion at 1 rad/s – in this chapter indicated with the symbol K_S – as also used as the evaluation frequency in the motion fidelity criteria proposed by Sinacori [1977] and Schroeder [1999], due to its ability to capture both the effects of filter gain and break frequency settings. For the first-order filter defined by Eq. (8.1), K_S is easily calculated from the values of K_{mf} and ω_{mf} through:

$$\begin{aligned}
 K_S &= |H_{mf}(j\omega)|_{\omega=1 \text{ rad/s}} \\
 &= \frac{K_{mf}}{\sqrt{\omega_{mf}^2 + 1}}
 \end{aligned} \tag{8.4}$$

The prediction equations derived in Chapter 5 allow for estimating the values of the parameters of the behavioral pilot model introduced in Section 8.2.2 and the disturbance and target open-loop crossover frequencies and phase margins that might result for a certain motion filter setting based on its value of K_S . These equations were derived to provide a

prediction of these parameters based on their values that are representative for pilot tracking behavior with one-to-one motion cues ($K_S = 1$), similar to the method described in Section 8.2.4.1. These prediction equations, which are taken from Chapter 5, are given by:

$$\hat{\omega}_{c,d}(K_S) = \omega_{c,d}(1) [0.23 (K_S - 1) + 1] \quad (8.5)$$

$$\hat{\omega}_{c,t}(K_S) = \omega_{c,t}(1) \quad (8.6)$$

$$\hat{\varphi}_{m,d}(K_S) = \varphi_{m,d}(1) [-0.10 (K_S - 1) + 1] \quad (8.7)$$

$$\hat{\varphi}_{m,t}(K_S) = \varphi_{m,t}(1) \quad (8.8)$$

$$\hat{K}_v(K_S) = K_v(1) [0.19 (K_S - 1) + 1] \quad (8.9)$$

$$\hat{T}_L(K_S) = T_L(1) [-0.29 (K_S - 1) + 1] \quad (8.10)$$

$$\hat{K}_m(K_S) = K_m(1) \quad (8.11)$$

$$\hat{\tau}_v(K_S) = \tau_v(1) [0.069 (K_S - 1) + 1] \quad (8.12)$$

$$\hat{\tau}_m(K_S) = \tau_m(1) \quad (8.13)$$

$$\hat{\omega}_{nm}(K_S) = \omega_{nm}(1) [0.058 (K_S - 1) + 1] \quad (8.14)$$

$$\hat{\zeta}_{nm}(K_S) = \zeta_{nm}(1) \quad (8.15)$$

For instance, in Eq. (8.5), the prediction equation for the disturbance crossover frequency, the value of $\omega_{c,d}$ that is representative for $K_S = 1$ is indicated as $\omega_{c,d}(1)$. Note from Equations (8.5) to (8.15), that only the disturbance open-loop crossover frequency $\omega_{c,d}$ and phase margin $\varphi_{m,d}$, the pilot visual gain K_v , lead time-constant T_L , visual delay τ_v , and neuromuscular system natural frequency ω_{nm} are predicted to change under varying motion cueing settings. For the other behavioral parameters, the experimental data collected in Chapter 5 did not show a sufficiently large or consistent variation with K_S to permit the formulation of a prediction equation. Note that the numerical factor in Equations (8.5) to (8.15) defines the percentage change in the value of the considered metrics over the full range of K_S . For instance, Eq. (8.5) indicates that the disturbance crossover frequency is expected to be 23% lower for $K_S = 0$ than for $K_S = 1$.

As the roll tracking task considered in this chapter is identical to the task performed in the experiment that is described in Chapter 6, the reference values for $K_S = 1$ to use with Equations (8.5) to (8.15) can simply be taken from the experimental measurements collected there. These values are listed in Table 8.1, in the columns labeled “Current”.

8.3 Experiment Setup

8.3.1 Apparatus

The experiment described in this chapter was conducted in the SIMONA Research Simulator (SRS) at Delft University of Technology. This simulator has a six degree-of-freedom hydraulic hexapod motion system capable of a maximum cabin roll of ± 26 degrees. The time delay of the motion system is 30 ms [Berkouwer et al., 2005].

During the experiment, the participants were seated in the right pilot seat. Control inputs were given using a Moog FCS Ecol-8000 electrical sidestick. The sidestick was set to operate as a force stick, where the force put on the stick by the participant was used as the control input. The sidestick was locked in place in the neutral position for both the pitch and roll axes by implementing a 1,000 N break-out force. As was the case for the in-flight and simulator tracking tasks described in Chapter 6, the pilot control inputs (indicated with u in Fig. 8.1) could be between ± 2.5 V. The applied force-output voltage characteristic was set to 14 N/V to match the experiment of Chapter 6.

For presenting the tracking error to the participants, use was made of the same visual display that was used for the experiment of Chapter 6. This display, which presented the tracking error (e_s , see Fig. 8.1) as the rotation of a target line with respect to a fixed aircraft symbol as shown in Fig. 8.3, was depicted on the primary flight display (PFD) directly in front of the participants. The update rate of the PFD was 60 Hz and the PFD latency, including the projection, was measured to be 25 ms [Stroosma et al., 2007].

To mask the acoustic noise made by the motion-base actuators, participants wore a noise-canceling headset. As opposed to the experiment described in Chapter 6, no recorded aircraft engine noise was played over the headphones to further cancel the actuator noise. The reason for this was that the modest roll motion excursions and velocities achieved during this experiment hardly produced any audible actuator movement.

8.3.2 Controlled Element

The controlled element in this experiment was a linearized model of the combined fly-by-wire control system and Cessna Citation II roll dynamics that were controlled in the tracking tasks evaluated in Chapter 6. The transfer function of this controlled element, which was determined from time-domain measurements of δ_c and ϕ from the in-flight tracking tasks of Chapter 6, is given by:

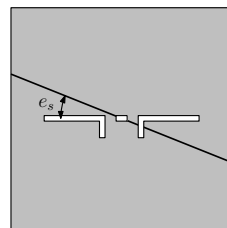


Figure 8.3. Compensatory roll tracking display.

$$\begin{aligned}
 H_c(s) &= \frac{\phi(s)}{\delta_c(s)} = K_\phi \frac{T_\phi s + 1}{s \left(\frac{s^2}{\omega_\phi^2} + \frac{2\zeta_\phi}{\omega_\phi} s + 1 \right)} e^{-\tau_\phi s} \\
 &= 0.29 \frac{0.51s + 1}{s \left(\frac{s^2}{2.70^2} + \frac{2 \cdot 0.81}{2.70} s + 1 \right)} e^{-0.09s}
 \end{aligned} \tag{8.16}$$

As explained in more detail in Chapter 6 and Appendix E, the controlled element dynamics of the form given by Eq. (8.16) represent a minimum parameter form that accurately captures the combined FBW system, including the control system delay incurred from using this FBW system dynamics, and the aircraft roll dynamics over the frequency range of interest for the considered tracking task. Due to the fact that $\omega_\phi > 1/T_\phi$, $H_c(s)$ in this experiment is approximately K/s for frequencies below ω_ϕ and approximately K/s^2 at frequencies exceeding ω_ϕ . As ω_ϕ is in the 2-5 rad/s frequency range where the pilot-vehicle system crossover frequency is expected for compensatory tracking [McRuer et al., 1965], this implies that pilot lead equalization is likely to be adopted to compensate for the approximately double integrator dynamics of this controlled element at higher frequencies.

8.3.3 Forcing Functions

The target and disturbance forcing function signals used for the experiment were both quasi-random multisine signals, which both consisted of $N_{d,t} = 10$ different sinusoids, as defined by:

$$f_{d,t}(t) = \sum_{k=1}^{N_{d,t}} A_{d,t}(k) \sin [\omega_{d,t}(k)t + \phi_{d,t}(k)] \tag{8.17}$$

The forcing function signals were generated for a measurement interval T_m of 81.92 seconds, with a 100 Hz data rate. To avoid spectral leakage over the measurement window T_m and to ensure two independent forcing function signals, which is required to allow for estimating separate describing functions for the pilot visual and motion responses using spectral methods [Stapleford et al., 1967], the sinusoid frequencies were calculated as an integer multiple of the measurement time base frequency $\omega_m = 2\pi/T_m$ according to $\omega_{d,t}(k) = n_{d,t}(k)\omega_m$. Note that the integer factor $n_{d,t}(k)$ defines the number of times the sinusoids fit into T_m .

Both f_t and the effective disturbance of the roll attitude induced by f_d – that is, f_d filtered by the controlled element dynamics $H_c(s)$, see Fig. 8.1 – were exactly those also used in the experiment of Chapter 6. Both signals had a time-domain variance of 0.4 deg². The numerical properties of the sinusoid frequency factors $n_{d,t}(k)$, frequencies $\omega_{d,t}(k)$, amplitudes $A_{d,t}(k)$, and phases $\phi_{d,t}(k)$ for both f_d and f_t as used in this experiment are listed in Table 8.2. Note that the amplitudes and phases listed for f_d have been pre-shaped with the inverse controlled element dynamics as given by Eq. (8.16). Due to the fact that these controlled element dynamics were slightly different from those used for the experiment of Chapter 6, also slightly different values of $A_{d,t}(k)$ and $\phi_{d,t}(k)$ are listed in Table 8.2 than are reported for this previous experiment.

Table 8.2. Experiment target and disturbance forcing function properties.

disturbance, f_d				target, f_t			
n_d	ω_d , rad/s	A_d , V	ϕ_d , rad	n_t	ω_t , rad/s	A_t , deg	ϕ_t , rad
5	0.384	0.0153	1.372	6	0.460	0.698	1.288
11	0.844	0.0245	5.763	13	0.997	0.489	6.089
23	1.764	0.0240	1.257	27	2.071	0.220	5.507
37	2.838	0.0213	7.416	41	3.145	0.119	1.734
51	3.912	0.0214	8.248	53	4.065	0.078	2.019
71	5.446	0.0237	5.407	73	5.599	0.049	0.441
101	7.747	0.0293	-1.171	103	7.900	0.031	5.175
137	10.508	0.0387	0.490	139	10.661	0.023	3.415
171	13.116	0.0502	1.216	194	14.880	0.018	1.066
226	17.334	0.0741	1.677	229	17.564	0.016	3.479

To minimize the initial controlled element stabilization required at the start of a tracking run, both the target and disturbance forcing functions were faded in, using a linear fade-in, over the first three seconds of each run.

8.3.4 Simulator Motion Cueing

During the experiment, pilots were presented with pure rotational roll motion cues (no coordinated lateral cueing), which were generated by passing the controlled element roll motion through the first-order high-pass filter given by Eq. (8.1). As was also the case for the experiment described in Chapter 6, the participants were seated at the right pilot position during the experiment. The supplied roll was defined to be around an axis of rotation that was 1.0 m above and 0.34 m left of the right pilot position, as is also the case in DUT's Cessna Citation II laboratory aircraft (see Chapter 6). This ensured that the lateral and vertical accelerations at the pilots' heads that resulted directly from the offset with respect to the axis of roll rotation were equivalent to those in the real aircraft.

During the first seconds of each run, which were not considered for data analysis, the simulator cabin was pre-positioned to the trim pitch attitude of 4.34 deg, equal to the pitch attitude the Citation laboratory aircraft had during the in-flight measurements described in Chapter 6. At the end of each tracking run, the simulator was brought back to the neutral cueing position of 0 deg cabin pitch and roll.

8.3.5 Independent Variables

The experiment described in this chapter compares measurements of pilot tracking behavior taken for ten different settings of the roll motion filter given by Eq. (8.1). Fig. 8.4 shows the different experimental conditions, indicated with solid black square markers and labeled C0-C9, in the graphical representation of the simulator fidelity criterion proposed for rotational simulator motion by Sinacori [1977] and Schroeder [1999]. The details of these ten motion filter settings are listed in Table 8.3. Fig. 8.4 further shows the roll motion filter settings that were used in a number of previous studies, among which are also the investigations that

explicitly measured roll tracking behavior for a number of different motion cueing settings summarized in Section 8.2.3. White-, gray-, and black-filled markers indicate pure gain, first-order washout, and second-order washout filter settings, respectively. The details of each of these roll motion cueing settings taken from literature can be found in the table in Fig. 8.4.

As can be verified from Fig. 8.4, the roll motion cueing settings evaluated in this chapter consist of nine conditions that are distributed over the high- and medium-fidelity regions as defined by Schroeder [1999], supplemented with a reference fixed-base single-loop tracking condition C0. Conditions C1 to C9 represent a factorial variation in motion filter gain K_{mf} and break frequency ω_{mf} , where three different levels are considered for each motion filter parameter. As can be verified from Table 8.3, motion filter gains of 0.5, 0.75, and 1 are considered, while ω_{mf} is varied from 0 rad/s (no washout) to 0.5 and 1 rad/s.

Table 8.3. Experimental conditions.

condition	K_{mf}	ω_{mf}	description	
C0	0.0		no motion	evaluated in Ch. 6
C1	0.5	0 rad/s	no washout, low gain	
C2	0.75		no washout, medium gain	
C3	1.0		no washout, high gain	evaluated in Ch. 6
C4	0.5	0.5 rad/s	medium washout, low gain	evaluated in Ch. 6
C5	0.75		medium washout, medium gain	
C6	1.0		medium washout, high gain	evaluated in Ch. 6
C7	0.5	1 rad/s	strong washout, low gain	
C8	0.75		strong washout, medium gain	
C9	1.0		strong washout, high gain	

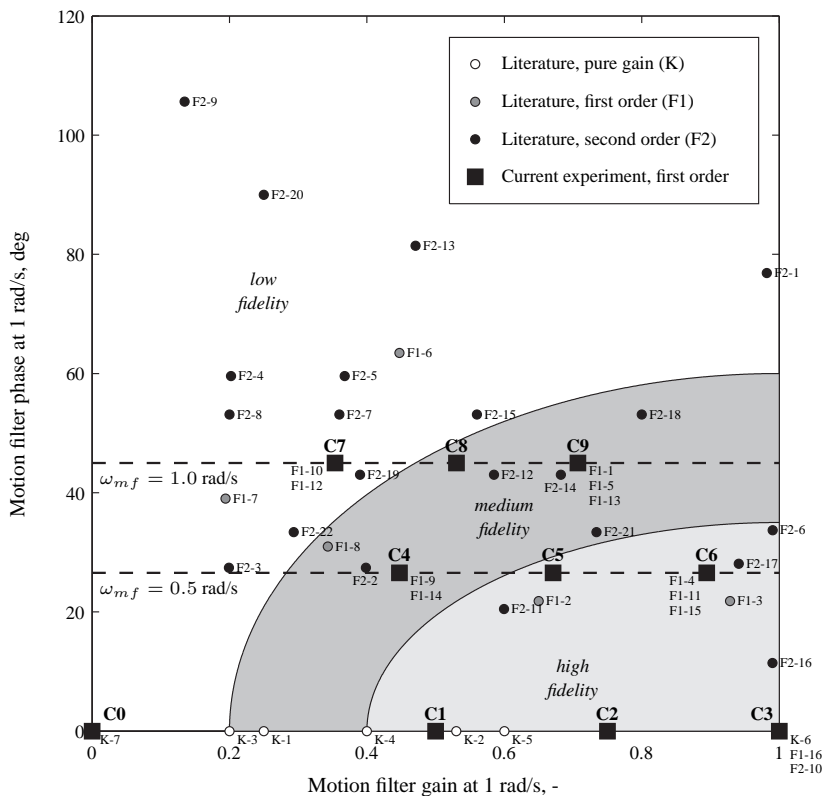
As also indicated in Table 8.3, for four of the ten roll motion cueing conditions evaluated in this chapter measurements of pilot roll tracking behavior were also collected in the experiment of Chapter 6. A side-by-side comparison of the results obtained for the overlapping conditions of both these experiments is provided in Appendix I.

8.3.6 Participants

Six of the seven DUT Cessna Citation II pilots who participated in the experiment described in Chapter 6 were asked to also perform the current simulator experiment. At the time of the experiment, one of these pilots was still employed as an airline pilot, but was no longer active on the Cessna Citation II. The participants' flight experience ranged from 1,500 to over 14,000 hrs on a multitude of different aircraft. Their ages ranged from 35 to 73 years ($\mu = 51.3$ years, $\sigma = 15.5$ years).

8.3.7 Experimental Procedure

The participants performed the entire experiment on one day. Before starting the experiment, they received an extensive briefing on the scope and objective of the experiment. They were informed that they would be subjected to the different motion cueing settings



Motion Filter Settings From Literature					
Symbol	Reference	Condition	Symbol	Reference	Condition
K-1	Bray [1996]		F2-1	Jex et al. [1978]	W2
K-2	Jex et al. [1978]	A	F2-2	Sinacori [1977]	A
K-3	Schroeder [1999]	Roll gain 0.2	F2-3	Sinacori [1977]	B
K-4	Schroeder [1999]	Roll gain 0.4	F2-4	Sinacori [1977]	C
K-5	Schroeder [1999]	Roll gain 0.6	F2-5	Sinacori [1977]	D
K-6	Schroeder [1999]	Roll gain 1.0	F2-6	Schroeder et al. [1996]	
K-7	Chapters 6 & 7	(0,0)	F2-7	Chung et al. [1998]	High fidelity
F1-1	Jex et al. [1978]	W1	F2-8	Chung et al. [1998]	Medium fidelity
F1-2	Jex et al. [1978]	W1.A	F2-9	Chung et al. [1998]	Low fidelity
F1-3	Jex et al. [1979]		F2-10	Mikula et al. [1999]	A1
F1-4	Stapleford et al. [1969]	Roll pole at 0.5 rad/s	F2-11	Mikula et al. [1999]	A2
F1-5	Stapleford et al. [1969]	Roll pole at 1.0 rad/s	F2-12	Mikula et al. [1999]	A3
F1-6	Stapleford et al. [1969]	Roll pole at 2.0 rad/s	F2-13	Mikula et al. [1999]	A4
F1-7	Schroeder et al. [1998]	Small motion	F2-14	Chung [2008]	Medium fidelity
F1-8	Gouverneur et al. [2003]		F2-15	Chung [2008]	Typical
F1-9	Reid and Nahon [1986a]	CW1	F2-16	Van Gool [1978]	R(0.1)
F1-10	Reid and Nahon [1986a]	CW2	F2-17	Van Gool [1978]	R(0.25)
F1-11	Pool et al. [2009b]		F2-18	Van Gool [1978]	R(0.5)
F1-12	Chapter 7	(0.5,1)	F2-19	Schroeder et al. [1998]	Large motion
F1-13	Chapter 7	(1,1)	F2-20	Reid and Nahon [1986a]	CW3
F1-14	Chapters 6 & 7	(0.5,0.5)	F2-21	Beukers et al. [2010]	high gain
F1-15	Chapters 6 & 7	(1,0.5)	F2-22	Beukers et al. [2010]	low gain
F1-16	Chapter 6	(1,0)			

Figure 8.4. The roll motion cueing settings considered in the current experiment and different settings evaluated in literature compared to the rotational simulator motion fidelity criterion proposed by Sinacori [1977] with modified fidelity regions as suggested by Schroeder [1999].

listed in Table 8.3. The main instruction they received before the experiment was that it was their task to minimize the roll tracking error, that is, to minimize the excursion of the target line on the compensatory display shown in Fig. 8.3.

In addition, the pilots were asked to provide a subjective motion fidelity rating for each run using the same verbal analog scale (VAS) also used for the experiments described in Chapters 6 and 7. Furthermore, they were also encouraged (but not required) to provide further verbal feedback of their opinions on the different motion conditions throughout the experiment. These subjective comments were recorded by the experimenter and can be found in Appendix H, for reference.

Immediately after the pilots received their instructions the experiment started. Each tracking run lasted 90 s, of which the final 81.92 s were used as the measurement data. The first 8.08 s of each run were not considered for data analysis. During this run-in time the forcing function signals were faded in (first three seconds, see Section 8.3.3), the simulator was tilted back to a trim pitch attitude of 4.34 deg (see Section 8.3.4), and the pilots were performing initial stabilization of the controlled element after the run start. The full 90 s runs were logged at a frequency of 100 Hz.

After a 90 s tracking run ended, the simulator was rotated back to 0 deg pitch and roll attitude. The pilots were then asked to give a subjective motion fidelity rating for the run they had just completed on the supplied rating form. After they had filled out the rating form and provided further feedback of their opinion on the motion cueing setting they had just been subjected to, pilots were informed of their performance for the last run, expressed in terms of the root mean square of the tracking error signal e .

The pilots performed the tracking task for the different roll motion cueing settings listed in Table 8.3 in randomized blocks of all ten of the experimental conditions. Typically, two blocks of all ten experimental conditions were completed in between breaks. These breaks were typically short (max. 20 minutes), but a longer lunch break was taken halfway the experiment.

No planned division between training and measurement runs was made before the experiment. Pilots' performance for the tracking task was monitored by the experimenter during the entire experiment. When a participant had familiarized himself with the tracking task and had attained a consistent level of tracking performance, five repetitions of each experimental condition were collected, after which the experiment was terminated. On average, a total of eight to nine repetitions of each experimental condition, corresponding to 80-90 tracking runs, were performed by each participant.

8.3.8 Dependent Measures

A number of different dependent measures are considered for evaluating the level of roll motion fidelity as evaluated with the current experiment. First of all, the subjective motion fidelity ratings collected using the VAS rating scale are analyzed as a reference metric for pilots' subjective impression of simulator motion fidelity. As explained in more detail in Chapter 6, on this rating scale the pilots were to indicate how well they believed the supplied motion cues to correspond to what they would expect in the aircraft (0-100%, along a 10 cm scale).

The main focus of the current chapter, however, is on a number of dependent measures that are commonly considered to evaluate changes in pilot tracking behavior. First of all, the time-domain variances of the error signal e and the pilot control signal u are considered as measures of the attained levels of tracking performance and control activity, respectively. In addition, the use of two independent multisine forcing function signals allows for separating the contributions of the target, disturbance, and remnant signals to these signal variances [Jex et al., 1978]. These variance contributions are used to separate possibly different effects of the applied variation in motion cueing on disturbance-rejection and target-following performance. To the same end, measured values of the disturbance and target open-loop system crossover frequencies and phase margins are also considered as dependent measures.

Finally, using the recorded time traces of e , ϕ_{mf} , and u the parameters of the multimodal pilot model introduced in Section 8.2.2 are estimated using the time-domain identification procedure described by Zaal et al. [2009a]. The seven pilot model parameters are used to quantify the true changes in pilot tracking behavior that underlie the observed variations in tracking performance and open-loop system dynamics. Furthermore, using the estimated model parameters, the relative contribution of the roll motion feedback provided to the pilots on their control inputs is evaluated by considering the modeled output of the pilot visual and motion responses, indicated with u_v and u_m in Figures 8.1 and 8.2.

8.3.9 Hypotheses

The current experiment evaluates roll tracking behavior for a wide variation in the settings of a first-order high-pass roll motion filter. For the behavioral evaluation of simulator motion fidelity performed in this chapter, a high level of motion fidelity is obtained if pilot tracking behavior is not significantly adapted compared to what is observed for the one-to-one cueing condition C3. For degraded roll motion fidelity, which could either result from decreased K_{mf} or increased ω_{mf} , it is expected that pilot tracking behavior will adapt towards the single-loop behavior measured for condition C0. Based on the previous roll tracking measurements taken in the experiment of Chapter 6, the main dependent measures that will show this adaptation are the pilot control activity (σ_u^2), the disturbance open-loop crossover frequency $\omega_{c,d}$ and phase margin $\varphi_{m,d}$, the pilot model visual gain K_v , and the visual lead time constant T_L .

For a motion filter with $K_{mf} = 1$ and $\omega_{mf} = 0.5$ rad/s (condition C8 of the current experiment), the experiment of Chapter 6 showed no differences in pilot tracking behavior compared to the condition with one-to-one roll motion cues. This is consistent with the previous results of Stapleford et al. [1969], Jex et al. [1978], and Van Gool [1978], which all indicated no effect of filter break frequency settings up to 0.5 rad/s on pilot tracking behavior and performance. In addition, as can be verified from Fig. 8.4, this further complies with the motion fidelity criterion proposed by Schroeder [1999], as condition C8 is clearly within the high-fidelity region of this criterion. In the experiment of Chapter 6, significant adaptation of tracking behavior was observed for a reduced filter gain of 0.5, that is, condition C4 of the current experiment, which is also only a medium-fidelity setting according to the criterion of Schroeder [1999].

Based on these previous findings, it is expected that no significant adaptation to the applied change in motion filter dynamics is observed for the conditions that remain closest to

the one-to-one condition and fall well within the high-fidelity region proposed by Schroeder [1999]. As can be verified from Fig. 8.4, this would at least be expected for conditions C2 and C8, while this may also still hold for C1 and C6, which are much closer to the medium-fidelity boundary. Being the only experimental condition shown in Fig. 8.4 in the low-fidelity region, the control signal variance and pilot behavioral parameters are expected to be closest to the single-loop measurements of condition C0 for condition C5. For all other conditions, significantly reduced pilot gains and increased visual lead time constants are expected to signal reduced simulator fidelity.

When comparing the different experimental conditions against the criterion boundaries proposed by Schroeder [1999] (see Fig. 8.4), it can be observed that for the different settings evaluated in this experiment this motion fidelity criterion predicts a slightly stronger effect of increasing ω_{mf} than of decreasing K_{mf} . Increasing ω_{mf} over the range considered in this experiment is seen to bring the motion filter settings closer to the low-fidelity region than is observed over the range of considered filter gains. It should be noted that this somewhat contradicts the linear prediction equations derived from a modest amount of experimental measurement data in Chapter 5, Equations (8.5) to (8.15). The predictor in these equations, K_S , reduces more rapidly over the range of considered motion filter gains ($K_S = 0.5$ for condition C1 with $K_{mf} = 0.5$ and $\omega_{mf} = 0$ rad/s) than over the considered values for the filter break frequency ($K_S = 0.71$ for condition C9 with $K_{mf} = 1$ and $\omega_{mf} = 1$ rad/s). Furthermore, Schroeder et al. [2000] report – based on experiments performed by Bray [1985] and Schroeder [1999] – that the motion filter break frequency typically affects target tracking, while reductions in motion filter gain are stated to mainly affect tasks in which an external disturbance is to be regulated. For these reasons, the effects of variations in K_{mf} and ω_{mf} as measured in this experiment, which considers a combined target-following and disturbance-rejection task, are expected to be about equally large and significant.

8.4 Results

This section presents the results of the experiment that was performed in the SRS to evaluate pilot tracking behavior for the ten different roll motion cueing conditions listed in Table 8.3. The measurement data are presented as the means over the data collected for the six participants, with error bars indicating the 95% confidence intervals of the means. The data have been corrected for between-subject variability before calculating the 95% percent confidence intervals. A two-way repeated-measures analysis of variance (ANOVA) was used to evaluate the effects of the tested variation in K_{mf} and ω_{mf} on the considered dependent measures. Note that for this statistical analysis all data except for the single-loop measurements (condition C0, (0,0)) were considered, yielding a set of nine conditions with a factorial evaluation of effects of gain and break frequency variations. Before analyzing data with an ANOVA, data were checked for normality using a Kolmogorov-Smirnov test. In addition, Mauchly's test of sphericity was performed to check if the assumption of sphericity was met. If for a certain dependent measure the sphericity assumption was not met, the conservative Greenhouse-Geisser sphericity correction was applied for the interpretation of the ANOVA results.

8.4.1 Subjective Motion Fidelity Ratings

Fig. 8.5 shows the subjective motion fidelity ratings collected using the VAS rating scale for the ten conditions of the experiment. In Fig. 8.5 the black square markers with variance bars indicate the mean and 95% confidence interval of the collected ratings over all subjects. The individual subject data for the motion fidelity ratings is also shown in Fig. 8.5, using gray markers with different symbols for the different participants. As indicated by the titles in the figure, the data for the different settings for ω_{mf} are separated by the vertical black lines.

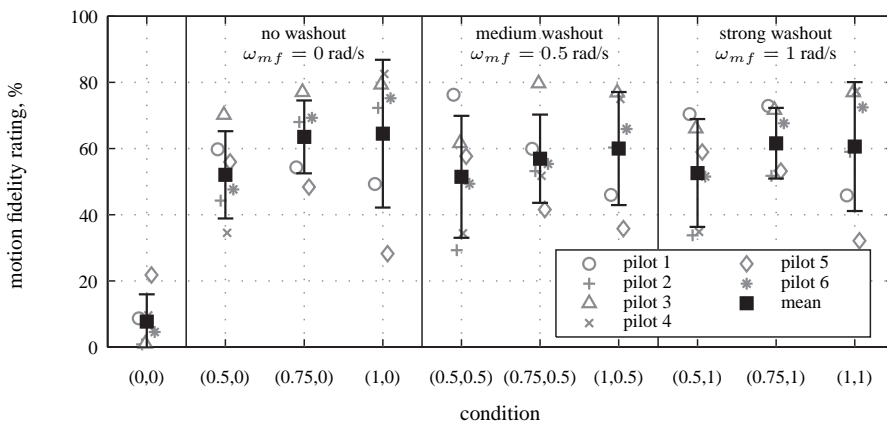


Figure 8.5. Mean measured subjective motion fidelity ratings.

Fig. 8.5 shows that the participants all gave the single-loop condition (0,0) the lowest motion fidelity ratings. Furthermore, for all three considered ω_{mf} settings the average motion fidelity ratings are seen to increase with around 10% with increasing K_{mf} (from left to right). Between the different washout levels the difference in the mean fidelity ratings is found to only be comparatively minor, where mainly the results for conditions (0.5,0.5)-(1,0.5) (medium washout) are found to be slightly lower than those for the corresponding no washout conditions. However, as is clear from Fig. 8.5, the spread in the subjective rating data is significant.

One of the reasons for this large spread in the subjective rating data is that pilots 1 and 5 consistently gave the highest fidelity ratings to the conditions with $K_{mf} = 0.5$, while, as was expected, the other pilots rated the conditions with the highest filter gains the best. As can be verified from the subjective pilot comments collected in Appendix H, pilots 1 and 5 claimed that the motion cues perceivable for conditions where $K_{mf} = 0.75$ or 1 were “exaggerated” compared to what they would expect in the real aircraft. It should be noted that these rating results obtained for both pilots are not consistent with the ratings they provided for the experiment described in Chapter 6.

As expected from the comparatively large spread in the subjective ratings, when considering the data for all conditions except (0,0) no statistically significant variation due to

the different values of K_{mf} and ω_{mf} is found. This implies that, even though some effect of the applied variation in the motion filter gain and break frequency seems to be visible in Fig. 8.5, no conclusions regarding the level of simulator motion fidelity can be drawn from this collected subjective rating data.

8.4.2 Tracking Performance and Control Activity

Fig. 8.6 shows the average measured error and control signal variance for the different experimental conditions. The presentation in Fig. 8.6 is different from that used for Fig. 8.5 to more clearly indicate the effects of the variation in motion filter gain and break frequency. The data are plotted as a function of K_{mf} and the data for the different values of ω_{mf} are shown with differently colored markers. Black, gray, and white markers correspond to data for $\omega_{mf} = 0, 0.5,$ and 1 rad/s, respectively. Table 8.4 lists the corresponding ANOVA results. Note again that these ANOVA results are based on the nine conditions with roll motion feedback, that is, those with K_{mf} equal to 0.5 or higher.

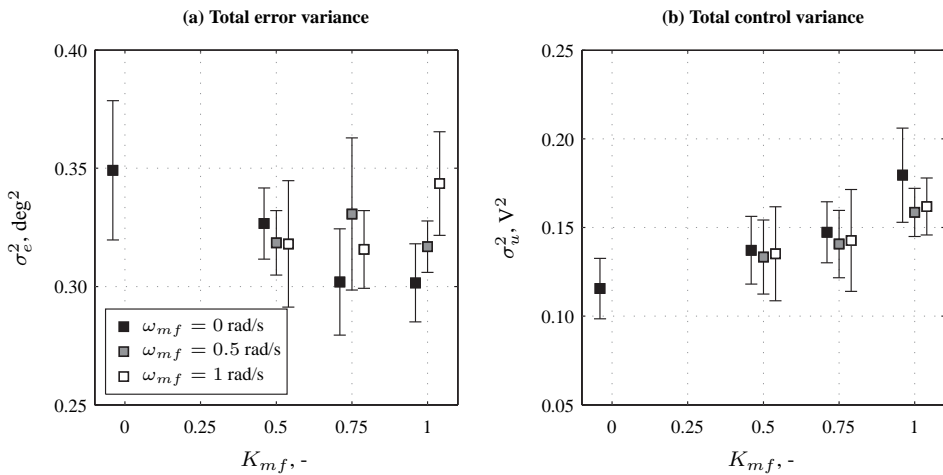


Figure 8.6. Mean error and control signal variances.

Table 8.4. Two-way repeated-measures ANOVA results for the tracking error and control signal variances.

Dependent measures	Factors								
	K_{mf}			ω_{mf}			$K_{mf} \times \omega_{mf}$		
	df	F	Sig.	df	F	Sig.	df	F	Sig.
σ_e^2	2,10	0.41	—	2,10	4.40	**	4,20	2.67	—
σ_u^2	2,10	10.03	**	2,10	1.00	—	4,20	0.37	—

** = significant ($p < 0.05$) gg = Greenhouse-Geisser sphericity correction
 — = not significant ($p \geq 0.05$)

Fig. 8.6(a) shows that for the no-washout conditions ($\omega_{mf} = 0$ rad/s) the pilots were able to more accurately perform the tracking task (lower σ_e^2) with increasing K_{mf} . For both $K_{mf} = 0.75$ and 1 the tracking error variance is on average found to be 15% lower than measured for the single-loop condition C0 ($K_{mf} = 0$). For $K_{mf} = 0.5$, the decrease in σ_e^2 compared to the single-loop measurements is found to be approximately half of the decrease observed for the highest motion filter gains.

For the conditions with washout, indicated with the gray and white filled markers in Fig. 8.6(a), this decrease in σ_e^2 with increasing K_{mf} is not visible. For $\omega_{mf} = 0.5$ rad/s tracking performance is found to be approximately equal for motion filter gains of 0.5 and 1, while for $\omega_{mf} = 1$ rad/s tracking performance is seen to degrade for $K_{mf} = 1$ almost to the same level as measured for single-loop tracking. Overall, for the highest two motion filter gain settings tracking performance is found to be consistently worse for $\omega_{mf} = 0.5$ and 1 rad/s than for the no-washout conditions. This effect of ω_{mf} on σ_e^2 is found to be statistically significant, as can be verified from Table 8.4. No overall significant effect of K_{mf} on the tracking error variance is observed, which is a result of the inconsistent effect of the applied motion filter gain variations over the different settings of ω_{mf} .

For the control signal variance Fig. 8.6(b) shows an almost linear increase in σ_u^2 with increasing K_{mf} for $\omega_{mf} = 0$ rad/s. This increase in control signal variance with increasing motion amplitude is highly consistent with previous experimental results, for instance those reported in [Zaal et al., 2009b, 2011] and Chapters 4, 5, and 6. This increased σ_u^2 indicates pilots respond with larger control inputs in the presence of larger amplitude physical motion stimulation. Fig. 8.6(b) shows that this trend is found to persist for the conditions with roll washout, even though a slight reduction in σ_u^2 compared to the no-washout measurements is observed for $\omega_{mf} = 0.5$ and 1 rad/s, which is especially visible for $K_{mf} = 1$. The observed increase in control activity with increasing motion filter gain is found to be statistically significant, as can be verified from Table 8.4.

Figures 8.7(a), (c), and (e) depict the disturbance, target, and remnant components of the total tracking error variance depicted in Fig. 8.6(a). Figures 8.7(b), (d), and (f) show the same three components of the control signal variance σ_u^2 . These different components have been determined through separation in the frequency domain [Jex et al., 1978]. The corresponding statistical analysis results are listed in Table 8.5.

Fig. 8.7(a) indicates a clear decrease in the disturbance component of σ_e^2 with increasing K_{mf} , especially for $\omega_{mf} = 0$ and $\omega_{mf} = 0.5$ rad/s. Furthermore, a smaller effect of ω_{mf} on $\sigma_{e,d}^2$ is also observed, showing higher error variances due to the disturbance signal for increased filter break frequencies. Again, as also concluded from the total error variance results presented in Fig. 8.6, this effect of ω_{mf} is especially visible for $K_{mf} = 1$. The ANOVA results presented in Table 8.5 indicate that both these effects of K_{mf} and ω_{mf} on $\sigma_{e,d}^2$ are statistically significant.

The target error variance component, for which the data are depicted in Fig. 8.7(c), is found to remain comparatively constant with the applied variation in motion filter settings at around 0.15 deg^2 . The data for $K_{mf} = 0.75$ and 1 show slightly elevated values of $\sigma_{e,t}^2$, indicating slightly worse target tracking performance, for the conditions with washout. However, as can be verified from Table 8.5 this is not a statistically significant effect. The remnant component data depicted in Fig. 8.7(e) show a variation over the different experimental conditions that matches the trends observed for $\sigma_{e,t}^2$, only with higher spread. As

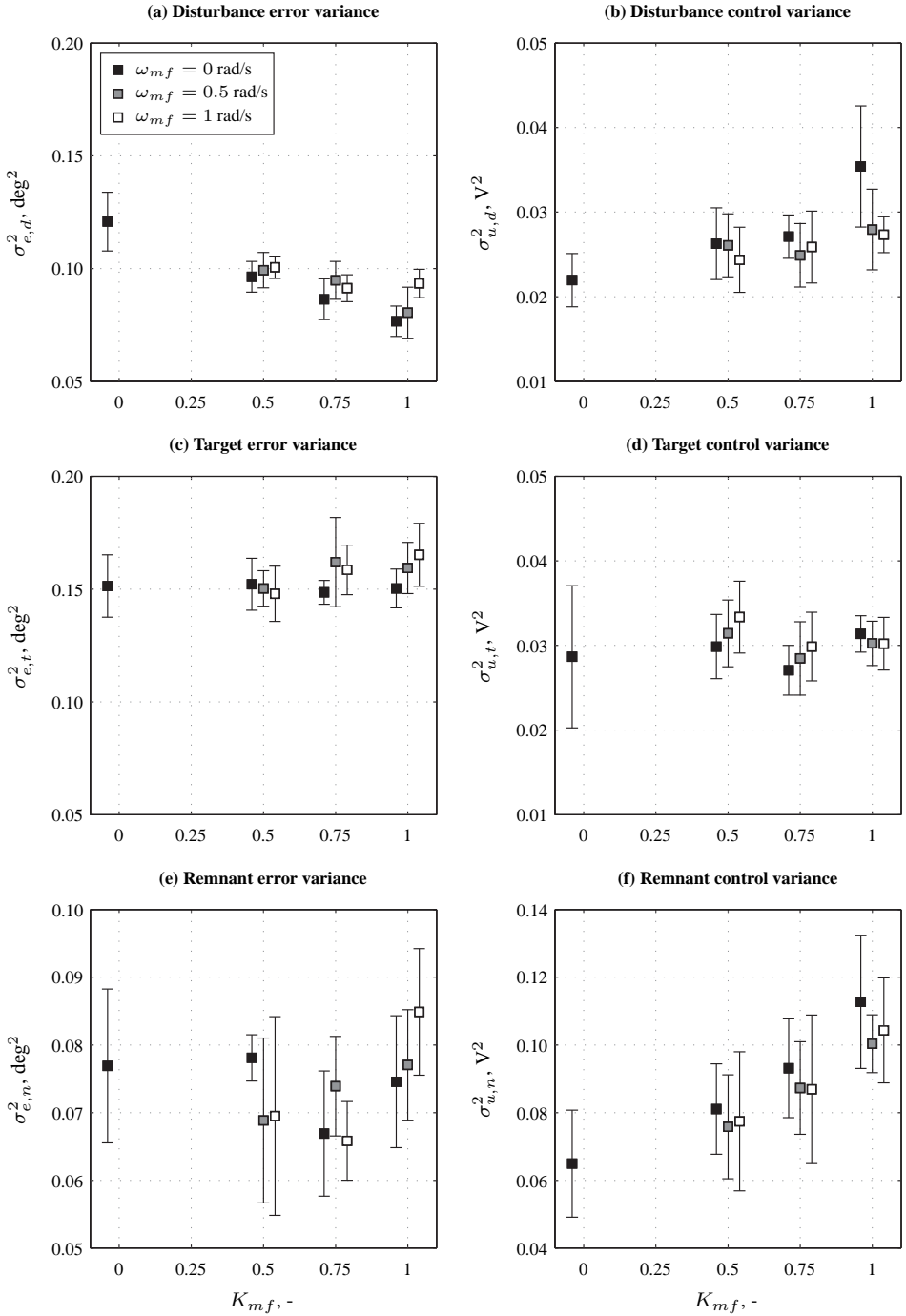


Figure 8.7. Disturbance, target, and remnant components of the error and control signal variances.

Table 8.5. Two-way repeated-measures ANOVA results for tracking error and control signal variance components.

Dependent measures	Factors								
	K_{mf}			ω_{mf}			$K_{mf} \times \omega_{mf}$		
	df	F	Sig.	df	F	Sig.	df	F	Sig.
$\sigma_{e,d}^2$	2,10	28.43	**	2,10	14.78	**	4,20	1.49	–
$\sigma_{e,t}^2$	2,10	1.95	–	2,10	1.44	–	4,20	1.78	–
$\sigma_{e,n}^2$	1.1,5,3 ^{gg}	3.06	–	2,10	0.01	–	4,20	2.64	–
$\sigma_{u,d}^2$	2,10	4.38	**	2,10	3.76	–	4,20	2.26	–
$\sigma_{u,t}^2$	2,10	4.82	**	2,10	1.35	–	4,20	0.67	–
$\sigma_{u,n}^2$	2,10	10.80	**	2,10	1.02	–	4,20	0.11	–

** = significant ($p < 0.05$) gg = Greenhouse-Geisser sphericity correction

– = not significant ($p \geq 0.05$)

can be verified from Table 8.5, no significant effects of the variation in motion filter gain and break frequency were observed for $\sigma_{e,n}^2$.

Table 8.5 shows that all three components of the control signal variance are significantly affected by the tested variation in the motion filter gain K_{mf} . Both the disturbance and remnant components – $\sigma_{u,d}^2$ and $\sigma_{u,n}^2$, respectively, which are presented in Figures 8.7(b) and (f) – are seen to show an increasing trend with K_{mf} , as was also observed for the total control signal variance in Fig. 8.6. For $\sigma_{u,t}^2$ the slightly lower values observed for $K_{mf} = 0.75$ compared to the other motion filter gains settings cause the significant effect listed in Table 8.5. Despite the fact that some effects of the applied variation in filter break frequency are observed – for instance, both $\sigma_{u,d}^2$ and $\sigma_{u,n}^2$ are found to be slightly lower for all values of K_{mf} than the variance components measured for the no-washout conditions – no statistically significant effects of ω_{mf} are observed for the control signal variance component data.

8.4.3 Crossover Frequencies and Phase Margins

Fig. 8.8 shows the average measured crossover frequencies and phase margins of the disturbance and target open-loop dynamics, as given by Equations (8.2) and (8.3). The corresponding ANOVA results for $\omega_{c,d}$, $\omega_{c,t}$, $\varphi_{m,d}$, and $\varphi_{m,t}$ are presented in Table 8.6.

For the conditions without washout ($\omega_{mf} = 0$ rad/s), the disturbance crossover frequency is found to show an almost linear increase with increasing motion filter gain K_{mf} , as can be verified from Fig. 8.8(a). Note that this increase in $\omega_{c,d}$ is considerable, with more than 1 rad/s separating the disturbance crossover frequencies measured for the no-motion and one-to-one roll motion conditions. For all settings of K_{mf} , increasing the filter break frequency is seen to result in a relative reduction in $\omega_{c,d}$. Furthermore, this relative decrease in crossover frequency with increasing ω_{mf} is found to become larger with increasing K_{mf} . This is especially visible for the $\omega_{mf} = 1$ rad/s data, which are found to remain approximately constant at around 2.1 rad/s for all considered values of the motion filter gain. As

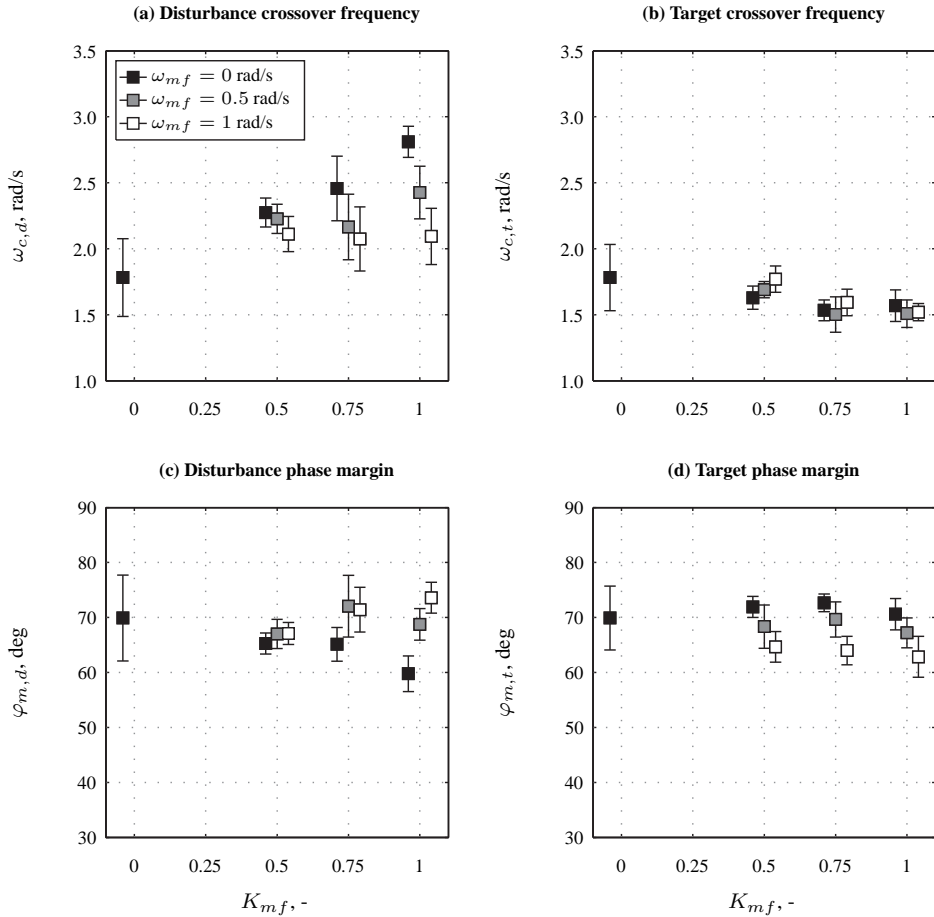


Figure 8.8. Mean disturbance and target open-loop crossover frequencies and phase margins.

Table 8.6. Two-way repeated-measures ANOVA results for crossover data.

Dependent measures	Factors								
	K_{mf}			ω_{mf}			$K_{mf} \times \omega_{mf}$		
	df	F	Sig.	df	F	Sig.	df	F	Sig.
$\omega_{c,d}$	2,10	11.47	**	1,6,5,39 ^{gg}	18.09	**	4,20	3.56	**
$\omega_{c,t}$	2,10	15.06	**	2,10	4.68	**	4,20	1.41	—
$\varphi_{m,d}$	2,10	4.74	**	2,10	24.44	**	4,20	5.61	**
$\varphi_{m,t}$	2,10	1.92	—	2,10	39.74	**	4,20	0.20	—

** = significant ($p < 0.05$) gg = Greenhouse-Geisser sphericity correction
 — = not significant ($p \geq 0.05$)

can be verified from Table 8.6, these effects of K_{mf} and ω_{mf} on the measured disturbance crossover frequencies are all statistically significant. The same holds for the degrading effect of K_{mf} on $\omega_{c,d}$ with increasing filter break frequency, judging from the statistically significant effect of the interaction between both motion filter parameters, $K_{mf} \times \omega_{mf}$.

The same variation with both motion filter parameters observed for $\omega_{c,d}$ is also found for the corresponding disturbance phase margin, see Fig. 8.8(c). For $\omega_{mf} = 0$ rad/s, a decrease in $\varphi_{m,d}$ of around 10 deg is observed between $K_{mf} = 0$ and $K_{mf} = 1$. Compared to the no-washout data, the presence of washout is found to result in an increase in $\varphi_{m,d}$. For $K_{mf} = 0.5$ and $K_{mf} = 0.75$ this increase in $\varphi_{m,d}$ is found to be approximately equal for both settings of ω_{mf} , but for $K_{mf} = 1$ the disturbance phase margin is found to increase with increasing ω_{mf} . On average, $\varphi_{m,d}$ for the condition with $K_{mf} = 1$ and $\omega_{mf} = 1$ rad/s (C9) is found to be even higher than the mean value measured for the single-loop condition with $K_{mf} = 0$. The ANOVA results for $\varphi_{m,d}$ listed in Table 8.6 show that the effects of K_{mf} , ω_{mf} , and their interaction are all statistically significant. Note that the significant effects of both the motion filter gain and break frequency on $\omega_{c,d}$ and $\varphi_{m,d}$ are consistent with the significant effects of both motion filter parameters on the disturbance tracking error component $\sigma_{e,d}^2$ observed from Fig. 8.7.

Fig. 8.8(b) shows that a slight decrease in the target open-loop crossover frequency is observed with increasing motion filter gain, a trend that is found to be statistically significant (see Table 8.6). Furthermore, $\omega_{c,t}$ is also found to be significantly affected by the applied variation in filter break frequency, where mainly for $K_{mf} = 0.5$ comparatively higher target crossover frequencies are found when $\omega_{mf} > 0$ rad/s than for the condition without washout. Note, however, that compared to the effect of K_{mf} this effect of ω_{mf} is comparatively minor.

The measured target open-loop phase margins presented in Fig. 8.8(d) only show a small (and not statistically significant, see Table 8.6) effect of K_{mf} , as for all motion filter break frequency settings $\varphi_{m,t}$ is found to be slightly lower for $K_{mf} = 1$ than for all other filter gain settings. A highly significant effect of varying ω_{mf} is, however, observed from Fig. 8.8(d). With increasing motion filter break frequency settings, the target phase margin is found to consistently decrease compared to the conditions without washout ($\omega_{mf} = 0$ rad/s), independent of the filter gain setting. As can be verified from Table 8.6, this effect of ω_{mf} on $\varphi_{m,t}$ is highly statistically significant. Note from comparison with the tracking error data shown in Fig. 8.7 that the significant effects of K_{mf} and ω_{mf} on the crossover frequency and phase margin of the target open-loop response do not result in a change in the level of target tracking performance.

8.4.4 Pilot Control Behavior

In this chapter, the multimodal pilot model shown in Fig. 8.2 is used to analyze changes in pilot tracking behavior due to the applied variation in roll motion filter gains and break frequencies. From this pilot model analysis, two sets of results are presented here. First, the estimated pilot model parameters are used to explicitly show changes in pilot tracking behavior over the different experimental conditions. Furthermore, the estimated pilot parameters are used to evaluate and compare the relative contribution of the supplied visual and physical motion cues for all considered motion filter settings.

8.4.4.1 Pilot Model Parameter Estimates

Figures 8.9 and 8.10 show the values of all seven model parameters and the pilot visual lead gain $K_v T_L$ that were estimated from time-domain measurements of pilot tracking behavior for all experimental conditions. The corresponding ANOVA results are presented in Table 8.7.

Fig. 8.9(a) and (b) show the increase in pilot visual gain and decrease in visual lead time constant with increasing motion filter gain that are consistently reported in a number of different tracking experiments, see Chapter 5. Furthermore, the presented data show that increasing ω_{mf} attenuates both these effects, as for the conditions with $\omega_{mf} = 0.5$ and 1, consistently lower values of K_v and higher values of T_L are measured. Overall, these results indicate that pilots performed reduced visual lead equalization for conditions with higher motion filter gains and lower filter break frequencies. Both these observations are highly consistent with the hypothesis that with decreasing motion fidelity measured tracking behavior was expected to increasingly approximate behavior representative for single-loop tracking (no motion). As can be verified from Table 8.7, the effect of K_{mf} on both these parameters is highly significant, while the effect of the motion filter break frequency is only found to be statistically significant for T_L (for K_v the ANOVA indicates $F(2, 10) = 3.10$, $p = 0.09$).

Fig. 8.9(c) shows the estimated values of the pilot visual lead gain $K_v T_L$. Due to the fact that the high-frequency response of $H_{p_v}(s)$ is dominated by the lead term, this parameter indicates the gain of the pilot visual response at frequencies well above T_L . As can be verified from Fig. 8.9(c), on average a slight decrease with increasing K_{mf} and increase with increasing ω_{mf} are observed for the visual lead gain. Both these observations suggest pilots put more weight on their response to visual lead information under conditions of degraded motion fidelity. The ANOVA results, however, show that both effects are not found to be statistically significant. The same holds for the identified values of the pilot motion gain K_m shown in Fig. 8.9(d). These do not show consistent variation over the different settings of the motion filter gain and break frequency and considerable spread.

As can be verified from the prediction equations for both pilot time delays derived in Chapter 5 (Equations (8.12) and (8.13)), τ_v is typically found to increase with increasing motion fidelity, while τ_m is found to be relatively independent of variations in motion fidelity. Fig. 8.9(e) shows that for this experiment the estimated pilot visual delays are found to increase with increasing K_{mf} , with around 20 ms separating the values of τ_v for $K_{mf} = 0$ and 1. This effect of K_{mf} is found to be independent of the applied variation in ω_{mf} and is, as can be verified from Table 8.7, statistically significant. As can be verified from Fig. 8.9(e) and Table 8.7, the pilot visual delay is found to be unaffected by the applied variation in ω_{mf} . For τ_m , Fig. 8.9(f) shows no clear variation with K_{mf} . For $K_{mf} = 0.5$ and 0.75, the presented data show a slight increase in τ_m with increasing filter break frequency. Note, however, that this effect is comparatively small, especially with respect to the spread in the data, and that for the unity-gain filter conditions the opposite trend is observed. Overall, the pilot motion delay was found to show no statistically significant effect of both the applied variation in K_{mf} and ω_{mf} .

Fig. 8.10 shows the estimated values of the two parameters of the neuromuscular actuation model $H_{nm}(s)$. As can be verified from Table 8.7, also no significant effects of the

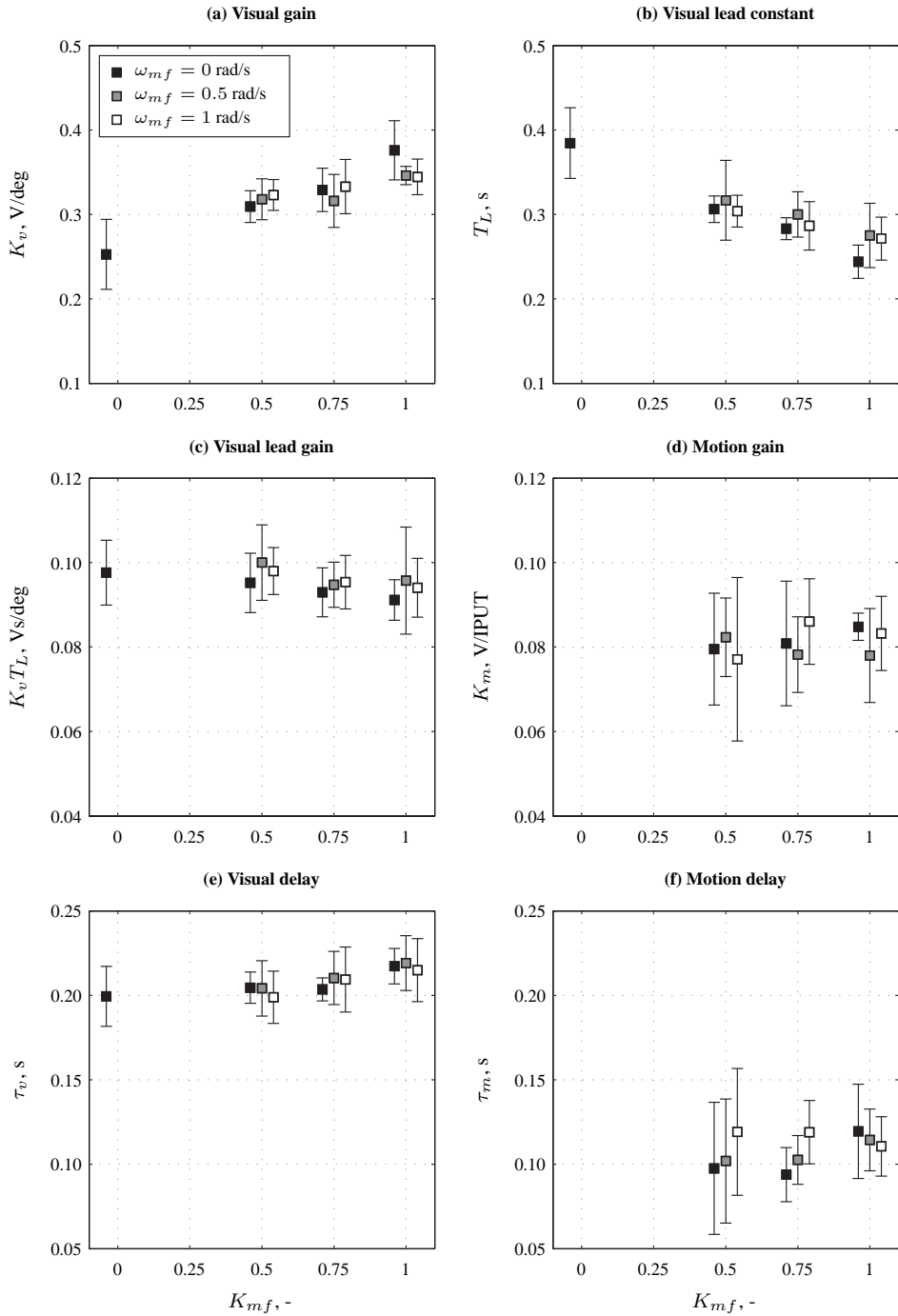


Figure 8.9. Mean estimated multimodal pilot model parameters.

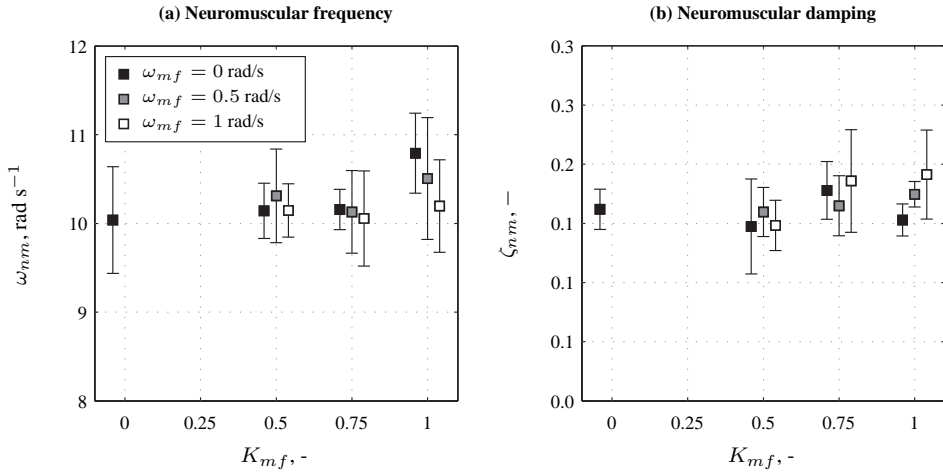


Figure 8.10. Mean estimated pilot model neuromuscular actuation model parameters.

Table 8.7. Two-way repeated-measures ANOVA results for the estimated multimodal pilot model parameters.

Dependent measures	Factors								
	K_{mf}			ω_{mf}			$K_{mf} \times \omega_{mf}$		
	df	F	Sig.	df	F	Sig.	df	F	Sig.
K_v	2,10	10.87	**	2,10	3.10	-	4,20	1.25	-
T_L	2,10	6.74	**	2,10	4.53	**	4,20	0.59	-
$K_v T_L$	1.0,5.1 ^{gg}	1.03	-	1.1,5.6 ^{gg}	1.56	-	4,20	0.10	-
K_m	1.1,5.6 ^{gg}	0.21	-	2,10	0.48	-	4,20	0.50	-
τ_v	2,10	4.58	**	2,10	0.27	-	4,20	0.24	-
τ_m	1.1,5.4 ^{gg}	0.96	-	2,10	0.75	-	4,20	0.79	-
ω_{nm}	2,10	3.16	-	1.0,5.2 ^{gg}	2.45	-	4,20	0.63	-
ζ_{nm}	2,10	3.38	-	2,10	2.08	-	4,20	1.12	-

** = significant ($p < 0.05$) gg = Greenhouse-Geisser sphericity correction
 - = not significant ($p \geq 0.05$)

considered variation in motion filter gain and break frequency are found for ω_{nm} and ζ_{nm} . Fig. 8.10(a) does show increased values of ω_{nm} for $K_{mf} = 1$, which is consistent with the findings from Chapter 4, where higher neuromuscular actuation natural frequencies were reported for increased motion amplitudes. As can be verified from Fig. 8.10(a), here the increase in ω_{nm} is found to be attenuated with increasing filter break frequency (and hence decreasing roll motion amplitudes). However, this effect of ω_{mf} is not observed for the other settings of K_{mf} .

8.4.4.2 Pilot Model Quality of Fit

To assess the quality of the fits of the multimodal pilot model to the measured data, the variance accounted for (VAF) was calculated for all pilot model fits with respect to the averaged time-domain measurements of the control signal u , as also done in [Nieuwenhuizen et al., 2008; Zaal et al., 2009a] and Chapters 2, 4, and 6. The VAF is a measure of how well the output of a model describes the corresponding measured signal, in this case the pilot control signal u , in the time domain. Fig. 8.11 shows the average VAF values obtained for all conditions of the experiment. Table 8.8 presents the corresponding results of a two-way repeated measures ANOVA performed on the VAF data.

Fig. 8.11 shows that for all experimental conditions the pilot model VAF was found to be between 70 and 80% on average, a result that is highly consistent with previously reported results (see, for instance, [Zaal et al., 2009a] and Chapters 4 and 6). Still, as can be verified from Table 8.8, significant changes in the pilot model VAF are observed over the different experimental conditions. First, a significant effect of K_{mf} on the VAF is found, which results from the lower model VAFs obtained for the highest two motion filter gain settings. Second, the significant interaction ($K_{mf} \times \omega_{mf}$) listed in Table 8.8 is explained by the fact that for $K_{mf} = 0.5$ the VAF is found to increase with increasing ω_{mf} , while for $K_{mf} = 1$ the opposite trend is observed and for $K_{mf} = 0.75$ no effect of the filter break frequency is observed. Notwithstanding the statistical significance of both these results, the differences in pilot model VAF over the different experimental conditions do not suggest a marked reduction in the quality of fit for any of the experimental conditions.

8.4.4.3 Pilot Model Control Signal Variance Contributions

The estimated values of the pilot model parameters presented in Figures 8.9 and 8.10 are used in this chapter to explicitly evaluate changes in pilot tracking behavior. As not only the pilot dynamics, but also the supplied visual and motion feedback signals vary over the different experimental conditions, these pilot model parameters do not directly allow for quantitative evaluation of the relative contributions of visual and motion information on the control inputs given by the pilots. For this reason, the obtained pilot model parameters sets were used together with the corresponding recorded time traces of e_s and $\dot{\phi}_s$ to calculate the contributions of the pilot model visual and motion channels to the total model output. These visual and motion contributions are indicated with u_v and u_m in Fig. 8.2. The means and 95% confidence intervals of the time-domain variances of these two signals ($\sigma_{u_v}^2$ and $\sigma_{u_m}^2$, respectively), as well as their fraction $\sigma_{u_m}^2 / \sigma_{u_v}^2$ are presented in Fig. 8.12. The corresponding ANOVA results for these three metrics shown in Fig. 8.12 are listed in Table 8.8.

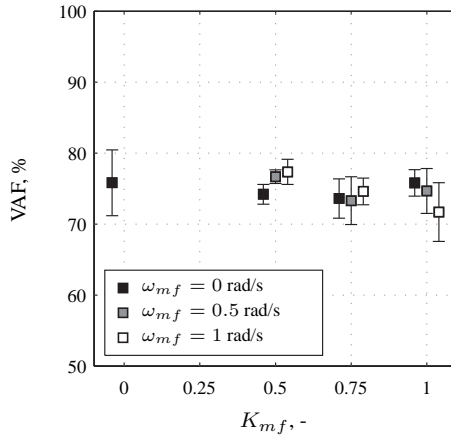


Figure 8.11. Mean pilot model variance accounted for.

Table 8.8. Two-way repeated-measures ANOVA results for pilot model VAF and control signal variances.

Dependent measures	Factors								
	K_{mf}			ω_{mf}			$K_{mf} \times \omega_{mf}$		
	df	F	Sig.	df	F	Sig.	df	F	Sig.
VAF	2,10	5.11	**	2,10	0.13	—	4,20	3.04	**
$\sigma_{u_e}^2$	2,10	3.00	—	1,1,5,4 ^{gg}	0.34	—	4,20	0.77	—
$\sigma_{u_m}^2$	1,1,5,4 ^{gg}	23.01	**	2,10	4.52	**	4,20	2.76	—
$\sigma_{u_m}^2/\sigma_{u_e}^2$	2,10	20.54	**	2,10	6.03	**	4,20	1.70	—

** = significant ($p < 0.05$) gg = Greenhouse-Geisser sphericity correction
 — = not significant ($p \geq 0.05$)

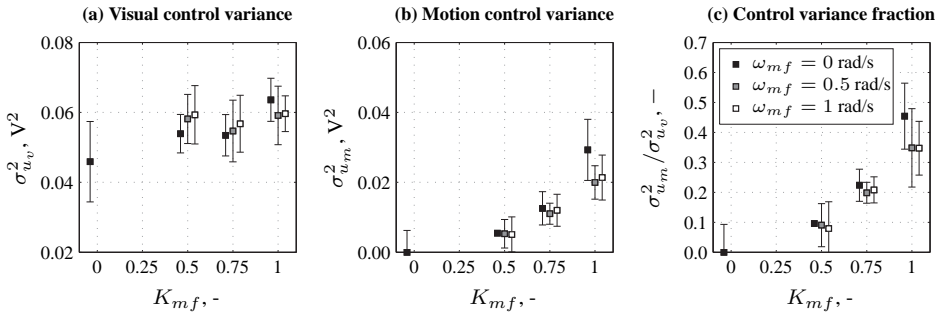


Figure 8.12. Mean pilot model visual and motion channel control signal variance contributions and their fraction.

Fig. 8.12(a) shows that compared to the no-motion condition ($K_{mf} = 0$), all experimental conditions with motion feedback show higher average visual control variance contributions. This is consistent with the increased control activity and pilot visual gain observed when motion feedback is available. As can also be verified from Table 8.8, $\sigma_{u_v}^2$ is not found to differ significantly over the different roll motion filter settings.

The motion control variance data shown in Fig. 8.12(b), however, show a clear increasing trend with increasing motion filter gain. Note that this increase in the contribution of u_m is not achieved through increased values for the pilot motion gain K_m (see Fig. 8.9), but results from the increased roll motion amplitudes for conditions with higher values of K_{mf} . Furthermore, Fig. 8.12(b) also shows that compared to the no-washout conditions ($\omega_{mf} = 0$ rad/s), the conditions with roll washout show reduced values of $\sigma_{u_m}^2$. Table 8.8 shows that both these effects are statistically significant. Due to the fact that the visual control variance is found to remain approximately constant, the control variance fraction data shown in Fig. 8.12(c) shows the same trend observed for $\sigma_{u_m}^2$ and the same statistically significant effects of K_{mf} and ω_{mf} . Fig. 8.12(c) thereby indicates that the relative contribution of the pilot motion response $H_{p_m}(s)$ decreases both with decreasing K_{mf} and increasing ω_{mf} . Note, however, that the effect of motion filter gain variations is found to be considerably stronger than that of the different tested values for ω_{mf} .

8.4.5 Comparisons with Offline Prediction Data

In Section 8.2.4, two different methods for predicting changes in some of the considered behavioral metrics were introduced. The first was meant to allow for separating the effects of variations in washout and pilot dynamics on the resulting open-loop system crossover frequencies and phase margins, by assuming no behavioral adaptation compared to one-to-one motion and assessing changes in open-loop dynamics solely resulting from variations in $H_{mf}(s)$. The second allowed for prediction of the different considered behavioral metrics based on the motion filter gain at 1 rad/s (K_S) for each experimental condition. This section presents the results of both these prediction tools, making use of previous measurements of roll tracking behavior from the experiment described in Chapter 6, and compares their results with the obtained experimental measurements.

Fig. 8.13 shows this comparison between experimental measurements and prediction results for the crossover frequencies and phase margins of the disturbance and target loops. The experimental data is depicted with black square markers and variance bars indicating the mean and 95% confidence interval of the data. The offline prediction results for the no-adaptation analysis and the linear predictions defined by Equations (8.5) to (8.8) are indicated a dashed black line and a solid gray line, respectively. It should be noted that both predictions were made based on data from the experiment of Chapter 6 for the condition with one-to-one roll motion cueing (1,0), hence the equal values of both predictions for this condition.

Fig. 8.13(a) shows that for the disturbance crossover frequency $\omega_{c,d}$, the results of both offline analyses correspond reasonably well. Both analyses predict a reduction in $\omega_{c,d}$ with reducing K_{mf} and a further drop in disturbance crossover frequency with increasing filter break frequency. As can be observed from Fig. 8.13(a), however, the collected experimental measurements show a much stronger effect of the variation in K_{mf} for the no-washout

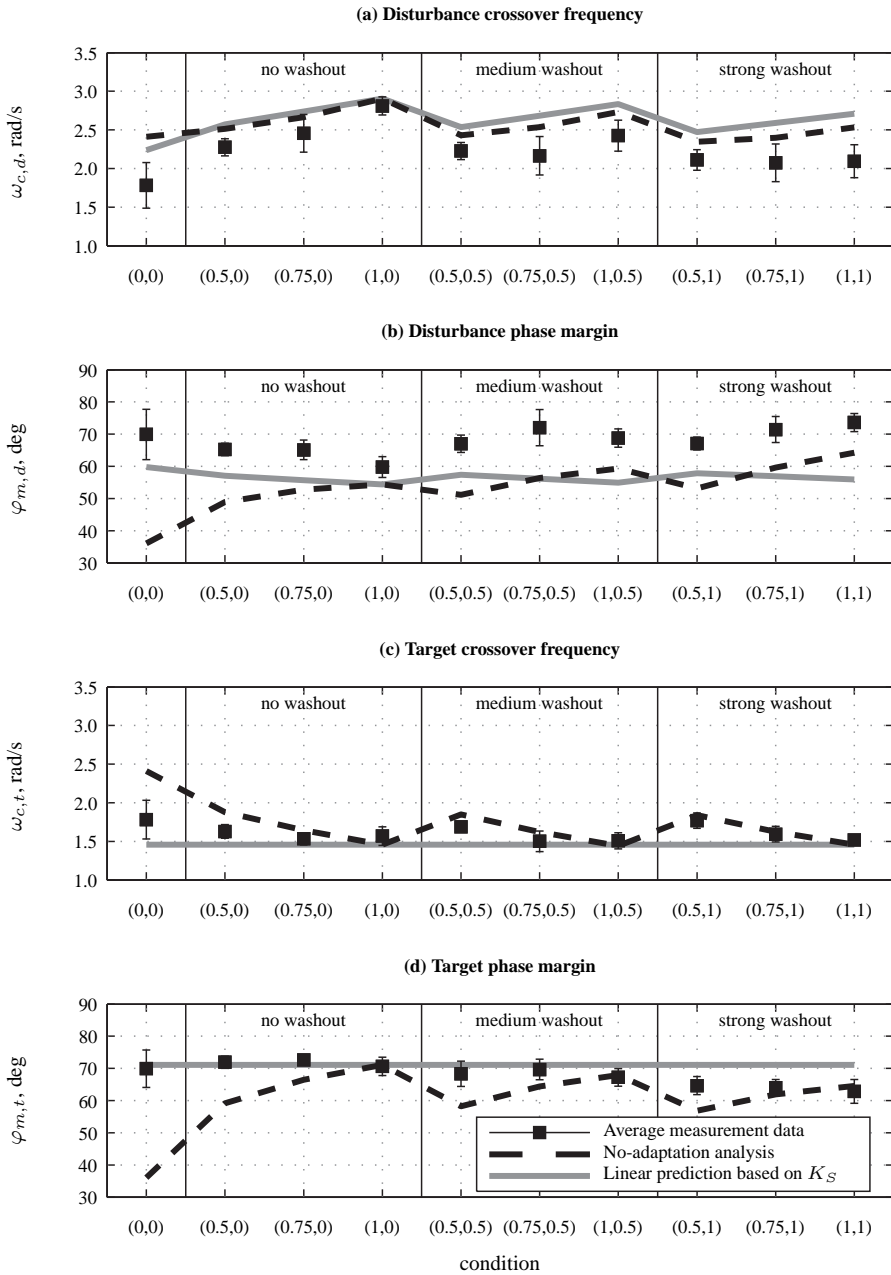


Figure 8.13. Comparison of measured disturbance and target open-loop crossover frequencies and phase margins with offline prediction results.

conditions and a much stronger effect of the applied variation in ω_{mf} on $\omega_{c,d}$ than predicted by both analyses. The reducing effect of K_{mf} for the conditions with higher values of ω_{mf} is also not sufficiently predicted by Eq. (8.5). The observed differences between the experimental measurements and the no-adaptation analysis results shown in Fig. 8.13(a) do suggest a change in pilot tracking behavior both due to K_{mf} and ω_{mf} .

For the disturbance open-loop phase margin, Fig. 8.13(b) shows nearly perfectly opposite predictions from both offline analyses. Assuming no pilot adaptation, $\varphi_{m,d}$ would be expected to show a decreasing trend with both decreasing K_{mf} and increasing ω_{mf} . The linear prediction equation obtained from previous measurements (Eq. (8.7)), however, shows a more modest increase in $\varphi_{m,t}$ with degrading simulator motion fidelity. Overlooking the offset between experimental measurements and prediction results, Fig. 8.13(b) shows that for the no-washout conditions the linear prediction provided by Eq. (8.7) describes the trend in the experimental measurements best, as an average increase in $\varphi_{m,d}$ of around 10 deg is observed between conditions (1,0) and (0,0). For the conditions with washout, the effect of K_{mf} on the disturbance phase margin is, however, found to be better captured by the no-adaptation analysis results. These results suggest that the prediction equation for $\varphi_{m,d}$ (Eq. (8.7)) should be extended to incorporate a stronger effect of ω_{mf} .

As shown in Fig. 8.13(c), the no-adaptation analysis predicts a marked increase in target open-loop crossover frequency with decreasing K_{mf} , but no effect of ω_{mf} on $\omega_{c,t}$. On the other hand, no change in target crossover frequency is predicted based on the findings of Chapter 5. The experimental measurements confirm the invariance with ω_{mf} and the effect of decreasing K_{mf} predicted by the no-adaptation analysis. However, the increase in $\omega_{c,t}$ is found to be smaller than would result from only changing the motion filter dynamics, hence suggesting adaptation of pilot dynamics to changes in the motion filter gain.

For the target open-loop phase margin, the linear prediction equation suggests that $\varphi_{m,t}$ remains constant over the different experimental conditions. If the pilots would not adapt their control strategy compared to the (1,0) condition, however, Fig. 8.13(d) shows that the target phase margin would decrease markedly with decreasing K_{mf} and increasing ω_{mf} . As can be verified from Fig. 8.13(d), no effect of motion filter gain variations is observed for $\varphi_{m,t}$, as for all settings of K_{mf} the target phase margin is found to be approximately equal for all values of ω_{mf} . The experimental measurement data shows that $\varphi_{m,t}$ is found to decrease with increasing filter break frequency, however, which is not consistent with the invariance with K_S suggested by the prediction equation derived for $\varphi_{m,t}$ in Chapter 5 (Eq. (8.8)).

Fig. 8.14 shows the comparison of the measured data and the prediction results for the four pilot model parameters for which linear prediction equations were defined in Chapter 5: the pilot visual gain K_v , the visual lead time-constant T_L , the pilot visual delay τ_v , and the neuromuscular actuation natural frequency ω_{nm} . Note from the dashed black lines presented in Fig. 8.14 that, by definition, the no-adaptation analysis assumes no change in pilot model parameters over the different experimental conditions. Comparison of the no-adaptation analysis data with the current experimental measurements for the (1,0) condition indicates that the values of K_v and T_L are highly consistent with the measurements of the experiment described in Chapter 6. The pilot visual delay and the neuromuscular actuation natural frequency are, however, found to be slightly lower and higher, respectively, than the reference measurements from Chapter 6 on which both predictions are based.

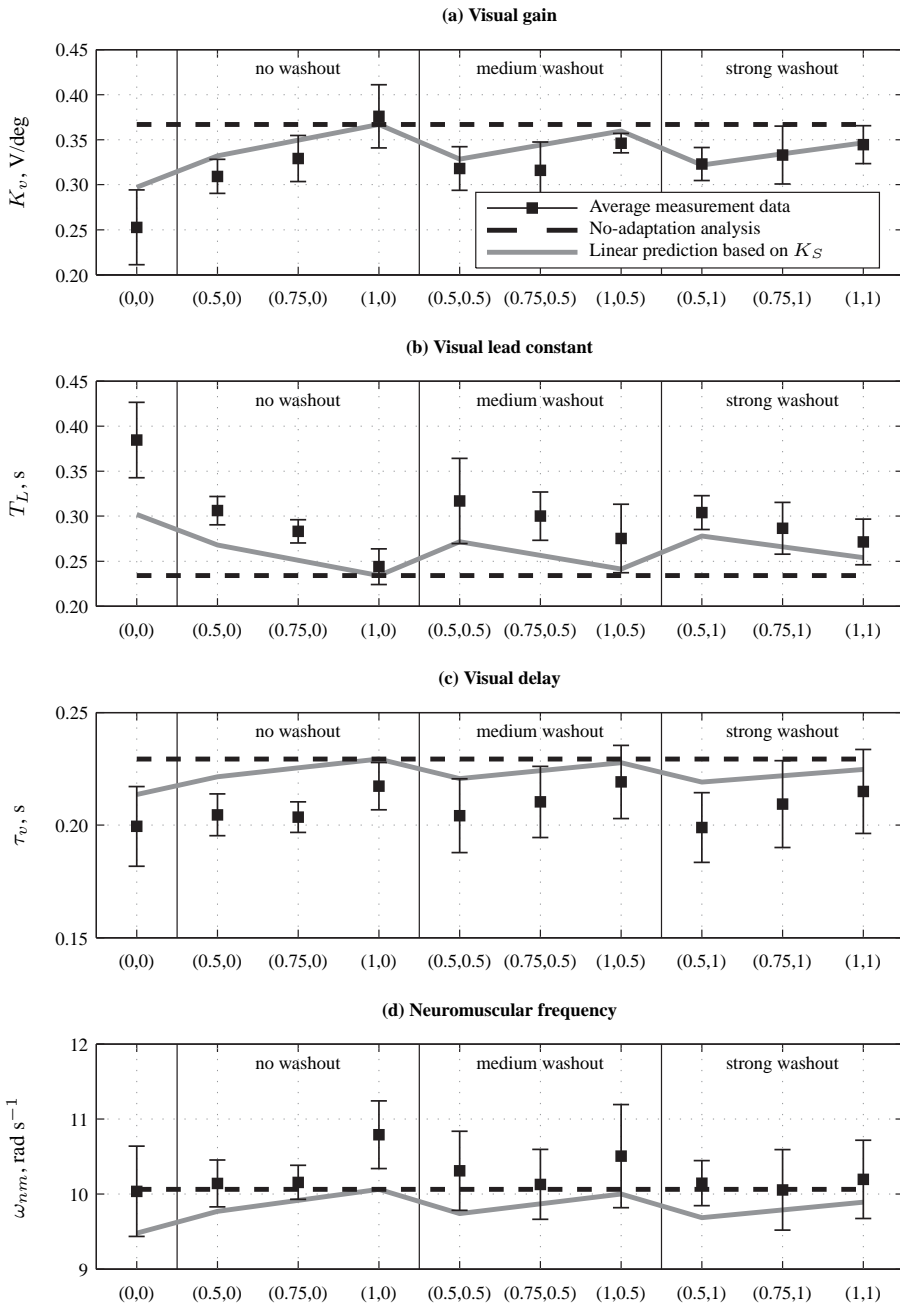


Figure 8.14. Comparison of the estimates for selected multimodal pilot model parameters with offline prediction results.

The linear predictions of the change in the pilot model parameters shown in Fig. 8.14, as given by Equations (8.9), (8.10), (8.12), and (8.14) are seen to reflect the general trend in the measured pilot model parameters well. This is especially true for the pilot visual gain shown in Fig. 8.14(a), for which Eq. (8.9) is seen to provide a decent prediction. Despite the fact that the magnitude of the predictions for τ_v and ω_{nm} is off due to the difference in the current experimental measurements compared to those of Chapter 6, the predicted increasing trend with increasing K_{mf} and decreasing ω_{mf} is confirmed by the current experimental measurements. Finally, for the visual lead time constant, see Fig. 8.14(b), the measured data from the current experiment suggests a markedly stronger effect of variations in both K_{mf} and ω_{mf} on the pilot visual lead time constant than predicted by Eq. (8.10). For the no-washout conditions, the increase in T_L with decreasing K_{mf} is seen to be around twice as strong as suggested by the linear prediction. Overall, however, the linear predictions based on the value of K_S for each experimental condition are found to provide an acceptable prediction of the measured changes in pilot tracking behavior.

8.4.6 Comparisons with In-Flight Tracking Measurements

Both for the current experiment and for the roll tracking experiment described in Chapter 6 the strongest effects of the applied variations in roll motion cueing were found on the crossover frequency and phase margin of the disturbance open-loop transfer function and, from pilot model analysis, the pilot visual gain and lead time constant. A quantitative comparison of these observed trends from both experiments, and a comparison with the corresponding in-flight tracking measurements taken in the experiment of Chapter 6, are shown in Fig. 8.15. Figures 8.15(a) and (b) show the difference (“ Δ ”) in K_v (vertical axis) and T_L (horizontal axis) with respect to the collected in-flight measurements for all roll motion filter conditions evaluated in both experiments. Each white circular marker indicates the mean difference in the pilot visual gain and lead time constant compared to the in-flight measurements for one evaluated condition, while each ellipse gives an indication of the spread in the measurements. The horizontal axis of each ellipse indicates the 95% confidence interval of the T_L data, while the vertical axis is defined by the 95% confidence interval of the measured K_v . In the same format, Figures 8.15(c) and (d) visualize the discrepancies in $\omega_{c,d}$ and $\varphi_{m,d}$ with respect to the in-flight measurements from Chapter 6.

Fig. 8.15(a) shows the comparison with the in-flight tracking measurements for the two pilot visual equalization parameters (K_v and T_L) for the four simulator roll motion settings evaluated in the experiment of Chapter 6. Compared to the in-flight measurements, a reduction in K_v and an increase in T_L are observed for the no-motion condition (0,0), while for both simulator conditions with unity motion filter gains, (1,0) and (1,0.5), pilot visual gains and lead time constants were found to be higher and lower than for the in-flight condition, respectively. Overall, Fig. 8.15(a) shows a trend towards the top left of the figure with increasing simulator motion fidelity.

As can be verified from Fig. 8.15(b), a highly similar effect of roll motion fidelity on K_v and T_L is observed for the current experiment data. The results for the conditions for one-to-one roll motion (1,0) and no-motion (0,0) are found to be highly consistent with those measured in the experiment of Chapter 6. The data for all conditions with attenuated roll motion are found to be in between the measurements taken for these two extremes

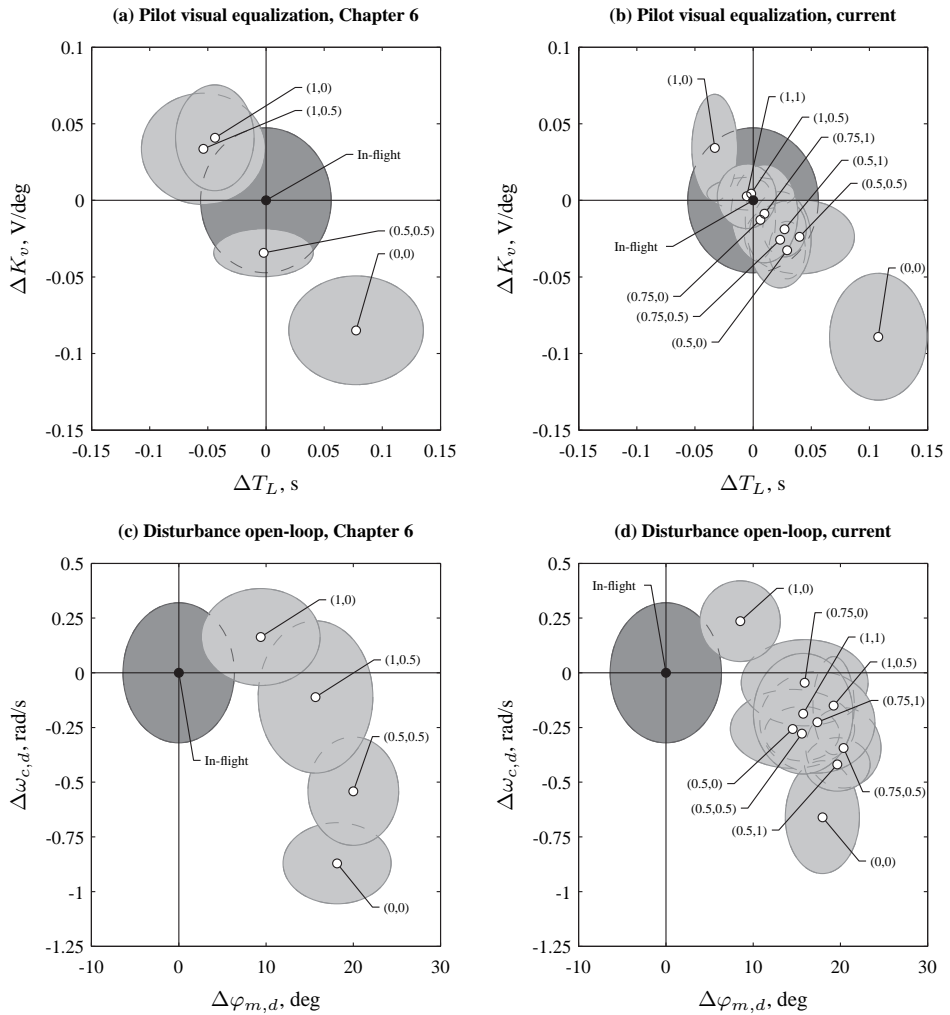


Figure 8.15. Discrepancies with respect to in-flight tracking measurements for all conditions of the experiment from Chapter 6 and the current experiment for the pilot visual gain K_v , the visual lead time constant T_L and the disturbance crossover frequency $\omega_{c,d}$ and phase margin $\varphi_{m,d}$.

in the evaluated roll motion filter settings. Confirming the dominant effect of the motion filter gain, Fig. 8.15(b) shows that the combinations of K_v and T_L for the roll motion filter settings with high values of K_{mf} are typically the closest to the data for the (1,0) condition, while those collected for $K_{mf} = 0.5$ are all closest to the single-loop measurements.

Of further note is the difference in measured visual equalization parameters for the high-fidelity (1,0.5) condition between the data from both experiments. In the experiment of Chapter 6, pilot tracking behavior for this condition was found to be equivalent to that measured with one-to-one roll motion. The current experiment data show a much larger difference in tracking behavior between (1,0) and (1,0.5). Finally, note that due to the considerable spread in the in-flight visual equalization measurements it is still difficult to draw conclusions on which roll motion cueing settings yield tracking behavior that differs significantly from that measured in real flight. As can be verified from Fig. 8.15(b), the means for all conditions except (0,0) are within the 95% confidence interval ellipse of the in-flight data. The values of K_v and T_L measured for conditions (1,0.5), (1,1), (0.75,0), and (0.75,1) are, however, found to be closest to the average of the in-flight measurements.

Figures 8.15(c) and (d) show the same consistency with respect to the in-flight tracking measurements for the disturbance open-loop crossover frequency and phase margin as observed for K_v and T_L . For both experiments, the data for the no-motion condition (0,0) is found to be on the lower right, indicating reduced values of $\omega_{c,d}$ and increased phase margins compared to the in-flight measurements. Furthermore, both experiments also show consistently higher crossover frequencies for one-to-one roll motion cueing in the simulator (1,0) and also a consistent increase in $\varphi_{m,d}$ of around 10 deg. Also the measurements of $\omega_{c,d}$ and $\varphi_{m,d}$ for all conditions with attenuated roll motion are again found to be between those for the no-motion and one-to-one motion conditions. As can be verified from Figures 8.15(c) and (d), for both experiments a motion condition where roll motion is slightly attenuated compared to the one-to-one, such as (0.75,0), is found to result in the best match with the crossover frequencies measured in real flight. Note, however, that in terms of the disturbance open-loop phase margin the (1,0) condition shows measured values closest to the values obtained for the in-flight tracking measurements.

8.5 Discussion

This chapter described the results of an experiment that was performed to evaluate the effects of varying roll motion filter gain and break frequency settings on pilot roll tracking behavior. The objective of this experiment was to identify and quantify the adaptation of pilot tracking behavior, through the fitting of a multimodal pilot model to time traces recorded during a tracking task, in response to combinations of motion filter gains and break frequencies. For this evaluation, simulator roll motion that ranged from high to low motion fidelity according to the motion fidelity criteria proposed by Sinacori [1977] and Schroeder [1999] was considered. The collected behavioral measurements were intended to contribute to the development of a motion filter parameter tuning strategy that can be applied to optimize simulator motion fidelity from a behavioral standpoint.

Based on previous experimental results, such as those described in Chapters 5 and 6, pilot tracking behavior was expected to adapt increasingly more towards a control strategy

resembling single-loop (no motion feedback) tracking behavior with decreasing roll motion fidelity. For the considered roll tracking task, this change in pilot tracking behavior was expected to be mainly visible in reduced pilot control activity, lower disturbance open-loop crossover frequencies and increased phase margins, and decreased pilot visual gains and increased visual lead equalization compared to measurements taken with one-to-one roll motion. The behavioral measurements collected for the ten different roll motion filter settings considered in this chapter confirm these suspected effects and all the corresponding metrics were found to show a statistically significant effect of at least one of the varied motion filter parameters. The apparent consistency in the behavioral metrics that are affected by washout filter variations, and their relative change due to these changes in motion filter dynamics, in these different experiments provide some confidence in the development of a framework for optimizing behavioral simulator motion fidelity.

With respect to the effects of variations in motion filter gain and break frequency on pilot behavior, Schroeder et al. [2000] have reported that disturbance rejection is most severely affected by reductions in the gain of the supplied motion cues, while increased washout mainly affects behavior and performance in target-following tasks. For the combined target-following and disturbance-rejection task considered in this chapter, both the applied variations in motion filter gain and break frequency are found to significantly affect disturbance-rejection performance. Highly significant changes in the tracking errors at the disturbance forcing function frequencies and the crossover frequency and phase margin of the disturbance open-loop are observed with both variations in motion filter gain and break frequency. Furthermore, despite the fact that no effect of the variation in either motion filter parameter is observed on the tracking errors that are correlated with the target forcing function signal, pilot control activity at the target forcing function frequencies and the crossover frequency of the target open-loop response are both found to increase significantly with increasing motion filter gain. The results of the current experiment therefore suggest that for control tasks that combine target following and disturbance rejection, such a clear separation of the effects of gain attenuation and motion washout as proposed by Schroeder et al. [2000] might not be present.

In the experiment described in Chapter 6, in which pilot tracking behavior was measured for a limited number of four different roll motion cueing settings, behavioral measurements indicated equivalent control behavior for the condition with one-to-one simulator roll motion and when the simulator roll motion was attenuated by a first-order filter with unity gain and a break frequency of 0.5 rad/s. This finding is consistent with earlier experiments that evaluated pilot tracking behavior with varying roll motion cueing settings [Jex et al., 1978; Van Gool, 1978], which also reported that pilot control behavior and tracking performance were not significantly affected by the presence of washout filters with break frequencies up to 0.5 rad/s. The current experiment, in which behavioral measurements during pilot roll tracking were collected for comparatively large number of different roll motion cueing settings, shows results that are not in agreement with these previous measurements. Even for comparatively small changes in washout settings, such as between one-to-one motion and a unity gain filter with a break frequency of 0.5 rad/s, a change in pilot tracking behavior is observed. Therefore, the current experimental measurements suggest that pilot adaptation to washout filter dynamics involves the continuous adaptation to even slight variations in washout dynamics, as opposed to pilot behavior remaining constant over a certain range

of washout settings, where reducing motion fidelity induces a more discrete change in behavior after a certain threshold is crossed. If this is indeed the case, this would complicate the formulation of an objective motion fidelity criterion based on measurements of tracking behavior such as those presented in this chapter, as then subjective interpretation is still required for defining when a behavioral adaptation can be considered significant. Evaluation of an even wider variation in motion filter dynamics, for instance including higher filter break frequencies than the maximum value of 1 rad/s considered in the current experiment or higher order washout filters, is needed, however, to confirm the full nature of this behavioral adaptation process.

Comparison of the current experimental data with the in-flight and simulator measurements of pilot roll tracking behavior from the experiment described in Chapter 6 showed good correspondence between the results of both experiments. The flight simulator measurements of pilot tracking behavior for conditions without simulator motion (single-loop) and with one-to-one simulator roll motion were found to be equivalent for both experiments, with closely matching measured values for the pilot visual gain, visual lead time constant, and the disturbance open-loop crossover frequency and phase margin. For this reason, comparison of the current measurements with the in-flight roll tracking measurements from Chapter 6 shows the same differences with pilot tracking behavior – that is, slightly higher pilot visual gains and crossover frequencies – measured with one-to-one roll motion cueing as reported for the comparison made in Chapter 6. Despite the fact that the differences between the different evaluated roll motion cueing settings are comparatively small and the spread in the measurements relatively large, the best agreement with the in-flight tracking measurements for important behavioral metrics such as the pilot visual gain and lead time constant is observed for motion filter settings that only slightly attenuate the simulator roll motion. For the current experimental measurements the adopted pilot visual equalization dynamics were found to be closest to those measured in real flight for the condition with a unity-gain roll motion filter with a 0.5 rad/s break frequency.

Finally, for comparison with the collected experimental measurements, this chapter evaluated two offline prediction tools. The first, which is based on the offline evaluation of the direct effect of changes in washout dynamics on the disturbance and target open-loop dynamics, was found to provide useful for interpreting measured changes in crossover frequencies and phase margins. By separately evaluating the effects of washout filter parameter variations on these metrics, thereby assuming no change in pilot tracking behavior compared to a condition with one-to-one motion, the added effect of changes in pilot tracking behavior on these crossover frequencies and phase margins could be properly identified. On the other hand, the linear prediction equations derived from collected measurements of pilot tracking behavior for different motion cueing settings in Chapter 5 were found to provide an acceptable estimate of changes in pilot tracking behavior for the roll motion filter settings evaluated in this chapter. When using measured data for roll tracking with one-to-one motion feedback from the experiment of Chapter 6 for the prediction, a reasonably good prediction of pilot behavioral parameters for all other experimental conditions evaluated in the current experiment was obtained. In some instances, the measured effects of motion filter parameter variations were, however, found to be somewhat larger than those predicted by these equations, most notably for the pilot visual gain and lead time constant. The current experimental measurements especially suggest a stronger effect of motion filter break fre-

quency variations on a number of considered dependent measures – such as the disturbance open-loop crossover frequency, the target open-loop phase margin, and the pilot visual lead time constant – than suggested by these linear predictions.

8.6 Conclusions

This chapter described the results of an experiment in which multimodal pilot roll tracking behavior was measured in a moving-base flight simulator for ten different settings of a first-order roll motion filter. A factorial variation in motion filter gain and break frequency settings was considered in order to evaluate the individual and combined effects of changes in these parameters on pilot tracking behavior. In accordance with previous experimental results, both a decrease in the motion filter gain and an increase in the motion filter break frequency were found to result in adaptation of pilot tracking behavior compared to behavior measured with one-to-one roll motion. This behavioral adaptation was mainly apparent from a reduction in the gain with which pilots responded to visual error information and an increase in visual lead equalization. For the ten considered roll motion filter settings, pilot tracking behavior was found to be more strongly affected by the applied variation in motion filter gains than by the considered range of filter break frequencies. A comparison of the current simulator measurements with behavioral roll tracking measurements from a recent in-flight experiment showed that drawing conclusions with respect to behavioral simulator motion fidelity based on these results is still difficult, especially due to the comparatively small behavioral variations, the relatively large spread in the data, and the low number of collected samples. Nonetheless, measured pilot tracking behavior for conditions with only slightly attenuated roll motion compared to one-to-one, most notably for the condition with a unity-gain filter and a low filter break frequency of 0.5 rad/s, was found to on average show the smallest behavioral discrepancies with the in-flight measurements.

9

Conclusions and Recommendations

In this final chapter, an overview of all experimental results and the conclusions drawn from them in the preceding chapters of this thesis is provided. For example, an attempt is made to draw generalized conclusions with respect to the evaluation of simulator motion fidelity from a behavioral perspective. Furthermore, the main limitations and challenges of the cybernetic approach that is adopted in this thesis are highlighted and discussed. Finally, this chapter will provide some recommendations for further research into human manual control behavior and simulator motion cueing.

9.1 Conclusions

Many of the difficulties encountered in the formulation of adequate requirements for simulator motion cueing have been argued to result from the limited understanding of human motion perception processes and how human multimodal manual control behavior is affected by variations in the motion cues presented in moving-base flight simulators [Ray, 1996; Wu and Cardullo, 1997; Hosman, 1999]. For this reason, the goal of the research described in this thesis was to evaluate flight simulator motion fidelity from a *behavioral perspective*, by explicitly measuring how skill-based pilot manual control behavior changes as a result of variations in simulator motion cueing settings and by comparing the observed behavioral discrepancies to true in-flight measurements of pilot control behavior.

The novelty of the approach taken in this thesis for evaluating simulator motion fidelity lies in the adopted *cybernetic approach*, in which the contributions of visual and physical motion information to the control responses of pilots during manual tracking tasks are measured, separated, and *quantified objectively* through fitted multimodal pilot models. Furthermore, pilots' use of physical motion feedback for control tasks performed in *real flight* was measured explicitly, to be used as a baseline for comparison with the control behavior observed for the same control tasks in a flight simulator environment.

9.1.1 Modeling and Identification of Manual Control Behavior

The mathematical models of pilot manual control behavior used for quantifying changes in control behavior are a critical element in the adopted cybernetic approach. The multimodal pilot models utilized in this thesis are based on the *Precision Model* proposed by McRuer et al. [1965] for modeling compensatory tracking behavior with only visual error feedback. The inclusion of pilots' responses to physical motion feedback is achieved with an additional, parallel, pilot motion response model similar to those proposed by Stapleford et al. [1969], Jex et al. [1981], Hess [1990b], Van der Vaart [1992], and Hosman [1996]. The resulting multimodal pilot model has indeed been found capable of accurately describing pilot manual control dynamics in a wide variety of tracking tasks with physical motion feedback in earlier investigations [Jex et al., 1981; Van der Vaart, 1992; Hosman, 1996; Zaal, 2011]. In this thesis, two additions to these known models of human manual control behavior, which were found to be required for the behavioral analysis of some of the considered control tasks, are described.

First, as described in **Chapter 2**, the available models of compensatory tracking behavior were found to lack the required freedom to capture the pilot equalization dynamics adopted during tracking tasks where the controlled element dynamics were the elevator-to-pitch dynamics of a Cessna Citation jet aircraft. For modeling the combination of low-frequency lag and high-frequency lead equalization performed by pilots for such controlled element dynamics, it was therefore proposed to add an additional lead term to the traditional compensatory pilot model's lead-lag equalization characteristic. Pilot models that included this additional lead term were found to describe measured pilot control dynamics more accurately in both the time and frequency domains. Furthermore, it was shown that this additional lead term was essential for the correct interpretation of the effect of physical motion feedback on pilot manual control behavior. This extension to the available models

for compensatory tracking behavior has been applied for modeling compensatory tracking behavior in a number of later experiments, including the pitch tracking experiment described in Chapter 4 of this thesis and the related experiments described by Zaal [2011].

In addition to this proposed extension to the available models of compensatory pilot control dynamics, **Chapter 3** describes an effort to develop mathematical models of pilot control behavior for control tasks where forcing function signals consisting of multiple ramp-like changes in target attitude are considered instead of quasi-random multisine signals. For such ramp-tracking tasks, especially when performed with a pursuit display on which this ramp signal is displayed explicitly, pilots likely adopt a partly pursuit or even pre-cognitive control strategy [Wasicko et al., 1966; McRuer et al., 1968; Allen and McRuer, 1979; Hess, 1981]. It is proposed to model the manual control behavior adopted during such ramp-tracking tasks with a traditional model of compensatory tracking behavior, supplemented with an additional linear feedforward operation on the ramp reference signal to account for the open-loop control inputs and pursuit tracking behavior used for performing these ramp maneuvers. Using measurements of ramp-tracking behavior for control tasks without physical motion feedback, it was found that when the ramp signal was sufficiently strong with respect to the external disturbances that were to be attenuated pilots indeed utilized a control strategy that was no longer purely compensatory. Under such conditions, the proposed combined compensatory and feedforward pilot model was found to provide a consistently more accurate fit of the measured control inputs than a purely compensatory pilot model. The same pilot model extension was therefore also applied for quantifying pilot control behavior in the roll attitude ramp-tracking tasks with physical motion feedback in Chapter 7.

9.1.2 Effects of Motion Filter Settings on Tracking Behavior

The main objective of this thesis is to indicate which simulator motion cueing settings yield the highest level of behavioral simulator motion fidelity, that is, yield the best match of pilot control dynamics between flight simulator and real flight. An important step towards this goal is the collection of measurements of pilot tracking behavior under varying motion cueing settings, as this allows for analyzing the discrepancies that occur in pilot control behavior due to degraded simulator motion fidelity. In this thesis, a number of experiments that were performed in the SIMONA Research Simulator (SRS) at Delft University of Technology are described in which such changes in pilot tracking behavior due to variations in the supplied physical simulator motion cues were measured.

Chapter 4 describes an experiment performed in the SRS to evaluate the effects of variations in pitch and heave motion cueing on pilot pitch attitude tracking behavior. During aircraft pitch maneuvering with a conventional fixed-wing aircraft, relatively strong vertical heave motion cues are typically perceivable at the pilot station in addition to the rotational pitch motion. To evaluate the effects of both these cues on pilot control behavior, the presence of these pitch and heave motion cues was varied independently in this experiment. This experiment focused on the component of the total heave motion that directly results from the distance between the center of aircraft pitch rotation and the aircraft cockpit and that is hence directly proportional to the aircraft pitch rotation. For cueing this heave motion component, a number of different motion cueing conditions were considered, ranging

from one-to-one presentation, to scaled-down heave motion, and heave motion attenuated by a third-order high-pass filter. Analysis of pilot manual control behavior using estimated multimodal pilot model parameters showed that highly similar pilot control dynamics were adopted in the presence of either simulator pitch or heave motion, if these motion cues were both presented without attenuation. Furthermore, a strong effect of variations in simulator heave motion cueing settings on pilot tracking behavior was observed. When the fidelity of the supplied heave motion cues was reduced, either by decreasing the heave motion cueing gain or by attenuating the aircraft heave motion with a third-order high-pass washout filter, pilot tracking behavior was found to clearly show adaptation towards behavior representative for tracking without physical motion feedback (single-loop tracking), indicative of reduced usage of the supplied motion feedback.

A number of investigations predating the work described in this thesis have been performed in which the effects of variations in high-pass simulator motion filter settings on pilot tracking behavior and performance were evaluated explicitly, using behavioral metrics equivalent to those considered in this thesis. **Chapter 5** provided an overview of ten of these experiments and described an effort to compile the data of these different experiments in order to identify consistent across-experiment trends. The compiled experimental measurements showed consistently enhanced tracking performance with increasing simulator motion fidelity. In addition, simulator motion that better approximated the true aircraft motion was found to result in tracking behavior with higher pilot visual response gains, reduced visual lead equalization, and increased pilot visual response delays. Using the motion filter gain at 1 rad/s – which is also used as a metric of simulator motion fidelity in the well-known motion fidelity criteria proposed by Sinacori [1977] and Schroeder [1999] – as the predictor variable, linear regression models were fit to the compiled behavioral measurements. From these linear regressions, a set of equations was deduced with which changes in pilot tracking performance and behavior due to the selection of certain high-pass motion filter setting can be predicted. In Chapter 8 these equations were used to predict changes in pilot tracking behavior for the wide range of different roll motion filter settings considered in the experiment described there. Despite the fact that the observed trends in the measurements were found to be slightly stronger than those predicted by the derived equations, a reasonably adequate prediction of the changes in pilot tracking behavior was still found to be obtained with these linear prediction equations.

The roll attitude tracking experiments of **Chapters 6–8** showed relative changes in pilot control dynamics as a result of the considered variations in roll motion cueing that were highly consistent with those reported in Chapter 5. These three experiments evaluated pilot roll tracking behavior for a wide variation in the gain and break frequency settings of a first-order high-pass roll motion filter. Overall, these three experiments confirmed many of the behavioral changes due to varying motion cueing settings identified in Chapter 5. Both for the roll tracking tasks with only multisine forcing functions considered in Chapters 6 and 8 and for the roll ramp-tracking task evaluated in Chapter 7, behavioral analysis with multimodal pilot models showed reduced pilot gains and increased visual lead equalization for conditions with decreased simulator motion fidelity. In the roll ramp-tracking task of Chapter 7 pilots further showed increased latency in their feedforward response for conditions where the roll motion was lower fidelity. The experiment described in Chapter 8, which considered the widest variation in roll motion filter settings, suggested that pilot tracking

behavior in the considered target-following and disturbance-rejection task is affected more strongly by the scaling of the supplied roll motion, as controlled by the motion filter gain, than by increasing roll washout. This is, for instance, consistent with the effects of motion attenuation on pilot control behavior reported by Schroeder et al. [2000], who state that variations in motion filter gain most strongly affect pilot control behavior in control tasks where external disturbances are to be mitigated.

In conclusion, all these different experiments that evaluated the effects of varying simulator motion filter settings on pilot tracking behavior show a strong consistency in their results despite considerable differences in important task variables, such as the considered controlled element dynamics and forcing function settings. Clear differences between tracking behavior for tasks without physical motion feedback and tracking behavior for tasks with one-to-one, or closest to one-to-one, simulator motion are observed in all cases. Furthermore, measured tracking behavior for conditions with attenuated and filtered simulator motion is typically found to be somewhere in between these two extreme cases. The most notable behavioral adaptation observed with varying simulator motion fidelity is found to occur in pilots' responses to visually presented tracking errors. Reducing the objective level of simulator motion fidelity is found to yield a decreased gain of pilots' visual responses. In addition, a strong increase in the amount of visual lead equalization and a decrease in the delay of the visual response suggest a control strategy with increased pilot workload under conditions with low-fidelity motion cueing.

9.1.3 In-Flight and Simulator Tracking Behavior Comparisons

As the experiments described in **Chapters 6–8** show, the collection of true in-flight reference measurements of the evaluation of simulator motion fidelity described in this thesis was largely successful. For both the multisine tracking task described in Chapters 6 and 8 and for the combined multisine and ramp tracking task of Chapter 7, pilot control behavior closely resembling that observed in the simulator parts of these experiments was observed for the in-flight measurements collected with the Cessna Citation II laboratory aircraft. Furthermore, important behavioral metrics such as the pilot visual response gain and lead time constant from the in-flight tracking tasks were found to best match those obtained when simulator motion cues were presented close to one-to-one. However, some notable behavioral discrepancies between the in-flight and simulator tracking tasks, which were much larger than thought to be attributable to differences in the supplied motion feedback, were still observed. The most notable of these differences in tracking behavior were an increased visual response delay and slightly decreased pilot visual and motion response gains for the in-flight tracking tasks compared to the conditions with the objectively highest level of simulator motion fidelity.

Due to the known adaptability of pilot tracking behavior to all factors that affect the control task that is to be performed, extreme care was taken to verify the equivalence of the experiment setups in the SRS and the laboratory aircraft. As this equivalence was even explicitly verified with additional reference measurements of pilot tracking behavior, the observed behavioral discrepancies between these in-flight and simulator tracking tasks are thought to have resulted from differences in *operator-centered variables* such as motivation and stress, which are impossible to fully control in an experimental setting. Rather than

purely representing a behavioral adaptation to the different motion cues perceived in real flight compared to those presented in the simulator, the observed behavioral discrepancies might also be (partially) attributable to a failure to properly isolate the effect of the variations in the supplied motion feedback. If, as for instance argued by Schroeder and Grant [2010], pilots do not perform control tasks with the same level of motivation or intensity in real flight and in a flight simulator, then this may also result in behavioral discrepancies similar to those observed in the experiments of Chapters 6 and 7. The success of the application of the cybernetic approach to the comparison of in-flight and simulator measurements of pilot tracking behavior – in-flight to simulator comparisons in general – hinges on the assumption that *only* the task variables that are manipulated in this comparison induce behavioral adaptation. The experimental results described in this thesis suggest that this main assumption may in fact be violated.

9.1.4 The Cybernetic Approach

The cybernetic, model-based approach used in this thesis was found to provide a valuable method for measuring, quantifying, and assessing the effects of simulator motion fidelity on pilot control behavior. The method based on multimodal pilot models allowed for clear and objective quantification of changes in pilot tracking behavior under varying simulator motion cueing settings. Furthermore, these observed differences in manual control behavior indicated stronger and much more consistent effects of varying simulator motion fidelity than were obtained from subjective motion fidelity ratings. In addition, compared to earlier comparisons of in-flight and simulator measurements of pilot tracking behavior [Smith, 1966; Newell and Smith, 1969; Mooij, 1973; Van Gool and Mooij, 1976; Steurs et al., 2004], the use of *multimodal* pilot models was found to allow for superior quantification of the effects of physical aircraft motion feedback on pilot tracking behavior.

Despite being an elegant and insightful method for evaluating the effects of simulator motion cueing settings on pilot tracking behavior, the cybernetic approach as adopted in this thesis is not the most straightforward method to apply. First of all, collecting measurements of pilot tracking behavior is a time-consuming affair, because of the required amount of task familiarization and training, the collection of repeated measurements to ensure stationary behavior, and the considerable number of samples and hence participants required to obtain meaningful results. Not counting test runs and tracking runs that were not completed, a total amount of 3,516 tracking runs were logged over the different main experiments described in this thesis. Per participant, this yields an average of 113 tracking runs that were performed for each experiment. In addition to the extensive required data collection, application of the cybernetic approach is further complicated due to the overdetermined multimodal pilot models that are required for describing pilots' cumulative responses to visual and physical motion cues. For this reason, considerable knowledge of mathematical modeling, simulation, and the implementation of optimization techniques, such as the time-domain identification procedure described by Zaal et al. [2009a], is required for correct and meaningful implementation of the proposed approach.

The multimodal pilot models considered in this thesis include two independent parallel model channels that explicitly account for pilots' responses to visually presented tracking errors and physical motion feedback, respectively. This thesis shows that such models are

highly valuable for evaluating and quantifying the extent to which visual and physical motion stimuli are utilized during skill-based manual control. However, these multimodal pilot models are still a heavily simplified control-theoretical representation of the complex motion perception, multisensory integration, and control input generation processes that actually occur during manual control in multimodal environments [Zacharias and Young, 1981; Van der Steen, 1998; Bos et al., 2001; Bos and Bles, 2002; Berger, 2006; De Vrijer et al., 2008; Butler et al., 2010]. For this reason, the increased understanding of these low-level perceptual processes that can be gained from analysis with these multimodal pilot models is still severely limited. This is for instance clear from the fact that in the models of pilot control behavior used in this thesis, the contributions the different modalities that play a role in physical motion perception – the vestibular, the tactile, the proprioceptive, and perhaps even the auditory modalities [Gum, 1973; Borah et al., 1988; Zaichik et al., 1999] – can not be considered separately. As the semicircular canals have been argued to be dominant motion sensor for perceiving physical angular motion [Young, 1966; Hosman and Van der Vaart, 1978], the contributions of these different modalities are instead lumped into a pilot motion response that is modeled to purely result from this dominant vestibular modality. A similar problem occurs with the separation of the effects of multiple physical motion stimuli on pilot tracking behavior, such as the correlated pitch and heave motion cues considered in Chapter 4. One of the main limitations of the cybernetic approach is the difficulty of distinguishing between such clearly distinct contributions to physical motion perception and its effect on manual control behavior. Theoretically, further separation of these different contributions to the pilot motion responses modeled in this thesis may be possible by using additional forcing function signals to ensure unique excitation of the different associated modalities. When measuring human manual control behavior, however, the available room for such manipulation of perceived information through the use of additional forcing function signals is limited, as this will affect the adopted control strategy itself [McRuer and Jex, 1967a; Zaal et al., 2009c]. Furthermore, perturbing the information perceived through a single modality compared to all others will affect the perceived realism of the presented stimuli, as these are normally consistent across different modalities in the real world.

This thesis describes a number of experiments in which measurements of manual tracking behavior were collected with active Cessna Citation II pilots as subjects (Chapters 6–8) and with subjects that were non-pilots or had only limited piloting experience (Chapters 2, 3, and 4). Overall, the experiments that evaluated the effects of physical motion feedback and of differences in the cueing of this physical motion feedback on the adopted control strategy show results that are highly consistent over the experiments performed with pilot and non-pilot subjects. A similar agreement between the results of tracking experiments performed with pilots and non-pilot subjects has, for instance, previously been reported by Jex et al. [1981]. The main reason for this equivalence in tracking behavior, and the consistency in the relative effects of experimental manipulation on this tracking behavior, for pilots and non-pilot subjects is thought to be the nature of the considered tracking tasks themselves. Compared to more low-bandwidth control tasks, the high-bandwidth tracking tasks considered in this thesis do not allow for much variability in control behavior without a severe degradation in task performance and closed-loop stability. Given enough time for learning, both pilots and non-pilots will therefore end up with highly comparable control

dynamics for these tasks. The comparatively “universal” adaptation to changes in motion cueing settings observed in the experiments described in this thesis further suggests that there is no reason to discount experiments in which the participants were non-pilots on this basis. This is especially valuable, given the severely limited amount of experimental data available for evaluating simulator motion fidelity from a behavioral perspective.

9.2 Recommendations

The evaluation of behavioral simulator fidelity performed in this thesis was limited to single-axis aircraft attitude tracking tasks. Even though such single-axis tracking tasks allow for studying elementary skill-based manual control behavior, such tasks typically do not account for much of the complexity of manual control in operational environments. Given the known adaptability of human manual control behavior, it is therefore difficult to predict to what extent the conclusions drawn from studying single-axis tracking behavior, as done in this thesis to evaluate simulator motion cueing fidelity, translate to true operational manual control tasks. Despite the tremendous complexity and extreme multidimensionality of that problem, it is strongly recommended that in future research into manual control behavior significant effort is dedicated to bringing our knowledge of pilot control behavior in true manual aircraft control tasks up to par with our current knowledge of single-axis tracking behavior. Some important research questions that need to be addressed for increasing our understanding of manual control behavior in real manual flying tasks, and how it relates to single-axis tracking, are, for instance:

1. In single-axis tracking tasks, pilots have their full attention available for controlling one degree-of-freedom. In real flight, it is typically not a single degree-of-freedom that is being controlled, but attention needs to be paid to the full aircraft position and attitude. Some experiments have suggested that if more than one degree-of-freedom is being controlled, pilots adapt their control dynamics and the level of control performance may degrade compared to the situation where the different degrees-of-freedom are controlled individually [Bergeron, 1970; Hess and Siwakosit, 2001]. Dividing attention over multiple degrees-of-freedom may therefore also affect the pilots’ reliance of physical motion feedback during manual control, which has not yet been studied extensively.
2. During real flight, pilots typically control and stabilize the aircraft attitude as an inner loop, where the aircraft position in space is actually being controlled in outer, navigation, loops [Hosman et al., 2001; Nieuwenhuizen et al., 2009; Zeyada and Hess, 2003; Mulder et al., 2004]. Even though convincing effects of physical motion feedback on pure inner-loop control behavior have been reported in numerous studies, the extent to which these effects persist when an additional outer loop is to be closed by pilots, and if motion feedback also contributes to outer-loop control itself, is as of yet largely unknown.
3. In the tracking tasks considered in this thesis, only a part of the multisensory environment available during real flight (heads-down display and physical motion) was

presented to allow for the isolated studying of the effects of physical motion feedback on manual control behavior. One of the gross simplifications compared to many real-world applications is the omission of immersive outside visual and peripheral visual cues, whose presence have also been shown to have an effect on pilot tracking behavior [Hosman, 1996; Van der Vaart, 1992; Zaal et al., 2006]. Given that the information on the vehicle motion that is perceivable through physical motion feedback and from such additional visual cues is largely equivalent, the effects of degraded simulator motion fidelity on pilot manual control behavior may also be affected by the presence of these additional visual cues.

The application of a cybernetic model-based approach as utilized in this thesis to such more complex and realistic manual control tasks requires the current state of behavioral models and corresponding analysis methods to be extended significantly. In addition to the challenge of developing mathematical models capable of capturing the simultaneous closure of multiple loops by the pilot, an additional issue with the modeling of pilot control behavior in realistic flying tasks is that the adopted control behavior is most likely no longer continuous and stationary, as it is forcibly made to be during single-axis compensatory tracking tasks. This implies that the modeling of manual control behavior for such realistic flying tasks will require behavioral models with *time-varying* and *nonlinear* elements. Even though an extensive body of literature is available on approaches to the modeling and identification of systems with time-varying and nonlinear dynamics, with respect to studying human manual control behavior such time-varying modeling and identification techniques have received only modest attention [Phatak and Bekey, 1969; Boer and Kenyon, 1998; Thompson et al., 2001; Hess, 2009; Zaal et al., 2011]. An emphasis on the development of such time-varying analysis methods for application to manual control behavior is therefore strongly recommended.

With the increasing number of functions performed by automatic control systems, and their ever increasing reliability, some have argued that the amount of skill-based manual aircraft control required of pilots might diminish in the future, leaving pilots with the task of mainly operating at the knowledge-based and rule-based levels in supervising the available automation. Still, given the perhaps impossible task of preparing automation for the myriad of system failures and unanticipated events that may occur, which human operators to this day are better capable of coping with than any available control algorithms or automation, it is still unlikely that humans will soon be taken out of the control loop entirely [Westbrook, 1959; Young, 1969; Flach, 2011]. As stated by Young in a 1969 paper: “*Man’s adaptability as a controller is frequently cited as the primary reason for incorporating him in complex vehicle control loops*”. For this reason, it is recommended to increase the emphasis on the explicit studying of the adaptive mechanisms that allow human operators to cope with sudden changes in important task variables during manual control, and the limits of their performance in doing so.

The experiments described in this thesis considered motion cueing in one or two coupled degrees-of-freedom, where different motion cueing settings were mostly defined as different settings of the gain and break frequency of linear high-pass motion filters. Even though such high-pass filters are the cornerstone of most motion cueing algorithms [Schmidt and Conrad, 1970; Reid and Nahon, 1985; Telban et al., 2000] and characterize the main distor-

tions of simulator motion cues compared to real flight, much more advanced simulator motion cueing algorithms have been developed and are frequently applied in flight simulation. An example of such more advanced motion cueing solutions are the different approaches that have been proposed to obtain the best possible cueing and coordination of simulator roll and lateral specific force cues for coordinated lateral aircraft maneuvers [Schmidt and Conrad, 1970; Jex et al., 1981; Ariel and Sivan, 1984; Chung et al., 1998; Mikula et al., 1999; Schroeder, 1999; Van Biervliet, 2007]. A significant amount of research has also been dedicated to the development of nonlinear adaptive motion filter algorithms, in which the strength of the motion attenuation is updated on-line through an adaptive optimization scheme [Parrish et al., 1975; Riedel and Hofmann, 1978; Ariel and Sivan, 1984; Nahon et al., 1992; Naseri and Grant, 2005]. As opposed to non-adaptive algorithms, such adaptive motion filters eliminate the requirement of having to tune a motion filter algorithm for the worst possible case. Thereby such algorithms have the capacity to always ensure high-fidelity cueing for low-amplitude motion and only attenuating the supplied simulator motion when it is in fact required. Finally, it has been proposed in a number of publications to integrate the motion cueing algorithm with the motion base control software, thereby yielding a closed-loop motion cueing implementation that can explicitly account for the effect of simulator motion system dynamics on the supplied motion cues [Idan and Nahon, 1999; Grant et al., 2007; Chang et al., 2009]. Despite the fact that for the experiments described in this thesis only the effects of linear high-pass washout filter settings on pilot tracking behavior were quantified using the adopted cybernetic approach, there are no restrictions that would preclude the application of the same cybernetic approach to the evaluation, comparison, and validation of the these more advanced motion cueing implementations. Such comparison of these different approaches to simulator motion cueing using behavioral measurements is one of the major items that future research into simulator motion fidelity should focus on.

In this thesis, the proposed method for evaluating flight simulator motion fidelity based on measured pilot manual control behavior was limited to the comparison of in-flight measurements of manual control behavior and equivalent measurements collected in a flight simulator environment under a limited number of different pre-defined simulator motion cueing settings. If baseline in-flight behavioral measurements are available, the adopted cybernetic approach, however, also allows for true optimization of simulator motion cueing and motion filter parameter settings. Such motion cueing optimization can for instance be performed through an iterative scheme consisting of the following steps:

- collection of behavioral measurements under a number of different motion cueing conditions,
- evaluation of the resulting behavioral discrepancies with respect to real flight,
- identification of the motion cueing settings that yield the smallest behavioral discrepancies, and
- formulation of a new set of motion cueing conditions to evaluate.

Note that in this thesis only a single iteration of steps 1-3 was performed, corresponding to the evaluation of Block ③, the “ Δ ” block, and Block ④ shown in Fig. 1.8, respectively.

Though not attempted in this thesis, such further iterative optimization of simulator motion cueing strategies and motion filter parameter settings based on the minimization of behavioral discrepancies compared to real flight is considered a valuable approach for improving flight simulator motion cueing and should be explored in more depth in future research.

For the experiments described in Chapters 6 and 7, significant discrepancies between pilot control behavior measured in real flight and in a simulator environment were observed that were found to not be attributable to differences in factors external to the pilots. With the adopted cybernetic approach and the setup of these experiments, it is not possible to distinguish between changes in pilot control behavior that result from differences in, for instance, the supplied motion feedback and operator-centered factors such as motivation, stress, or workload. Schroeder and Grant [2010] also suggest that this may be a crucial factor in the type of experiments as described in this thesis, due to the typically adopted assumption that other than adapting to the applied variation in the task variable under consideration, the pilot is an otherwise constant element in the pilot-vehicle control system. The observed discrepancies between real-flight pilot control behavior and that measured in a simulator environment suggests that perhaps pilot control dynamics may in fact also be affected by such factors internal to the pilots themselves. Though extremely difficult to achieve in a controlled experiment, given the aims of most in-flight to simulator comparisons of pilot control behavior it is still strongly recommended to attempt to explicitly characterize and quantify possible differences in behavior that may result from such pilot-centered factors.

The experiments described in this thesis have shown that for a comparatively wide range of control tasks pilot manual control behavior is affected by variations in simulator motion cueing. Despite the fact that the observed changes in manual control behavior were considerable, the collected measurements can not be used to argue that the manual control skills developed during training with degraded physical motion feedback will degrade transfer to conditions with true aircraft motion, which may in fact be the question that is of interest to much of the flight simulator community. The results presented in this thesis do show that pilots will likely adapt their behavior if transferred to an environment with different fidelity motion feedback. The extent to which this adaptation is easily, straightforwardly, and quickly achieved, or requires extensive re-familiarization with the new situation, can, however, not be deduced from the reported experimental results. A number of researchers have suggested that this question is best answered by performing transfer-of-training and quasi-transfer-training studies [Caro, 1973; Bürki-Cohen et al., 1998; Hosman et al., 2001; Go et al., 2003; Nusseck et al., 2008; Sparko et al., 2010; Koglbauer et al., 2011; De Winter et al., 2012]. Most of the currently reported transfer-of-training studies only consider metrics of task performance for evaluating differences in training. More structural investigation of the underlying behavioral adaptation asked from pilots when transferred to an environment where important cues are presented differently, which would provide increased insight into the perceptual and control behavioral mechanisms that play a role in this adaptation, could be provided by utilizing a cybernetic approach as adopted in this thesis.

References

- Advani, S. K. and Hosman, R. J. A. W. (2006). Revising Civil Simulator Standards – An Opportunity for Technological Pull. In *Proceedings of the AIAA Modeling and Simulation Technologies Conference and Exhibit, Keystone (CO)*, number AIAA-2006-6248.
- Advani, S. K., Nahon, M. A., Haeck, N., and Albronda, J. (1999). Optimization of Six-Degrees-of-Freedom Motion Systems for Flight Simulators. *Journal of Aircraft*, 36(5):819–826.
- Advani, S. K., Schroeder, J. A., and Burks, B. (2010). What Really Can Be Done in Simulation to Improve Upset Training? In *Proceedings of the AIAA Modeling and Simulation Technologies Conference, Toronto, Canada*, number AIAA-2010-7791.
- Allen, L. D. (1993). Evolution of Flight Simulation. In *Proceedings of the AIAA Flight Simulation Technologies Conference, Monterey (CA)*, number AIAA-1993-3545.
- Allen, R. W. and Jex, H. R. (1968). An Experimental Investigation of Compensatory and Pursuit Tracking Displays with Rate and Acceleration Control Dynamics and a Disturbance Input. NASA Contractor Report NASA CR-1082, National Aeronautics and Space Administration, Washington, D.C.
- Allen, R. W. and McRuer, D. T. (1979). The Man/Machine Control Interface–Pursuit Control. *Automatica*, 15(6):683–686.
- Allerton, D. J. (2009). *Principles of Flight Simulation*. John Wiley and Sons, Ltd.
- Allerton, D. J. (2010). The impact of flight simulation in aerospace. *The Aeronautical Journal*, 114(1162):747–756. Paper No. 3581.
- Anonymous (1980). Fidelity of Simulation for Pilot Training. AGARD Advisory Report AGARD-AR-159, Advisory Group for Aerospace Research and Development, North Atlantic Treaty Organization. Edited by David L. Key.
- Anonymous (2003). Aeroplane Flight Simulators. JAR-STD 1A, Joint Aviation Authorities (JAA).
- Anonymous (2005). Aeroplane Flight Simulator Evaluation Handbook – International Standards for the Qualification of Aeroplane Flight Simulators. Technical report, Royal Aeronautical Society, 4 Hamilton Place, London. Third edition.

- Anonymous (2009). Manual of Criteria for the Qualification of Flight Simulation Training Devices. Volume 1 – Airplanes. ICAO Doc 9625, International Civil Aviation Organization. Third edition.
- Aponso, B. L., Beard, S. D., and Schroeder, J. A. (2009). The NASA Ames Vertical Motion Simulator – A Facility Engineered for Realism. In *Proceedings of the Royal Aeronautical Society Spring 2009 Flight Simulation Conference, London, UK*.
- Ariel, D. and Sivan, R. (1984). False Cue Reduction in Moving Flight Simulators. *IEEE Transactions on Systems, Man, and Cybernetics*, SMC-14(4):665–671.
- Ashkenas, I. L. (1986). Collected Flight and Simulation Comparisons and Considerations. In *AGARD Conference Proceedings Number 408, Flight Simulation*, volume AGARD-CP-408, pages 26–1–26–34. Advisory Group for Aerospace Research and Development, North Atlantic Treaty Organization.
- Ashkenas, I. L. and McRuer, D. T. (1962). A Theory of Handling Qualities Derived from Pilot-Vehicle System Considerations. *Aerospace Engineering*, 21(2):60–102.
- Baarspul, M. (1990). A Review of Flight Simulation Techniques. *Progress in Aerospace Sciences*, 27(1):1–120.
- Beerens, G. C., Damveld, H. J., Mulder, M., Van Paassen, M. M., and Van der Vaart, J. C. (2009). Investigation into Crossover Regression in Compensatory Manual Tracking Tasks. *Journal of Guidance, Control, and Dynamics*, 32(5):1429–1445.
- Benson, A. J. (1990). Sensory Functions and Limitations of the Vestibular System. In Warren, R. and Wertheim, A. H., editors, *Perception and Control of Self-Motion*, pages 145–170. Lawrence Erlbaum, Hillsdale, NJ, USA.
- Berger, D. R. (2006). *Sensor Fusion in the Perception of Self-Motion*. PhD thesis, Institute of Neural Information Processing, Faculty of Engineering and Computer Science, Ulm University, Germany.
- Bergeron, H. P. (1970). Investigation of Motion Requirements in Compensatory Control Tasks. *IEEE Transactions on Man-Machine Systems*, MMS-11(2):123–125.
- Berkouwer, W. R., Stroosma, O., Van Paassen, M. M., Mulder, M., and Mulder, J. A. (2005). Measuring the Performance of the SIMONA Research Simulator’s Motion System. In *Proceedings of the AIAA Modeling and Simulation Technologies Conference and Exhibit, San Francisco (CA)*, number AIAA-2005-6504.
- Beukers, J. T., Stroosma, O., Pool, D. M., Mulder, M., and Van Paassen, M. M. (2010). Investigation into Pilot Perception and Control During Decrab Maneuvers in Simulated Flight. *Journal of Guidance, Control, and Dynamics*, 33(4):1048–1063.
- Boer, E. R. and Kenyon, R. V. (1998). Estimation of Time-Varying Delay Time in Nonstationary Linear Systems: An Approach to Monitor Human Operator Adaptation in Manual Tracking Tasks. *IEEE Transactions on Systems, Man, and Cybernetics – Part A: Systems and Humans*, 28(1):89–99.

- Borah, J., Young, L. R., and Curry, R. E. (1988). Optimal Estimator Model for Human Spatial Orientation. *Annals of the New York Academy of Sciences*, 545:51–73.
- Borst, C., Sjer, F. A., Mulder, M., Van Paassen, M. M., and Mulder, J. A. (2008). Ecological Approach to Support Pilot Terrain Awareness After Total Engine Failure. *Journal of Aircraft*, 45(1):159–171.
- Bos, J. E. and Bles, W. (2002). Theoretical Considerations on Canal-Otolith Interaction and an Observer Model. *Biological Cybernetics*, 86(3):191–207.
- Bos, J. E., Bles, W., and Hosman, R. J. A. W. (2001). Modeling Human Spatial Orientation and Motion Perception. In *Proceedings of the AIAA Modeling and Simulation Technologies Conference and Exhibit, Montreal, Canada*, number AIAA-2001-4248.
- Bray, R. S. (1964). A Piloted Simulator Study of Longitudinal Handling Qualities of Supersonic Transports in the Landing Maneuver. NASA Technical Note NASA TN D-2251, National Aeronautics and Space Administration, Ames Research Center, Moffett Field (CA).
- Bray, R. S. (1985). Visual and Motion Cueing in Helicopter Simulation. Technical Memorandum NASA-TM-86818, NASA Ames Research Center, Moffett Field (CA).
- Bray, R. S. (1996). *Vertical Flight Training: An Overview of Training and Flight Simulator Technology with Emphasis on Rotary-Wing Requirements*, chapter 10: Cockpit Motion in Helicopter Simulation, pages 247–255. Number NASA-RP-1373. National Aeronautics and Space Administration, Ames Research Center, Moffett Field (CA).
- Brown, Y. J., Cardullo, F. M., and Sinacori, J. B. (1989). Need-Based Evaluation of Simulator Force and Motion Cueing Devices. In *AIAA Flight Simulation Technologies Conference and Exhibit, Boston (MA)*, number AIAA-1989-3272.
- Bryan, G. H. (1911). *Stability in Aviation. An Introduction to Dynamical Stability as applied to the Motion of Aeroplanes*. Macmillan and Co., Ltd., St. Martin's Street, London.
- Bürki-Cohen, J., Go, T. H., and Longridge, T. (2001). Flight Simulator Fidelity Considerations for Total Air Line Pilot Training and Evaluation. In *Proceedings of the AIAA Modeling and Simulation Technologies Conference and Exhibit, Montreal (CA)*, number AIAA-2001-4425.
- Bürki-Cohen, J., Soja, N. N., and Longridge, T. (1998). Simulator Platform Motion – The Need Revisited. *International Journal of Aviation Psychology*, 8(3):293–317.
- Butler, J. S., Smith, S. T., Campos, J. L., and Bühlhoff, H. H. (2010). Bayesian integration of visual and vestibular signals for heading. *Journal of Vision*, 10(11).
- CAE (2009). CAE 7000 Series full-flight simulator: The customized solution for a seamless training experience. <http://www.cae.com/en/sim.products/cae.7000.series.asp>. Visited: 10 November 2009.

- Cameron, N., Thomson, D. G., and Murray-Smith, D. J. (2003). Pilot modelling and inverse simulation for initial handling qualities assessment. *The Aeronautical Journal*, 107(1074):511–520. Paper No. 2792.
- Caro, P. W. (1973). Aircraft Simulators and Pilot Training. *Human Factors*, 15(6):502–509.
- Chang, Y.-H., Liao, C.-S., and Chieng, W.-H. (2009). Optimal motion cueing for 5-DOF motion simulations via a 3-DOF motion simulator. *Control Engineering Practice*, 17(1):170–184.
- Chernikoff, R., Birmingham, H. P., and Taylor, F. V. (1955). A Comparison of Pursuit and Compensatory Under Conditions of Aiding and No Aiding. *Journal of Experimental Psychology*, 49(1):55–59.
- Chung, W. W. Y. (2000). A Review of Approaches to Determine the Effectiveness of Ground-Based Flight Simulations. In *Proceedings of the AIAA Modeling and Simulation Technologies Conference, Denver (CO)*, number AIAA-2000-4298.
- Chung, W. W. Y. (2008). A Preliminary Investigation of Achievable Motion Cueing in Ground-Based Flight Simulators for Upset Recovery Maneuvers. In *Proceedings of the AIAA Modeling and Simulation Technologies Conference and Exhibit, Honolulu (HI)*, number AIAA-2008-6868.
- Chung, W. W. Y., Robinson, D. J., Wong, J., and Tran, D. (1998). Investigation of Roll-Lateral Coordinated Motion Requirements with a Conventional Hexapod Motion Platform. In *Proceedings of the AIAA Modeling and Simulation Technologies Conference and Exhibit, Boston (MA)*, number AIAA-1998-4172.
- Cohen, J. (1977). *Statistical Power Analysis for the Behavioral Sciences*. Academic Press, Inc., 111 Fifth Avenue, New York.
- Conrad, B., Douvillier, J. G., and Schmidt, S. F. (1973). Washout Circuit Design for Multi-Degrees-Of-Freedom Moving Base Simulators. In *Proceedings of the AIAA Visual and Motion Simulation Conference, Palo Alto (CA)*, number AIAA-1973-929.
- Damveld, H. J. (2009). *A Cybernetic Approach to Assess the Longitudinal Handling Qualities of Aeroelastic Aircraft*. PhD thesis, Delft University of Technology, Faculty of Aerospace Engineering.
- Damveld, H. J., Abbink, D. A., Mulder, M., Mulder, M., Van Paassen, M. M., Van der Helm, F. C. T., and Hosman, R. J. A. W. (2009). Measuring the Contribution of the Neuromuscular System During a Pitch Control Task. In *Proceedings of the AIAA Modeling and Simulation Technologies Conference, Chicago (IL)*, number AIAA-2009-5824.
- Damveld, H. J., Beerens, G. C., Van Paassen, M. M., and Mulder, M. (2010). Design of Forcing Functions for the Identification of Human Control Behavior. *Journal of Guidance, Control, and Dynamics*, 33(4):1064–1081.

- De Vrijer, M., Medendorp, W. P., and Van Gisbergen, J. A. M. (2008). Shared Computational Mechanism for Tilt Compensation Accounts for Biased Verticality Percepts in Motion and Pattern Vision. *Journal of Neurophysiology*, 99:915–930.
- De Vroome, A. M., Valente Pais, A. R., Pool, D. M., Van Paassen, M. M., and Mulder, M. (2009). Identification of Motion Perception Thresholds in Active Control Tasks. In *Proceedings of the AIAA Modeling and Simulation Technologies Conference, Chicago (IL)*, number AIAA-2009-6243.
- De Winter, J. C. F., Dodou, D., and Mulder, M. (2012). Training Effectiveness of Whole Body Flight Simulator Motion: A Comprehensive Meta-Analysis. *International Journal of Aviation Psychology*, 22(2):164–183.
- Dehouck, T. L., Mulder, M., and Van Paassen, M. M. (2006). The Effects of Simulator Motion Filter Settings on Pilot Manual Control Behaviour. In *Proceedings of the AIAA Modeling and Simulation Technologies Conference and Exhibit, Keystone (CO)*, number AIAA-2006-6250.
- Drop, F. M. (2011). Feed Forward Behavior in Manual Control Tasks With Predictable Target Signals. Master's thesis, Delft University of Technology.
- Durlach, N., Allen, G., Darken, R., Garnett, R. L., Loomis, J., Templemann, J., and von Wiegand, T. E. (2000). Virtual Environments and the Enhancement of Spatial Behavior: Towards a Comprehensive Research Agenda. *Presence: Teleoperators and Virtual Environments*, 9(6):593–615.
- Elkind, J. I. (1956). *Characteristics of Simple Manual Control Systems*. PhD thesis, Massachusetts Institute of Technology.
- Ellerbroek, J., Stroosma, O., Mulder, M., and Van Paassen, M. M. (2008). Role Identification of Yaw and Sway Motion in Helicopter Yaw Control Tasks. *Journal of Aircraft*, 45(4):1275–1289.
- Feddersen, W. E. (1962). The Role of Motion Information and Its Contribution to Simulation Validity. Report D228-429-001, Bell Helicopter Company.
- Ferguson, S. W., Clement, W. F., Cleveland, W. B., and Key, D. L. (1984). Assessment of Simulation Fidelity Using Measurements of Piloting Technique in Flight. In *40th American Helicopter Society Annual Forum, Arlington (VA), May 16-18*, pages 67–92.
- Fernandez, C. and Goldberg, J. M. (1971). Physiology of Peripheral Neurons Innervating Semicircular Canals of the Squirrel Monkey. II. Response to Sinusoidal Stimulation and Dynamics of Peripheral Vestibular System. *Journal of Neurophysiology*, 34(4):661–675.
- Field, A. (2005). *Discovering Statistics Using SPSS*. ISM Introducing Statistical Methods. SAGE Publications Ltd., second edition.

- Field, E. J., Armor, J. B., and Rossitto, K. F. (2002a). Effects of Pitch Instantaneous Center of Rotation Location on Flying Qualities. In *Proceedings of the AIAA Modeling and Simulation Technologies Conference and Exhibit, Monterey (CA)*, number AIAA-2002-4799.
- Field, E. J., Armor, J. B., Rossitto, K. F., Schroeder, J. A., and Weingarten, N. C. (2002b). Comparison of In-Flight and Ground Based Simulations of Large Aircraft Flying Qualities. In *Proceedings of the AIAA Atmospheric Flight Mechanics Conference and Exhibit, Monterey (CA)*, number AIAA-2002-4800.
- Flach, J. M. (2011). Complexity: learning to muddle through. *Cognition, Technology & Work*.
- Go, T. H., Bürki-Cohen, J., Chung, W. W. Y., Schroeder, J. A., Saillant, G., Jacobs, S., and Longridge, T. (2003). The Effects of Enhanced Hexapod Motion on Airline Pilot Recurrent Training and Evaluation. In *Proceedings of the AIAA Modeling and Simulation Technologies Conference and Exhibit, Austin (TX)*, number AIAA-2003-5678.
- Gorsira, M. F. B. (1993). Development of a Control System Design for the Elevator Flight Controls of the Citation II. Master's thesis, Delft University of Technology.
- Gouverneur, B., Mulder, J. A., Van Paassen, M. M., Stroosma, O., and Field, E. J. (2003). Optimisation of the SIMONA Research Simulator's Motion Filter Settings for Handling Qualities Experiments. In *Proceedings of the AIAA Modeling and Simulation Technologies Conference and Exhibit, Austin (TX)*, number AIAA-2003-5679.
- Grant, P. R. (1996). *The Development of a Tuning Paradigm for Flight Simulator Motion Drive Algorithms*. PhD thesis, University of Toronto, Institute for Aerospace Studies.
- Grant, P. R., Advani, S. K., Liu, Y., and Haycock, B. (2007). An Iterative Learning Control Algorithm for Simulator Motion System Control. In *Proceedings of the AIAA Modeling and Simulation Technologies Conference and Exhibit, Hilton Head (SC)*, number AIAA-2007-6471.
- Grant, P. R. and Reid, L. D. (1997a). Motion Washout Filter Tuning: Rules and Requirements. *Journal of Aircraft*, 34(2):145–151.
- Grant, P. R. and Reid, L. D. (1997b). PROTEST: An Expert System for Tuning Simulator Washout Filters. *Journal of Aircraft*, 34(2):152–159.
- Grant, P. R. and Schroeder, J. A. (2010). Modelling Pilot Control Behaviour for Flight Simulator Design and Assessment. In *Proceedings of the AIAA Guidance, Navigation, and Control Conference, Toronto, Canada*, number AIAA-2010-8356.
- Grant, P. R., Yam, B., Hosman, R. J. A. W., and Schroeder, J. A. (2006). Effect of Simulator Motion on Pilot Behavior and Perception. *Journal of Aircraft*, 43(6):1914–1924.
- Groen, E. L., Smaili, M. H., and Hosman, R. J. A. W. (2007). Perception Model Analysis of Flight Simulator Motion for a Decrab Maneuver. *Journal of Aircraft*, 44(2):427–435.

- Groen, E. L., Valenti Clari, M. S. V., and Hosman, R. J. A. W. (2001). Evaluation of Perceived Motion during a Simulated Takeoff Run. *Journal of Aircraft*, 38(4):600–606.
- Groen, E. L., Wentink, M., Valente Pais, A. R., Mulder, M., and Van Paassen, M. M. (2006). Motion Perception Thresholds in Flight Simulation. In *Proceedings of the Modeling and Simulation Technologies Conference and Exhibit, Keystone, Colorado, Aug. 21-24*, number AIAA-2006-6254.
- Gum, D. R. (1973). Modeling of the Human Force and Motion-Sensing Mechanisms. Technical Report AFHRL-TR-72-54, Air Force Human Resources Laboratory, Wright-Patterson Air Force Base (OH).
- Gundry, A. J. (1977). Thresholds to Roll Motion in a Flight Simulator. *Journal of Aircraft*, 14(7):624–631.
- Hagiwara, T., Advani, S. K., Funabiki, K., Wakairo, K., Muraoka, K., and Nojima, T. (2008). Evaluating an Objective Method for Motion Cueing Fidelity. In *Proceedings of the AIAA Modeling and Simulation Technologies Conference and Exhibit, Honolulu (HI)*, number AIAA-2008-6542.
- Hall, I. A. M. (1963). Study of the Human Pilot as a Servo Element. *Journal of the Royal Aeronautical Society*, 67:351–360.
- Heffley, R. K. (1982). Pilot Models for Discrete Maneuvers. In *Proceedings of the AIAA Guidance and Control Conference, San Diego (CA)*, number AIAA-1982-1519, pages 132–142.
- Heffley, R. K., Clement, W. F., Ringland, R. F., Jewell, W. F., Jex, H. R., McRuer, D. T., and Carter, V. E. (1981). Determination of Motion and Visual System Requirements for Flight Training Simulators. Technical Report 546, U.S. Army Research Institute for the Behavioral and Social Sciences.
- Heffley, R. K. and Schulman, T. M. (1981). A Comparison of Landing Maneuver Piloting Technique Based on Measurements Made in an Airline Training Simulator and in Actual Flight. In *Proceedings of the Seventeenth Annual Conference on Manual Control*, pages 223–234.
- Heffley, R. K., Schulman, T. M., Randle, Jr., R. J., and Clement, W. F. (1982). An Analysis of Airline Landing Flare Data Based on Flight and Training Simulator Measurements. STI Technical Report 1172-1R, Systems Technology, Inc., Mountain View (CA).
- Hensen, R. H. A., Van de Molengraft, M. J. G., and Steinbuch, M. (2002). Frequency Domain Identification of Dynamic Friction Model Parameters. *IEEE Transactions on Control Systems Technology*, 10(2):191–196.
- Hess, R. A. (1981). Pursuit Tracking and Higher Levels of Skill Development in the Human Pilot. *IEEE Transactions on Systems, Man, and Cybernetics*, SMC-11(4):262–273.
- Hess, R. A. (1990a). Analyzing Manipulator and Feel System Effects in Aircraft Flight Control. *IEEE Transactions on Systems, Man, and Cybernetics*, 20(4):923–931.

- Hess, R. A. (1990b). Model for Human Use of Motion Cues in Vehicular Control. *Journal of Guidance, Control, and Dynamics*, 13(3):476–482.
- Hess, R. A. (1995). A Model-Based Analysis of Handling Qualities and Adverse Aircraft-Pilot Coupling in High Angle of Attack Flight. In *Proceedings of the 1995 IEEE International Conference on Systems, Man & Cybernetics, Vancouver, Canada*, pages 2663–2669.
- Hess, R. A. (2006). Simplified approach for modelling pilot pursuit control behaviour in multi-loop flight control tasks. *Proceedings of the Institution of Mechanical Engineers, Part G: Journal of Aerospace Engineering*, 220(2):85–102.
- Hess, R. A. (2009). Modeling Pilot Control Behavior with Sudden Changes in Vehicle Dynamics. *Journal of Aircraft*, 46(5):1584–1592.
- Hess, R. A. and Malsbury, T. (1991). Closed-loop Assessment of Flight Simulator Fidelity. *Journal of Guidance, Control, and Dynamics*, 14(1):191–197.
- Hess, R. A., Malsbury, T., and Atencio, Jr., A. (1993). Flight Simulator Fidelity Assessment in a Rotorcraft Lateral Translation Maneuver. *Journal of Guidance, Control, and Dynamics*, 16(1):79–85.
- Hess, R. A. and Marchesi, F. (2009). Analytical Assessment of Flight Simulator Fidelity Using Pilot Models. *Journal of Guidance, Control, and Dynamics*, 32(3):760–770.
- Hess, R. A. and Mnich, M. A. (1986). Identification of Pilot-Vehicle Dynamics from In-Flight Tracking Data. *Journal of Guidance, Control, and Dynamics*, 9(4):433–440.
- Hess, R. A. and Siwakosit, W. (2001). Assessment of Flight Simulator Fidelity in Multiaxis Tasks Including Visual Cue Quality. *Journal of Aircraft*, 38(4):607–614.
- Hettinger, L. J. and Haas, M., editors (2003). *Virtual and Adaptive Environments – Applications, Implications, and Human Performance Issues*. Lawrence Erlbaum Associates, Inc.
- Hosman, R. J. A. W. (1996). *Pilot's Perception and Control of Aircraft Motions*. PhD thesis, Delft University of Technology, Faculty of Aerospace Engineering.
- Hosman, R. J. A. W. (1999). Are Criteria for Motion Cueing and Time Delays Possible? In *Proceedings of the AIAA Modelling and Simulation Technologies Conference and Exhibit, Portland (OR)*, number AIAA-1999-4028.
- Hosman, R. J. A. W., Grant, P. R., and Schroeder, J. A. (2005). Pre and Post Pilot Model Analysis Compared to Experimental Simulator Results. In *AIAA Modeling and Simulation Technologies Conference and Exhibit, San Francisco (CA)*, number AIAA-2005-6303.
- Hosman, R. J. A. W., Hamman, B., Lehman, C., Pelchat, Y., and Schroeder, J. A. (2001). Summary of the Panel Discussion on Motion Cueing Requirements. In *Proceedings of the AIAA Modeling and Simulation Technologies Conference & Exhibit, Montreal, Canada*, number AIAA-2001-4253.

- Hosman, R. J. A. W. and Stassen, H. G. (1999). Pilot's perception in the control of aircraft motions. *Control Engineering Practice*, 7:1421–1428.
- Hosman, R. J. A. W., Van de Moesdijk, G. A. J., and Van der Vaart, J. C. (1979). Optimization and Evaluation of Linear Motion Filters. In *Fifteenth Annual Conference on Manual Control*, pages 213–242, Dayton (OH). Wright State University.
- Hosman, R. J. A. W. and Van der Vaart, J. C. (1978). Vestibular Models and Thresholds of Motion Perception. Results of Tests in a Flight Simulator. Internal Report LR-265, Delft University of Technology, Faculty of Aerospace Engineering.
- Idan, M. and Nahon, M. A. (1999). Off-Line Comparison of Classical and Robust Flight Simulator Motion Control. *Journal of Guidance, Control, and Dynamics*, 22(5):702–709.
- Jategaonkar, R. V. (2006). *Flight Vehicle System Identification: A Time Domain Methodology*, volume 216 of *AIAA Progress in Astronautics and Aeronautics Series*. American Institute of Aeronautics and Astronautics, first edition.
- Jex, H. R., Jewell, W. F., and Magdaleno, R. E. (1979). Effects of Various Lateral-Beam-Motion Washouts on Pilot Tracking and Opinion in the “LAMAR” Simulator. In *Proceedings of the Fifteenth Annual Conference on Manual Control*, pages 244–266. Wright State University, Dayton (OH).
- Jex, H. R., Magdaleno, R. E., Jewell, W. F., Junker, A. M., and McMillan, G. (1981). Effects on Target Tracking of Motion Simulator Drive-Logic Filters. Report AFAMRL-TR-80-134, Air Force Aerospace Medical Research Laboratory, Wright-Patterson Air Force Base (OH).
- Jex, H. R., Magdaleno, R. E., and Junker, A. M. (1978). Roll Tracking Effects of G-vector Tilt and Various Types of Motion Washout. In *Proceedings of the Fourteenth Annual Conference on Manual Control*, pages 463–502.
- Johnston, D. E. and Aponso, B. L. (1988). Design Considerations of Manipulator and Feel System Characteristics in Roll Tracking. Technical Report NASA CR-4111, National Aeronautics and Space Administration, Ames Research Center.
- Junker, A. M. and Replegle, C. R. (1975). Motion Effects on the Human Operator in a Roll Axis Tracking Task. *Aviation, Space, and Environmental Medicine*, 46(6):819–822.
- Kaljouw, W. J., Mulder, M., and Van Paassen, M. M. (2004). Multi-loop Identification of Pilot's Use of Central and Peripheral Visual Cues. In *Proceedings of the AIAA Modeling and Simulation Technologies Conference and Exhibit, Providence (RI)*, number AIAA-2004-5443.
- Knotts, L. H. and Bailey, R. E. (1988). Ground Simulator Requirements Based on In-Flight Simulation. In *Proceedings of the AIAA Flight Simulation Technologies Conference, Atlanta (GA)*, number AIAA-1988-4609, pages 191–197.

- Koglbauer, I., Kallus, K. W., Braunstingl, R., and Boucsein, W. (2011). Recovery Training in Simulator Improves Performance and Psychophysiological State of Pilots During Simulated and Real Visual Flight Rules Flight. *The International Journal of Aviation Psychology*, 21(4):307–324.
- Kosut, R. L. (1979). Nonlinear Optimal Cue-Shaping Filters for Motion Base Simulators. *Journal of Guidance, Control, and Dynamics*, 2(6):486–490.
- Krendel, E. S. and McRuer, D. T. (1960). A Servomechanics Approach to Skill Development. *Journal of the Franklin Institute*, 269(1):24–42.
- Lam, T. M., Mulder, M., Van Paassen, M. M., Mulder, J. A., and Van der Helm, F. C. T. (2009). Force–Stiffness Feedback in Uninhabited Aerial Vehicle Teleoperation with Time Delay. *Journal of Guidance, Control, and Dynamics*, 32(3):821–835.
- Lee, B. P., Rodchenko, V. V., Zaichik, L. E., and Yashin, Y. P. (2003). Simulation-To-Flight Correlation. In *Proceedings of the AIAA Modeling and Simulation Technologies Conference and Exhibit, Austin (TX)*, number AIAA-2003-5823.
- Levison, W. H. (1978). A Model for the Pilot’s Use of Roll-Axis Motion in Steady-State Tracking Tasks. BBN Report 3808, Bolt Beranek and Newman Inc., Cambridge (MA).
- Levison, W. H. and Junker, A. M. (1977). A Model for the Pilot’s use of Motion Cues in Roll-Axis Tracking Tasks. BBN Report 3528, Bolt Beranek and Newman Inc., Cambridge (MA).
- Lilliefors, H. W. (1967). On the Kolmogorov-Smirnov Test for Normality with Mean and Variance Unknown. *Journal of the American Statistical Association*, 62(318):399–402.
- Ljung, L. (1999). *System Identification Theory for the User*. Prentice Hall, Inc., second edition.
- Lombaerts, T. J. J., Smaili, M. H., Stroosma, O., Chu, Q. P., Mulder, J. A., and Joosten, D. A. (2009). Piloted Simulator Evaluation Results of New Fault-Tolerant Flight Control Algorithm. *Journal of Guidance, Control, and Dynamics*, 32(6):1747–1765.
- Lubbers, B. (2009). A Model of the Experimental Fly-By-Wire Flight Control System for the PH-LAB: Performing Flight Tests, System Identification and Parameter Estimation. Master’s thesis, Delft University of Technology.
- Maine, R. E. and Iliff, K. E. (1986). AGARD Flight Test Techniques Series Volume 3 on Identification of Dynamic Systems – Applications to Aircraft Part 1: The Output Error Approach. AGARDograph No. 300 AGARD-AG-300-VOL.3 PART I, North Atlantic Treaty Organization (NATO).
- McRuer, D. T. (1980). Human Dynamics in Man-Machine Systems. *Automatica*, 16(3):237–253.

- McRuer, D. T. (1988). Pilot Modeling. In *AGARD-LS-157 Advances in Flying Qualities*, pages 2–1–2–30. North Atlantic Treaty Organisation, Advisory Group for Aerospace Research and Development.
- McRuer, D. T., Ashkenas, I. L., and Guerre, C. L. (1960). A Systems Analysis View of Longitudinal Flying Qualities. Technical Report WADD-TR 60-43, Wright Air Development Division, Wright Patterson Air Force Base (OH).
- McRuer, D. T., Graham, D., Krendel, E. S., and Reisener, W. J. (1965). Human Pilot Dynamics in Compensatory Systems, Theory Models and Experiments with Controlled Element and Forcing Function Variations. Technical Report AFFDL-TR-65-15, Air Force Flight Dynamics Laboratory.
- McRuer, D. T., Hofmann, L. G., Jex, H. R., Moore, G. P., Phatak, A. V., Weir, D. H., and Wolkovitch, J. (1968). New Approaches to Human-Pilot/Vehicle Dynamic Analysis. Technical Report AFFDL-TR-67-150, Air Force Flight Dynamics Laboratory, Wright-Patterson Air Force Base (OH).
- McRuer, D. T. and Jex, H. R. (1967a). A Review of Quasi-Linear Pilot Models. *IEEE Transactions on Human Factors in Electronics*, HFE-8(3):231–249.
- McRuer, D. T. and Jex, H. R. (1967b). A Systems Analysis Theory of Manual Control Displays. In *Proceedings of the Third NASA-University Conference on Manual Control*, number NASA-SP-144, pages 9–28.
- McRuer, D. T. and Krendel, E. S. (1959). The Human Operator as a Servo System Element. *Journal of the Franklin Institute*, 267(5):381–403.
- McRuer, D. T. and Krendel, E. S. (1974). Mathematical Models of Human Pilot Behavior. AGARDograph AGARD-AG-188, Advisory Group for Aerospace Research and Development.
- Mehra, R. K. (1974). Optimal Input Signals for Parameter Estimation in Dynamic Systems – Survey and New Results. *IEEE Transactions on Automatic Control*, 19(6):753–768.
- Meiry, J. L. (1967). The Vestibular System and Human Dynamic Space Orientation. Technical Report NASA CR-628, Massachusetts Institute of Technology, Cambridge (MA).
- Mikula, J., Tran, D., and Chung, W. W. Y. (1999). Motion Fidelity Criteria for Roll-Lateral Translational Tasks. In *Proceedings of the AIAA Modeling and Simulation Technologies Conference and Exhibit, Portland (OR)*, number AIAA-1999-4329.
- Mitchell, D. G., Aponso, B. L., and Klyde, D. H. (1992). Effects of Cockpit Lateral Stick Characteristics on Handling Qualities and Pilot Dynamics. Technical Report NASA-CR-4443, National Aeronautics and Space Administration.
- Mooij, H. A. (1973). In-Flight Measured Human Pilot Describing Function and Remnant for Pitch Attitude Control. In *Proceedings of the Ninth Annual Conference on Manual Control*, pages 543–555. Massachusetts Institute of Technology, Cambridge (MA).

- Mulder, J. A. (1986). *Design and evaluation of dynamic flight test manoeuvres*. PhD thesis, Delft University of Technology, Faculty of Aerospace Engineering.
- Mulder, M. (1999). *Cybernetics of Tunnel-in-the-Sky Displays*. PhD thesis, Delft University of Technology.
- Mulder, M., Lubbers, B., Zaal, P. M. T., Van Paassen, M. M., and Mulder, J. A. (2009). Aerodynamic Hinge Moment Coefficient Estimation Using Automatic Fly-by-Wire Control Inputs. In *Proceedings of the AIAA Modeling and Simulation Technologies Conference and Exhibit, Chicago (IL)*, number AIAA-2009-5692.
- Mulder, M. and Mulder, J. A. (2005). Cybernetic Analysis of Perspective Flight-Path Display Dimensions. *Journal of Guidance, Control, and Dynamics*, 28(3):398–411.
- Mulder, M., Van Paassen, M. M., and Boer, E. R. (2004). Exploring the Roles of Information in the Control of Vehicular Locomotion: From Kinematics and Dynamics to Cybernetics. *Presence: Teleoperators and Virtual Environments*, 13(5):535–548.
- Nahon, M. A., Reid, L. D., and Kirdeikis, J. (1992). Adaptive Simulator Motion Software with Supervisory Control. *Journal of Guidance, Control and Dynamics*, 15(2):376–383.
- Naseri, A. R. and Grant, P. R. (2005). An Improved Adaptive Motion Drive Algorithm. In *Proceedings of the AIAA Modeling and Simulation Technologies Conference and Exhibit, San Francisco (CA)*, number AIAA-2005-6500.
- Neilson, P. D., O'Dwyer, N. J., and Neilson, M. D. (1988). Stochastic Prediction in Pursuit Tracking: An Experimental Test of Adaptive Model Theory. *Biological Cybernetics*, 58(2).
- Newell, F. D. and Smith, H. J. (1969). Human Transfer Characteristics in Flight and Ground Simulation for a Roll Tracking Task. Technical Report NASA TN D-5007, National Aeronautics and Space Administration, Washington, D.C.
- Nieuwenhuizen, F. M. (2012). *Changes in Pilot Control Behaviour across Stewart Platform Motion Systems*. PhD thesis, Delft University of Technology, Faculty of Aerospace Engineering.
- Nieuwenhuizen, F. M., Zaal, P. M. T., Mulder, M., Van Paassen, M. M., and Mulder, J. A. (2008). Modeling Human Multichannel Perception and Control Using Linear Time-Invariant Models. *Journal of Guidance, Control, and Dynamics*, 31(4):999–1013.
- Nieuwenhuizen, F. M., Zaal, P. M. T., Teufel, H. J., Mulder, M., and Bülthoff, H. H. (2009). The Effect of Simulator Motion on Pilot Control Behaviour for Agile and Inert Helicopter Dynamics. In *Proceedings of the 35th European Rotorcraft Forum, Hamburg, Germany*.
- Nusseck, H.-G., Teufel, H. J., Nieuwenhuizen, F. M., and Bülthoff, H. H. (2008). Learning System Dynamics: Transfer of Training in a Helicopter Hover Simulator. In *Proceedings of the AIAA Modeling and Simulation Technologies Conference and Exhibit, Honolulu (HI)*, number AIAA-2008-7107.

- Parrish, R. V., Dieudonne, J. E., Bowles, R. L., and Martin, Jr., D. J. (1975). Coordinated Adaptive Washout for Motion Simulators. *Journal of Aircraft*, 12(1):44–50.
- Parrish, R. V. and Martin, Jr., D. J. (1976). Comparison of a Linear and a Nonlinear Washout For Motion Simulators Utilizing Objective and Subjective Data from CTOL Transport Landing Approaches. Technical Report NASA TN D-8157, National Aeronautics and Space Administration, Langley Research Center, Hampton (VA).
- Pew, R. W., Duffendack, J. C., and Fensch, L. K. (1967). Sine-Wave Tracking Revisited. *IEEE Transactions on Human Factors in Electronics*, HFE-8(2):130–134.
- Phatak, A. V. and Bekey, G. A. (1969). Model of the Adaptive Behavior of the Human Operator in Response to a Sudden Change in the Control Situation. *IEEE Transactions on Man-Machine Systems*, MMS-10(3):72–80.
- Pool, D. M., Mulder, M., Van Paassen, M. M., and Van der Vaart, J. C. (2008a). Effects of Peripheral Visual and Physical Motion Cues in Roll-Axis Tracking Tasks. *Journal of Guidance, Control, and Dynamics*, 31(6):1608–1622.
- Pool, D. M., Zaal, P. M. T., Damveld, H. J., Van Paassen, M. M., and Mulder, M. (2009a). Pilot Equalization in Manual Control of Aircraft Dynamics. In *Proceedings of the 2009 IEEE International Conference on Systems, Man, and Cybernetics, San Antonio (TX)*, pages 2480–2485.
- Pool, D. M., Zaal, P. M. T., Mulder, M., Van Paassen, M. M., and Mulder, J. A. (2008b). Parameter Estimation of Multimodal Pilot Models for Manual Target-following Tasks. In *Proceedings of the 27th European Annual Conference on Human Decision-Making and Manual Control*.
- Pool, D. M., Zaal, P. M. T., Van Paassen, M. M., and Mulder, M. (2009b). Identification of Roll Attitude Control Behavior During Turn Maneuvers. In *Proceedings of the AIAA Modeling and Simulation Technologies Conference and Exhibit, Chicago (IL)*, number AIAA-2009-6029.
- Pool, D. M., Zaal, P. M. T., Van Paassen, M. M., and Mulder, M. (2010). Effects of Heave Washout Settings in Aircraft Pitch Disturbance Rejection. *Journal of Guidance, Control, and Dynamics*, 33(1):29–41.
- Pouliot, N. A., Gosselin, C. M., and Nahon, M. A. (1998). Motion Simulation Capabilities of Three-Degree-of-Freedom Flight Simulators. *Journal of Aircraft*, 35(1):9–17.
- Praamstra, F. J., Zaal, P. M. T., Pool, D. M., Ellerbroek, J., Mulder, M., and Van Paassen, M. M. (2008). Function of Attitude Perception in Human Control Behavior in Target Tracking Tasks. In *Proceedings of the AIAA Modeling and Simulation Technologies Conference and Exhibit, Honolulu (HI)*, number AIAA-2008-6845.
- Rasmussen, J. (1983). Skills, Rules, and Knowledge; Signals, Signs, and Symbols, and Other Distinctions in Human Performance Models. *IEEE Transactions on Systems, Man, and Cybernetics*, SMC-13(3):257–266.

- Ray, P. A. (1996). Quality Flight Simulation Cueing: Why? In *Proceedings of the AIAA Flight Simulation Technologies Conference, San Diego (CA)*, number AIAA-1996-3488, pages 138–147.
- Reid, L. D. (1970). An Investigation into Pursuit Tracking in the Presence of a Disturbance Signal. In *Proceedings of the Fifth Annual NASA University Conference on Manual Control*, volume NASA SP-215, pages 129–169.
- Reid, L. D. and Nahon, M. A. (1985). Flight Simulation Motion-Base Drive Algorithms. Part 1: Developing and Testing the Equations. Technical Report UTIAS 296, University of Toronto, Institute for Aerospace Studies.
- Reid, L. D. and Nahon, M. A. (1986a). Flight Simulation Motion-Base Drive Algorithms. Part 2: Selecting the System Parameters. Technical Report UTIAS 307, University of Toronto, Institute for Aerospace Studies.
- Reid, L. D. and Nahon, M. A. (1986b). Flight Simulation Motion-Base Drive Algorithms. Part 3: Pilot Evaluations. Technical Report UTIAS 319, University of Toronto, Institute for Aerospace Studies.
- Riedel, S. A. and Hofmann, L. G. (1978). Investigation of Nonlinear Motion Simulator Washout Schemes. In *Proceedings of the Fourteenth Annual Conference on Manual Control*, pages 521–532. University of Southern California.
- Ringland, R. F. and Stapleford, R. L. (1971). Motion Cue Effects on Pilot Tracking. In *Seventh Annual Conference on Manual Control*, pages 327–338.
- Rolfe, J. M. and Staples, K. J. (1986). *Flight Simulation*. Cambridge University Press.
- Schmidt, S. F. and Conrad, B. (1970). Motion Drive Signals for Piloted Flight Simulators. Technical Report NASA CR-1601, National Aeronautics and Space Administration, Ames Research Center.
- Schroeder, J. A. (1993). Simulation Motion Effects on Single Axis Compensatory Tracking. In *Proceedings of the AIAA Flight Simulation Technologies Conference, Monterey (CA)*, number AIAA-1993-3579, pages 202–213.
- Schroeder, J. A. (1996). Evaluation of Simulation Motion Fidelity Criteria in the Vertical and Directional Axes. *Journal of the American Helicopter Society*, 41(2):44–57.
- Schroeder, J. A. (1999). Helicopter Flight Simulation Motion Platform Requirements. Technical Report NASA-TP-1999-208766, National Aeronautics and Space Administration.
- Schroeder, J. A., Chung, W. W. Y., and Hess, R. A. (2000). Evaluation of a Motion Fidelity Criterion with Visual Scene Changes. *Journal of Aircraft*, 37(4):580–587.
- Schroeder, J. A., Chung, W. W. Y., Tran, D., Laforce, S., and Bengford, N. J. (1998). Pilot-Induced Oscillation Prediction with Three Levels of Simulation Motion Displacement. In *Proceedings of the AIAA Atmospheric Flight Mechanics Conference and Exhibit, Boston (MA)*, number AIAA-1998-4333.

- Schroeder, J. A. and Grant, P. R. (2010). Pilot Behavioral Observations in Motion Flight Simulation. In *Proceedings of the AIAA Guidance, Navigation, and Control Conference, Toronto, Canada*, number AIAA-2010-8353.
- Schroeder, J. A., Tischler, M. B., Watson, D. C., and Eshow, M. M. (1996). *Vertical Flight Training: An Overview of Training and Flight Simulator Technology with Emphasis on Rotary-Wing Requirements*, chapter 9: Simulation Validation in the Frequency Domain, pages 203–246. Number NASA-RP-1373. National Aeronautics and Space Administration, Ames Research Center, Moffet Field (CA).
- Sentouh, C., Chevrel, P., Mars, F., and Claveau, F. (2009). A Sensorimotor Driver Model for Steering Control. In *Proceedings of the 2009 IEEE International Conference on Systems, Man, and Cybernetics*, pages 2462 – 2467.
- Shirley, R. S. and Young, L. R. (1968). Motion Cues in Man-Vehicle Control – Effects of Roll-Motion Cues on Human Operator’s Behavior in Compensatory Systems with Disturbance Inputs. *IEEE Transactions on Man-Machine Systems*, 9(4):121–128.
- Sinacori, J. B. (1973). A Practical Approach to Motion Simulation. In *Proceedings of the AIAA Visual and Motion Simulation Conference, Palo Alto (CA)*, number AIAA-1973-931.
- Sinacori, J. B. (1977). The Determination of Some Requirements for a Helicopter Research Simulation Facility. Technical Report NASA-CR-152066, Systems Technology Inc., Mountain View (CA).
- Sinacori, J. B. (1978). Piloted Aircraft Simulation Concepts and Overview. STI Technical Report 1074-2, Systems Technology, Inc., Mountain View (CA).
- Sivan, R., Ish-Shalom, J., and Huang, J.-K. (1982). An Optimal Control Approach to the Design of Moving Flight Simulators. *IEEE Transactions on Systems, Man, and Cybernetics*, SMC-12(6):818–827.
- Smith, H. J. (1966). Human Describing Functions Measured in Flight and on Simulators. In *Proceedings of the Second Annual NASA-University Conference on Manual Control*, pages 279–292.
- Sparko, A. L., Bürki-Cohen, J., and Go, T. H. (2010). Transfer of Training from a Full-Flight Simulator vs. a High Level Flight Training Device with a Dynamic Seat. In *Proceedings of the AIAA Guidance, Navigation, and Control Conference, Toronto, Canada*, number AIAA-2010-8218.
- Spithost, S. P. (1993). Modelvorming van de Primaire Besturingssystemen van het Cessna Citation II Laboratoriumvliegtuig en een Beschouwing over de Hydraulische Aandrijving van deze Systemen. Master’s thesis, Delft University of Technology.
- Stapleford, R. L., McRuer, D. T., and Magdaleno, R. E. (1967). Pilot Describing Function Measurements in a Multiloop Task. *IEEE Transactions on Human Factors in Electronics*, 8(2):113–125.

- Stapleford, R. L., Peters, R. A., and Alex, F. R. (1969). Experiments and a Model for Pilot Dynamics with Visual and Motion Inputs. Technical Report NASA CR-1325, Systems Technology, Inc., Hawthorne (CA).
- Steurs, M., Mulder, M., and Van Paassen, M. M. (2004). A Cybernetic Approach to Assess Flight Simulator Fidelity. In *Proceedings of the AIAA Modelling and Simulation Technologies Conference and Exhibit, Providence (RI)*, number AIAA-2004-5442.
- Stewart, D. (1966). A Platform With Six Degrees of Freedom. *Institution of Mechanical Engineers, Proceedings 1965-1966*, 180 Part I(15):371–378.
- Stroosma, O., Damveld, H. J., Mulder, J. A., Choe, R., Xargay, E., and Hovakimyan, N. (2011). A Handling Qualities Assessment of a Business Jet Augmented with an L1 Adaptive Controller. In *Proceedings of the AIAA Guidance, Navigation, and Control Conference, Portland (OR)*, number AIAA-2011-6610.
- Stroosma, O., Van Paassen, M. M., and Mulder, M. (2003). Using the SIMONA Research Simulator for Human-machine Interaction Research. In *Proceedings of the AIAA Modeling and Simulation Technologies Conference and Exhibit, Austin (TX)*, number AIAA-2003-5525.
- Stroosma, O., Van Paassen, M. M., Mulder, M., and Postema, F. N. (2007). Measuring Time Delays in Simulator Displays. In *Proceedings of the AIAA Modeling and Simulation Technologies Conference and Exhibit, Hilton Head (SC)*, number AIAA-2007-6562.
- Sturgeon, W. R. (1981). Controllers for Aircraft Motion Simulators. *Journal of Guidance, Control, and Dynamics*, 4(2):184–191.
- Takasaki, G. M. and Fenton, R. E. (1977). On the Identification of Vehicle Longitudinal Dynamics. *IEEE Transactions on Automatic Control*, 22(4).
- Telban, R. J., Cardullo, F. M., and Houck, J. A. (1999). Developments in Human Centered Cueing Algorithms for Control of Flight Simulator Motion Systems. In *Proceedings of the AIAA Modeling and Simulation Technologies Conference and Exhibit, Portland (OR)*, number AIAA-1999-4328.
- Telban, R. J., Cardullo, F. M., and Kelly, L. C. (2005a). Motion Cueing Algorithm Development: New Motion Cueing Program Implementation and Tuning. Technical Report NASA CR-2005-213746, National Aeronautics and Space Administration, Langley Research Center.
- Telban, R. J., Cardullo, F. M., and Kelly, L. C. (2005b). Motion Cueing Algorithm Development: Piloted Performance Testing of the Cueing Algorithms. Technical Report NASA CR-2005-213748, National Aeronautics and Space Administration, Langley Research Center.
- Telban, R. J., Wu, W., and Cardullo, F. M. (2000). Motion Cueing Algorithm Development: Initial Investigation and Redesign of the Algorithms. Contractor Report NASA-CR-2000-209863, NASA Langley Research Center, Hampton (VA).

- Teufel, H. J., Nusseck, H.-G., Beykirch, K. A., Butler, J. S., Kerger, M., and Bülthoff, H. H. (2007). MPI Motion Simulator: Development and Analysis of a Novel Motion Simulator. In *Proceedings of the AIAA Modeling and Simulation Technologies Conference and Exhibit, Hilton Head (SC)*, number AIAA-2007-6476.
- Thompson, P. M., Klyde, D. H., and Brenner, M. J. (2001). Wavelet-Based Time-Varying Human Operator Models. In *Proceedings of the AIAA Atmospheric Flight Mechanics Conference and Exhibit, Montreal (CA)*, number AIAA-2001-4009.
- Tustin, A. (1947). The Nature of the Operator's Response in Manual Control, and its Implications for Controller Design. *Journal of the Institution of Electrical Engineers – Part IIA: Automatic Regulators and Servo Mechanisms*, 94(2):190–206.
- Valente Pais, A. R., Van Paassen, M. M., Mulder, M., and Wentink, M. (2010). Perception Coherence Zones in Flight Simulation. *Journal of Aircraft*, 47(6):2039–2048.
- Valente Pais, A. R., Wentink, M., Van Paassen, M. M., and Mulder, M. (2009). Comparison of Three Motion Cueing Algorithms for Curve Driving in an Urban Environment. *Presence: Teleoperators & Virtual Environments*, 18(3):200–221.
- Van Biervliet, F. (2007). Method to Control the Movements of a Flight Simulator and Flight Simulator Implementing Such a Method. International Patent. Application number PCT/EP2006/009841.
- Van der Steen, F. A. M. (1998). *Self-Motion Perception*. PhD thesis, Delft University of Technology, Faculty of Aerospace Engineering.
- Van der Vaart, J. C. (1992). *Modelling of Perception and Action in Compensatory Manual Control Tasks*. PhD thesis, Delft University of Technology, Faculty of Aerospace Engineering.
- Van Gool, M. F. C. (1978). Influence of Motion Washout Filters on Pilot Tracking Performance. In *Piloted Aircraft Environment Simulation Techniques*, number AGARD-CP-249, pages 19–1 – 19–5.
- Van Gool, M. F. C. and Mooij, H. A. (1976). A Comparison of In-Flight and Ground-Based Pitch Attitude Tracking Experiments. In *Proceedings of the Twelfth Annual Conference on Manual Control*, pages 443–454.
- Van Paassen, M. M. (1994). *Biophysics in Aircraft Control, A Model of the Neuromuscular System of the Pilot's Arm*. PhD thesis, Delft University of Technology, Faculty of Aerospace Engineering.
- Van Paassen, M. M. and Mulder, M. (1998). Identification of Human Operator Control Behaviour in Multiple-Loop Tracking Tasks. In *Proceedings of the Seventh IFAC/IFIP/IFORS/IEA Symposium on Analysis, Design and Evaluation of Man-Machine Systems, Kyoto Japan*, pages 515–520.

- Van Paassen, M. M., Stroosma, O., and Delatour, J. (2000). DUECA - Data-Driven Activation in Distributed Real-Time Computation. In *Proceedings of the AIAA Modeling and Simulation Technologies Conference and Exhibit, Denver (CO)*, number AIAA-2000-4503.
- Van Wieringen, A. T., Pool, D. M., Van Paassen, M. M., and Mulder, M. (2011). Effects of Heave Washout Filtering on Motion Fidelity and Pilot Control Behavior for a Large Commercial Airliner. In *Proceedings of the AIAA Modeling and Simulation Technologies Conference, Portland (OR)*, number AIAA-2011-6323.
- Wasicko, R. J., McRuer, D. T., and Magdaleno, R. E. (1966). Human Pilot Dynamic Response in Single-loop Systems with Compensatory and Pursuit Displays. Technical Report AFFDL-TR-66-137, Air Force Flight Dynamics Laboratory.
- Wentink, M., Bles, W., Hosman, R. J. A. W., and Mayrhofer, M. (2005). Design & evaluation of spherical washout algorithm for Desdemona simulator. In *Proceedings of the AIAA Modeling and Simulation Technologies Conference and Exhibit, San Francisco (CA)*, number AIAA-2005-6501.
- Westbrook, C. B. (1959). Pilot's Role in Space Flight. AGARD Report 252, Advisory Group for Aeronautical Research and Development, North Atlantic Treaty Organization.
- Wiener, N. (1961). *Cybernetics or Control and Communication in the Animal and the Machine*. The M.I.T. Press, Cambridge, Massachusetts, second edition.
- Wu, W. and Cardullo, F. M. (1997). Is There an Optimum Motion Cueing Algorithm? In *Proceedings of the AIAA Modeling and Simulation Technologies Conference and Exhibit, New Orleans (LA)*, number AIAA-1997-3506, pages 23–29.
- Yamashita, T. (1989). Precognitive behavior in tracking of targets with 2 sine waves. *Japanese Psychological Research*, 31(1):20–28.
- Yamashita, T. (1990). Effects of Sine Wave Combinations on the Development of Precognitive Mode in Pursuit Tracking. *The Quarterly Journal of Experimental Psychology*, 42A(4):791–810.
- Young, L. R. (1966). Some Effects of Motion Cues on Manual Tracking. In *Second Annual NASA-University Conference on Manual Control, Massachusetts Institute of Technology, Cambridge (MA), February 28 – March 2, 1966*, pages 231–240.
- Young, L. R. (1969). On Adaptive Manual Control. *Ergonomics*, 12(4):635–674.
- Zaal, P. M. T. (2011). *Pilot Control Behavior Discrepancies Between Real and Simulated Flight Caused by Limited Motion Stimuli*. PhD thesis, Delft University of Technology, Faculty of Aerospace Engineering.
- Zaal, P. M. T., Nieuwenhuizen, F. M., Mulder, M., and Van Paassen, M. M. (2006). Perception of Visual and Motion Cues During Control of Self-Motion in Optic Flow Environments. In *Proceedings of the AIAA Modeling and Simulation Technologies Conference and Exhibit, Keystone (CO)*, number AIAA 2006-6627.

- Zaal, P. M. T., Pool, D. M., Chu, Q. P., Van Paassen, M. M., Mulder, M., and Mulder, J. A. (2009a). Modeling Human Multimodal Perception and Control Using Genetic Maximum Likelihood Estimation. *Journal of Guidance, Control, and Dynamics*, 32(4):1089–1099.
- Zaal, P. M. T., Pool, D. M., De Bruin, J., Mulder, M., and Van Paassen, M. M. (2009b). Use of Pitch and Heave Motion Cues in a Pitch Control Task. *Journal of Guidance, Control, and Dynamics*, 32(2):366–377.
- Zaal, P. M. T., Pool, D. M., Mulder, M., and Van Paassen, M. M. (2008). New Types of Target Inputs for Multi-Modal Pilot Model Identification. In *Proceedings of the AIAA Modeling and Simulation Technologies Conference and Exhibit, Honolulu (HI)*, number AIAA-2008-7106.
- Zaal, P. M. T., Pool, D. M., Mulder, M., and Van Paassen, M. M. (2009c). Multimodal Pilot Control Behavior in Combined Target-Following Disturbance-Rejection Tasks. *Journal of Guidance, Control, and Dynamics*, 32(5):1418–1428.
- Zaal, P. M. T., Pool, D. M., Mulder, M., Van Paassen, M. M., and Mulder, J. A. (2010). Identification of Multimodal Pilot Control Behavior in Real Flight. *Journal of Guidance, Control, and Dynamics*, 33(5):1527–1538.
- Zaal, P. M. T., Pool, D. M., Postema, F. N., In 't Veld, A. C., Mulder, M., Van Paassen, M. M., and Mulder, J. A. (2009d). Design and Certification of a Fly-By-Wire System with Minimal Impact on the Original Flight Controls. In *Proceedings of the AIAA Guidance, Navigation, and Control Conference and Exhibit, Chicago (IL)*, number AIAA-2009-5985.
- Zaal, P. M. T., Pool, D. M., Van Paassen, M. M., and Mulder, M. (2011). Comparing Multimodal Pilot Pitch Control Behavior Between Simulated and Real Flight. In *Proceedings of the AIAA Modeling and Simulation Technologies Conference, Portland (OR)*, number AIAA-2011-6475.
- Zacharias, G. L. and Young, L. R. (1981). Influence of Combined Visual and Vestibular Cues on Human Perception and Control of Horizontal Rotation. *Experimental Brain Research*, 41(9):159–171.
- Zaichik, L. E., Rodchenko, V. V., Rufov, I. V., Yashin, Y. P., and White, A. D. (1999). Acceleration Perception. In *Proceedings of the AIAA Modeling and Simulation Technologies Conference and Exhibit, Portland (OR)*, number AIAA-1999-4334.
- Zeyada, Y. and Hess, R. A. (2003). Computer-Aided Assessment of Flight Simulator Fidelity. *Journal of Aircraft*, 40(1):173–180.
- Zollner, H. G. H., Pool, D. M., Damveld, H. J., Van Paassen, M. M., and Mulder, M. (2010). The Effects of Controlled Element Break Frequency on Pilot Dynamics During Compensatory Target-Following. In *Proceedings of the AIAA Guidance, Navigation, and Control Conference, Toronto, Canada*, number AIAA-2010-8092.



Pilot Visual Response Modeling

This Appendix provides some additional motivation for the models used for describing pilots' responses to visually presented tracking errors as used, for example, in Chapters 5, 6, and 8 of this thesis. The focus lies on indicating why this model structure, which lumps the contributions of all different delays that may be induced in the pilot's response into a single delay parameter, is desirable from a model identification point of view, as opposed to a more complete and extensive model for pilots' visual responses.

A.1 Introduction

The approach for evaluating simulator motion fidelity proposed in this thesis is centered around models of pilot tracking behavior. These models typically consist of separate visual and motion channels that account for pilots responses to visually presented tracking errors and information available from physical motion feedback, respectively. For the Cessna Citation roll dynamics considered as the controlled element in the experiments described in Chapters 6–8, and for many other controlled elements relevant for aerospace applications, it is known that pilots perform visual lead equalization to compensate for the controlled element dynamics over a frequency range where these are approximately K/s^2 [McRuer et al., 1965]. Note that if lead equalization is performed, pilots' responses to visual tracking errors approximate a derivative-proportional (DI) controller, that is, a controller responding to both error magnitude (proportional) and error rate (derivative).

In this thesis, the model structure used for modeling the pilot visual response is based on the Precision Model proposed by McRuer et al. [1965]. This model consists of a gain-

lead equalization transfer function that accounts for the lead equalization performed of a certain frequency range, a single pure delay term, and a second-order model for the neuromuscular actuation dynamics. Other researchers, such as Jex et al. [1978] and Hosman [1996], have proposed pilot models in which pilots' responses to the tracking error and the tracking error rate are separated in parallel model channels. Hosman [1996] further shows using data from stimulus-response experiments that the delay in perceiving error magnitude and is different from the delay incurred in the perception of error rate from a visual display, where the latter is found to be around 0.1 s higher. Intuitively, such a model that separates the proportional and derivative contribution to pilot control inputs and accounts for possible different processing delays incurred in these contributions perhaps seems more appropriate for modeling pilots' responses to visually presented tracking errors than the minimum parameter form represented by the Precision Model.

In addition to the appropriateness of the used model, a second aspect that is important for the research described in this thesis is the accuracy with which the applied pilot models can be identified from measurements of pilot tracking behavior. This Appendix evaluates the identifiability of a pilot visual response model as proposed by Hosman [1996] and compares it to the results obtained with the model based on the Precision Model proposed by McRuer et al. [1965] as applied in this thesis. Pilot model simulations of the two-channel model proposed by Hosman with known parameters are used to directly compare the accuracy with which both models can be fit to the same data.

This Appendix is structured as follows. First, the different models for pilots' responses to visually presented tracking errors will be introduced in Section A.2. Then, Section A.3 explains the analysis into the identifiability of both models described in this Appendix. The results of this analysis will be presented in Section A.4.

A.2 Pilot Model Structures

The models for pilots responses to visually presented tracking errors as applied in this thesis are typically of the following form, which is based on the Precision Model proposed by McRuer et al. [1965]:

$$H_{pe}(j\omega) = K_{pv} [1 + T_L j\omega] e^{-j\omega\tau_v} H_{nm}(j\omega) \quad (\text{A.1})$$

Note that compared to the definition of the Precision Model in [McRuer et al., 1965], the model given by Eq. (A.1) does not include the very low-frequency lead-lag term proposed by McRuer et al. for capturing the low-frequency phase droop observed in their measured describing functions. The model of Eq. (A.1) consists of a gain-lead equalization term that models pilot lead equalization for frequencies larger than $1/T_L$ rad/s. The delay parameter τ_v captures the delay in the pilot's response and the frequency response function $H_{nm}(j\omega)$ models the combined manipulator and neuromuscular actuation dynamics. In this thesis, these neuromuscular dynamics are modeled as a second-order mass-spring-damper system with two parameters:

$$H_{nm}(j\omega) = \frac{\omega_{nm}^2}{(j\omega)^2 + 2\zeta_{nm}\omega_{nm}j\omega + \omega_{nm}^2} \quad (\text{A.2})$$

The model of Eq. (A.1) represents a minimal-parameter form that is capable of capturing typical pilot visual response dynamics for controlled elements for which lead equalization is adopted. Alternatives to this model have also been proposed in literature. One example, which explicitly separates pilots' responses to the tracking error and to tracking error rate, was proposed by Hosman [1996] and is depicted in Fig. A.1.

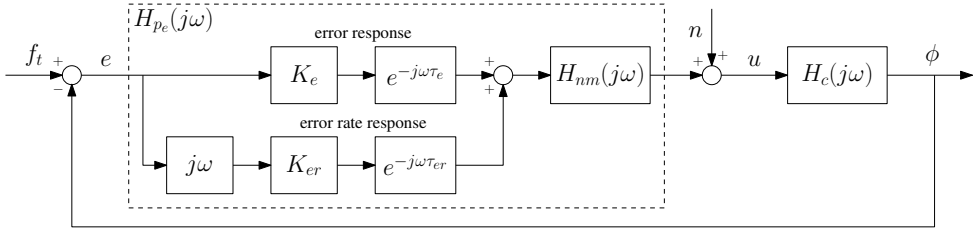


Figure A.1. Alternative pilot visual response model as proposed by Hosman [1996].

Fig. A.1 depicts a schematic representation of a pilot engaged in a single-loop (only visual error information is presented) target-following task. The controlled element dynamics are depicted with the $H_c(j\omega)$ block, and the model for the pilot visual control dynamics $H_{pe}(j\omega)$ is enclosed in the dashed rectangular area. Note that the model of Fig. A.1 shows two parallel channels that capture pilots' responses to the tracking error e and to the error rate \dot{e} . Hosman [1996] proposed to model both these responses with a pure gain and time delay, as also indicated in Fig. A.1. Note that the information processing delay present in the definition of Hosman's model and which affects the output of both channels is here assumed to be included in both τ_e and τ_{er} . From Fig. A.1 the following equation for $H_{pe}(j\omega)$ can be derived:

$$\begin{aligned}
 H_{pe}(j\omega) &= [K_e e^{-j\omega\tau_e} + K_{er} j\omega e^{-j\omega\tau_{er}}] H_{nm}(j\omega) \\
 &= K_e \left[e^{-j\omega(\tau_e - \tau_{er})} + \frac{K_{er}}{K_e} j\omega \right] e^{-j\omega\tau_{er}} H_{nm}(j\omega)
 \end{aligned}
 \tag{A.3}$$

Note from Eq. (A.3) and Fig. A.1 that this model is largely equivalent to the model given by Eq. (A.1), except for the additional delay term that allows for taking into account a difference in perceptual and processing latency between both response channels. Despite the fact that explicit separation of pilots' responses to visually presented tracking errors and error rate as depicted in Fig. A.1 could be of interest for manual control research, this model form poses a problem when attempting fit it to typical measurements of pilot tracking behavior.

A.3 Analysis Setup

A.3.1 Pilot Model Simulations

To evaluate the accuracy with which the parameters of the two pilot model forms given by Equations (A.1) and (A.3) can be estimated from measured data, this Appendix describes the results of an offline analysis performed in Matlab. Pilot model simulations of the roll attitude double integrator control tasks described in [Hosman, 1996], using the target forcing function signal from that study, a sum of 10 sinusoids. The pilot model parameters for the simulations were taken from [Hosman, 1996] for the condition of his experiment where only the central visual (compensatory) display was present (target-following task data) and are listed in Table A.1.

Table A.1. Pilot model simulation parameters.

Parameter	K_e	K_{er}	τ_e	τ_{er}	ω_{nm}	ζ_{nm}	K_n	T_n
Unit	—	s	s	s	rad/s	—	—	s
Value	0.31	0.47	0.25	0.35	10.0	0.5	8.0	0.1

To assess identifiability for these pilot model parameters, pilot model simulations were performed for 100 different realizations of the remnant signal n (see Fig. A.1). Remnant was modeled as Gaussian noise with zero mean and unity standard deviation, simulated through the fourth-order low-pass remnant filter given by:

$$H_n(j\omega) = \frac{K_n}{(1 + T_n j\omega)^4} \quad (\text{A.4})$$

The form of this remnant model and the value of T_n were derived from data from a later experiment [Pool et al., 2008a] that replicated the results of Hosman [1996]. The remnant gain K_n was set to ensure 10% of the variance in the simulated pilot control signal u could be attributed to the remnant signal n . The values of K_n and T_n are listed in Table A.1.

A.3.2 Data Analysis

Pilot model simulation data was generated using the model proposed by Hosman, with the additional delay parameter compared to the model given by Eq. (A.1). As will be shown using this simulation data, the model proposed by Hosman is an overdetermined model for which it is not possible to estimate both delay terms reliably. This is first evaluated by assessing the sensitivity of the overall model dynamics to changes in both pilot model delay parameters. In addition, using the time-domain identification procedure described in Zaal et al. [2009a] the parameters of the pilot model shown in Fig. A.1 are then estimated from the simulated data. For reference, also the pilot model as adopted in this thesis (Eq. (A.1)) is fit to the same pilot model simulation data.

A.4 Results

A.4.1 Delay Sensitivity Analysis

To assess the sensitivity of the model depicted in Fig. A.1 to changes in the values of both the delay parameters τ_e and τ_{er} , Fig. A.2 shows the frequency response of this model as calculated from Eq. (A.3). Fig. A.2(a) shows the Bode magnitude of the model, which clearly shows the gain-lead dynamics and the high-frequency peak resulting from the neuromuscular actuation model. The Bode phase response of the model with the true values for τ_e and τ_{er} is depicted in Figures A.2(b) and (c) with a solid black line. The gray lines in Figures A.2(b) and (c) depict the phase response for extreme variations in the value of τ_e and τ_{er} , respectively. Dashed gray lines indicate the model phase response for the case where the delay parameter is set to 0, while the solid gray lines correspond to an extremely large 1 s delay.

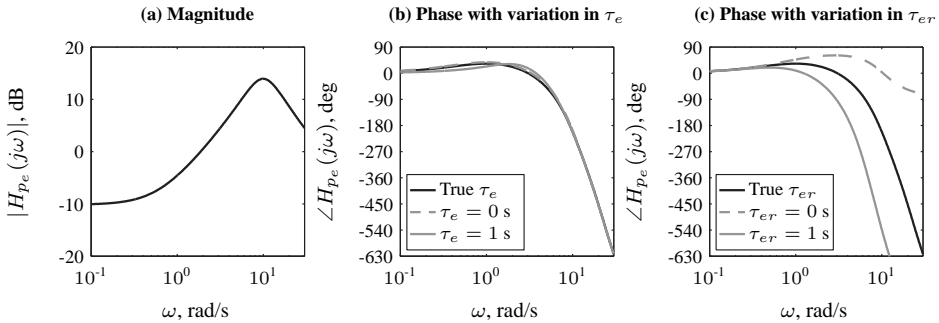


Figure A.2. Pilot model frequency responses for a variation in τ_e and τ_{er} .

Fig. A.2 shows that the total model frequency response is a lot less sensitive to variations in τ_e than to changes in τ_{er} . This is readily explained as the frequency response of the model is calculated as the vectorial sum of the frequency responses of the parallel error and error rate responses. At high frequencies, the error rate response magnitude is much larger than the error response magnitude, hence the total model output at high frequencies is dominated by $K_{er}j\omega e^{-j\omega\tau_{er}}$. As the effect of both delay parameters is mainly felt at these higher frequencies, the model is comparatively insensitive to variations in τ_e .

This is further evaluated using the pilot model simulation data. For all 100 realizations of the simulation data, the model variance accounted for (VAF) was calculated for τ_e and τ_{er} varying from 0 to 1 s. Only one delay parameter was varied and all other model parameters were fixed at their true values. Fig. A.3 shows the average variation in VAF for varying values of the error delay τ_e and the error rate delay τ_{er} . Fig. A.3 confirms the observations made from Fig. A.2, as a clear effect of varying τ_{er} on the model output is observed, while the effect of τ_e is much less pronounced. The model VAF is seen to only change less than 5% when varying τ_e between 0 and twice its true value.

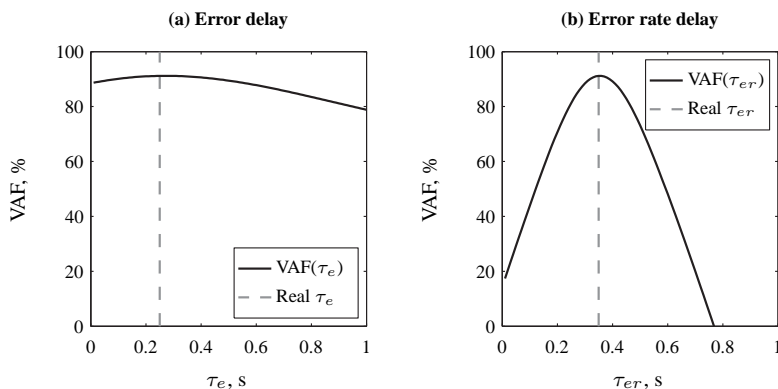


Figure A.3. Average variation in pilot model VAF with the value of the error and error rate delay parameters.

A.4.2 Delay Identifiability Analysis

The previous section showed that an analysis of the sensitivity of the pilot model to changes in the value of both delay parameters suggests that the model is relatively insensitive to changes in the error delay τ_e . It is likely that this may lead to problems when attempting to identify the model from measurements of pilot tracking behavior. Figures A.4 and A.5 show the results of fitting the pilot models given by Equations (A.3) and (A.1) to the pilot model simulation data. Again, note that in both cases pilot model simulation data generated with the model of Eq. (A.3) was used.

The rightmost graphs in Figures A.4 and A.5 show the true parameter value used for the simulation data as a dashed black line. The individual estimates of the parameters for both models are indicated with gray markers, while the mean and standard deviation are presented as black markers with variance bars. The two histograms indicate the distributions of the parameter estimates obtained for both models. Again, dashed black lines indicate the true value of the parameter, while the solid black line indicates the mean of the distribution. Note that for the model given by Eq. (A.1) the equivalent value of K_{er} was calculated by multiplying the obtained estimates of K_v and T_L . In addition, the results of estimating τ_v are presented in the graph for τ_{er} . Consequently, no data is presented in Fig. A.4(i) for the Eq. (A.1) model.

Figures A.4 and A.5 show that parameter estimates for the model of Eq. (A.1) are typically more consistent than those obtained for the more elaborate model of Eq. (A.3) and are on average closer to the true simulation parameter setting. This is especially notable for the error rate gain K_{er} and the neuromuscular damping ratio ζ_{nm} , as can be verified from Figures A.4(d) to (f) and A.5(d) to (f). The parameter for which identification results show the most spread, however, is the error delay τ_e . The estimated values for this parameter almost cover the entire range of 0 to 1 s and the average estimated value of τ_e is found to be more than twice as high as the true value used for generating the simulation data. The identification results shown in Fig. A.4(h) thereby confirm that the parameter τ_e is not identifiable for the selected case, because of its severely limited effect on the pilot model response.

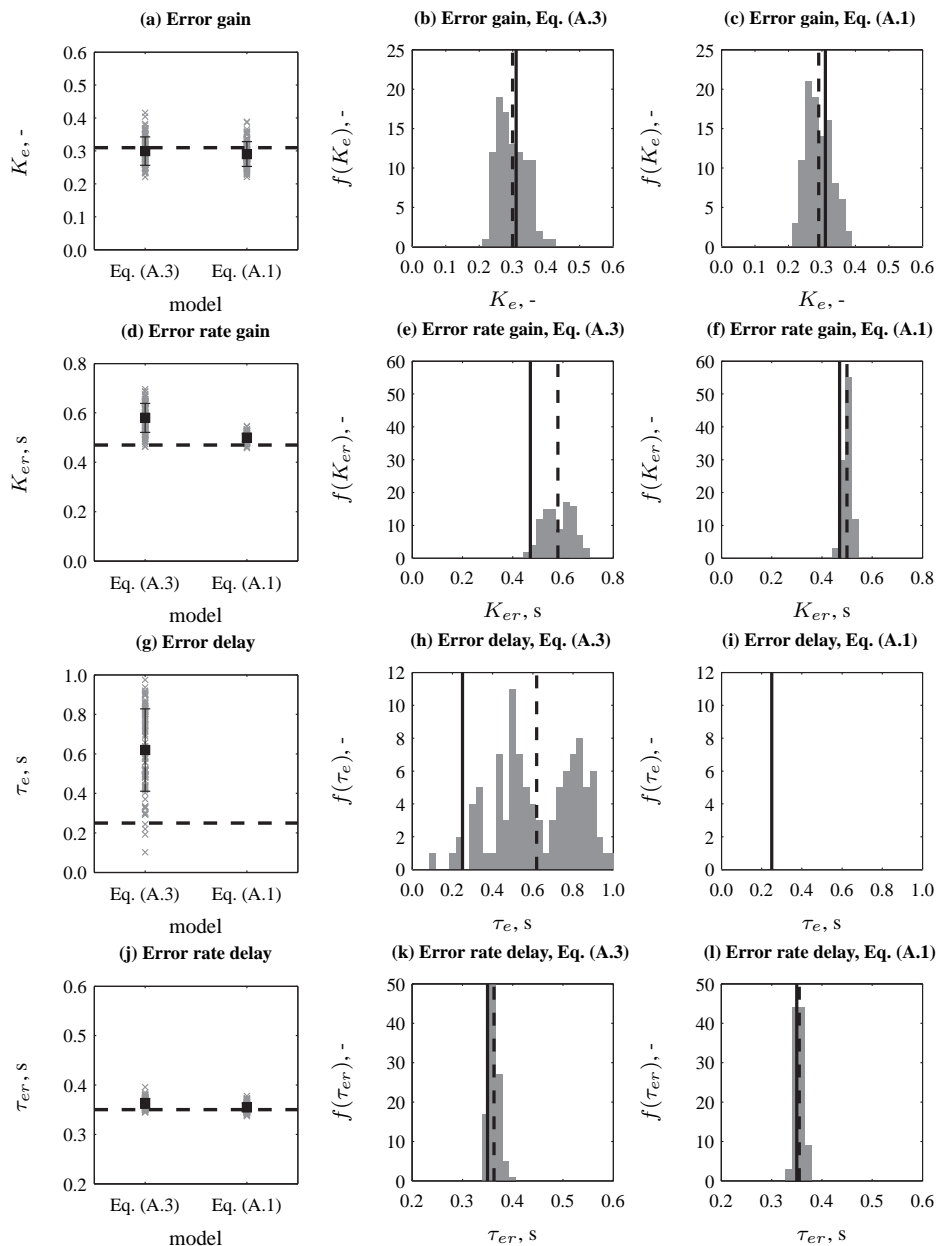


Figure A.4. Estimated values and their distributions for the parameters of the pilot models of Equations (A.3) and (A.1) based on 100 pilot model simulation realizations.

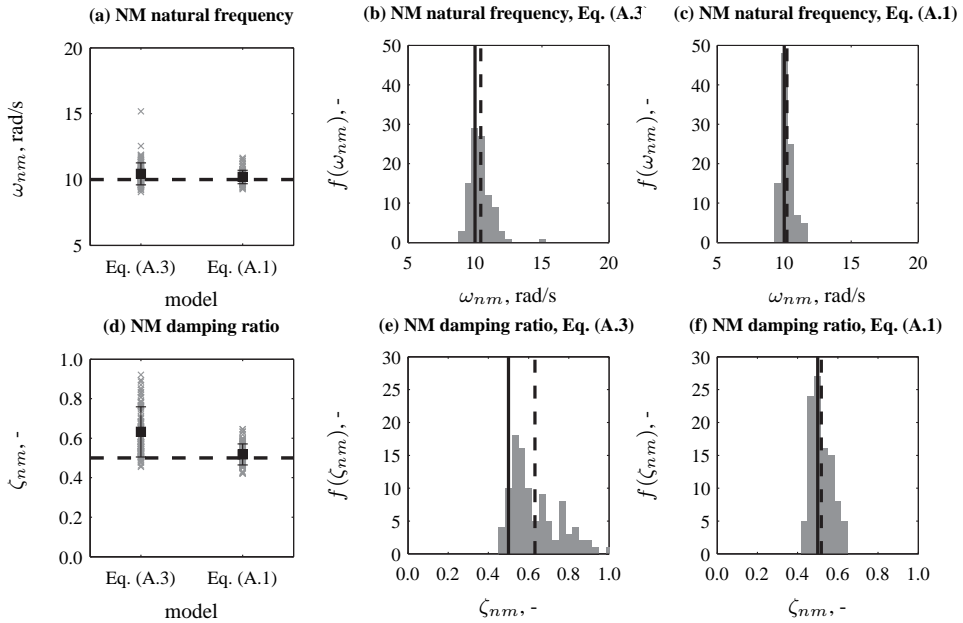


Figure A.5. Estimated values and their distributions for the parameters of the neuromuscular (NM) system model of Eq. (A.2) based on 100 pilot model simulation realizations.

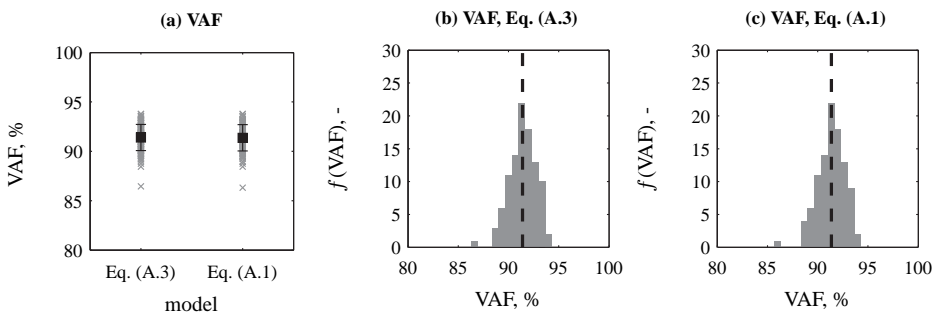


Figure A.6. Fitted pilot model variance accounted for for the models of Eq. (A.2) based on 100 pilot model simulation realizations.

Finally, Fig. A.6 presents the VAF of the achieved pilot model fits corresponding to the parameter estimates shown in Figures A.4 and A.5. As can be verified from Fig. A.6, the accuracy with which both models describe the simulated data that was generated using the model of Eq. (A.3) is found to be equivalent. On average, the VAF for the fits of the model of Eq. (A.3) is equal to 91.39%, whereas for the model of Eq. (A.1) an average VAF of 91.37% is obtained.

The results presented in Figures A.4 to A.6 confirm that the error delay parameter τ_e only has a negligible contribution to the overall model response and that its omission in the model of Eq. (A.1) does not lead to an appreciable degradation in the accuracy with which typical measured pilot error response data can be modeled. Moreover, for estimating the model parameters from measured data the omission of this extra parameter is even highly preferable, as the estimates obtained for some of the other model parameters are found to become more consistent and reliable.

A.5 Conclusions

The application of pilot models for quantifying changes in pilot behavior that result from variations in simulator motion cueing requires a pilot model structure that can be fitted reliably to measurements of pilot tracking behavior. The results presented in this Appendix show that, in this respect, accounting for different perceptual and processing delays for pilots' responses to visually presented tracking errors and tracking error rate for controlled elements for which lead equalization is performed is not feasible. The observable pilot dynamics, which are dominated by the response to error rate at higher frequencies, show only a negligible effect of the error delay, which is therefore typically not identifiable. Having this non-observable parameter in the model is further seen to yield errors in the estimation of the remaining model parameters. This is the reason for modeling pilots' visual responses using a pilot model based on McRuer et al.'s Precision Model, which only includes a single lumped delay parameter, for the work described in this thesis.

B

Pilot Model Identification Using Ramp Target Signals

Chapter 3 considered possible changes from purely compensatory control behavior that can result from the use of deterministic target forcing functions consisting of multiple ramp-like changes in reference attitude. A second important aspect with respect to the application of such alternative forcing function signals is the provided excitation of the pilot-vehicle system. As detailed in [Zaal et al., 2009a], the typical multimodal pilot models used for analyzing pilot tracking behavior with physical motion feedback are overdetermined, due to control-theoretically equivalent terms in the visual and motion channels of such models. In order to be able to reliably separate pilot visual and motion responses, these alternative target forcing functions still need to provide sufficient excitation to differentiate the effects of both pilot operations.

This appendix addresses this problem by using pilot model simulation data, generated using a pilot model fitted to data from a previous experiment, to evaluate the the excitation provided by the type of ramp forcing function signals considered in this thesis in Chapters 3 and 7. This is done by evaluating ramp signals with different ramp rates of change and comparing obtained results with those obtained with a quasi-random multisine target signal as used successfully in many previous investigations.

The contents of this appendix have been published as:

Pool, D. M., Zaal, P. M. T., Van Paassen, M. M., and Mulder, M., "Identification of Multimodal Pilot Models Using Ramp Target and Multisine Disturbance Signals", *Journal of Guidance, Control, and Dynamics*, 34(1), pp. 8697, 2011.

B.1 Introduction

Pilot manual control behavior can be modeled successfully using quasi-linear models that consist of linear response functions and a remnant signal to account for nonlinearities [McRuer et al., 1965; McRuer and Jex, 1967a; Hosman, 1996; Van der Vaart, 1992; Pool et al., 2010]. The modeling and identification of pilot dynamics requires measurements that are typically taken from control tasks in which manual control action is induced using target and disturbance forcing function signals [McRuer and Jex, 1967a; Stapleford et al., 1969; Jex et al., 1978]. These target and disturbance signals represent the reference trajectory that needs to be followed and external disturbances that are to be attenuated, respectively. The characteristics of these forcing function signals heavily influence the actual control behavior that is adopted and the quality of pilot model identification results. For instance, McRuer et al. [1965] indicate that random-appearing forcing function signals are required for inducing skill-based manual control. In addition, commonly used multimodal pilot model identification techniques make use of multiple independent quasi-random multisine forcing functions to be able to separate the responses to multiple cues [Stapleford et al., 1969].

Quasi-random target and disturbance forcing function signals have frequently been combined in tracking tasks to allow for separate modeling of pilot visual and vestibular responses [Stapleford et al., 1969; Nieuwenhuizen et al., 2008; Pool et al., 2009a]. Even though accurate estimates of multimodal pilot model parameters can be obtained with these identification techniques if multiple quasi-random forcing function signals are applied, this approach results in control tasks that can be considered as less representative for real-life piloting tasks. Perturbing the controlled element using a (low-pass) quasi-random disturbance signal is not objectionable due to its similarity to turbulence. The following of a quasi-random multisine target signal, however, is often indicated to be unlike any control task performed in-flight.

As indicated in [Zaal et al., 2009a], time-domain estimation techniques for identification of multimodal pilot models put less severe constraints on the design of forcing functions. Rather than requiring an independent forcing function signal for each model channel as needed for application of the method described in [Stapleford et al., 1969], data sets used for time-domain model identification only need to be “persistently exciting” [Ljung, 1999]. This reduced requirement on forcing function design theoretically allows for alternative types of forcing functions to be used to excite a pilot-vehicle system for multimodal pilot model identification. For example, an aircraft pitch or roll attitude control task where a multisine disturbance signal is combined with a target signal consisting of multiple discrete ramps and steps in target attitude may also yield identifiable measurements of pilot behavior. Such target signals also yield more realistic manual control tasks, similar to in-flight maneuvers such as a turn entry or altitude change, while flying in turbulence [Zaal et al., 2008; Pool et al., 2009b].

Two distinct challenges, however, arise when control behavior is analyzed using such deterministic reference signals. First, the quasi-random nature of the target signal is lost and the deterministic nature of multiramp signals may yield precognitive (feed-forward) or pursuit-tracking control behavior [McRuer and Jex, 1967a; Wasicko et al., 1966; Allen and McRuer, 1979; Hess, 1981, 2006]. As for instance argued in [McRuer and Jex, 1967a] and [Wasicko et al., 1966], control behavior in a pursuit-tracking situation is found to be a com-

bination of pursuit (feed-forward) and compensatory (error reducing) control operations. Therefore, depending on further details of control task design, predictable forcing function signals could yield a deviation from purely compensatory control, to which the multimodal pilot models that have been used to analyze control behavior [Zaal et al., 2008; Pool et al., 2009b; Zaal et al., 2010] need to be adapted.

A second distinct challenge lies in the fact that it is unknown if such alternative forcing function signals provide enough excitation of the combined pilot-vehicle system – that is, yield data sets that are sufficiently informative – to allow for reliable separation of pilots' visual and vestibular responses [Zaal et al., 2009a]. This appendix investigates this latter issue by evaluating the accuracy of model identification results for control tasks where a reference signal consisting of multiple ramp-like changes in target attitude is followed. Unlike the experimental approach to evaluating such alternative forcing functions taken in [Zaal et al., 2008; Pool et al., 2009b; Zaal et al., 2010], this appendix will make use of pilot model simulations – based on experimental measurements taken from [Zaal et al., 2008] – to assess the accuracy and reliability of pilot model identification results. For this analysis a model of purely compensatory multimodal pilot control is used, yielding a typical multimodal pilot model identification problem as for instance also analyzed in [Nieuwenhuizen et al., 2008] and [Zaal et al., 2009a]. Feed-forward control strategies resulting from the use of deterministic input signals are not considered in the adopted pilot model for two reasons. First, experimental measurements supporting the presence of such control behavior are sparse and appropriate models for describing this feed-forward have not yet been validated. Moreover, the presence of feed-forward control operations is largely independent of the problem of separating pilot compensatory visual and vestibular responses as studied here. As will be shown in this appendix, increased excitation of the pilot-vehicle system is obtained for increased steepness of the ramps in such alternative forcing function signals. Therefore, the effects of ramp signal steepness on the multimodal pilot model identification problem are evaluated by comparing estimation results for signals with different levels of ramp steepness.

This appendix first gives an overview of the multimodal pilot model identification problem, including a description of the pilot model and identification algorithm used for estimating the model parameters. Then, Section B.3 provides an analysis of the excitation provided by signals consisting of a number of ramps using frequency-domain methods. Details of the pilot model simulations, the different forcing function settings that are evaluated, and the settings of the identification algorithm are given in Section B.4. Section B.5 presents the main results of the identification performed on the data from the pilot model simulations. The appendix ends with a discussion and conclusions.

B.2 The Pilot Model Identification Problem

B.2.1 Control Task

During manual control tasks in a multimodal environment, human operators may utilize information perceived through different perceptual modalities for feedback [Hosman, 1996]. In addition, they may use this information to achieve compensatory control, pursuit control,

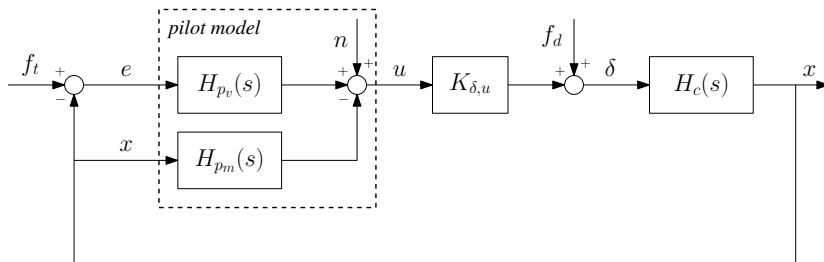


Figure B.1. Schematic representation of a multimodal attitude control task with visual and vestibular motion feedback.

precognitive control, or any combination of these modes of control operation [McRuer and Jex, 1967a]. In this appendix, pilot control behavior during compensatory attitude control (tracking) tasks is investigated, based on the control task performed in the experiment described in [Zaal et al., 2008]. Fig. B.1 shows a schematic representation of a pilot-vehicle system where a pilot performs compensatory control. Physical motion feedback, which has been shown to make a significant contribution to pilot control in multimodal environments in a number of previous investigations [Meiry, 1967; Shirley and Young, 1968; Stapleford et al., 1969; Jex et al., 1978], is included as a second feedback channel, $H_{p_m}(s)$.

Target and disturbance forcing function signals are indicated in Fig. B.1 with the symbols f_t and f_d , respectively. These signals represent the reference trajectory that is to be followed and the external disturbances (turbulence) that are to be attenuated by the pilot. Pilot control action is shown to be the sum of the pilot's compensatory (visual) and motion responses, $H_{p_v}(s)$ and $H_{p_m}(s)$. The inputs to the visual and motion channels of the pilot model are the tracking error e and the state of the controlled element x , respectively. An additional remnant signal n is added to the responses of the linear pilot model channels to model the nonlinear (uncorrelated) portion of the pilot control signal, u .

In the schematic representation shown in Fig. B.1, the dynamics of the controlled element are represented by $H_c(s)$. In the experiment of Zaal et al. [2008] acceleration control was considered. Therefore, the transfer function of the controlled element used in this appendix is given by:

$$H_c(s) = \frac{K_c}{s^2} \quad (\text{B.1})$$

In Fig. B.1, the symbol $K_{\delta,u}$ represents the scaling gain between the pilot control deflection u and the input to the controlled element δ . The numerical values that were used for the controlled element gain K_c and the control scaling gain $K_{\delta,u}$ in the experiment of Zaal et al. [2008] – which are also applied in the current evaluation – will be specified in Section B.4.

B.2.2 Pilot Model

Human manual control behavior is inherently time-varying and nonlinear. For carefully designed control tasks, and specifically for compensatory control tasks as the one studied

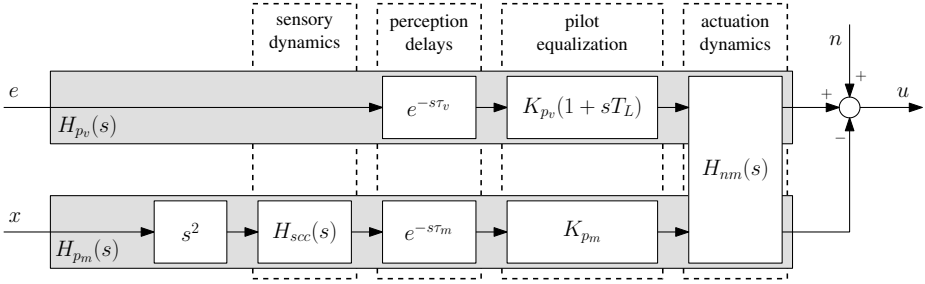


Figure B.2. Quasi-linear multimodal pilot model for compensatory attitude control.

in this appendix, pilot control behavior can be successfully captured using quasi-linear pilot models [McRuer et al., 1965; McRuer and Jex, 1967a]. During compensatory manual control tasks, pilots are known to adapt their control strategy to the dynamics of the controlled element to achieve approximately single integrator open-loop dynamics over a wide frequency range around gain crossover [McRuer et al., 1965]. For the double integrator dynamics defined by Eq. (B.1) this implies that pilots will need to generate lead starting at frequencies below crossover to compensate for the second-order dynamics of $H_c(s)$. In addition, the presence of physical motion cues has been shown to affect pilot control behavior and task performance in numerous occasions [Meiry, 1967; Stapleford et al., 1969; Jex et al., 1978; Hosman, 1996; Pool et al., 2010], especially for controlled elements that require pilots to perform significant lead equalization [Shirley and Young, 1968].

An appropriate quasi-linear multimodal pilot model that captures both compensatory visual control strategies and the effect of physical motion feedback on pilot control – as depicted in Fig. B.1 – is shown in Fig. B.2. Note that the pilot visual and motion responses are modeled as separate parallel channels, which have the tracking error e and the system attitude x as inputs. Furthermore, note that the linear responses of both channels consist of contributions from the human motion sensory dynamics, pilot equalization dynamics, and pilot limitations such as perceptual delays and the dynamics of the neuromuscular system. Similar pilot models have been applied in many earlier studies into human manual control behavior in vehicle control tasks [Van der Vaart, 1992; Hosman, 1996; Pool et al., 2009a, 2010].

As shown in Fig. B.2, it is assumed that the semicircular canals, which are part of the human vestibular organ in the inner ear, are the dominant motion sensor for perception of physical angular motion. The semicircular canals are sensitive to angular accelerations and their dynamics can be described by [Hosman, 1996]:

$$H_{scc}(s) = K_{scc} \frac{1 + 0.11s}{(1 + 5.9s)(1 + 0.005s)} \quad (\text{B.2})$$

The time constants of the semicircular canal dynamics given by Eq. (B.2) are assumed to be constants. The main free parameters of the pilot model shown in Fig. B.2 are the visual and motion perception gains, K_{pv} and K_{pm} , the corresponding perceptual time delays, τ_v and τ_m , and the visual lead constant T_L . The neuromuscular actuation dynamics, depicted as $H_{nm}(s)$ in Fig. B.2, are modeled as a second-order mass-spring-damper system:

$$H_{nm}(s) = \frac{\omega_{nm}^2}{s^2 + 2\zeta_{nm}\omega_{nm}s + \omega_{nm}^2} \quad (\text{B.3})$$

Previous experiments have shown that the characteristic frequency ω_{nm} and damping factor ζ_{nm} of the neuromuscular system tend to vary considerably for different control tasks [Pool et al., 2009a] and motion cueing settings [Pool et al., 2010]. Therefore, both are also considered as free pilot model parameters, which gives a total of seven pilot model parameters that are to be estimated when fitting the model of Fig. B.2 to measured data.

B.2.3 Parameter Estimation Procedure

This appendix focuses on the reliability with which the parameters of multimodal pilot models can be identified. The main problem that is encountered when the parameters of models like the one depicted in Fig. B.2 are estimated from measurement data is that these models are overdetermined [Zaal et al., 2009a]. This overdetermined model structure results from the fact that the semicircular canals are hypothesized to integrate perceived angular accelerations in the frequency range of interest to manual control [Hosman, 1996], thereby yielding an additional source of pilot lead. Previous experiments have shown that pilots adopt a control strategy in which the available motion cues are used to reduce the amount of lead that is generated visually, but that pilot visual lead equalization does not fully disappear [Pool et al., 2009a, 2010]. As pointed out in [Zaal et al., 2009a], this may cause parameter estimation algorithms to return sets of model parameters that, for instance, attribute all pilot lead to either the visual or the vestibular pilot model channels, sometimes without significantly degrading the goodness-of-fit. To be able to draw valid conclusions on pilots' use of physical motion information during manual control, however, it is essential that the visual and vestibular contributions to the measured pilot control behavior can be separated reliably.

As described in detail in [Nieuwenhuizen et al., 2008] and [Zaal et al., 2009a], different identification methods are available for estimating the parameters of multimodal pilot models from measurement data. Frequency-domain methods, such as those based on Fourier coefficients [Stapleford et al., 1969] and linear time-invariant models [Nieuwenhuizen et al., 2008], first estimate nonparametric describing functions of the observed pilot control behavior. Then, in a second step, the parameters of the pilot model are identified by fitting the model to this frequency-domain data. Alternatively, time-domain parameter estimation methods, such as the maximum likelihood estimation (MLE) procedure described in [Zaal et al., 2009a], estimate pilot model parameters directly from time-domain measurements.

The success of the frequency-domain estimation methods is highly dependent on the design of the experiment forcing functions [Nieuwenhuizen et al., 2008; Zaal et al., 2009a], f_t and f_d in Fig. B.1. In fact, they require independent target and disturbance signals for successful estimation of the visual and motion describing functions in the first step [Stapleford et al., 1969], which is usually achieved by using two multisine forcing function signals with interleaving frequencies.

For time-domain estimation methods, there is no requirement for independent forcing functions, but the different inputs to the pilot model (e and x in Fig. B.2) should be "persistently exciting" [Zaal et al., 2009a; Ljung, 1999]. This implies that for control tasks in

which a disturbance signal f_d is to be attenuated, an additional target forcing function is still needed to provide enough excitation – that is, to induce differences in e and x – to allow for reliable multimodal pilot model identification. However, unlike for the frequency-domain estimation methods, the target signal is not required to be an independent multisine signal. Therefore, multimodal pilot model identification with MLE [Zaal et al., 2009a] theoretically allows for the use of target forcing function signals consisting of multiple ramp-like changes in target attitude, instead of a quasi-random target signal [Zaal et al., 2009a, 2008]. It is, however, as of yet unknown if such alternative forcing function signals provide enough excitation of the pilot-vehicle system to allow for reliable estimation for the overdetermined multimodal pilot model [Zaal et al., 2009a; Pool et al., 2009b], and how ramp signal design affects the accuracy of model identification results.

B.3 Ramp Forcing Function Characteristics

Ramp- and step-like input signals are successfully applied for the identification of unknown system dynamics in engineering disciplines other than multimodal pilot model identification [Takasaki and Fenton, 1977; Hensen et al., 2002; Mulder et al., 2009]. As for instance pointed out in [Mehra, 1974; Maine and Iliff, 1986; Jategaonkar, 2006], the type of excitation used for gathering the data on which system identification is to be performed significantly influences the accuracy and reliability with which model parameters can be estimated. In many previous investigations into multimodal pilot control behavior, quasi-random target forcing function signals have been found to yield sufficient excitation to provide accurate pilot model identification results [Nieuwenhuizen et al., 2008; Zaal et al., 2008; Pool et al., 2009a, 2010]. This section uses such a quasi-random multisine target signal taken from previous research [Zaal et al., 2008] as a baseline for comparing the excitation provided by signals consisting of ramp or step-like changes in target attitude. In addition, the effects of one of the design parameters that is thought to affect the excitation provided by such alternative forcing functions signals – that is, the steepness of the ramps – are evaluated in both the time and frequency domain.

B.3.1 Fourier Transforms of Ramps and Steps

Fig. B.3 depicts time traces of the basic building blocks of the ramp and step forcing function signals that are evaluated in this appendix. Fig. B.3 shows signals consisting of a single step $s(t)$ and of a single ramp $r(t)$, which ends at the same final magnitude as the step. Note that the magnitudes of both the ramp and step are equal to A , and that the ramp takes a time T to reach that final value.

Due to the fact that the pilot model defined in Fig. B.2 describes pilot dynamics over a relatively wide frequency range (0.1-20 rad/s), sufficient excitation over this frequency range is required for reliable identification of the model. To evaluate the power distributions (spectra) of the step and ramp signals shown in Fig. B.3, the Fourier transform can be applied to $s(t)$ and $r(t)$ as is done in Eq. (B.4) and Eq. (B.5), respectively.

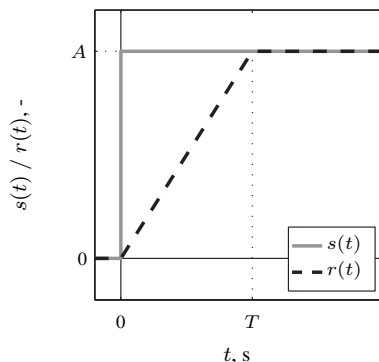


Figure B.3. Example time traces of single ramp and step signals.

$$s(t) = \begin{cases} 0 & t < 0 \\ A & t \geq 0 \end{cases} \iff S(s) = \frac{A}{s} \quad (\text{B.4})$$

$$r(t) = \begin{cases} 0 & t < 0 \\ \frac{A}{T}t & 0 \leq t < T \\ A & t \geq T \end{cases} \iff R(s) = \frac{A/T}{s^2}(1 - e^{-sT}) \quad (\text{B.5})$$

Eq. (B.4) indicates that the Fourier transform of the step signal $s(t)$ is an integrator with a gain equal to A . Similarly, the Fourier transform of the ramp signal $r(t)$ is approximately equal to a double integrator with a gain of A/T . Note that this Fourier analysis of $s(t)$ and $r(t)$ already reveals that step signals provide significantly more high-frequency excitation than ramps signals, whose amplitude distribution decays with frequency at a rate of 40 dB per decade, compared to 20 dB per decade for $S(s)$. Eq. (B.4) and Eq. (B.5) further show that the power in both $s(t)$ and $r(t)$ increases when A is increased, that is when the magnitude of the changes in the commanded signal is larger. In addition, it can be verified from Eq. (B.5) that the magnitude of $R(s)$ is inversely proportional to T , which implies more signal power for steeper ramps.

The Fourier analysis of ramp and step signals presented here indicates that the amount of excitation provided by such signals can be manipulated with the parameters that define the magnitude of ramps or steps, and the steepness of the ramps. In the remainder of this appendix, the effect of the final parameter, ramp steepness, will be evaluated further. Signals with step-like changes such as $s(t)$ will be treated as ramp signals with ramps of infinite steepness.

B.3.2 Comparison with Multisine Signal

This section evaluates how the excitation provided by multiramp signals – that is, the total amount of power such signals hold and how this power is distributed over the frequency

content of the signal – compares to that of the quasi-random multisine signals that are often applied for multimodal pilot model identification. Multisine forcing functions are typically constructed according to:

$$f_{d,t}(t) = \sum_{k=1}^{N_{d,t}} A_{d,t}(k) \sin [\omega_{d,t}(k)t + \phi_{d,t}(k)] \quad (\text{B.6})$$

The subscripts d and t in Eq. (B.6) refer to the disturbance and target forcing functions f_d and f_t , respectively (see Fig. B.1). Eq. (B.6) indicates that these quasi-random multisine forcing functions are constructed as the sum of a number ($N_{d,t}$) of individual sinusoids. The amplitudes, frequencies and phases of each sinusoid are indicated with the symbols $A_{d,t}(k)$, $\omega_{d,t}(k)$ and $\phi_{d,t}(k)$, respectively. The multisine forcing functions that are used in this appendix are those from a previous experiment [Zaal et al., 2008]. The detailed characteristics of these signals – that is, the amplitude, frequency and phase distributions defined in Eq. (B.6) – will be defined in Section B.4.2. Here, the time trace and the corresponding Fourier transform of the multisine target signal from [Zaal et al., 2008] will be used for comparison with the proposed multiramp signals.

B.3.2.1 Time Domain

Fig. B.4 depicts the multisine target forcing function from the experiment described in [Zaal et al., 2008] in gray. It also shows three examples of the ramp forcing functions that are investigated in this appendix.

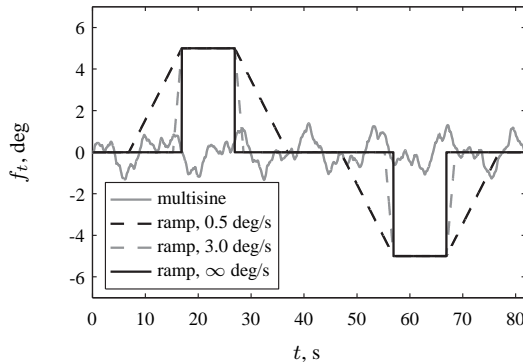


Figure B.4. Time traces of multisine and multiramp target forcing function signals.

Note that these ramp signals, all consisting of one positive and one negative excursion in commanded target value, are highly similar to those evaluated in previous investigations [Zaal et al., 2008; Pool et al., 2009b; Zaal et al., 2010]. Furthermore, note that the amplitude of the excursions (A in Fig. B.3) is chosen to be equal to 5 deg for all ramp signals. Fig. B.4 also shows the effect of ramp signal steepness: here signals with steepness values of 0.5 deg/s and 3.0 deg/s, in addition to an infinitely steep ramp (step), are depicted.

B.3.2.2 Frequency Domain

From the comparison of the signal time traces in Fig. B.4 the multisine target signal appears to provide a distinctly different and significantly more high-frequency excitation than the ramp signals. This is further evaluated by comparing the frequency content of the forcing function signals of Fig. B.4 in the frequency domain. Fig. B.5 shows the absolute value of the Fourier transform of the multisine target signal. For reference, the magnitude distribution of unity-gain single and double integrators are shown alongside.

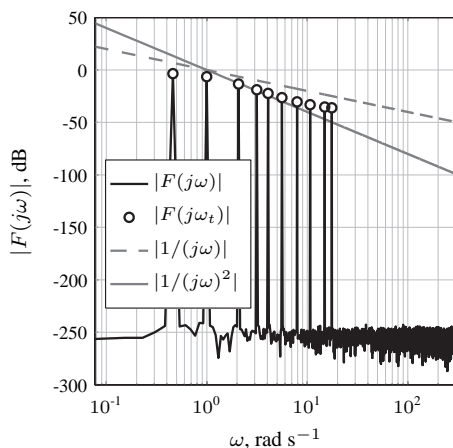


Figure B.5. Absolute value of Fourier transform of the multisine forcing function used by Zaal et al. [2008].

Note from Fig. B.5 that the multisine target signal only provides excitation at the frequencies of the sinusoids that make up the signal (indicated with the circular markers). At all other frequencies, the multisine signal provides no power. The multisine signal amplitudes follow a low-pass distribution, as the amplitude of the sinusoid with the lowest frequency is around 0 dB, where this is reduced to around -40 dB for the highest frequency sinusoid. Such a distribution of sinusoid amplitudes, with reduced power at higher frequencies, was proposed by McRuer et al. [1965] to yield signals that were not too difficult to track, but still allowed for measurement of high-frequency pilot dynamics. Forcing function signals with the same amplitude distribution as depicted in Fig. B.5 have been used successfully in many later investigations [Pool et al., 2009a, 2010; Zaal et al., 2010].

Fig. B.6 shows the absolute values of the Fourier transforms of the three ramp signals depicted in Fig. B.4. Note that the single and double integrators shown in Fig. B.5 are also depicted here, but that unlike Fig. B.5 the vertical axes of these graphs only span [-150,50] dB.

Comparison of Fig. B.6(a) and (b) with Fig. B.6(c) shows that the Fourier transforms of the signal time traces depicted in Fig. B.3 abide by Eqs. (B.4) and (B.5), respectively. For both ramp signals the absolute value of the Fourier transform is found to be approximately proportional to $|1/(j\omega)^2|$, where increased ramp signal steepness clearly yields increased

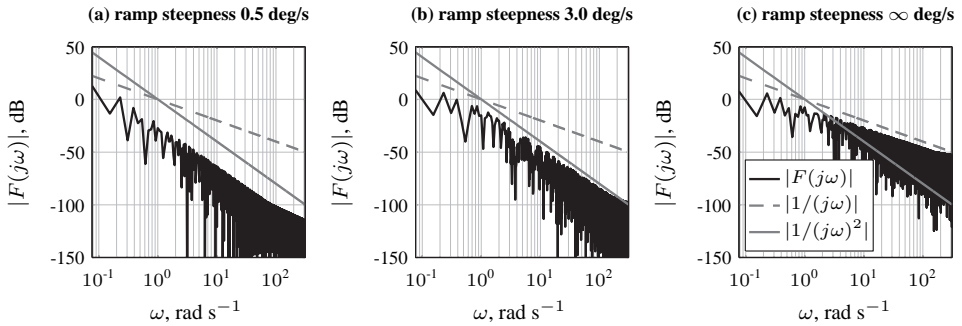


Figure B.6. Comparison of the absolute value of the Fourier transform for three values of ramp forcing function signal steepness.

signal power as predicted by Eq. (B.5). Fig. B.6(c) shows that for infinitely steep ramps, the signal amplitudes vary approximately proportional with $|1/j\omega|$, yielding comparatively more high-frequency power than Figures Fig. B.6(a) and (b) show for the ramp signals with lower steepness. Fig. B.6 thus shows that the steepness of the ramps in the alternative forcing function signals evaluated in this appendix affects the (high-frequency) excitation provided by such signals.

Direct comparison of the excitation provided by multisine and multiramp signals is difficult. This is due to the fact that the signal power is distributed over a limited number of discrete frequencies for signals consisting of a number of sinusoids, while for multiramp signals power is distributed more evenly over all frequencies (compare Figures B.5 and B.6). To still allow for some comparison, the absolute values of the Fourier transforms of the different forcing function signals depicted in Figures B.5 and B.6 have been averaged over a number of neighboring frequencies around the multisine signal sinusoid frequencies. As can be observed from Fig. B.7, this yields ten frequency bins (light gray shaded areas) over which the signal power is averaged. Note that these ten bins together contain all frequencies of the signals' Fourier transforms up to a frequency of 20 rad/s. For the multisine signal, the resulting averaged power distribution $|\bar{F}(j\omega)|$ (the gray line in Fig. B.7) still follows the signal's low-pass characteristic.

The same frequency-domain averaging was also performed on the ramp signal Fourier transforms depicted in Fig. B.6. Fig. B.8 shows a comparison of the averaged signal power $|\bar{F}(j\omega)|$ for the different forcing function signals. The average power of the multisine target forcing function signal is depicted a solid gray line, as also done in Fig. B.7. Note again from Fig. B.8 that increased ramp signal steepness results in increased signal power over the full frequency range. In addition, the comparison with $|\bar{F}(j\omega)|$ for the multisine signal shown in Fig. B.8 indicates that the ramp signal with a steepness of 3.0 deg/s already provides slightly more averaged power. This shows that, depending on the selection of ramp signal parameters, such ramp signals can provide excitation similar to that achieved with a multisine signal over the complete frequency range of interest, or even better.

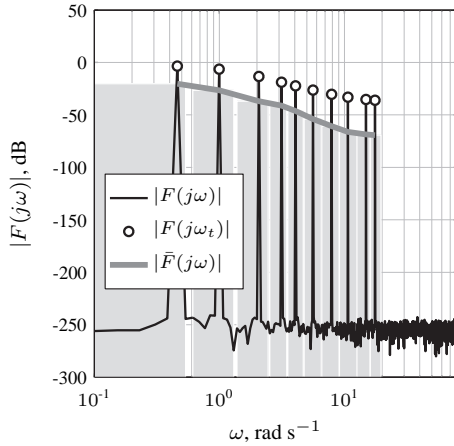


Figure B.7. An example of the averaged frequency-domain power calculation, and definition of the frequency bins, for the multisine forcing function.

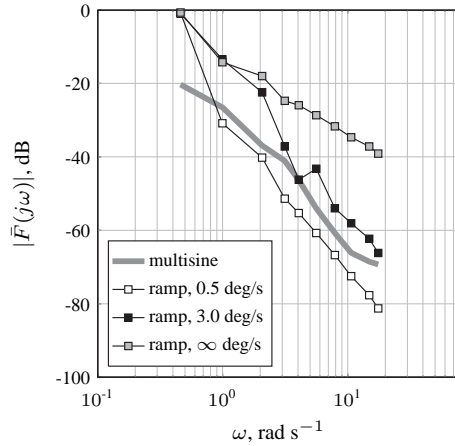


Figure B.8. A comparison of the averaged frequency-domain power for multisine and ramp signals with 0.5, 3.0, and ∞ deg/s steepness.

B.4 Method

To evaluate the identifiability of multimodal pilot models when using alternative target forcing functions as depicted in Fig. B.3, simulations of multimodal pilot control in a control task similar to the one described by Zaal et al. [2008] are used. This approach, where the exact pilot dynamics are known, allows for quantification and comparison of estimation bias and variance for different forcing function settings and ramp signal steepnesses.

B.4.1 Pilot Model Simulations

To gather the data for testing the accuracy of multimodal pilot model identification results, simulations of the closed-loop control task depicted in Fig. B.1 were performed. The gain of the acceleration control dynamics (Eq. (B.1)) was set to $K_c = 4$ and the stick input gain $K_{\delta,u}$ was chosen to be equal to 0.2865. The pilot visual and motion responses were simulated using the multimodal pilot model depicted in Fig. B.2. Identified values from the experiment of Zaal et al. [2008] were used for the pilot model parameters. These parameter values are listed in the top data row of Table B.1.

Pilot remnant n , which is typically modeled as filtered white noise [Zaal et al., 2009a], was generated by passing white noise through a fourth-order low-pass filter:

$$H_n(s) = \frac{K_n}{(1 + sT_n)^4} \quad (\text{B.7})$$

The chosen remnant filter gain K_n and lag time constant T_n (see Table B.1) were again based on data from [Zaal et al., 2008]. The remnant gain was chosen to yield a remnant

Table B.1. Pilot model parameters and identification upper and lower bounds.

Parameter Unit	Pilot Model							Remnant	
	K_{pv}	T_L	K_{pm}	τ_v	τ_m	ω_{nm}	ζ_{nm}	K_n	T_n
	—	s	—	s	s	rad/s	—	—	s
Value	1.2	0.6	4.0	0.25	0.20	11.5	0.3	0.15	0.06
Identification lower bound	0.0	0.0	0.0	0.0	0.0	5.0	0.0	—	—
Identification upper bound	5.0	10.0	10.0	1.0	1.0	20.0	1.0	—	—

contribution of 20% to the total pilot control input signal variance, that is, $\sigma_n^2/\sigma_u^2 = 0.2$ [Zaal et al., 2009a]. By using different white noise sequences, 100 different realizations of the multimodal control task were simulated.

B.4.2 Forcing Functions

Multisine target and disturbance forcing functions were generated according to Eq. (B.6). Both f_t and f_d consisted of 10 sinusoids, whose properties (frequencies, amplitudes and phases) are listed in Table B.2. Note that these forcing function signals are the same as those described in [Zaal et al., 2008].

Table B.2. Multisine forcing function properties.

target, f_t				disturbance, f_d			
n_t	ω_t	A_t	ϕ_t	n_d	ω_d	A_d	ϕ_d
—	rad/s	deg	rad	—	rad/s	deg	rad
6	0.460	1.353	4.437	5	0.383	0.048	-2.088
13	0.997	0.946	2.769	11	0.844	0.175	1.238
27	2.071	0.427	1.809	23	1.764	0.381	-3.895
41	3.145	0.230	3.544	37	2.838	0.502	3.138
53	4.065	0.154	3.687	51	3.912	0.581	-2.807
73	5.599	0.096	3.209	71	5.446	0.684	-1.808
103	7.900	0.061	4.286	101	7.747	0.866	-1.563
139	10.661	0.044	2.992	137	10.508	1.152	-2.953
194	14.880	0.035	5.391	171	13.116	1.496	-2.626
229	17.564	0.032	2.006	226	17.334	2.212	0.864

The disturbance signal was scaled to yield a low-pass disturbance of the controlled element output x with a variance of 1.5 deg^2 . Similarly, the target signal was scaled to have a variance of 0.375 deg^2 , that is, a quarter of the power of the disturbance signal. Similar fractions of target and disturbance signal power have been successfully applied in many previous experiments [Zaal et al., 2008; Pool et al., 2009a, 2010].

Five different ramp target forcing functions like those depicted in Fig. B.3 were defined, each with a different steepness of the ramps in the signals. The values for the rate of change of the ramps that were selected were: 0.5, 1.0, 3.0, 10.0 and $\infty \text{ deg/s}$. Note that ramps with 1.0 deg/s steepness were considered in [Zaal et al., 2008] and [Zaal et al., 2010] and that Pool et al. [2009b] evaluated both 1.0 and 3.0 deg/s ramp signals.

The multisine disturbance signal was present during all simulations of the control task of Fig. B.1 considered here. The target forcing function was varied over seven different conditions: the five different ramp forcing functions, supplemented with a multisine target

signal condition and a condition with a zero target signal, for reference. The latter two conditions will be referred to in the following as “MS” and “NO”. Ramp target conditions are indicated with a capital “R”, followed by the value of the ramp rate of change, that is, “R3.0” indicates the signal with 3 deg/s ramps.

B.4.3 Identification Procedure

For the seven different control task settings described in Section B.4.2, the known parameters of the multimodal pilot model have been estimated from the simulated time traces. The time-domain maximum likelihood estimation algorithm described in [Zaal et al., 2009a] was used for the identification. As also described in [Zaal et al., 2009a], an initial estimate of the model parameters was generated through the use of a genetic algorithm, which optimizes the model parameters for 100 iterations. The upper and lower bounds that were used for each parameter in this step of the estimation algorithm are listed in Table B.1. For each realization of simulation data, this genetic optimization was performed ten times. The best parameter estimate, as indicated by the corresponding lowest value of the likelihood function, was then further refined using an unconstrained Gauss-Newton optimization [Zaal et al., 2009a]. For each of the target forcing function settings, this gives a total of 100 estimated parameter sets, that is, one corresponding to each remnant realization.

B.4.4 Dependent Measures and Hypotheses

For a well-defined identification problem, repeated maximum likelihood estimates of model parameters will have an approximately Gaussian (normal) distribution [Mulder, 1986; Zaal et al., 2009a], where the mean and standard deviation of the distribution are related to the bias and variance in the parameter estimates, respectively. Therefore, the first dependent measure that is considered here is normality of the set of 100 parameter estimates obtained for the 100 different realizations of the simulated multimodal control task. The statistical Lilliefors test [Lilliefors, 1967] – which compares a measured distribution to a Gaussian distribution with the same mean and standard deviation – is used to evaluate the normality of the obtained distributions of parameter estimates. In addition to testing the normality of the identified sets of parameters, the mean bias and variance of the model parameter estimates obtained for each of the seven configurations will be compared.

Due to the increased excitation provided by signals with steeper ramps (see Fig. B.6) it is expected that pilot model identification results will become more consistent – that is, their distributions will become more normal – and accurate as ramp signal steepness is increased. The bias and variance in the parameter estimates are expected to be largest for the condition without target signal (NO). Based on a comparison of Figures B.5 and B.6(c), it is expected that the ramp signals with the highest steepnesses could yield pilot model estimates with bias and variance that are very similar to that of the estimates for the multisine target condition (MS).

B.5 Results

B.5.1 Example Simulation Results

Figures B.9 and B.10 depict example time traces of pilot model simulations for the condition with a multisine target signal (MS) and the condition with the 1.0 deg/s ramp signal (R1.0), respectively. For both figures, (a) shows the target f_t and the controlled element state x (see Fig. B.1); (b) and (c) depict the pilot control signal u (and, for reference, the remnant signal n) and the tracking error signal e . Note that the actual simulation time was 90 seconds – with a measurement time of 81.92 seconds as defined in [Zaal et al., 2008], over which the model identification was performed – but that only 60 seconds of the simulation data are depicted here for clarity.

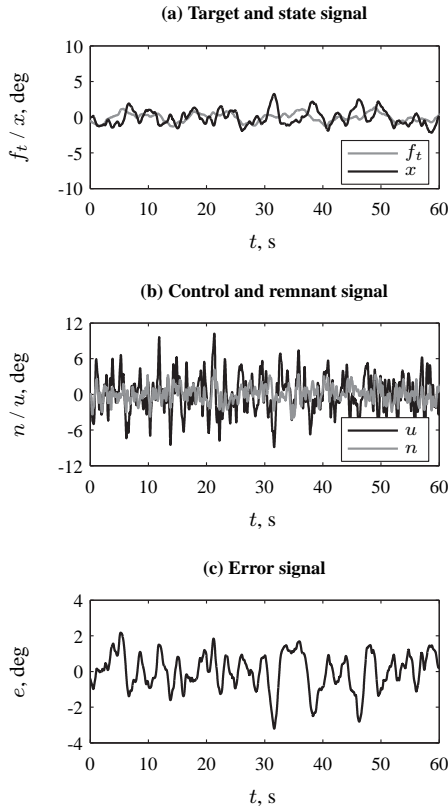


Figure B.9. Example pilot model simulation time traces for condition MS.

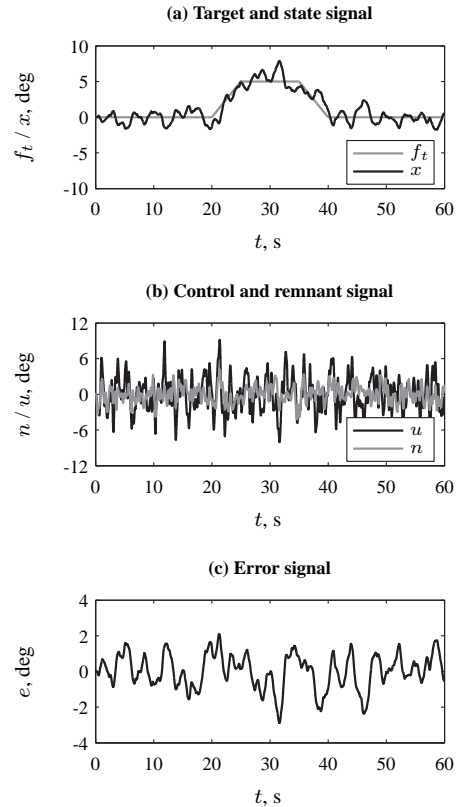


Figure B.10. Example pilot model simulation time traces for condition R1.0.

Figures B.9(a) and B.10(a) show the difference between the target signals used for these two conditions, and their effect on the controlled element state x . Note that the deviations of x from the reference trajectory defined by f_t predominantly result from the perturbations

introduced by the disturbance signal f_d . As can be verified from Figures B.9(b) and (c) and Figures B.10(b) and (c), the pilot control and tracking error signals (u and e , respectively) are found to be highly similar for both conditions, which is again due to the same disturbance signal that is attenuated by the pilot model in both conditions. Only minor differences in both these signals can be observed due to the different target forcing functions, mainly during the intervals where the ramp signal is increasing or decreasing.

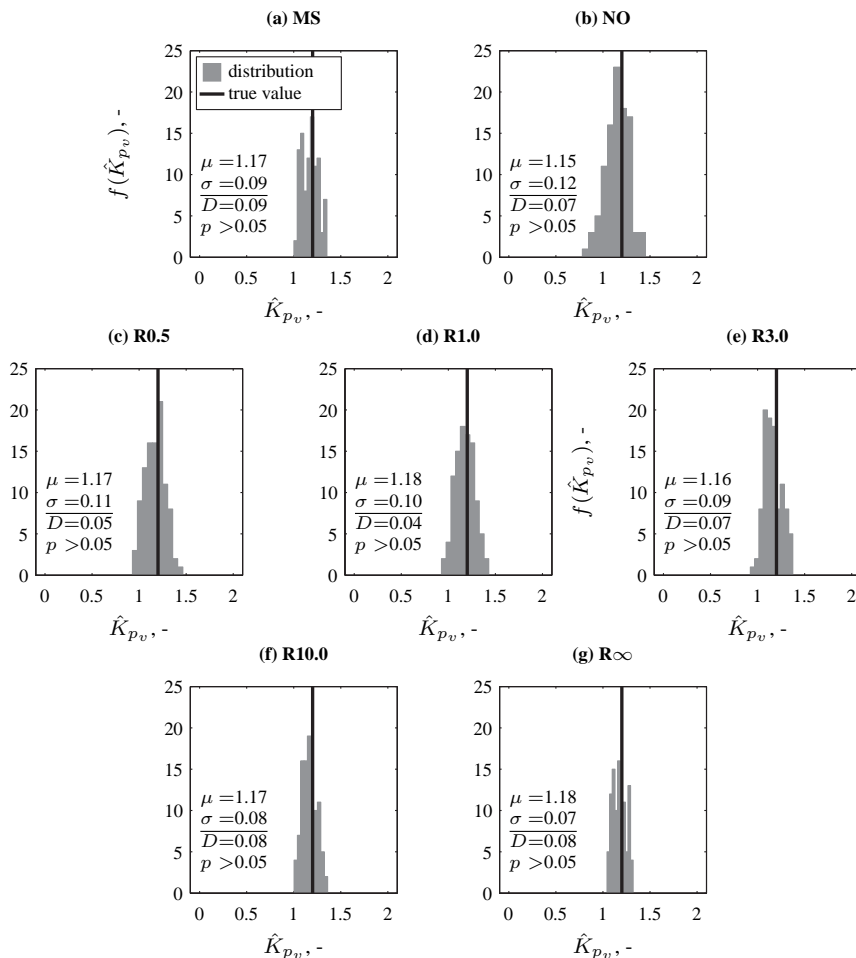


Figure B.11. Distribution of estimated values for the pilot visual gain \hat{K}_{p_v} compared to its actual value, $K_{p_v} = 1.2$. Mean μ and standard deviation σ of each distribution and the Lilliefors normality test statistic D and corresponding p -value are listed in each graph.

B.5.2 Pilot Model Estimation Results

Using the time traces of e , x and u as depicted in Fig. B.9 and B.10, the parameters of the pilot model were estimated using MLE. This yielded a set of model parameters for each of the 100 simulations of the control task considered here. The consistency of parameter estimation results was evaluated by investigating the distribution of the different attained solutions for the different target forcing function settings. Histograms of the 100 identified values of the pilot visual gain K_{p_v} , visual lead constant T_L , and motion gain K_{p_m} are depicted in Figures B.11 to B.13, respectively. The normality of the distributions shown in Figures B.11 to B.13 has been evaluated using the Lilliefors test. The values of the test statistic D and the corresponding p -values are indicated in each graph. Note that a p -value less than 0.05 is taken to indicate a significant deviation from normality. These figures also list the means μ and sample standard deviations σ of the presented distributions. The true values of the corresponding parameters, which were used for the pilot model simulations (see Table B.1), are depicted by the solid black lines.

For the evaluation of how the distributions of the estimated parameters are affected by the variation in target forcing function signal, the results for the condition with the multisine target signal (MS) as shown in Figures B.11–B.13(a) will be used as the baseline. As illustrated by these figures, the distribution of the estimated pilot model parameters that results from the use of a multisine target signal is typically not significantly different from a Gaussian distribution ($p > 0.05$), with a mean that is very close to the true parameter value. Especially for \hat{T}_L and \hat{K}_{p_m} , when no additional target signal is used (NO) the estimated parameter values show clearly non-Gaussian distributions of parameters and markedly larger spread (Figures B.12(b) and B.13(b)). This confirms that some additional target signal is indeed needed to ensure both inputs to the multimodal pilot model are “persistently exciting” [Ljung, 1999] and that the use of two independent multisine target and disturbance forcing function signals allows for obtaining reliable pilot model identification results [Stapleford et al., 1969; Nieuwenhuizen et al., 2008; Zaal et al., 2009a].

Figures B.11(c) to (g) show the distributions of \hat{K}_{p_v} for the ramp target signals with increasing ramp steepness. Based on the analysis of ramp signal characteristics in Section B.3, more consistent estimation results are expected with increasing ramp signals steepness, due to the increased excitation provided by signals with steeper ramps. As can be verified from Fig. B.11, the distributions of the estimates of the pilot visual gain K_{p_v} are indeed found to become narrower (lower σ), indicative of more consistent estimates, with increasing ramp forcing function steepness. Compared to the results obtained without an additional forcing function condition (NO) as shown in Fig. B.11(b), the overall improvement in the estimation of K_{p_v} is, however, found to be comparatively modest. In addition, for all target forcing function settings including the NO target condition, the distributions of \hat{K}_{p_v} are found to show no significant deviations from normality ($p > 0.05$). Fig. B.11 therefore illustrates that the accuracy with which the pilot visual gain can be estimated from measurement data is largely independent of the applied target forcing function signal.

The distributions of the estimated values for T_L and K_{p_m} depicted in Figures B.12 and B.13, however, show a significantly more marked effect of the variation in target forcing function and ramp signal steepness. This is an expected result, as difficulties with separating the visual and vestibular contributions (pilot lead) as defined in the overdetermined pilot

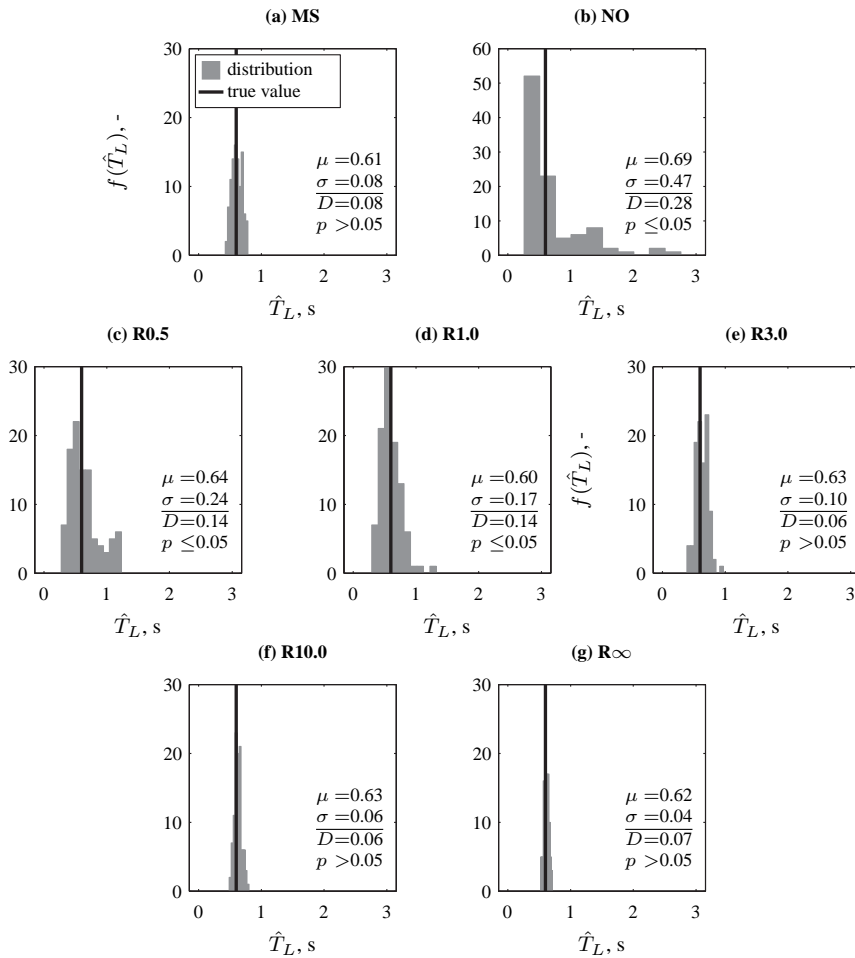


Figure B.12. Distribution of estimated values for the pilot lead time constant \hat{T}_L compared to its actual value, $T_L = 0.6$ s. Mean μ and standard deviation σ of each distribution and the Lilliefors normality test statistic D and corresponding p -value are listed in each graph.

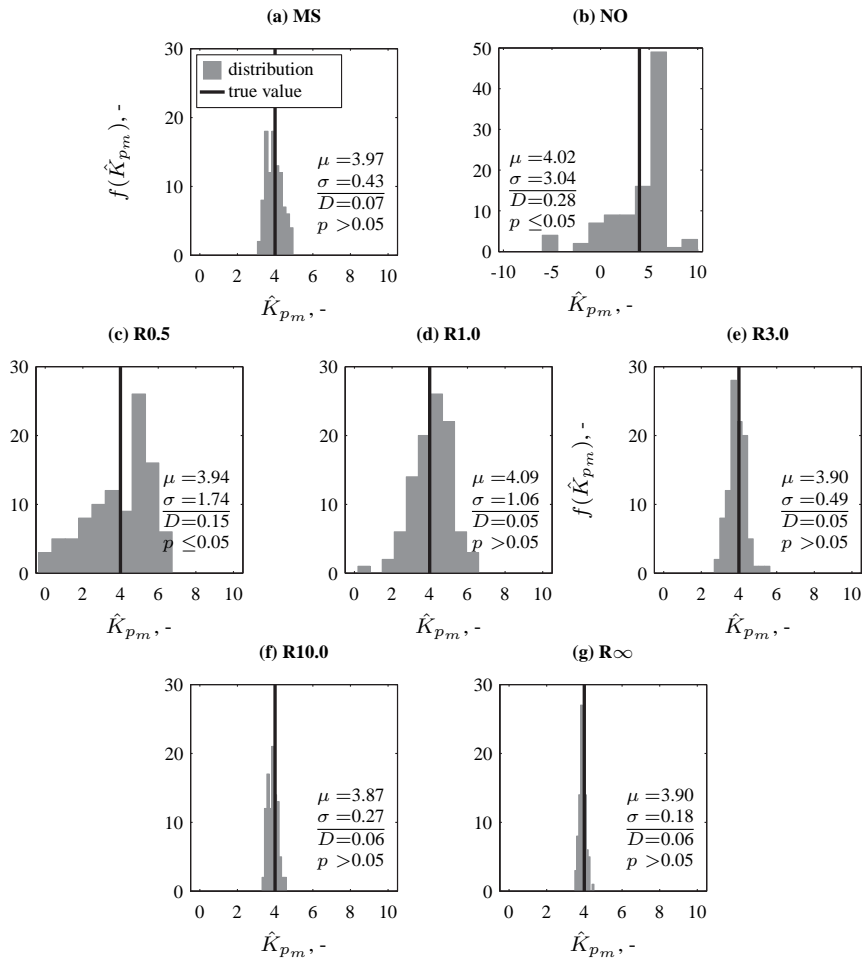


Figure B.13. Distribution of estimated values for the pilot motion gain \hat{K}_{p_m} compared to its actual value, $K_{p_m} = 4.0$. Mean μ and standard deviation σ of each distribution and the Lilliefors normality test statistic D and corresponding p -value are listed in each graph.

model will firstly affect the identified values of these two parameters [Zaal et al., 2009a]. For the low-steepness ramps and especially the R0.5 signal, the estimates of the visual lead constant and the pilot motion gain are found to be hardly more consistent than those found without an additional target signal (NO). Note the different ranges of the vertical axes in Figures B.12(b) and B.13(b), and the additional alternative x -axis scaling of the latter. Lilliefors test results also indicate that the distributions of \hat{T}_L and \hat{K}_{p_m} for these conditions are non-Gaussian ($p \leq 0.05$). As ramp signal steepness is increased, however, the values of the test statistic D are seen to consistently increase, indicating reducing deviations from normality, and the distributions of the estimates of T_L and K_{p_m} become increasingly narrower. As can be verified from subfigures (f) and (g) of Figures B.12 and B.13 by evaluating the shape of the distributions and the values of D and σ , parameter estimates are even more consistent than those found with the multisine target for the two signals with the steepest ramps, that is, R10.0 and R ∞ .

The histograms and corresponding statistical analysis depicted in Figures B.11 to B.13 show that the ramp signals proposed in this appendix indeed provide enough power to allow for reliable estimation of the overdetermined multimodal pilot model's parameters, as long as the steepness of the ramps is above a 3.0 deg/s. Fig. B.14 shows the biases¹ and standard deviations (σ in Figures B.11 to B.13) of the estimated parameter distributions as a function of the type of target signal for all seven pilot model parameters. Note that both the bias and standard deviation are normalized with respect to the true value of the pilot model parameter and expressed as a percentage. To allow for comparison with the baseline MS condition, a gray shaded area marks the bias obtained when using the multisine target signal (MS). Finally, solid black markers indicate the mean biases of those conditions for which the obtained distributions showed no significant deviations from normality, while white markers are used for those conditions for which the Lilliefors test indicated a deviation from normality.

The variance bars depicted in Fig. B.14 show that the spread in the estimates in all pilot model parameters reduces significantly when ramp signal steepness is increased. The more narrow distributions than found for the MS condition obtained for the steepest ramp signals, as shown in Figures B.12 and B.13, are confirmed here for the other pilot model parameters as well. For most model parameters, σ is found to be clearly lower for the R3.0 to R ∞ signals than for MS. Finally, note the typically non-normal distribution of parameter estimates and the comparatively large spread in the estimated parameter values obtained for the NO target condition and the R0.5 ramp signal: for instance for the visual lead constant T_L and the motion delay τ_m (Fig. B.14(b) and (e), respectively) the variance bars cover a range of at least $\pm 15\%$ of the true parameter value.

In addition to this increase in estimation consistency, the bias in most parameter estimates is also seen to reduce. Note that for the condition without an additional target signal (NO), the bias in the estimates is typically highest, on average reaching 15-20% for the visual lead constant T_L and the visual delay τ_v (Figs. B.14(b) and (d), respectively) and even going up to 60% of the true parameter value for the motion delay τ_m (Fig. B.14(e)). The decrease in bias for increased ramp steepness is perhaps most clearly visible for the estimates of both pilot model time delays, as can be verified from Figures B.14(d) and (e),

¹Note that bias is defined here as the difference between the mean of the estimated parameter values μ and the true parameter value as both depicted in Figures B.11 to B.13.

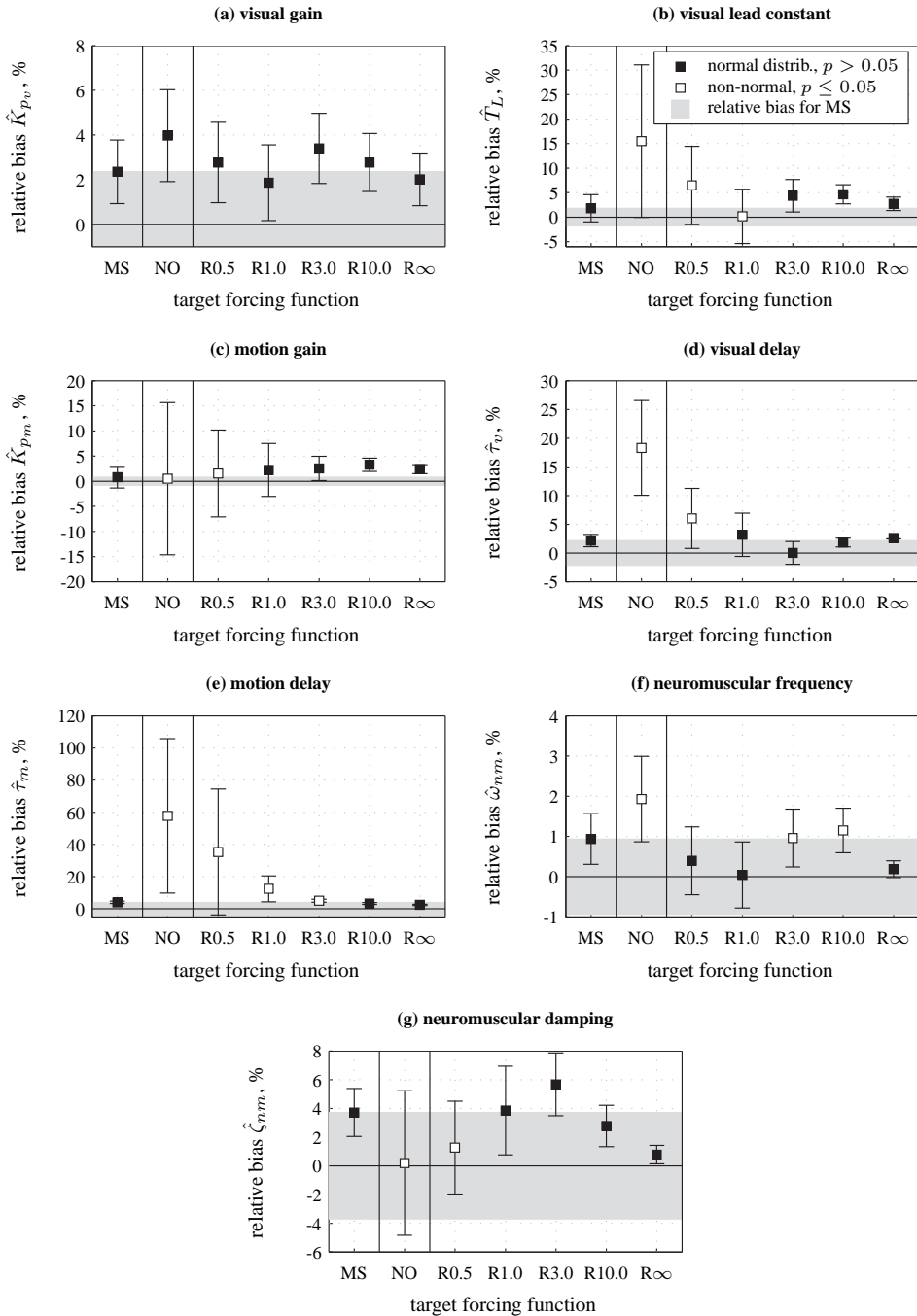


Figure B.14. Mean parameter estimate bias for different target forcing functions.

respectively. This can be explained by the fact that due to the phase roll-off caused by time delays, the biggest effect of these parameters is present at the higher frequencies. The increased high-frequency power in the forcing function signals for steeper ramps allows for more accurate estimation of these parameters. Note from Fig. B.14(d) and (e) that estimates for the steepest ramps are at least as accurate as those obtained for the MS condition.

Note that the results described here can provide an explanation for the comparatively low accuracy of the multimodal pilot model identification results found in some previous experimental evaluations in which ramp forcing function signals were evaluated [Zaal et al., 2008; Pool et al., 2009b; Zaal et al., 2010]. In these experiments, ramp forcing function signals with steepnesses of 1.0 and 3.0 deg/s were used. Figures B.11 to B.14 suggest that the excitation provided by such signals could be insufficient to guarantee accurate and reliable pilot model identification results.

B.6 Discussion

The focus of the presented research was not on the effects target forcing function signals that consist of multiple discrete ramp-like changes in reference value may have on pilot control behavior. Rather, this appendix investigated whether such signals provide enough excitation to allow for reliable identification of typical overdetermined multimodal pilot models. The overdetermined models that are typically used for modeling pilot multimodal control behavior put requirements on the design of the control task, and especially of the forcing function signals, to ensure pilot modeling can be applied for analysis of pilot control behavior. In particular, sufficient high-frequency forcing function power is required for identification of the high-frequency pilot dynamics that are present in typical multimodal pilot models.

From an analysis of the proposed ramp forcing function signals in the frequency domain, using frequency-domain descriptions obtained with the Fourier transform, it was found that one of the main factors affecting the power these signals hold at higher frequencies is the steepness of the ramps in the signal. For ramp signals, the signal power is inversely proportional with the square of the frequency, but increases approximately linearly with increased ramp signal steepness. For infinitely steep ramps, signal power is only inversely proportional to the frequency, yielding even more high-frequency excitation. Even though it is more distributed over all frequencies, on average signals consisting of multiple ramp-like changes were found to hold an amount of high-frequency power that is similar to that contained in multisine target signals that are typically used for multimodal pilot model identification.

Simulations of an attitude control task with acceleration control dynamics (double integrator) based on the results of a previous experiment [Zaal et al., 2008] were used to evaluate the accuracy of multimodal pilot modeling results for different target forcing function settings. For the selected control task – defined by the choice of controlled element dynamics, pilot model parameters and the disturbance signal f_d – a clear effect of ramp signal steepness was found on the accuracy of multimodal pilot model identification results. For ramps with steepnesses lower than 3.0 deg/s, estimated parameter values were found to have significantly higher bias and spread than those obtained with a multisine target signal.

Ramp signals with higher ramp steepnesses were, however, found to yield more reliable estimates of the multimodal pilot model parameters. This effect was visible in both the bias and standard deviation of the parameter estimates, but also in the distribution of these estimates. Using the Lilliefors test, it was shown that for conditions for which less accurate parameter estimates were obtained, distributions of parameter estimates also showed more frequent and larger deviations from normality.

The results presented in this appendix indicate that the proposed ramp forcing functions can allow for reliable pilot model identification for a typical multimodal pilot model identification problem. However, it can be expected that changes in the control task – that is, variations in controlled element dynamics, forcing functions, and the adopted pilot control behavior – will affect the accuracy with which pilot model parameters can be estimated. This implies that the conclusions drawn here with respect to the limits of ramp signal steepness that yield accurate estimation results may differ for other control task settings. As control task and forcing function design are found to affect pilot control behavior in numerous occasions [McRuer et al., 1965; Hosman, 1996], more research is required to investigate how the results described in this appendix are affected by changes in control task setup. In addition, whether the proposed ramp forcing function signals indeed provide more realistic control tasks than tracking tasks with two quasi-random forcing functions also needs to be evaluated in an experimental setting.

In this appendix, the assumption was made that pilot control behavior in a combined disturbance-rejection and ramp target signal following task could still be modeled using compensatory models of pilot control. As for instance argued in [Wasicko et al., 1966; Allen and McRuer, 1979; Hess, 1981], predictable forcing function signals may yield pursuit or precognitive contributions to control behavior during tracking. Especially if the same ramp signals are tracked a significant number of times, as was done in previous experimental investigations [Zaal et al., 2008; Pool et al., 2009b; Zaal et al., 2010], it is likely that pilots will develop a mental model of the control task and the forcing function signal that will allow for feed-forward control. If ramp signal design is varied, however, for instance by adopting randomized ramp amplitudes and durations, this would yield similar excitation to that provided by the signals considered in this appendix, but remove part of the predictability of the signal. This would then reduce the extent to which feed-forward control is supported. These effects of using such alternative forcing function signals for modeling pilot control behavior are planned to be addressed in future experimental investigations.

B.7 Conclusions

Time-domain pilot model identification techniques allow for the use of other forcing function signals than the quasi-random harmonic signals that are typically used for the identification of multimodal pilot control behavior in the frequency domain. This appendix evaluated the suitability of signals consisting of multiple ramp-like changes in reference value for use as the target forcing function during a manual attitude control task. The excitation and thereby the accuracy of multimodal pilot modeling results provided by such signals were evaluated using simulations of a typical multimodal pilot model in a control task from a previous human-in-the-loop experiment. The steepness of the ramps in such alternative

forcing functions was found to heavily affect the bias and variance of the resulting pilot model parameter estimates. Steeper ramps, which were shown to contain markedly more high-frequency power, yielded significantly more reliable identification results. For the signals with the steepest ramps (> 3 deg/s), estimates for most of the pilot model parameters were found to be more accurate and consistent than those obtained with a multisine target signal.

C

In-Flight Experiment Hardware Verification Tests

Due to the importance of the in-flight measurements of pilot tracking behavior (see Chapters 6 and 7) to the research described in this thesis, a significant amount of care was taken to ensure that all the hard- and software that was used to perform these experiments was functioning properly. The details of the experimental setup in the Cessna Citation II laboratory aircraft and the role of all hard- and software components are provided in Appendix D. This Appendix provides further details of the separate offline tests performed to evaluate the characteristics of three of the hardware components that were crucial to the success of these in-flight tracking experiments: the visual display used to present the tracking information to the pilots, the sidestick manipulator used for giving control inputs, and the vertical gyro used to measure the aircraft attitude to be used for the control tasks.

Note that despite the fact that only roll tracking data is described in this thesis, also behavioral measurements for pitch tracking task were collected in-flight, from which the results are presented in [Zaal et al., 2011] and [Zaal, 2011]. For this reason, this Appendix also covers some of the hardware characteristics important for the in-flight pitch tracking tasks.

C.1 Visual Display Delay Measurements

For human-in-the-loop experiments, especially those involving multimodal cueing conditions such as those collected in this thesis, knowledge of the delay with which information is presented to human operators is crucial for interpretation of the reported experimental results. Therefore, a custom visual delay measurement system was developed by Stroosma et al. [2007] for determining the delay of the various visual cueing systems of the simulator setups available at Delft University of Technology. This visual delay measurement system

uses a pair of shutter glasses that allows for (subjective) estimation of a time shift between the time data becomes available in the simulation software and the time it becomes visible on a visual display.

As described in more detail by Stroosma et al. [2007], this system is based around software that generates a sinusoidal signal, for which the frequency and the amplitude can be specified. This sinusoidal signal is used to drive the visual display that is to be tested. Together with this sinusoidal signal, the software generates a pulsing signal that is used to time the opening of the shutter glasses at a rate that is synchronous with the sinusoidal signal presented on the display. By shifting the pulsing signal in time until the shutter glasses open exactly at the zero-crossings of the sinusoidal signal on the display the delay in the visual presentation, including delays incurred from graphics calculations and hardware projection, can be estimated. The software used for this measurement system was implemented in DUECA (Delft University Environment for Communication and Activation, [Van Paassen et al., 2000]).

Before the experiments described in this thesis were performed, the delay of the visual cueing systems of the SIMONA Research Simulator (SRS) were determined using this visual delay measurement system. For the outside visual system, which was not used for any of the experiments described in this thesis, the delay was measured to be around 30 ms, while for the primary and secondary flight displays in the SRS a slightly lower delay of 20-25 ms was measured [Stroosma et al., 2007].

For correspondence of the control behavioral measurements collected in the Cessna Citation II laboratory aircraft and those taken in the SRS it was important to ensure the delays in the visual displays used for both experiments were equal. For determining the visual delay of the hardware used for the in-flight measurements, it was preferably to use exactly the same soft- and hardware as would be used during the actual experiments, as these all affect the total visual delay. Due to the fact that a computer with accurate high-frequency timing is required for driving the shutter glasses, an additional computer, other than the two Toshiba M700 touchscreen tablet computers of the Citation experiment setup (see Appendix D) was required, as these tablets lack the required hardware capabilities to perform this task. For this reason, a separate setup was used for measuring the visual delay, in which the tablet that performed the display generation during the in-flight experiments (*citefis*) was connected to the network of computers available in the Human-Machine Systems Laboratory (HMSLab) at Delft University of Technology. A schematic representation of the measurement setup is depicted in Fig. C.1.

As shown in Fig. C.1, the shutter glasses were connected to one of the real-time QNX machines available in the HMSLab (*dutmms4*). This computer also ran the DUECA module that generated the periodic test signals used for the visual delay test. Input (signal frequency and amplitude, shutter glasses delay and aperture, etc.) could be given from the experiment control station of the HMSLab (*dutmms1*) and through a joystick attached to this computer. As it would also do during the in-flight experiments, the *citefis* tablet only ran the *PFD* module, which was adapted slightly to present the signal generated by the visual delay measurement system.

The visual delay measurement was performed with a number of different frequencies for the sinusoidal signal (1, 2, 4, and 6 Hz). With all selected visual delay measurement test

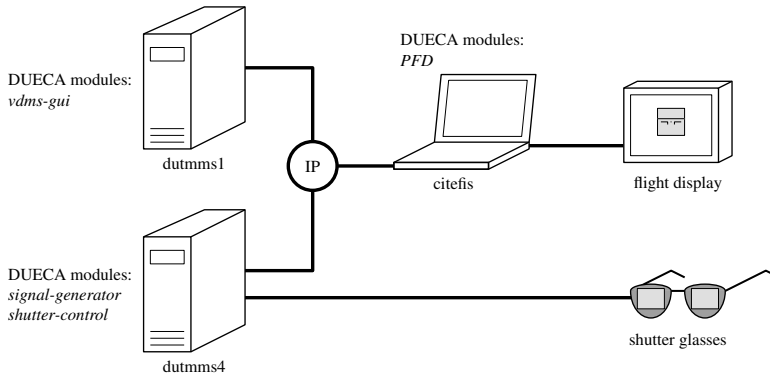


Figure C.1. Test setup used for the visual delay measurements.

frequencies, the visual delay of the setup used for the in-flight experiments was determined to be around 25 ms.

C.2 Force Stick Measurements

C.2.1 Static Force-Voltage Characteristic Measurements

For the in-flight experiments, a BG Systems JFf force stick was used for giving control inputs during the tracking tasks. This side stick was a force stick, meaning the output voltage, and hence the given control input, was proportional to the force applied to the manipulator. To evaluate the force-output voltage characteristics of this side stick, static force measurements have been taken at two occasions during the course of this research project. These measurements were taken by fixing the side stick with its grip aligned horizontally and suspending known weights from the grip to induce a known static force input. The results of these measurements, which were performed for both the pitch and roll axes of the stick, are depicted in Fig. C.2. Note that the first set of force-voltage characteristic measurements are indicated with star-shaped markers, while the second set of measurement data is depicted with open circles. Furthermore, note that the output voltages u_x and u_y could only attain values of $\pm 2.5V$.

Fig. C.2 shows that the force gradient was lower for the stick roll axis than for the pitch axis. This was by design, as it is more difficult to exert large forces on a side stick along the roll axis. Note, however, that the stiffness in pitch was increased after the first test flights with the system described by Zaal et al. [2010], to ensure that the force that would result in the stick hitting the mechanical end-stop would result in the maximum (positive or negative) output voltage. Note from Fig. C.2 that the static force-voltage characteristic measurements show largely linear force-output gradients of around 14 and 23 V/N for the stick roll and pitch axes, respectively.

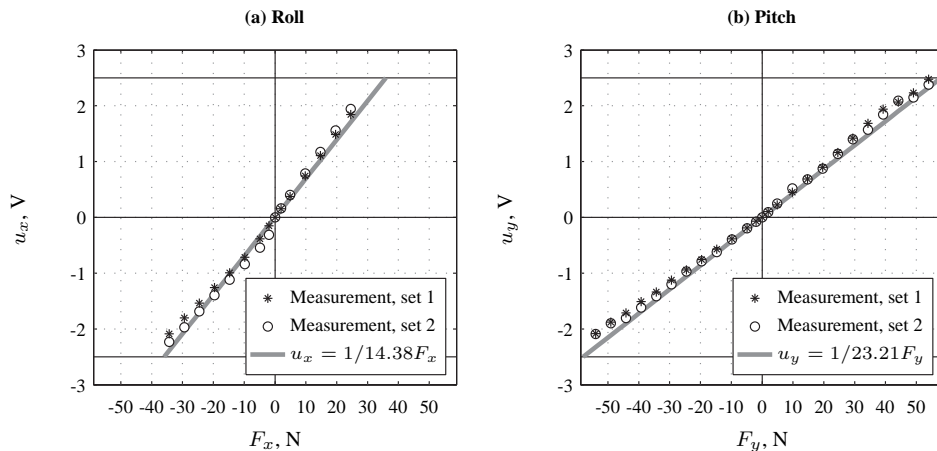


Figure C.2. Static Citation force stick measurements for the roll and pitch axes.

C.2.2 Force Stick Describing Function Measurements

To evaluate the dynamic characteristics of the side stick, measurements were performed on the Acutronic AC2266L calibration table that is available in the Calibration Laboratory at Delft University of Technology. For these measurements the side stick was fixed to the exact center of the rotational platform of the calibration table and rotated with its grip axis aligned horizontally. For a fixed rotational rate of the calibration table, gravity's pull would induce sinusoidal force inputs in the stick pitch and roll channels. The following rotational velocities were tested: 5, 25, 60, 120, 180, 230, 320, 450, 600, 850, and 1000 deg/s. Note that these rotational velocities yielded sinusoidal force inputs in both axes of the side stick with frequencies ranging from 0.0873 to 17.45 rad/s, that is, approximately the frequency range over which manual control behavior was measured in the in-flight experiments.

To collect the required measurements of the stick output voltages u_x and u_y together with the recorded state of the calibration table, the analog stick voltage outputs were read into the control cabinet of the calibration table and logged there. After some initial tests, it was found that the forces on the stick, and hence the measured output voltages remained very low due to the stick grip's relatively low weight. Therefore, 1 and 2 kg blocks of steel were manufactured, which could be mounted on the stick body instead of the stick grip. Measurements were taken at both these loading conditions for all 11 rotational velocity settings. From these measurements, the stick dynamics describing functions depicted in Fig. C.3 were calculated. Circular markers represent the describing function estimates, which were compiled from the separate rotational velocity measurements. The solid lines indicate the fits of a pure first-order lag model to these describing functions. The fitted first-order lag model is given by:

$$\hat{H}_s(j\omega) = \frac{K_s}{T_s j\omega + 1} \quad (\text{C.1})$$

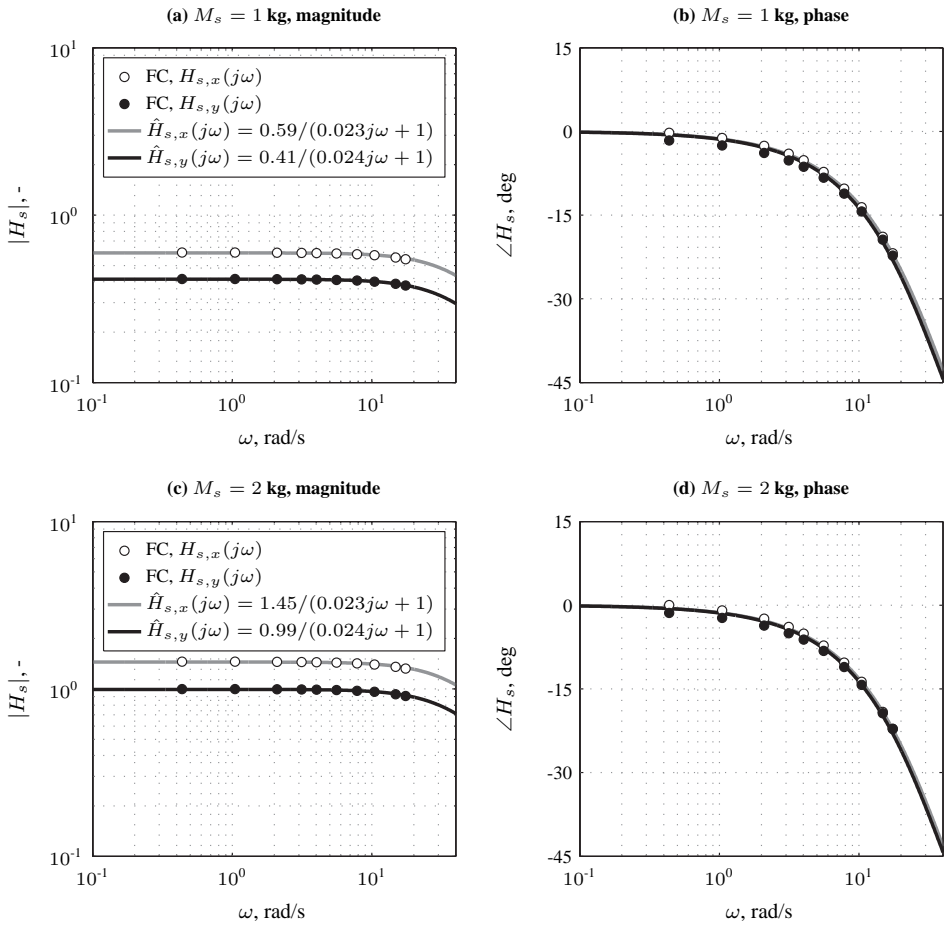


Figure C.3. Measured Citation force stick describing functions for stick pitch and roll axes under 1 and 2 kg loading conditions.

Note from Fig. C.3 that for both loading conditions and for both stick axes, the dynamic characteristics are found to be approximately those of a pure lag with a break frequency around 40 rad/s. The difference in amplitude between both loading conditions results from the different weights mounted on the stick – which is not simply a factor 2, mainly because of the center of gravity also shifted upwards for the heavier block, thereby further increasing stick forces – while the difference in gain between the stick pitch and roll axes results from the different stiffness of the stick in both axes (see Section C.2.1).

C.2.3 Stick Output Noise and Bias Characteristics

For the force stick used for the collecting the in-flight measurements of pilot tracking behavior, the output voltages u_x and u_y were between ± 2.5 V. The force measurements, and hence the resulting stick output voltages, were found to have significant bias and noise on them. This is illustrated in Fig. C.4, which shows time traces of the roll and pitch axis output voltages for a recorded measurement run in which no stick inputs were given by the pilot.

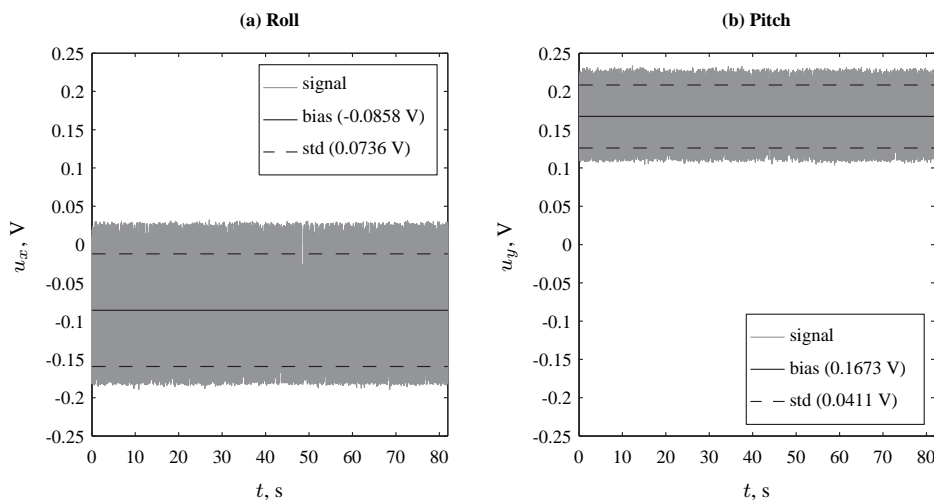


Figure C.4. Stick-free (no control) force stick roll and pitch output voltages.

As is clear from Fig. C.4 and the indicated values of the biases and standard deviations (stds) of the recorded signals, both the bias and the std were not negligible for both stick axes. Due to the fact that especially a bias in the stick output signals was not desired during the in-flight tracking tasks, the stick output biases were monitored during the experiments and it was made possible to cancel out the biases in u_x and u_y by adding control input offsets through the Experimental Control Interface (ECI) of the DUECA software (see Appendix D).

C.3 Gyro Describing Function Measurements

Perhaps the most important sensor for the pitch and roll attitude control tasks performed during the in-flight experiments is the vertical gyro (Honeywell VG-14 Three-Axis Reference SYNchro (Tarsyn)) that is used for measuring the aircraft pitch and roll attitude. As explained in Appendix D, the attitude measurements of this vertical gyro are collected in the on-board dSPACE computer of the Cessna Citation II laboratory aircraft, where they were used for calculating the tracking error that was to be minimized by the pilots during the tracking tasks. Due to its importance for the in-flight tracking measurements, the dynamic characteristics of this vertical gyro (referred to in the remainder of this section as “Tarsyn”) were evaluated using the Acutronic AC2266L calibration table in the Calibration Laboratory at Delft University of Technology. A schematic representation of the setup used for these tests is depicted in Fig. C.5.

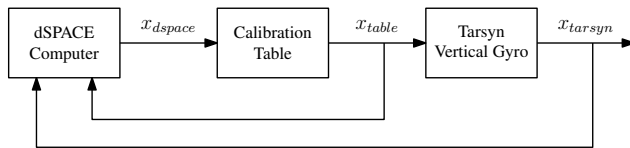


Figure C.5. Schematic representation of the test setup used for the Tarsyn vertical gyro describing function measurements.

For the calibration table tests, the Tarsyn gyro was mounted on the rotational platform of the calibration table. Similar to the setup in the laboratory aircraft, the dSPACE computer was used to read the gyro measurements. Specifically for these tests, the dSPACE computer was also used to generate a test signal x_{dSPACE} , see Fig. C.5. This test signal was then read into the control cabinet of the calibration table and used as a position reference signal for the calibration table’s pitch or roll axes. The calibration table and the gyro mounted on it would then move in either pitch or roll along a trajectory defined by x_{table} . Both the table attitude and measured Tarsyn attitude (x_{Tarsyn}) were fed back into the dSPACE computer, where all three signals depicted in Fig. C.5 were logged.

The test signal x_{dSPACE} that was used for these tests was equal to the target forcing function signal used for our in-flight experiments, scaled-up to yield maximum peak attitudes of up to 5 deg, and is depicted in Fig. C.6(a). Using this signal for these measurements allowed for evaluation of the Tarsyn dynamics over exactly the frequency range of interest to our in-flight experiments. Fig. C.6(b) depicts the spectrum of the test signal (calculated using 3 periods of the signal shown in Fig. C.6(a)). In addition, it depicts the corresponding spectrum of the attitude measured by the vertical gyro x_{Tarsyn} in black.

Measuring the three attitude signals depicted in Fig. C.5 allows for estimating the dynamics of both the calibration table’s response to a position reference signal, and of the Tarsyn gyro to the table’s response:

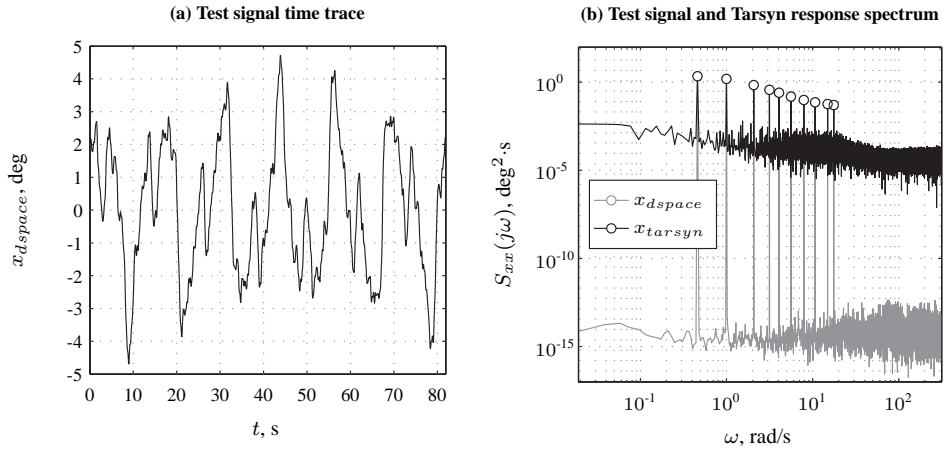


Figure C.6. Time trace of the test signal x_{dspace} used for measuring the Tarsyn describing functions and a comparison of its spectrum with that of an x_{tarsyn} measurement.

$$H_{table}(j\omega) = \frac{X_{table}(j\omega)}{X_{dspace}(j\omega)} \quad (C.2)$$

$$H_{tarsyn}(j\omega) = \frac{X_{tarsyn}(j\omega)}{X_{table}(j\omega)} \quad (C.3)$$

Fig. C.7 depicts the calibration table and Tarsyn describing function measurements obtained by applying Equations Eq. (C.2) and Eq. (C.3) to the collected measurements for the gyro pitch and roll axes. Note that the magnitude of both $H_{table}(j\omega)$ and $H_{tarsyn}(j\omega)$ is found to be very close to one over the complete range of tested frequencies. Fig. C.7 further shows that the response of the calibration table can be approximated as a delay of around 21 ms, while the Tarsyn response in both axes is near-perfect and is approximately equal to a pure gain with no appreciable phase distortion.

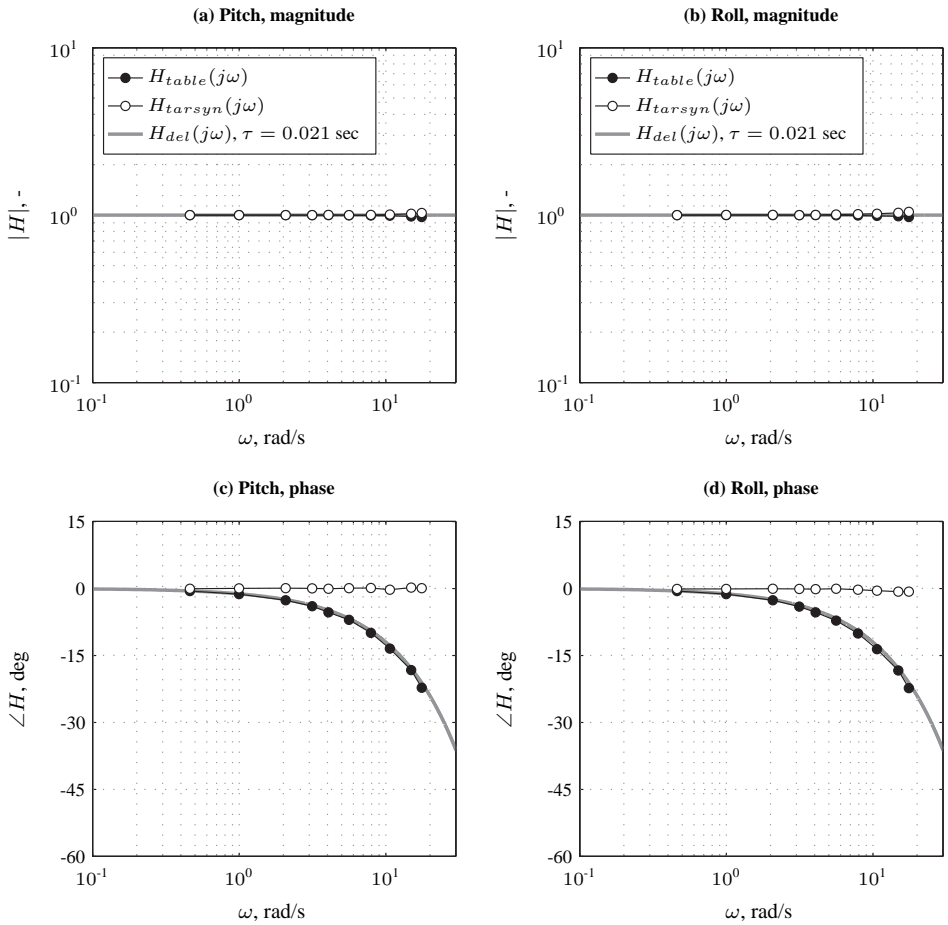


Figure C.7. Measured describing functions of the Tarsyn vertical gyro dynamics for roll and pitch attitude measurements.

D

In-Flight Experiment Software and Timing

This Appendix gives an overview of the software that was used to perform the in-flight tracking experiments described in Chapters 6 and 7. The first in-flight experiments for the research described in these chapters and the thesis by Zaal [2011] that were performed using this software were conducted in July-August 2009. After these experiments were completed, a timing error that resulted from the communication between different portions of the experiment software was discovered. As this timing error had resulted in significant extra delay in the control loop pilots closed in the in-flight tracking tasks, this timing problem was fixed and new in-flight measurements were taken in October and December 2010. The results of these second in-flight measurements are described in Zaal [2011] and Chapters 6 and 7. This Appendix provides an overview of the different software modules, and how they interact with the various hardware components of the experimental setup in the laboratory aircraft. Furthermore, this Appendix will explicitly show the cause and result of the incurred timing issues, and of some additional offline hardware tests performed to diagnose this problem.

D.1 July/August 2009 Experiments

D.1.1 Experiment Software Setup

The software used to perform the in-flight pitch and roll tracking tasks described in [Zaal, 2011; Zaal et al., 2011] and Chapters 6-7, respectively, consists of two separate parts, that run in parallel. First, most of the communication with the various hardware components that were important for the in-flight experiments was performed by dSPACE[®] software, imple-

mented in Matlab[®] Simulink[®], that ran on the real-time dSPACE computer that is a part of the custom Cessna Citation II laboratory aircraft Flight Test Instrumentation System (FTIS), see Fig. D.1. For more detailed descriptions of the different hardware components used for the experiments and FTIS, please refer to Chapter 6 and [Zaal et al., 2009d]. In addition to this dSPACE software, additional experiment software modules were developed in the Delft University Environment for Communication and Activation (DUECA) [Van Paassen et al., 2000], implemented in C++, and ran on two experimental computers (Toshiba M700 touch-screen tablet notebooks, see Fig. D.2). The DUECA portion of the experiment software was used for experiment control and condition selection, for generating the forcing function signals, for data logging, and for generating the visual displays presented to the pilots. The dSPACE and DUECA parts of the in-flight experiment software communicated and exchanged data through User Datagram Protocol (UDP) network communication. Fig. D.3 depicts a schematic representation of the structure of the total experiment software as used for the first in-flight experiments that were performed in July/August 2009.

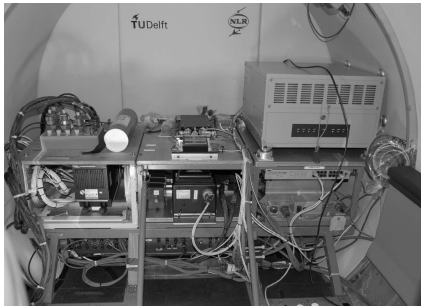


Figure D.1. The Flight Test Instrumentation System (FTIS) mounted in the back of the Cessna Citation II laboratory aircraft cabin (dSPACE computer at top right).



Figure D.2. The two Toshiba M700 touch-screen tablet notebooks in their mounts in the Cessna Citation II laboratory aircraft (*citefis* at left, *citecs* at right).

D.1.1.1 dSPACE Software

The main functions of the dSPACE part of the experiment software were to communicate data from DUECA to the experimental fly-by-wire (FBW) control system hardware in the laboratory aircraft and to collect measurement data from various analog and digital sensors installed in the aircraft. As can be verified from Fig. D.3, the dSPACE software performed the following six main activities, of which the details are provided in Table D.1.

As can be noted from Fig. D.3, these different activities within the dSPACE software were triggered at different frequencies. Some of the *Analog Receive* activities were performed at 50 Hz, while others ran at 5000 Hz. Note that the activities for sending and receiving UDP data both ran at 100 Hz, the same rate at which UDP packets were sent from DUECA (see Section D.1.1.3). The dSPACE software was triggered based on the internal clock of the dSPACE computer.

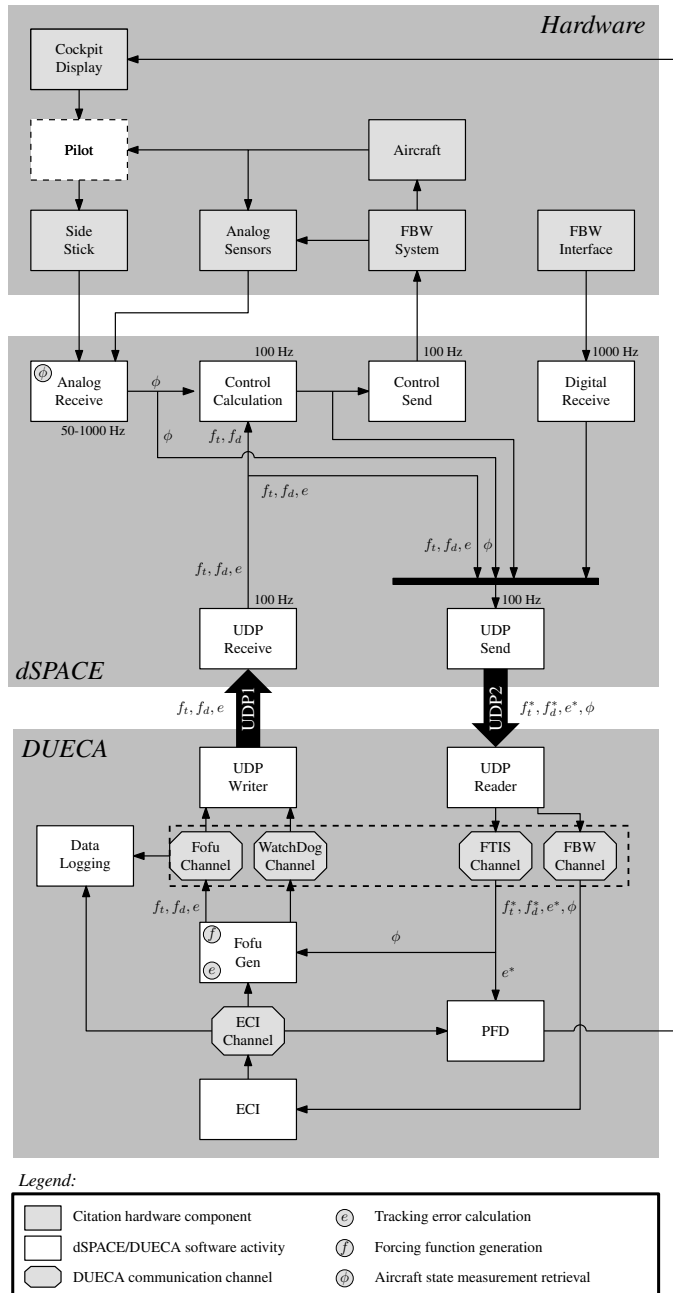


Figure D.3. DUECA and dSPACE software architecture as used for the July/August 2009 in-flight experiments.

Table D.1. dSPACE software activity definition and function.

dSPACE activity	Function
AnalogReceive	Receive data from a number of analog sensors (IMU, nose-boom alpha- and beta-vanes, GPS, vertical gyro, servo actuator synchro and tacho, etc.) and the custom <i>Side Stick</i> installed in the Citation cockpit for the in-flight experiments.
DigitalReceive	Receive data on the current state of the FBW system (channel selection and activation) from the <i>FBW Interface</i> mounted in the Citation cockpit.
ControlCalc	Calculate required control inputs to be sent to the FBW control system servo actuators based on stick inputs, forcing function signals from DUECA, and feedback of control system servo synchro position.
ControlSend	Transmit calculated control inputs to the servo amplifier circuit boards of the autopilot computer
UDPReceive	Receive important data from the DUECA software via UDP
UDPSend	Send all important data to the DUECA software via UDP

D.1.1.2 DUECA Software

As can be verified from Fig. D.3, some of the key activities in the experiment software were performed by a core of software modules implemented in DUECA. The main reason for this is that this approach allowed for using exactly the same software for, for instance, data logging and forcing function generation, as used for the corresponding simulator experiments performed in the SIMONA Research Simulator (SRS) (see Chapters 6-7). For the in-flight experiments, these DUECA software modules ran on two Toshiba M700 touch-screen notebooks with a Linux operating system. The first, referred to in the remainder of this appendix as *citefis* was used to generate the visual image of the compensatory or pursuit displays presented to the pilots during the tracking tasks. The second experiment computer, referred to as *citecs*, ran the rest of the DUECA modules. Table D.2 lists the DUECA software modules, as shown in Fig. D.3, and their corresponding functions during the in-flight experiments.

Communication between the DUECA modules that performed these different functions went through the DUECA *channels* that are indicated with the diamond-shaped boxes shown in Fig. D.3. A definition of these different DUECA channels is given in Table D.3.

The two UDP communication links between the DUECA and dSPACE software entities through the *UDPWriter* and *UDPReader* modules, indicated with *UDP1* and *UDP2* in Fig. D.3, will be treated in more detail in Section D.1.1.3. Note that the DUECA software was triggered on the internal clock of the *citecs* laptop and ran at 100 Hz, where the software triggering chain started with the *UDPReader* module. Furthermore, note from Fig. D.3 that the DUECA software drove one hardware element, that is, the cockpit display used to display the control task instruments. This external display was connected to the *citefis* tablet through a VGA cable. Finally, the DUECA experiment control interface (ECI) that allowed

Table D.2. DUECA software module definition and function.

DUECA module	Function	Ran on
FofuGen	Generate the target and disturbance forcing function signals used for the tracking tasks.	<i>citecs</i>
ECI	Provide an interface for experiment control and condition selection.	<i>citecs</i>
DataLogging	Log all relevant variables to files.	<i>citecs</i>
PFD	Generate a visual display image during the tracking tasks.	<i>citefis</i>
UDPWriter	Send important data to dSPACE software via UDP.	<i>citecs</i>
UDPReader	Receive important data from dSPACE software via UDP.	<i>citecs</i>

Table D.3. DUECA software channel definitions and functions.

DUECA channel	Channel type	Function
ECIChannel	Event	This channel is used to communicate experimental conditions selected by the experimenter from the experimental control interface to all other DUECA software modules.
FofuChannel	Stream	This channel contains the values of the target and disturbance forcing function signals and the corresponding tracking run time. Furthermore, it also contains the current value of the tracking error that is shown on the visual display.
WatchDogChannel	Stream	This channel is used to send a watchdog signal to the dSPACE software to indicate the DUECA software is still running properly. In addition, this channel is used to send information on the current state of the DUECA software to dSPACE. This information is used to verify if the DUECA software is in the correct state before the FBW system is switched on.
FTISChannel	Stream	This channel is used to send all data collected from the analog FTIS sensors and variables calculated from those measurements in dSPACE to DUECA. In the SRS experiments, the data in this channel was provided by the aircraft and FBW control system model described in Appendix E.
FBWChannel	Stream	This channel is used to communicate the current state of the experimental FBW system, as selected on the <i>FBW Interface</i> , from dSPACE to DUECA.

for selection of experimental conditions and for monitoring of several experiment and aircraft states during the in-flight tracking runs is shown in Fig. D.4.

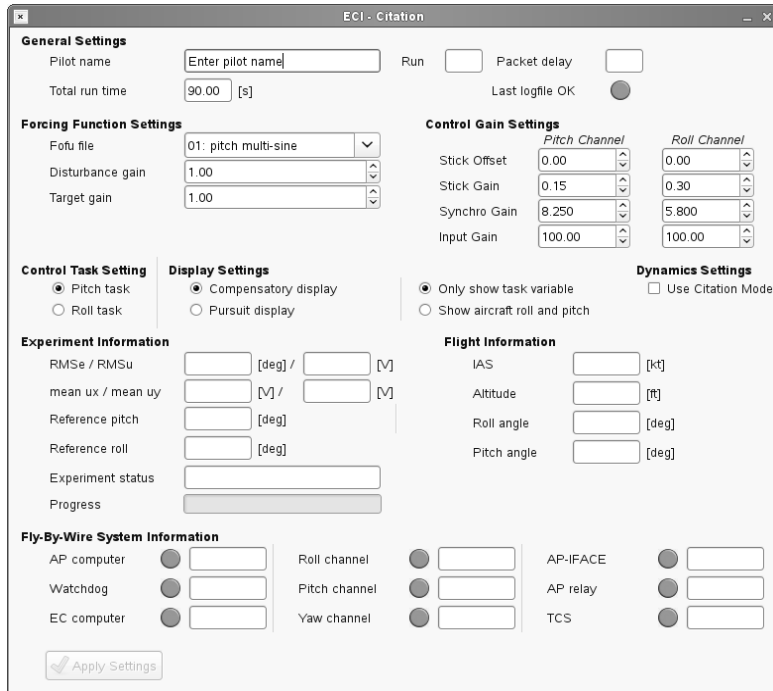


Figure D.4. DUECA software experimental control interface (ECI) used for condition selection and experiment monitoring during the in-flight experiments.

D.1.1.3 UDP Communication

The *UDP1* communication link between the DUECA and dSPACE software serves two main purposes. The first is communicating important data that is generated within the DUECA software – most notably the target and disturbance forcing function signals and experiment control variables – to the dSPACE software. A second important function of this UDP communication link is sending a watchdog signal to the dSPACE software, to indicate that the DUECA software is running properly. To achieve these two purposes, a DUECA *UDPWriter* module is used to send all data in the *FofuChannel* and the *WatchDogChannel* to dSPACE via *UDP1*, see Fig. D.3. The DUECA *UDPWriter* module sent data at a rate of 100 Hz, that is, the rate at which the DUECA simulation was running. As can be verified from Fig. D.3, the receiving dSPACE activity (*UDP Receive*) was also triggered at 100 Hz, and not on the incoming data packets.

The *UDP2* communication link was used for sending important data collected by the dSPACE computer to DUECA. A distinction is made between measurements of various states of the aircraft and the FBW control system, and currently selected settings of the

experimental FBW system. These two sets of variables were converted by a DUECA *UDPReader* module into two DUECA channels: the *FTISChannel* and the *FBWChannel*, respectively. Similarly to *UDP1*, both the UDP sending and receiving activities were ran at 100 Hz on the respective systems. Note that the DUECA *UDPReader* module was triggered on the internal DUECA clock, and not on the incoming UDP data packet stream.

D.1.1.4 Tracking Error Calculation

One of the most important functions the combined DUECA and dSPACE software was to perform was the cueing of physical aircraft motion and visual tracking error information during the in-flight control tasks. The motion of the aircraft was driven by both a disturbance forcing function signal generated in the *FofuGen* module in the DUECA software (see Fig. D.3) and by control inputs given through the installed *Side Stick*.

As indicated in Fig. D.3 by the symbol \odot , the tracking error that was presented on the display was calculated in the *FofuGen* module in DUECA. For this the target forcing function signal generated in that same module was used, in addition to the measured aircraft attitude received from dSPACE through *UDP2* and the DUECA *FTISChannel*. To make sure that the effects of the target and disturbance forcing function signals would affect the control task *synchronously*, the calculated tracking error was sent to dSPACE, together with the target and disturbance forcing function signals. As indicated with the superscript “*” in Fig. D.3, these signals were then looped back to DUECA, where e^* was then presented on the cockpit display.

D.1.2 Experiment Software Timing Issues

After performing the first in-flight experiments in July/August 2010, an issue with the experimental setup, either in the hardware or in the used software, in the laboratory aircraft was identified. The collected in-flight measurements of pilot tracking performance, control activity and further control behavioral metrics showed large discrepancies with measurements taken for the same control task in the SRS. After extensive testing of all hard- and software components of the experiment setup, this issue was found to result from the UDP communication between the DUECA and dSPACE parts of the experiment software (see Fig. D.3).

D.1.2.1 Software Timing Issues Evaluation

To illustrate the issue with the UDP communication link between the dSPACE and DUECA parts of the experiment software, Fig. D.5 depicts the number of time steps by which the disturbance forcing function signal was shifted between the variable f_d present in the DUECA *FofuChannel* and the variable f_d^* in the DUECA *FTISChannel*. The data presented in Fig. D.5 was calculated from all recorded measurement runs during the four flights performed in July/August 2009. Data from the two different pilots that performed the experiment on each flight are depicted in each graph and are indicated with differently colored markers.

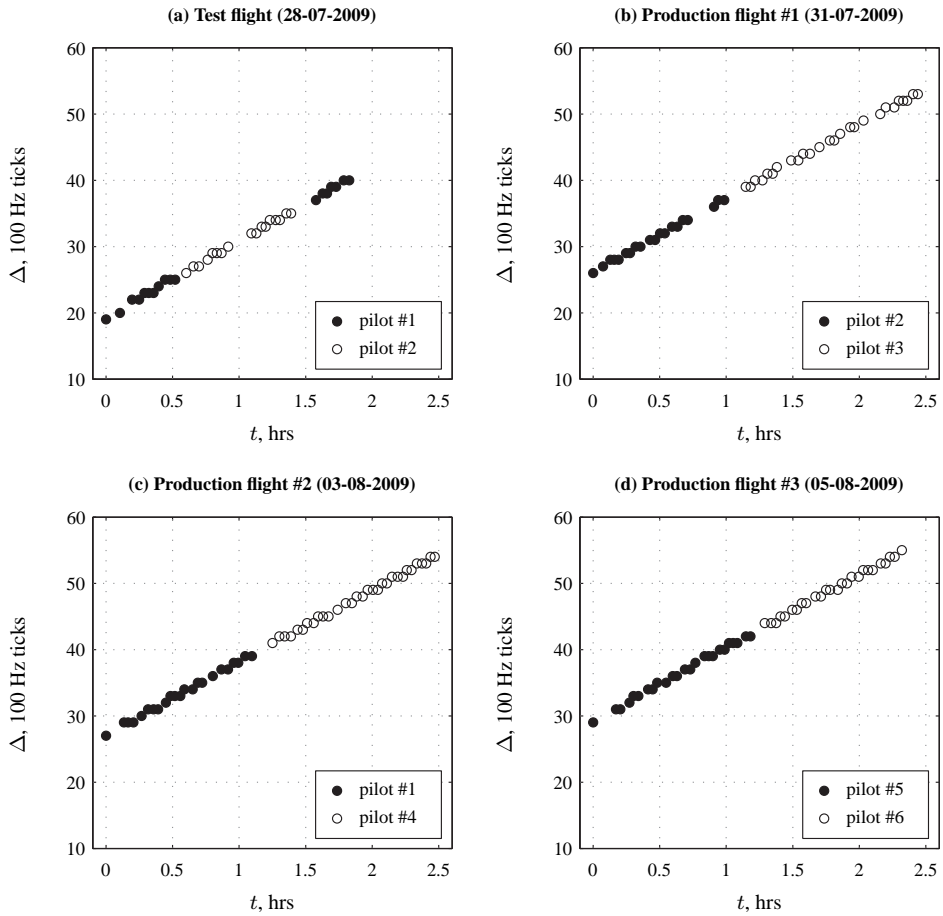


Figure D.5. Time shift Δ between disturbance signals in *FofuChannel* and *FTISChannel* during the July/August 2009 in-flight experiments.

Note from Fig. D.5 that the time shift between f_d and f_d^* increases with time, with a constant rate of about 10 ticks (equivalent to 0.1 s) per hour for all four flights. For some of the flights, the time shift increased to over 55 ticks (0.55 s), and some subjects only started their part of the experiment when Δ was already larger than 0.4 sec. Note that the fact that the time shifts do not start from 0 is a result of the fact that DUECA and dSPACE were typically already running since the start of the flight and that tracking task measurements were not started immediately.

D.1.2.2 Timing Issues Evaluation Test Setup

To further evaluate the timing problems encountered during the July/August 2009 experiments and to attribute these to either one of the UDP communication links (*UDP1* and *UDP2*, Fig. D.3), a test setup for diagnosing the timing issue was developed in an iron-bird setup that included the relevant components of the experimental setup. This setup made use of DUECA and dSPACE software that were equivalent to that used for the in-flight experiments. As indicated in Fig. D.6, however, the *FofuGen* module was adapted to send a test signal $f_s(t)$ from DUECA to dSPACE in two independent ways, in order to separate possible delays incurred in the *UDP1* and *UDP2* communication links. As can be verified from Fig. D.6, the test signal f_s was:

1. directly fed to the *Analog Receive* activity of the dSPACE software through one of the analog inputs normally used for receiving *Side Stick* inputs.
2. put on the *FofuChannel* in the variable e_{FOFU} and then sent to the dSPACE software via *UDP1* as also done during normal software operation.

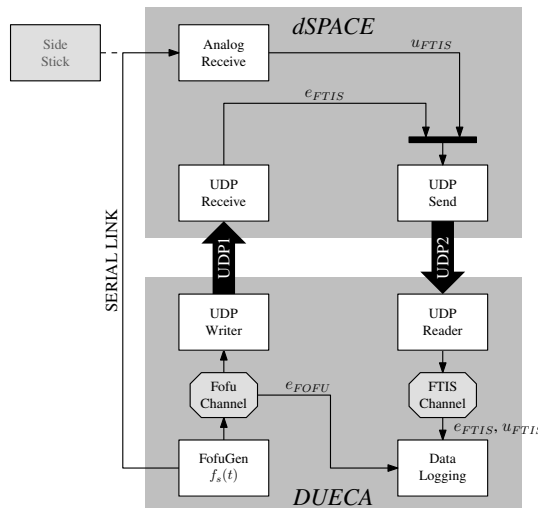


Figure D.6. Test setup used for identifying timing issues.

The two different instances of f_s within the dSPACE software, contained in the dSPACE software variables e_{FTIS} and u_{FTIS} (see Fig. D.6), were then sent back to DUECA via *UDP2*, where they ended up as the corresponding variables in the *FTISChannel*. By evaluating the time shift of these two signals coming back from dSPACE with respect to the test signal as generated in DUECA (e_{FOFU} in Fig. D.6), the following time shifts can be calculated:

$$\Delta 1 = \Delta(e_{FTIS}, e_{FOFU}) \quad (D.1)$$

$$\Delta 2 = \Delta(u_{FTIS}, e_{FOFU}) \quad (D.2)$$

Note from Fig. D.6 that $\Delta 1$ results from both *UDP1* and *UDP2* (in addition to lags induced by dSPACE and DUECA calculations), while $\Delta 2$ results only from *UDP2*, as f_s ends up in dSPACE through the SERIAL link undelayed.

The test signal f_s that was used for these ironbird tests is depicted in Fig. D.7(a). The value of f_s changes between +1 and -1 for increasing intervals, ranging from 1 to 20 time steps. Such a signal allows for clear and unambiguous determination of time shifts. Note that Fig. D.7(a) only depicts one period of the signal. For the measurements taken to evaluate $\Delta 1$ and $\Delta 2$, more than 20 periods of this signal were used.

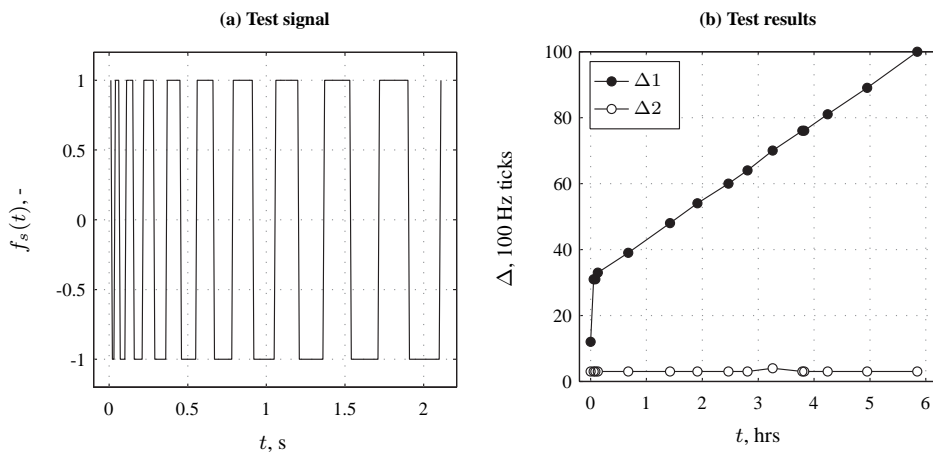


Figure D.7. Test signal used for measurement of software timing and the results of the timing test.

Fig. D.7(b) depicts the results of these ironbird measurements. The horizontal axis of this graph shows the time in hours from the starting of the DUECA software and the taking of the measurement. The data then shows the corresponding time lags $\Delta 1$ (black) and $\Delta 2$ (white) expressed in the number of (100 Hz) clock ticks. Fig. D.7(b) clearly shows that $\Delta 2$, which is only affected by *UDP2*, remains constant over the duration of running the software at around 3 ticks. $\Delta 1$, however, clearly shows a linear increase with time of around 10 ticks/hour, as also visible in Fig. D.5, and reaches a full second of delay within 6 hours

of running the software. Together with the data from the in-flight experiments depicted in Fig. D.5 this showed the timing issue resulted from the sending of UDP data from DUECA to dSPACE (*UDP1*).

Upon further inspection of the *UDP Receive* activity in the dSPACE software it was found that rather than returning the latest datagram received at a certain trigger of the dSPACE software, the datagram at the top of the circular buffer was read and used in the dSPACE software. With the uncoupled timing of the DUECA and dSPACE parts of the software, this caused datagrams to accumulate in the buffer over time, yielding the use of older data in dSPACE software compared to what was generated in DUECA.

D.2 October/December 2010 Experiments

D.2.1 Experiment Software Setup

To solve the software timing issue described in Section D.1.2, both the DUECA and dSPACE software were adapted for a second set of in-flight experiments, performed in October and December 2010. The adapted architecture of this second version of the in-flight experiment software is depicted in Fig. D.8. The main modifications with respect to Fig. D.3 are:

1. Adding a message counter to the UDP communication packets for communication monitoring
2. Synchronizing the DUECA clock with incoming UDP data from dSPACE
3. Modification of the *UDP Receive* activity in dSPACE
4. Moving the calculation of the tracking error from DUECA to dSPACE

D.2.1.1 Modifications to dSPACE Software

As can be verified from Fig. D.8, two additional activities were added to the dSPACE software compared to the software used for the July/August 2009 experiments (Fig. D.3). The first was the addition of the *Msg Counter* activity, which incremented an integer message counter variable every 100 Hz time step of the dSPACE software. This message counter was appended to the UDP data packets sent to DUECA (*UDP2*). The second was the calculation of the tracking error, which was moved to dSPACE from DUECA. More details of this tracking error calculation can be found in Section D.2.1.4.

The biggest modification to the dSPACE software, however, was made to the *UDP Receive* activity. To ensure datagrams could no longer accumulate in the circular buffer of the dSPACE network communication interface, this activity was now ran at double the rate at which UDP data was sent from DUECA, that is, at 200 Hz. In addition, the dSPACE Simulink[®] software used for reading data from the circular UDP buffer was modified to always read from the buffer until there were no more packets in the buffer, and then send through the latest received set of data. Note that this required storing of the latest received data in a local variable in the dSPACE software.

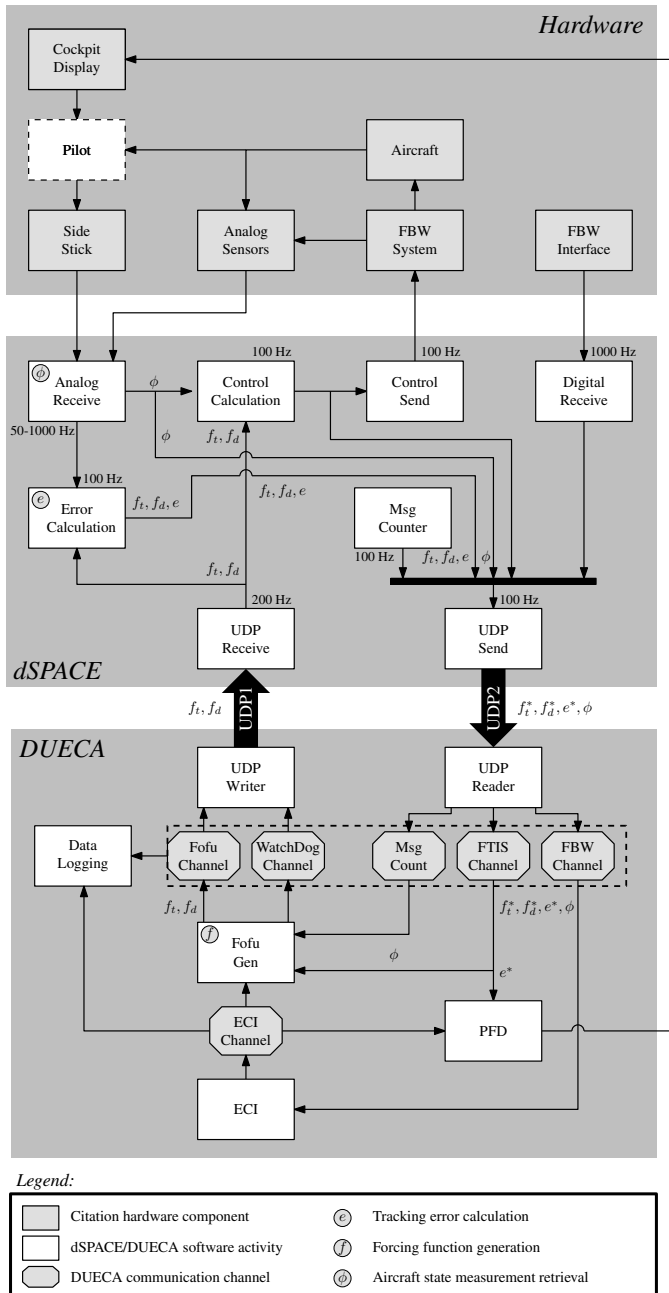


Figure D.8. DUECA and dSPACE software architecture as used for the October/December 2010 in-flight experiments.

D.2.1.2 Modifications to DUECA Software

Comparing Fig. D.8 with Fig. D.3, an extra channel was added to the DUECA software: the *MsgCount* channel. This channel was used to send the identification number of the latest data packet received through *UDP2* to the *FofuGen* module. Note that this identification number is generated in the *Msg Counter* activity in the dSPACE software. The *FofuGen* module adds the received counter to the *WatchDogChannel* that is sent back to dSPACE, where it is looped back to DUECA through *UDP2* and is appended to the *FTISChannel*. Comparison of the two received message counters (the one that is on the *MsgCount* channel and the counter in the *FTISChannel*) allows for direct evaluation of the time lags in the software communication and calculation cycle.

In addition, the settings of the DUECA *UDPReader* module were modified. The functionality built in this module was used to synchronize the internal clock used for triggering the DUECA software activities with the UDP data coming in from dSPACE. This ensures more synchronous operation of both parts of the software, leading to a lower probability of a communication error occurring.

D.2.1.3 Modifications to UDP Communication

Other than the changes to the UDP receiving activities of both DUECA and dSPACE, and the addition of a number of variables in the UDP packets going through *UDP1* and *UDP2*, the UDP communication itself was the same as in the July/August 2009 experiments.

D.2.1.4 Modifications to Tracking Error Calculation

As indicated in Fig. D.8 by the symbol \textcircled{e} , the calculation of the tracking error was moved from DUECA to dSPACE in the modified version of the experiment software. The reason for this is that this omits the extra looping of calculated tracking errors depicted in Fig. D.3. Fig. D.8 shows that now the target and disturbance forcing functions are sent from DUECA to dSPACE through *UDP1* and then used for calculating the tracking error and calculating the FBW control input, respectively, in the dSPACE software. The tracking error is then calculated using the measurements of aircraft attitude and sent to DUECA through *UDP2*.

D.2.2 Experiment Software Timing Verification

Using the two message counters added to the software for the October/December 2010 experiments (see Section D.2.1.2), the timing discrepancies introduced by the communication between DUECA and dSPACE can be evaluated explicitly for each time step. For all recorded runs of the experiments performed in October/December 2010 (four flights), Fig. D.9 depicts the maximum discrepancy Δ between the two message counters.

A comparison of the values of Δ shown Fig. D.9 with those depicted in Fig. D.5 shows that the increasing time shift was adequately taken care of with the measures described in Section D.2.1. For the large majority of the recorded runs, the maximum time shift was found to be between 2 and 4 ticks. Note that a minimum of 2 ticks is already expected, considering the fact that consecutive iterations of both the DUECA and the dSPACE software are included in the time difference between both counters. The results shown in Fig. D.9

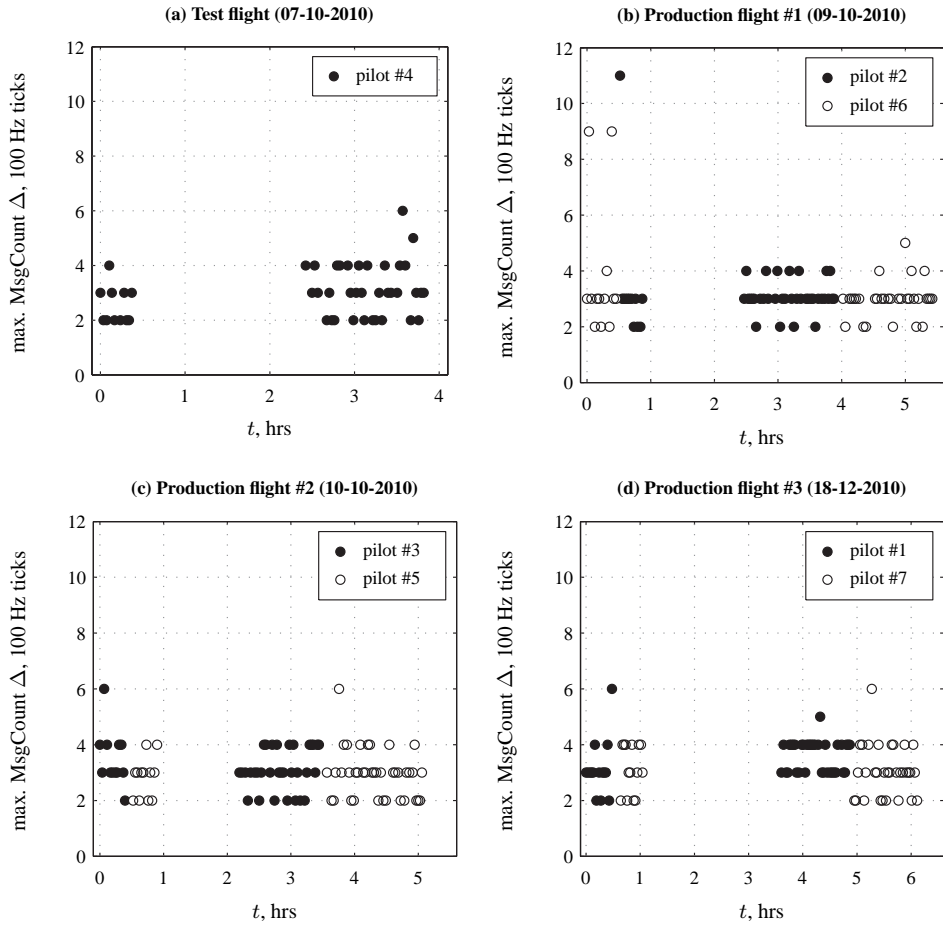


Figure D.9. Maximum MsgCount Δ for all three flights performed in October 2010 and the one flight performed in December 2010.

are summarized in Table D.4, which presents percentages for which the different values of Δ were found to occur. Note that in only 3% of the recorded runs, the maximum timing discrepancy was found to be more than 4 ticks, where that percentage was 100% during the July/August experiments (see Fig. D.5).

Table D.4. Distribution of maximum timing discrepancies (335 logged files).

Max. MsgCount Δ 100 Hz ticks	Occurrence %
2	22%
3	50%
4	25%
> 4	3%

For the 3 of the 11 experiment runs that made up the 3% for which $\max. \Delta > 4$, the difference between both message counters is plotted against time in Fig. D.10. For each run, the left graph shows the full time trace of the timing discrepancy Δ , while the right graph shows a detail of the largest peak in the signal. Note that even for these recorded runs, which represent the worst collected sets of data in terms of timing performance, the timing discrepancy is around 2 for the large majority of the measurement interval. Values of $\Delta > 2$ are depicted as white circular markers, while the maximum Δ occurring in each run is depicted with a black circle.

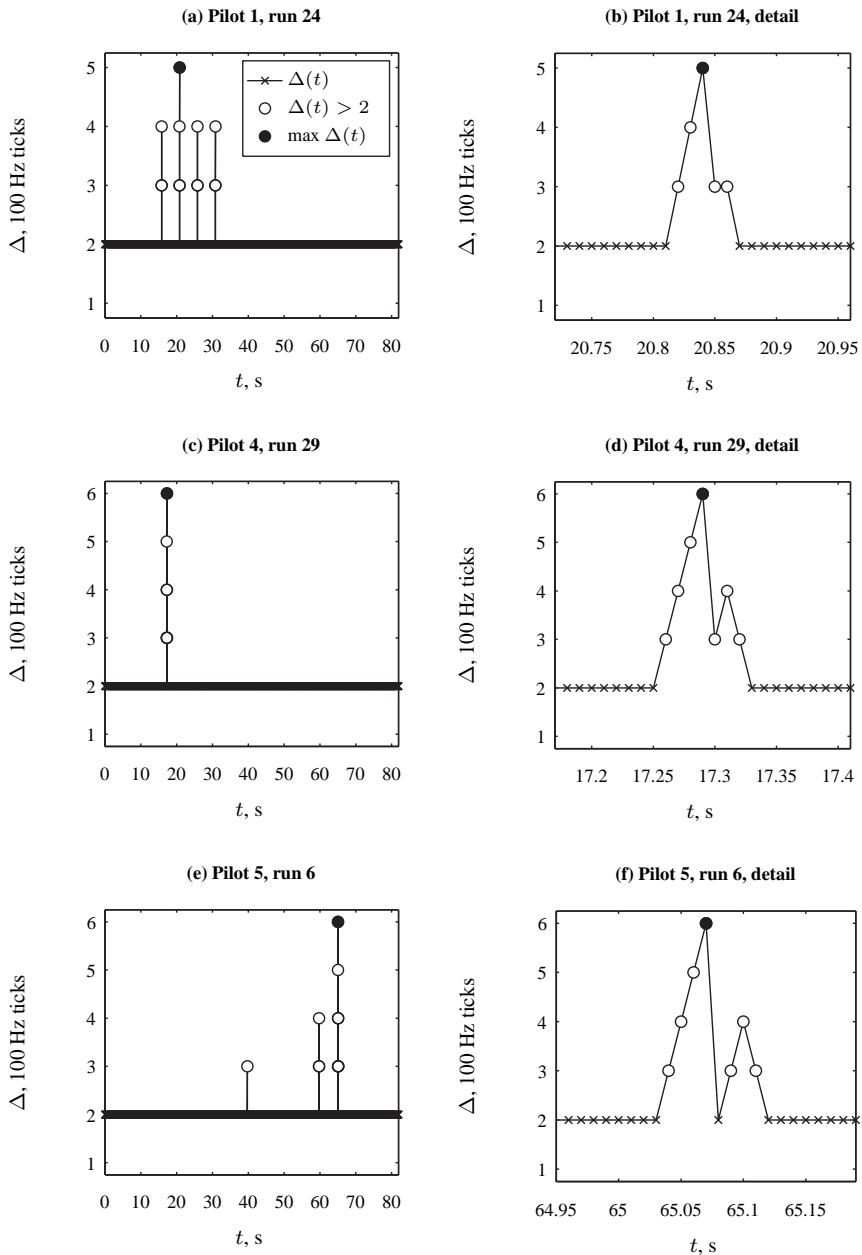


Figure D.10. Example timing discrepancies Δ as a function of time for the first three runs for which $\max. \Delta > 4$ as measured using the October/December 2010 experiment software.

E

Cessna Citation II Fly-By-Wire and Aircraft Dynamics Model

This Appendix describes the nonlinear simulation model of the combined Cessna Citation II fly-by-wire control system and aircraft dynamics used for performing the simulator parts of the experiments described in Chapters 6 and 7. This Appendix only covers the model developed for the aileron control system and Citation II roll dynamics as used for the roll tracking experiments described in this thesis. A similar model of the elevator control system and Citation II pitch dynamics, developed for the comparison of in-flight and simulator measurements of pilot pitch attitude tracking behavior described by Zaal [2011], is described there. In addition to a description of the different components of the combined fly-by-wire control system and aircraft dynamics model, this Appendix also provides a comparison of simulated model outputs to in-flight measurements of actual aircraft and control system responses.

E.1 Model Structure and Implementation

Fig. E.1 shows the structure of the developed model of the fly-by-wire (FBW) control system and the Cessna Citation II roll dynamics. The gray shaded areas in Fig. E.1 indicate three different components of the model, from left to right: a nonlinear structural model of the fly-by-wire control system, a flight dynamics model for evaluating the hinge moments acting on the left and right ailerons, and a (linear) model of the Cessna Citation II aircraft dynamics in response to an aileron input. The different submodels defined in Fig. E.1, and the symbols indicating the different forces and displacements by which these submodels are interrelated, will be defined in the remainder of this Appendix.

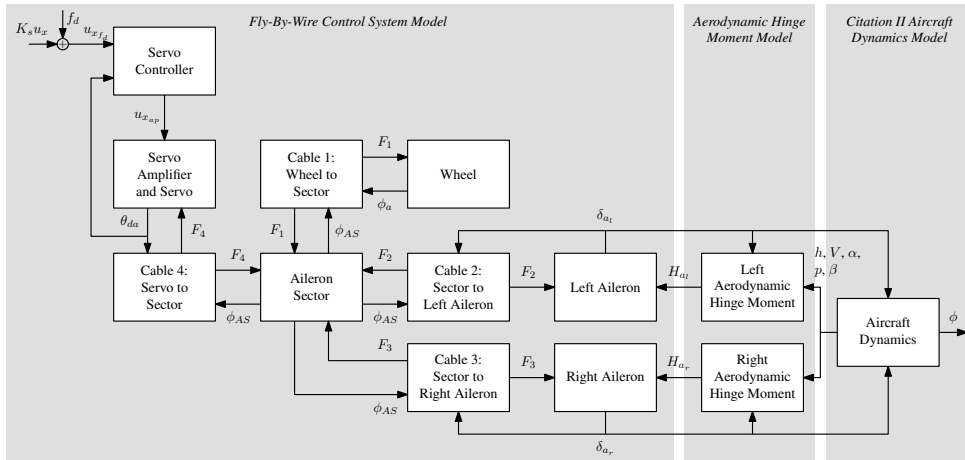


Figure E.1. Combined roll channel fly-by-wire control system and Cessna Citation II aircraft dynamics model structure.

The model shown in Fig. E.1 is based on earlier work into the modeling of the control system of the Cessna Citation II laboratory aircraft [Gorsira, 1993; Spithost, 1993; Lubbers, 2009; Mulder et al., 2009]. The complete model was developed in Matlab[®] and Simulink[®] and converted to C++ code using Real-Time Workshop[®] for implementation in the DUECA software (see Appendix D) used for performing the experiments in the SIMONA Research Simulator and the laboratory aircraft.

E.2 Fly-By-Wire Control System Model

As described in more detail in [Zaal et al., 2009d], the FBW control system implemented in the Cessna Citation II laboratory aircraft made use of the installed Honeywell automatic flight control system architecture. When active, the automatic flight control system can exert control forces on all control surfaces through electric Honeywell SM-200 servo actuators (see Fig. E.2) that are coupled to the cabling of the conventional aircraft controls. A mathematical model of this FBW control system implementation has been developed based on earlier models of the automatic flight control system of the Cessna Citation II laboratory aircraft [Gorsira, 1993; Spithost, 1993]. As can be verified from Fig. E.1, this model of the FBW control system is relatively detailed and contains submodels for all the different components of the real-life system.

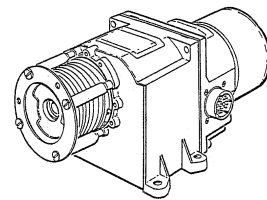


Figure E.2. The Honeywell SM-200 servo actuator.

During the experiments performed with the experimental FBW control system (Chapters 6 and 7), pilot control inputs to the fly-by-wire control system, indicated with the symbol u_x in Fig. E.1, were given using an additional sidestick that was installed in the Citation

cockpit. Furthermore, an external disturbance signal f_d , which was generated on an experimental computer, was also put on the aircraft using the FBW system. To achieve the appropriate FBW control system response to these external input signals, the *Servo Controller* shown in Fig. E.1 implemented the following proportional control law, which ensured that the aileron servo drum rotation θ_{da} accurately followed the total fly-by-wire control system input $K_s u_x + f_d$:

$$u_{x_{ap}} = K_{ap} [K_s u_x + f_d - K_{\theta_{da}} \theta_{da}] \quad (\text{E.1})$$

The *Servo Controller* proportional gain K_{ap} was set to 100. As can be verified from Fig. E.1, the resulting autopilot control input signal $u_{x_{ap}}$ formed the input to the *Servo Amplifier and Servo* system of the FBW control system. A schematic representation of this subsystem is depicted in Fig. E.3.

The model of the *Servo Amplifier and Servo* system shown in Fig. E.3 was developed by Gorsira [1993] based on physical measurements of the different hardware components of the automatic flight control system. The *Servo Amplifiers* are a set of electrical circuits that check and, if needed, limit the inputs given to the servo actuators. Based on the FBW control input signal $u_{x_{ap}}$, the *Servo Amplifiers* give a voltage input U_a to the armature of the servo actuator. The full details of the model for the *Servo Amplifiers* are described by Gorsira [1993].

The model of the servo actuator dynamics as shown in Fig. E.3 includes the effects of viscous friction forces on the rotation of the servo drum and the forces put on the servo actuator by the attached control system cabling (F_4). The output of the *Servo Amplifier and Servo* subsystem model is the servo drum rotation θ_{da} , which, as can be verified from Fig. E.1, drives all components of the conventional aircraft control system. A schematic representation of these different control system components is shown in Fig. E.4, with the FBW control system servo shown at the bottom of the figure.

As shown in Fig. E.4, for the aileron control system the servo actuator is connected to the *Aileron Sector* with a cable system here defined as *Cable 4* (see Fig. E.1). A rotation of the aileron sector induces a rotation of the left and right ailerons through the cable systems 2 and 3. Finally, also the conventional aircraft controls (*Wheel*) are connected to the aileron sector through *Cable 1*. As indicated in Fig. E.4, all four cable subsystems are modeled as spring-damper systems with stiffness and damping characteristics calculated from the material properties and lengths of the cables. Equations (E.2) to (E.9) define the model for the aileron control system depicted in Fig. E.4. The cable forces for the *Cable 1* to *Cable 4* systems are given by Equations (E.2) to (E.5), while the corresponding models for the *Wheel*, *Aileron Sector*, and *Left* and *Right Aileron* systems are given by Equations (E.6) to (E.9), respectively.

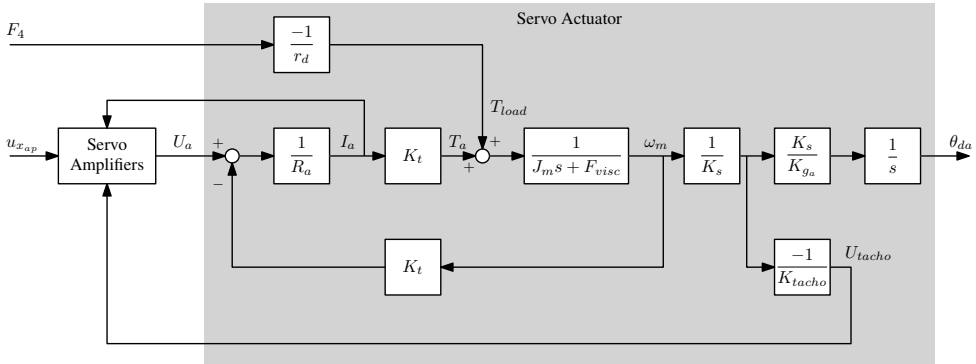


Figure E.3. Model of the electric aileron servo and servo amplifier subsystem.

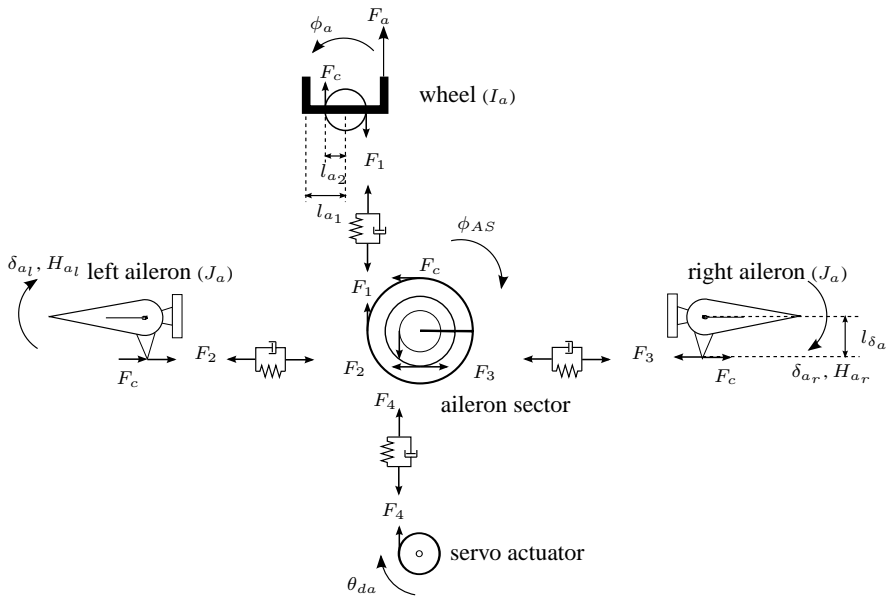


Figure E.4. Structural representation of the different aileron fly-by-wire control system model subsystems.

$$F_1 = l_{a_2} \left(c_{a_2} \phi_a + k_{a_2} \dot{\phi}_a \right) - R_{AS_b} \left(c_{a_2} \phi_{AS} + k_{a_2} \dot{\phi}_{AS} \right) \quad (\text{E.2})$$

$$F_2 = l_{\delta_a} \left(c_{a_1} \delta_{a_l} + k_{a_1} \dot{\delta}_{a_l} \right) - R_{AS_t} \left(c_{a_1} \phi_{AS} + k_{a_1} \dot{\phi}_{AS} \right) \quad (\text{E.3})$$

$$F_3 = -l_{\delta_a} \left(c_{a_1} \delta_{a_r} + k_{a_1} \dot{\delta}_{a_r} \right) + R_{AS_t} \left(c_{a_1} \phi_{AS} + k_{a_1} \dot{\phi}_{AS} \right) \quad (\text{E.4})$$

$$F_4 = R_d \left(c_{a_3} \theta_{da} + k_{a_3} \dot{\theta}_{da} \right) - R_{AS_b} \left(c_{a_3} \phi_{AS} + k_{a_3} \dot{\phi}_{AS} \right) \quad (\text{E.5})$$

$$\ddot{\phi}_a = \frac{1}{I_a} \left(F_a l_{a_1} + (F_2 - F_c) l_{a_2} \right) \quad (\text{E.6})$$

$$\ddot{\phi}_{AS} = \frac{1}{I_{AS}} \left(F_1 R_{AS_b} + F_2 R_{AS_t} - F_3 R_{AS_t} + F_4 R_{AS_b} - F_c R_{AS_b} \right) \quad (\text{E.7})$$

$$\ddot{\delta}_{a_l} = \frac{1}{J_a} \left(H_{a_l} + l_{\delta_a} F_2 - 1.5 \frac{R_{AS_b}}{R_{AS_t}} l_{\delta_a} F_c \right) \quad (\text{E.8})$$

$$\ddot{\delta}_{a_r} = \frac{1}{J_a} \left(H_{a_r} + l_{\delta_a} F_3 - 1.5 \frac{R_{AS_b}}{R_{AS_t}} l_{\delta_a} F_c \right) \quad (\text{E.9})$$

The model parameters of the different FBW control system subsystems defined above, which were used for the simulation model of these full nonlinear control system dynamics, are listed in Table E.1.

E.3 Aerodynamic Hinge Moment Model

As can be verified from Equations (E.8) and (E.9), the total moment that acts on both ailerons is the sum of the cable forces (F_2 and F_3 for the left and right ailerons, respectively), the Coulomb friction force F_c , and the aerodynamic hinge moments that work on the left and right ailerons, H_{a_l} and H_{a_r} , respectively. Due to the strong aerodynamic forces that act on both ailerons during flight, which results in considerable forces in all components of the aileron control system, a sufficiently accurate model of the aerodynamic hinge moment is required to accurately model the fly-by-wire control system dynamics. Using a typical aircraft flight dynamics model, the hinge moment is calculated from:

$$H_{a_l} = \frac{1}{2} \rho V^2 \bar{c}_a S_a C_{h_{a_r}} \quad (\text{E.10})$$

$$H_{a_r} = \frac{1}{2} \rho V^2 \bar{c}_a S_a C_{h_{a_l}} \quad (\text{E.11})$$

In Equations (E.10) and (E.11), ρ and V represent the air-density and airspeed, respectively. The aerodynamic chord \bar{c}_a and surface area S_a of the aileron, which are both known, see Table E.1. The hinge moment coefficients $C_{h_{a_l}}$ and $C_{h_{a_r}}$ are used to include the effects of variations in aircraft state on the aerodynamic hinge moments as given by Equations (E.10) and (E.11). As described in more detail by Mulder et al. [2009], the following models for the aileron hinge moment coefficients of both ailerons were assumed:

Table E.1. Fly-by-wire control system model parameters.

Submodel	Parameter	Description	Value	Unit
Servo Controller	K_{ap}	Servo controller proportional gain	100	—
Servo	r_d	Servo drum radius	0.0252	m
	R_a	Servo armature resistance	18	Ω
	K_t	Servo torque constant	0.22	(Nm/A)/(Vs/rad)
	J_m	Total servo inertia	$3.066 \cdot 10^{-5}$	kg m ²
	F_{visc}	Total servo viscous friction	$6.0 \cdot 10^{-5}$	N m s/rad
	K_s	Servo synchro gain	151.1	—
	K_{ga}	Servo gear ratio	38.9	—
	K_{tacho}	Servo tacho gain	0.0677	Vs/rad
Cables	c_{a1}	Cable 2 & 3 stiffness	26,833	N/m
	k_{a1}	Cable 2 & 3 damping coefficient	26	Ns/m
	c_{a2}	Cable 1 stiffness	30,060	N/m
	k_{a2}	Cable 1 damping coefficient	17.5	Ns/m
	c_{a3}	Cable 4 stiffness	90,180	N/m
	k_{a3}	Cable 4 damping coefficient	52.5	Ns/m
Yoke	I_a	Yoke inertia	0.03084	Nm/(rad/s ²)
	l_{a1}	Yoke outer arm	0.144	m
	l_{a2}	Yoke inner arm	0.055	m
Sector	I_{AS}	Aileron sector inertia	0.001	Nm/(rad/s ²)
	R_{AS_b}	Aileron sector outer arm	0.135	m
	R_{AS_t}	Aileron sector inner arm	0.095	m
Aileron	J_a	Aileron inertia	0.03778	Nm/(rad/s ²)
	$l_{\delta a}$	Aileron arm	0.079	m
	\bar{c}_a	Aileron aerodynamic chord	0.45677	m
	S_a	Aileron surface	1.22	m
	y_a	Aileron lateral offset	5.77	m
	b	Wing span	15.9	m

$$C_{h_{a_l}} = C_{h_0} - C_{h_\alpha} \alpha_l + C_{h_{\delta_a}} \delta_{a_l} + C_{h_{\dot{\delta}_a}} \dot{\delta}_{a_l} + C_{h_\beta} \beta \frac{b}{2V} \quad (\text{E.12})$$

$$C_{h_{a_r}} = C_{h_0} - C_{h_\alpha} \alpha_r + C_{h_{\delta_a}} \delta_{a_r} + C_{h_{\dot{\delta}_a}} \dot{\delta}_{a_r} + C_{h_\beta} \beta \frac{b}{2V} \quad (\text{E.13})$$

Equations (E.12) and (E.13) show that the hinge moment coefficients for the left and right ailerons are modeled as linear combinations of a baseline coefficient value C_{h_0} and contributions that depend on the angle of attack, aileron deflection δ_a and deflection rate $\dot{\delta}_a$, and the angle of sideslip β . Note that the hinge moment coefficients of the left and right ailerons depend on their respective angle of attack, aileron deflection, and aileron deflection rate, indicated with subscript l and r , respectively. The aileron angles of attack α_l and α_r account for differences in local angle of attack at the ailerons due to aircraft roll rates and are defined as:

$$\alpha_l = \alpha - \frac{2y_a}{b} \frac{pb}{2V} \quad (\text{E.14})$$

$$\alpha_r = \alpha + \frac{2y_a}{b} \frac{pb}{2V} \quad (\text{E.15})$$

In Equations (E.14) and (E.15), p denotes the aircraft roll rate, b is the aircraft wing span, and y_a indicates the lateral offset of the ailerons with respect to the aircraft roll axis in aircraft body axes. It should be noted that aircraft yaw rates can also affect the local angle of attack at the ailerons. As explained in more detail in [Mulder et al., 2009], however, this effect of aircraft yaw motion on α_l and α_r was found to be comparatively small and is therefore not taken into account in the hinge moment model.

In the model for the aerodynamic hinge moment, the baseline hinge moment coefficient C_{h_0} is used to ensure zero H_a for the trim condition used for the experiments ($\alpha_0 = 3.56$ deg, $\delta_{a_0} = 0$ deg, $\dot{\delta}_{a_0} = 0$ deg/s, and $\beta_0 = 0$ deg). For the remainder of the hinge moment coefficients listed in Equations (E.12) and (E.13) linear relations with the local angle of attack – α_l and α_r for the left and right ailerons, respectively – were estimated by Mulder et al. [2009] from measured flight test data. The estimated equations for C_{h_α} to C_{h_β} are given by:

$$C_{h_\alpha} = -0.120\alpha_{l,r} + 0.0159 \quad (\text{E.16})$$

$$C_{h_{\delta_a}} = -0.705\alpha_{l,r} + 0.0795 \quad (\text{E.17})$$

$$C_{h_{\dot{\delta}_a}} = -0.121\alpha_{l,r} + 0.0065 \quad (\text{E.18})$$

$$C_{h_\beta} = -0.0384 \quad (\text{E.19})$$

E.4 Citation II Aircraft Dynamics Model

As indicated in Fig. E.1, the model of the fly-by-wire control system described in Section E.2 is combined with a model of the Cessna Citation II aircraft dynamics. The air-

craft dynamics model consisted of linear transfer functions that related the required aircraft model states to the aileron deflection δ_a . These transfer functions were determined from in-flight measurements at the flight condition that was chosen for the in-flight experiments ($h = 17,000$ ft, $V = 160$ kt). For the roll attitude control tasks described in Chapters 6 and 7 the aircraft state variables that are important for the simulation model are the roll attitude ϕ , the roll rate p , and the sideslip angle β . The linear transfer function models for the response of these three aircraft states to an aileron input are given by:

$$H_{\phi, \delta_a}(s) = \frac{-15.4246(s + 2.038)}{s(s^2 + 4.646s + 7.937)} \quad (\text{E.20})$$

$$H_{p, \delta_a}(s) = \frac{-15.4246(s + 2.038)}{(s^2 + 4.646s + 7.937)} \quad (\text{E.21})$$

$$H_{\beta, \delta_a}(s) = \frac{0.02074(s + 10.4)(s - 10.37)(s + 0.02001)}{s(s + 0.6348)(s^2 + 0.9297s + 5.462)} \quad (\text{E.22})$$

E.5 Comparison of Model Responses and In-Flight Measurements

To illustrate the accuracy of the developed model for the combined FBW control system and Cessna Citation II aircraft dynamics, Fig. E.5 shows comparisons of model responses with corresponding in-flight measurements. In Fig. E.5, time traces of the roll attitude ϕ , the roll rate p , the aileron servo drum rotation θ_{da} , and the aileron deflection δ_a are depicted. For generating the model responses, the developed FBW control system model was simulated with the fly-by-wire control input u_x and external disturbance f_d that were recorded for the presented in-flight measurements as inputs. As is clear from the comparisons presented in Fig. E.5, the simulated responses of the developed FBW control system and Cessna Citation II aircraft dynamics model match the in-flight measurements well.

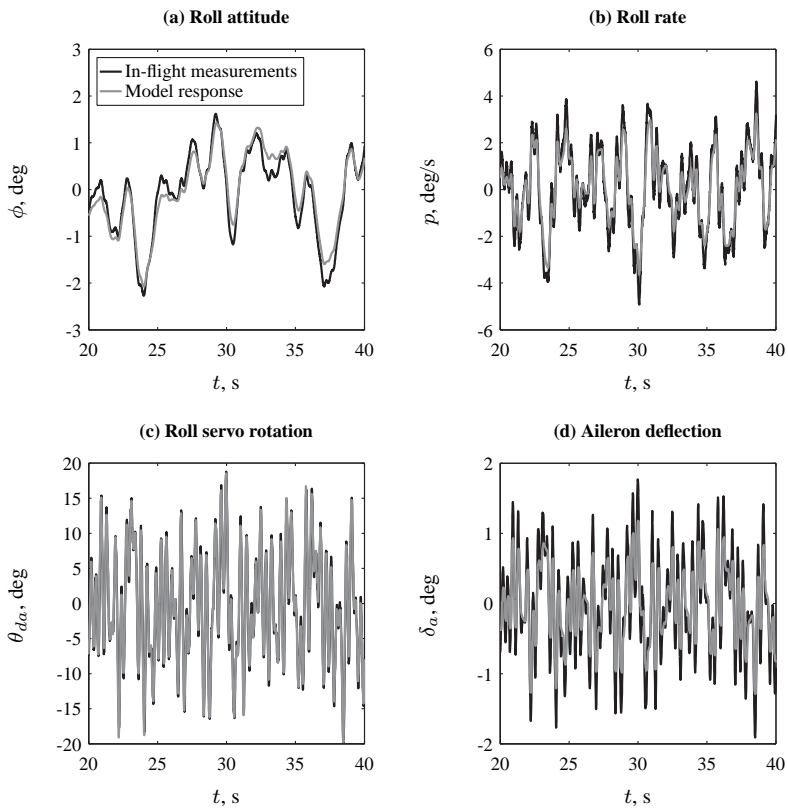


Figure E.5. Comparison of combined fly-by-wire control system and Cessna Citation II dynamics model response time traces with in-flight measurements.

F

Aircraft and Simulator Single-Loop Tracking Measurements

Chapter 6 describes a comparison of multimodal pilot roll tracking behavior measured in real flight and, for varying roll motion cueing settings, in a moving-base flight simulator. The in-flight portion of this experiment was performed using the Delft University of Technology Cessna Citation II laboratory aircraft. The simulator measurements were collected in the SIMONA Research Simulator (SRS) at Delft University of Technology. As described in Chapter 6, extreme care was taken to minimize differences in the experiment setups used for both parts of this combined in-flight and simulator experiment. In Chapter 6 the observed differences in pilot tracking behavior measured in both these experimental setups are used to draw conclusions on how pilots' use of physical motion feedback differs for a given simulator motion cueing setting compared to real flight. This Appendix describes a side-by-side comparison of reference measurements of single-loop (no motion feedback) pilot tracking behavior collected in both the experimental setups in the laboratory aircraft and the SRS. These reference single-loop measurements were performed to quantify possible differences in pilot control behavior resulting from remaining differences in the experimental setups used for both parts of the experiment. These observed differences in single-loop pilot tracking behavior were taken into account in the comparison of in-flight and simulator behavioral tracking measurements described in Chapter 6.

F.1 Introduction

This section presents the data from the comparison between single-loop tracking task measurements taken in the SRS and the Cessna Citation cockpit setups (conditions S0 and C0, respectively, see Table 6.3). The objective of this explicit comparison of control behavior measured in both experimental setups was to filter out possible differences in tracking behavior that resulted from the difference in experimental apparatus, rather than differences in motion cueing. Measured tracking performance and control activity, crossover frequencies and phase margins, and estimated behavioral pilot model parameters are compared. For all dependent measures, a dependent t-test is performed to evaluate statistically significant differences between the data from both experimental setups. It should be noted that if a sample for either S0 or C0 was found to be significantly different from a Gaussian distribution, a Wilcoxon signed-rank test was performed instead of a dependent t-test.

F.2 Tracking Performance and Control Activity

Fig. F.1 shows measured tracking performance and control activity, expressed in the variances of the tracking error signal e and the control signal u , respectively. As was also done in Fig. 6.24, the contributions of the disturbance and target forcing function signal to these signal variances were separated from the remnant contribution using a spectral method [Jex et al., 1978], and are presented separately. The variance bars indicate the 95% confidence interval of the mean total signal variance. The results of t-tests performed on the total signal variances, as well as the contributions of f_d , f_t , and n , are listed in Table F.1. Note that as the data for σ_e^2 and $\sigma_{e,n}^2$ were found to show distributions that deviated significantly from a Gaussian distribution (as tested using a KolmogorovSmirnov test), no t -statistics but the results of a Wilcoxon signed-rank test are listed for these variables.

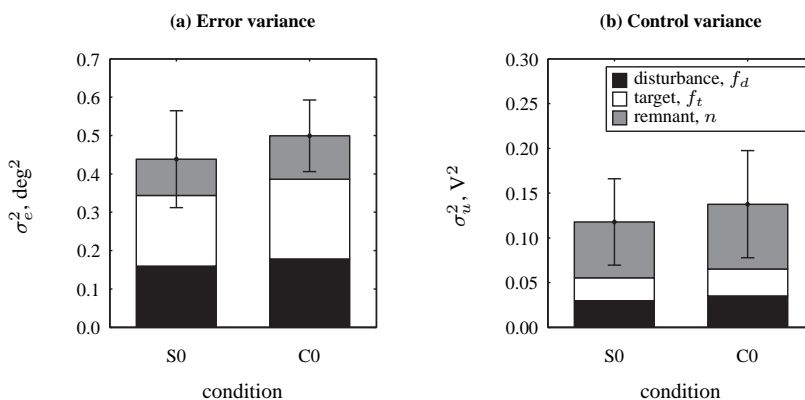


Figure F.1. Comparison of mean no-motion performance and control activity for single-loop SRS and Citation measurements (conditions S0 and C0).

Table F.1. Dependent t-test results for variance component data ($df = 6$).

Variable	Statistic, t	Sig.
σ_e^2	$T = 5^a$	—
σ_{e,f_d}^2	-2.28	—
σ_{e,f_t}^2	-1.54	—
$\sigma_{e,n}^2$	$T = 7^a$	—
σ_y^2	-1.09	—
σ_{u,f_d}^2	-1.27	—
σ_{u,f_t}^2	-1.39	—
$\sigma_{u,n}^2$	-0.85	—

^a = non-normal data, Wilcoxon signed-rank test results
 ** = highly-significant ($p < 0.05$)
 — = not significant ($p \geq 0.1$)

Fig. F.1 shows slightly higher σ_e^2 and σ_u^2 , indicating worse performance and higher control activity, for the measurements taken in the Cessna Citation setup (C0). The observed increase in both σ_e^2 and σ_u^2 are not found to result from one of the contributing signals in particular, as all three contributions to the total signal variance are slightly larger for C0 than for S0. As can be noted from the depicted variance bars, the observed differences are small compared to the spread in the measurements. As can be verified from Table F.1, the increase in variance is not found to be statistically significant for both σ_e^2 and σ_u^2 , and the different contributions to both signal variances.

F.3 Crossover Frequencies and Phase Margins

Fig. F.2 shows the measured single-loop crossover frequencies and phase margins for experimental conditions S0 and C0. In Fig. F.2 the data from the individual subjects is depicted with gray markers. The average of the data and the corresponding 95% confidence intervals are depicted with black markers and variance bars. Finally, Fig. F.2(a) and (b) also show the results of dependent t-tests performed on the measured crossover frequencies and phase margins, respectively.

The gray data in Fig. F.2 shows that for some subjects slightly lower crossover frequencies and slightly higher phase margins were measured for condition C0 than for S0. As also found for the tracking performance and control activity data, however, on average the measured values of ω_c and φ_m were found to be approximately equal to 1.5 rad/s and 60 deg, respectively, for both single-loop conditions, as is also confirmed by the t-test results presented in Fig. F.2.

F.4 Pilot Control Behavior

In the same format as Fig. F.2, Fig. F.3 presents the estimated values of the five parameters of the model for the pilot visual response $H_{p_v}(j\omega) - K_v, T_L, \tau_v, \omega_{nm}$, and ζ_{nm} – and the corresponding pilot model VAF. Note that as the estimates of T_L were not normally

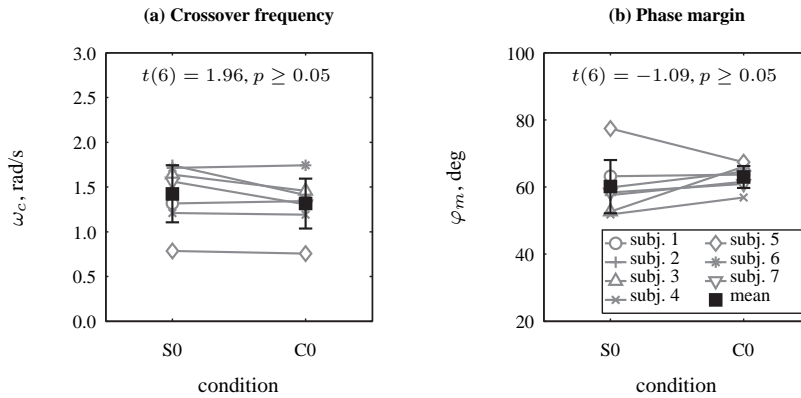


Figure F.2. Comparison of mean no-motion crossover frequencies and phase margins for single-loop SRS and Citation measurements (S0 and C0).

distributed, a Wilcoxon signed-rank test was performed on this data instead of dependent t-test.

With the exception of the neuromuscular actuation natural frequency ω_{nm} , only very small differences between the estimated parameters for conditions C0 and S0 can be observed in Fig. F.3. Only the values of ω_{nm} , which for C0 are on average found to be around 2 rad/s lower, are significantly different for both conditions. This difference in the value of ω_{nm} suggests a difference in the combined manipulator and human neuromuscular actuation dynamics between both experimental setups. This difference is believed to result from the usage of a different sidestick manipulator (see Section 6.4.1) and the difference in arm support and positioning with respect to manipulator supplied for both single-loop measurements. For S0, pilots' arms were supported by an armrest mounted on the right side of the right pilot seat in the SRS, while for C0 pilots would simply rest their arms on the cockpit geometry.

Expect for a difference in neuromuscular actuation dynamics, which is of secondary importance to our results and can be readily explained by a difference in cockpit geometry, all considered dependent measures show little differences for conditions S0 and C0. This is believed to give further confidence in the comparison of in-flight and flight simulator measurements of pilot tracking behavior as performed in this paper.

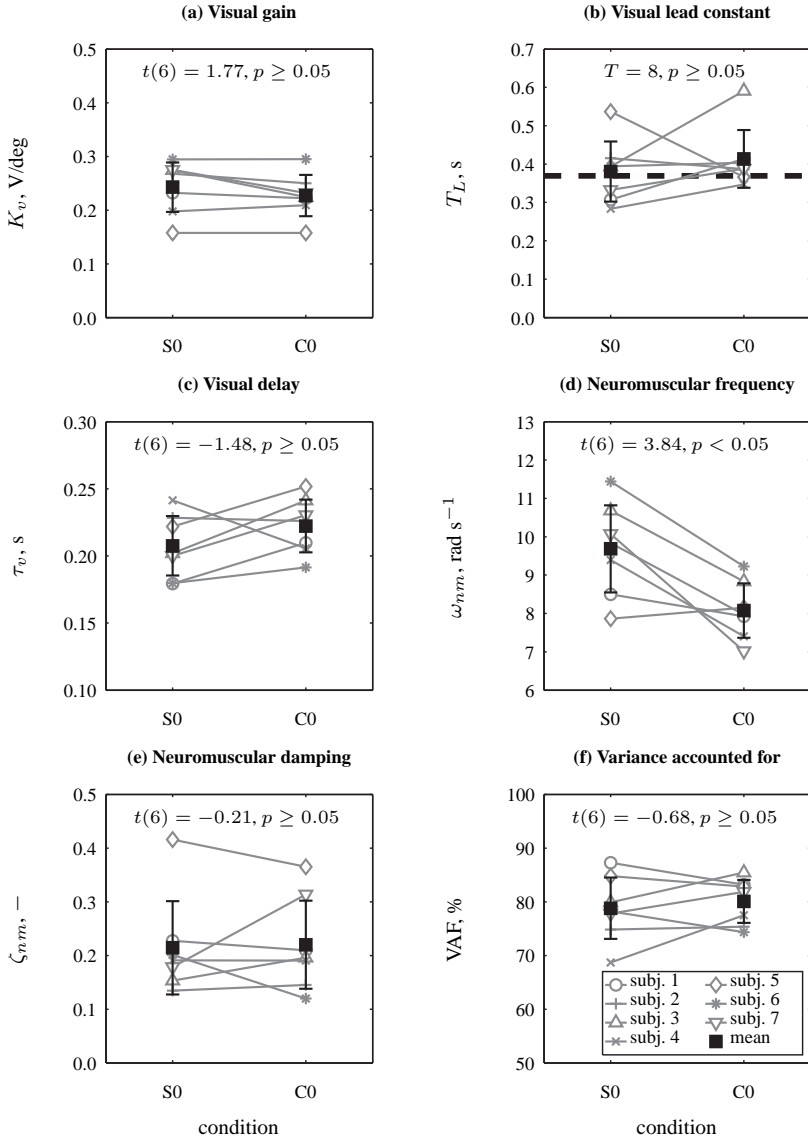


Figure F.3. Comparison of mean no-motion pilot modeling results for single-loop SRS and Citation measurements (conditions S0 and C0).

G

Simulator Hood Tracking Measurements

This Appendix summarizes the main results of a set of measurements collected in the SIMONA Research Simulator in March-April 2011 to verify the possible effect of the hood that was worn by our experiment pilots during the collecting of our in-flight measurements on their adopted control strategy. This Appendix presents measured tracking performance and control activity, pilot-vehicle system open-loop characteristics, and identified pilot model parameters for the three pilots for which these reference measurements were taken.

G.1 Introduction

As described by the excellent overview of all variables that affect a pilot-vehicle system compiled by McRuer and Jex [1967a], the manual control behavior that is adopted in a certain control task is a function a large number of factors both external and internal to the human operator performing the control task. The comparison of pilot tracking behavior measured in-flight and in a flight simulator for varying motion cueing settings as attempted in this thesis therefore is a highly intricate one. As described in [Zaal et al., 2011] and Chapter 6, where the results of the pitch and roll attitude tracking tasks performed for our evaluation of flight simulator motion fidelity are presented, a lot of care was taken to match important experimental variables in both measurement setups, to minimize the variation in pilot behavior due to all pilot-vehicle system variables except the available motion feedback. Of course, despite all these efforts we were still left with some unavoidable differences in the experimental setup, cockpit environment, and experimental procedures during the collection of behavioral measurements in-flight and those taken in the SIMONA Research Simulator (SRS).

One of these results remaining discrepancies results from the fact that to ensure only pilots' responses to the central visual cues (presented on the head-down display) and physical motion cues (presented through the true aircraft motion in the Citation and simulator motion cueing in the SRS) it was found necessary to constrain pilots' fields of view to only the head-down display during the in-flight measurements. The reason for this is that the in-flight cockpit environment could hypothetically yield the same information useful to some of the control tasks as provided through physical motion cues from a number of different sources:

- peripheral visual cues from the out-of-the-window view [Pool et al., 2008a],
- the changing angle of incidence of the sunlight in the aircraft cockpit under variations in aircraft attitude,
- the observable movement of the control column or control wheel, which were mechanically linked to the actuators that provided the Fly-By-Wire (FBW) control inputs.

To ensure that only pilots' responses to physical motion cues were measured it was therefore decided to have the pilots wear the hood depicted in Fig. G.1 during the in-flight experiments. This hood was a slightly extended version of the hood that was used in earlier in-flight experiments [Zaal et al., 2010] and effectively deprived the experiment pilots of all visual cues except for those presented on the head-down display.

(a) Close-up of the hood.



(b) The hood worn during Citation experiments.



Figure G.1. The field-of-view constraining hood that was used during the in-flight tracking tasks (a) and one of the pilots performing an in-flight tracking task while wearing the hood (b).

A crucial choice in the design of these experiments was to use this hood in during the in-flight control tasks, but to allow pilots to perform the simulator measurements without wearing the hood. Wearing the hood during the simulator tracking tasks would have been superfluous, as the three different additional cues that could not be controlled otherwise in the Citation cockpit were easily omitted in the simulator cockpit environment. Furthermore, all pilots indicated some level of discomfort after wearing the hood for extended periods of time. As the simulator sessions took markedly longer than the collection of the in-flight

measurements, due to the variation in motion cueing settings that needed to be evaluated in the flight simulator, and no effect of wearing the hood was expected after some preliminary tests in the SRS performed in July 2009, it was decided to refrain from the use of the hood during the simulator tracking tasks.

This Appendix summarizes the results of a set of reference measurements that were performed in the SRS in April 2011 to validate this choice in the experimental design by explicitly evaluating the possible effect of the hood on pilot behavior during the pitch and roll attitude tracking tasks. For both control tasks the motion cueing setting that yielded the highest pilot head accelerations were selected for these measurements: the unfiltered pitch-heave only condition for the pitch task and the 1-to-1 roll motion condition for the roll task. Measurements for both control tasks were collected both with the hood on (HD) and without (NHD). Three of the same pilots that also performed the other Citation and SRS control tasks were asked to perform these reference measurements. Care was taken to balance out these different conditions over the different participants, yielding the experimental design listed in Table G.1.

Table G.1. Experiment design.

Hood Test Subject #	Main Experiment Subject #	Session I		Session II	
1	6	Pitch, NHD	Pitch, HD	Roll, HD	Roll, NHD
2	1	Roll, NHD	Roll, HD	Pitch, HD	Pitch, NHD
3	3	Pitch, HD	Pitch, NHD	Roll, NHD	Roll, HD

This Appendix compares measured tracking performance, pilot-vehicle system crossover parameters, and pilot modeling results for these reference measurements with the results from the main experiments that are described in [Zaal et al., 2011] and Chapter 6. Note that here only the data collected for the same three pilots is used as the reference, yielding different mean data than obtained for the full experiment subject pool.

G.2 Tracking Performance and Control Activity

Tracking performance and control activity for tracking with and without hood are compared by evaluating the time-domain variances of the recorded tracking error and sidestick input signals, respectively. Furthermore, the relative contributions of the target and disturbance forcing functions and pilot remnant to these signal variances are computed using the spectral method proposed by Jex et al. [1978]. Fig. G.2 and G.3 show these variance distributions for the pitch and roll tracking tasks, respectively. The depicted variance bars depict the 95% confidence intervals over the data from the three subjects. In addition to the data from the reference experiment described here (HD and NHD conditions), for comparison also the results from the main experiment that compared in-flight and flight simulator performance are depicted for the same subjects. Note that the motion configuration for the HD and NHD conditions corresponded to the “PH” and “(1,0)” conditions for the pitch and roll tracking tasks, respectively. Finally, Table G.2 shows the corresponding results of a paired T-test

that was performed to evaluate possible differences between measurements for the HD and NHD conditions.

Fig. G.2(a) and Fig. G.3(a) show that for both the pitch and roll tracking tasks the attained level of tracking performance was highly similar to that observed from the corresponding previous measurements. When comparing tracking performance for the HD and NHD conditions, tracking is found to be slightly less accurate with the hood on. The variance decomposition bars suggest that this decrease in tracking performance results from a slight decrease in both the target and disturbance signal contributions. Table G.2 shows that the observed decrease in tracking performance can be shown to be statistically significant at the 95% level for the pitch tracking task, $T(2) = 4.46$, $p = 0.047$. It should be remarked that a marked decrease in tracking performance when wearing the hood was only observed for subject 1. This subject tends to lean forward during tracking to enhance his view of the head-down display to optimize his performance. When wearing the hood, this was no longer possible, resulting in a consistent decrease in performance for this subject. For the other two subjects no consistent decrease in performance was observed for either task.

Fig. G.2(b) and Fig. G.3(b) show that control activity was found to be markedly higher than observed from the corresponding previous measurements for both the pitch and roll tracking tasks. A clear explanation for this difference is not available, but it may result from the different setup of both experiments. However, the simulator conditions during the previous experiment were performed mixed, which could hypothetically make differences between conditions less extreme than would be observed if all conditions were evaluated separately, as was done in this reference experiment. Furthermore, a decrease in control activity is typically observed with experiment duration due to fatigue effects. Fig. G.2(b) and Fig. G.3(b) do show almost equal control activity for the HD and NHD conditions, which is confirmed by the T-test results shown in Table G.2.

G.3 Pilot-Vehicle System Crossover Parameters

G.3.1 Pitch Tracking

Fig. G.4 shows the crossover frequencies and phase margins of both the disturbance and target open-loop responses [Jex et al., 1978]. Again, the results of the main simulator fidelity experiment are also depicted for reference. Note that here individual subject results are presented in gray, while means and 95% confidence intervals over the three participants are depicted with black square markers and variance bars. Results of T-tests that were performed to evaluate possible differences in these parameters between condition HD and NHD are presented in Table G.3.

It is clear from Fig. G.4 that the adopted disturbance-loop crossover frequencies $\omega_{c,d}$ were around 1 rad/s higher than those measured in the earlier experiment for condition PH. In addition, the disturbance-loop phase margin is also to be consistently below the reference data. This suggests the pilots adopted a control strategy that results in a more high-gain disturbance-rejection loop, which would then be expected to yield better disturbance-rejection performance. This, however, is not apparent from Fig. G.2. The T-test results

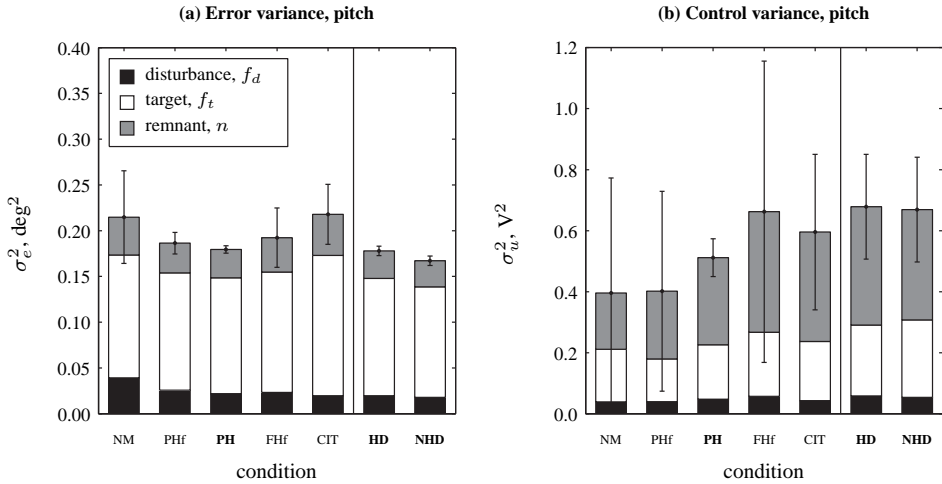


Figure G.2. Average pitch tracking error and control signal variance decompositions.

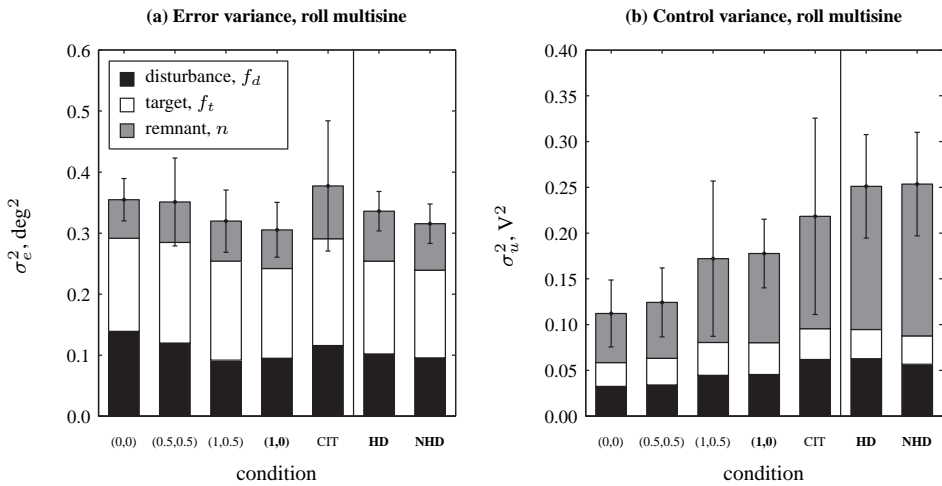


Figure G.3. Average roll tracking error and control signal variance decompositions.

Table G.2. T-test results for tracking performance and control activity data.

Measure	T	p	Sig.
Pitch, σ_e^2	4.46	0.047	*
Pitch, σ_u^2	0.12	0.917	—
Roll, σ_e^2	1.37	0.304	—
Roll, σ_u^2	-0.10	0.930	—

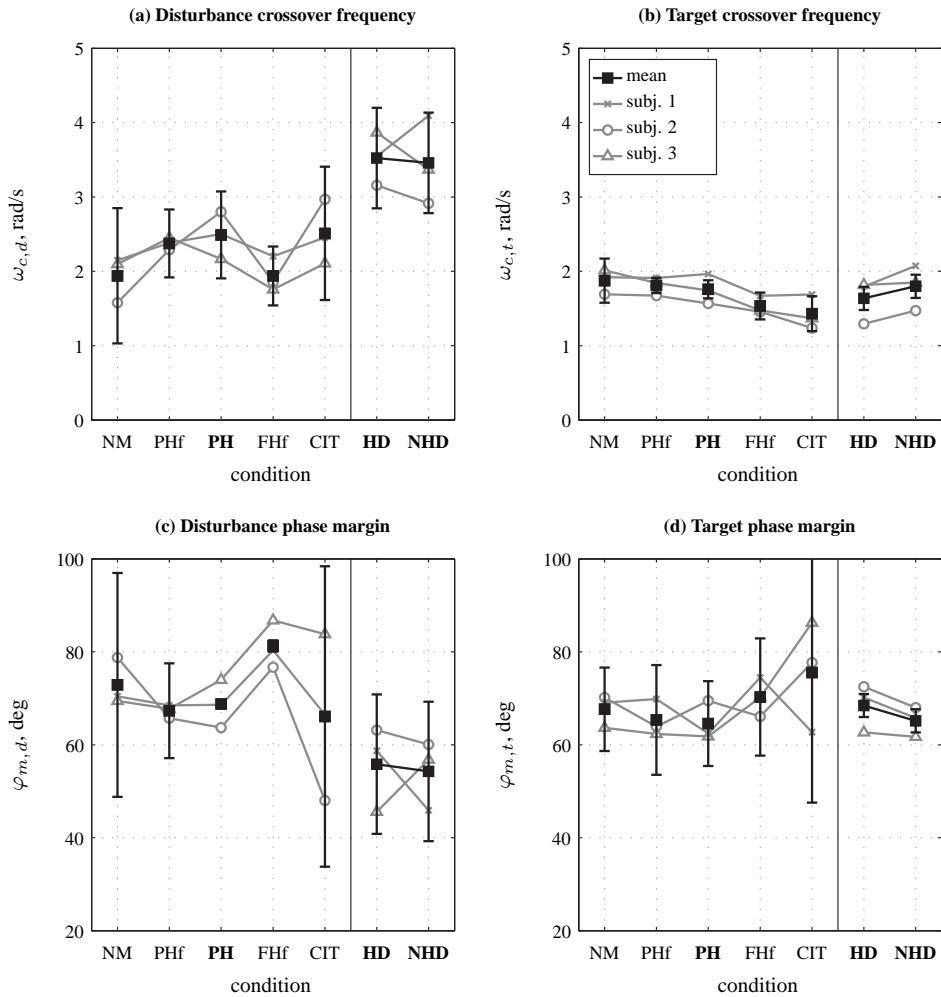


Figure G.4. Pitch tracking crossover data for "hood" experiment.

Table G.3. T-test results for pitch tracking task crossover parameters.

Measure	T	p	Sig.
$\omega_{c,d}$	0.20	0.857	—
$\omega_{c,t}$	-2.25	0.153	—
$\varphi_{m,d}$	0.22	0.845	—
$\varphi_{m,t}$	2.84	0.105	—

presented for $\omega_{c,d}$ and $\varphi_{m,d}$ in Table G.3 show no significant differences in these parameters for condition HD and NHD, as would be expected from Fig. G.4.

For the target-loop much better correspondence of the data for conditions HD and NHD with those of the previous experiment can be observed from Fig. G.4. However, for the target-loop data a slight increase in $\omega_{c,t}$ and a slight decrease in $\varphi_{m,t}$ can be observed for tracking without hood compared to condition HD. Though consistent, these differences are comparatively small – around 0.15 rad/s and 3 deg for $\omega_{c,t}$ and $\varphi_{m,t}$, respectively – and are not statistically significant as can be verified from Table G.3.

G.3.2 Roll Tracking

Fig. G.5 and Table G.4 show the same results as presented in Fig. G.4 and Table G.3, but then for the roll tracking task. As can be verified from Fig. G.5, the data collected for the HD and NHD conditions corresponds very well with the measurements for (1,0) from the previous experiment, except for consistently slightly higher target-loop phase margins (around 5 deg increase).

As can be verified from Fig. G.5(a) and Table G.4, no difference in disturbance-loop crossover frequency was observed between conditions HD and NHD. An average 3.5 deg increase in $\varphi_{m,d}$, however, was observed for the roll tracking task, which the T-test results indicate is statistically significant $T(2) = -8.97$, $p = 0.012$ due to the marked consistency over the different subjects. Note that this decrease in disturbance-loop phase margin is much smaller than the drop in $\varphi_{m,d}$ observed between conditions (1,0) and CIT.

The target-loop crossover frequencies and phase margins are found to remain approximately constant for conditions HD and NHD, as can be verified from Fig. G.5 and Table G.4.

G.4 Pilot Modeling Results

G.4.1 Pitch Tracking

Fig. G.6 presents the identified multimodal pilot model parameters for the pitch tracking task for the three subjects that performed the hood reference measurements. Again, the data from the original experiment is presented alongside the data from the HD and NHD conditions, for reference. Table G.5 lists the results of a paired T-test performed to check for possible differences in pilot model parameters between conditions HD and NHD.

As can be verified from Fig. G.6, identified pilot model parameters for conditions HD and NHD show good correspondence to the previous measurements for condition PH. Both pilot gains (K_v and K_m) are found to be slightly higher, and both the identified lead and lag time constants (T_L and T_I , respectively) are found to be slightly higher, than those measured for condition PH. These slight changes are consistent changes in pilot behavior that result from increased reliance on physical motion information [Pool et al., 2008a, 2010].

Only very small differences can be observed between the identified pilot model parameter estimates for conditions HD and NHD presented in Figs. G.6 and G.7. This is confirmed by the T-test results listed in Table G.5, which shows no significant difference between the identified values for both conditions for all pilot model parameters.

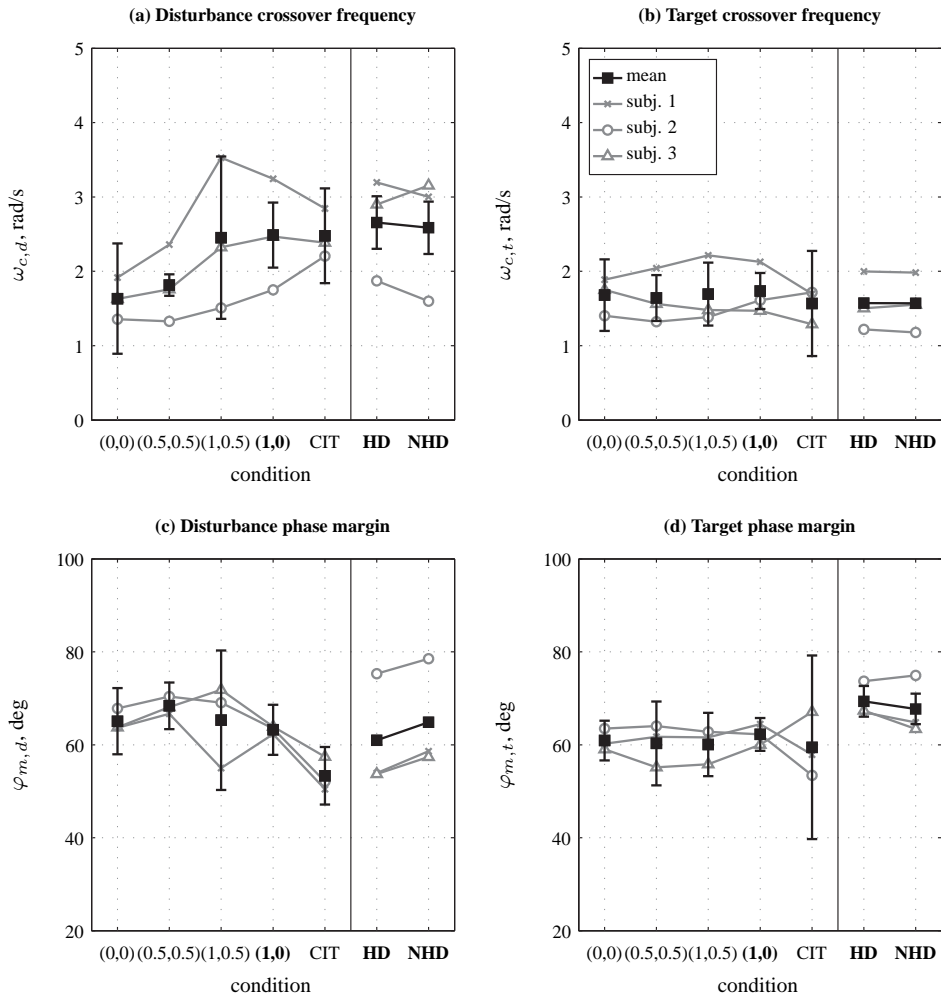


Figure G.5. Roll tracking crossover data for “hood” experiment.

Table G.4. T-test results for roll tracking task crossover parameters.

Measure	<i>T</i>	<i>p</i>	Sig.
$\omega_{c,d}$	0.43	0.711	—
$\omega_{c,t}$	0.10	0.930	—
$\varphi_{m,d}$	-8.97	0.012	*
$\varphi_{m,t}$	1.07	0.397	—

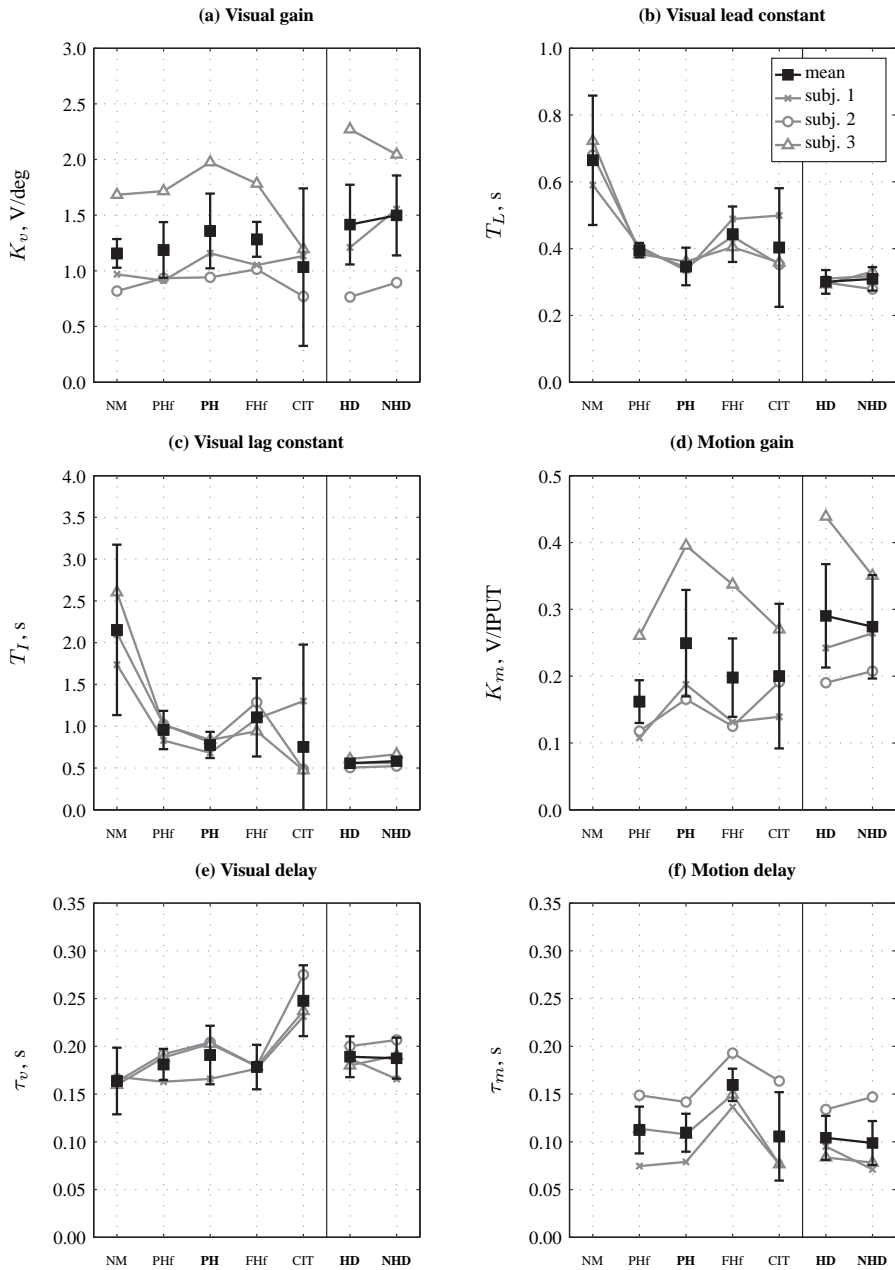


Figure G.6. Pitch tracking pilot model parameters.

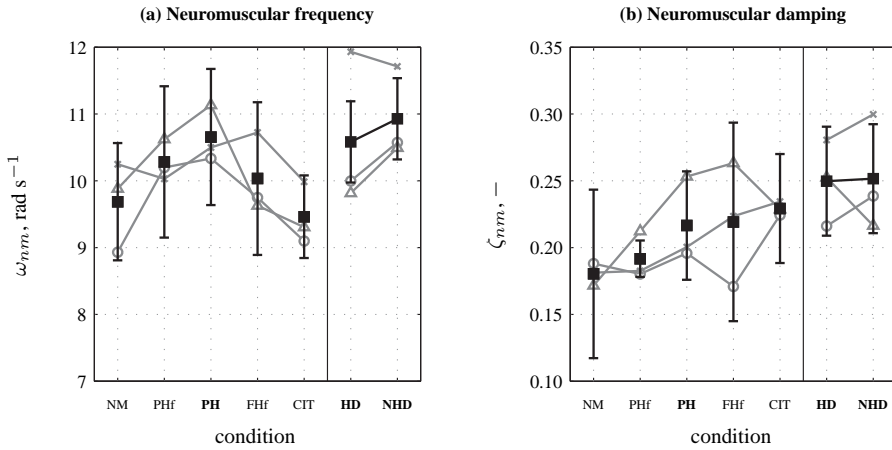


Figure G.7. Pitch tracking neuromuscular actuation model parameters.

Table G.5. T-test results for pitch tracking task pilot model parameters.

Measure	<i>T</i>	<i>p</i>	Sig.
K_v	-0.49	0.671	—
T_L	-0.54	0.642	—
T_I	-1.56	0.259	—
K_m	0.45	0.695	—
τ_v	0.15	0.894	—
τ_m	0.51	0.659	—
ω_{nm}	-1.22	0.346	—
ζ_{nm}	-0.10	0.929	—

Table G.6. T-test results for roll tracking task pilot model parameters.

Measure	<i>T</i>	<i>p</i>	Sig.
K_v	-0.78	0.517	—
T_L	0.44	0.700	—
K_m	-0.85	0.486	—
τ_v	0.21	0.852	—
τ_m	-0.26	0.820	—
ω_{nm}	-1.37	0.304	—
ζ_{nm}	-0.24	0.832	—

G.4.2 Roll Tracking

Fig. G.8 presents the identified multimodal pilot model parameters for the roll tracking task. Table G.6 lists the corresponding results of a paired T-test performed to check for possible differences in pilot model parameters between conditions HD and NHD.

Also for the roll tracking task the correspondence between the pilot model parameters identified for conditions HD and NHD and the reference measurements for the (1,0) condition is very good. As opposed to the observations made for the pitch task, here slightly lower pilot gains (K_v and K_m) and slightly higher visual lead time constants T_L are found for HD and NHD, but especially for the gain parameters the spread over the different subjects is too large to draw definitive conclusions.

Just as was found for the pitch tracking task, the identified pilot model parameter values presented in Figs. G.8 and G.9 show almost no differences between conditions HD and NHD, suggesting only minor effects of wearing the hood during tracking. This is again confirmed using the T-test results, which for the roll tracking data are presented in Table G.5 and which show no significant difference in the identified values for both conditions for any of the pilot model parameters.

G.5 Discussion

This Appendix presented the results of a series of reference measurements taken in the SRS for both pitch and roll tracking to evaluate the effect of wearing the field-of-view constraining hood, which was utilized for the in-flight measurements taken for these tasks, on the pilot behavior. The reason for performing this experimental verification was to exclude the possibility that part of the behavioral discrepancy observed between the flight simulator and in-flight data in [Zaal et al., 2011] and Chapter 6 could be attributed to this hood, rather than to differences in the supplied physical motion cues.

Using measurements of pilot tracking performance and control activity, pilot-vehicle system crossover characteristics, and identified multimodal pilot model parameters it was shown for both tasks that pilot behavior and performance were only marginally affected if subjects were wearing the hood. Even though slightly worse tracking performance was observed for both tracking tasks for the HD condition, the underlying differences in crossover characteristics and pilot model parameters were not found to reveal consistent and significant changes of pilot dynamics due to the wearing of the hood. At least, all observed changes were much smaller than the observed differences with the in-flight (CIT) measurements.

The results from these later simulator measurements, despite being performed by the same subjects that performed the simulator experiments in July-August 2009, showed some marked differences with the earlier simulator measurements. These differences may in part result from the different experimental setup used in both experiments (full randomization of conditions vs. per-condition evaluation), but they also indicate how difficult it is to use such “snapshots” of pilot behavior for drawing engineering conclusions, as pilot behavior is affected by so many variables that can not always be controlled in an experimental environment.

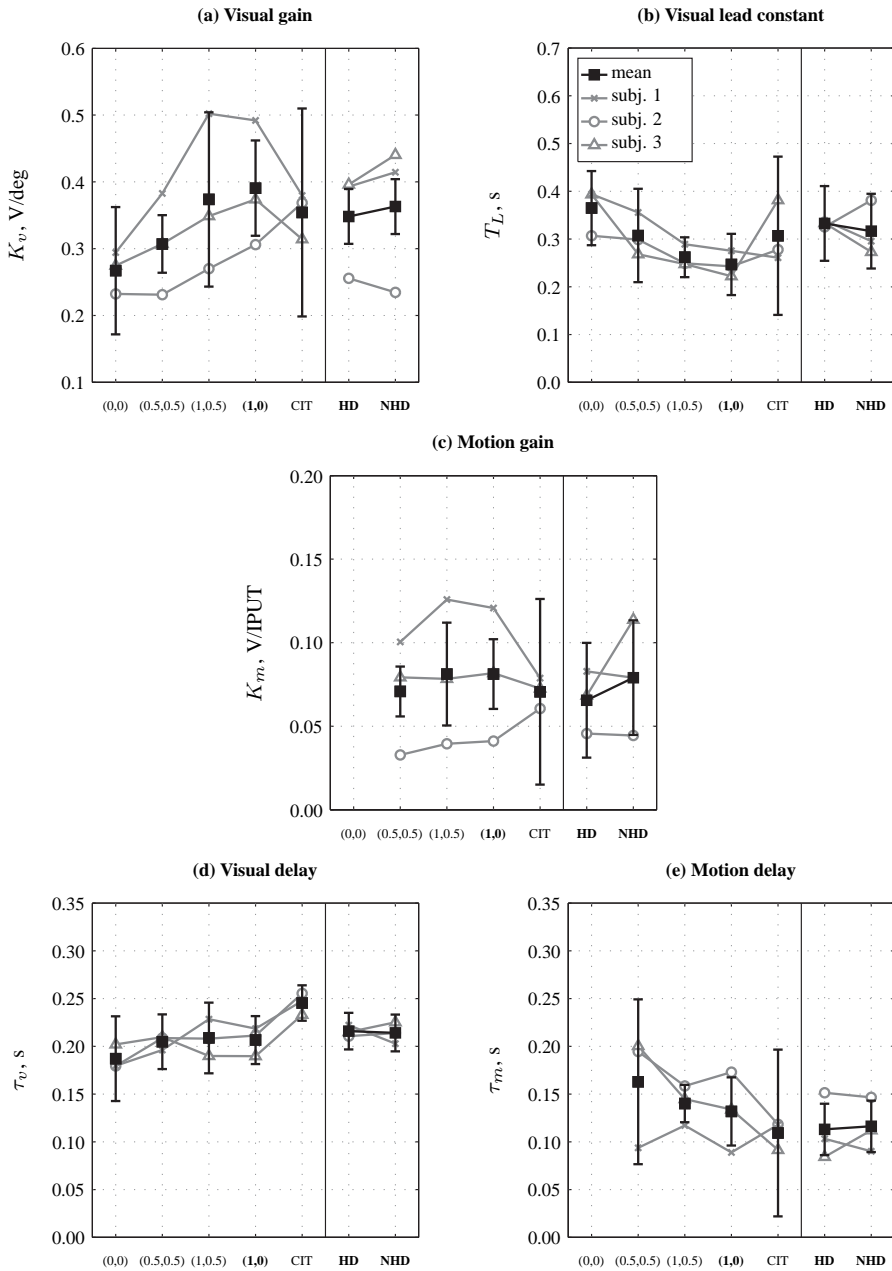


Figure G.8. Roll tracking pilot model parameters.

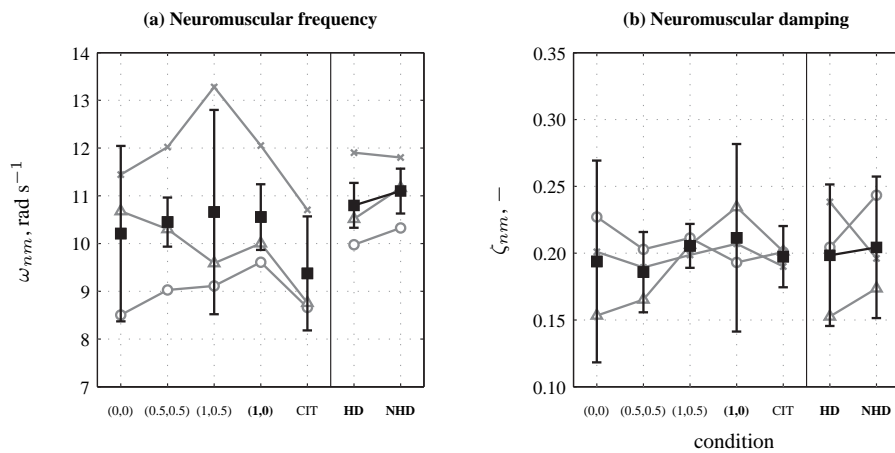


Figure G.9. Roll tracking neuromuscular actuation model parameters.

H

Motion Fidelity Pilot Comments

Chapter 8 described an experiment performed in the SIMONA Research Simulator in which pilot roll tracking behavior was measured for ten different roll motion cueing settings. The six pilots who performed this experiment were asked to give a subjective assessment of the level of simulator motion fidelity on a visual analogue rating scale (VAS) after each tracking run. Furthermore, they were encouraged (but not required) to provide comments on the motion cueing for the condition they had just evaluated. The pilot comments that were collected for all ten conditions of this experiment are included in this Appendix.

Each table in this Appendix lists the collected pilot comments for one of the conditions of the experiment described in Chapter 8, both in Dutch – in which nearly all comments were originally given – and in English. Furthermore, for each comment the corresponding information on the pilot, run number, and given fidelity rating also included for reference. The different experimental conditions are indicated with their identifier from Chapter 8 (C0-C9) and their motion filter gain and break frequency setting in the format (K_{mf} , ω_{mf}). In a number of comments, the pilots referred to, or made judgments relative to, the motion conditions they had evaluated before the run they were commenting on. In these instances, this previously evaluated condition is indicated in the comment between square brackets.

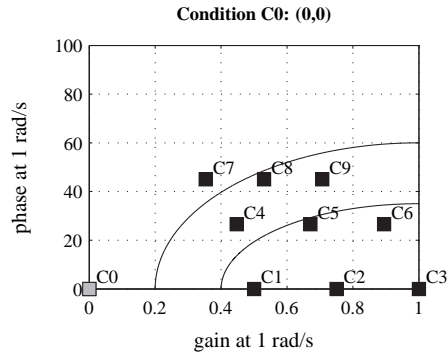
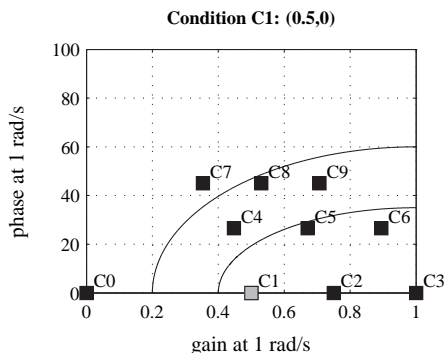


Table H.1. Motion fidelity pilot comments for condition C0 (0,0).

Comment (Dutch <i>English</i>)	Subject	Rating	Run
Categorie computerspelletjes. <i>Computer games category.</i>	4	9.9	36
Nintendo. <i>Nintendo.</i>	4	9.7	78
Dit lijkt wel helemaal geen motion cues, maakt het moeilijk. <i>This feels like no motion cues at all, makes it difficult.</i>	5	4.3	18
Geen motion cues, ook niet goed. <i>No motion cues, also not good.</i>	5	10.1	26
Geen cues, lastig. <i>No cues, difficult.</i>	5	12.1	35
Geen motion lijkt het, maar je hebt dan in ieder geval geen last van het teveel. <i>No motion it seems, but then at least you are not bothered by the excess.</i>	5	11.6	51
Lastig zonder motion cues. <i>Difficult without motion cues.</i>	5	14.5	54
Helemaal geen motion, dat is nou ook weer niet goed. <i>No motion at all, that is also not good.</i>	5	11.8	73

**Table H.2. Motion fidelity pilot comments for condition C1 (0.5,0).**

Comment (Dutch <i>English</i>)	Subject	Rating	Run
Iets te weinig rol informatie. <i>Slightly too little roll information.</i>	1	52.9	24
Te weinig rol. <i>Too little roll.</i>	1	64.6	37
Lateraal een haartje te sterk. <i>Lateral cues are slightly too strong.</i>	1	63.5	51
Rol een haartje te veel, maar lekker. <i>A little too much roll, but nice.</i>	1	77.0	53
Te zwak, vooral in rol. <i>Too weak, especially in roll.</i>	1	49.2	72
Te weinig rol. <i>Too little roll.</i>	1	45.4	78
Weinig beweging, maar OK. <i>Little motion, but OK.</i>	2	61.4	17
Wel goed. <i>Quite OK.</i>	2	84.9	32
Redelijk weinig, had wel het gevoel dat het redelijk klopte. <i>Rather little motion, did feel quite accurate though.</i>	2	67.5	51
Een iets minder filter, te weinig beweging. <i>A bit worse, too little motion.</i>	2	40.6	57
Een stuk minder dan de vorige [C3, (1,0)]. <i>A lot worse than the previous run [C3, (1,0)].</i>	2	27.2	80
Ietsje beter, maar niet wat het moet zijn. <i>A bit better, but not what it should be.</i>	4	35.2	23
Weer heel matig. <i>Again very poor.</i>	4	39.8	39
Weinig overeenkomst met de werkelijkheid. <i>Little agreement with reality.</i>	4	35.4	41
Een beetje laag op mijn schaal. <i>A bit low on my scale.</i>	4	29.8	66
Duidelijk onder de Balkenende-norm. <i>Clearly below Balkenende's norm.</i>	4	35.5	75
Lijkt iets grotere cues dan hiervoor [C7, (0.5,1)], redelijk realistisch. <i>A bit larger motion cues than the previous one [C7, (0.5,1)], reasonably realistic.</i>	5	52.9	21
Goede cues. <i>Good cues.</i>	5	62.5	22
Realistisch. <i>Realistic.</i>	5	54.7	34
Weinig motion, maar lijkt niet onrealistisch. <i>Little motion, but does not seem unrealistic.</i>	5	54.2	47
Cues klein maar fijn. <i>Cues small but nice.</i>	5	58.7	60
OK. <i>OK.</i>	5	57.7	71
OK. <i>OK.</i>	5	55.3	75
Een beetje lafjes, voelt allemaal gedempt aan. <i>A bit bland, it all feels muffled.</i>	6	46.9	13
Hier voel je niet zoveel van, alsof het rustiger weer is. <i>Here you do not feel very much, like the weather calmed down.</i>	6	56.4	30
Stuurt wel OK. <i>Controls quite OK.</i>	6	69.0	39
Het beweegt wel, maar het voegt allemaal zo weinig toe, het is allemaal zo gedempt. <i>It does move, but it all adds so little, it all feels so muffled.</i>	6	35.7	55

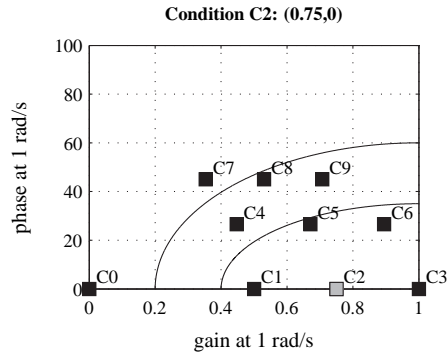


Table H.3. Motion fidelity pilot comments for condition C2 (0.75,0).

Comment (Dutch <i>English</i>)	Subject	Rating	Run
Iets te sterk in de laterale versnellingen. <i>Lateral accelerations are a little bit too strong.</i>	1	63.4	15
Te veel rol. <i>Too much roll.</i>	1	48.3	31
Lekker. <i>Very good.</i>	1	81.3	35
Te weinig gedempt, beweegt nog door terwijl je verwacht dat hij stopt. <i>Too little damping, you keep moving while you would expect it to stop.</i>	1	36.2	48
Te weinig rol demping. <i>Too little roll damping.</i>	1	45.2	69
Goede, maar niet zo goed als de vorige [C3, (1,0)]. <i>A good one, but not as good as the last one [C3, (1,0)].</i>	2	32.3	15
Wel een goede, kreeg een beetje gevoel voor de rolhoeken. <i>A pretty good one, I got a bit of a feel for the roll attitude.</i>	2	89.6	34
Mooi filtertje, geeft ook gevoel voor de rolhoek. <i>A nice little filter, also gives you some feel for the roll attitude.</i>	2	88.3	47
Een stuk beter, wel goed. <i>A lot better, quite good.</i>	2	77.6	72
Niet al te heftig, volgens mij wel aardig, goed. <i>Not too intense, I think this one is quite acceptable, good.</i>	2	78.9	76
Redelijke bewegingsrespons, het voelde goed. <i>A reasonable motion response, it felt good.</i>	4	76.3	24
Weer een hele lage in de responsie. <i>Again very low in terms of response.</i>	4	27.3	47
Een vrij matige respons. <i>A relatively poor response.</i>	4	55.1	57
Een beetje boven modaal. <i>A bit above average.</i>	4	79.9	69
Iets boven modaal. <i>A bit above average.</i>	4	80.7	71
Met cues gaat het beter, lijkt toch iets overdreven. <i>It goes better with cues, does seem a bit exaggerated.</i>	5	41.9	19
Iets overdreven? Niet helemaal zeker van. <i>A bit exaggerated? I am not really sure.</i>	5	41.9	28
OK, iets overdreven. <i>OK, a bit exaggerated.</i>	5	53.8	37
Iets te veel motion. <i>A bit too much motion.</i>	5	37.4	46
Voelt wel goed. <i>Feels about right.</i>	5	60.1	67
Realistisch, voelde wel weer goed. <i>Realistic, felt alright again.</i>	6	76.7	18
Stuurde ook wel OK. <i>Also controlled quite OK.</i>	6	71.7	52
Wel OK, maar het kan beter. <i>Quite OK, but could be better.</i>	6	53.9	63

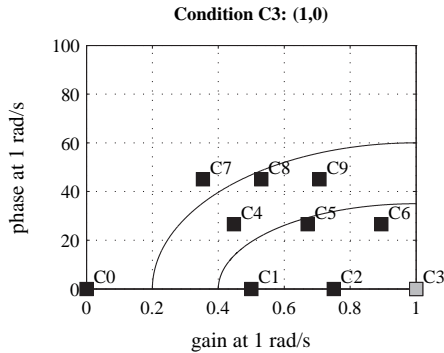


Table H.4. Motion fidelity pilot comments for condition C3 (1,0).

Comment (Dutch <i>English</i>)	Subject	Rating	Run
Niet zo best, lateraal te weinig demping. <i>Not too great, too little lateral damping.</i>	1	45.9	20
Rol OK, lateraal te veel. <i>Roll OK, too much lateral motion.</i>	1	52.6	28
Lateraal te veel. <i>Lateral too much.</i>	1	50.6	46
Te sterk lateraal. <i>Too strong laterally.</i>	1	36.7	54
Te sterk. <i>Too strong.</i>	1	50.3	63
Te veel laterale beweging. <i>Too much lateral motion.</i>	1	50.2	79
Hefdig, hoge gain, wel goed de effecten van de disturbance en de target te scheiden. <i>Intense, high gain, does allow for separating the effects of the disturbance and the target though.</i>	2	75.5	13
Het nerveuze filter. <i>The nervous filter.</i>	2	37.9	41
Aardig goed, niet het beste dat we gehad hebben. <i>Reasonably good, not the best we have had.</i>	2	76.8	52
Vooral wat zijdelingse versnellingen, niet zo'n geweldig filter. <i>Mainly lateral accelerations, not a very good filter.</i>	2	46.5	61
Een wat beter filter. <i>This filter is a bit better.</i>	2	76.2	68
Een redelijk goed filter, ik voelde de rolhoek goed. <i>A reasonably good filter, I really felt the roll angle.</i>	2	82.8	79
Ook wel een goede. <i>Also quite a good one.</i>	2	80.2	86
Wel lekker. <i>Quite nice.</i>	3	89.0	15
Dat voelde meer als een echt vliegtuig. <i>That felt more like a real aircraft.</i>	4	81.6	27
Voelde goed, een beetje als "thuis". <i>Felt good, a bit like "home".</i>	4	81.8	32
Een behoorlijke respons. <i>A reasonable response.</i>	4	83.9	48
Iets boven matig. <i>A little better than poor.</i>	4	78.9	58
Een goede score op mijn schaal. <i>A good score on my scale.</i>	4	88.6	70
Nou, 80 procent op de schaal van Zaal. <i>Well, 80 percent on Zaal's scale.</i>	4	80.9	76
Wat te uitgesproken cues. <i>The cues are a bit too pronounced.</i>	5	35.3	15
Iets overdreven, lijkt het. <i>A bit exaggerated, it seems.</i>	5	43.4	31
Overdreven. <i>Exaggerated.</i>	5	23.8	33
Motion goed voelbaar, wel te veel. <i>Motion well perceivable, but too much.</i>	5	27.0	49
Te veel. <i>Too much.</i>	5	29.3	61
Goed te vliegen, maar wel te veel motion. <i>Very flyable, but too much motion.</i>	5	15.6	78
Hier voel je vooral de verstoring, waar je bij andere condities vooral de respons van het vliegtuig op je eigen inputs voelt. <i>Here you mainly feel the disturbance, where for some of the other conditions you mainly feel the response of the aircraft to your own inputs.</i>	6	71.9	24
Een beetje nerveus, wel prettig. <i>A bit nervous, quite agreeable.</i>	6	96.8	34
Hiermee kon ik prima sturen. <i>This allowed me to control just fine.</i>	6	77.5	48
Het stuurt toch fijner als hij gewoon wiebelt. <i>For the control task it is nicer when it rocks from side to side.</i>	6	82.6	60

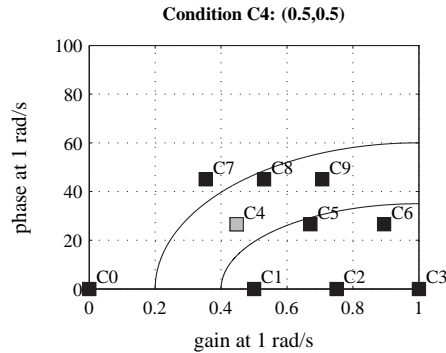


Table H.5. Motion fidelity pilot comments for condition C4 (0.5,0.5).

Comment (Dutch English)	Subject	Rating	Run
Wel OK. <i>Quite OK.</i>	1	78.7	45
Wiebelt iets te veel, rol demping te laag. <i>Rocks and jolts a bit too much, roll damping too low.</i>	1	50.2	57
Goede motion. <i>Good motion.</i>	1	91.8	70
Goed. <i>Good.</i>	1	79.2	85
Lekker rustig, misschien een beetje te. <i>Nice and calm, perhaps a bit too calm.</i>	2	33.6	21
Alleen wat geschok, had er niet erg veel aan. <i>Only some jolting and bumping, it did not really help me.</i>	2	22.2	29
Niet erg veel van te merken. <i>Not really noticeable.</i>	2	37.3	37
Weinig beweging, had er niet al te veel aan. <i>Not a lot of motion, did not help me very much.</i>	2	35.3	50
Weinig van te merken. <i>Not very noticeable.</i>	2	25.5	53
Relatief weinig beweging. <i>Relatively little motion.</i>	2	26.1	73
Volgens mij gebeurde er niet zo veel. <i>I do not think a lot happened.</i>	2	8.8	89
In het begin dacht ik "dat is echt 20 procent van de beweging", maar later dacht ik "hij is toch wel OK". <i>In the beginning I thought "this really is just 20 percent of the motion", but later I thought "this one is quite OK anyway".</i>	3	59.1	16
Voor de stuurtaak plezierig, maar een beetje gevoelig. <i>Nice for the control task, but a little sensitive.</i>	4	31.7	16
Weer slechter dan de vorige [C3, (1,0)]. <i>Worse than the previous one [C3, (1,0)].</i>	4	30.2	28
Een lage score wat de bewegingsrespons betreft. <i>A low score for the motion response.</i>	4	28.9	33
Een beetje matig in de reactie op de inputs. <i>A bit poor in terms of response to inputs.</i>	4	33.3	50
Een lage respons. <i>A low response.</i>	4	30.2	55
Vrij laag op de respons-schaal. <i>Relatively low on the response-scale.</i>	4	32.8	62
Ietsje beneden modaal. <i>A bit below average.</i>	4	47.1	80
Kleinere, meer realistische cues, alleen rol. <i>Smaller, more realistic cues, pure roll.</i>	5	59.2	14
Redelijk realistisch. <i>Reasonably realistic.</i>	5	58.8	29
OK. <i>OK.</i>	5	64.9	42
Cues ongeveer goed. <i>Cues about right.</i>	5	72.2	57
OK. <i>OK.</i>	5	63.2	69
Moelijk te vliegen. <i>Difficult to fly.</i>	5	32.6	86
Beter dan de vorige [C7, (0.5,1)]. <i>Better than the previous one [C7, (0.5,1)].</i>	6	60.2	16
Alsof je op een Tempur matras ligt, zacht, je voelt alleen de grote bewegingen, niet realistisch. <i>Like you are lying on a Tempur mattress, soft, you only feel the large motions, not realistic.</i>	6	33.8	31
Hier ben ik niet zo kapot van, alsof je tussen sponzen aan het sturen bent, een beetje gedempt. <i>I do not really like this one, it feels like your controlling in between sponges, a bit muffled.</i>	6	39.7	38
Weinig feedback. <i>Little feedback.</i>	6	60.2	44
Te weinig, niet zo prettig. <i>Too little, not very agreeable.</i>	6	33.4	68

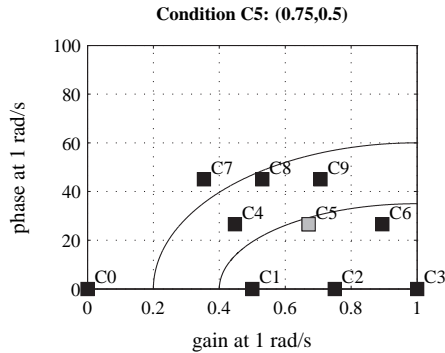


Table H.6. Motion fidelity pilot comments for condition C5 (0.75,0.5).

Comment (Dutch English)	Subject	Rating	Run
Goed. <i>Good.</i>	1	78.9	14
Demping te laag. <i>Damping too low.</i>	1	54.3	29
Te weinig demping. <i>Too little damping.</i>	1	54.6	38
Laterale demping iets te laag. <i>Lateral damping a little too low.</i>	1	68.9	52
Laterale demping te laag. <i>Lateral damping too low.</i>	1	37.1	61
Wel redelijk. <i>Decent.</i>	1	65.6	64
Lekkere motion. <i>Nice motion.</i>	1	74.4	76
Ook een goede, duidelijk onderscheid tussen de disturbance en de target, gain goed, realistisch. <i>Also a good one, clear distinction between the disturbance and target, gain OK, realistic.</i>	2	82.6	16
Aangenaam filter, niet veel beweging, wel realistisch. <i>A pleasant filter, not a lot of motion, but it is realistic.</i>	2	71.4	25
Wat minder, wat schokkerig, niet het gevoel dat ik er iets aan had. <i>A bit worse, a bit jolty, I do not believe it helped me at all.</i>	2	34.4	43
Ik voelde vooral wat zijdelingse versnellingen. <i>I mainly felt some lateral accelerations.</i>	2	34.3	59
Beter. <i>Better.</i>	2	69.1	71
Een beetje een erg snelle respons. <i>The response was a bit too fast.</i>	4	22.4	19
Matig tot redelijk. <i>Poor to reasonable.</i>	4	58.6	34
Matig wat respons betreft. <i>Mediocre in terms of response.</i>	4	46.7	42
Vrij laag in de score. <i>A relatively low rating.</i>	4	43.8	51
Weer redelijk laag op de schaal. <i>Again quite low on the scale.</i>	4	33.0	63
70 procent op de respons schaal. <i>70 percent on the response scale.</i>	4	77.6	79
Iets overdreven motion cues. <i>Slightly exaggerated motion cues.</i>	5	39.0	17
Nog te veel. <i>Still too much.</i>	5	35.9	25
Redelijk, iets te veel? <i>Reasonable, a bit too much?</i>	5	44.6	36
Motion, ongeveer goed. <i>Motion, about right.</i>	5	62.4	52
Lijkt iets te veel en onrealistisch te zijn. <i>Seems to be a bit too much and unrealistic.</i>	5	49.8	56
Te veel motion vergeleken met de kist denk ik. <i>Too much motion compared to the aircraft I believe.</i>	5	26.5	65
Duidelijke motion cues, meer cues dan realistisch? <i>Clear motion cues, more cues than realistic?</i>	5	25.2	82

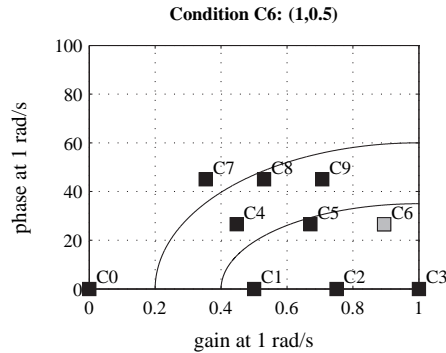
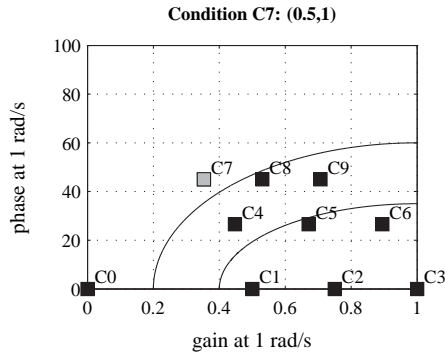


Table H.7. Motion fidelity pilot comments for condition C6 (1,0.5).

Comment (Dutch <i>English</i>)	Subject	Rating	Run
Lateraal niet goed gedempt, stuur soms op basis van wat ik voel in plaats van wat ik zie. <i>Lateral damping is no good, I sometimes control based on what I feel instead of what I see.</i>	1	28.8	13
Te veel laterale cues. <i>Too much lateral cues.</i>	1	33.6	23
Te veel laterale cues. <i>Too much lateral cues.</i>	1	36.2	32
Rol OK, lateraal te sterk. <i>Roll OK, too strong laterally.</i>	1	48.4	49
Rol goed, lateraal te sterk. <i>Roll good, too strong laterally.</i>	1	49.2	58
Allebei (rol en lateraal) te sterk. <i>Both (roll and lateral) too strong.</i>	1	36.6	67
Lateraal te sterk. <i>Lateral too strong.</i>	1	59.2	83
Lateraal te sterk. <i>Lateral too strong.</i>	1	37.4	86
Veel beweging, niet zo fraai. <i>A lot of motion, not too pretty.</i>	2	15.2	22
Het nerveuze filter. <i>The nervous filter.</i>	2	30.1	28
Redelijk goed, maar wat veel bewegingen. <i>Reasonably correct, but a bit too much motion.</i>	2	76.4	40
Vrij veel beweging, maar verder wel goed. <i>Quite a lot of motion, however; it still feels good.</i>	2	78.8	49
Wel aangenaam, wat weinig beweging. <i>Quite pleasant, but rather little motion.</i>	2	79.9	55
Niet echt behulpzaam, ik vond de beweging een beetje tegenvallen. <i>Did not really help, I found the motion a bit disappointing.</i>	2	38.0	64
Een beter filter. <i>A better filter.</i>	2	69.5	85
Hier kon ik tenminste wat mee. <i>This is at least one I could work with.</i>	3	84.7	22
Lekker wat beweging. <i>A good amount of motion.</i>	3	86.5	26
Komt behoorlijk overeen met de werkelijkheid. <i>Agrees quite well with reality.</i>	4	85.9	20
Aan de gevoelige kant. <i>Relatively sensitive.</i>	4	35.8	21
De score was misschien minder goed, maar ik zat wel in een vliegtuig. <i>The tracking score may not have been too good, but I was flying an aircraft.</i>	4	82.2	37
Redelijke respons. <i>Reasonable response.</i>	4	85.9	43
Vloog wel weer als een vliegtuig. <i>This one flew like an aircraft again.</i>	4	83.8	56
Boven gemiddeld. <i>Above average.</i>	4	72.3	64
Gemiddelde respons. <i>Moderate response.</i>	4	51.9	72
Nog steeds wat te veel beweging. <i>Still too much motion.</i>	5	46.4	12
Te veel. <i>Too much.</i>	5	17.6	24
Te veel. <i>Too much.</i>	5	24.0	32
Te veel motion, onrealistisch. <i>Too much motion, unrealistic.</i>	5	25.2	48
Ongeveer OK. <i>About OK.</i>	5	59.9	59
Vliegt goed, maar niet als de echte kist, te overdreven motion. <i>Flies well, but not like the real aircraft, motion too exaggerated.</i>	5	19.3	85
Wel prettig. <i>Quite agreeable.</i>	6	72.3	29
Er was wel motion, maar het voegde niet zo veel toe. <i>There was motion, but it did not really add anything.</i>	6	40.0	56
Qua motion kan er wel iets meer in. <i>Could be a bit more in terms of motion.</i>	6	62.8	83
Fijn. <i>Nice.</i>	6	76.3	93

**Table H.8. Motion fidelity pilot comments for condition C7 (0.5,1).**

Comment (Dutch English)	Subject	Rating	Run
Lekker. <i>Very good.</i>	1	74.0	26
Rol OK, lateraal iets te sterk. <i>Roll OK, lateral a bit too strong.</i>	1	60.9	71
Niet goed. <i>Not good.</i>	1	49.6	80
Weinig beweging, niet zo realistisch. <i>Little motion, not very realistic.</i>	2	28.7	19
Niet onaardig. <i>Not bad.</i>	2	66.7	26
Ik had er niet veel aan. <i>It did not really help me.</i>	2	34.8	33
Weinig motion, niet al te realistisch. <i>Little motion, not very realistic.</i>	2	23.2	45
Motion is niet heel erg duidelijk aanwezig, niet echt een hulp. <i>The motion is not very clearly perceivable, not a big help.</i>	2	39.9	70
Behoorlijke directe respons. <i>A reasonably direct response.</i>	4	29.2	12
Geringe overeenstemming met de werkelijkheid. <i>Little agreement with reality.</i>	4	27.0	26
Zeer matig. <i>Very poor.</i>	4	36.2	38
Matig wat betreft de reactie op de inputs. <i>Mediocre in terms of response to the inputs.</i>	4	34.5	44
Beneden matig. <i>Past poor.</i>	4	36.7	59
Weer een matige respons. <i>Again a poor response.</i>	4	34.2	67
Beneden modaal. <i>Below average.</i>	4	33.2	73
Redelijk realistisch. <i>Reasonably realistic.</i>	5	62.0	20
Komt meer in de buurt van de realiteit. <i>This comes closer to reality.</i>	5	57.6	27
Niet te veel, niet te weinig, ongeveer goed. <i>Not too much, not too little, about OK.</i>	5	58.4	44
OK. <i>OK.</i>	5	66.6	68
OK. <i>OK.</i>	5	61.9	83
Niet zo best, het lijkt alsof je de verstoringen niet voelt, alleen wat je zelf stuurt. <i>Not too good, it seems as if you do not feel the disturbances, only what you control yourself.</i>	6	35.3	15
Dat voelde alweer beter, kostte alweer bijna geen moeite. <i>That felt better again, almost took no effort at all.</i>	6	74.5	23
Niet eens zo slecht, niet zo duidelijk als je zou willen. <i>Not even that bad, not as clear as you would like though.</i>	6	68.1	62
Qua motion niet zoveel aan. <i>Not very interesting in terms of motion.</i>	6	33.3	79

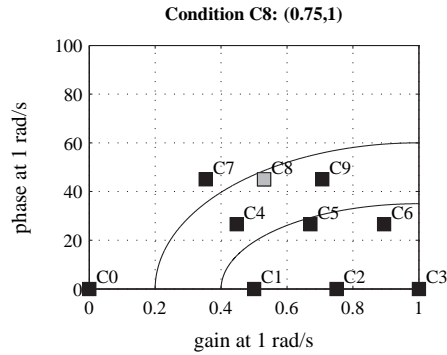
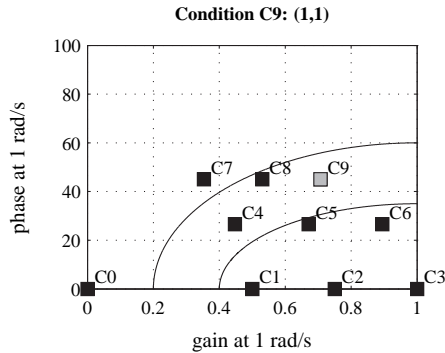


Table H.9. Motion fidelity pilot comments for condition C8 (0.75,1).

Comment (Dutch <i>English</i>)	Subject	Rating	Run
Te veel rol. <i>Too much roll.</i>	1	58.7	17
Rol demping te laag, lateraal OK. <i>Roll damping too low, lateral is OK.</i>	1	55.0	50
Goed. <i>Good.</i>	1	81.2	68
Weinig gain, niet zo heftig. <i>Low gain, not very intense.</i>	2	71.0	24
Realistisch filter, geeft gevoel voor de rolhoek. <i>A realistic filter, provides a sensation of the roll attitude.</i>	2	80.6	39
Niet de beste, ook niet de slechtste. <i>Not the best, but also not the worst.</i>	2	59.1	83
In het begin dacht ik dat het wel OK was, aan het einde niet meer. Wel beter dan de vorige [C7, (0.5,1)]. <i>In the beginning I thought this one was OK, at the end I thought it was not. Still better than the previous one [C7, (0.5,1)].</i>	4	64.9	13
Matig tot redelijk. <i>Poor to reasonable.</i>	4	66.5	29
Matige bewegingsrespons. <i>A middling motion response.</i>	4	53.3	35
Deze krijgt een hele matige beoordeling. <i>This one receives a very poor rating.</i>	4	25.6	46
Licht matig. <i>A bit poor.</i>	4	36.6	60
Iets onder modaal. <i>A bit below average.</i>	4	71.6	68
Een klein beetje als een vliegtuig. <i>A little bit like an aircraft.</i>	4	75.7	74
Voelt beter, maar nog steeds als te veel beweging. <i>Feels better, but still comes across as too much motion.</i>	5	50.8	16
Motion cues helpen wel, maar lijken onrealistisch (te groot). <i>The motion cues do help, but they seem unrealistic (too large).</i>	5	36.7	23
Overdreven. <i>Exaggerated.</i>	5	23.8	43
Motion OK. <i>Motion OK.</i>	5	68.4	64
OK. <i>OK.</i>	5	55.4	77
Niet zoveel feedback in de motion. <i>Not a lot of feedback in the motion.</i>	6	35.0	22

**Table H.10. Motion fidelity pilot comments for condition C9 (1,1).**

Comment (Dutch <i>English</i>)	Subject	Rating	Run
Te heftig, vooral lateraal. <i>Too severe, especially lateral.</i>	1	24.1	11
Iets te veel rol. <i>A little too much roll.</i>	1	63.4	27
Net iets te veel rol. <i>Just a little too much roll.</i>	1	68.2	36
Te sterke beweging. <i>Motion is too strong.</i>	1	36.3	44
Lateraal te sterk. <i>Lateral motion too strong.</i>	1	45.4	66
Matig, lateraal te sterk. <i>Mediocre, lateral too strong.</i>	1	28.2	81
Te weinig rol. <i>Too little roll.</i>	1	51.5	87
Nerveus filtertje. <i>A nervous filter.</i>	2	25.8	18
Niet slecht, maar wel minder goed dan de vorige [C2, (0.75,0)]. <i>Not bad, but still worse than the previous one [C2, (0.75,0)].</i>	2	70.8	35
Veel beweging, te veel. <i>A lot of motion, too much.</i>	2	71.7	46
De bewegingen waren wat random. <i>The motion was a bit random.</i>	2	24.8	54
Een hoop geschok en gedoe. <i>A lot of jolting, a bit of a hassle.</i>	2	32.8	81
Een goed filter om mee te eindigen. <i>A good filter to end with.</i>	2	84.9	95
Voor de stuurtaak plezierig, maar niet in overeenstemming met de werkelijkheid. <i>For the control task this one is nice, but it does not feel realistic.</i>	4	75.0	14
Begint weer op een vliegtuig te lijken. <i>This starts to feel like an aircraft again.</i>	4	82.7	30
Matige respons. <i>A poor response.</i>	4	64.9	31
Een vrij goede respons. <i>A reasonably good response.</i>	4	82.7	49
Deze krijgt een redelijke score. <i>This one receives a reasonable rating.</i>	4	78.8	52
Dat begint weer op een vliegtuig te lijken. <i>That starts to feel like an aircraft again.</i>	4	78.9	65
De respons was goed. <i>A good response.</i>	4	82.4	77
Te veel beweging. <i>Too much motion.</i>	5	38.6	11
Motion cues, maar te veel. <i>Motion cues, but too much.</i>	5	18.1	30
Te veel beweging om realistisch te zijn. <i>Too much motion to be realistic.</i>	5	15.1	40
Ongeveer goed. <i>About right.</i>	5	59.9	53
Cues, wel te veel. <i>Cues, too much though.</i>	5	22.7	58
Te veel om realistische motion te zijn. <i>Too much to be realistic motion.</i>	5	13.7	70
Voelde wel weer beter. <i>That felt a bit better.</i>	6	69.4	17
Minder realistisch dan de vorige [C3, (1,0)]. <i>Less realistic than the previous one [C3, (1,0)].</i>	6	67.1	49
De motion voelde wel goed. <i>The motion felt quite good.</i>	6	86.1	88



Roll Tracking Replicated Condition Comparison

Chapter 6 describes the results of an experiment where pilot roll tracking behavior is measured in real flight and compared to control behavior measured for four different roll motion cueing settings in the SIMONA Research Simulator. Six of the seven Cessna Citation pilots who performed this combined in-flight and simulator experiment also were the participants for the experiment described in Chapter 8, in which a nearly identical roll tracking task was performed for a much larger number of different roll motion cueing settings. In this Appendix the different roll motion cueing settings are referred to using symbols of the same form also used in Chapters 6 and 8, $(K_{m,f}, \omega_{m,f})$, which indicate the combination of motion filter gain $K_{m,f}$ and filter break frequency $\omega_{m,f}$ used for a certain condition. The four overlapping conditions between both experiments – a no-motion condition (0,0), a one-to-one roll motion condition (1,0), and two conditions with a first-order roll motion filter, both with a break frequency of 0.5 rad/s and filter gains of 1 (1,0.5) and 0.5 (0.5,0.5) – allow for direct comparison of the results obtained in both experiments.

This Appendix provides this side-by-side comparison of the subjective motion fidelity ratings given by the pilots in both experiments, in addition to a comparison of the typical behavioral metrics considered in this thesis: tracking performance, control activity, pilot-vehicle system crossover frequencies and phase margins, and identified pilot model parameters. Furthermore, two-way repeated measures ANOVAs are performed on the combined data from both experiments to identify possible effects of the applied variation in motion cueing and the different experimental data sets. Note that the numbering of the different pilots for whom data were collected in both experiments is the same as in Chapter 8.

I.1 Subjective Evaluations

Fig. I.1 shows the subjective motion fidelity ratings obtained from the experiments described in Chapters 6 and 8. The mean ratings obtained from both these experiments are depicted with white and black-filled markers, respectively. Note that the mean data for the first experiment is different from the averages presented in Chapter 6, due to the fact that the data from one subject is not considered for the comparison made in this Appendix. The individual subject data from both experiments is presented in gray in Fig. I.1, for reference. Finally, Table I.1 presents the results of a two-way repeated measures ANOVA, with the different experiments and motion cueing settings as factors, that was performed on this fidelity rating data and on all other dependent measures analyzed in this Appendix.

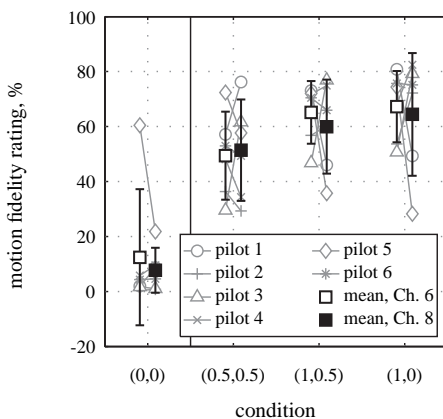


Figure I.1. Subjective motion fidelity rating comparison for the data from the experiments described in Chapters 6 and 8.

Fig. I.1 shows that on average the motion fidelity ratings taken in both experiments correspond well and show the same trend over the different motion conditions. This is confirmed by the ANOVA results (see Table I.1), which only indicate a highly significant effect of the variation in motion cueing on the motion fidelity ratings.

Still, when considering the ratings given by individual subjects (gray data in Fig. I.1) some differences between the data from both experiments are observed. For instance, pilot 5 rated the different motion conditions very differently in both experiments. First, pilot 5 was the only participant to consistently rate the no-motion (0,0) condition at around 60%, where all other subjects rated below 10%, in the experiment described in Chapter 6. For the experiment of Chapter 8 he rated the same condition much lower, on average at around 20%, thereby yielding much lower between-subjects variance for the (0,0) condition. Furthermore, both pilots 1 and 5 consistently rated the (1,0) and (1,0.5) condition lower than the lower-fidelity (0.5,0.5) condition in the experiment of Chapter 8. Note that this contradicts the results collected in the experiment of Chapter 6, where they both gave the conditions with unity-gain roll motion the highest fidelity ratings. As can be verified from the pilot

Table I.1. Two-way repeated-measures ANOVA results for all behavioral metrics.

Dependent measures	Factors								
	experiment			motion			experiment × motion		
	df	F	Sig.	df	F	Sig.	df	F	Sig.
Ratings	1,5	0.13	–	1.4,7.2 ^{gg}	26.82	**	1.6,8.0 ^{gg}	0.26	–
σ_e^2 (N)					n.a.				
$\sigma_{e,d}^2$	1,5	5.26	–	3,15	30.41	**	3,15	2.00	–
$\sigma_{e,t}^2$	1,5	3.10	–	3,15	0.41	–	3,15	1.05	–
$\sigma_{e,n}^2$ (N)					n.a.				
σ_u^2	1,5	3.64	–	1.2,6.2 ^{gg}	14.30	**	3,15	5.06	**
$\sigma_{u,d}^2$	1,5	15.88	**	3,15	9.21	**	3,15	5.81	**
$\sigma_{u,t}^2$	1,5	0.63	–	1.2,5.8 ^{gg}	1.37	–	3,15	0.60	–
$\sigma_{u,n}^2$	1,5	2.30	–	1.1,5.4 ^{gg}	12.31	**	1.1,5.6 ^{gg}	4.14	–
$\omega_{c,d}$	1,5	0.55	–	3,15	29.56	**	3,15	1.14	–
$\omega_{c,t}$	1,5	3.01	–	3,15	2.78	–	3,15	0.20	–
$\varphi_{m,d}$	1,5	0.09	–	3,15	8.67	**	3,15	1.06	–
$\varphi_{m,t}$	1,5	0.85	–	3,15	6.81	**	3,15	0.11	–
K_v	1,5	0.16	–	3,15	20.99	**	3,15	2.86	–
T_L	1,5	4.55	–	3,15	14.85	**	3,15	0.69	–
$K_v T_L$	1,5	1.17	–	3,15	0.21	–	3,15	0.67	–
K_m	1,5	0.88	–	2,10	0.50	–	2,10	0.92	–
τ_v	1,5	0.37	–	3,15	2.06	–	3,15	1.36	–
τ_m	1,5	5.14	–	3,15	0.03	–	3,15	1.32	–
ω_{nm}	1,5	0.34	–	3,15	3.13	–	1.2,6.1 ^{gg}	0.34	–
ζ_{nm}	1,5	3.25	–	3,15	3.81	**	3,15	2.05	–

** = significant ($p < 0.05$) gg = Greenhouse-Geisser sphericity correction
 – = not significant ($p \geq 0.05$) (N) = Issues with data normality

comments in Appendix H, both pilots insisted during the experiment of Chapter 8 that both the roll and lateral motion cues supplied in the (1,0) and (1,0.5) conditions were exaggerated and larger in magnitude than they would expect in the aircraft.

I.2 Tracking Performance and Control Activity

Fig. I.2 shows a comparison of the total tracking error and control signal variances measured in both experiments. Fig. I.2(a) indicates all pilots achieved lower tracking errors in the experiment of Chapter 8, yielding a marked difference in the average tracking performance measured for both experiments. The decrease in σ_e^2 is especially notable for pilot 2, who compared to the other pilots recorded relatively high tracking error variances in the experiment described in Chapter 6. Due to the data from pilot 2, the distribution of the tracking error variance data differs significantly from a normal distribution for all compared conditions. For this reason, no two-way repeated-measures ANOVA could be performed to analyze the σ_e^2 results. Due to the fact that no nonparametric tests for two-way repeated-measures analyses are available, no statistical analysis results for the comparison of the total tracking error variance measured in both experiments are therefore listed in Table I.1.

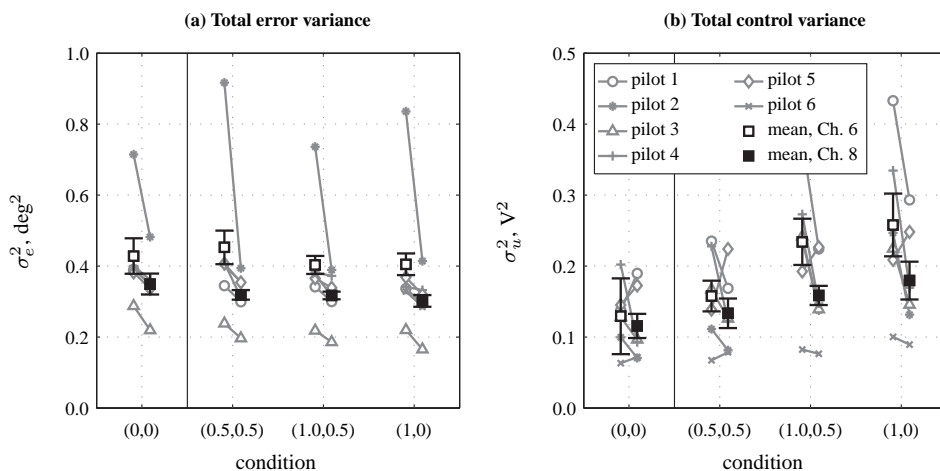


Figure I.2. Total tracking performance and control activity comparison for the data from the experiments described in Chapters 6 and 8.

The control signal variance data shown in Fig. I.2(b) shows the same increasing trend with increasing motion fidelity for both experiments. This effect of the variation in motion cueing settings is found to be highly significant, as can be judged from Table I.1. Fig. I.2(b) further shows control activity was higher for the experiment of Chapter 6, especially for the conditions with high roll motion gains, (1,0.5) and (1,0). The increase in control activity was found to be comparatively less for the experiment of Chapter 8 than for the measurements from the experiment described in Chapter 6. This is also reflected in the ANOVA results,

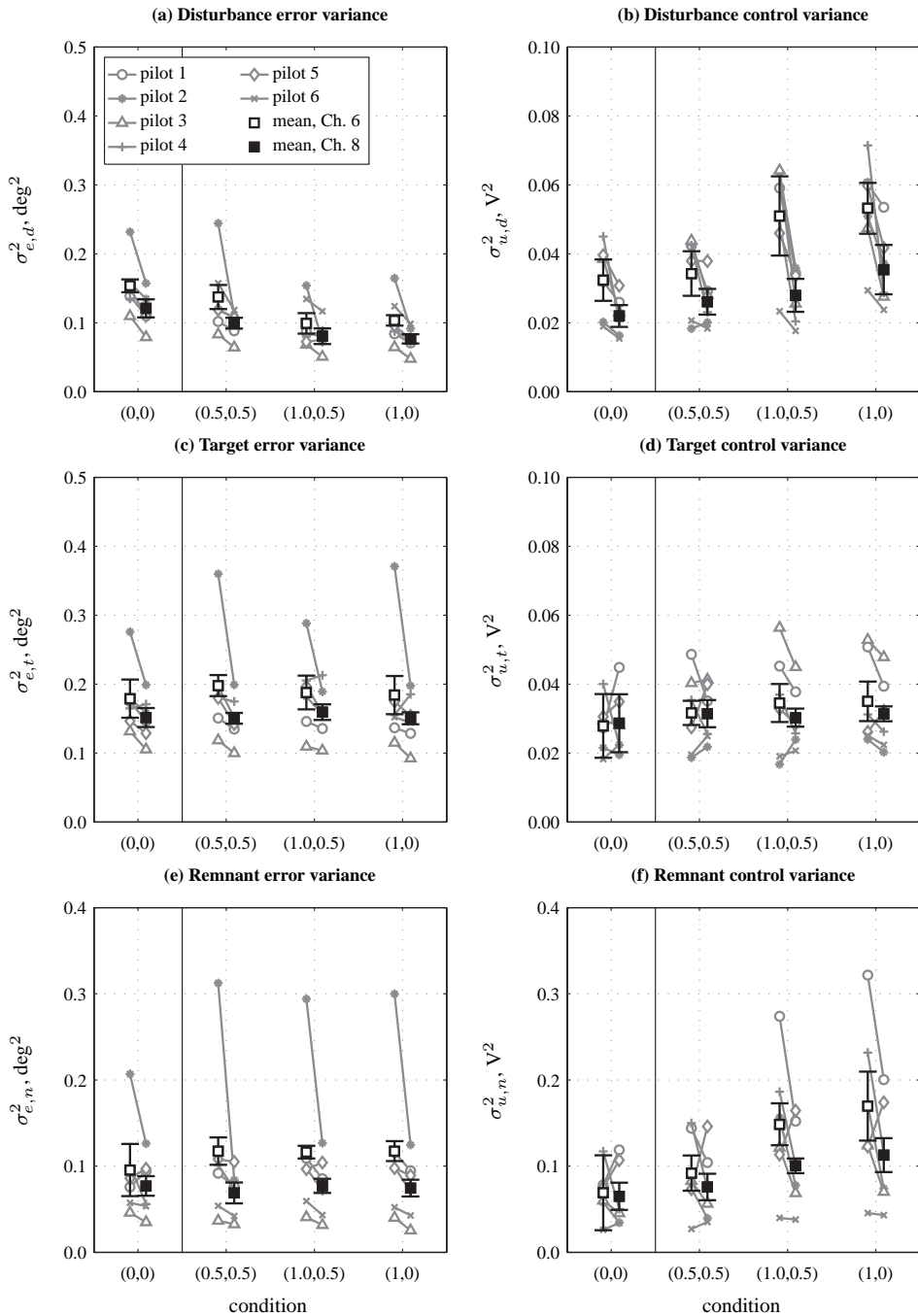


Figure I.3. Comparison of the different components of the tracking error and control signal variances measured in the experiments described in Chapters 6 and 8.

which show a significant interaction between the effect of motion cueing variations and the different experiment data sets.

Fig. I.3 shows the same comparison for the three different components (disturbance, target, and remnant) that together yield the total error and control signal variances shown in Fig. I.2. This variance component data shows largely the same trends also observed in Fig. I.2. Tracking errors resulting from all three components are found to be lower for the experiment of Chapter 8, where the marked improvement in tracking performance for pilot 2 is visible in all components. Note that due to the data from pilot 2 also the $\sigma_{e,n}^2$ data from the experiment of Chapter 6 was found to not be normally distributed. Hence, no statistical analysis results for this remnant component of the tracking error variance are listed in Table I.1.

Equivalent to the observation made for the total control signal variance from Fig. I.2(b), the different components of the control signal variance are also found to be lower for the data from experiment of Chapter 8, especially $\sigma_{u,d}^2$ and $\sigma_{u,n}^2$. The difference in the disturbance component of σ_u^2 between both experiments is even found to be statistically significant (see Table I.1), as is the difference in the increase over the different motion conditions (interaction in Table I.1).

I.3 Crossover Frequencies and Phase margins

Fig. I.4 shows the measured crossover frequencies and phase margins of the disturbance and target open-loop responses for both experiments. As can be verified from Fig. I.4(a) and (c), the observed increase in $\omega_{c,d}$ and decrease in $\varphi_{m,d}$ with increasing roll motion fidelity are both consistent over the data from the two experiments and are both found to be statistically significant (see Table I.1), as also concluded in Chapter 6 based on data from the same four experimental conditions. Furthermore, the increase in target open-loop phase margin $\varphi_{m,t}$ observed for the (1,0.5) and (1,0) conditions in both experiments, which was not found to be significant for only the data from Chapter 6, is found to be statistically significant when the data from both experiments are combined.

The only consistent difference observed between the data from both experiments is that the target-loop crossover frequency $\omega_{c,t}$ is found to be around 0.2 rad/s higher for all conditions in the experiment of Chapter 8, as can be verified from Fig. I.4(b). The ANOVA results of Table I.1, however, show that this difference in $\omega_{c,t}$ is not statistically significant.

I.4 Pilot Control Behavior

Fig. I.5 shows the identified parameter values for the pilot visual gain K_v , visual lead time constant T_L , visual lead gain $K_v T_L$, pilot motion gain K_m and the pilot visual and motion delays (τ_v and τ_m) from both experiments. Fig. I.6 shows the two remaining parameters of the fitted pilot model (see Section 6.2.2): the neuromuscular actuation model natural frequency ω_{nm} and damping ratio ζ_{nm} .

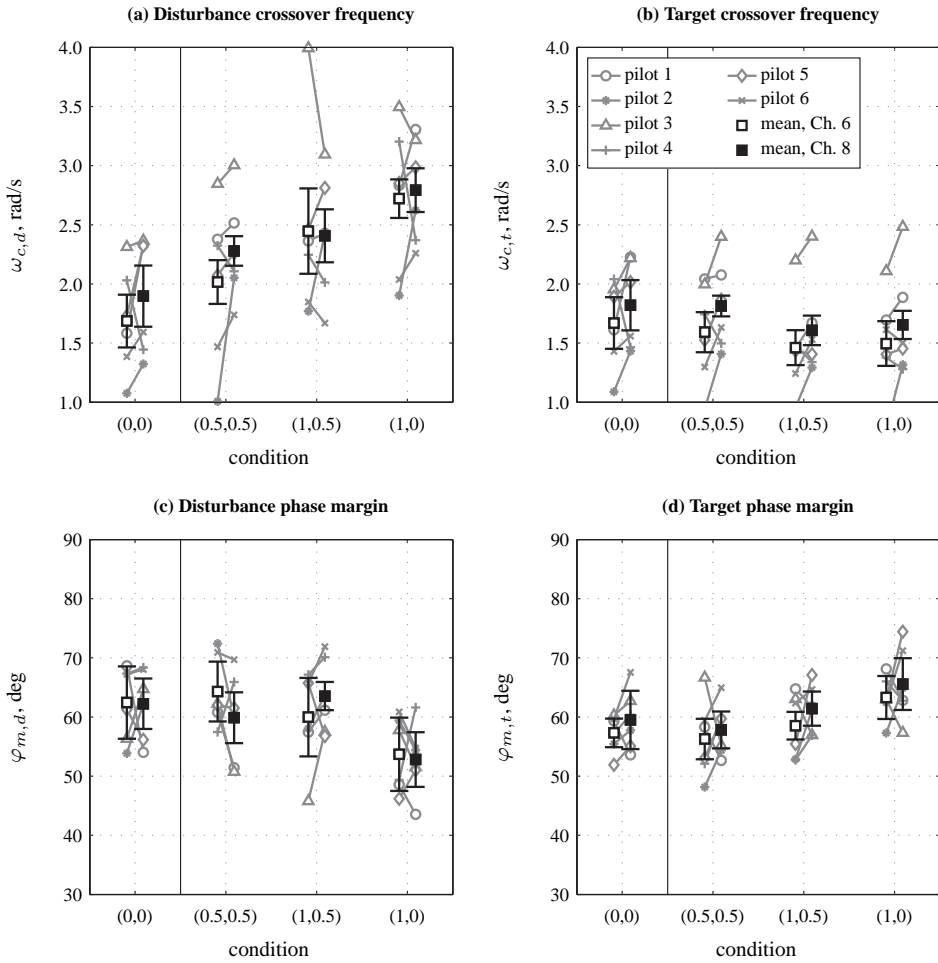


Figure I.4. Comparison of the disturbance and target open-loop crossover frequencies and phase margins measured in the experiments described in Chapters 6 and 8.

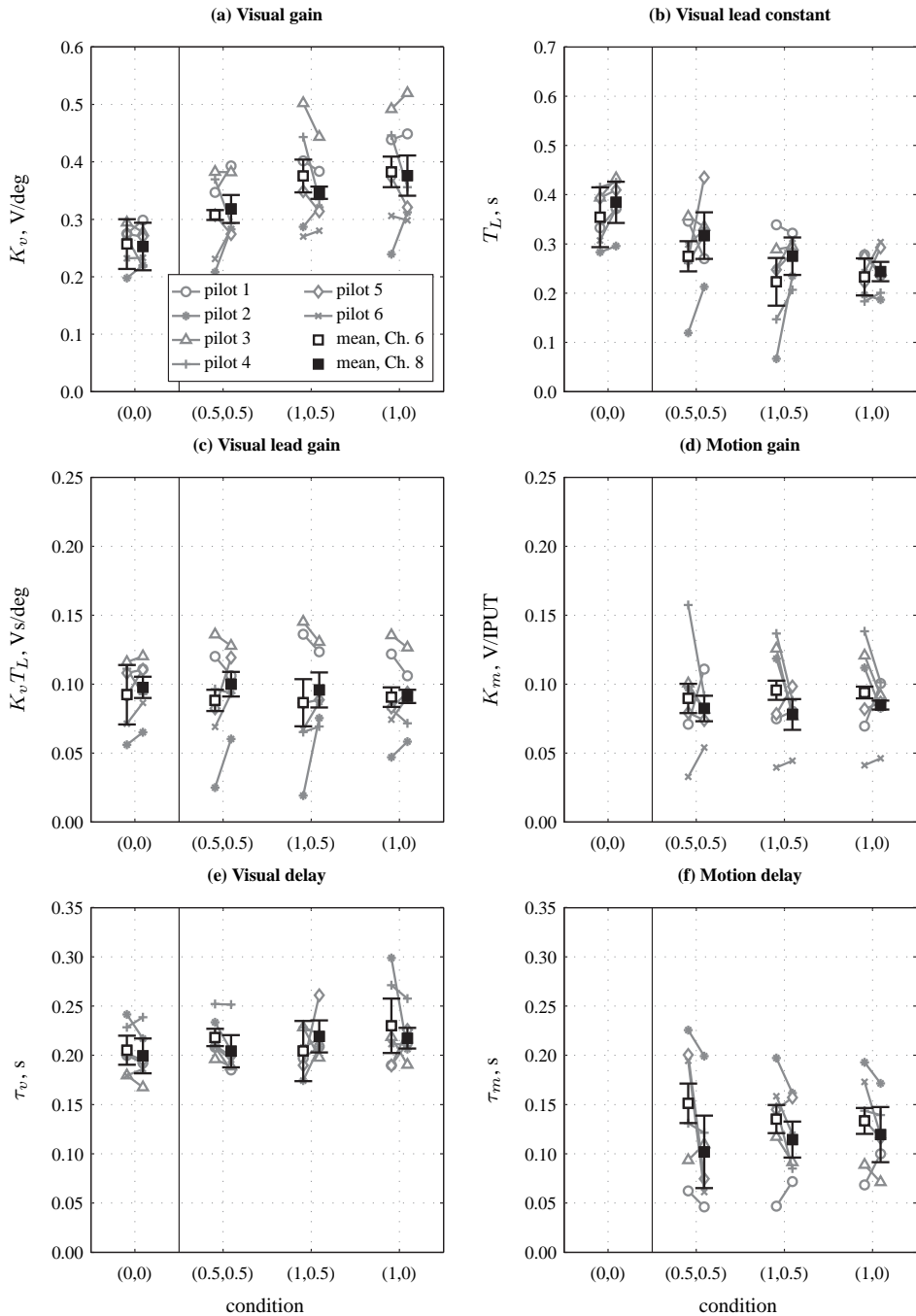


Figure I.5. Comparison of the identified multimodal pilot model parameters for the experiments described in Chapters 6 and 8.

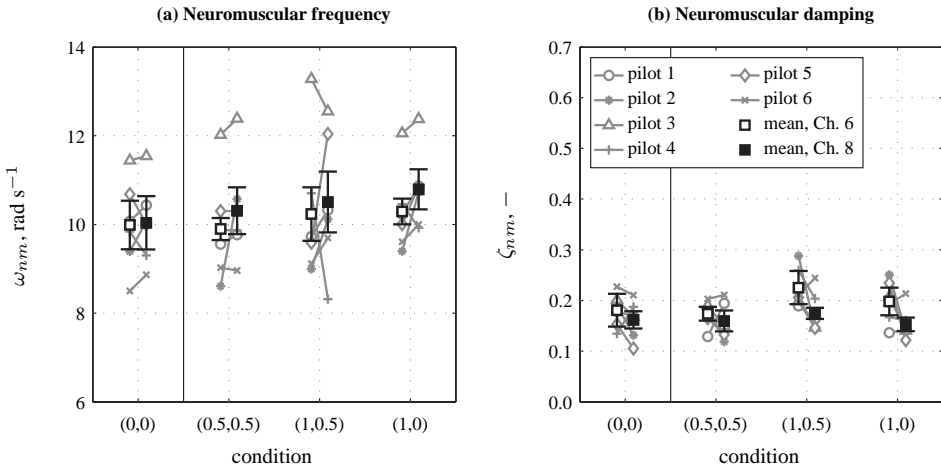


Figure I.6. Comparison of the identified neuromuscular actuation model parameters for the experiments described in Chapters 6 and 8.

Overall, the data from both experiments show the same trends over the different roll motion settings. As also concluded from Chapter 6, the most pronounced effects on pilot tracking behavior are found to be the increase in K_v and decrease in T_L with increasing motion fidelity. As can be verified from Table I.1, both these effects are found to be highly significant. Also for the neuromuscular damping ratio ζ_{nm} , for which slightly increased values are observed for the (1,0) condition and especially (1,0.5) in both experiments, a significant effect of the variation in motion cueing is present.

Figures I.5 and I.6 show only a number of small differences in identified pilot model parameters for the compared experiments. For the experiment described in Chapter 8, visual lead time constants are found to be consistently lower for all conditions except (1,0). In addition, pilot motion gains and time delays are also found to be slightly lower than found for the experiment of Chapter 6 for all experimental conditions. However, as can be verified from Table I.1, none of these differences can be concluded to be statistically significant for the small data set available for this comparison.

I.5 Conclusions

The comparison of the roll tracking data collected for the four overlapping conditions of the experiments described in Chapters 6 and 8 performed in this Appendix shows trends in the considered dependent measures that are highly consistent over the data from both experiments. This is especially true for the measured crossover frequencies and phase margins and the identified pilot model parameters. Still, some between-experiment variation is clearly visible from the comparison made in this Appendix, most notably for the subjective fidelity ratings and measured tracking performance and control activity. Especially for the tracking error and control signal variances, which are both consistently found to be lower for the

experiment of Chapter 8, differences between the data from both experiments are observed. Despite the fact that these observed differences are only found to be statistically significant for the disturbance control variance component, the results presented in this Appendix do suggest that the typical subjective and objective metrics considered for evaluating flight simulator motion fidelity in this thesis are still affected, to a certain extent, by day-to-day variability.

Nomenclature

Latin Symbols

A_d	disturbance forcing function sinusoid amplitude	deg or V
A_t	target forcing function sinusoid amplitude	deg
a_z	heave acceleration	m/s ²
a_{zcg}	c.g. heave acceleration	m/s ²
$a_{z\theta}$	pitch heave acceleration	m/s ²
D	normality test statistic	-
e	tracking error signal	deg
F	ANOVA test statistic	-
f_d	disturbance forcing function	deg or V
f_t	target forcing function	deg
f_x, f_y, f_z	longitudinal, lateral, and vertical specific forces	m/s ²
$H(s)$	transfer function	
$H(j\omega)$	frequency response function	
H_c	controlled element dynamics	
$H_{e,fd}$	closed-loop disturbance-to-error dynamics	
$H_{e,ft}$	closed-loop target-to-error dynamics	
H_{eq}	pilot equalization dynamics	
H_{eqt}	pilot feedforward equalization dynamics	
H_{mf}	motion filter dynamics	
H_{nm}	neuromuscular actuation dynamics	
H_{ol}	open-loop dynamics	
$H_{ol,d}$	disturbance open-loop dynamics	
$H_{ol,t}$	target open-loop dynamics	
H_p	pilot response dynamics	
H_{paz}	pilot heave motion response	
H_{pe}	pilot error response	
H_{pv}	pilot visual response	
H_{pm}	pilot motion response	
H_{pt}	pilot feedforward target response	
$H_{p\theta}$	pilot pitch response	
H_{pp}	pre-position filter dynamics	
H_{sc}, H_{scc}	semicircular canal dynamics	
H_{sm}	simulator motion cueing system dynamics	
H_{sv}	simulator visual cueing system dynamics	
$H_{\ddot{y},x}$	controlled element motion dynamics	
H_{θ,δ_e}	elevator-to-pitch dynamics	
h	altitude	ft

j	imaginary unit	
K	gain	-
K_c	controlled element gain	-
K_{ap}	autopilot input gain	-
K_m	pilot motion response gain	deg/ips or V/IPUT
$K_{m,f}$	motion filter gain	-
K_p	pilot gain	-
K_{pe}	pilot error response gain	-
K_{pt}	pilot feedforward response gain	-
K_S	motion filter gain at 1 rad/s	deg
K_s	stick input scaling gain	-
K_t	pilot feedforward response gain	-
K_v	pilot visual response gain	- or V/deg
$K_{\delta_e,u}$	control input to elevator scaling gain	-
K_{θ,δ_e}	elevator-to-pitch dynamics gain	-
K_ϕ	aircraft roll dynamics gain	-
L	likelihood function	-
l	distance between aircraft c.g. and pilot station	m
N	number of data points	-
N_d	number of disturbance forcing function sinusoids	-
N_t	number of target forcing function sinusoids	-
n_d	disturbance forcing function frequency integer factor	-
n_t	target forcing function frequency integer factor	-
n	pilot remnant signal	deg or V
p	roll rate	deg/s
p	statistical p -value	-
q	pitch rate	deg/s
R	Pearson's correlation coefficient	-
r	yaw rate	deg/s
$S_{x,x}$	Spectrum of x	
s	Laplace variable	
T	time constant	s
T_K, T'_K	low-frequency lag-lead time constants	s
T_L	visual lead time constant	s
T_m	measurement interval	s
T_N	neuromuscular lag time constant	s
T_r	roll subsidence mode time constant	s
T_I	visual lag time constant	s
T_{I_t}	pilot feedforward lag time constant	s
$T_{sc1}, T_{sc2}, T_{sc3}$	semicircular canal time constants	s
T_{θ_2}	short-period mode lead time constant	s
T_ϕ	aircraft roll dynamics lead time constant	s
t	time	s
u	pilot control signal	deg or V
u_{ap}	autopilot input signal	V
V	airspeed	kt
X	generic dependent measure	
X_s, Y_s, Z_s	simulator body axes	
x	controlled element output	deg or m

Y	generic predictor variable	
y	controlled element motion output	deg/s ² or m/s ²
Z	generic dependent measure	
z	vertical position (heave)	m

Greek Symbols

α	linear regression coefficient	-
α	statistical significance level	-
β	linear regression constant	-
Δ	discrepancy operator	
δ_a	aileron deflection	deg
δ_c	controlled element input	deg
δ_e	elevator deflection	deg
ζ_d	dutch roll mode damping ratio	-
ζ_n	motion filter damping ratio	-
ζ_{nm}	neuromuscular damping ratio	-
ζ_{sp}	short-period mode damping ratio	-
ζ_ϕ	aircraft roll dynamics damping ratio	-
θ	pitch attitude	deg
μ	mean	
σ	standard deviation	
σ^2	variance	
φ_m	phase margin	deg
$\varphi_{m,d}$	disturbance phase margin	deg
$\varphi_{m,t}$	target phase margin	deg
ϕ	roll attitude	deg
ϕ_d	disturbance forcing function sinusoid phase shift	rad
ϕ_S	motion filter phase shift at 1 rad/s	deg
ϕ_t	target forcing function sinusoid phase shift	rad
τ	time delay	s
τ_e	effective time delay	s
τ_e	pilot error response delay	s
τ_m	pilot motion response delay	s
τ_t	pilot feedforward response delay	s
τ_v	pilot visual response delay	s
τ_ϕ	aircraft roll dynamics delay	s
χ^2	χ^2 test statistic	-
ψ	yaw attitude	deg
ω	frequency	rad/s
ω_b	additional motion filter break frequency	rad/s
ω_c	crossover frequency	rad/s
$\omega_{c,d}$	disturbance crossover frequency	rad/s
$\omega_{c,t}$	target crossover frequency	rad/s
ω_d	disturbance forcing function sinusoid frequency	rad/s
ω_d	dutch roll mode natural frequency	rad/s
$\omega_{m,f}$	motion filter break frequency	rad/s
ω_m	measurement interval base frequency	rad/s
ω_n	motion filter break frequency	rad/s

ω_{nm}	neuromuscular frequency	rad/s
ω_{sp}	short-period mode natural frequency	rad/s
ω_t	target forcing function sinusoid frequency	rad/s
ω_ϕ	aircraft roll dynamics natural frequency	rad/s

Subscripts

0	trim
<i>d</i>	disturbance
<i>m</i>	motion
<i>m.f</i>	motion filter
<i>n</i>	remnant
<i>nm</i>	neuromuscular
<i>ol</i>	open loop
<i>p</i>	pilot
<i>ref</i>	reference
<i>t</i>	target
<i>s</i>	simulator
<i>v</i>	visual

Acronyms

ANOVA	analysis of variance
ARX	auto-regressive models with an exogeneous input
DUECA	Delft University Environment for Communication and Activation
FBW	fly-by-wire
FC	Fourier coefficients
FTIS	flight test instrumentation system
LCD	liquid crystal display
MLE	maximum likelihood estimation
MSE	mean square error
RMS	root mean square
SCC	semicircular canals
SOP	Successive Organization of Perception
SRS	SIMONA Research Simulator
VAF	variance accounted for
VAS	visual analogue scale

Samenvatting

Objectieve Bepaling van de Waarheidsgetrouwheid van de Beweging van Vluchtsimulatoren met een Cybernetische Aanpak

Daan M. Pool

Het gebruik van vluchtsimulatoren is wijdverbreid in de luchtvaart, waar zij onder andere worden toegepast voor het trainen van piloten en bij aan de luchtvaart gerelateerd onderzoek. Het feit dat vluchtsimulatoren een flexibel, veilig, efficiënt en relatief goedkoop alternatief bieden voor het uitvoeren van deze activiteiten in een echt vliegtuig is de belangrijkste reden voor hun brede toepassing. Doordat de beweging van een echt vliegtuig resulteert in duidelijk voelbare krachten op de lichamen van piloten wordt het nabootsen van dit soort *bewegingsstimuli* al sinds de ontwikkeling van de allereerste simulatoren als een belangrijk onderdeel van vluchtsimulatie gezien. Door technische, praktische en financiële beperkingen is het echter niet haalbaar om de beweging van een vliegtuig volledig na te bootsen in een vluchtsimulator.

De mate waarin een vluchtsimulator er in slaagt om de vliegervaring zoals die tijdens een echte vlucht wordt beleefd na te bootsen wordt meestal de *waarheidsgetrouwheid* van die simulator genoemd. Naast de dynamische capaciteiten van het bewegingssysteem van een vluchtsimulator wordt de waarheidsgetrouwheid van de in een simulator te voelen beweging het sterkst beïnvloed door het toegepaste *bewegingsalgoritme*. Zulke bewegingsalgoritmen worden in het aandrijven van de bewegingssystemen van vluchtsimulatoren gebruikt om de echte vliegtuigbewegingen te transformeren naar een gereduceerde vorm van die bewegingen die *wel* kan worden nagebootst met het bewegingssysteem van de simulator. Zo wordt de echte vliegtuigbeweging vaak ingeperkt door vermenigvuldiging met een *verkleiningsfactor*. Daarnaast worden vaak ook *hoogdoorlaatfilters* toegepast om de simulatorbewegingen verder te beperken. De mate waarin bewegingsalgoritmen zorgen voor verschillen tussen de echte vliegtuigbewegingen en de beweging die voelbaar is in een vluchtsimulator wordt bepaald door de waarden van de *parameters* van zulke algoritmen, zoals de toegepaste *verkleiningsfactoren* en *kantelfrequenties* van de hoogdoorlaatfilters. Het verlagen van de verkleiningsfactoren en het verhogen van de kantelfrequenties zorgt voor grotere verschillen tussen de echte vliegbewegingen en de aangeboden bewegingsinformatie in een simulator.

Het is bekend dat een hoge waarheidsgetrouwheid van de gepresenteerde bewegingsstimuli niet nodig is voor alle toepassingen van vluchtsimulatoren. Voor het ontwikkelen van *elementaire handmatige vliegvaardigheden* en *vaardigheidsgebaseerd stuurgedrag* bij piloten wordt echter aangenomen dat een dergelijke hoge waarheidsgetrouwheid van de simulatorbewegingen *wel* cruciaal is. De huidig beschikbare richtlijnen met betrekking tot het behalen van een afdoende waarheidsgetrouwe simulatorbewegingen zijn echter puur gebaseerd op de eigenschappen van de hard- en software waarmee deze bewegingsstimuli worden gegenereerd. Geen van deze richtlijnen neemt op adequate wijze de eigenschappen van de *menselijke bewegingsperceptie* in acht, ook al dragen die in belangrijke mate bij aan de werkelijke waarheidsgetrouwheid. De belangrijkste reden hiervoor is de nog altijd gebrekkige kennis van het bewegingsperceptieproces en de manier waarop piloten de informatie uit alle beschikbare stimuli benutten tijdens het handmatig besturen van een vliegtuig.

In dit proefschrift wordt daarom de waarheidsgetrouwheid van de in vluchtsimulatoren aangeboden bewegingsinformatie beoordeeld volgens de definitie van *gedragswaarheidsgetrouwheid*. Dat wil zeggen dat de waarheidsgetrouwheid wordt afgelezen aan de capaciteit van simulatoren om *handmatig stuurgedrag* zoals dat tijdens het besturen van een echt vliegtuig toegepast wordt te ondersteunen en te induceren. Dit doel wordt bereikt door het systematisch analyseren van de veranderingen die optreden in het stuurgedrag van piloten als gevolg van beperkingen in de in vluchtsimulatoren aangeboden bewegingsinformatie. Voor deze bepaling van de gedragswaarheidsgetrouwheid wordt in dit proefschrift gebruik gemaakt van een zogeheten *cybernetische aanpak*. Hierbij worden veranderingen in het stuurgedrag van piloten expliciet gekwantificeerd door middel van *multimodale pilootmodellen* die de reacties van piloten op informatie die is waargenomen via de *visuele en vestibulaire modaliteiten* kunnen beschrijven. Door met daarvoor geschikte *schattingstechnieken* de parameters van dit soort multimodale pilootmodellen te schatten op basis van verzamelde metingen van handmatig stuurgedrag wordt een methode verkregen waarmee veranderingen in het multimodale stuurgedrag van piloten *objectief* kunnen worden bepaald. In dit proefschrift wordt deze cybernetische aanpak gebruikt om vaardigheidsgebaseerd gedrag dat is gemeten in een *echt vliegtuig* direct te vergelijken met het stuurgedrag van piloten gemeten in een *vluchtsimulator* voor variërende instellingen van de bewegingsalgoritmen. Van de simulatorinstellingen waarbij de kleinste verschillen in stuurgedrag worden gemeten ten opzichte van het stuurgedrag in een echt vliegtuig kan dan worden gezegd dat ze resulteren in de hoogste gedragswaarheidsgetrouwheid.

De effecten van verminderde waarheidsgetrouwheid van de bewegingsinformatie in vluchtsimulatoren op het handmatige stuurgedrag van piloten worden in dit proefschrift bepaald voor vaardigheidsgebaseerde *tracking-taken*. De reden voor deze keuze is dat is aangetoond dat het stuurgedrag van piloten voor dit specifiek soort stuurtaken voldoende linear en stationair is om het modeleren ervan met *quasi-lineaire regeltheoretische modellen* toe te staan. Bij de tracking-taken in dit proefschrift wordt het stuurgedrag van piloten geïnduceerd met twee *stoorsignalen*, die als een doelsignaal dat gevolgd dient te worden en een externe verstoring op het bestuurde vliegtuig worden geïmplementeerd. Er wordt in dit proefschrift een onderscheid gemaakt tussen twee soorten tracking-taken. De eerste zijn tracking taken met twee onafhankelijke *quasi-willekeurige multisinus stoorsignalen*, waarvoor bekend is dat ze het scheiden van de reacties van piloten op waargenomen visuele en bewegingsstimuli mogelijk maken. In het tweede onderzochte type tracking-taak wordt

een quasi-willekeurig multisinus verstoringssignaal gecombineerd met een *deterministisch* volgsignaal dat bestaat uit meerdere hellingsvormige veranderingen in de doelstandhoek. Dit levert een stuurtaak op die meer overeenkomt met echte handmatige vliegtaken dan de onderzochte tracking-taken met twee multisinus stoorsignalen. In een dergelijke *hellingsvolgtaak* gebruiken piloten wel een andere stuurstrategie dan tijdens tracking-taken met quasi-willekeurige stoorsignalen. Een uitbreiding van de beschikbare multimodale pilootmodellen met een voorwaartskoppeling die wordt aangedreven door het deterministische volgsignaal wordt daarom in dit proefschrift voorgesteld en toegepast voor het beschrijven van menselijk stuurgedrag in hellingsvolgtaken.

Dit proefschrift beschrijft een aantal experimenten, allen uitgevoerd in de SIMONA onderzoekssimulator van de Technische Universiteit Delft, waarbij het vaardigheidsgedreven stuurgedrag van piloten is gemeten voor een aantal verschillende instellingen van de aangeboden simulatorbeweging. De grootste en meest consistente veranderingen in het stuurgedrag van piloten door toenemende inperking van de simulatorbewegingen door bewegingsalgoritmen zijn zichtbaar in de stuurdynamica waarmee piloten reageren op visuele feedback. Een gezamenlijke analyse van de metingen uit een aantal simulatorexperimenten die beschreven zijn in dit proefschrift en in eerdere publicaties van andere onderzoekers laat zien dat piloten gemiddeld 20% minder sterk reageren op visuele stimuli wanneer er geen bewegingsinformatie beschikbaar is in vergelijking met het geval waar de volledige vliegtuigbeweging voelbaar is. Daarnaast neemt met afnemende bewegingswaarheidsgetrouwheid de hoeveelheid visuele lead equalisatie door piloten gemiddeld toe met ongeveer 30% en neemt de tijdsvertraging in de reactie op visuele informatie enigszins af. De stuurdynamica van piloten waarmee ze reageren op bewegingsstimuli zijn in vergelijking veel minder gevoelig voor variërende simulatorbewegingsinstellingen.

De belangrijkste mijlpaal voor het onderzoek dat wordt beschreven in dit proefschrift is de directe vergelijking van het multimodale stuurgedrag van piloten tussen stuurtaken die zijn uitgevoerd in een *echt vliegtuig* en in een *vluchtsimulator*. Metingen aan het stuurgedrag van piloten in een echt vliegtuig zijn voor twee verschillende rolhoek tracking-taken, één met twee multisinus stoorsignalen en één hellingsvolgtaak, verzameld met behulp van het Cessna Citation II laboratoriumvliegtuig van de Technische Universiteit Delft. Om te voorkomen dat verschillen in belanghebbende aspecten van de opstellingen waarin het stuurgedrag van piloten gemeten is, zoals de karakteristieken van de gebruikte visuele displays, sidesticks en de bestuurde vliegtuig- en besturingssysteemdynamica, de geïsoleerde vergelijking van het effect van variërende bewegingsinformatie op het stuurgedrag van piloten in de weg zou staan is al het mogelijke gedaan om de meetopstellingen in het laboratoriumvliegtuig en de SIMONA simulator zo goed mogelijk overeen te laten komen.

Uit de analyse van het stuurgedrag van piloten tijdens de stuurtaken die zijn uitgevoerd in een echt vliegtuig was duidelijk dat gebruik werd gemaakt van de beschikbare bewegingsinformatie. Gemeten pilootdynamica verschilden overduidelijk van het stuurgedrag dat is gemeten voor dezelfde stuurtaken in de SIMONA simulator wanneer daar geen bewegingsstimuli beschikbaar waren. In vergelijking met metingen voor bewegingsinstellingen die resulteerden in simulatorbewegingen die de echte vliegtuigbewegingen zeer goed benaderden werden de stuurtaken in het vliegtuig echter minder precies uitgevoerd en met flink lagere stuuractiviteit. Geschatte pilootmodelparameters lieten zien dat alle piloten in het vliegtuig minder sterk reageerden op zowel visuele als bewegingsinformatie, gemiddeld

gezien een grotere tijdsvertraging in hun respons op visuele informatie hadden en een lagere natuurlijke frequentie van hun neuromusculaire dynamica aannamen. Het verschil in de neuromusculaire dynamica kon met extra stuurgedragmetingen worden terugherleid naar de verschillen in de sidestick en de stoel waarin de piloten zaten in beide opstellingen. De rest van de geobserveerde afwijkingen in stuurgedrag kon echter niet worden verklaard door overblijvende verschillen tussen de experimentele omgeving in vliegtuig en simulator. Het feit dat de beschikbare bewegingsinformatie voor deze metingen zeer nauw overeen kwam suggereert dat de geobserveerde gedragsverschillen het resultaat zijn van factoren die intern aan de piloot zijn, zoals bijvoorbeeld motivatie en stress, die deze vergelijking van menselijk stuurgedrag beïnvloed hebben. Deze experimentele resultaten benadrukken daardoor nogmaals de complexiteit van dit soort vergelijkingen tussen vlucht en vluchtsimulator.

De cybernetische aanpak voor het beoordelen van de waarheidsgetrouwheid van de bewegingsinformatie die wordt aangeboden in vluchtsimulatoren, zoals gebruikt in dit proefschrift, heeft laten zien waardevol inzicht te geven in de manier waarop het stuurgedrag van piloten zich aanpast aan veranderingen in de aangeboden bewegingsinformatie. Met deze aanpak is onweerlegbaar aangetoond dat het vaardigheidsgebaseerde stuurgedrag van piloten verandert als gevolg van de gekozen instellingen van bewegingsalgoritmen. Ondanks de verschillen tussen beide rolhoek stuurtaken waarvoor het stuurgedrag tussen vlucht en vluchtsimulator expliciet is vergeleken, leidt de analyse van dat stuurgedrag voor beide taken tot dezelfde conclusies wat betreft de gedragswaarheidsgetrouwheid. Voor beide taken kwam het multimodale stuurgedrag van piloten het best overeen met dat gemeten in een echt vliegtuig voor die experimentele condities waar de minste verschillen in de bewegingsinformatie ten opzichte van de echte vlucht optraden. Deze overeenkomst was met name duidelijk te zien in die parameters die de veranderingen in het stuurgedrag van piloten als gevolg van veranderingen in de aangeboden bewegingsinformatie het best karakteriseren, zoals de versterkingsfactor en lead tijdsconstante van de visuele responsdynamica. Alle experimentele resultaten beschreven in dit proefschrift suggereren daarom dat het hoogste niveau van gedragswaarheidsgetrouwheid bereikt wordt als de bewegingsstimuli die piloten gebruiken voor het uitvoeren van vaardigheidsgebaseerde stuurtaken met *zo min mogelijk inperkingen door hoogdoorlaatfilters* in vluchtsimulatoren worden aangeboden.

Het is belangrijk dat in verder onderzoek aandacht wordt geschonken aan het uitbreiden van de methoden die gebruikt zijn in dit proefschrift voor toepassing op echte handmatige vliegtuigstuurtaken. Hiervoor zal een aanmerkelijke uitbreiding van de huidige kennis op het gebied van het modelleren van menselijk stuurgedrag nodig zijn, en ook van de methoden en de schattingsalgoritmen die gebruikt kunnen worden voor het bestuderen van dit gedrag. Verder wordt het ten zeerste aanbevolen om de gevolgen van de door beperkingen in de aangeboden simulatorbewegingen geïnduceerde gedragsveranderingen voor het trainen van piloten in vluchtsimulatoren expliciet te analyseren. Dit kan gedaan worden door de hier gebruikte cybernetische aanpak toe te passen op de analyse van het *ontwikkel*en van vaardigheidsgebaseerd stuurgedrag in simulatoren en hoe dat *aangeleerde* gedrag *overdraagt* naar echte vliegtuigbesturing.

Acknowledgments

Even though there is only one name on the cover of this thesis, a lot of other people made significant contributions, either direct or indirect, to its realization and completion. I am very grateful to my family, friends, and colleagues for their continuous help and support throughout this five-year process.

First of all, I would like to thank Max Mulder, my promotor, for giving me the opportunity to pursue my Ph.D. degree at the Control & Simulation Division in Delft. I am very thankful for the fact that Max selected me to work on his VIDI scholarship funded simulator fidelity research project, together with another Ph.D. student, Peter Zaal. Even though we have had some setbacks in our work on this project, especially in the preparation for and execution of the planned in-flight experiments, Max deserves a lot of credit for always succeeding in keeping me motivated and ensuring I kept pushing on. I would also like to express my gratitude to Max for being one of the most approachable supervisors I have heard of, allowing me to drop in for questions frequently and whenever I had them, even well outside of regular office hours.

Another person who greatly contributed to the research described in this thesis is my co-promotor René van Paassen. René is who we all go to with the most difficult questions about our research and at moments when we are truly stuck. He always provides us with the perfect answers to those questions, even though it may take us “mortals” a couple of weeks or months to reach the same level of insight that is natural to René and fully comprehend them. I would also like to thank René for his tireless reviewing of my writings and always managing to provide some extremely sharp comments that I never saw coming, but have greatly improved the quality of a large number of my papers.

I would further like to thank the rest of the scientific staff of the Control & Simulation Division for their contributions to this thesis. I am much indebted to Bob Mulder and Ping Chu for sharing some of their knowledge of system identification and parameter estimation and for their help in the development of the time-domain identification procedure that has allowed for obtaining the majority of the experimental results described in this thesis. In addition, I would also like to sincerely thank Hans van der Vaart for providing me with very detailed and highly useful comments on many of the papers that are included in this thesis.

During much of my Ph.D. time I have worked closely together with Peter Zaal, who was the first Ph.D. student to start working on Max’s VIDI project and with whom I was therefore in a little club known around the office as the “*VIDI boys*”. Peter, thanks a lot for the innumerable interesting discussions, hilarious moments around the office, and the very fruitful cooperation: sometimes 1+1 really is equal to 3. I would also like to sincerely thank

you for still providing me with valuable feedback on my part of the VID I research while you had already moved on to working for NASA after completing your own thesis.

Since the very first week of my Ph.D. research, Peter and I have occupied a double office at C&S with Herman Damveld and Rita Valente Pais. Herman and Rita, I am very thankful for your company and friendship over these past years and for the innumerable experiences we have exchanged regarding our respective research projects, working in research, and life in general. Furthermore, I would like to thank Herman, who joined the work on the VID I project in my third year, for all his advice and for providing significant aid in identifying and resolving a major issue with the experimental setup used for the in-flight experiments. And Rita, it has been awesome sharing a leaky office, an alternative radio station, four “*PhD Comics*” calendars, and the extremely limited leg-room available under our joined desks with you all of these years.

The people and working environment at the Control & Simulation Division are largely responsible for the fact that I had a truly great time during my Ph.D. in Delft. I would therefore sincerely like to thank all my fellow Ph.D. students and all other colleagues at the Control & Simulation Division. I will always have fond memories of our discussions and talks (both those work-related and those not so much), Friday afternoon drinks, very frequent and obligatory coffee breaks, annual C&S barbecues, poker nights, and wonderful conference trips.

With respect to the work described in this thesis, I am forever indebted to the Citation pilots – Xander in ’t Veld, Hessel Benedictus, Bob Mulder, Hans Mulder, Alwin Kraeger, Tjipke van Netten, and Arun Karwal – who agreed to be the participants in our numerous in-flight and simulator experiments. Without these experiments, which must have seemed to be endlessly repetitive and torturously long-winded to you, the writing of this thesis would not have been possible at all. The same holds, of course, for all “non-pilots” who have been subjects in the experiments described in this thesis – Erik-Jan van Kampen, René van Paassen, Jan Comans, Ferdinand Postema, Joost de Winter, Michel de Koning, Arjan van Wieringen, and Frank Drop – or who have participated in some of the other experiments that I have been involved in.

Many of the experiments described in this thesis could also never have been performed without Andries Muis, Ferdinand Postema, Alwin Damman, Menno Klaassen, Harold Thung, Cor Dam, Kees van Woerkom, Fred Toomen, Olaf Stroosma, and Henk Lindenburg. Every time a piece of hard- or software that was key to an experiment in the SIMONA Research Simulator, the Cessna Citation laboratory aircraft, or the Human-Machine Systems lab failed, needed to be repaired, or was to be newly developed from scratch, the Control & Simulation Division’s technical staff has truly been there for me, on numerous occasions.

I would also like to acknowledge the members of the *users committee* that has evaluated my work on this VID I project throughout these years: Sunjoo Advani, Filip van Biervliet, Eddy van Duivenbode, Ruud Hosman, Rob Ruigrok, and Mark Wentink. The often refreshingly practical feedback I have received from this group of flight simulation experts at our periodic meetings has really helped me to always keep the bigger picture in mind while working out the very detailed and specific research questions that I as a researcher found very interesting.

I believe I have been very lucky with the large number of M.Sc. students I have been allowed to supervise during their final M.Sc. research projects at the Control & Simulation

Division. In chronological order: Folkert Praamstra, Hans Beukers, Aniek de Vroome, Sjoerd Breur, Arjan van Wieringen, Frank Drop, Hugo Zollner, Mareijn Willems, Niek Beckers, Vincent Laurens, Martin Kers, Maxim Vos, and Joost van der Heiden. For me, supervising you guys has been one of the most rewarding experiences during the course of my Ph.D. work and I just hope that you have learned as much from working with me as I have from working with you. For this reason, I would also sincerely like to thank Hans van der Steen for giving me the unique opportunity of helping with the supervision of one of his M.Sc. students, Angelique Remmers, at the Neuroscience department of the Erasmus Medical Center.

Spending much of my time as a Ph.D. student sitting behind my computer to prepare experiments, to analyze measurement data, or to put some of the words in this thesis on paper, I was often in dire need of some distraction from my work. For providing me with an especially valuable distraction, I would greatly like to thank my awesome H3 teammates, coach, and all the other great people at Punch Basketball in Delft with whom I have had the pleasure of standing on or hanging around a basketball court over the last years.

Of course, I am also extremely grateful to my parents, my brother, and the rest of my family for supporting me through all the ups and downs of this Ph.D. research project. Without your unconditional love and support I would never have been able to achieve this.

And then finally, Kim – or my “*moppie*” as some of my office mates perhaps know you best – thank you for being there for me, always. The last years have been awesome, though somewhat crazy at times, with both of us pursuing our Ph.D.’s at the same time. Extra special gratitude goes out to Kim for starting a bet with me on the number of pages my thesis would end up counting: even though I lost the bet (badly), who knows how long this thesis would otherwise have ended up to be. . .

Daan Pool

Rotterdam, September 2012

Curriculum Vitae

Daan Marinus Pool was born on January 3, 1983 in Purmerend, The Netherlands. From 1995 to 2001 he attended the Openbare Scholengemeenschap (OSG) West-Friesland in Hoorn, where he obtained his Gymnasium diploma (*summa cum laude*).

In 2001 he enrolled as a student at the Faculty of Aerospace Engineering at Delft University of Technology. As a part of his Aerospace Engineering studies, he performed an internship at Elektronik System GmbH (ESG) in Munich, Germany, where he worked on the flight model of a fixed-base CH-53 simulator. In April 2007 he obtained his M.Sc. degree in Aerospace Engineering at the Control and Simulation Division (*cum laude*), receiving an additional accreditation for completing the Delft University of Technology *Honours Track*. His final thesis work investigated the effects of peripheral visual and physical motion information on manual control of aircraft roll attitude.

In May 2007 he started his Ph.D. research at the Control and Simulation Division of the Faculty of Aerospace Engineering at Delft University of Technology. His research, as described in this thesis, involved the development of an objective method for evaluating flight simulator motion cueing fidelity based on measurements of pilots' manual control behavior.

Since June 2012, after the completion of his Ph.D. thesis, Daan has been working as a Research Scientist with the Human Perception, Cognition and Action group at the Max Planck Institute for Biological Cybernetics in Tübingen, Germany. In Tübingen, he is mainly involved with ongoing research into human motion perception and flight simulator motion cueing. In addition, Daan remains affiliated with the Control and Simulation Division at Delft University of Technology, where he continues to supervise a number of M.Sc. students during their final graduation research projects.



Publications

- Pool, D. M.**, Damveld, H. J., Van Paassen, M. M., and Mulder, M. Effects of Motion Filter Gain and Break Frequency Variations on Pilot Roll Tracking Behavior. *Journal of Guidance, Control, and Dynamics*. To be submitted.
- Pool, D. M.**, Damveld, H. J., Van Paassen, M. M., and Mulder, M. Prediction of Behavioral Pilot Model Parameters for Given Motion Filter Settings. *Journal of Guidance, Control, and Dynamics*. To be submitted.
- Pool, D. M.**, Zaal, P. M. T., Damveld, H. J., Van Paassen, M. M., and Mulder, M. Evaluating Simulator Motion Fidelity using In-Flight and Simulator Measurements of Roll Tracking Behavior. *Journal of Guidance, Control, and Dynamics*. To be submitted.
- Drop, F. M., **Pool, D. M.**, Damveld, H. J., Van Paassen, M. M., and Mulder, M. Identification of the Feedforward Component of Manual Control in Tasks with Predictable Target Signals. *IEEE Transactions on Systems, Man, and Cybernetics – Part B*. Under review.
- Zaal, P. M. T., **Pool, D. M.**, Van Paassen, M. M., and Mulder, M. (2012). Comparing Multimodal Pilot Pitch Control Behavior Between Simulated and Real Flight. *Journal of Guidance, Control, and Dynamics*, 35(5):1456–1471.
- Valente Pais, A. R., **Pool, D. M.**, De Vroome, A. M., Van Paassen, M. M., and Mulder, M. (2012). Pitch Motion Perception Thresholds During Passive and Active Tasks. *Journal of Guidance, Control, and Dynamics*, 35(3):904–918.
- Pool, D. M.**, Valente Pais, A. R., De Vroome, A. M., Van Paassen, M. M., and Mulder, M. (2012). Identification of Nonlinear Motion Perception Dynamics Using Time-Domain Pilot Modeling. *Journal of Guidance, Control, and Dynamics*, 35(3):749–763.
- Pool, D. M.**, Zaal, P. M. T., Van Paassen, M. M., and Mulder, M. (2011). Identification of Multimodal Pilot Models Using Ramp Target and Multisine Disturbance Signals. *Journal of Guidance, Control, and Dynamics*, 34(1):86–97.
- Pool, D. M.**, Zaal, P. M. T., Damveld, H. J., Van Paassen, M. M., Van der Vaart, J. C., and Mulder, M. (2011). Modeling Wide-Frequency-Range Pilot Equalization for Control of Aircraft Pitch Dynamics. *Journal of Guidance, Control, and Dynamics*, 34(5):1529–1542.

- Zaal, P. M. T., **Pool, D. M.**, Mulder, M., Van Paassen, M. M., and Mulder, J. A. (2010). Identification of Multimodal Pilot Control Behavior in Real Flight. *Journal of Guidance, Control, and Dynamics*, 33(5):1527–1538.
- Pool, D. M.**, Zaal, P. M. T., Van Paassen, M. M., and Mulder, M. (2010). Effects of Heave Washout Settings in Aircraft Pitch Disturbance Rejection. *Journal of Guidance, Control, and Dynamics*, 33(1):29–41.
- Beukers, J. T., Stroosma, O., **Pool, D. M.**, Mulder, M., and Van Paassen, M. M. (2010). Investigation into Pilot Perception and Control During Decrab Maneuvers in Simulated Flight. *Journal of Guidance, Control, and Dynamics*, 33(4):1048–1063.
- Zaal, P. M. T., **Pool, D. M.**, Mulder, M., and Van Paassen, M. M. (2009). Multimodal Pilot Control Behavior in Combined Target-Following Disturbance-Rejection Tasks. *Journal of Guidance, Control, and Dynamics*, 32(5):1418–1428.
- Zaal, P. M. T., **Pool, D. M.**, Chu, Q. P., Van Paassen, M. M., Mulder, M., and Mulder, J. A. (2009). Modeling Human Multimodal Perception and Control Using Genetic Maximum Likelihood Estimation. *Journal of Guidance, Control, and Dynamics*, 32(4):1089–1099.
- Zaal, P. M. T., **Pool, D. M.**, De Bruin, J., Mulder, M., and Van Paassen, M. M. (2009). Use of Pitch and Heave Motion Cues in a Pitch Control Task. *Journal of Guidance, Control, and Dynamics*, 32(2):366–377.
- Pool, D. M.**, Mulder, M., Van Paassen, M. M., and Van der Vaart, J. C. (2008). Effects of Peripheral Visual and Physical Motion Cues in Roll-Axis Tracking Tasks. *Journal of Guidance, Control, and Dynamics*, 31(6):1608–1622.